UNIVERSITÉ DE STRASBOURG

Thèse d'Habilitation à Diriger des Recherches

Contribution à l'étude des catalogues sismiques, mouvements forts et aléa sismique: Cas des séismes du Moyen Orient

Présentée par:

Mehdi Zaré

À l'Université de Strasbourg

Soutenue le 1er Février 2017

Membres du Jury:

Prof. Mustapha Meghraoui	Université de Strasbourg, France	Garant
Prof. Aldo Zollo	Université de Naples, Italie	Rapporteur
Dr. Wolfgang Brüstle	Regierungspräsidium Freiburg, Germany	Rapporteur
Prof. Alessia Maggi	Université de Strasbourg, France	Rapporteur
Dr. Pierre-Yves Bard	Université de Grenoble (ISTerre), France	Examinateur
Dr. Jacques Hinderer	Université de Strasbourg, France	Examinateur

UNIVERSITÉ DE STRASBOURG

Thesis of Habilitation for Direction of Researches

Contribution to the study of the seismicity, strong motion catalogues and seismic hazard assessment of the Middle East earthquakes

Presented by:

Mehdi Zaré

At the University of Strasbourg

Defended at February 1, 2017

Members of Jury:

Prof. Mustapha Meghraoui	University of Strasbourg, France	Guarantor
Prof. Aldo Zollo	University of Naples, Italy	Reporter
Dr. Wolfgang Brüstle	Regierungspräsidium Freiburg, Germany	Reporter
Prof. Alessia Maggi	University of Strasbourg, France	Reporter
Dr. Pierre-Yves Bard	University of Grenoble (ISTerre), France	Examiner
Dr. Jacques Hinderer	University of Strasbourg, France	Examiner

Résumé

Dans cette thèse, je présente mes travaux de recherche les plus importants menés sur la sismicité des catalogues, les bases de données de mouvement du sol et l'analyse des risques sismiques en Iran et dans d'autres zones actives du Moyen-Orient et de l'Asie du sud. L'accent dans cette thèse est mis sur les grands facteurs de contrôle pour la détermination de la source sismique, les paramètres de la sismicité et les modèles de mouvement du sol. Après chaque séisme (comme en 1990, le tremblement de terre de Manjil, M_w=7.3, et, en 2003, le tremblement de terre de Bam, M_w=6.5), il y a des discussions sur la fiabilité des cartes de zonage de l'aléa sismique et une comparaison entre l'enregistrement et la prédiction des mouvements du sol. Ceci montre l'importance des données d'entrée et le niveau de connaissance des paramètres de sources sismiques dans les régions à risque (géométrie et mécanique des failles, les périodes de retour, etc..).

La thèse est organisée en 8 chapitres qui présentent un résumé de mes travaux de recherche et publications sur des sujets incluant les catalogues de sismicité, les mouvements forts, le développement des relations d'atténuation des risques sismiques et leur analyse. En outre, un résumé des études de reconnaissance de certains tremblements de terre destructeurs (depuis 2003) et les enseignements qui en découlent, ainsi que ma formation de recherche en matière de supervision de thèse sont décrits. En outre, une nouvelle recherche sur la sismicité et les mouvements sismiques de la banque de données de l'Asie du sud est proposée dans ce manuscrit.

Mehdi Zaré

Novembre 2016

Abstract

In this thesis, I present the most important research works I conducted on the seismicity catalogs, strong ground motion databases and seismic hazard analysis of Iran and other active zones in the Middle East and south Asia. An emphasis in this thesis is to represent the important controlling factors for the seismic source determinations, seismicity parameters and ground motion models. After each earthquake (such as the 1990, Manjil earthquake; Mw=7.3, and 2003, Bam earthquake; Mw=6.5) there are some discussions on the reliability of the seismic hazard zoning maps and a comparison between the recorded and previously assessed ground motions. This draws attention to the importance of input dataset and the level of knowledge of the seismic source parameters in the potential seismic regions (geometry and mechanical of faults, return periods, etc...).

The thesis is organized in 8 chapters that present a summary of my research works and published papers on the subjects including seismicity catalogues, strong motion processing, development of attenuation relationships and seismic hazard analysis. In addition, a summary of reconnaissance studies of some important and destructive earthquakes (since 2003) and lessons learned from them, as well as my research formation in terms of supervision of Ph.D. thesis are described. Furthermore, a new research on seismicity and strong motion databank of the south Asia is proposed in this manuscript.

Mehdi Zaré

November 2016

چکیده

در این رساله، مهم‌ترین کارهای پژوهشی اینجانب در زمینه لرزه‌خیزی، پردازش و آنالیز داده‌های جنبش نیرومند زمین و همچنین تحلیل خطر زمین‌لرزه که طی سال‌های اخیر در ایران و سایر مناطق فعال در خاورمیانه و آسیای جنوبی انجام شده است، ارائه می‌شود. در متن حاضر، بیشترین تاکید بر معرفی مهم‌ترین عوامل کنترل‌کننده در تعیین سرچشمه‌های لرزه‌زا، پارامترهای لرزه‌خیزی و مدل‌های جنبش نیرومند زمین است. پس از رخداد برخی از زلزله‌های مخرب ایران (مانند زلزله 1990 منجیل با بزرگای M_w=7.3 و زلزله 2003 بم با بزرگای M_w=6.5) بحث‌های متعددی درمورد میزان کارائی نقشه‌های پهنه‌بندی زلزله و مقایسه بین سطوح جنبش نیرومند ثبت شده و پیش‌بینی شده به راه افتاده است. این مساله بر توجه به اهمیت مجموعه داده‌های ورودی و میزان شناخت ما از پارامترهای چشمه‌های لرزه‌ا در مناطق لرزه‌خیز (مانند هندسه و مکانیک گسل، دوره بازگشت و ...) تاکید می‌کند.

رساله حاضر در 8 فصل ساماندهی شده است. در این نوشتار، خلاصه‌ای از مهم‌ترین مقالات و کارهای پژوهشی اینجانب در زمینه کاتالوگ‌های لرزه‌خیزی، پردازش داده‌های جنبش نیرومند، توسعه روابط کاهندگی و تحلیل خطر زمین‌لرزه آورده شده است. به‌علاوه، به خلاصه‌ای از مطالعات شناسایی مهم‌ترین زلزله‌های مخرب در ایران و جهان (از سال 2003 تاکنون) که موردبازدید قرار گرفته‌اند، و به درس‌های آموخته شده از این زلزله‌ها نیز اشاره گردیده است. در پایان، ساختار کارهای پژوهشی اینجانب در قالب راهنمایی رساله‌های دانشجویان دکترا نیز تشریح شده و یک پروپوزال پژوهشی جهت مطالعه بانک داده‌های لرزه‌خیزی در جنوب آسیا در قالب HDR ارایه می‌شود.

مهدی زارع

نوامبر 2016- آذر 1395

e

Table of Contents

Introduction

In this section, I present the motivations and the importance of the research subject as well as the outline, objectives and the structure of this thesis. It should be noted that all the sections and sentences in *italics* throughout the text are excerpts from articles (or websites) which are mentioned along with their corresponding references.

Motivations and importance of the research subject

From the seismotectonic point of view, the Iranian Plateau and the Middle-East region are exposed to high seismic activity and are greatly influenced by the continental convergence between the Arabian and the Indian plates to the NE and northward with respect to the Eurasian plate. According to the regional tectonic regime of the Iranian plateau, the focal mechanism solutions of the most earthquakes are compressional, strike-slip or a combination of these two mechanisms (Fig. 1).

Reilinger et al., (2006) showed that there is counterclockwise rotation in the crust including the Arabian plate, Zagros and central Iran, Turkey, and the Aegean relative to Eurasia with rates of about 20–30 mm/yr. (Fig. 2). Central Turkey has an internal deformation <2 mm/yr, while surrounded by the right-lateral North Anatolian fault on the north (24±1 mm/yr) and by the left-lateral East Anatolian fault on the southeast (9±1 mm/yr). Relative to Eurasia, the southwestern Aegean-Peloponnisos moves toward the SSW at 30±2 mm/yr in a coherent fashion with low internal deformation (<2 mm/yr) (McClusky et al., 2000). The similar measurements in the Iranian continent and northern Oman performed by Vernant et al., (2004) indicate that most of the shortening is accommodated by the Makran subduction zone (19.5±2 mm/yr) and less by the Kopet-Dag (6.5±2 mm/yr). The Central Iranian Block moves consistently with internal deformation smaller than 2 mm/yr. In the western part of Iran, distributed deformation occurs among several fold and thrust belts. Between the Central Iranian Block and the Arabian Plate, the central Zagros accommodates about 7±2 mm/yr of north–south shortening. North of the Central Iranian Block, the Alborz mountain range accommodates 8±2 mm/yr of north–south compression. According to the GPS measurements by Wang et al. (2001), the southern parts of the Himalaya show northward movement (N19°-22°E) at a rate of 36 to 38 mm/yr with respect to stable Eurasia. Bangalore in southern India has a northward velocity of 35.9±1 mm/yr. The maximum velocity (38 mm/yr) in the northern Ganges plains approximates the rate of convergence between the Indian and Eurasian plates. All these GPS analysis indicate high rates of

deformation in the Middle-East region and the Iranian Plateau, so that the region is exposed to all-round pressures caused by the collision of lateral tectonic plates.

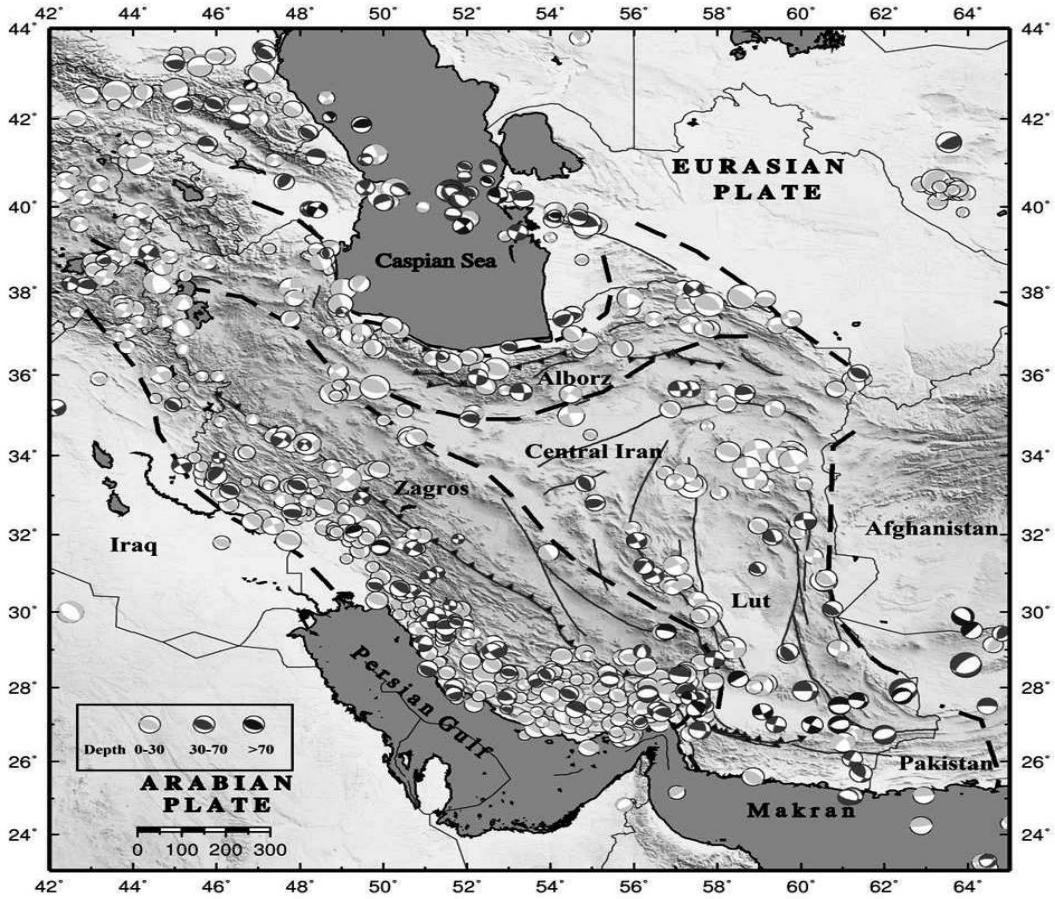

Fig 1. Focal mechanism of the main earthquakes recorded in Iran during the last century. Dashed lines: borders of the 3 main tectonic zones of Iran. Solid line: major faults (adapted from Shahvar et al., 2013).

Therefore, the geodetic, seismic and tectonic studies in the region confirm the existence of a complex active tectonic framework with high deformation rates, a part of which expresses in terms of earthquakes. This region experiences different earthquake magnitudes each year, some of them may reach M_w8 (e.g. 27 November 1945 M_w8.1 Makran earthquake). Many destructive earthquakes with magnitude≥7.0 have occurred during the last century such as the 1909 Silakhor (M_w.7.3), 1930 Salmas (M_w.7.1), 1962 Bou'in-Zahra (M_w.7.1), 1968 Dasht-e-Bayaz (M_w.7.4), 1978 Tabas (M_w.7.4), 1990 Manjil (M_w.7.4),1997 Ghaen (M_w.7.3), 2003 Bam (M_w.6.6), 2013 Savaran (M_w.7.8) earthquakes in Iran, 1939 Erzincan (M_w.7.8), 1970 Gediz (M_w.7.2), 1976 Çaldıran–Muradiye (M_w.7.0), 1999 Izmit (M_w.7.6), 1999 Düzce (M_w.7.2), 2011 Van (M_w.7.1) earthquakes in Turkey, the Nuweiba

earthquake south of the Dead Sea fault and in the Gulf of Aquaba in Egypt, the 1935 Quetta (M_w.7.7), 1945 Balochistan (M_w.8.1), 2005 Balakot (M_w.7.6), 2011 Dalbandin (M_w.7.2) and 2013 Awaran (M_w.7.7) earthquakes in Pakistan, and the 2002 Hindu-Kush (M_w.7.4) and 2015 Hindu-Kush (M_w.7.5) earthquakes in Afghanistan (Fig. 3).

Taking into account the seismotectonic framework and high seismicity with destructive earthquakes as well as the large population density settled in the earthquake-prone areas, the necessity for the development of a database with field investigations for the seismic hazard and risk assessment is critical.

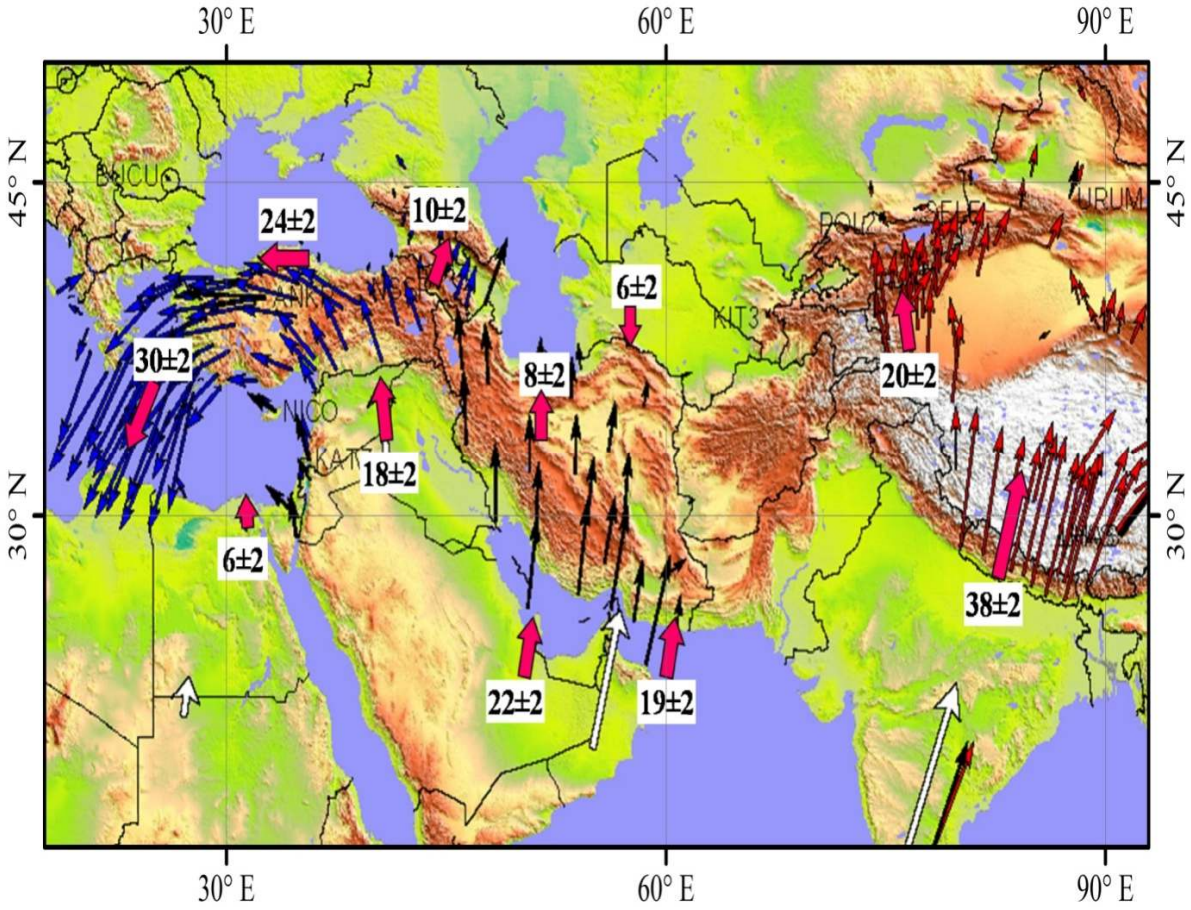

Fig 2. Horizontal velocity field for a major part of Alpine-Himalayan chain. The blue vectors are by Reilinger et al., (2006) and McClusky et al. (2000) and the red vectors are by Wang et al. (2001). The black vectors are by Vernant et al. (2004). The white vectors are the Nuvel1-A plate velocity model by DeMets et al. (1994).

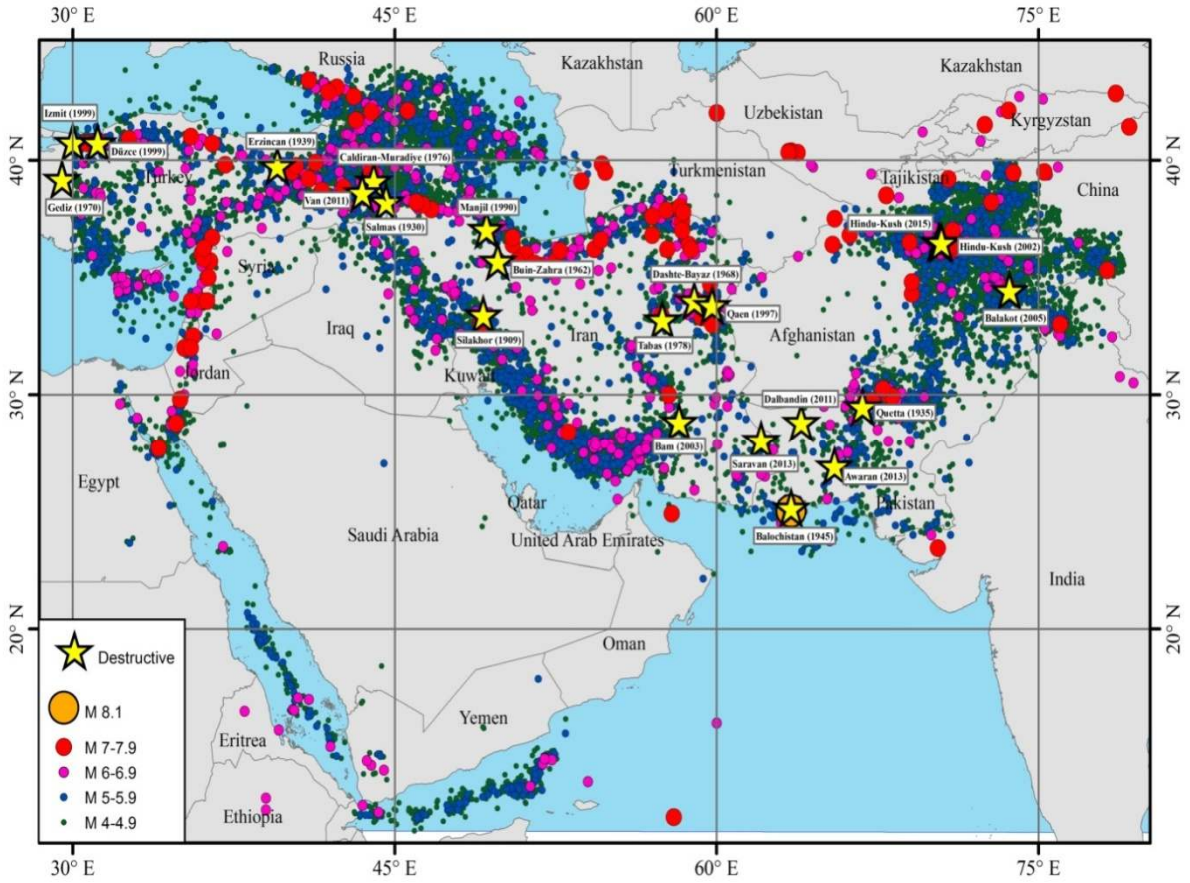

Fig. 3. Seismicity map of the Middle East region before declustering represented by epicenters of earthquakes ($4 \leq M_w$). Yellow stars indicate some of the destructive seismic events (with $6.5 \leq M_w$) during the last century. Source of data: EMME earthquake catalogue (Zare et al., 2014).

After some earthquake (such as the 1978 M_w7.4 Tabas earthquake, 1990 M_w7.3 Manjil earthquake and 2003 M_w6.5 Bam earthquake), several questions were raised on the reliability of the seismic hazard zoning maps and on the comparison between the recorded and previously assessed ground motions. I will exemplify some important events where the hazard maps failed to predict the high hazard levels. Such examples indicate the importance of the accuracy of the input dataset and the level of knowledge of the seismic source parameters in the study regions (fault geometry and mechanics, return periods of large and destructive earthquakes, etc...).

Related efforts

I will describe different approaches in the study of seismicity and seismic hazard analysis in a specific chapter. The application of most popular seismic hazard analysis methods such as the

Deterministic Seismic Hazard Analysis (DSHA) as well as the Probabilistic Seismic Hazard Analysis (PSHA) in the study region is explained. It should be noted that reliable seismic hazard studies depend on having a robust earthquake catalogue, good knowledge on the tectonic framework and rate of active deformation, and relevant attenuation model. The better input for hazard analysis results in more reliable the parameters and the seismic hazard assessments, so that precise input data such as comprehensive catalogues, seismicity parameters as well as characteristic of seismotectonic zones lead to decrease uncertainties of the analysis. There have been several efforts to prepare uniform earthquake catalogues of the Middle-East and Iran in the recent years such as a new earthquake catalogue of the Middle East region which has been developed consisting historical, early and modern instrumental events recorded between 1250 B.C. and 2006 (Zare et al., 2014). This effort was undertaken under the framework of Global Earthquake Model (GEM) and Earthquake Model of Middle East (EMME) projects and the final goal was to establish a unified catalogue of seismicity by incorporating regional and international data to be used for homogeneous estimation of seismic hazard in the region. In addition, two seismicity catalogues including a uniform catalogue for the Iranian earthquakes with a moment magnitude range of M_W 3.5–7.9, from the third millennium BC until April 2010 (Karimiparidari et al., 2013) as well as a unified instrumental catalogue for the Iranian Plateau (1900–2011) with $M_w \geq 4$ (Shahvar et al., 2013) were prepared in the framework of supervision of Ph.D. thesis performed at the International Institute of Earthquake Engineering and Seismology (IIEES). In this regard, I also present the way of compiling raw metadata and the reason of declustering the most important recent catalogues as the comprehensive available databank. Throughout my previous research topics, I noticed that there is not enough strong-motion metadata in most parts of the study region, except in some parts of Iran and Turkey that contribute to improving the DSHA and PSHA studies. Uncertainties associated with the seismic hazard analysis and level of success of the Poisson method in the region is also presented.

In conclusion, I mention that the seismic hazard studies in the Middle-East and south Asia have been initiated using deterministic approaches, continued with probabilistic approaches and finally linked to the spectral zoning maps. The trend in hazard mapping appears to cover the intensity assessment, realistic acceleration and the neo-deterministic approaches; the development of site specific seismic hazard analysis for the region should be based on the detailed integrated site characteristics database.

Outline

In this thesis, I present the most important research works I conducted on the seismicity catalogues, strong ground motion databases and seismic hazard analysis of Iran and other active zones in the Middle East and south Asia. An emphasis in this thesis is to represent the important controlling factors for the seismic source determinations, seismicity parameters and ground motion models. In this manuscript, a summary of reconnaissance studies of some important and destructive earthquakes (since 2003) and lessons learned from them, as well as my research formation in terms of supervision of Ph.D thesis are described. Furthermore, a new research on seismicity and strong motion databank of the south Asia is proposed in this manuscript.

Objectives

The scope of this thesis is to represent the context and a critical review of the seismic hazard studies that I performed during the last 17 years. This will represent the necessity of the development and re-evaluation of and seismicity parameters and seismic hazard studies in the Middle East region; with a special reference to the seismic hazard assessments performed in Iran. The presentation of the studies cover from challenges of development of earthquake seismicity and strong motion databases toward the development of regional attenuation models and uncertainty considerations for hazard analysis.

Thesis structure

The thesis has been organized in 8 chapters that present a summary of my research works and published papers on the subjects including seismicity catalogues, strong motion processing, development of attenuation relationships and seismic hazard analysis (SHA) and etc.

In the ***chapter 1***, the methodology of the studies about seismicity and seismic hazard analysis is described. In this regard, the necessity of a time-dependent as compared with a time-independent seismic hazard analysis as well as the importance of Poisson distribution in the seismicity catalogues are presented briefly. It should be considered that there are not enough strong-motion metadata in the region of study, while there are relatively proper data in some parts such as Iran and Turkey. The application of most popular seismic hazard analysis approaches such as the Deterministic Seismic Hazard Analysis (DSHA) as well as

the Probabilistic Seismic Hazard Analysis (PSHA) are also discussed. I also discuss uncertainties which originated from the lack of knowledge about the seismic sources and their effects on the final SHA results.

An accurate earthquake catalog results in more reliable outputs in seismic hazard analysis. In this respect, there have been several efforts to prepare uniform earthquake catalogs of the Middle-East and Iran in the recent years which are described in the ***chapter 2***. In this section, the existing seismic networks within the region are first pointed out briefly. Then, the way of compiling and the reason of declustering the most important recent catalogs as the comprehensive available databanks are explained.

In the ***chapter 3***, I highlight the results of strong motion processing and especially the data analysis of the Iranian and Turkish strong-motion networks. The main outcome is to obtain strong motion catalogues with the seismic parameters of site conditions, the frequency band of seismic records, peak values of acceleration, velocity and displacements, source parameters (magnitude, epicentral and macroseismic distances), intensity and fault plane solutions whenever possible. The aim is to obtain with other regional dataset, a homogenous and good quality database to be incorporated in the SHA. Furthermore, the strong-motion processing of some case studies such as the earthquakes of Bam, Iran (M_w=6.5, 2003), Gorkha, Nepal (M_w=7.8, 2015) and etc are expressed and discussed.

Since the attenuation relations are one of the most essential elements of any seismic hazard analysis, in the ***chapter 4***, I have tried to summarize the researches, which I involved with during the last two decades for developing regional attenuation equations for Iran and other regions. In this respect, different PGA, spectral acceleration and intensity equations, with a recent development of intensity-strong motion predictive equations in Iran are described. The regional attenuation equations would lead to have less uncertainties in the seismic hazard assessments of Iran.

In the ***chapter 5***, I first review a state-of-the-art on the seismic hazard assessments during four decades in Iran. Then, I discuss the previous and current challenges in SHA studies of Iran, e.g. the sufficiency of seismotectonic data in the region of study and what we did not know about the faulting and site conditions before the major earthquakes such as the 1978 Tabas, 1990 Manjil and 2003 Bam for finalizing the seismic hazard zoning programs in Iran. Subsequently, my most important studies on seismotectonic and sources, magnitude

assessments as well as the recent seismic hazard zoning in Iran and some parts of Asia (including Malaysia, Singapore and Iraq) are summarized.

In the ***chapter 6***, a combination of lessons learned from in-situ earthquakes damages and subsequent phenomena observed during reconnaissance studies in different earthquake-affected areas are presented. In this regard, selected topics such as the data acquisition in earthquake recognitions, the analysis of recorded strong motions, the determination of physical damage, the near-field effects associated with directivity and fling-step, and the importance of these analysis in hazard zoning provide some insights into the seismic hazard assessment. These studies are the results of field investigations that I performed following the fourteen important recent earthquakes in Iran and other countries in the Middle East. The field studies start from the 2003 Bam (Iran) earthquake, continue with the 2003 Boumerdès-Zemmouri (Algeria), 2005 Balakot (Pakistan), 2009 Padang (Indonesia), 2009 Southeastern Tehran (Iran), 2010 Kuh-Zar (Iran), 2011 Tohoku (Japan), 2011 Van (Turkey), 2012 Varzeghan (Iran) twin events, 2013 Shonbeh (Iran), 2013 Saravan (Iran), 2013 Bashagard (Iran), 2014 Mormori (Iran) earthquakes and finally ends to the 2015 Gorkha (Nepal) earthquake. The thesis shows a synthesis of the main observations and comparison of local SHA and scenarios between the different regions.

The thesis contains also a research proposal on the regional seismic database (earthquake catalogue and strong motion database) for the South Asia region which is described the ***chapter 7***. One of the goals of this study is to devise methodologies for the seismic risk evaluation and loss estimation that are tailored for different cities in the South Asia and Caucasus. There are some vulnerable and densely populated regions in south Asia (i.e. in Afghanistan, some regions of Pakistan, Nepal, etc..) where the seismic hazard and risk are high, but the quality of accessible knowledge on seismicity, seismic source parameters and strong ground motion are poorly known, a situation not acceptable to perform a meaningful seismic hazard and risk assessment. To this end, the ground-motion models that provide hazard evaluation associated should yield accurate ground motion estimates with low dispersion through simple functional forms that use the essential geophysical and seismological information. Based on this fact, the perspective and strategy of the work plan is to develop a consistent seismicity catalogue, strong motion dataset, detailed seismic source model and regional ground-motion prediction models (GMPEs). These need to be based on

the assumption that the tectonic regimes, seismicity rates and data availability are extremely variable.

In summary, my future research plan includes the following items:

- Compilation of existing seismicity catalogues
- Reevaluating the historical earthquake catalogues
- Incorporating the new sources of information
- Assembly of strong ground-motion database
- Development of predictive model for peak ground motion and spectral values
- Evaluation of site amplification and soil linear and nonlinear behavior

Finally, in the ***Chapter 8***, I present the research formation of my works and a summary of the researches in form of supervision or co-supervision of doctoral thesis of my former Ph.D students.

Chapter 1: Methodology

> ... All models are approximations. Essentially, all models are wrong, but some are useful. However, the approximate nature of the model must always be borne in mind."
>
> *Box, George E. P.; Norman R. Draper (1987). Empirical Model-Building and Response Surfaces, p. 424, Wiley. ISBN 0471810339.*

In this chapter, advantages and disadvantages of using seismic hazard maps, time-dependent and time-independent analysis, as well as the well known DSHA, PSHA and NDSHA approaches are described. Finally I take a brief look to the uncertainties associated with the PSHA studies.

1-1. Seismic hazard analysis. Yes or No?

Active geologic structures in the current geological epoch (Holocene, about 12,000 years old) are known as the seismic source zones which can create an earthquake with maximum magnitude. Determination of the potential seismic fault and source zones, their characteristics and mechanisms as well as the calculation of their maximum magnitude and seismicity rates are of important issues. In this respect, seismic hazard analysis is an efficient tool used to evaluate the potential seismic hazard in an area. Usually, a team of geologists, seismologists, engineering seismologists and earthquake engineers are involved to collectively produce an update of the probabilistic seismic hazard model in a national scale. Different seismic hazard maps propose various types of ground motion or intensity information to their users.

Confidence in scientific models is confirmed by validation of the model's predictions. Experience of some destructive earthquakes such as the 2011 Tohoku (M_w=9.1), 2008 Wenchuan (M_w=7.9), 2010 Haiti (M_w=7.0) as well as the 2002 Bam (M_w=6.5), 1978 Tabas (M_w=7.4) and 1990 Manjil (M_w=7.4) earthquakes of Iran, all of which occurred in areas predicted by earthquake hazard map to be relatively safe, indicates that in several cases, such hazard maps clearly failed to predict the actual strong motions.

Fig 1-1 shows the hazard map of Japan which was prepared in 2010 before the 2011 Tohoku earthquake. In their interesting review article on the reasons of the usual failure of earthquake hazard maps, Stein et al., (2012) declare that *"the Japanese hazard map predicted less than a 0.1% probability of shaking with intensity "6-lower" (on the Japan Meteorological Agency -JMA- intensity scale) in the next 30 years. In other words, such shaking was expected on average only once in the next 30,000 years. However, within two years, such shaking occurred"*.

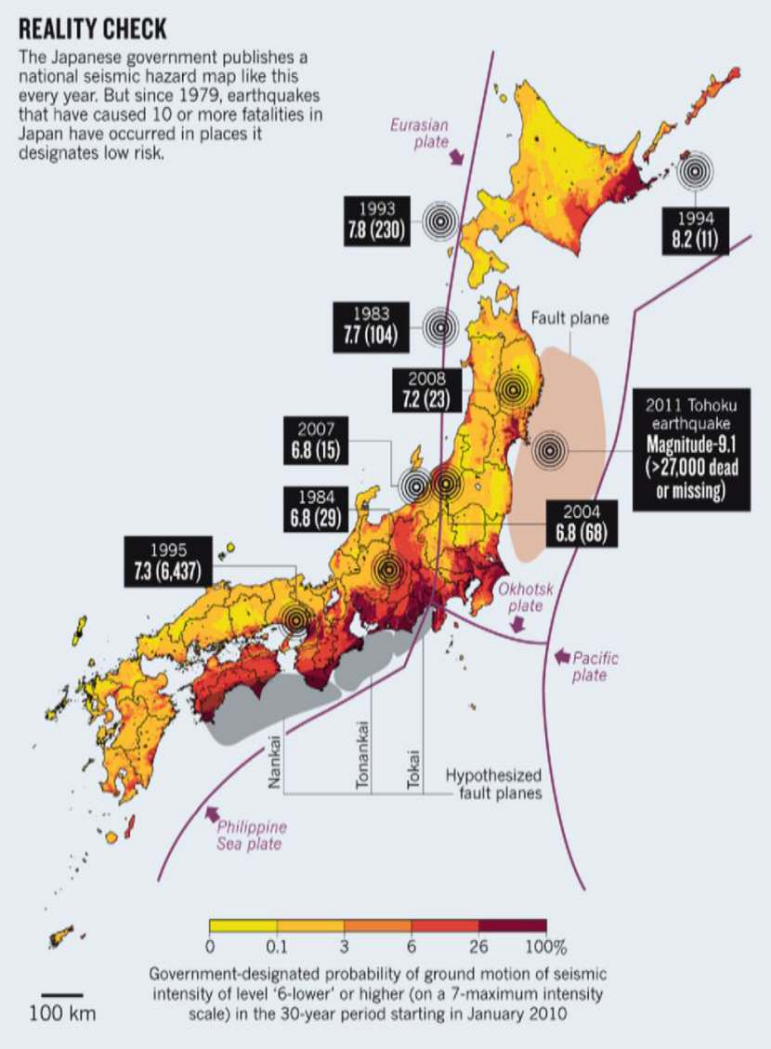

Fig. 1-1. Comparison between hazard levels in the government hazard map of Japan and earthquakes caused 10 or more fatalities since 1979 (Geller, 2011).

The occurrence of the catastrophic 2011 Tohoku, Japan earthquake (M_w=9.1), draw the attention of many researches to the inefficiency of the existing seismic hazard maps and the necessity to revise such maps based on updated data and improved methods. A number of factors that may cause errors in seismic hazard maps have been mentioned in a published article by Stein et al (2012). These factors are: bad physics, bad assumptions, bad data and bad luck (black swans).

1-2. Time-dependent and time-independent seismic hazard analysis

1-2.1. Time-independent SHA

Hazard maps can be produced by either a time-dependent or time-independent analysis. Until now, most of the seismic hazard maps, containing the hazard models of Iran and the Middle-East region, have been mainly prepared based on the time-independent assessments. The probability of the occurrence of an earthquake in time-independent models are assumed to follow a Poisson distribution. Poisson process describes number of occurrences of an event during a given time interval or spatial region as follows:

1) The number of occurrences in one time interval are independent of the number that occur in any other time interval.
2) Probability of occurrence in a very short time interval is proportional to length of interval.
3) Probability of more than one occurrence in a very short time interval is negligible.

1-2.2. Time-dependent SHA

One of the most important tasks involved in seismic hazard assessment is the examination of the temporal and spatial patterns of earthquake occurrence. Anagnos and Kiremidjian (1988) compiled a review of the basic assumptions of the various earthquake occurrence models involved in hazard analysis. The widespread application of probabilistic hazard analysis has been based on the memoryless Poisson model of earthquake occurrence for several reasons (Gardner and Knopoff, 1974; McGuire and Barnhard, 1981).

Modeling of faults in laboratory experiments (Byerlee and Brace, 1968; Brune, 1973) has indicated that the elastic rebound theory suggests that the times of occurrence and magnitudes of a sequence of earthquakes in a given source may not be stochastically independent. For this reason, several attempts have been made for studying time-dependent seismicity at faults (Papaioannou and Papazachos, 2000). The probability of the occurrence of an earthquake in time-dependent models are assumed to follow a renewal model, i.e., a log-normal, Brownian passage time (BPT), or other probability distribution in which the probability of the event depends on the time since the last event. (Petersen et al., 2007). In Figs. 1-2 and 1-3, time-independent and time-dependent seismic hazard maps for the state of California (by Petersen et al., 2007) are depicted.

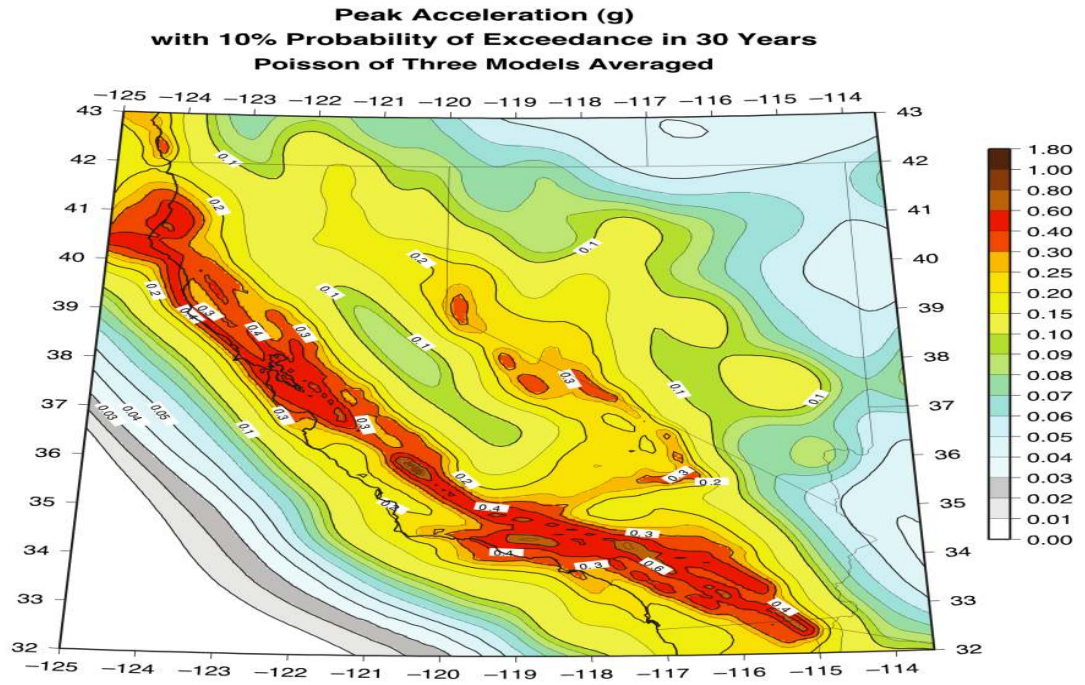

Fig. 1-2. *"Time-independent (Poisson) map for rock site condition and a 10% probability of exceedance in 30 years"* (Petersen et al., 2007).

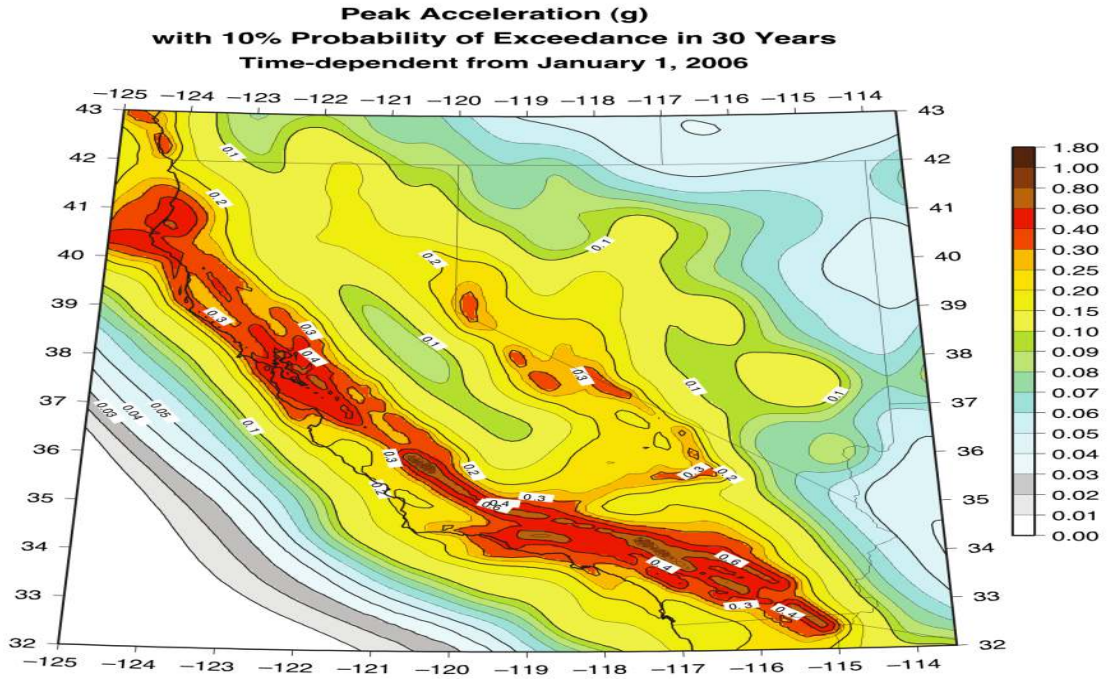

Fig. 1-3. *"Time-dependent map for rock site condition and a 10% probability of exceedance in 30 years"* (Petersen et al., 2007).

1-3. Seismic Hazard Analysis Approaches

There are different methods applied in seismic hazard analysis. In this part, three of the most important methods consisting of the Deterministic Seismic Hazard Analysis (DSHA), Probabilistic Seismic Hazard Analysis (PSHA) and Neo-Deterministic Seismic Hazard Analysis (NDSHA) are explained briefly.

1-3.1. Deterministic Seismic Hazard Analysis (DSHA)

DSHA is the earliest, easiest and simplified approach to carry out seismic hazard analysis. For a worst case scenario, DSHA is more useful. To evaluate seismic hazard deterministically for a particular site or region, all possible sources of seismic activity must be identified and their potential for generating strong ground motion must be evaluated. It is used widely for nuclear power plants, large dams, large bridges, hazardous waste containment facilities and also as a 'cap' for PSHA (Puri and Jain, 2016). According to Reiter (1990), the steps in the process of a DSHA study indicated by Shah et al. (2012), are as follows (Fig. 1-4):

1) Identification of seismic sources
2) Calculation of the nearest distance between source and the site of interest
3) Determination of controlling earthquake
4) Calculation of the maximum hazard

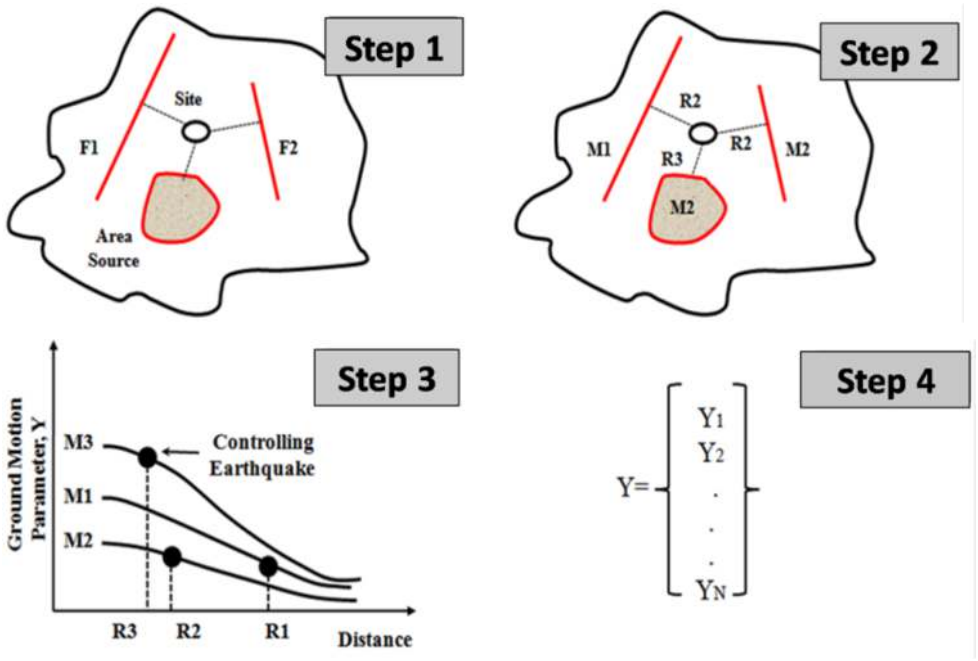

Fig. 1-4. Four-step process of a deterministic seismic hazard assessment (DSHA)

1-3.2. Probabilistic Seismic Hazard Analysis (PSHA)

Since a DSHA study takes the worst possible earthquake scenario into account, the approach is mainly used only for some critical structures such as dams, power plants and bridges (especially in near-field regions). A DSHA study calculates the maximum hazard due to the occurrence of the biggest earthquake in the nearest distance to a critical structure for a long life span. Thus, for the average life span of the most of the typical buildings, the results of a DSHA model imposes large costs. The Probabilistic Seismic Hazard Analysis (PSHA) have been known as the most popular approach which considers the different probabilities in the hazard calculations.

Here, a general procedure of a PSHA analysis is pointed out based on the educational materials taken from the Pacific Earthquake Engineering Research Center (PEER) website (http://peer.berkeley.edu/course_modules/eqrd/index.htm?c227top.htm&227cont.htm&EQDef/eqdef7.htm): *"the PSHA follows a similar process to the DSHA, but the uncertainty is quantified by a probability distribution at each step. Distributions are determined for the magnitude of each earthquake on each source $f_M(m)$, the location of the earthquake in or along each source $f_R(r)$, and the prediction of the response parameter of interest $P[pga>pga'|m,x]$. For example, for a given earthquake "x" of magnitude M and distance R:*

$$P[pga>pga'] = P[pga>pga'|x]\ P[x] \tag{1-1}$$

For all earthquakes:

$$P[pga>pga'] = \iint P[pga>pga'|m,r] f_m(m) f_R(r)\ dm\ dr \tag{1-2}$$

The PSHA computes the likelihood of occurrence of potential seismic hazard events and the intensity of ground shaking produced by those events at the sites being analyzed. A PSHA considers the contribution from all potential sources of earthquake shaking collectively and the likelihood of those events. In this approach, uncertainty is treated explicitly and annual probability of exceeding specified ground motions is computed. The hazard analysis covers the following related components (Fig. 1-5):

1) Definition of the nature and locations of earthquake sources.
2) Seismicity and frequency-magnitude relationships for the sources.
3) Attenuation of ground motion with distance from the sources.
4) Determination of exceedance probability at given sites.

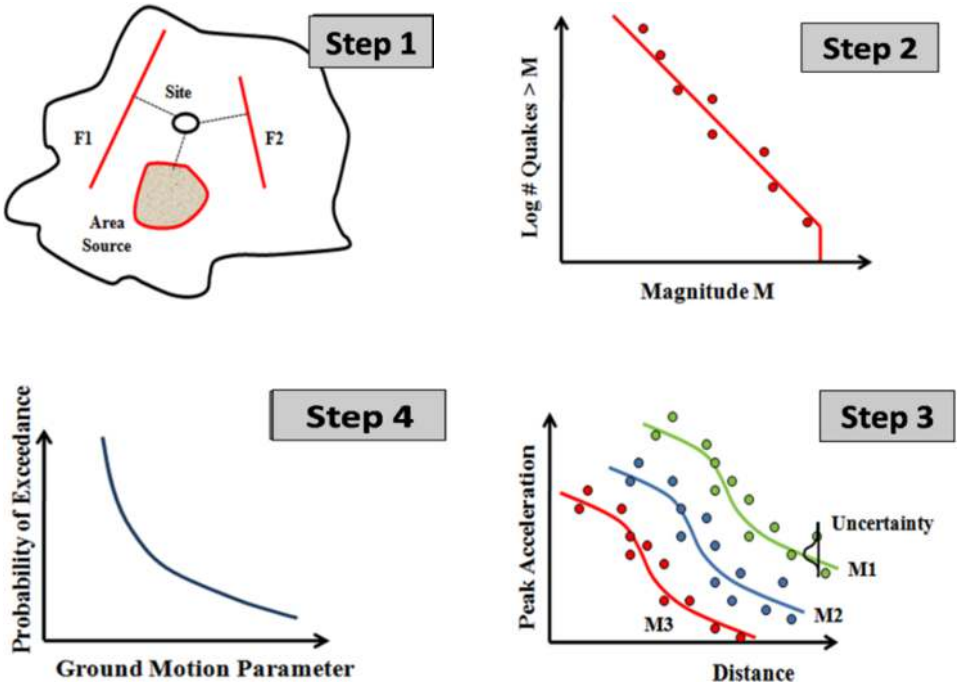

Fig. 1-5. Four-step process of a probabilistic seismic hazard assessment (PSHA)

Many authors have expressed criticisms of the probabilistic method (e.g. Castanos and Lomnitz, 2002; Klugel, 2007a; Wang, 2008), on the grounds that the probabilistic results are not very realistic nor reliable. Experience of several recent events, such as 1995 Kobe, Japan, 2001 Gujarat, India, 2003 Bam, Iran, 2008 Sichuan, China and 2010 Haiti shows the shortcomings, however, the probabilistic approach is still applied world-wide for hazard assessment (e.g. GSHAP and EMME) and also for national seismic codes.

1-3.3. Neo-Deterministic Seismic Hazard Analysis (NDSHA)

The procedure for the NDSHA addresses some issues largely neglected in probabilistic hazard analysis, namely how crustal properties affect propagation and attenuation of wave trains: ground motion parameters are not derived from overly simplified attenuation functions, but rather from synthetic time histories. In fact, synthetic seismograms can be computed to model ground motion at sites of interest, using knowledge of the physical process of earthquake generation and wave propagation in realistic inelastic media. The signals are efficiently generated by the modal summation technique (Panza et al., 2001).

Synthetic signals can be produced in short time and at a very low cost/benefit ratio, to be used as seismic input in subsequent engineering analysis aimed at the computation of the full

non-linear seismic response of the structures or to simply estimate the earthquake damaging potential.

Taking into account the source characteristics and the relevant bedrock models, the NDSHA can be applied at national scale, computing seismograms at the nodes of a grid with the desired spacing, or at local scale, considering the path and the geological and geotechnical conditions at the site, as well. The flowchart of the standard neo-deterministic procedure at national scale is shown in Fig. 1-6 (Zuccolo, 2010).

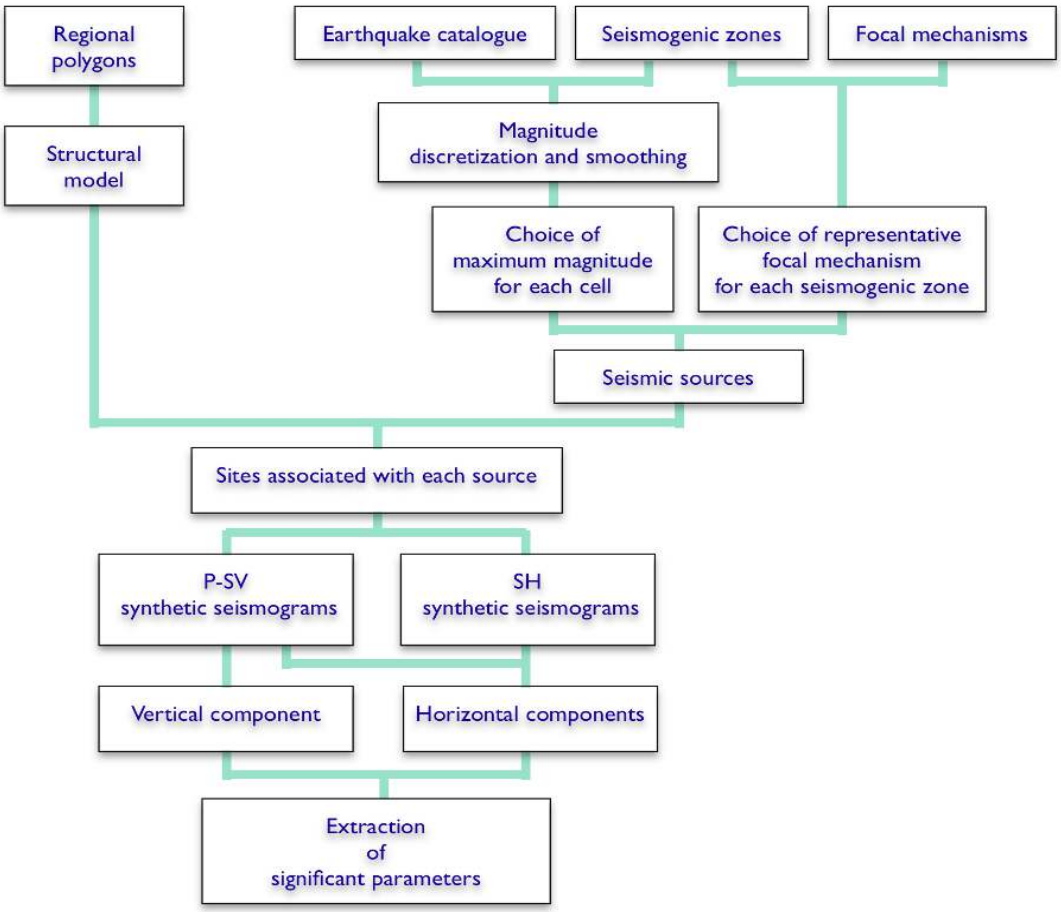

Fig. 1-6. Flow-chart of the standard neo-deterministic procedure for seismic hazard assessment at national scale (Zuccolo, 2010).

1-4. Uncertainties in PSHA

As mentioned before, PSHA characterizes uncertainty in location, size, frequency, and effects of earthquakes, and combines all of them to compute probabilities of different levels of

ground shaking. Uncertainties are mostly divided to epistemic uncertainty (from limited data and knowledge.) and aleatory variability (innate randomness in a process).

A usual way to treat epistemic uncertainty is the use of logic trees. An example of a logic tree is shown in Fig. 5-13 in the section 5-5-1 for the recent seismic hazard analysis of Iran (Zare et al., 2015). As can be seen, it consists of a series of branches that describe alternative models and/or parameter values with a set of weights located at the tips. These weights represent the relative credibility of each model and must sum to unity at each branch. Representing current scientific judgment on the merit of the alternative models, the weights are based on data collected from analogous regions, simplified physical models, and empirical observations.

Recent PSHA logic tree included:

- Cascadia interplate
- attenuation relationships
- up dip boundaries
- down dip boundaries
- return periods
- segmentation models
- maximum magnitude approaches
- terminal branches

Chapter 2: Database and Seismicity Catalogs

2-1. Introduction

In this chapter, I explain the seismicity databases and catalogs acquired for the Iranian Plateau as well as the Middle-East region. These seismicity catalogs have been prepared through research collaboration with my scientist colleagues and Ph.D students. At first, I will briefly review the instrumental seismicity databases consisting of the most important global, regional and national seismic networks as well as resources of the historic earthquakes within Iran and the Middle East region in brief. The importance and necessity of earthquake data in form of uniform catalogs, the qualities of catalogs as well as declustering and its needs is then represented. In the following, I will describe the most comprehensive uniform seismicity catalogs compiled in the recent years as a basic data in order to conduct seismic hazard studies in Iran and the Middle-East. The Poisson distribution of the Iranian declustered earthquake catalog is also investigated. In addition, catalogs of the Iranian earthquake intensities, one as a catalog of the earthquakes with maximum intensities (I_{max}) in Iran and the other studies such as an Iranian earthquake intensity database for the time period of 1975 - 2000 are then discussed. It should be noted that since the strong motion records are essential data for engineering purposes, I will describe the strong motion data acquisition and processing in an individual investigation in the Chapter 3. Finally, I will discuss the uncertainties associated with the seismicity datasets and catalogs and explain that why more work must be continued.

2-2. Seismicity Databases

The great progress made in seismology in the past 50 years has been stimulated principally by the availability of steadily improving data obtained by seismic networks. In the following, the most important active global, regional and national seismic networks are briefly described. These datasets provide basic data for compiling new uniform seismicity catalogs.

2-2.1. Global Agencies

The most important global agencies that record and report Iranian earthquakes are as following:

- ISC, International Seismological Centre UK: The ISC center collects and recalculates earthquake parameters from national and local agencies (from 1900 to now). Earthquake data related to Iran and the Middle-East are available from 1909 (ISC, 2016).

- EHB, Bob Engdahl: Indeed, the EHB catalog is a recalculated version of the ISC Bulletin based on an improved algorithm for hypocenter calculation by Engdahl et al. (1998). This databank includes 141,478 seismic events occurred during 1960 to 2008.
- NEIC, National Earthquake Information Center: This center reports the epicenter of the recorded earthquakes from 1973 to the present (USGS website; NEIC Bulletins US, 2016).
- HRVD, Harvard Centroid Moment Tensor (CMT) Catalog: This catalog provides focal mechanism database from January, 1976, to about 6 months before the present (Harvard CMT Catalog website; Harvard CMT Catalog, 2016).

2-2.2. Regional Agencies

There are several seismic datasets belonging to the countries of the Middle East region, among which the most important networks are listed below. These catalogs were provided through the meetings for the Earthquake Model of the Middle East region (EMME) project.

- The Armenian catalogs are reporting only mb as the magnitude value. Regarding their report, they had used the data from the new catalog of strong earthquake in USSR (NCUS SR) for the events up to 1975. The other source of data is the Russian Space System Cooperation (RSSC) catalog.
- The main sources for Georgia data are SMCG and EDIG.
- The National Center of Geophysical Research (NCGR) was established in 1975 by the National Council of Scientific Research (CNRS) in Lebanon. Nowadays, the seismic national network of this country with title of "Geophysical Research Arrays of Lebanon (GRAL)" is expanding.
- The main source of all Turkey's records is "ISK" prepared by the Kandilli Observatory, Bogazici University in Istanbul. The institute provides both broad-band and strong motion data recorded for throughout Turkey.
- The main source for the seismic monitoring and tsunami early earning in Pakistan is the Pakistan Meteorological Department (PMD). The PMD started recording events since 1954 using analogue equipments and then replaced all the paper equipments with the digital ones since 2005.

- More than 20 short period digital stations which account as the Syrian National Seismological Network (SNSN) were established in 1995.
- Egyptian National Seismograph Network (ENSN) has started its work in 2003.
- Kuwait National Seismic Network (KNSN) was established in 1996 and has started to monitor the seismicity of this small country.

2-2.3. National Agencies

- *IRSC*: The Iranian Seismological Centre, University of Tehran: The IRSC was the first research center responsible for recording the seismic events in Iran. The center installed the first seismic station in Tehran in 1958. Until 1995, several analogue stations were in work in order to record earthquakes throughout the country. Since then, *digital seismographs including three-component short-period, medium-band or broad-band seismometers were added to the network. Today, the IRSC network comprises 115 digital stations* (http://irsc.ut.ac.ir/istn.php). The IRSC website provides data online from 2006 up to the present. M_N, a magnitude scale based on Lg wave (Nuttli, 1973), is provided by IRSC (Rezapour, 2005).
- *IIEES*: Broadband Seismic Network of Iran, International Institute of Earthquake Engineering and Seismology: the broadband Seismic network of Iran was designed and operated in 1998, including 4 stations in Ashtian, Naien, Hashtgerd and Zahedan. Until the end of 2016, the number of seismic stations had been increased to 26 (IIEES, 2016). The seismic stations of IIEES and IRSC networks are depicted in Fig. 2-1.

2-2.4. Historic Datasets of the Middle East region

"A History of Persian Earthquakes" (Ambrasys and Melville, 1982), "The seismicity of Egypt, Arabia and the Red Sea" (Ambraseys et al., 2005), "Earthquakes in the Mediterranean and Middle East" (Ambraseys, 2009), and "The SHARE European Earthquake Catalogue (SHEEC) 1,000–1,899" (Stucchi et al., 2012) are considered as the main resources of historical earthquake information on the Middle-East region.

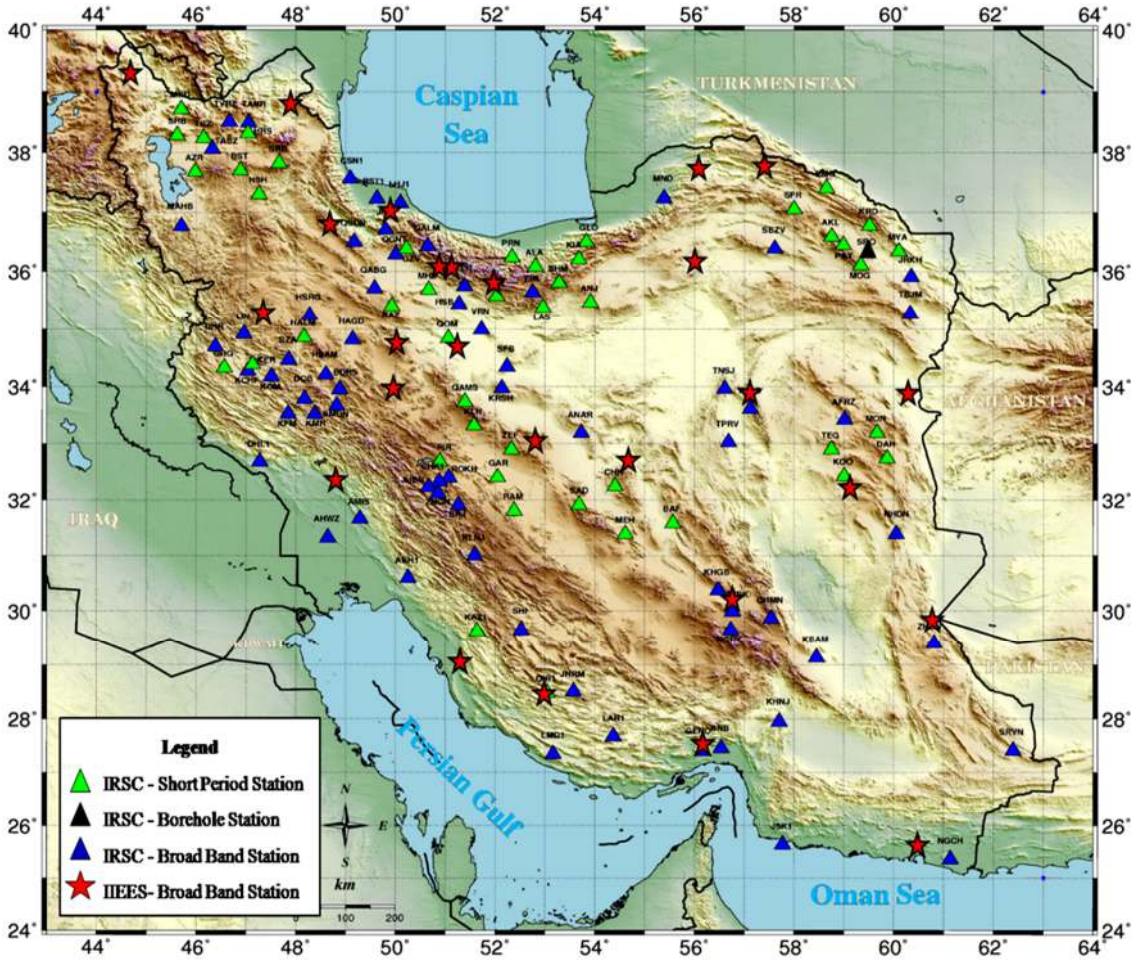

Fig. 2-1. Seismic Networks of Iran

2-3. Catalogs

A uniform and comprehensive earthquake catalog, which contains both historic and instrumental earthquake data, is an essential tool in any seismic hazard analysis in each region. Prehistoric and historic events are those for which no instrumental recording was possible and they are related to the time mostly before 1900. The sources of information to identify prehistoric and historic earthquakes are usually paleoseismic investigations, archaeological information and qualitative descriptions. Instrumental earthquakes are those which have been recorded by seismic instruments mostly after 1900. The instrumental catalogs are mainly divided into two time sections: early instrumental (before 1960-1964) and modern instrumental (since 1964) catalogs.

Earthquake catalogs should be declustered for time-independent seismic hazard analysis. In this regard, seismicity declustering is important because: (1) from mechanism viewpoint, mainshock as independent earthquakes are assumed to be mostly caused by secular, tectonic

loading or, in the case of seismic swarms, by stress transients that are not caused by previous earthquakes, while earthquakes that depend on each other like aftershocks, foreshocks, or multiples, correspond to earthquakes triggered by static or dynamic stress changes, seismically-activated fluid flows, after-slip, etc., hence by mechanical processes that are at least partly controlled by previous earthquakes (van Stiphout et al., 2012) and (2) mainshocks are considered as the realization of a point process modeled by a generalized Poisson distribution, since it is a condition for use of probability functions in the probabilistic seismic hazard analysis (PSHA) method (Cornell, 1968).

The first algorithm for declustering a seismic catalog was defined by Knopoff in 1964. In this algorithm, the occurrence of time intervals in which an excessive number of earthquakes occurred was taken to be an identifying marker that an aftershock sequence was present in the interval. This procedure lead to non-Poisson results for the main shock residual Gardner and Knopoff (1974).

In 1974, Gardner and Knopoff introduced a window-based method named the mainshock-window algorithm. The conceptual idea of this method is to distinguish dependent events which are located within the specified space-time windows belonging to a mainshock. Therefore, for each mainshock in the catalog with magnitude M, the subsequent shocks are identified as aftershocks if they occur within a specified time interval T(M), and within a distance interval L(M).

In 1985, Reasenberg introduced a clustering approach for identifying aftershocks by linking earthquakes to clusters according to spatial and temporal interaction zones. In this regard, a space-time window defined based on the Omori law, is calculated for all the seismic events, not only the mainshocks and then the aftershocks are linked to an earthquake cluster. Earthquake clusters thus typically grow in size when processing more and more earthquakes.

There are also other approaches such as stochastic declustering methods (e.g. Vere-Jones, 1970; Zhuang et al., 2002; Marsan and Lengline, 2008); waveform similarity approach (Barani et al., 2007); single-link cluster analysis (e.g. Frohlich and Davis,1990; Davis and Frohlich,1991) and others. Defined algorithms by Gruenthal (pers. comm.) and Uhrhammer (1986) are also some of the most applied methods for declustering in the ZMAP software under Matlab. Among these different proposed algorithms, the methods proposed by Gardner and Knopoff (1974) or Reasenberg (1985) are the most popular methods due to their simplicity. In the following, I present and describe the most important catalogs prepared for the Middle-East region and Iran.

2-3.1. Recent developments of the Middle East catalog (EMME catalog)

** **Source Article:** **Zaré M**., Amini H., Yazdi P., Sesetyan K., Demircioglu M.B., Kalafat D., Erdik M., Giardini D., Asif Khan M. and Tsereteli N., (2014), "Recent developments of the Middle East catalog", Journal of Seismology, Vol 18., pp.749–772, DOI: 10.1007/s10950-014-9444-1.*

In this section, I present the developments of the Middle East earthquake catalog (EMME catalog), an analysis taken from the published article by Zaré et al (2014) which was established in the framework of the Global Earth model (GEM) and the Earthquake Model of the Middle East (EMME) project. In this study, a new uniform catalog of earthquakes in the Middle East region was developed in order to prepare a reliable and most complete collection of available information of seismicity in this region. In addition, some of the seismicity information, i.e., number of events, range of magnitudes, and magnitude completeness (Mc) and seismicity depths of this region were also determined.

Earthquake database:

The first step for preparing a uniform earthquake catalog is to acquire all the available databases in the study region. The databases used in this research include both global (NEIC, ISC and EHB) and local networks (IIEES, IRSC, KOERI). Moreover, some published earthquake catalogs were also used including, *"A History of Persian Earthquakes" (Ambrasys and Melville, 1982), "The seismicity of Egypt, Arabia and the Red Sea" (Ambraseys et al., 2005), and "Earthquakes in the Mediterranean and Middle East" (Ambraseys, 2009).*

Uniform catalog:

To preparing a unified catalog, we need to uniform all of the magnitudes to one scale. For this purpose, all events with two magnitudes from mb, ML, Ms, and Mw were considered. After finding appropriate relations between them, the magnitude of all events was converted to Mw. The results of the derived relationships are represented in Table 2-1.

Now, in this catalog, all of the magnitude scales were unified using regional conversion equations between mb, Ms, ML, and Mw and were converted to magnitude in Mw scale. After omitting events with zero magnitudes and erroneously large depth (Wyss et al., 2001), there will be a catalog with 28,244 events from all of historical and instrumental events, in

Mw magnitude scale. This catalog contains events with magnitudes 4.0–8.1 between 1250 B.C. and 2006 of which 22,427 events occurred between 1976 and 2006 in the last 30 years.

Table 2-1. Relationship between Ms, Ml, mb, and Mw in the Middle East region by comparing the recorded magnitude of the events.

Magnitude type	Conversion relation	Boundary	R^2	Number	σ	
mb, Mw	Mw = 0.87 mb + 0.83	3.5≤mb≤6.0	0.88	16,752	0.3	This study
	Mw = 0.85(±0.04) mb + 1.03(±0.23)	3.5≤mb≤6.2	0.53	39,784	0.29	Scordilis
Ms, Mw	Mw = 0.66 Ms + 2.11	2.8≤Ms≤6.1	0.94	4,123	0.28	This study
	Mw = 0.93 Ms + 0.45	6.2≤Ms≤8.2	0.88	129		
	Mw = 0.67 (±0.005) Ms + 2.07(±0.03)	3.0≤Ms≤6.1	0.77	23,921	0.17	Scordilis
	Mw = 0.99 (±0.02) Ms + 0.08(±0.13)	6.2≤Ms≤8.2	0.81	2,382	0.2	
Ml, Mw	Mw = 1.01 Ml – 0.05	4.0≤Ml≤8.3	0.98	2,271	0.25	This study

Declustering catalog:

The Middle East catalog was first declustered with the Gardner and Knopoff (1974), Gruenthal (pers. comm.), Uhrhammer (1986), and Reasenberg (1985) algorithms. These declustered catalogs contain 10,131; 7,272; 16,569; and 24,530 events, respectively. Then, we used the merged declustered catalog with omitting foreshocks and aftershocks by Stefan Wiemer's ZMAP package for MATLAB to apply Gruenthal's algorithm, resulting in a minimum number of events in the catalog after declustering, in order to be sure that the dependent events are eliminated from the catalog of the mainshocks. Finally, there are 378; 1,058; and 5,837 events in the period before 1900 (historical earthquake), 1901–1963 (early instrumental earthquake), and 1964–2006 (modern instrumental earthquake).

Seismicity information:

The database of the Middle East region after declustering present a set of uniform information for 7,272 earthquakes including historical and instrumental recorded events from 1250 B.C. through 2006. After the declustering, there is only one event with magnitude more than 8 in this region (Mw=8.1, 1945), which belongs to the Makran subregion. Moreover, the number of events between 7–8, 6–7, and 5–6 are 125, 444, and 1,897 using Gruenthal algorithm. M=4.0 is selected to be the minimum magnitude in adding data from different catalogs for the Earthquake Model of the Middle East catalog. Thus, maximum and minimum

magnitudes in the catalog would be 4.0 and 8.1, respectively (Fig. 2-2).

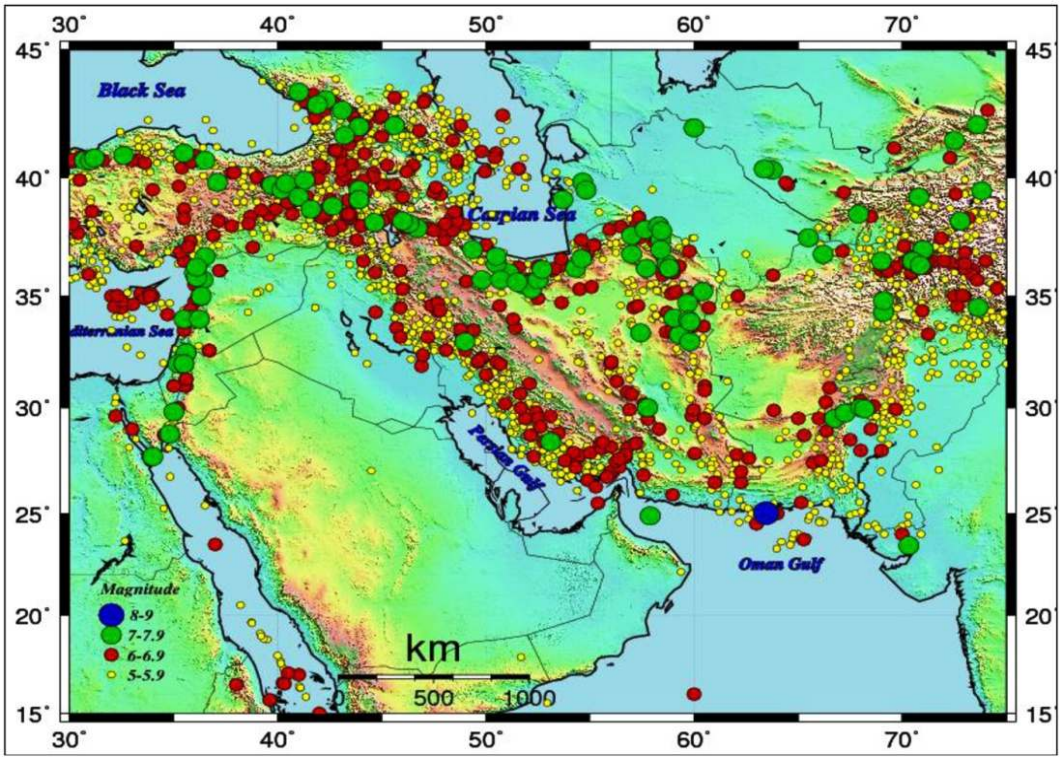

Fig. 2-2. Catalog of the Middle East region from 1220 B.C. to 2006, with Mw≥5.0. Magnitudes between 5–6, 6–7, 7–8, and more than 8 are shown in yellow, red, green and blue, respectively.

As felt by humans, the magnitude of completeness for historical period of time is around 6 and 7. For instrumental earthquakes, depending on the region and accuracy of seismogram recorded, Mc can be presented by recorded events which have different value. In this investigation for the Middle East region and each subregion, Mc was calculated using two main methods: the traditional and common method based on the cumulative frequency–magnitude distribution (Gutenberg and Richter, 1944; Richter, 1958) and seismological analysis of the frequency-magnitude distribution in the software ZMAP (Wiemer 2001; Dixon et al.,2005). The Mc for each subregion of Middle East is presented in Table 2-2. Based on this table, the Mc was determined as 4.9 for five out of nine subregions, where the least value of Mc was found to be 4.2. The total threshold of magnitude based on all Middle East earthquake data was calculated as 5.5, 5.0, 4.5, and 4 (or less than 4) for the time periods before 1950, 1963, 1975, and 2000, respectively.

For recent investigation in Middle East region, the events with erroneously large depth and with magnitude zero were omitted. Moreover, we omitted the events with depth of 33,

because this is an assumption that depth for the events do not determine in an exact value. Examination of the focal depth within the Middle East region imply that the location discrepancies for larger earthquakes are considerably less than discrepancies for smaller events and there is no significant improvement in location determination with respect to the occurrence time of earthquakes in the period of 1800 to 2006 in this region. Averages of depth for each subregion are estimated using the software ZMAP (Wiemer, 2001) (Table 2-2). The average of teleseismic depths in all regions is less than 15 km. Totally, majority of depth for Kopeh–Dogh and Central Iran, Zagros, and Alborz–Azarbayjan is approximately 15, 13, and 11 km, respectively; all of them have depths with more than 10 km. Majority of depth for Afghanistan–Pakistan, Caucasus, Makran, and Turkey (after 30° E) is 9 km and Saudi Arabia has depth of 8 km.

Table 2-2. Some of the information on seismicity for each section, Magnitude (maximum and Mc), Depth (maximum and with depth of zero)

Number	Name of Section	Magnitude		Depth		Average Depth	Start year	Depth reported by Mirzaei et al (1997)
		Mc	M_{max}	Max	= 0			
1	Afghanistan-Pakistan	4.9	7.9	300	184	9	818	
2	Kopeh-Dogh	4.9	7.6	46	80	15	10	7~35
3	Central-Iran	4.9	7.7	106	91	15	734	8~20
4	Makran	4.8	8.1	164	19	9	1483	Up to 60
5	Zagros	4.9	7.4	185	147	13	859	8~15
6	Alborz-Azarbayjan	4.3	7.8	92	419	11	550 B.C.	7~35
7	Caucasus	4.2	7.0	165	67	9	1,250 B.C.	
8	Turkey (after 33˚E)	4.4	7.7	169	375	9	995	
9	Saudi Arabia	4.9	7.5	101	109	8	31 B.C.	

2.3.2. Iranian earthquakes, a uniform catalog with moment magnitudes (3rd millennium BC - 2010)

** **Source Article:** Karimiparidari S., **Zaré M.**, Memarian H. and Kijko A., (2013), "Iranian earthquakes, a uniform catalog with moment magnitudes", Journal of Seismology, Vol.17, pp.897–911. DOI:10.1007/s10950-013-9360-9.*

In this section, I present the developments of a uniform catalog with moment magnitudes (3rd millennium BC - 2010), an analysis taken from the published article by Karimiparidari et al (2013). The aim of this study was to develop an updated seismicity catalog for Iran, which would be as accurate as possible. In this respect, all available national and international databanks were used to compile the new catalog. Earthquakes that have occurred within a magnitude range of M_W 3.5–7.9, from the third millennium BC until April 2010 were included. To achieve this purpose, several orthogonal regressions (OR) between different magnitude types were developed using overlapping events as input data, which led to define a procedure for creating a uniform catalog. The final catalog includes more than 10,000 earthquakes, in which all dependent events (foreshock and aftershocks) were detected based on the well-known procedure described by Gardner and Knopoff (1974). The seismicity parameters were also calculated for the six main seismotectonic zones of Iran, i.e., Zagros, Alborz, Central Iran, Kope Dagh, Azerbaijan, and Makran.

Sources and data:

There are two main sources of information on historic Iran earthquakes, one compiled by Ambraseys and Melville (1982) and the other by Berberian (1994). Moinfar et al. (1994) collected a set of historical and instrumental earthquake data which was referred in this study to confirm the magnitude of some events. Some of the obstacles encountered during research were that the catalogs cover different time periods. The instrumental data were compiled from several national and international agencies including IIEES, IRSC and BHRC as national sources as well as ISC, NEIC, EHB, HRVD and MOS as global datasets (for more explanation about these national and international agencies, see *section 2-2*).

Table 2-3 shows the catalogs used for this study. The authors had to set some priority for both the magnitude and the location of an event in order to choose specific data from the collected information. The first assumption was that earthquake magnitudes available from global catalogs are more accurate than those provided by the local catalog for the same

earthquake. In addition, an obvious criterion for catalog selection was magnitude uncertainty; earthquake magnitudes were selected from catalogs that provide the most reliable magnitudes with the lowest uncertainty (Wang et al. 2009). The HRVD catalog has higher priority than other catalogs because of reporting moment magnitude. The location of seismic events was selected according to the procedure proposed by Wang et al. (2009). Table 2-4 shows the applied strategy used in the determination of earthquake magnitude, location, and intensity.

Table 2-3. Available catalogs used for different time periods

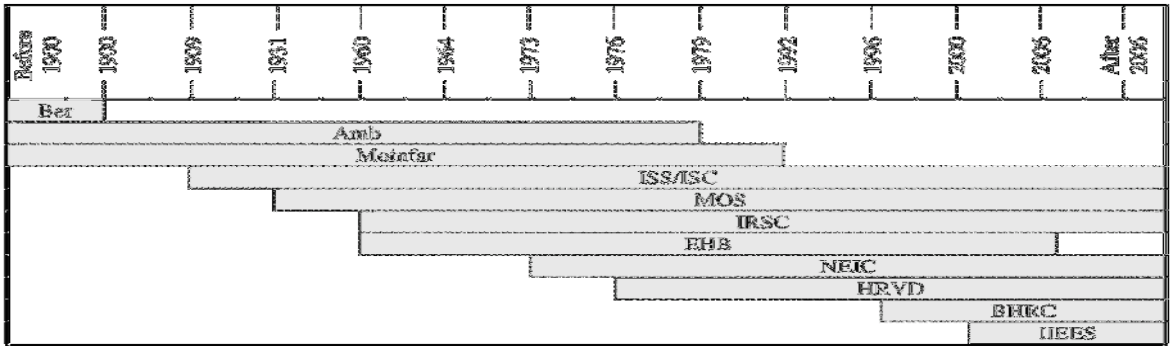

Amb: Ambraseys and Melville (1982); *Ber*: Berberian (1994); *BHRC*: Building and Housing Research Centre (2010); *EHB*: Bob Engdahl (from ISC, 2010); *HRVD*: Harvard Centroid Moment Tensor Catalog (2010); *IIEES*: International Institute of Earthquake Engineering and Seismology (2010); *IRSC*: The Iranian Seismological Centre, University of Tehran (2010); *ISC*: International Seismological Centre (2010); *Moinfar*: Moinfar et al. (1994); *MOS*: Institution of the Russian Academy of Sciences (2010); *NEIC*: National Earthquake Information Center (2010).

Table 2-4. Priority to choose magnitude and location from international and national databanks

Magnitude Priority	Location Priority	Intensity Priority
HRVD	EHB	Amb
Amb	Amb	Ber
ISC	IIEES	
NEIC	IRSC	
MOS	BHRC	
IIEES	ISC	
IRSC	NEIC	
BHRC	HRVD	
Ber	Ber	
Moinfar	MOS	
	Moinfar	

Estimating the moment magnitude:

In this study, the moment magnitude (Mw) was chosen as the standard, since it has a strong physical foundation, and most of the ground motion prediction equations use Mw magnitude

as an input parameter. The authors, therefore, developed several relationships between moment magnitude and other magnitude types in order to convert them into Mw (Table 2-5). Orthogonal Regression (OR) was used to account for the effects of measurement error in both the variables. After converting all magnitudes into Mw, all earthquakes with Mw<3.5 were removed from the newly compiled catalog. In order to create a uniform catalog in terms of Mw magnitude, the following procedure was applied:

1. If M_w is available: use M_w.
2. If M_w is not available and $6.1 \leq M_S \leq 7.4$: use Eq. 2-2.
3. If M_w is not available and $3.5 \leq mb \leq 6.0$: use Eq. 2-3.
4. If M_w and mb are not available and $3.0 \leq M_S < 6.1$: use Eq. 2-1.
5. If M_w and M_S are not available and $6.0 < mb$: first use Eq. 2-4, then use Eq. 2-1 or 2-2.
6. If M_w, M_S, and mb are not available and $3.5 \leq M_N \leq 6.3$: use Eq. 2-5.
7. If M_L is the only available magnitude and $3.4 \leq M_L \leq 6.3$: use Eq. 2-6.

Table 2-5. Developed relations for transition of M_S, m_b, M_L and M_N to M_w

Parameter Transition	Magnitude Range	Relation		RMSE
M_S to M_w	$3.0 \leq M_S \leq 6.1$	$M_w = 0.623642\ (\pm 0.015) \times M_S + 2.289902\ (\pm 0.076)$	(2-1)	0.19
M_S to M_w	$6.1 \leq M_S \leq 7.4$	$M_w = 0.988974\ (\pm 0.054) \times M_S + 0.040903\ (\pm 0.355)$	(2-2)	0.15
m_b to M_w	$3.5 \leq m_b \leq 6.0$	$M_W = 1.137129\ (\pm 0.026) \times m_b - 0.500249\ (\pm 0.134)$	(2-3)	0.27
m_b to M_S	$6.0 < m_b$	$M_S = 1.572622\ (\pm 0.022) \times m_b - 3.071216\ (\pm 0.092)$	(2-4)	0.47
M_N to M_w	$3.5 \leq M_N \leq 6.3$	$M_w = 0.738540\ (\pm 0.044) \times M_N + 1.409211\ (\pm 0.226)$	(2-5)	0.20
M_L to M_w	$3.4 \leq M_L \leq 6.3$	$M_w = 0.696736\ (\pm 0.047) M_L + 1.621469\ (\pm 0.230)$	(2-6)	0.32

Fig. 2-3 depicts all the earthquakes of the catalog of Iran and its vicinity over the time span from the third millennium BC to 2010.

Seismicity parameters:

The area-characteristic seismicity parameters, the maximum magnitude, M_{max}, the b value of Gutenberg– Richter, and the mean seismic activity rate λ were calculated for each of the six seismotectonic zones of Iran. The M_{max}, b, and λ parameters were calculated by Matlab code, which takes into account the latest extension of the procedure developed by Kijko and Sellevoll (1989, 1992). The applied procedure takes into account the incompleteness of the seismic event catalog, the uncertainty of earthquake magnitudes, and the approximate nature of distributions describing the seismicity of the area (Kijko 2010).

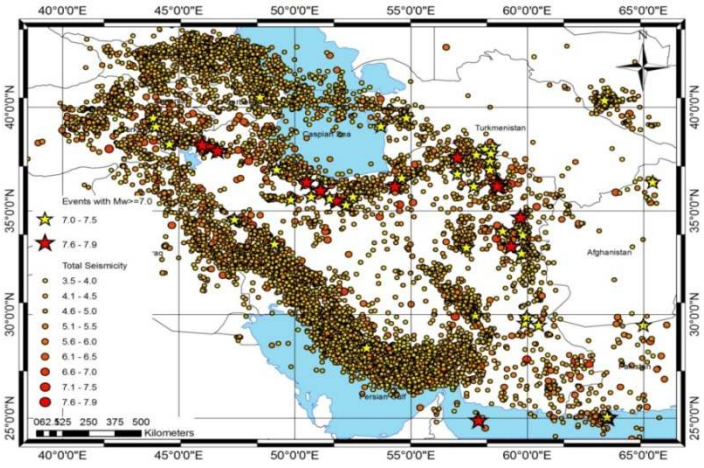

Fig. 2-3. Map showing a total cataloged earthquakes for the period third millennium to 2010

In order to calculate the level of completeness for the instrumental part of the newly compiled catalog, the authors applied the maximum curvature, MAXC, technique (Wyss et al. 1999; Wiemer and Wyss 2000) by ZMAP (Wiemer 2001). In this method, the maximum value of the first derivative of the frequency–magnitude curve is computed which matches the magnitude bin with the highest frequency of events in the noncumulative frequency–magnitude distribution (FMD) (Mignan and Woessner 2012). The magnitude of completeness is in the range of 4.4 to 4.5; these values are used as the magnitude threshold in the calculation of seismicity parameters.

Earthquake events are classified to prehistoric, historic, and complete catalogs, each with specific uncertainty. The magnitude uncertainty of prehistoric and historic catalogs varies from 0.3 to 0.7 based on the quality of reported event. This uncertainty changes from 0.1 up to 0.4 in the complete catalogs based on the time which the earthquake occurred and the magnitude. The estimated M_{max}, b value, and λ are as shown in Table 2-6. The authors could not calculate the M_{max} for the Makran zone because of the lack of data.

Table 2-6. Seismicity parameters for six seismotectonic zones of Iran

Zone Name	*b* value	λ	$M_{max\ calculated}$	$M_{W\ (max\ observed)}$
Alborz Mountain Range	1.15±0.04	3.03±0.26 (M_W =4.4)	7.8±0.4	7.7
Central Iran	1.13±0.05	2.30±0.28 (M_W =4.5)	7.7±0.4	7.6
Zagros Mountain Range	1.20±0.03	9.65±0.58 (M_W =4.4)	7.5±0.2	7.4
Kope Dagh	1.05±0.06	1.37±0.26 (M_W =4.5)	7.7±0.5	7.6
Azerbaijan	1.07±0.04	0.71±0.18 (M_W =4.5)	7.9±0.4	7.7
Makran	1.08±0.07	2.04±0.34 (M_W =4.5)	–	8.0

2-3.3. A unified seismic catalog for the Iranian plateau (1900-2011)

** **Source Article:** Shahvar M.P, **Zaré M.**, and Castellaro S., (2013), "A Unified Seismic Catalog for the Iranian Plateau (1900–2011)", Seismological Research Letters, Vol.84, No.2, pp. 233-249, doi: 10.1785/0220120144.*

In this section, I present the developments of a uniform catalog for the Iranian plateau (1900-2011), an analysis taken from the published article by Shahvar et al. (2013). In this research, a unified and homogeneous catalog was presented for the Iranian plateau (Mw ≥4), created by merging data from two local catalogs and seven international agencies, each one covering the magnitude scale and period illustrated in Fig. 2-4. The moment magnitude (Mw) is chosen as reference for its physical meaning (Kanamori, 1977) and because it does not saturate. In this attempt to convert different magnitude scales to Mw, regression relations that take into account errors on both variables are used, and a specific statistical analysis shows that the region under study (24°N–42°N, 43°W–66°E) is better described when subdivided into two tectonic domains, Zagros and Alborz–Central Iran, characterized by different regression relations. The unified catalog for the Iranian plateau, spanning 1900–2011, is finally presented also in a declustered form for time-independent seismic hazard estimates.

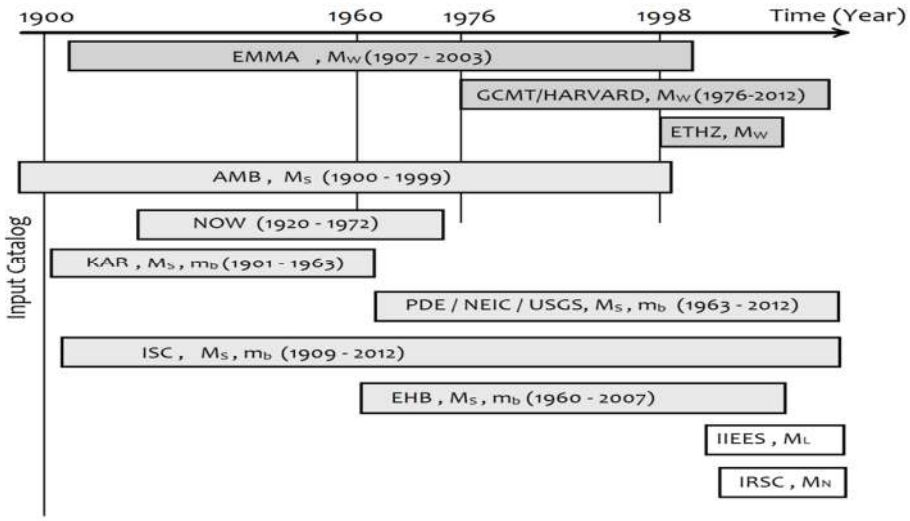

Fig. 2-4. Earthquake magnitude scales provided by the catalogues used to compile a unified catalogue for Iran between 1900 and 2012.

Regional differences in magnitude conversion relations:

The Iranian Plateau is wide, and there could exist statistically different magnitude conversion relations for different tectonic domains. In a previous study by Mirzaei et al. (1997), Ms–mb

conversion relations were derived separately for four tectonic regions, namely, Alborz, Zagros, Makran, and Central Iran. We used the Tukey (J. W. Tukey, unpublished manuscript, 1953; Kramer, 1956) honest significant difference method to compare the 95% confidence interval of different population marginal means. This technique compares the means of two or more samples based on the one-way analysis of variance (ANOVA) and the Student's t-distribution (Tukey, 1991). Results showed that the parameters for Alborz and Central Iran do not differ in a statistically significant way. The two zones will therefore be considered as a unique zone, called Alborz–Central Iran. On the opposite, the Ms–mb, ML–MN, and Mw–mb relations are found to differ significantly for the Alborz–Central Iran and the Zagros region, which will therefore be treated separately.

New magnitude conversion relations:

Standard least-square regression (SR) is still the most-used method to derive magnitude conversion relations (e.g. Mirzaei et al., 1997, for Iran; Bindi et al., 2005, for Italy; Braunmiller et al., 2005, for Switzerland; Chen and Tsai, 2008, for Taiwan; Yadav et al., 2009, for India). However, its basic assumptions, that is, (1) the independent variable (x) is measured with no error and (2) the measurement error on the dependent variable (y) is normally distributed and its variance is nearly constant across the observations (Draper and Smith, 1998), are rarely satisfied in practice (Castellaro et al., 2006). To derive the conversion laws between magnitude types, we also apply the orthogonal regression (OR), and because the ratio between the variable variance (η) is not known, we assume it to be η=1, with the limitations described in Castellaro and Bormann (2007) and Gutdeutsch et al. (2011). Results of the regression relations for each couple of magnitudes using the OR, SR and Inverse Standard least-squares Regression (ISR) are shown in Table 2-7.

Priority order:

The Kullback–Leibler (KL) divergence is a nonsymmetrical measure of the difference between two probability distributions. Scherbaum et al. (2009) introduced a quantity (LLH, which is the negative average sample log likelihood of the model g), based on the second term of the KL divergence. This is defined as

$$\mathrm{LLH}: = -\frac{1}{N}\sum_{i=1}^{N}\log_2 g(x_i),$$

In which N is the number of observations x. We have ranked the candidate models for our calculated magnitude conversion according to their relative LLH divergence, thus creating a priority-order list.

Table. 2-7. Regression relations for each couple of magnitudes. The chosen regression for each magnitude couple is shown by bold.

Coefficient of relationships	Adjusted R^2	Root mean square error
Regression relation between M_S - M_W ($M_S < 6.1$)		
SR : $M_W \leftarrow 0.589\ (\pm0.012)M_S + 2.420\ (\pm0.055)$	0.872	0.145
ISR : $M_S \leftarrow 1.483\ (\pm0.029)M_W - 2.996\ (\pm0.152)$	0.678	0.230
OR : $M_W = 0.611(\pm0.010)\ M_S + 2.314\ (\pm0.047)$	**0.871**	**0.124**
Regression relation between M_S - M_W ($M_S \geq 6.1$)		
SR : $M_W \leftarrow 0.887\ (\pm0.047)M_S + 0.656\ (\pm0.316)$	0.862	0.171
ISR : $M_S \leftarrow 1.004\ (\pm0.043)M_W + 0.072\ (\pm0.285)$	0.848	0.179
OR : $M_W = 0.949\ (\pm0.029)\ M_S + 0.243\ (\pm0.192)$	**0.858**	**0.126**
Regression relation between m_b-M_W Alborz-Central Iran region		
SR : $M_W \leftarrow 1.107\ (\pm0.052)m_b + 0.117\ (\pm0.273)$	0.780	0.213
ISR : $m_b \leftarrow 0.665\ (\pm0.034)M_W + 1.556\ (\pm0.186)$	**0.860**	**0.207**
OR : $M_W = 1.303\ (\pm0.034)m_b - 1.292\ (\pm0.178)$	0.759	0.153
Regression relation between m_b - M_W Zagros region		
SR : $M_W \leftarrow 0.917\ (\pm0.023)m_b + 0.507\ (\pm0.115)$	0.796	0.341
ISR : $m_b \leftarrow 0.869\ (\pm0.022)M_W + 0.568\ (\pm0.111)$	**0.806**	**0.274**
OR : $M_W = 1.030\ (\pm0.017)m_b - 0.057\ (\pm0.082)$	0.784	0.223
Regression relation between M_L - M_W		
SR : $M_W \leftarrow 0.701(\pm0.036)\ M_L + 1.656(\pm0.176)$	0.793	0.190
ISR: $M_L \leftarrow 1.138\ (\pm0.059)\ M_W - 0.904(\pm0.296)$	0.664	0.242
OR : $M_W = 0.763(\pm0.029)\ M_L + 1.355\ (\pm0.142)$	**0.787**	**0.153**
Regression relation between M_N - M_W		
SR : $M_W \leftarrow 0.768(\pm0.035)M_N + 1.272(\pm0.183)$	0.816	0.197
ISR: $M_N \leftarrow 1.067(\pm0.049)\ M_W - 0.430\ (\pm0.257)$	0.745	0.233
OR : $M_W = 0.834(\pm0.028)\ M_N + 0.932\ (\pm0.143)$	**0.810**	**0.154**
Regression relation between M_N–M_L Alborz-Central Iran region		
SR : $M_L \leftarrow 0.921\ (\pm0.012)M_N + 0.125\ (\pm0.044)$	0.849	0.19
ISR : $M_N \leftarrow 0.922\ (\pm0.012)M_L + 0.432\ (\pm0.042)$	0.848	0.19
OR : $M_L = 0.999\ (\pm0.009)M_N - 0.160\ (\pm0.032)$	0.842	0.137
Regression relation between $M_N - M_L$ Zagros region		
SR : $M_L \leftarrow 0.945\ (\pm0.009)M_N + 0.123\ (\pm0.032)$	0.871	0.181
ISR : $M_N \leftarrow 0.922\ (\pm0.009)M_L + 0.350\ (\pm0.030)$	0.875	0.179
OR : $M_L = 1.014\ (\pm0.006)M_N - 0.123\ (\pm0.023)$	0.867	0.13
Regression relation between m_b–M_S Alborz-Central Iran region		
SR : $M_S \leftarrow 1.285\ (\pm0.027)m_b - 1.653\ (\pm0.124)$	0.746	0.436
ISR : $m_b \leftarrow 0.581\ (\pm0.012)M_S + 2.100\ (\pm0.052)$	0.885	0.293
OR : $M_S = 1.576\ (\pm0.016)m_b - 2.965\ (\pm0.072)$	0.708	0.251
Regression relation between $m_b - M_S$ Zagros region		
SR : $M_S \leftarrow 1.071\ (\pm0.021)m_b - 0.866\ (\pm0.095)$	0.648	0.414
ISR : $m_b \leftarrow 0.606\ (\pm0.012)M_S + 2.081\ (\pm0.047)$	0.801	0.311
OR : $M_S = 1.420\ (\pm0.013)m_b - 2.415\ (\pm0.060)$	0.579	0.26

We have tested four regression relations (450 data pairs for Ms–Mw, 532 for mb–Mw, 108 for M_N–Mw, and 98 for M_L–Mw) and three different models (OR, SR, and ISR) for each. Results are summarized in Table 2-8a. SR and OR give very close results in the Ms–Mw relation. ISR shows instead better performances in the mb–Mw model. OR appears to be the best estimator in the relations involving M_N and M_L. The global Ms–Mw and mb–Mw relations determined by Scordilis (2006) are also investigated (Table 2-8b). These, being based on large databases and wider derivations, exhibit larger LLH.

We now apply the method to 70 events for which M_L, M_N, and Mw are available and find (Table 2-8c) that OR applied to M_N performs better in estimating Mw rather than M_L. Between mb and Ms in estimating Mw , lower dispersion is provided by Ms.

As a final step, the proposed ranking criterion is applied to 50 events reported in five different magnitude scales (Mw, Ms, mb, M_L, and M_N). Table 2-8d shows the LLH of the events for the resulting 14 relations. Ms–Mw OR, characterized by the lowest LLH, has to be considered the best model. This is followed by the Mw–M_N OR.

The procedure we have followed practically consists of the calculation of the best available regression model. An alternative procedure would consist of the calculation of a weighted mean Mw from the original magnitudes.

Table. 2-8. Average log-likelihood (LLH) values. Equations with the lowest LLH value (bold) are the best performers

Relation	Regression type	LLH
(a) M_S-M_W (n=429)	**OR**	**0.512**
	SR	0.533
	ISR	4.541
	Scordilis (2006)	0.582
m_b-M_W (n=583)	OR	0.879
	SR	0.846
	ISR	0.729
	Scordilis (2006)	1.038
M_N-M_W (n=106)	OR	0.687
	SR	0.695
	ISR	0.689
M_L-M_W (n=98)	OR	0.657
	SR	0.668
	ISR	0.798
(b) M_S-M_W (n=407)	**OR**	**0.486**
	SR	0.516
	ISR	5.012
	Scordilis (2006)	0.559
m_b-M_W (n=407)	OR	0.874
	SR	0.855
	ISR	0.788
	Scordilis (2006)	1.039

Relation	Regression type	LLH
(c) M_N-M_W (n=70)	**OR**	**0.669**
	SR	0.675
	ISR	0.671
M_L-M_W (n=70)	OR	0.682
	SR	0.689
	ISR	0.764
(d) M_S-M_W (n=50)	**OR**	**0.523**
	SR	0.543
	ISR	5.712
	Scordilis (2006)	0.534
m_b-M_W (n=50)	OR	0.6685
	SR	0.7301
	ISR	0.6089
	Scordilis (2006)	0.8919
M_N-M_W (n=50)	OR	0.7079
	SR	0.7119
	ISR	0.7104
M_L-M_W (n=50)	OR	0.6507
	SR	0.6747
	ISR	0.761

2-3.4. Poisson distribution of the Iranian Declustered Earthquake Catalog

** **Source Article:** **Zaré M**., Karimiparidari S., Memarian H., Kamranzad F., (2016), "Poisson distribution of the Iranian declustered earthquake catalog", Arab J Geosci (2016) 9:737, DOI 10.1007/s12517-016-2765-3.*

In this section, I present the poisson distribution of the ıranian declustered earthquake catalog, an analysis taken from the published article by Zaré et al. (2016). To test whether a declustered catalog collects independent events, we have to answer the question: can we disprove, to a certain level of significance, the null hypothesis that the declustered data set is drawn from the Poisson distribution? Therefore, failing to disprove the null hypothesis shows that the dataset can be consistent with the expected model.

The goal of this research was to check the independence of the Iranian mainshocks based on Poisson model. But, before testing the Poisson distribution of mainshocks, it is essential to extract the mainshocks from a seismicity catalog using an appropriate declustering technique. To achieve this, it was first tried to modify and localize the coefficients of the space-time windows in the well-known and largely adopted declustering algorithm by Gardner and Knopoff (1974). Due to the comprehensiveness of the seismic catalog prepared by Karimiparidari et al. (2013) which covers a homogeneous moment magnitude ranged between Mw=3.5–7.9, and dating from the third millennium BC to April 2010, this catalog was selected to determine the new modified space-time declustering windows for the Iranian seismic sequences as well as to investigate the Poisson distribution of the mainshocks.

Localization of the coefficients of the space-time windows for declustering:

According to Gardner and Knopoff (1974), the window-based declustering is a simple method by which time intervals and spatial distances corresponding to dependent events are determined as a function of the mainshock magnitudes. It is highly recommended to modify the coefficients of the declustering space-time windows based on the local observations in an area, in order to decrease the possible errors in the removal of independent events and making the mainshock distributions better follow the Poisson distribution.

To modify and localize the coefficients of the space-time windows for the Iranian earthquake sequences, twenty one of the well-documented earthquake sequences with the mainshock magnitudes ranged between Mw=5.4-7.0 were extracted from the Iranian

earthquake catalog (Karimiparidari et al., 2013). In order to have an idea about the earthquake clusters, the new space-time windows were initially selected in a double size of the windows defined by Gardner and Knopoff (1974). Then, by mapping these initial selected earthquake clusters, each seismic event that was near to the mainshock in terms of time and distance, was selected visually as a dependent event. The specified space-time intervals for each mainshock are shown in the Table 2-9. Based on this table, an exponential lub or envelope was fitted to the time and space of aftershock sequences. To develop an acceptable relation for the time window, the magnitude of mainshocks was divided into two parts: events with M_W<6.5 and events with 6.5≤ M_W. The new temporal equations were defined as below:

$$T = 0.2496 * e^{1.2803 M_w} \qquad M_w < 6.5$$

$$T = 324.86 * e^{0.1727 M_w} \qquad M_w \geq 6.5$$

Where T is the time in days and M_w is the moment magnitude of the mainshock.

By fitting a suitable lub to the spatial data, the new space window is also defined as below:

$$R=10*e^{0.286 M_w}$$

Where R is the distance in kilometers.

Table 2-9. Selected earthquake sequences and specified space-time distances of aftershocks to mainshock for each sequence.

Date			Location		Mw	Days after mainshock that aftershocks occurred	Distance from mainshock that aftershocks occurred (Km)
Year	Month	Day	Latitude	Longitude			
1981	7	28	29.97	57.77	7.1	852	56
1977	3	21	27.58	56.36	7.0	1072	46
1972	4	10	28.41	52.79	6.8	1052	67
1998	3	14	30.14	57.59	6.6	711	54
2003	12	26	28.9	58.28	6.5	927	58
1990	4	21	28.15	55.61	6.4	835	53
1999	3	4	28.27	57.21	6.4	609	58
1999	5	6	29.52	51.91	6.3	763	58
2005	2	22	30.72	56.78	6.3	595	31
2008	9	10	26.94	55.72	6.1	490	-
1993	3	1	29.14	52.64	6.0	410	34
2006	2	28	28.13	56.79	6.0	293	35
1983	7	12	27.60	56.40	5.9	285	30
2005	11	27	26.79	55.81	5.8	191	36
2006	3	25	27.50	55.62	5.8	120	51
1998	8	11	29.88	51.66	5.8	175	36
2003	7	10	28.33	54.16	5.6	288	37
1988	3	30	30.85	50.18	5.6	127	35
2002	9	25	32.06	49.32	5.5	157	39
1990	12	16	29.02	51.31	5.5	120	37
1998	11	13	27.80	53.64	5.4	172	37

The results of the new modified space-time windows in the current study were then compared to Gardner and Knopoff's (1974) windows in the Fig.2-5. According to this figure, using the Iranian earthquake sequences has led to introduce a bigger spatial window for the new model in comparison to the Gardner and Knopoff's (1974) window. In addition, the new modified time window shows two different trends: (1): For M_W<6.5, the modified time window greatly corresponds to the Gardner and Knopoff's time window. (2): For 6.5≤ M_W, aftershocks occur during a longer time interval than the Gardner and Knopoff's time window.

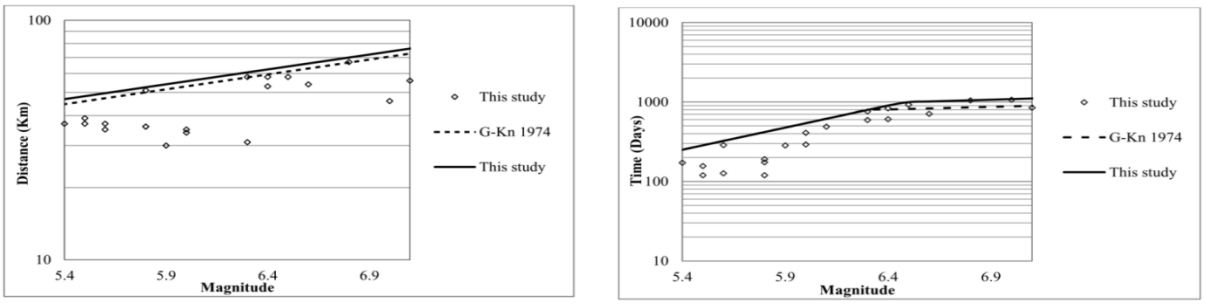

Fig. 2-5. Comparison of the new modified space-time windows of this study to the Gardner and Knopoff's (1974) windows.

Checking the independence of mainshocks in the declustered catalog:

In order to control the independence of mainshocks, the events of the Iranian catalog (Karimiparidari et al., 2013) in the time span of 1964-2010 with M_w=3.5-7.4 were used. Then, the new modified space-time windows defined in this study were applied to the seismic catalog in the seven well-known seismotectonic zones of Iran. After declustering, to control whether the mainshocks follow a Poisson distribution or the distribution of the inter-event times are exponential, the Kolmogorov–Smirnov (KS) test was used. The time interval of 10 days was considered. To control the validity of the method, the KS-test was performed on the both primary (non-declustered) and mainshock (declustered) seismic catalogs. The results of the aftershock removal, the test of the magnitude of completeness and the one-sample KS-test on the both primary and mainshock catalogs have been presented in Table 2-10.

The results show that by using the modified space-time windows, 36%, 29% 45%, 26%, 19%, 36% and 56% of the data have been removed in Alborz mount ranges, Azarbaijan, Central Iran, Kopet Dagh, Makran, North-West Zagros mountains and the South-East Zagros mountains, respectively. The P-values over 0.05 indicate that there is no significant difference between the two datasets. In this study, it shows that there is no significant difference between the type of the statistical distribution of the earthquakes with the type of

experimental distribution (Poisson or exponential). In this respect, the results of the one-sample KS-test show that the primary catalogs generally does not follow the Poisson distribution in the most seismotectonic zones. The primary catalog of Kopet Dagh is close to a Poisson distribution with the P-value of 0.05 and the primary catalog of Makran is the only exception that completely follows the Poisson distribution with the P-value of 0.52. The Poisson distribution of the primary catalog of Makran before the aftershock removal is likely due to lack of enough data in this seismotectonic zone. The results of the KS-test on the successful declustered inter-event times indicates that the inter-event times of the all catalogs follow an exponential distribution (Table 2-11). Results of the one-sample KS-test show that all the declustered catalogs in the seismotectonic zones follow the Poisson distribution.

Table 2-10. The results of the aftershock removal, test of the magnitude of completeness and one-sample KS-test on the primary and declustered catalogs for 7 seismotectonic zones of Iran.

Seismotectonic Zone	Total No. of Events	No. of Mainshocks	Mag. Threshold (Mw)	Poisson Parameters (Mean)		Most Extreme Differences		Kolmogorov -Smirnov Z		Asymp. Sig. (P-Value)	
				Primary Catalog	Mainshock Catalog	Primary Catalog	Mainshock Catalog	Primary Catalog	Mainshock Catalog	Primary Catalog	Mainshock Catalog
Alborz Mountain Range	507	325	4.2	0.27	0.12	0.069	0.003	2.81	0.12	0	1
Azerbaijan	738	526	4.2	0.38	0.15	0.06	0.004	2.45	0.15	0	1
Central Iran	1266	698	3.9	0.71	0.32	0.171	0.03	7.02	1.23	0	0.1
Kopet Dagh	351	260	4.1	0.18	0.11	0.033	0.005	1.35	0.22	0.05	1
Makran	306	249	4.2	0.17	0.1	20	0.005	0.82	0.19	0.52	1
NW Zagros Mountains	1853	1192	4.5	1.06	0.32	0.14	0.017	5.75	0.69	0	0.74
SE Zagros Mountains	2559	1280	4.4	1.47	0.35	0.203	0.015	8.32	0.61	0	0.86

Table 2-11. Results of the one-sample KS-test on inter-event times for 7 seismotectonic zones of Iran.

Seismotectonic Zone	N (no. of inter-event times)	Exponential parameter (Mean)	Most Extreme Differences	Kolmogorov-Smirnov Z	Asymp. Sig. (P-Value)
Alborz Mountain Range	195	86.24	0.058	0.81	0.53
Azerbaijan	249	67.42	0.056	0.88	0.43
Central Iran	274	60.83	0.049	0.81	0.53
Kopet Dag	172	97.83	0.071	0.94	0.35
Makran	168	99.3	0.053	0.69	0.73
NW Zagros Mountains	516	32.62	0.048	1.09	0.19
SE Zagros Mountains	565	29.75	0.04	0.96	0.32

2-3.5. Catalog of the earthquakes with maximum intensities (I_{max}) in Iran

** **Source Article:** Amini H., **Zaré M**. and Gasperini P., (2016), "Catalogue of the earthquakes with maximum intensities (Imax) in Iran", Submitted.*

In this section, I present a recent effort on preparing a catalog of the earthquakes with maximum intensities (I_{max}) in Iran, an analysis taken from the under review article by Amini et al. (2016). Intensity can be used for determining the location and size of the earthquakes (*e.g.* Gasperini et al., 1999) occurred when or where there were no available instruments. The MSK (Medvedev–Sponheuer–Karnik), MMI (Modified Mercalli Intensity), and EMS (European Macroseismic Scale) intensity scales are three 12-degree intensity scales applied in Iran. Another scale, used for most of the historical and some of the instrumental earthquakes, was proposed by Ambraseys and Melville (1982) (called AMS in this study) and has only 5 degrees because its authors believed that macroseismic information in Iran was not detailed enough for applying a 12-degree scale. In the AMS scale, degree I corresponds to the strongest effects and degree V to the weakest ones.

In this study, we attempt to reconcile the maximum intensity assessments made by various authors in different intensity scales in order to prepare a uniform dataset as much homogeneous as possible for Iran region. To this aim, at first, all information is collected from the literature in terms of the descriptions of effects and/or assessed intensity values. In cases when descriptions are not available from sources, the intensity values assessed by various authors in different scales are converted to the EMS, using tables of correspondence. Reports of environmental effects are also considered by the ESI scale so that include in the maximum intensity dataset as many earthquakes as possible.

Datasets:

The sources used for collecting the information mainly consist of books, articles as well as web reports provided by different Iranian research centers (i.e. IIEES, BHRC, Geological Survey of Iran (GSI), and National Geoscience Database of Iran). The intensity information available to us consist of a) reports including descriptions, with or without intensity values for about 350 earthquakes, and b) reports with only intensity values for about 150 earthquakes. Moreover, in this study, the information of about 1110 Macroseismic Data Points (MDPs) of 37 earthquakes, which have more complete descriptions, is also considered to obtain more reliable comparison between different intensity scales.

Most of the Iranian intensity reports were provided by Berberian (1976; 1977; 1981) in the MMI scale, by Ambraseys and Melville (1982) in the AMS scale, by Ambraseys (2001) in the MSK scale, and by Zare and Memarian (2003) in the EMS scale.

Choice of the Intensity Scale for Iran region:

The EMS is the most recent intensity scale with detailed damage descriptions on different categories of buildings. In this study, this scale is selected as a basic scale to assess the intensity values. In many cases, there is not enough information to assess an intensity value using EMS scale, but there are descriptions of effects on ground and environment, which were almost totally removed from the EMS scale. As for many Iranian earthquakes this is the only information available, we also use the ESI (Environmental Seismic Intensity) scale that was properly designed to account for such environmental effects. The joint use of these two scales can be seen as the application of a combined EMS-ESI scale.

Converting intensities from other scales to the homogeneous EMS-ESI scale:

To get homogeneous maximum intensity estimates in cases when no descriptions of effects but only intensity values are reported on available sources, we derived tables of correspondence between the different scales used by various authors and the EMS-ESI scale. To this aim, we compared our intensity estimates for earthquakes having descriptions, with those made by different authors for the same earthquakes. As the estimation of intensity from written sources depends on subjective interpretations and on the evaluation of the reliability of sources, we also compared estimates made by Zare and Memarian (2003) in the EMS scale with those made by us in the EMS-ESI scale for the same earthquakes.

For each degree of the EMS-ESI scale, the averages of intensity assessed by various authors in different scales are shown in Table 2-12 using a) data with information only concerning the maximum effects (I_{max}) and b) data with information on single localities (MDPs). We can note that using I_{max} data, there are several inconsistencies in which for an increase of EMS-ESI degree, the average intensity decreases in EMS and MSK scales, and increase in AMS scale. For example, considering the AMS scale and I_{max}, the average intensities 1.86 and 2.04 are related to the degree IX and X of EMS-ESI scale respectively. This means that with increasing intensity in the EMS-ESI scale, the intensity of the AMS is increasing instead of decreasing as it should be. Similarly, the average intensities of degree VIII in both the EMS and the MSK scales, instead of increasing with respect to degree VII,

are decreasing. Also, the average intensity of MSK for degree XI of EMS-ESI scale is decreasing with respect to the value of degree X. Such inconsistencies disappear or strongly reduce when using instead MDPs data. Then, in the following, we consider only the comparisons made using MDPs data.

Table 2-12. Averages of intensities in AMS, MMI, EMS and MSK scales for each degree of the EMS-ESI scale using only I_{max} (a) and MDPs (b).

EMS-ESI	a) Using I_{max}				b) Using MDPs			
	AMS	MMI	EMS	MSK	AMS	MMI	EMS	MSK
VI	3.93	5.92	6.10	5.93	4.00	4.00	5.00	7.00
VII	3.65	6.51	7.41	7.11	2.85	6.83	7.20	7.00
VIII	3.32	7.06	7.08	7.00	2.71	7.42	7.25	7.67
IX	1.86	7.79	8.08	8.67	2.03	7.50	8.25	8.72
X	2.04	8.12	8.50	9.00	1.89	8.10	8.20	8.62
XI	1.25	8.89	8.50	8.50	1.50	8.89	10.33	9.50

Preparing a homogeneous intensity dataset:

When descriptions are available, the intensity value of each MDP or I_{max} is assessed directly from them in the EMS-ESI intensity scale. For the earthquakes with MDPs, I_{max} is simply computed as the maximum intensity over all MDPs. If only intensity values in various scales are available from sources, the homogeneous intensity is computed as the average of EMS-ESI intensity estimations made by us for MDPs having intensity estimates from various sources in the MMI, EMS, MSK and AMS scales (Tables 2-13 a, b, c and d, respectively). In Tables 2-13 a, b, c and d, we also report the standard deviations with respect to the EMS-ESI averages as well as the rounded integer value (in Roman numerals) that we actually use for the conversion to the EMS-ESI scale.

We can observe that MMI intensities (Table 2-13 a) are for most degrees underestimated by a degree with respect to our EMS-ESI assessments. Conversely the EMS intensities (Table 2-13 b) are substantially coincident with our re-assessments. For the MSK scale (Table 2-13 c), we observe the underestimation by one degree for degrees VII and VIII of the EMS-ESI and coincidence for others degrees. In Fig. 2-6, all earthquakes with assessed or converted I_{max} (512 earthquakes) for the new intensity catalog are mapped with different colors and sizes depending on I_{max}. The maximum intensity assessed in previous works was X, whereas we assessed intensity XI for some localities or areas where the descriptions indicate total destruction of buildings or particularly strong environment effects. Note that degree XI is actually included in degree I of the AMS by Ambraseys and Melville (1982).

The numbers of earthquakes with maximum (XI) and minimum (IV) I_{max} are 22 and 30,

respectively. I_{max} VIII with 171 earthquakes and I_{max} XI with 22 earthquakes have maximum and minimum number of assessments, respectively. Number of earthquakes with intensity for period of year before 1900, 1901-1964, and 1965-2013 are 237, 88, and 187, respectively. Most of the information before 1900 has intensity values in the AMS scale that in this study are converted to the values in the 12-degree EMS-ESI scale.

Table 2-13. Correspondence between the degrees of (a): MMI and EMS-ESI (b): EMS and EMS-ESI, (c): MSK and EMS-ESI and (d): AMS and EMS-ESI scales.

(a)

MMI	Average	Std	EMS-ESI
III	4.20	-	IV
IV	4.47	0.70	IV
V	5.31	0.79	V
VI	6.56	0.79	VII
VII	7.99	0.79	VIII
VIII	8.88	0.74	IX
IX	9.77	0.70	X
X	10.3	0.70	X

(b)

EMS	Average	Std	EMS-ESI
IV	5.21	-	V
V	4.93	0.70	V
VI	6.30	0.74	VI
VII	7.50	0.70	VII
VIII	8.09	0.79	VIII
IX	9.47	-	IX

(c)

MSK	Average	Std	EMS-ESI
IV	4.06	0.70	IV
V	5.09	0.70	V
VI	6.71	0.70	VII
VII	7.68	0.70	VIII
VIII	8.94	0.74	IX
IX	9.80	0.74	X
X	10.2	0.74	X

(d)

AMS	Average	Std	EMS-ESI
I	10	0.70	X
II	9.45	0.79	IX
III	8.03	0.79	VIII
IV	6.36	0.74	VI
V	4.18	0.70	IV

*Average: EMS-ESI intensity average; Std: standard deviation of EMS-ESI intensity with respect to the average; EMS-ESI: intensity average rounded to the nearest integer.

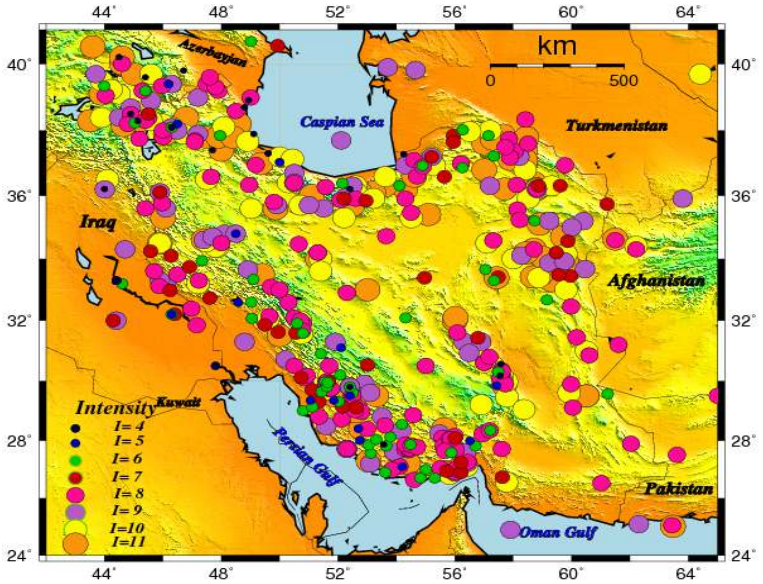

Fig. 2-6. Map of intensity catalog of the Iranian Plateau with 512 earthquakes. Each value of intensity is shown in different color and size.

2-3.6. The Iranian earthquake intensity database: 1975 - 2000

** **Source Article:** **Zaré M**. and Memarian H., (2002), "The Iranian earthquake intensity database: 1975-2000", 9th International Congress of the International Association of Engineering Geology and the Environment, pp.2894-2903.*

In this section, I present the Iranian earthquake intensity database: 1975 - 2000, an analysis taken from the published article by Zaré and Memarian (2002). The data on the intensities of the Iranian earthquakes (1975-2000) are investigated, along with the existing damage reports, in order to provide a catalogue of the intensity information to be used as the basis of developing an attenuation law. The data reported in different scales are unified under the European Macroseismic Scale (EMS-98). A catalogue of 470 intensity estimations comprising source and site specifications and a quality factor for each data is prepared (for the full catalog, refer to Zare and Memarian, 2002). The sources of information on the earthquake intensities in Iran consist of the reports by different Iranian research centers, scientific articles, historical books, the remnants of the monuments and archeological locations. The evaluation of the strong motions in the areas such as Iran could be performed even for the event occurred in the past. This is important for the seismic hazard and risk assessment. The intensity estimations have however the uncertainties, because they are qualitative in its nature and meanwhile it should be investigated through the eye witnesses.

In the present study a catalog for the recent earthquakes since 1975 until 2000 is prepared to be used as the basis for the intensity attenuation law for Iran. The macroseismic intensity investigations in Iran are carried out after the great and moderate earthquakes (usually after the destructive events). The homogenization of the reported intensities and estimation an intensity value for the damage reports of the moderate events with no reported intensity evaluation was the first step of this work. We have then looked for the earthquake source data for which the intensities were reported. In this paper, we will present first how we gathered the intensity reports and the information on source and site conditions. The sources of uncertainties in such evaluations are discussed as well.

Catalog of earthquake intensities:

The intensity reports for the recent Iranian earthquakes with an acceptable level of confidence are selected to form the catalog of the intensity values of recent earthquakes in Iran. This catalog comprises the information for the localities of reported or estimated intensity values

and the earthquake source specifications. The greater events are reported by several reconnaissance group. Different iso-intensity maps are reported for such earthquakes, in which the intensity estimations contradict sometimes with each other. These reports comprise the intensity estimations in different scales; mainly the MMI, MSK and a 5- degrees scale developed by Ambraseys and Melville (1982) for the Iranian earthquakes. The scale chosen as the basis for the present study was the EMS-98 (Grunthal, 1998) . It is tried to invert the other scales to EMS-98: most of the MSK estimations are not essentially different than that of EMS-98; the other scales were correlated with MSK and EMS-98 using the correlation charts (Japan TC-4, 1992) and the explanatory chart of the EMS-98 (Grunthal, 1998). The recent earthquakes (1975-2000) were chosen for this study, since the details on the casualties exist in more details, and the result could be directly compared with the accelerometric studies recently performed in Iran (Zaré 1999, Zaré et al 1999).

To provide the database for the present study, a bibliography was performed on the reconnaissance and damage reports on the recent Iranian earthquakes (i.e. Moinfar and Naderzadeh 1990, Berberian et al 1992). The information on the geotechnical conditions in different locations of the intensity estimations were gathered and the results of the observations (whenever existed) were entered to the catalog. The surface observations were not chosen to be the basis of surface geology conditions, since the misleading are expected using such observations to classify the soil conditions (Zaré et al, 1999).

Surface Geology:

The effects of the surface geology on the strong ground motions are previously studied in Iran, in the stations of the accelerometric network (Zaré et al, 1999). According to the mentioned study, the site conditions are classified according to their H/V ratio. This ratio is chosen based on the locations of the broadened H/V spectral ratios and the value of its amplitude. In brief, site category 1 corresponds to rock and hard alluvial sites, with Vs>800 m/s over 1st 30m depth and site amplification fundamental frequency (f_0) over 15 Hz. The site category 2 relates to alluvial sites; thin soft alluviums, with 500<Vs<700 over 1st 30m depth, and 5<f_0<15 Hz. The site category 3 corresponds to soft gravel and sandy sites, with 300<Vs<500 over 1st 30m depth and 2<f_0<5Hz. Finally the site category 4 relates to soft soil sites; thick soft alluviums with Vs<300m/s over 1st 35m depth and f_0<2Hz. In the present study, we couldn't specify the site conditions in the exact location of the intensity observation or estimation. It is however decided to include only the sites with a known H/V spectral ratio

(where at least a well recorded accelerogram is obtained), and then to generalize the classification to two categories ("1" stands for hard soil conditions classes; 1 and 2, and "2" stands for soft soil conditions 3 and 4).

Source Parameters:

The source parameters, investigated in the present study, are the earthquake macroseismic epicenter, the data of the mainshock (UTC time), magnitude (in different scales; mb, Ms, ML and Mw, based on the available data), focal depth (using mostly the teleseismic estimations and in some cases the relocated hypocenters) and the focal mechanisms (based on the Harvard seismology Web site, 2001). The macroseismic epicenter is chosen as the location of the greatest damages (where the highest intensity values is assigned; I_0). This location could be near to, or coincided with, the real epicenter (whenever the region is densely populated) or far from it (when the region is sparsely populated; in the central and eastern Iran, where the great deserts exist). The macroseismic intensities (I_0) are plotted against the observed intensities in Fig. 2-7. The Mw magnitude (and the magnitudes in other scales; ML, mb, Ms which are scaled to Mw) are plotted in Fig. 2-8 against I_0.

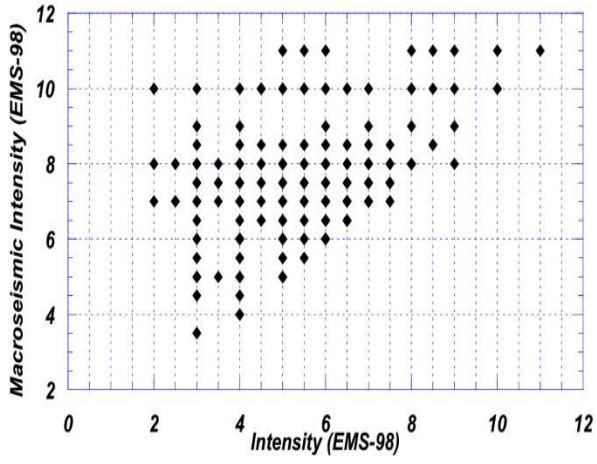

Figure 2-7. The macroseismic epicentral intensities against observed intensities for the studied earthquakes.

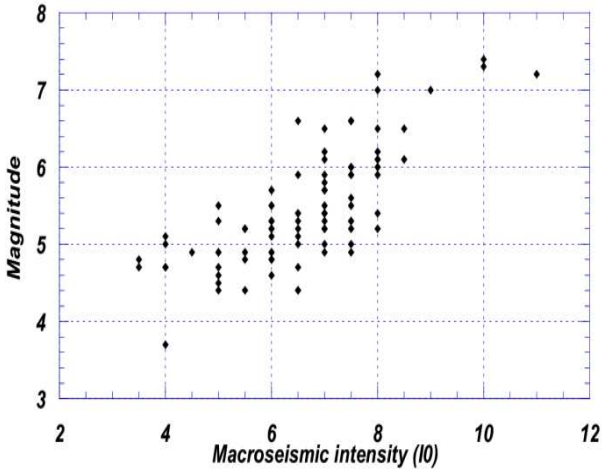

Figure 2-8. The Magnitudes against macroseismic epicentral intensities for the studied earthquakes.

Different macroseismic intensities could cause the intensities up to that degree (i.e. for I_0=V, the intensities up to V could be observed; Fig. 2-7). The relationship of earthquake magnitudes and the macroseismic intensities, given in Fig. 2-8, could be shown with a linear regression which gives the best correlation coefficients. The relationship is:

$$I_0 = 1.45\ M - 1.22$$

The standard deviation for this relationship is 0.81 and the correlation coefficient is 0.81. Using this formula, for a magnitude 6.0, the macroseismic epicentral intensity could reach to VII+ (mean value) and VIII+ (mean plus one sigma standard deviations).

Distance

The definition of distance is one of the most important factors, especially for the attenuation formulas. The macroseismic epicenter distance is the nearest distance between the location of the felt intensity and the macroseismic epicenter (where the maximum intensity is felt). The epicentral distance is the nearest distance between the location of the felt intensity and the instrumentally located epicenter. According to the importance of the event and precision of the field observations, location of the instrumentally located epicenter and the macroseismic observed intensity could be different (the greater the magnitude of the event and the more precise the observations, the locations of these two epicenters are nearer to each other).

Intensity Values and Quality Factor

The intensity values are reported either in MMI or in MSK scales. The intensity values were unified to EMS-98, which is a 12 degree European macroseismic scales developed essentially based on MSK (its old version). The bar charts are used to find the equivalent of the MMI values in the MSK and EMS-98 scales. The values in MSK could be directly taken as EMS-98 values, since there is no major difference between these two scales (at least in the scales of our observations). The Quality factors are assigned in four levels (from “A” to “D”). The quality level of “D” (the basic level of the data) was assigned, when at least a location of macroseismic intensity and an intensity value could be assigned (no more information existed). Level “C” is assigned when the quality of a magnitude and instrumental epicenter location were reported but the doubt existed on the location of the intensity observations and other source parameter. Level “B” was when all information was available from the intensity observation locations and the source parameters, but the location of the macroseismic intensity and/or the level was uncertain. The quality level “A” introduces the best information quality. For the magnitudes greater than 7.0, most of the data in the final catalog presented in this paper have the “A” level of quality. The worse cases are the magnitudes less than 5.0, when the most uncertain information exist.

2-4. Uncertainties associated with seismicity catalog

For a catalog, a clear description and evaluation of uncertainty of earthquake parameters is effective. Based on a number of local and regional seismographic stations, station distribution and velocity models, there are apparent uncertainties in different earthquake parameters. Value of uncertainty is decreased during the time until now. By comparing some of location, depth and magnitude, which are reported by different seismological centers, we can assess uncertainties for each earthquake and center.

The feasibility of selecting 'reference events' (events where the hypocenters can be considered known to high accuracy) was investigated by Sweeney (1996) in continental regions from global bulletins such as those published by the ISC and NEIC that contains predominantly teleseismic arrival time data. Sweeney (1996) suggested when the largest azimuthal gap between stations surrounding the epicenter is less than 200° and at least 50 first-arriving P phases are used, locations from these catalogs have an accuracy of 10–15 km. Sweeney (1998) revised these selection criteria for teleseismic networks with an azimuthal gap of less than 90° and with at least 50 first-arriving P phases that were used in the location he found 15 km (or better) epicenter accuracy.

Accuracy of focal depths for earthquakes is important in understanding tectonics of a region and for evaluating earthquake hazards (Maggi et al. 2002). There is no complete reliable evidence of intermediate focal depth of earthquakes. The assessment of depth is a controversial issue, even for modern instrumental earthquakes.

Analysis of events with independently known coordinates indicates that most Preliminary Determination of Epicenters (PDE) determinations are accurate to a few tenths of a degree in epicentral position and 25 km in depth. Because of these uncertainties, verbal descriptions of locations in news releases are rounded to the nearest 5 miles and/or 10 km (Sipkin et al., 2000).

Engdahl et al. (1998), by using travel-time tables (Kennett et al., 1995), produced a "groomed" ISC catalog. Myers and Schultz (2001), when the largest azimuthal gap is less than 90°, estimated the epicentre accuracy in the EHB catalog which is 15 km or better at the 95% confidence level for events not in subduction zones.

Ambraseys (2001) claimed for the eastern Mediterranean (Middle East) region that the instrumental locations before the early 1970s had low accuracy. International Seismological Summary (ISS)/ISC locations are systematically shifted by 10–30 km to the N or NE from

their macroseismic epicenters, a bias which is unlikely to be due to systematic errors in the macroseismic positions.

According to Yunatci (2010), the macroseismicity catalog for Turkey has revealed that the location uncertainty of focal points of events can reach over 10 kilometers. Due to moment magnitude estimates, the average value of magnitude being equal to 0.17 magnitude units assigned as the constant value of parameter uncertainty in the current GMPE model. Then, we will have at least 20 km and 0.17 uncertainty for location and magnitude.

Mirzaei et al, (1997), based on quality and quantity of available information determined uncertainty of earthquake parameter for Iran in three periods of time: for historical period (pre 1900) uncertainty in depth, location and magnitude represent in 30 km, 100 km and 0.4 to 0.8 respectively; for early instrumental period (1900-1963) 20 km and 0.3 to 0.5 was calculated for location and magnitude; and for modern instrumental period (1964-1994) location errors for moderate and major earthquakes are about 15 and 10 km and direct assignment of Ms may contain 0.2 to 0.4 magnitude units of error and Ms values from the conversion of mb suffer 0.45 to 0.67 magnitude units of uncertainty.

The magnitude of completeness (Mc) is another seismicity parameter that may consist of different levels of uncertainties. The Mc is theoretically defined as the lowest magnitude at which 100 % of the earthquakes in a space–time volume are detected (Rydelek and Sacks, 1989) which might be studied in the specific time windows. Determination Mc of instrumental earthquake catalogs is an essential and compulsory step for any seismicity analysis (Mignan and Woessner, 2012). Ambraseys (2001) explained that it is unlikely that all small and perhaps a few moderate shocks in the early part of the twentieth century in Afghanistan, Africa, and offshore would have been recorded, the available twentieth-century data for the whole region are almost complete only for moderate earthquakes or greater (Ambraseys, 2001).

2-5. Comments and Replies on two papers

In this section, two comments and replies published on the papers of EMME earthquake catalog (Zare et al., 2014) and Iranian seismic catalog during 1900-2011 (Shahvar et al., 2013) are discussed.

2-5.1. Comment on 'A Unified Seismic Catalog for the Iranian Plateau (1900–2011)'

** **Source Article:** Mirzaei N., Shabani E., and Mousavi Bafrouei S.H., (2014), 'Comment on "A Unified Seismic Catalog for the Iranian Plateau (1900–2011)" by Mohammad P. Shahvar, **Mehdi Zare**, and Silvia Castellaro', Seismological Research Letters, 85, 179-183.*

Here, some comments proposed by Mirzaei et al. (2014) on our previously published paper entitled 'A Unified Seismic Catalog for the Iranian Plateau (1900–2011) by Shahvar et al. (2013)' are summarized in the following points:

- *Shahvar et al. (2013) claim that the Iranian plateau can de facto be divided into two domains only because seismicity in the Alborz and Central Iran zones show statistically undistinguishable features.*
- *It is stated by Shahvar et al. (2013) that the continental Arabian shield subducts beneath the Zagros belt. However, local seismograph networks have found no reliable depths in the Zagros deeper than about 20 km.*
- *In contrast to what Shahvar et al. (2013) state that "displacement occurs mostly through strike-slip mechanisms parallel to the axis of the Zagros range"; the Zagros belt is a broad zone of continuing compressional deformation that experiences horizontal shortening of the basement on reactivated normal faults that stretched and thinned the basement of a continental margin on which the Mesozoic sedimentary was deposited.*
- *Shahvar et al. (2013) derived the magnitude conversion relation M_s–M_w for $M_s \geq 3{:}6$, on the other hand this relation is used later to convert $M_s \geq 2{:}7$ to M_w. In addition, it is not clear that how magnitude uncertainties are assessed to the unified M_w. The total magnitude uncertainty can be defined as $\sigma_{total} = (\sigma^2_{original} + \sigma^2_{conversion})^{1/2}$ in which $\sigma_{original}$ scale uncertainty and $\sigma_{conversion}$ is the uncertainty after any con-version from one scale to another. The uncertainties reported by Shahvar et al. (2013) do not comply with a rule, for instance, the uncertainty for m_b 4:0 and m_b 6:1 is considered as 0.3 magnitude units, equally".*

2-5.2. Reply to "Comment on 'A Unified Seismic Catalog for the Iranian Plateau (1900–2011)'"

* ***Source Article:*** *Shahvar M.P., **Zaré M**., and Castellaro S., (2014), "Reply to "Comment on 'A Unified Seismic Catalog for the Iranian Plateau (1900–2011)' by Mohammad P. Shahvar, Mehdi Zaré, and Silvia Castellaro" by Noorbakhsh Mirzaei, Elham Shabani, and Seyed Hasan Mousavi Bafrouei", Seismological Research Letters Volume 85, pp. 184-185. doi: 10.1785/0220130144.*

We hereby reply to the comments of Noorbakhsh Mirzaei, Elham Shabani, Seyed Hasan Bafrouei (hereafter NES) on our paper published in Seismological Research Letters 84 (2), 233– 249 (hereafter Shahvar et al., 2013). Our work originated from the lack of a uniform catalog of earthquakes in Iran (both for the fact that data are dispersed among several catalogs and for the fact that they report magnitudes with different scales), which makes research on seismicity and seismic hazard very difficult.

Regarding the comments on the number of zones used to define magnitude conversion relations, it has to be noted (but we think this was already clear from the text) that our subdi-vision was not based on tectonic arguments but naturally came out from the application of statistics to the data. We started from the six main seismotectonic areas defined by Rham (2009) but found that: (1) the Makran and Kopet–Dagh areas reported too few M_w data to perform any meaningful analysis, and (2) no statistically significant differences between the Alborz and Central Iran zones appeared for any magnitude con-version relation. These two areas could also belong to two different tectonic settings but this is completely irrelevant to our analysis: they show the same conversion relations and it makes no sense to treat them separately to the aim of our paper. The Ockham's razor principle, on which the scientific method is based, forces us to use—among the many possible models— the one that explains the observations using the lowest amount of parameters. This choice is also supported by the results of the same Mirzaei et al. (1997) who found the same relation by treating the Central Iran and Alborz zones as separate. On the opposite side, the M_s–m_b, M_L–M_N, and M_w–m_b relations were found to differ significantly for the Alborz–Central Iran and the Zagros region, which have therefore been treated separately.

About the comments on the depths, the values reported in our paper are the maximum depths described by the different agencies.

For what concerns the choice of the Zagros area, we have followed Alavi (1994, 2004), Agard et al. (2005), Ghasemi and Talbot (2006), and Rham (2009). Alavi (1994, which is one of the most cited papers), states:

> The Zagros orogenic belt of Iran is the result of the opening and closure of the Neo-Tethys oceanic realm, and consists, from northeast to southwest, of three parallel tectonic subdivisions: (1) the Urumieh-Dokhtar Magmatic Assemblage; (2) the Sanandaj-Sirjan Zone; and (3) the Zagros Simply Folded Belt.

The NES statement according to which Karimiparidari et al. (2013) established magnitude conversion relations for six separate zones appears to us to be incorrect, because Karimiparidari et al. (2013) computed the conversion relations for whole Iranian plateau, with no segmentation (a subdivision into six areas was used only to calculate the seismicity parameters, not the magnitude conversion relations).

The NES comment on our presumed wrong data entries ("event number 1420 is reported with M_w 5.8 instead of 5.3; or event number 2031 is reported with M_w 4.6 instead of 5.1") is not correct. The event number 1420 (9 December 1971) is reported as an M_w 5.8 (M_0 5:623413 × 10^{24}) by Earthquake Mechanisms of the Mediterranean Area (EMMA) and Talebian and Jackson (2004). In our catalog the event number 2031 (11 February 1978) is reported with M_w 5.1 (M_o 6:559931 × 10^{23} by EMMA, and Jackson and McKenzie, 1984). The event number 7056 (8 November 2011) and the event number 6789 (9 February 2011), are reported under the ID 17525142 and 16852124 in the International Seismological Centre (ISC) catalog. The other events incorrectly reported by National Earthquake Information Center (NEIC) were removed.

Reporting the history of seismic networks (who, when, and why initiated them) was definitely not pertinent to our paper and this information can easily be found in the seismological network manuals for the interested readers. Regarding the comments on the uncertainty estimation, as described in the section Uncertainty Estimation, the final uncertainties include the contribution to the total error (often unfortunately neglected!) deriving from the original magnitude uncertainties. This makes it clear that magnitude values cannot and should never be written with more than two significant digits (see also Bormann, 2002).

2-5.3. Comment on 'Recent developments of the Middle East catalog' by Zare et al (2014).

** **Source Article:** Mousavi, S.M, (2016), Comment on "Recent developments of the Middle East catalog" by **Zare et al**., Journal of Seismology.*

Here, some comments proposed by Mousavi (2016) on our previously published paper titled 'Recent developments of the Middle East catalog' by Zare et al (2014)' are summarized in the following points:

- *The provided Mc map for entire region (Figure 12a of Zare et al. 2014) does not reflect the temporal variation of the Mc in individual subregions. In many cases such as in studies of temporal seismicity rate variations, the temporal consistency of reporting is more important than the level of completeness (Habermann, 1982).*
- *If we plot all earthquakes with magnitudes 4.0 and 4.1 for a time period from1900 to 1970 (Fig. 2-9-a) almost all events are limited to Azerbaijan and Caucasus subregions, while there is just one event in Turkey and one in Afghanistan-Pakistan subregion. Table 8 (of Zare et al. 2014) reports that Central Iran, Makran and Turkey are complete for events with Mw≤4.0 within the same period of time. As another example, we plot all events with 4.0<Mw ≤4.3 for time period of 1900 to 1990 (Fig. 2-9b). Although all regions have been reported to be complete for this magnitude range and time period, but distribution of event density is not homogeneous throughout the region. A high concentration of earthquakes with this magnitude range is observable at Caucasus and northwest of Alborz-Azerbaijan subregions around longitudes 40°-47° (herein Caucasus-Azerbaijan region).*
- *In Table 8 (of Zare et al. 2014) beginning year of complete reporting of earthquakes with Mw≤4.0 in Makran subregion is 1970. But the starting time of completeness for events with 4.0<Mw≤4.5 in the same region is reported to be 1975.*
- *We have determined minimum (smaller values between two) and conservative (higher one in two alternatives) magnitude cutoffs (Table 2-14). These are the lowest magnitude level above which detection is unaffected within a time period between the center year and the time of next significant rate change.*

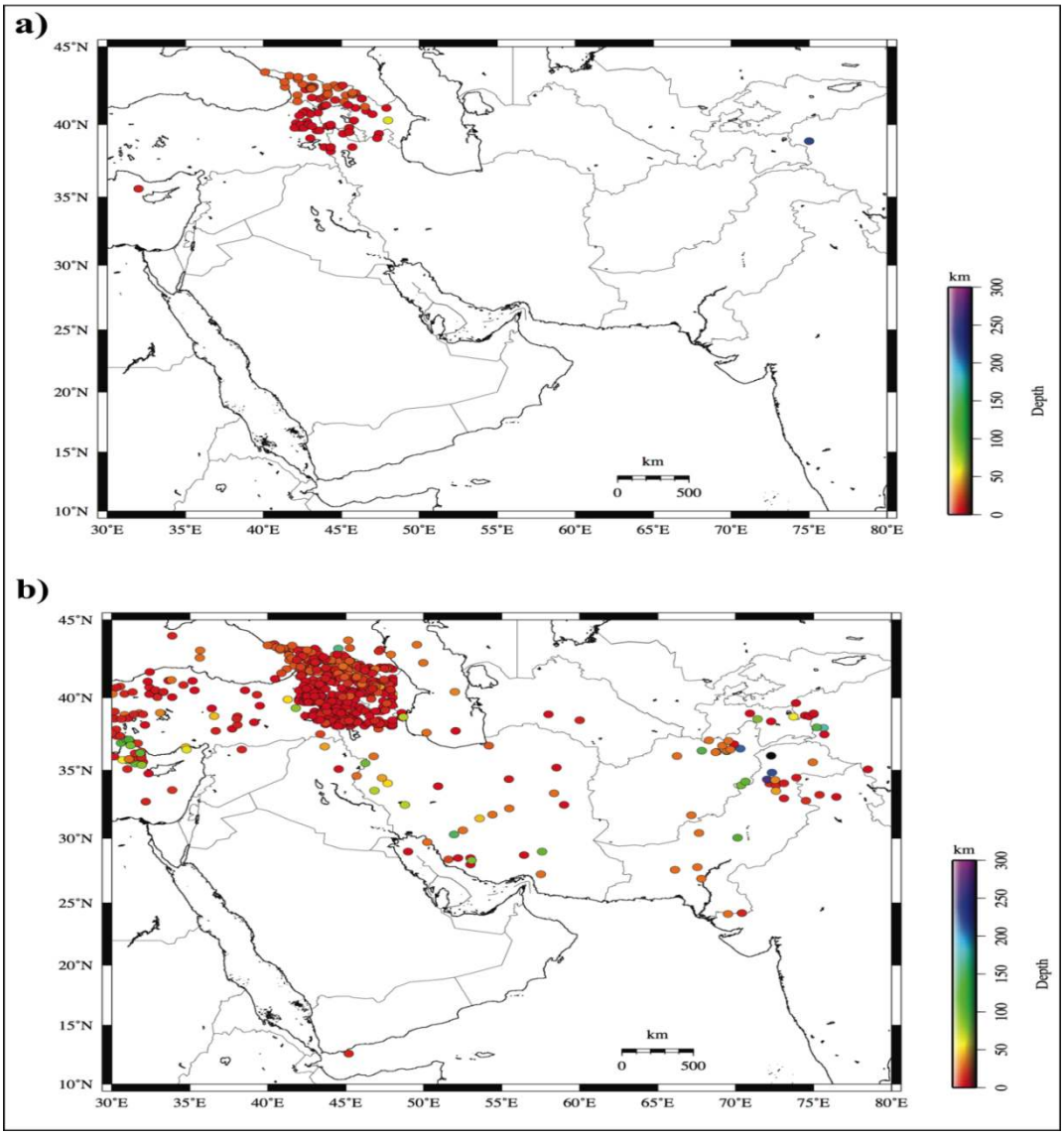

Fig. 2-9. *a) All earthquakes with magnitudes 4.0 and 4.1 for a time period between 1900 and 1970. b) Events with 4.0 < Mw≤4.3 for a time period of 1900 to 1990. All events are color-coded based on their depth.*

Table 2-14. *Cutoff values based on magnitude signature plots and minimum magnitude of completeness estimated using maximum curvature (MAXC), 90% goodness of fit (GFT), and entire magnitude range (EMR) methods".*

Time Period (Year)	Minimum Cutoff (Mw)	Conservative Cutoff (Mw)	Mc (MAXC)	Mc (GFT)	Mc (EMR)
1900-1927	6.5	6.5	5.4	5.2	5.5
1927-1963	6.5	6.5	4.8	5.1	4.9
1963-1973	5.5	5.5	4.8	4.8	4.9
1973-1995	4.7	4.9	4.9	4.8	4.9
1995-2001	4.6	4.6	4.3	4.2	4.6
2001-2006	4.3	4.9	4.2	4.2	4.5

2-5.4. Reply to "Comment on 'Recent developments of the Middle East catalog'"

* ***Source Article:*** ***Zaré M****., Amini H., Yazdi P, Sesetyan K, Demircioglu M.B., Kalafat D., Erdik M., Giardini D., Asif Khan M. and Tsereteli N., (2016), Reply to "comment on 'recent developments of the Middle East catalog'", Journal of Seismology, pp 1–3, doi:10.1007/s10950-016-9626-0.*

We hereby reply to the comments of S. Mostafa Mousavi (2016) (hereafter Mousavi, 2016) on our paper published in *Journal of Seismology* (2014) 18:749–772 (hereafter Zare et al., 2014). We thank the reader for the time spent and attention given to the paper, however, we think that he has carried out a new individual and independent study which can be interesting, but it seems not to be relevant to our work and it might be reviewed and qualified in a separate review process. In this regard, two major ambiguity of his work can be noted:

1) It seems that our paper's (Zare et al., 2014) purpose has been considerably misunderstood by Mousavi (2016). He discusses that the magnitude of completeness (Mc) is not temporally and spatially homogeneous throughout the EMME catalog and he focuses on exploring any artifactual changes associated with significant seismicity rate changes and minimum magnitude of homogeneity (mminh) of the dataset in order to determine homogeneous parts of the catalog. As we clearly mentioned in the introduction and in the conclusion, the main objective of our paper was to provide a reliable and most complete collection of available information of seismicity as a uniform catalog of earthquakes in the Middle East region. This dataset consists of the all existing historical, early and modern instrumental events with moment magnitude (M_w) equal to or greater than 4.0 over a wide range of time (1250 B.C to 2006). In this respect, we tried to perform a preliminary refinement and organize the raw metadata. We then put the records of this geographical area (the Middle East) together within a homogeneous catalog in which different magnitude scales were unified to the M_w scale by defining new regional conversion equations. Obviously, this does not mean that the whole data have a same accuracy or to what extent there are rate changes in the spatial-temporal distributions throughout a regional scale. We also tried to provide some extra information like the number of events, range of magnitudes, range of Mc and the range of seismicity depth based on this unified catalog in order to have a general overview about these parameters. The EMME catalog as a comprehensive databank allows users to analyze different seismicity parameters such as the spatial-temporal changes of seismicity rates, variation

of Mc and so on, based on their intended application. Therefore, Mousavi's (2016) analysis about the spatial-temporal heterogeneity of Mc throughout the EMME catalog is not consistent with our intention.

2) In the last part of the Mousavi's (2016) commentary, he calculates the minimum magnitude of homogeneity (mminh) and the parameter Mc with regard to the time periods of artifactual changes in the seismicity. Although this part is not relevant to our work and we do not wish to referee the claims proposed by Mousavi (2016), we may draw attention to the fact that the relation between the parameters mminh and Mc is not clear. More importantly, his final results about the Mc estimation for the six time periods (presented in the Table 2-14 of Mousavi, 2016), are generally in a good agreement with the average values of Mc during the same time periods in the Figure 12-b of Zare et al. (2014). Accordingly, the advantage of investigating the homogeneity of the catalog is not obvious at this level of study.

We hereby highlight some points that seem to be important. We appreciate Mousavi (2016) for his attention to some mistakes made in the Figure 12-a and the Table 8 of Zare et al. (2014). In the Figure 12-a of Zare et al., (2014), the map of Mc for the Middle East region has been prepared for the modern instrumental period as it has been written above of the figure in red, while the time period has been mentioned as "1250 B.C to 2006" in the caption and we hereby correct the caption of the figure to the "1964 to 2006". For this reason, the values on the map (Figure 12-a) do not correspond to the values in the Table 7 of Zare et al. (2014). In the Table 8 of Zare et al. (2014), the header of the second column should be changed from $M_w \leq 4.0$ to $M_w = 4.0$, since it is the minimum magnitude available in the EMME catalog. In addition, the beginning year of complete reporting of earthquakes should be corrected to 1900 for the Alborz-Azerbaijan zone in the magnitude range of $4.0 < M_w \leq 4.5$. For the Makran zone, the value is corrected to 1975 and 1970 for the magnitude of $M_w = 4.0$ and $4.0 < M_w \leq 4.5$, respectively.

As we mentioned in the section 3-3 (of Zare et al., 2014), for the Middle East region and each subregion (defined in that article), Mc was calculated using two main methods. The first one was the traditional and common method of the cumulative frequency–magnitude distribution of Gutenberg and Richter (1944) and Richter (1958). The second method was the frequency magnitude distribution using the software ZMAP (Wiemer, 2001) in which the Mc was calculated based on the Maximum Curvature (MAXC) technique (Wiemer and Wyss, 2000).

We add that the sensitive Mc estimations are crucial for the short-term earthquake forecasting like in the study indicated by the reviewer (Mignan et al. 2013), where the entire catalog of rather short durations (e.g. post 1970) is used above the Mc for earthquake forecast, and in these cases the temporal and spatial fluctuations in Mc should be studied. In the kind of work carried out in the EMME project where the final aim was to assess the long term seismic hazard, we use a catalog of several hundreds of years and the completeness periods of different magnitude ranges vary over time and over regions. This is why we propose completeness ranges for different magnitude bins for different regions of the study area. The Mc here only reflects the minimum magnitude below which the catalog is completely unusable. Correct estimation of Mc is surely important here as well because optimistic estimations (low Mc), even if associated with a short (recent) period of completeness may result in decreasing the estimated b values.

Finally, according to Mousavi's (2016) statements, some of the provided figures and explanations by Zare et al., (2014) (e.g. Figure 12-a) do not reflect the temporal variation of the Mc; In response to this comments, we strongly emphasize that it was not the aim of our study. In addition, it seems that some mistakes have been made in the selection of proper time windows as well as magnitude ranges in the Figure 2-14 (by Mousavi, 2016), so that attention to the differences in the beginning year of complete reporting of earthquakes for each section and thus, the data selection corresponding to equal overlapping time-intervals of complete reporting as well as considering the inherent differences in seismicity rates and characteristics of the Middle East's sub-regions were neglected in his comparisons.

We acknowledge the reader's attention, but for all the above reasons, we feel that the results of our paper are not affected in any way by the comments.

2-6. Conclusion

According to Ambraseys et al. 2002, the historical record confirms that some regions of the Middle East that are active today (e.g., the North Anatolian fault zone) were also active 2,500 years ago, demonstrating the long-term nature of their seismicity. It also shows that some regions that are, at present, quiescent (such as the Jordan Rift Valley), are capable of generating relatively large earthquakes. For some of these events, this is consistent with their known active tectonic environment.

It should be also noticed that in the historical period, many moderate and almost all of the small events were missed out. In addition, although after installation of the World Wide Seismic Standard Network (WWSSN) seismograms in the Middle East and around the world and by improving the seismograms in this time, we have fairly good information for earthquake events now, but it is still necessary to develop seismic networks by large number of seismographs with more accuracy, in order to have a better monitoring of earthquakes as well as a good evaluation of seismicity parameters. Since the assessment of seismicity of each region may be strongly inferred from the recorded events as database, more works must to be done to complete the data and enhance the qualities of catalogs and to improve our knowledge of earthquakes in the study region as well as to reduce uncertainties associated to seismicity catalogs as the input data of seismic hazard analysis.

Main articles of this chapter:

Zaré M., Amini H., Yazdi P., Sesetyan K., Demircioglu M.B., Kalafat D., Erdik M., Giardini D., Asif Khan M. and Tsereteli N., (2014), "Recent developments of the Middle East catalog", *Journal of Seismology*, Vol 18., pp.749–772, DOI: 10.1007/s10950-014-9444-1.

Karimiparidari S., **Zaré M**., Memarian H. and Kijko A., (2013), "Iranian earthquakes, a uniform catalog with moment magnitudes", *Journal of Seismology*, Vol.17, pp.897–911. DOI:10.1007/s10950-013-9360-9.

Shahvar M.P, **Zaré M**., and Castellaro S., (2013), "A Unified Seismic Catalog for the Iranian Plateau (1900–2011)", *Seismological Research Letters*, Vol.84, No.2, pp. 233-249, doi: 10.1785/0220120144.

Zaré M., Karimiparidari S., Memarian H., Kamranzad F., (2016), "Poisson distribution of the Iranian declustered earthquake catalog", Arab J Geosci (2016) 9:737, DOI 10.1007/s12517-016-2765-3.

Amini H., **Zaré M**. and Gasperini P., (2016), "Catalogue of the earthquakes with maximum intensities (Imax) in Iran", *Submitted*.

Zaré M. and Memarian H., (2002), "The Iranian earthquake intensity database: 1975-2000", *9th International Congress of the International Association of Engineering Geology and the Environment*, pp.2894-2903.

Mirzaei N., Shabani E., and Mousavi Bafrouei S.H., (2014), "Comment on "A Unified Seismic Catalog for the Iranian Plateau (1900–2011)" by Mohammad P. Shahvar, Mehdi Zare, and Silvia Castellaro", Seismological Research Letters Volume 85, pp. 179-183.

Shahvar M.P., **Zaré M**., and Castellaro S., (2014), "Reply to "Comment on 'A Unified Seismic Catalog for the Iranian Plateau (1900–2011)' by Mohammad P. Shahvar, Mehdi Zaré, and Silvia Castellaro" by Noorbakhsh Mirzaei, Elham Shabani, and Seyed Hasan Mousavi Bafrouei", Seismological Research Letters Volume 85, pp. 184-185. doi: 10.1785/0220130144

Mousavi, S.M, (2016), Comment on "Recent developments of the Middle East catalog" by Zare et al., Journal of Seismology.

Zaré M., Amini H., Yazdi P, Sesetyan K, Demircioglu M.B., Kalafat D., Erdik M., Giardini D., Asif Khan M. and Tsereteli N., (2016), Reply to "comment on 'recent developments of the Middle East catalog'", Journal of Seismology, pp 1–3, doi:10.1007/s10950-016-9626-0

Chapter 3: Strong Ground Motion

3-1. Introduction

In this chapter, I first introduce the worldwide, regional and national strong motion networks in brief. Then, I will describe the researches on the strong motion databases and catalogs of Iran or other regions in the Middle East, which I was involved in. Then, I will describe the strong motion processing related to three selected earthquakes and databases (2002 Bam, Iran and 2015 Gorkha, Nepal). In the last part, some extra studies on strong motion analysis are summarized.

3-2. Accelerometric Databases

There are global, regional and local strong motion networks which attend to record the real-time strong motion data. In the following, the most important global, regional and local strong motion networks and databases from which the waveform of earthquakes is available are briefly discussed.

3-2.1. Center for Engineering Strong-Motion Data (CESMD)

According to the published paper by Haddadi et al. (2012), *"the CESMD is a cooperative effort between the California Geological Survey and the USGS. The CESMD website allows users to view and download records from recent or archived historical earthquakes, or to search for and download records selected based on various parametric values. Currently there are two domains in which to search for data: U.S. Structural and Ground Response and Worldwide Ground Response at Virtual Data Center (VDC; sponsored by COSMOS). The main differences between the holdings accessible through these two alternatives are that, for the VDC, the magnitude range is limited to greater than ~M5, and the most recent earthquakes at VDC are from August, 2007"*.

3-2.2. PEER

As it is described in the Pacific Earthquake Engineering Research Center (PEER) website (http://ngawest2.berkeley.edu/), *"the web-based Pacific Earthquake Engineering Research Center (PEER) ground motion database provides tools for searching, selecting and downloading ground motion data. All downloaded records are unscaled and as-recorded (unrotated). Due to copyright issues, a strict limit has been imposed on the number of records*

that can be downloaded within a unique time window. The current limit is set at approximately 200 records every two weeks, 400 every month. Abusive downloads will result in further restrictions. The database and web site are periodically updated and expanded".

In 2003, the Pacific Earthquake Engineering Research Center (PEER) initiated a large research program to develop next generation ground motion prediction equations (GMPEs or "attenuation relationships") for shallow crustal earthquakes in active tectonic regions (now called NGAWest1). The project concluded in 2008 and provided several important products, including a strong-motion database of recorded ground motions and a set of peer-reviewed GMPEs (Power et al. 2008). Many researchers, practitioners, and organizations throughout the world are now using the NGA-West1 models and the NGA-West1 database for research and engineering applications.

3-2.3. Databases of Euro-Mediterranean region

The first coordinated collection of pan-European strong-motion data was established within the framework of the European Strong- Motion Database (ESD), supported by the European Commission during the 5th Framework Program (1998–2002). The latest database version (Ambraseys, Douglas, et al., 2004; Ambraseys, Smit, et al., 2004) contains about 2000 strong-motion records in the time span 1973–2008.

The summary of the evolution of teh strong-motion data archiving in Europe since 1998.is shown in Fig. 3-1. *The ESM database is the recent effort which is complementary to the Rapid Response Strong-Motion Database, also developed in the framework of Project NERA (see Cauzzi et al., 2016). RRSM allows rapid access to earthquake information, peak-ground-motion parameters, and response spectral amplitudes within minutes after an earthquake with magnitude ≥3.5. Data are exclusively obtained from EIDA and are automatically processed and published on the Web without manual checks. The complete data collection dates back to 2005"* (Luzi et al., 2016). Fig. 3-1

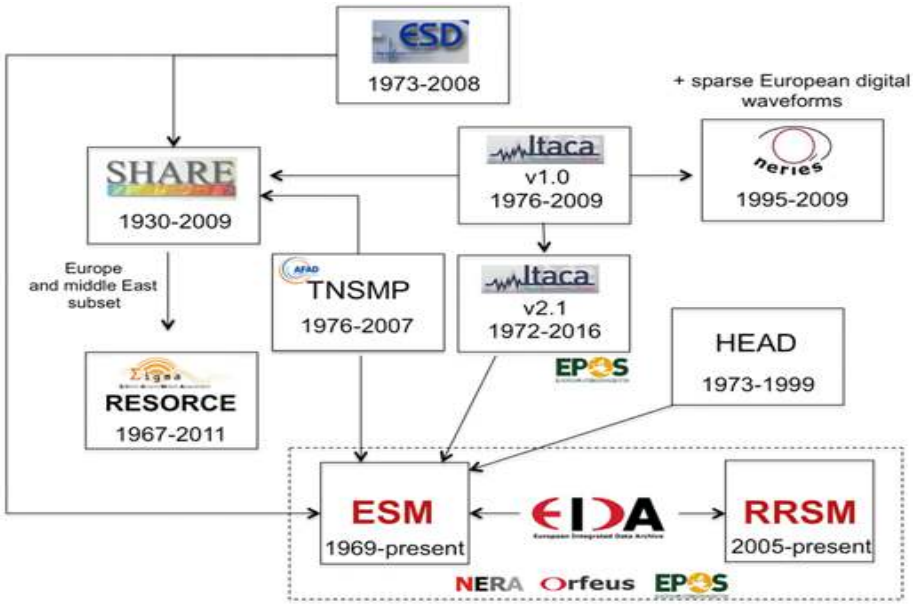

Fig. 3-1. Strong-motion data collection in Europe and strong-motion data flows (time intervals are relative to the dataset).

3-2.4. Iran strong motion network (ISMN)

Iran strong motion network (ISMN) was established by the Road, Housing & Urban Development Research Center (under Ministry of Road & Urban Development) in 1973. Until 1992, 276 SMA-1 analog accelerographs were installed throughout the country. After the devastating 1990 Manjil earthquake, this network was developed using digital SSA-2 and CMG-5TD instruments. First installation of the digital accelerographs was done in the village of Sefidabeh after the earthquake of February 22, 1992. Between 1992 and 1998, more than 1,100 units of SSA-2 digital accelerographs were added. Until November 2016, the ISMN databank includes approximately 11,000 three-component accelerograms recorded at more than 1,140 digital active stations (http://ismn.bhrc.ac.ir/) (Fig. 3-2). Most of these stations are concentrated in seismically active or in densely populated and industrialized areas, providing significant data for scholars to conduct a wide range of studies about earthquakes in Iran. Among the records of ISMN, there are some of the most important and distinct accelerograms in the world. For example, an uncorrected peak ground acceleration (PGA) over 1g is related to 20 June 1994 Zanjiran earthquake (mb= 6.1) recorded at Zanjiran station. The accelerogram of 16 September 1978 Tabas earthquake (M_w=7.4) is considered as the most important record of Iran, since it shows PGA=0.9g recorded in 3 km distance from the fault, along with near-fault effect and a long 50-seconds strong motion duration. Another

important record belongs to the 26 December 2003 Bam earthquake (Mw=6.5) with a vertical PGA of about 989 cm/s2. This recorded PGA on vertical component with near-fault effects has made this accelerogram as one of the most specific records of the country. Other distinct records consists of June 20, 1990, Manjil earthquake (M_w=7.3) as well as the August 11, 2012, Varzeghan earthquake (Mw=6.5), which was recorded by 40 instruments, having a PGA=0.54g.

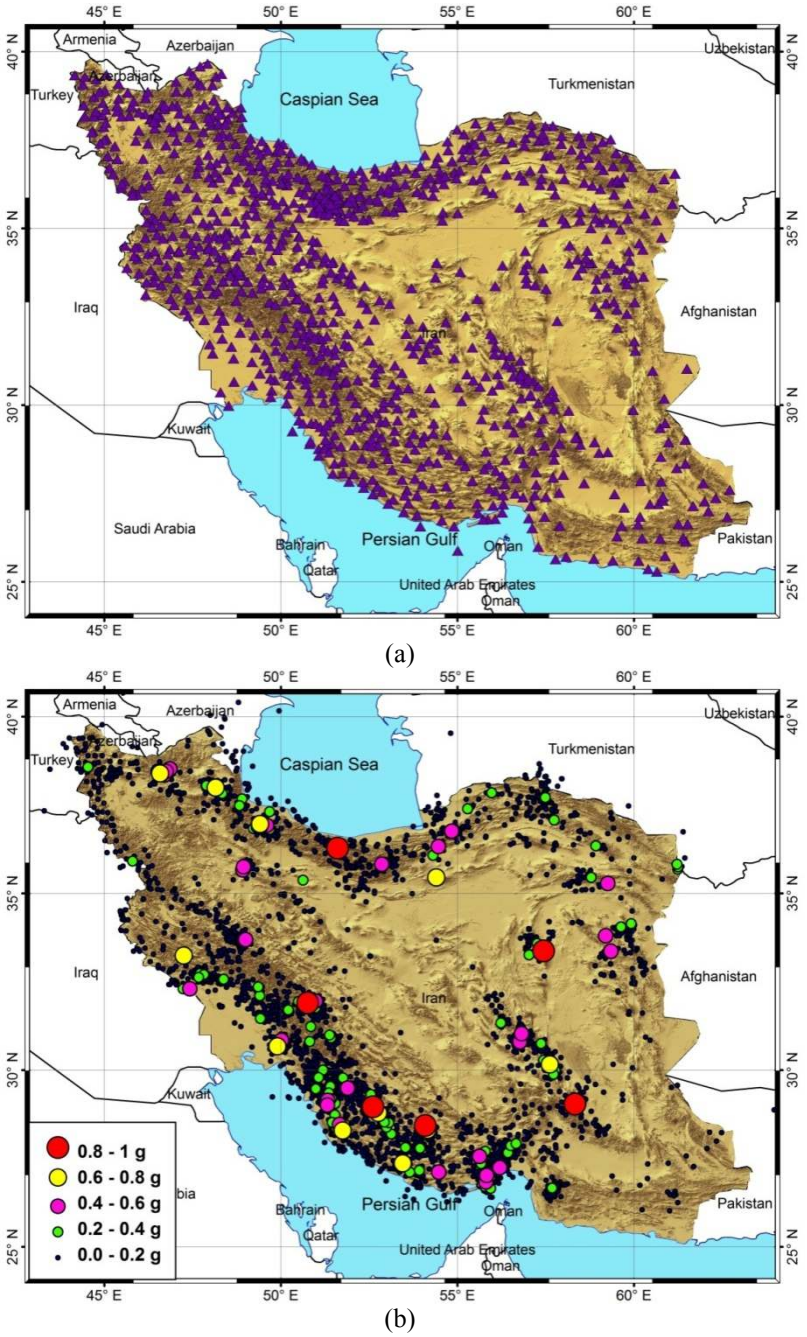

(a)

(b)

Fig. 3-2. Map of (a): 1,140 active strong motion stations and (b): 11,000 accelerograms (recorded during 1973 to October 2016) of the ISMN.

3-3. Strong Motion Catalogs

In this part, I describe the goals and procedures of preparing four strong motion catalogs for the pan-European region, Turkey and Iran.

3-3.1. Engineering strong-motion database: a platform to access pan-European accelerometric data

** **Source Article:** H Luzi L, Puglia R, Russo E, D'Amico M, Felicetta C, Pacor F, Lanzano G, Ceken U, Clinton J, Costa G, Duni L, Farzanegan E. Guéguen P, Ionescu C, Kalogeras I, Özener H, Pesaresi D, Sleeman R, Strollo A. and **Zaré M**, (2016), "The engineering strong-motion database: A platform to access pan-European accelerometric data", Seismological Research Letters, 87(4): 987-997. doi: 10.1785/0220150278.*

In the following section, I present the recent study on the pan-European strong-motion database, an analysis taken from the published article by Luzi et al. (2016). ESM is a database developed to provide end users only with quality-checked, uniformly processed strong-motion data and relevant parameters of the Euro-Mediterranean records since 1969. Several information such as earthquake and station information as well as 23,000 three-component raw and processed waveforms of events with magnitude ≥ 4.0 is accessible through the ESM website (http://esm.mi.ingv.it/). In addition, online processing tools are also available for users (e.g. Fig. 3-3). About 60%, 15% and 25% of waveforms are manually processed, automatically processed or judged of bad quality, respectively. The manual processing of acceleration time series is performed based on the general procedure described in Paolucci et al. (2011).

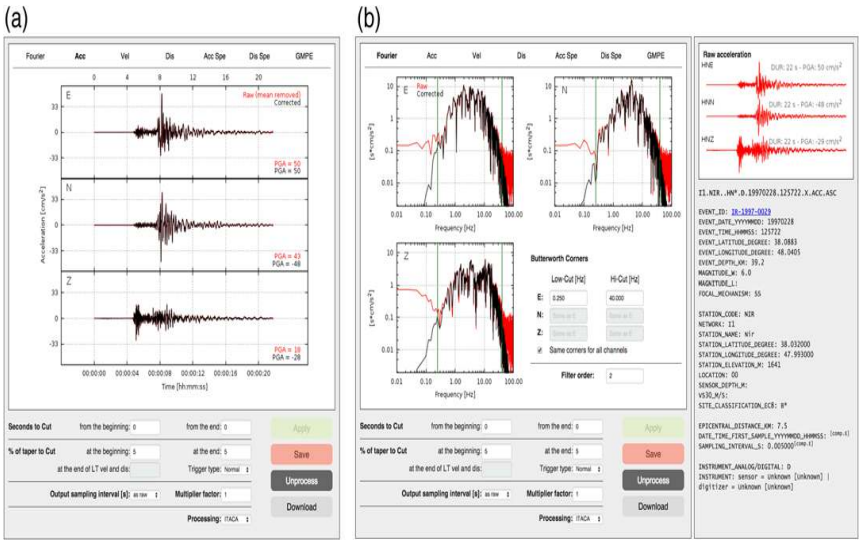

Fig. 3-3. Three components of the ground motion recorded at NIR (Iran) on 28 February 1997 at 12:57:22 GMT (M_w6.0): (a) superimposed unprocessed and processed acceleration time series; (b) Fourier spectra of unprocessed and processed acceleration time series.

3-3.2. Strong motion data processing of the Iranian earthquakes (2004-2014)

** **Source Article:** **Zaré M.**, Kamranzad F. and Farzanegan E., (2017), "Processing and Preliminary Analysis Iranian Strong Motion Database: 2004-2014; A", 16 world conference on earthquake engineering (WCEE), Santiago, Chile, 9-13 January 2017.*

Since 2004 till the end of 2014, more than 6,000 three-component accelerograms were recorded in the ISMN. In this study, 140 accelerograms corresponding to nine important earthquakes ($5.5<M_w$) (Table 3-1) in the time span of 2004-2014 were processed and analyzed. In this study, accelerograms having magnitude $M_w>6$ with epicentral distance less than 20 km, were processed as well.

Table. 3-1. List of selected earthquakes and the related accelerograms (2004-2014)

No	Date	Mw	Macroseismic epicenter	No. selected accelerograms
1	05/28/2004	6.4	Firouz abad- Kojour	22
2	02/22/2005	6.5	Dahuiyeh Zarand	8
3	03/31/2006	5.9	Darb Astane Silakhor	14
4	06/18/2007	5.7	Kahak Qom	18
5	08/11/2012	6.2	Ahar- Varzeghan	47
6	04/09/2013	6	Shonbe Bushehr	10
7	04/16/2013	7.8	Saravan, Sistan	4
8	05/11/2013	6.2	Goharan-Bashagerd	3
9	08/18/2014	6	Mormori	14
			Total =	**140**

All the individual acceleration time series were processed manually following the "general procedure described in Paolucci et al. (2011). According to the procedure, baseline correction was first applied. Then, waveforms were filtered and processed, and acceleration, velocity, and displacement time series were released, together with the values of PGA, PGV and PGD. The frequency contents of the most records showed dominant amplitudes between frequencies 0.2 and 10 Hz. Subsequently, the significant duration of these strong motion records was also calculated based on 5-95% of the Arias intensity method (Trifunac and Brady, 1975).

Site types of accelerograph stations were also classified according to the frequency band of the fundamental frequency. The fundamental frequency of each site can be evaluated using horizontal to vertical (H/V) Fourier amplitude spectral ratio, so that for each site, the highest

clear peak of the smoothed H/V curve is used to recognize the fundamental frequency. By application of this method and according to the site classification proposed by Zare et al, (1999) for Iran (Table 3-2), the site type of each accelerograph station was evaluated. It should be noted that the site type of some stations of ISMN has been also recognized by geotechnical surveys or based on shear wave velocity in the top 30m depth of soil profiles. These values were compared to the H/V results in order to increase the accuracy of site type determinations. According to this procedure, the numbers of the selected records were 3, 37, 67 and 33 for the site classes 1, 2, 3 and 4, respectively.

Table. 3-2. Proposed classification of site effects for Iran (Zare et al., 1999).

Site Class	V_{S30} (m/s)	Fundamental Frequencies
I (Rock)	700<	F≥15 Hz
II (Hard Alluvium)	500-700	5≤F<15 Hz
III (Soft Alluvium, Sand)	300-500	2≤F<5 Hz
IV (Soft Soil, Clay)	<300	F<2Hz

The final catalog consists of the calculated ground-motion parameters, such as PGA, PGV, PGD, duration and site classes for the 140 selected accelerograms belonging to nine earthquakes recorded in 2004-2014. This catalog provides a basis for the good quality/recent strong motion records in Iran and can be used for further studies such as development of new attenuation relations.

In addition, 8 three-component records belonging to earthquakes with a magnitude of Mw>6 and the epicentral distance less than 20 km, were also processed. Results of these near-field accelerograms are shown in Table 3-3.

Table. 3-3. Results of data processing for 8 selected near-field accelerograms

Earthquake		Station					H1 (N-S)			Vertical			H2 (E-W)			duration	Site Type
Date	Mw	Name	X	Y	Record No.	Epi. Dist.	HP	LP	PGA	HP	LP	PGA	HP	LP	PGA		
05/28/2004	6	Poul	51.6	36.4	3330/01	14	0	50	283.9	0	50	247.4	0	50	164.1	14	2
10/07/2004	6	Agh Ghala	54.4	37.2	3556/01	19	0	45	48.79	0	45	82.87	0	45	70.08	27	4
02/22/2005	7	Zarand	56.6	30.8	3671/01	18	0	50	309.6	0	50	314.3	0	50	244	20	3
09/10/2008	6	Tabl	55.8	26.8	4675/01	12	0	25	93.24	0	35	72.51	0	35	89.02	20.5	3
09/10/2008	6	Tomban	55.9	26.8	4686/03	9	0	50	588.6	0	50	305.9	0	50	561.6	6.8	4
08/11/2012	6	Ahar	46.9	38.5	5520/01	18	0	50	200	0	50	98.45	0	50	282.3	13.3	2
08/11/2012	6	Varzaqan	46.9	38.5	5579/01	19	0	50	439.5	0	50	242.2	0	50	356.7	8.4	3
08/11/2012	6	Varzaqan	46.6	38.5	5579/04	11	0	50	535	0	50	219.7	0	50	553.3	8.7	3

3-3.3. Strong motion data of the 1994-2002 earthquakes in Iran: a catalogue of 100 selected records with higher qualities in the low frequencies

** **Source Article:** **Zaré M**., (2004), "Strong Motion Data of the 1994-2002 Earthquakes in Iran: A Catalogue of 100 Selected Records with Higher Qualities in the Low Frequencies", Journal of Seismology and Earthquake Engineering (JSEE), Vol. 6 No. 2, pp.1-17.*

In this section, I present a strong motion catalogue of 100 selected records with higher qualities in the low frequencies of the 1994-2002, an analysis taken from the published article by Zaré (2004). In this study, the recorded strong motion data in Iran since 1994 till the end of 2002 were studied in order to investigate the well recorded (high signal to noise ratio) accelerometric data, especially in the long period ranges. In this regard, first the procedure of data processing and selection of the records is presented, and then the strong motion parameters estimated based on selected records are discussed.

(*Note*: The final catalog is accessible in the paper by Zare (2004). In this catalog, the records are presented based on their code (assigned by the ISMN) station name, site class, band-pass filter selected for each record, PGA (the greatest of three components), the event's date, coordinates, epicentral region, reported magnitude, focal depths, focal mechanisms and the hypocentral distances).

In this study, the significant signal to noise ratio (R_{sn}) was acceptable if it exceeds a given threshold equal to or greater than 3. The signal to noise ratio (R_{sn}) is computed (as estimated by Theodulidis and Bard (1995)) as:

$$R_{sn}(f) = \frac{S(f)/\sqrt{t_s}}{N(f)/\sqrt{t_n}} \qquad (3\text{-}1)$$

A site classification for the territory of Iran has been proposed by Zare et al., 1999 (Table 3-2.). The 100 selected records in this study were assessed on the basis of this classification. Therefore, the number of the selected records were 46, 10, 16 and 28 for the site classes 1, 2, 3 and 4 respectively.

The response spectra for different site classes are distinguished. As it is clear in Fig. 3-4a, b, c and d, the softer the site, the longer the predominant period of response spectra will be. "The predominant periods were calculated as 0.09, 0.1, 0.13 and 0.2 seconds for the site classes 1, 2, 3 and 4, respectively (on the horizontal components). These values were also calculated as 0.08, 0.06, 0.11 and 0.15 seconds for the site classes 1, 2, 3 and 4, respectively (on the vertical components).

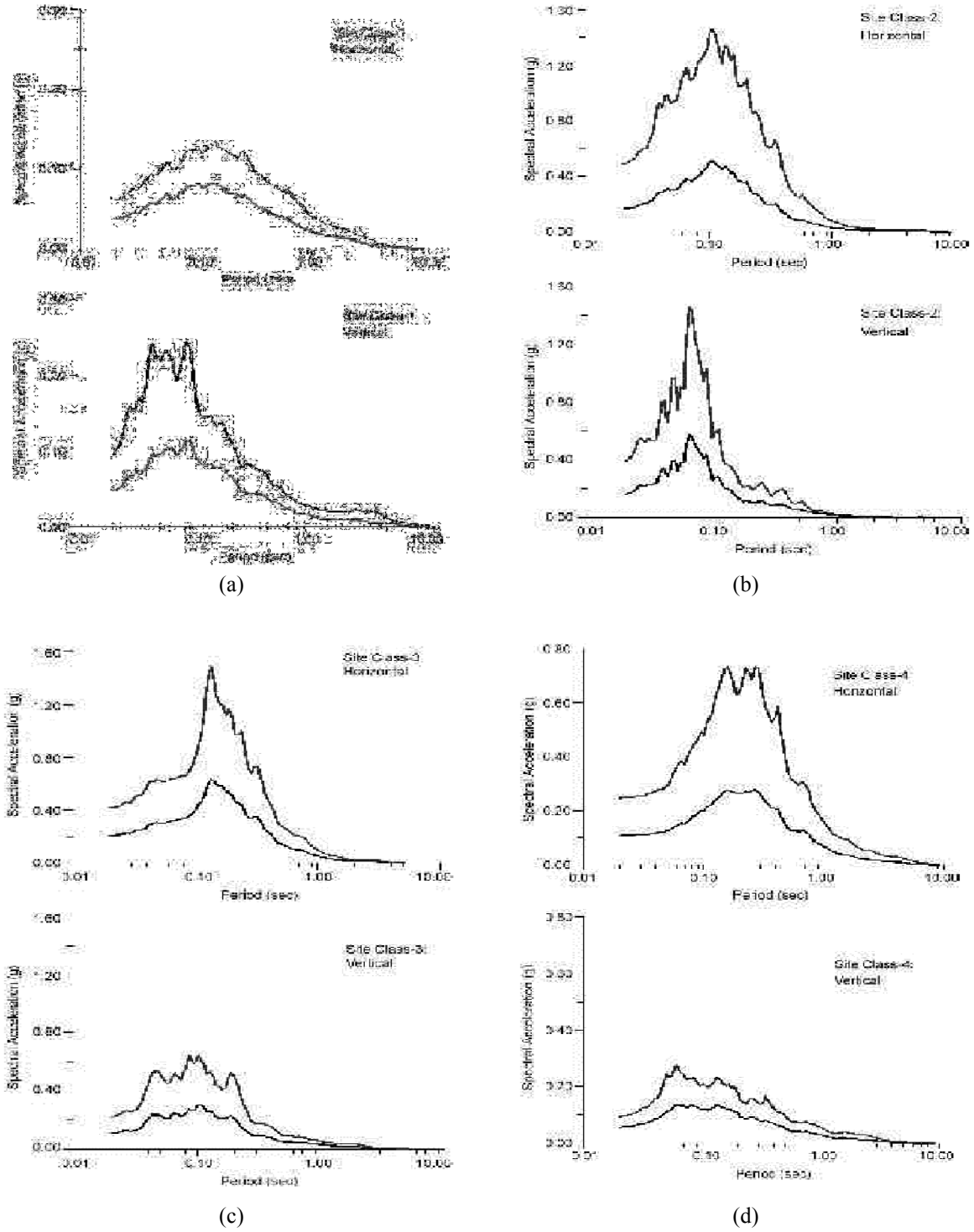

Fig. 3-4. The mean and mean plus sigma response spectra (Horizontal; up, and vertical; down) for: (a)= site class "1"; (b)= site class "2"; (c)= site class "3" and (d)= site class "4".

3-3.4. Strong motion dataset of Turkey: data processing and site classification

** **Source Article:** **Zaré M**., and P.-Y. Bard, (2002), "Strong Motion Dataset of Turkey: Data Processing and Site Classification", Soil Dynamics and Earthquake Engineering, Vol. 22., No.8, Pages 703-718.*

In this section, I present the strong motion processing and site classification of Turkey, an analysis taken from the published article by Zaré and Bard (2002).

Extracting the most reliable records:

Among the records available from June 2000, we selected our database according to the following criteria:

- Knowledge of magnitude and source location (for developing the attenuation laws);
- S/N ratio greater than 3–4;
- PGA greater than 0.05 m/s^2.

Data correction:

The data correction (after baseline correction) is carried out through the following steps:

1) Determination of the appropriate frequency band: A threshold of 3 for S/N ratio was selected to determine the frequency band [f_{HP}, f_{LP}], where the information is meaningful.

2) Spectrum shape: the Fast Fourier Transform (FFT) was calculated. According to the theoretical shape of the far field Fourier spectrum of acceleration, a ω^2 increase is expected in the region below the 'corner frequency' (f_c) and a decaying shape at high frequencies beyond the 'maximum frequency' (f_{max}) with a plateau in between.

3) Filtering and integration: A band pass filter with a Butterworth filter of order 2 was then applied.

Site effects:

In brief, site categories have been shown in Table 3-2. The results of our H/V study for the Turkish strong motion stations are shown in Fig. 3-5 for site classes 1–4.

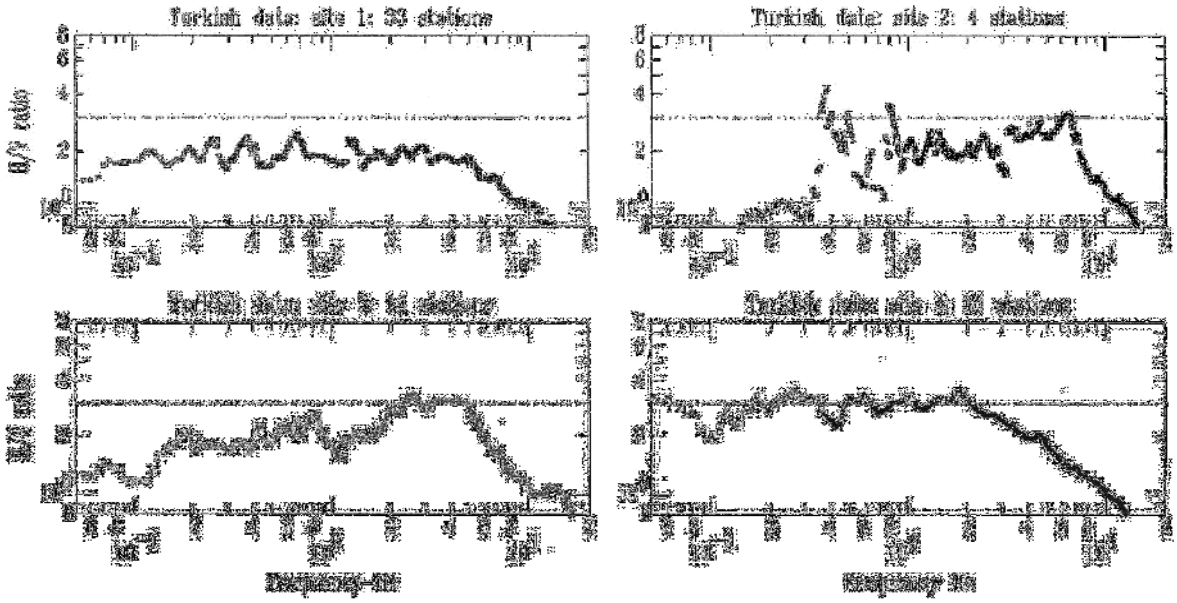

Fig. 3-5. The mean H/V ratio for the 4 site categories, site class 1, 33 stations; site class 2, 4 station; site class 3, 14 stations and site class 4, 30 stations.

Sources of uncertainties:

Some sources of uncertainties during this study may originate from the following

1) The instrumental and macroseismic epicentral distances: The estimated hypocentral distances are compared with the teleseismic hypocentral distances in Fig. 3-6.

2) Focal depths

3) The integration of the filtered records:

4) The earthquake intensities:

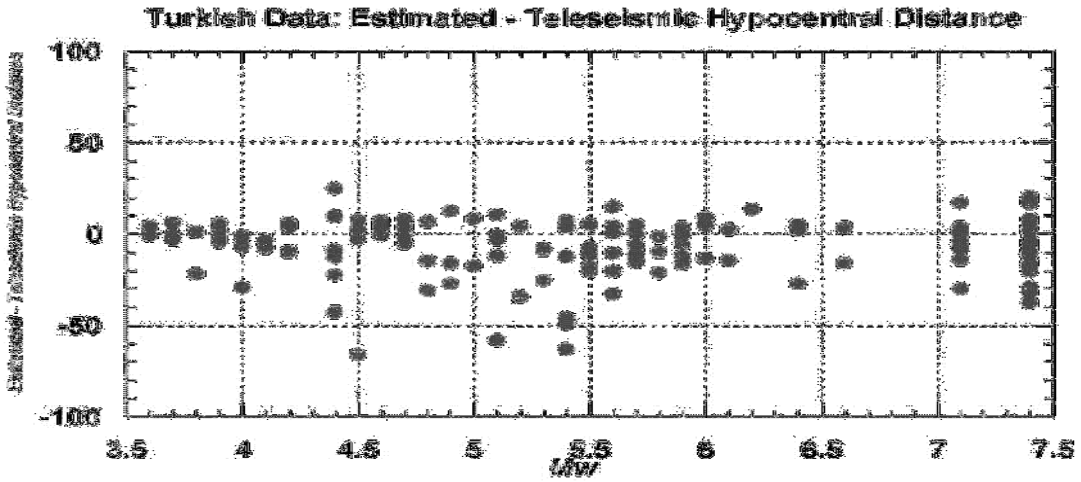

Fig. 3-6. The residual of the estimated and teleseismic (calculated based on the epicentral distance and focal depth) distances against magnitude.

3-4. Strong Motion Processing for Some Selected Earthquakes

In this section, my studies on the strong motion processing of the two important earthquakes occurred in the last decade, including M_w7.8 2015 Gorkha Nepal earthquake as well as the M_w6.5 Bam Iran earthquake, are explained.

3-4.1. April 25, 2015 Gorkha, Nepal earthquake (M_w7.8)

** **Source Article:** **Zaré M**., Kamranzad F., Mona Lisa., and Rajaure, (2016), "A Seismological Overview of the 25 April 2015, Mw7.8 Nepal Earthquake", submitted.*

An intense earthquake -also known as the Gorkha earthquake- with magnitude of M_w7.8 and 15km shallow depth struck the central Nepal on 25 April 2015 (11:46 A.M. in local time). In this study, it was tried to analyze the available strong motion data of the mainshock and eight of its aftershocks recorded at a strong motion station (named KATNP) in Kathmandu. With respect to the geological condition and probable site amplification in the location of the KATNP station, horizontal to vertical spectral ratios are calculated and compared. In addition, considering the low angle of the fault plane (about 10°), it may exist near-source directivity effect in the vertical component of the April 25, 2015 mainshock. Hence, vertical to horizontal spectral ratios are also calculated to obtain the results.

Strong Ground Motion Analysis:

Currently, strong motion records for the 25 April, 2015 M_w7.8 Nepal mainshock and eight of the larger aftershocks are available by the Center for Engineering Strong Motion Data (CESMD) (www.strongmotioncenter.org). These very important accelerograms are the only publicly available data which were recorded at the KATNP station in the center of Kathmandu (27.712N and 85.316E) (Table 3-4). Prior to ground motion data analysis and estimation, it is important to review typical site conditions in Kathmandu, as they affect ground motion intensity significantly (Goda et al., 2015).

1) KATNP Station, Kathmandu Valley Basin and Soil conditions

Kathmandu basin is filled by more than 500m thick lacustrine and fluvial sediments which belong to Pliocene to Pleistocene (Moribayashi and Maruo, 1980; Yoshida and Gautum, 1988; Sakai et al., 2002). Additionally, shear wave velocity up to a depth of 30m (V_{30}) is estimated to be about 180-360 m/s in Kathmandu which belongs to soft deposits (JICA, 2002;

Wald and Allen, 2007). The KATNP station is located about 60 km from the 25 April 2015 earthquake epicenter but only perhaps 15 km from the fault and very near to several historic monument (e.g., Durbar Square) and severely damaged areas of Kathmandu. The ground water might be observed in the western Kathmandu and the KATNP site with 3 to 6 meters depth. This site condition might be effective for the greater damages during the mainshock of the 2015 earthquake in the western Kathmandu and especially along the Bishnumati River.

Table 3-4. List of available strong motion records of the 25 April 2015 earthquake and 8 of its aftershocks at KATNP station in Kathmandu.

Date	M	Time (GMT)	Lat (N)	Long (E)	Epi. Dist to KATNP (km)
25 April 2015	7.8	06:11:46.6	28.15	84.71	77
25 April 2015	6.6	06:45:47.8	28.19	84.87	69
25 April 2015	5.5	06:57:06.9	27.91	85.65	40
25 April 2015	5.3	08:56:26.0	27.64	85.50	20
25 April 2015	5.6	23:16:30.7	27.81	84.87	45
26 April 2015	6.7	07:09:36.2	27.78	86.00	68
26 April 2015	5.3	16:26:34.7	27.76	85.77	45
12 May 2015	7.3	07:05:38.0	27.84	86.08	77
12 May 2015	6.3	07:37:15.1	27.62	86.17	85

2) Site Amplification Frequencies

Considering the geology of Kathmandu basin, seismic waves can be amplified by site effects. Paudyal at al., (2012) studied the local amplification effect of soil layers on ground motion in the Kathmandu Valley using microtremor analysis. They showed that *"the predominant frequencies vary from 0.5 Hz to 8.9 Hz in their study area, whereas the second resonance frequency varies from 4 Hz to 6 Hz in the center and northern part of the Kathmandu valley"* Paudyal at al., (2012). After the occurrence of 2015 Gorkha earthquake, Galetzka et al. (2015) also studied the slip pulse and resonance of Kathmandu basin using Global Positioning System (GPS) measurements. Based on their method, they found that the 2015 earthquake rupture excited the Kathmandu basin and the whole-basin resonance at a period of 4 to 5 seconds caused the collapse of tall structures, including cultural artifacts.

To determine site and source effects based on strong motion analysis method, we first processed the available accelerograms of the April 25, 2015 mainshock and eight of its large aftershocks which were recorded at KATNP station. Then, we calculated the Fourier Amplitude Spectrums (FAS). In this regard, baseline correction, high-pass and low-pass

filtering were applied to the acceleration time histories to reduce probable noises. The processed data are listed in Table 3-5. The study on the amplification functions at the KATNP station became possible by calculating the horizontal to vertical (H/V) ratios based on the 25 April 2015 mainshock and the following eight aftershock data. For each record, FAS of north-south (N) and east-west (E) components and average of them (H_{avg}) were divided to the FAS of vertical (Z) component. Thus, the N/Z, E/Z and H_{avg}/Z spectral ratio curves were obtained (Fig. 3-7). Comparing the spectral ratios of the mainshock and aftershocks indicates that there is a low-frequency (high-period) peak of ground motion in the range of 0.2 to 0.3Hz (period of 3.3-5s) and a second peak of 2 to 3 Hz in the all horizontal to vertical ratios. Our obtained result from the strong motion analysis is in a good agreement with the study by Galetzka et al. (2015) which was carried out based on GPS method.

Table 3-5. Calculated parameters of processed strong motion records at the KATNP station.

Date	M	East-West Component (E)					North-South Component (N)					Vertical Component (Z)				
		Frequency Band (Hz)		PGA (cm/s2)	PGV (cm/s)	PGD (cm)	Frequency Band (Hz)		PGA (cm/s2)	PGV (cm/s)	PGD (cm)	Frequency Band (Hz)		PGA (cm/s2)	PGV (cm/s)	PGD (cm)
		HP	LP				HP	LP				HP	LP			
25/04/2015	7.8	0.03	50	145.7	108.6	135	0.03	50	172.8	101.7	120	0.03	50	188.9	53.7	68.86
25/04/2015	6.6	0.03	50	45.59	10.65	5.71	0.03	50	47.09	13.29	7.60	0.03	50	45.12	4.74	2.58
25/04/2015	5.5	0.04	50	14.77	0.57	0.20	0.07	50	14.16	0.53	0.16	0.08	50	5.20	0.28	0.06
25/04/2015	5.3	0.1	50	61.07	3.19	0.39	0.1	50	36.92	2.18	0.40	0.05	50	72.46	2.31	0.19
25/04/2015	5.6	0.1	50	35.63	1.99	0.25	0.08	50	33.36	2.42	0.21	0.08	50	12.86	0.65	0.12
26/04/2015	6.7	0.03	50	54.18	8.14	3.56	0.04	50	64.95	8.64	4.17	0.1	50	38.20	4.50	1.66
26/04/2015	5.3	0.1	50	6.72	0.83	0.29	0.07	50	4.42	0.51	0.17	0.09	50	3.12	0.33	0.08
12/05/2015	7.3	0.03	50	73.39	12.16	7.60	0.03	50	85.54	13.35	7.9	0.03	50	75.56	9.81	4.82
12/05/2015	6.3	0.06	50	13.67	2.23	1.06	0.07	50	11.26	1.13	0.41	0.03	50	9.23	0.73	0.31

Considering the nodal plane with 295 azimuth and 10° dip to the north, a directivity as the source effect may be expected in the vertical component of the mainshock. Thus, vertical to horizontal ratios containing Z/N and Z/E of the mainshock and the aftershocks were calculated in the log-log curves (Fig. 3-8). For the M_w7.8 mainshock, two peaks in the vertical to horizontal ratios are presented at the frequency around 0.7-0.8 Hz and 1.5-2 Hz (especially in the Z/E spectra), while the peaks are not repeated on the aftershock ratios. The peaks on the V/H spectral ratio can probably be attributed to evidently a mainshock source

effect (near-source rupture directivity effect). Thus, the strong shaking on the vertical component and this amplification (due to source directivity) might be causative for intensifying the slop instabilities, landslides and snow avalanches during the mainshock.

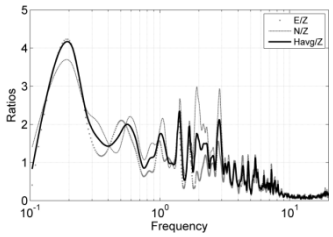

Mainshock M7.8 (25-4-2015)

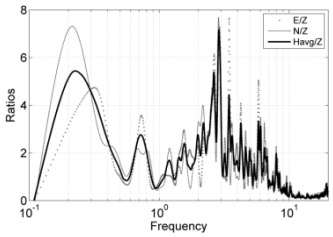

Aftershock M6.6 (25-4-2015)

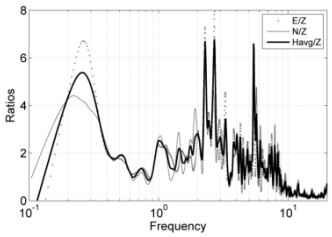

Aftershock M5.5 (25-4-2015)

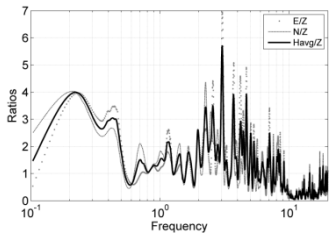

Aftershock M5.3 (25-4-2015)

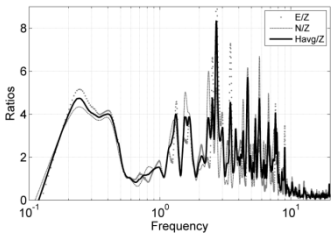

Aftershock M5.6 (25-4-2015)

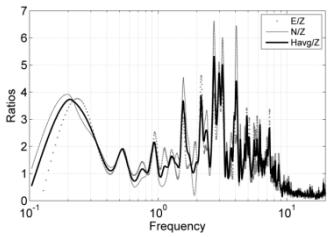

Aftershcok M6.7 (26-4-2015)

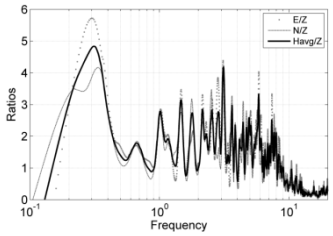

Aftershock M5.3 (26-4-2015)

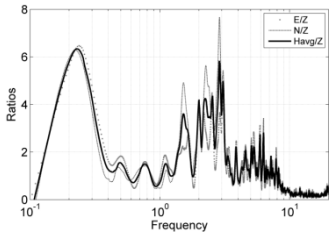

Aftershock M7.3 (2015-5-12)

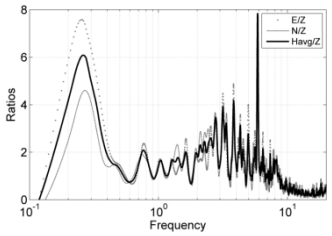

Aftershock M6.3 (12-5-2015)

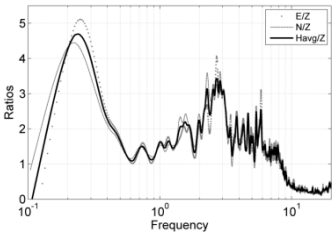

Average of all records

Fig. 3-7. Horizontal to vertical spectra of the 25 April 2015 earthquake, 8 of its aftershocks and an average of all the records (E/Z ratio in gray dotted-line, N/Z ratio in gray dashed-line and H_{avg}/Z in black line).

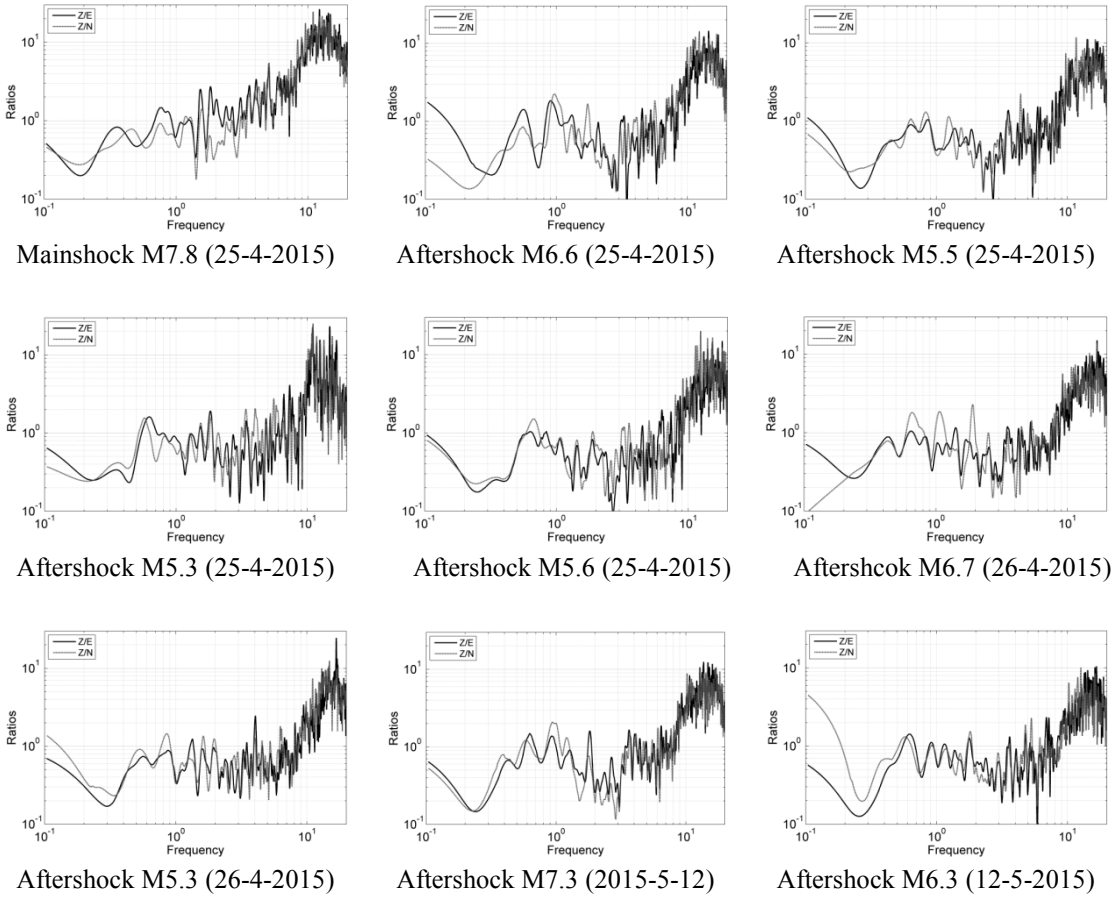

Mainshock M7.8 (25-4-2015) | Aftershock M6.6 (25-4-2015) | Aftershock M5.5 (25-4-2015)

Aftershock M5.3 (25-4-2015) | Aftershock M5.6 (25-4-2015) | Aftershcok M6.7 (26-4-2015)

Aftershock M5.3 (26-4-2015) | Aftershock M7.3 (2015-5-12) | Aftershock M6.3 (12-5-2015)

Fig. 3-8. Vertical to horizontal spectra of the 25 April 2015 mainshock and aftershocks (E/Z ratio in black line and N/Z ratio in gray dashed-line).

3-4.2. December 26, 2002 Bam, Iran earthquake (M_w6.5)

** **Source Article:** **Zaré M**. and H. Hamzehloo, (2005), "Strong Motion study on Bam Earthquake of 26 December 2003", Earthquake Spectra, Special Issue on Bam earthquake.*

The Bam earthquake of 26 December 2003 M_w6.5 occurred at 01:56:56 GMT, 05:26:56 local time near the city of Bam in the southeast of Iran. The strong motions of this event were recorded at 23 stations of the national Iranian Strong Motion Network (ISMN). The strong motion records were studied and processed and these preliminary results are presented based primarily on the mainshock and aftershock records obtained at Bam station. All of the strong motion data obtained during the Bam earthquake were recorded by digital Kinemetrics SSA-2

accelerographs. The attenuation of the strong motion was studied based on the records with good signal-to-noise ratio at six stations.

Strong motion data processing:

The record obtained at Bam station ─after band-pass filtering between 0.11 and 40Hz─ shows a PGA of 775 and 623 cm/s^2 for the east-west and north-south horizontal components, respectively, and 992 cm/s^2 for the vertical component. This processing was performed based on the estimation of the signal-to-noise ratio. The FFT showed more energy at longer periods for the fault-normal horizontal component.

A comparison of the H/V ratio obtained at Bam station during the mainshock and 13 aftershocks, which occurred in the first 24 hours after the earthquake (Fig. 3-9) shows very low-frequency amplification between 0.1 and 0.2 Hz, which is evident in the main shock, but not evident in the aftershocks. This may be taken as evidence for the vertical directivity effect (Lay and Wallace, 1995). This vertical directivity might be explained in the Bam earthquake by rupture propagation from depth to the surface, with an inclination towards the north. A strong fault-normal east-west motion was created during the mainshock as well. The demolished walls and buildings of Bam are representative of such effects in the up-down vertical and east-west directions fault-normal. The Bam residents that survived the earthquake told reconnaissance team members that they felt strong up-down displacements during the mainshock. The site class, however, may be taken for Class 3 since the site fundamental frequency was about 2 to5 Hz (equal to a site condition having the average V_{30} of about 300 to 500 m /s, Zare et al. 1999).

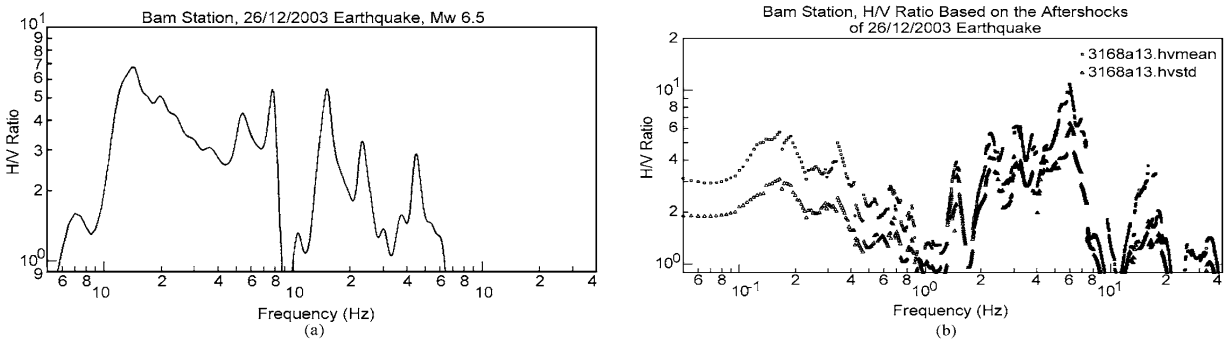

Fig. 3-9. H/V ratio for (a) the main shock, and (b) aftershocks recorded at Bam strong motion station.

The velocity and displacement time histories of the Bam record obtained based on single and double integration of the Bam accelerogram are shown in (Fig. 3-10). The time histories show a great pulse, especially in the fault-normal component E-W direction.

The spectral accelerations for 5% damping are shown in Fig. 3-11 for the three-component acceleration recorded at Bam station. The predominant period is the period corresponding to the highest peak in a response spectrum. The response spectrum in Fig. 3-11 shows predominant periods of 0.1 second for vertical and 0.2 second for 2 horizontal components. Fig. 3-11 also shows higher spectral ordinates for the vertical and for the fault-normal components of motion.

The records obtained at the BHRC stations around the epicenter were also processed and the acceleration time histories obtained at Bam, Abaragh, Mohammadabad-e-Maskun, Jiroft, and Sirch stations were selected for the detailed strong motion studies. These records were filtered according to their corresponding signal-to-noise ratio, and the band-pass filters selected are shown in Table 3-6.

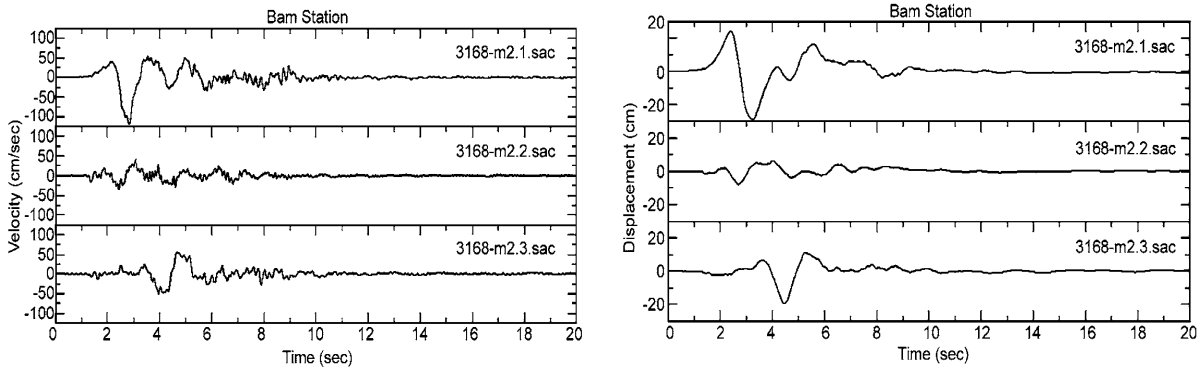

Fig. 3-10. Velocity and displacement time histories based on single and double integration of the accelerogram recorded in Bam.

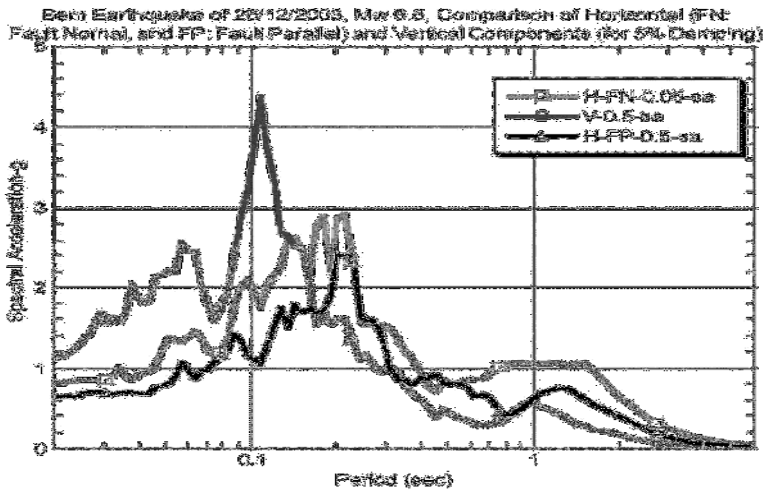

Fig. 3-11. Response spectra for the damping value of 5% are compared for horizontal (fault normal) vertical and horizontal (fault parallel) components.

Table 3-6. Strong motion parameters estimated for the five selected records.

Rec.	Station	Y (N)	X (E)	Site	BP Filter (Hz)	PGA (cm/s^2)			PGV (cm/s)			PGD (cm)			Fc (Hz)	F_{max}-H	F_{max}-V	Hypocentral Distance (Km)
						H1	V	H2	H1	V	H2	H1	V	H2				
3161	Sirch	30.24	57.57	1	0.1-25	30.2	14	29.2	2.4	1	2.3	0.4	0.2	0.3	0.4	8	15	152
3162-1	Mohammadabad	29.97	57.88	4	0.1-40	120	69.2	71	10.4	3.1	3.3	2.1	0.6	0.8	0.4	6	8	48
3168-2	Bam	29.12	58.38	3	0.11-40	992	775	623	92.3	32.3	72.6	26.4	6.3	16	0.3	9	18	12
3170-2	Jiroft	28.68	57.76	4	0.1-25	39.6	30.5	27.3	3.6	1.3	2.1	0.9	0.4	5.1	0.45	3.5	5	76
3176-1	Abaragh	29.38	57.97	1	0.1-40	163	83.2	107.7	8.2	8.1	10.2	2.8	2.6	2.2	0.25	18	25	56

BP= Bandpass; HPGA= Horizontal Peak Ground Acceleration; HPGV= Horizontal Peak Ground Velocity; HPGD= Horizontal Peak Ground Displacement.

SH-wave analysis:

The analyses of teleseismic and strong ground motion data have been used by different investigators to infer and identify the complex rupture process and subevents (Campos et al. 1994; Sarkar et al. 2003). It is expected that the energy releases from these subevents will be identifiable in the near field strong motion data and an attempt can be made to study their properties. For this purpose, a method of Sarkar et al. 2003 has been used to estimate fault plane parameters using strong ground motion data pertaining to SH-wave only. This method is based on a point source representation and non-linear least-square formulation that estimates the strike, dip, and rake of the causative fault and a grid search technique that provides separate estimates of the strike, dip, and rake. The analysis confines to SH-waves because these are minimally affected by crustal heterogeneity (Haskell, 1960). Further, use of SH-waves minimizes the need for corrections for the mode conversion at the free surface and other heterogeneities disregarded in the model used here. The spectral amplitudes at various stations were measured at the longest wavelength (lowest frequency) permitted by the data (Sarkar et al. 2003). This was done in order that the point source approximation could be as appropriate as possible.

The observed spectral amplitudes of the acceleration were picked at a common frequency, *f*, on all stations for a particular event, which lies in the flat portions of the spectra, and were then converted into the corresponding values of the spectral displacements. The values were then corrected for geometrical divergence. The corresponding theoretical estimates of SH-wave amplitudes of displacement were obtained from the formulae for the radiation pattern of SH-waves in a full space (Aki and Richards 1980; Lay and Wallace 1995). The error function E (strike, dip, and rake) is written as:

$$E\ (\text{strike, dip, rake}) = \Sigma_i\ (A_{oi} - A_{ti})^2 \qquad (3\text{-}6)$$

Here A_{oi} and A_{ti} denote the observed and theoretical amplitudes of the near field SH-wave displacement at the selected frequency at the i^{th} station. The summation is over all stations that recorded the particular subevent. The nonlinear Newton technique has been used to simultaneously obtain those values of strike, dip, and rake that minimize E (strike, dip, rake) in the least square sense.

For appropriate selection of SH-wave components of the recorded data the radial (L) and transverse (T) components of recorded acceleration and displacement are suitably rotated so that corresponding estimates along and perpendicular to the azimuth direction are obtained. The rotated transverse components provide acceleration and displacement data of SH-waves, recorded at each station.

In the absence of a common time code, it was not feasible to locate independently the hypocenters of the two subevents on the basis of the accelerogram data. However, a master event technique was employed to estimate the hypocentral location of the sub-event from where the S1 phase of energy possibly radiated. Generally, a value of two-thirds is assumed for the ratio between vertical and horizontal peak accelerations. In re-cent earthquakes, however, it has been observed that in the near field there is often a potential for a significant vertical component of ground shaking. The Bam station recorded vertical peak acceleration of 956cm/s^2, which is larger than for the two horizontal components. It seems that at Bam station, a strong up-down motion occurred which was also reported by the observers.

At the time of an earthquake, damage is maximum in the epicentral region, where the ground experiences intense shaking. Therefore, it is assumed here that the chosen master event, namely the subevent corresponding to the release of the S2 phase was located near 58.35° and 29.09° at depth of 8 km (below the Bam strong motion station). Considering this as location of S2 phases, acceleration time histories from the four stations viz. Bam, Abaragh, Mohammadbad, and Jiroft (Table 3-7) have been used to estimate that the S1 phase of energy was released from 29.02°N, 58.30°E, at a depth of 8 km depth, about 8 second before the release of the S2 phase of energy.

The acceleration spectra were obtained for each of the S1 and S2 phases using relevant time windows on the appropriately rotated transverse component accelerograms. These spectra were obtained using Fast Fourier Transform along with a Hamming-Turkey window so as to reduce the effect of data truncation. Several variations were performed on the

window sizes and placement to confirm the stability of these spectra in terms of their general structure and frequency content. The spectra for S1 and S2 are shown in Figures 14 and 15.

The fault plane solution corresponding to the S1 subevent estimated using spectra at four stations is as follows: strike= 174°N, dip= 85°, rake= 170°. The standard error of estimate is 0.50. This event was surmised to have occurred at 29.02°N, 58.30°E, 10km.

For the causative fault of the S2 subevent, spectral data from four stations have been used to estimate the following parameters: strike= 172°N, dip= 65°, rake= 110°. The standard error of estimate is 0.18. It was estimated earlier that the epicenter of this event was located at 29.09°N, 58.34°E km and occurred about 8 seconds after the event S1.

The total fault plane parameters, considering the SH-wave spectra including both S1 and S2, are as follows: strike= 172°, dip= 72°, rake= 156°. The standard error of estimate is 0.32.

Table 3-7. Salient features of recording stations

Station	Lat.	Long.	Elev.	L/T direction
Abaragh	29.34	57.94	1644	72/ 162
Bam	29.09	58.35	1094	278/ 8
Jiroft	28.67	57.74	275	240/ 330
Mohammadabad	28.90	57.89	1961	350/ 80

Conclusions:

The strong motions records observed in the Bam earthquake are representative of a very strong, but short, earthquake that had large vertical and fault-normal near-fault effects. The following conclusions have emerged from the analysis of strong ground motion data for the Bam earthquake:

- The Bam earthquake was a complex earthquake. The SH-wave accelerograms exhibited distinct phases corresponding to the energy released from two separate events.
- Two strong phases of energy are seen on the accelerograms. The first was interpreted to represent a starting subevent with right-lateral strike slip mechanism and located south of Bam. The event corresponding to the second release of energy was interpreted to be released 8 seconds after the first subevent. The mechanism of the second subevent was a reverse mechanism.

3-5. Analysis of Strong Motion Records

3-5.1. Site effects and classification of Iran accelerographic stations

** **Source Article:** **Zaré M.,** and Sinaiean, F., (2014), "Site Effects and Classification of Iran Accelerographic Stations", Geodynamics Research Inter-national Bulletin, (Special Issue on Intra- Plate Earthquakes), Vol. (I) - No. 02, pp.15-23.*

In this study, about 3,200 reliable three-component accelerograms in 620 stations from 1994 to 2003, were selected as the database. We applied shallow refraction and H/V spectral ratio methods for site classification. The first method determines the mean shear wave velocity called Vs-30 and the second scheme will present the fundamental frequency (FF) of vibration in each specific site. The H/V spectral ratio is computed for all the stations but we managed to carry out the geoseismic measurements just in 64 stations, which were located in Boushehr, Kerman, Qazvin, Mazandaran, Tehran and Zanjan provinces and there were the results of 10 stations studied by Zare et. al., (1999). The number of the recorded accelerograms, the importance of the registered earthquakes, the peak values of acceleration and abnormal recorded ground motions were the main criteria considered in station selecting for shallow refraction investigations and mean Vs-30 measurements. Then, we tried to compare the results of Vs-30 obtained from geoseismic measurements and H/V spectral ratio using the recorded accelerograms to modify the previous criteria for a fast and reliable classification. The final results show the convenience of the newly- defined criteria that could be used with more confidence for the stations with more records.

Results and discussion

The H/V spectral ratio was computed using different windows of earthquake records such as S, Coda and S-Coda waves and the whole signal including P and S wave windows. Considering the limitations of recording the wave arrivals and discrimination of different wave windows, we examined the whole recorded signal (P-S wave windows) in comparison with S and S-Coda windows for H/V computation and found that the results are nearly the same. We tried to find a FF-based reliable criterion for classifying the soil types of 620 accelerographic stations in which a total number of 3200 strong motion accelerograms were recorded from 1994 to 2003. Moreover, 74 stations with computed Vs-30 were investigated to find a correlation between Vs-30 and the estimated FF. Based on the computed Vs-30, the

studied stations are categorized in four groups I, II, III and IV. The classification of NEHRP (2000), Iranian Building Codes (standard 2800) and Zare (1999) are proposed in this study. The mean FF is estimated for all stations using the H/V spectral ratio, but because of the discrepancy in the number of accelerograms, source parameters and path effect, the obtained results do not have the same quality and reliable confirmation.

Fig. 3-12 to 3-14 signify the correlation between the estimated FF and site class for the stations with different number of records. In the first place, all stations for which the shear wave velocity were measured, even if they have just one record, were considered. As it is clear, a single record cannot be representative of site characteristics, and it reflects a combination of site, source and path effects that cannot be separated. Increasing the number of records will minimize the source and path effects by averaging and the consequential is mainly representative of the site effect. We tried to find a correlation between the site class estimated by Vs-30 and FF resulted in H/V spectral ratio. The obtained results from different classifications proposed in NEHRP (2000) and Zare (1999) and standard 2800 (2003), show differences in few stations and another scale will lead to different result. Although this correlation help us to find the boundaries of 2.0 Hz, 2.0 to 5.0 Hz, 5.0 to 8.0 Hz and 8.0Hz., high overlaps of the defined boundaries made us find a direct correlation between the measured Vs-30 and the estimated NF. This idea enabled us to define new criteria for site classification which are presented in Table 3-8.

Fig. 3-15 shows that these defined criteria cover more than 75% of the studied stations, even if there was a single good quality record with the possibility of estimating H/V spectral ratio. These boundaries are considered as site classification criteria which were considered in this research and Fig. 3-16 shows a better separation of site classes by using the new defined criteria.

Table 3-8. New criteria defined for sit e classifications

Site Class	Vs-30 (m/sec)	FF(Hz)
I	$750 \leq$ Vs-30	$8.0 \leq$ NF
II	$500 \leq$ Vs-30 < 750	$5.0 \leq$ FF < 8.0
III	$250 \leq$ Vs-30 < 500	$2.0 \leq$ FF < 5.0
IV	Vs-30 < 250	NF < 2.0

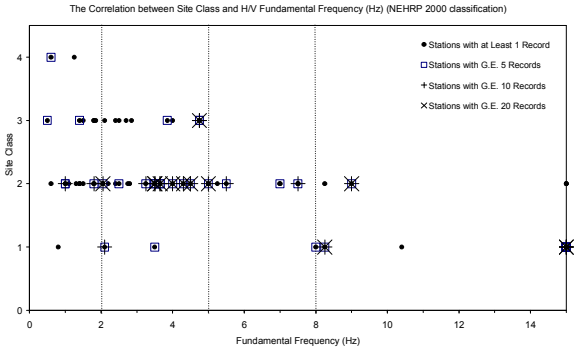

Fig. 3-12. Comparison of site class (NEHRP 2000 criterion) and FF estimated using H/V spectral ratio. The effect of considering the stations with more recorded accelerograms is shown.

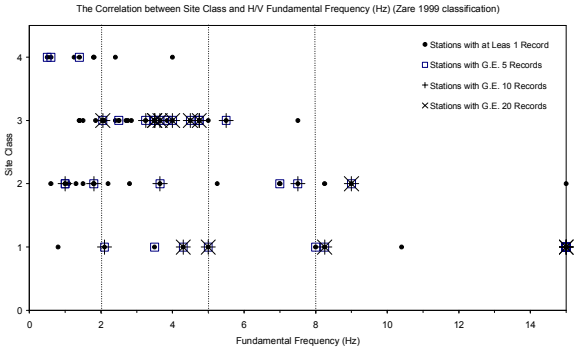

Fig. 3-13. Comparison of site class (Zare 1999 criterion) and FF estimated using H/V spectral ratio. The effect of considering the stations with more recorded accelerograms is shown.

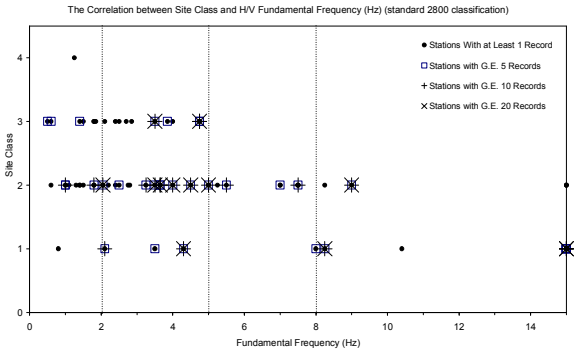

Fig. 3-14. Comparison of site class (standard 2800 criterion) and FF estimated using H/V spectral ratio. The effect of considering the stations with more recorded accelerograms is shown.

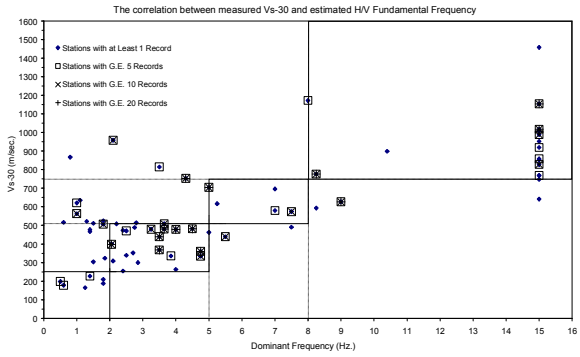

Fig. 3-15. Defining the new limits for Vs-30 and FF boundaries

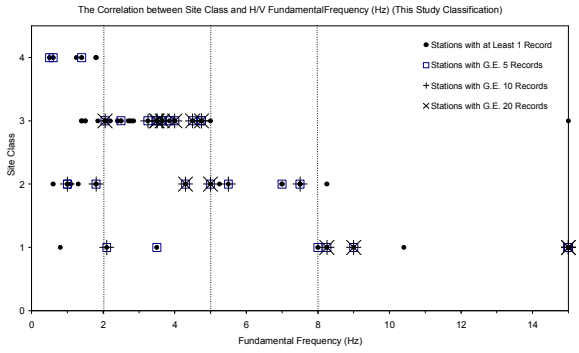

Fig. 3-16. Comparison of site class (this study critera) and FF estimated using H/V spectral ratio. A better separation of classes and lower overlap is seen.

3-5.2. Applying empirical methods in site classification, using response spectral ratio (H/V): A case study on Iranian strong motion network (ISMN)

** **Source Article:** Ghasemi, H., **Zaré M**, Y. Fukushima and F. Sinaiean, (2009), "Applying empirical methods in site classification, using response spectral ratio (H/V): A case study on Iranian strong motion network (ISMN)", Soil Dynamics and Earthquake Engineering, Vol.29, pp.121-132.*

In this section, I present the empirical methods in site classification, using response spectral ratio (H/V): a case study on Iranian strong motion network (ISMN), an analysis taken from the published article by Ghasemi et al. (2009). Here, three different empirical schemes have been considered to classify the ISMN stations.

Method 1:

In Method 1, first the average H/V spectral ratio of records at each station is determined, and then the first (long period) dominant peak is taken as the natural period of the site. To classify strong motion stations, the natural period at each station is compared with site-dependent period ranges recommended by JRA (1980). The overall success rates of the classification scheme for SC-I, SC-II and SC-III are 57, 43 and 42 percentages, respectively. Similar success rates for Method 1 have been obtained by Zhao et al. (2006) as well. However, the classification accuracy, using peak periods, is strongly related to the number of records.

Method 2:

Zhao et al. (2006) proposed an automatic classification based on the probabilistic distribution of spectral shapes. They empirically illustrated that the method is more effective in SC-I, SC-III and SC-IV sites than in SC-II ones for Japan stations. The results of the present study are consistent with those presented by Zhao et al. (2006), i.e. the more success rates are of SC-I and SC-III sites and the least one is of SC-II sites. Higher success rates for SC-II as well as SC-I and SC-III sites are expected, if additional information such as borehole measurements were available for ISMN stations. As an example, Zhao et al. (2006) showed that the success rates for different site classes can be enhanced by considering another classification limit, i.e. ‘‘if the site class assigned to a site according to the S-wave travel time in the top 20 m is higher than that assigned by H/V ratios, the site class determined by the S wave travel time

should be selected.'' By applying this restrain, they observed a considerable improvement in the SC-II sites. The exact classification overall rate of Method 2 is higher than Method 1.

Method 3:

In this study, a site classification index (SI) is designed as

$$SI_k = 1 - 6\sum \frac{d_i^2}{n(n^2-1)} \tag{3-7}$$

where d_i is the difference between each rank of corresponding values of x_k and y, x_k the mean H/V ratio curve for the site class, y the mean H/V ratio curve for the site of interest, and n the total number of periods. In fact, the proposed SI is Spearman's rank correlation coefficient (Press et al., 2011), which is statistically a nonparametric (distribution-free) rank to be proposed as a measure of the association strength between two variables. In this study, it is used to measure the correlation between average HVRS curves for the site of interest and mean HVRS ones for different site classes without making any assumptions about the frequency distribution. The range of Spearman correlation is from -1 to 1. The SI=1 indicates a perfect positive correlation between x and y. As in Method 2, SI is calculated for each site class for a certain site; the site class with the largest value of SI is assigned to this site. The accuracy rates of this scheme are 73%, 43% and 70% for SC-I, SCII and SC-III, respectively.

Application of the proposed classification scheme:

In the present study, for further applicability control of the proposed SI, 347 ISMN strong motion stations, having more than three records at each station, are selected. The strong motion stations are then classified following the third methodology described before. Fig. 3-18d shows the average H/V response spectral ratio for ISMN site classes. The vertical dashed lines represent the limits of period intervals for each site class. The peak periods in spectral ratios are consistent with those recommended by JRA (1980) at 0.13, 0.26 and 0.44 s for SC-I, SC-II and SC-III sites, respectively. The overall shapes and amplitudes of average H/V spectral ratios are remarkably different for different site classes. The mean H/V spectral ratio and 84 percentile curves are plotted in Fig. 3-18a, b and c for SC-I, SC-II and SC-III sites, respectively. The results of each site class are fairly consistent with those obtained by Zhao et al. (2006) and, which confirm the acceptability of classification results of this research.

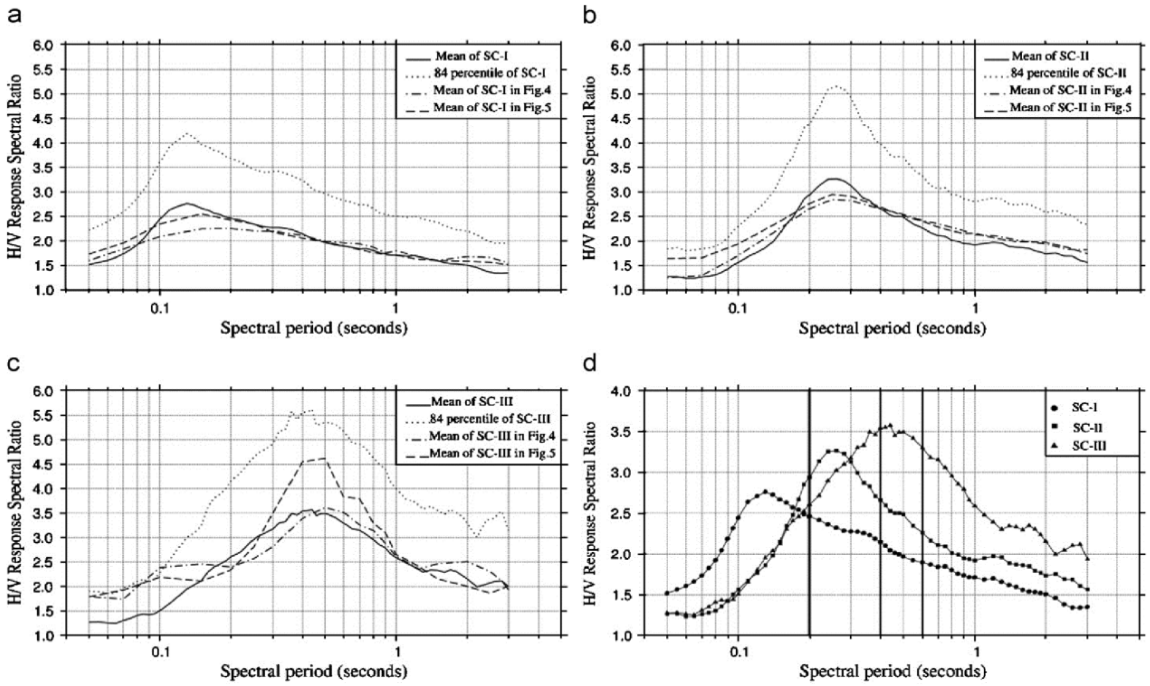

Fig. 3-18. (a–c) Comparing response spectral ratios of ISMN strong motion data with the mean H/V response spectral ratios obtained in this study and the mean H/V response spectral ratios determined by Zhao et al (2006). for Japanese strong motion sites. The dashed lines indicate 84 percentile of each site class. (d) Average H/V spectral ratios for the site classes assigned in this study. The vertical thick

3-5.3. Smooth spectra of horizontal and vertical ground motions for Iran

** **Source Article:** Ghasemi H, **Zaré M** and F. Sinaeian, (2009), "Smooth Spectra of Horizontal and Vertical Ground Motions For Iran", ISET Journal of Earthquake Technology, Paper No. 500, Vol. 46, No. 1, March 2009, pp. 1–17.*

In this section, I present the a study on the smooth spectra of horizontal and vertical ground motions for Iran, an analysis taken from the published article by Ghasemi et al. (2009). In this study, *"a set of strong-motion records, located at the near-field regions during the earthquakes with moment magnitudes equal to or larger than 6, were selected. To consider the effects of strong motions, only those records for which the maximum horizontal ground accelerations are greater than 0.05g were used.*

The smooth spectra of numerous horizontal and vertical ground motions were computed via their corresponding peak ground motion parameters. In order to validate the results, as obtained by analyzing the Iranian strong-motion records, the ratio between the smoothed and actual response spectra is calculated for each ground motion. Fig. 3-19 shows

the median spectral ratio for horizontal and vertical ground motions; the shaded area corresponds to ± 1 standard deviation about the median. The closeness of the median ratio of actual and smoothed SVs to unity for all natural periods confirms accuracy of the results obtained in this study. Here, a t-test of the hypothesis is also performed, i.e., the data points in each period range come from a united distribution. The results indicate that the null hypothesis cannot be rejected in wide period ranges.

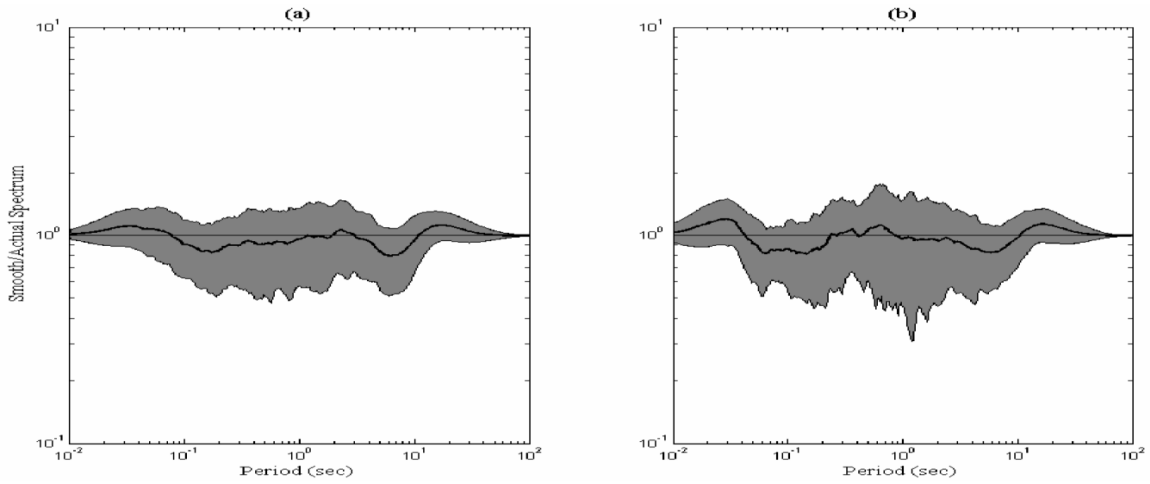

Fig. 3-19. *Median ratios between the 5%-damping smooth spectrum and the actual spectra of (a) horizontal and (b) vertical ground motions (the shaded area corresponds to ± 1 standard deviation about the median)*

3-5.4. Spectral demand curves based on the selected strong motion records in Iran

** **Source Article:** **Zaré M**., (2007), "Spectral Demand Curves Based on the Selected Strong Motion Records in Iran", Journal of Seismology and Earthquake Engineering (JSEE), Vol. 7, No.3. pp.111-123.*

In this section, I present my study on the spectral demand curves based on the selected strong motion records in Iran, an analysis taken from the published article by Zaré (2007). In this study, the spectral demand curves were prepared based on 89 selected records (with signal to noise ratio in the frequency range of less than 0.3Hz and a PGA greater than 50cm/sec^2). According to the H/V ratio method, site classification was determined so that the number of selected records were 22, 16, 25 and 26 for the site classes 1, 2, 3 and 4, respectively. The discussion on the developed results are summarized as:

- ❖ Alborz-Central Iran has the highest spectral displacement (Sd) in comparison with other site classes, see Figs. 3-27 and 3-28. However, the mean demand curves of site class-4 in Alborz-Central Iran shows systematic increase in the spectral displacement comparing to those of site classes-2 and 3, see Fig. 3-28.
- ❖ Based on the existing reliable and selected data for this study, the demand curves and Sd show no significant increase in site classes 2 and 3 in comparison with site class-1, see Figs. 3-27 and 3-28.
- ❖ The near fault demand curves in Fig. 3-27, show that horizontal component spectra have greater values than that of vertical one caused by the directivity effect which induced long period pulses of SH waves in fault-normal horizontal component of the motion.
- ❖ Such difference between the frequency content of the horizontal and vertical components in the near-fault distances is especially evident for spectral displacement ordinates, when the values of horizontal components represent twice the vertical one, see Fig. 3-28.

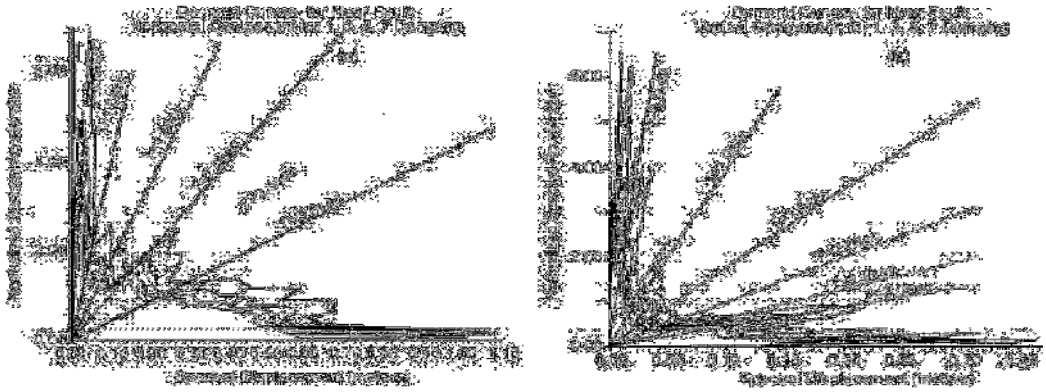

Fig. 3-27. Mean demand curve for the near-fault conditions, for a) horizontal and b) vertical components.

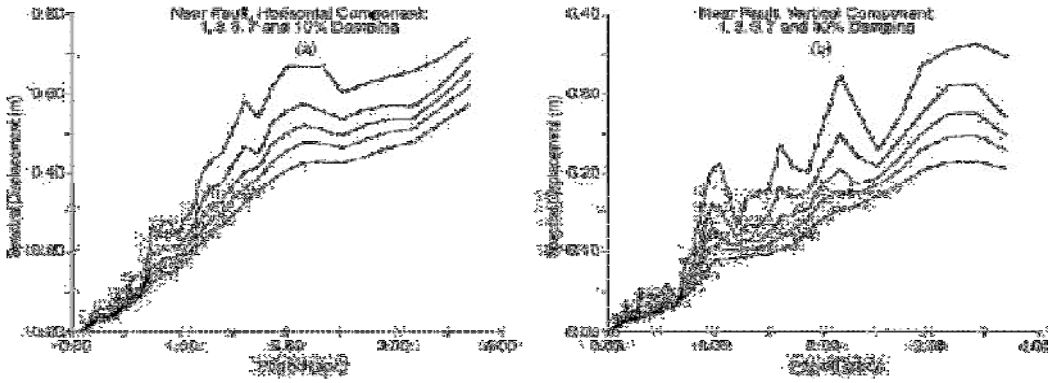

Fig. 3-28. Mean spectral displacement for the near-fault conditions, for a) horizontal and b) vertical components.

3-5.5. Doppler Effect observed on the recorded strong ground motions in Iran and Turkey

** **Source Article:** **Zaré M**., (2002), "Doppler Effect Observed on the Recorded Strong Ground Motions in Iran and Turkey", Journal of Seismology and Earthquake Engineering, Vol.4, No. 2 and 3, pp.21-36.*

In this section, I present my study on the Doppler Effect observed on the recorded strong ground motions in Iran and Turkey, an analysis taken from the published article by Zare (2002). The strong motion specifications, site class, the applied filter, peak acceleration (after filtering) and the observed intensity are presented in Table 1 of Zare (2002). The earthquake source specifications (epicenter location, Magnitude scales, and the values for different distance definitions, focal depth and mechanisms) as well as the corner and maximum frequencies and the values of rise and rupture times are given in Table 1 of Zare (2002) for 10 selected records.

The earthquake of Tabas (16/06/1978, central Iran), Kocaeli (17/08/1999, M_w7.4 Marmara Sea region, NW Turkey) and Kaynasli (12/11/1999, M_w7.1, Bolu area, NW Turkey) were selected to be discussed. *"This selection was based on the availability of a pair of records obtained in opposite ends of the earthquake fault rupture.*

- *The FFT of the amplitudes displacements are compared for different components of Tabas and Deyhuk records in Fig. 3-29. The greater amplitudes for Tabas record is evident, while the f_{c1} and f_{c2} are placed in different frequencies. Tabas was much closer to the active part of the rupture than Deyhuk, and the rupture propagation towards Tabas is supported by the observed much higher f_{c1} in this station. The displacements for the first 20 seconds of the displacement time-histories (DTH) in Tabas and Deyhuk are compared however in Fig. 3-30. A great difference is observable between these two records; the evident greater amplitudes and even the trapezoid type pulses in about 16 to 18 seconds correspond to Tabas DTH. This could be interpreted to the rupture directivity towards the Tabas, during the Tabas earthquake"* (Zare, 2002).

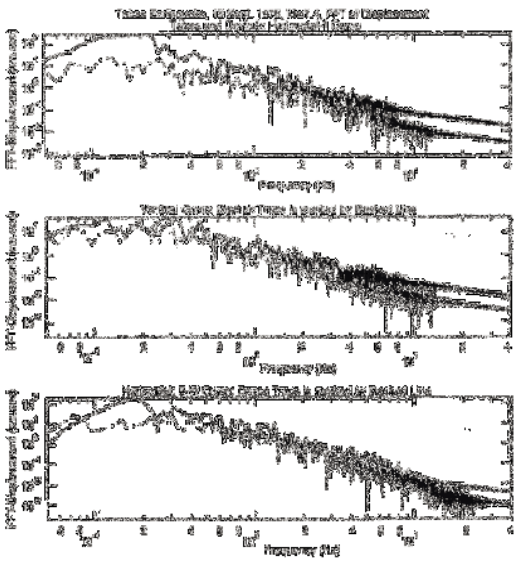

Fig. 3-29. The FFT of displacements are compared for Tabas and Deyhuk records for different components: the upper and lower are the horizontal components and the middle one is the vertical component (the Deyhuk traces are shown with dashed lines).

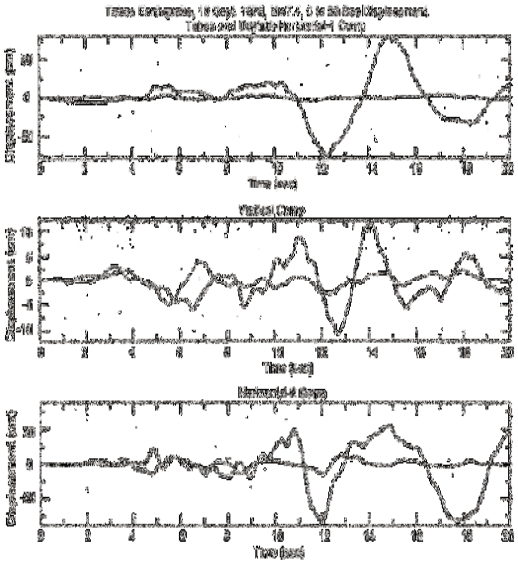

Fig. 3-30. The displacement time-histories are compared for Tabas and Deyhuk records for different components: the upper and lower are the horizontal components and the middle one is the vertical component (the Deyhuk traces are shown with dashed lines).

- *"The FFT of the amplitude of displacements for different components of Yarimca and Duzce records are compared in Fig. 3-31. The shapes of these spectra are more or less similar in different frequencies. This similarity could be followed in the waveform of the DTH's of these two records, see Fig. 3-32. This is suggested to be related to the bilateral directivity in the Kocaeli earthquake.*
- *"The FFT of the amplitudes of displacements in Duzce and Bolu records are compared for different components in Fig. 3-33. The level of the Fourier amplitude of displacements in Duzce shows greater values than that of Bolu. The wave forms of DTH's for these two locations are compared in Fig. 3-34, where the difference is evident especially for the horizontal components; the displacements were greater in Duzce, but the rupture time was found to be shorter in Bolu.*

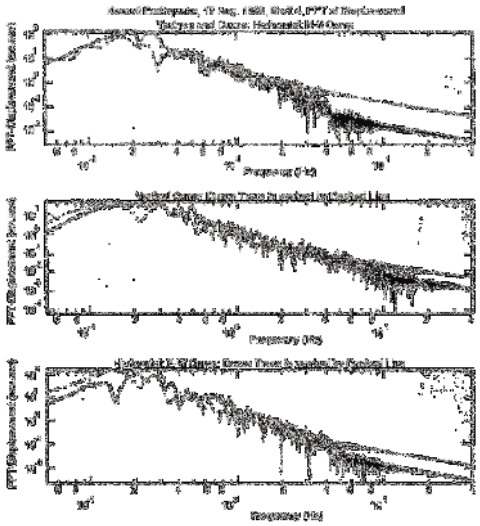

Fig. 3-31. The FFT of displacements are compared for Yarimca and Duzce records for different components: the upper and lower are the horizontal components and the middle one is the vertical component (the Duzce traces are shown with dashed lines).

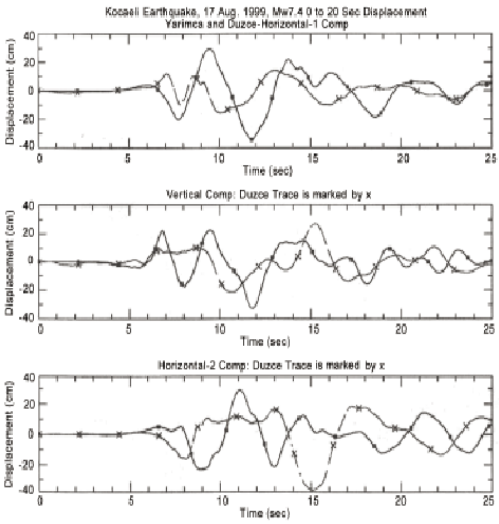

Fig. 3-32. The displacement time-histories are compared for Yarimca and Duzce records for different components: the upper and lower are the horizontal components and the middle one is the vertical component (the Duzce traces are shown in dashed lines).

❖

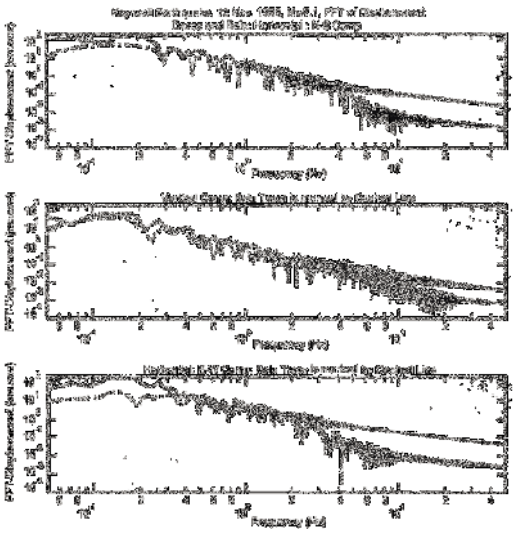

Fig. 3-33. The FFT of displacements are compared for Duzce and Bolu records for different components: the upper and lower are the horizontal components and the middle one is the vertical component (the Bolu traces are shown with dashed lines).

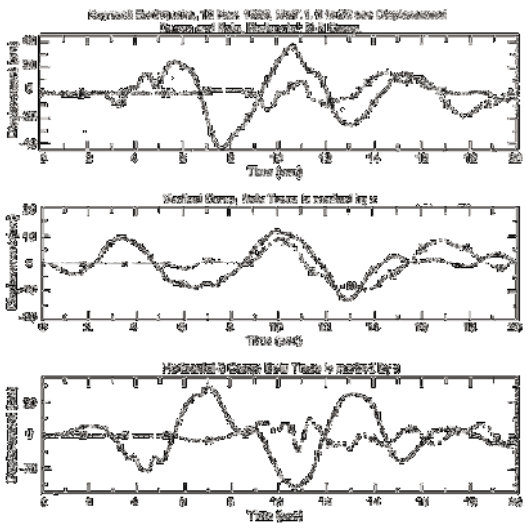

Fig. 3-34. The displacement time-histories are compared for Duzce and Bolu records for different components: the upper and lower are the horizontal components and the middle one is the vertical component (the Bolu traces are shown with dashed lines).

3-5.6. Site characterizations for the Iranian strong motion network

** **Source Article:** **Zaré M**., P.-Y. Bard and M. Ghafory-Ashtiany, (1999), "Site characterization for the Iranian Strong Motion Network", Soil Dynamics and Earthquake Engineering, Vol. 18, No.2, pp. 101-123.*

Twenty-six sites of the Iranian strong motion network, having provided numerous records of good quality, were selected for a site effect study with the objective of obtaining a reliable site categorization for later statistical work on Iranian strong motion data. For each site, superficial Vp and Vs profiles were measured with refraction techniques, microtremor recordings were obtained and analyzed with the H/V technique and the available three-component accelerograms by the receiver function technique. The aggregation of these results allows the proposition of a four-class categorization based on the H/V spectral ratio of strong ground motions, which demonstrate a satisfactory correlation with the S-wave velocity profile. Iran has a particular geological and meteorological situation compared to other seismic countries such as Japan or California, a mountainous country with dry weather conditions and a low water table in most areas. These conditions result in a relatively small number of sites with low frequency amplification, while many sites exhibit moderate amplifications in the intermediate and high frequency range.

Fifty sites were studied. These sites were chosen from a database of 279 records (already processed and developed (Zare et al., 1998)). The sites were chosen on the basis of the number and quality of corresponding records, as well as on the amplitude of the recorded motion and its dependence with a great earthquake (to compare cases of the same events). The site studies were carried out with different methods: geoseismic tests to determine the compressional and shear waves in a profile under the station, microtremor studies (with SS-1 instruments and SSR-1 sensors) and geoelectric studies. Finally, the geological site observations were performed to understand the geologic frame in each local-ity (type of the superficial layers, the depth of the water table, etc...). Among the fifty aforementioned sites, in 24 sites microtremor tests were applied, the geoseismic tests were performed in the 26 more important sites. In all of the sites, the obtained strong motion records are studied to obtain their horizontal to vertical spectral ratio (receiver function for the strong motions; RF SMS). Calculating the same ratio for micro-tremors (H/V ratio for the microtremors; H/V MTS), we were able to compare the H/V ratio for noises and earthquakes. No geotechnical

boring was done through this study and no data of this type was found in the location of the stations.

The relatively good relationship between the S-wave velocity profiles and the RF results allowed us to propose a multi-class site categorization based on the RF curves which is simply based on the amplitude and level of the highest peak on the RF curve (Table 3-10). According to these criteria, the 26 studied sites are classified and presented later. On the other hand, there are the cases where the RF amplitude is not equal to 4 (as it is defined earlier), but passes 3. In these cases it observes the results of other tests (if available) to distinguish the site conditions. In such intermediate cases, we have used the Vs and Vp profiles and the microtremor results to decide on the case. However, if the peaks did not approach 3 at all, that site is classified as rock site (class 1).

Table 3-10. The four class site categorization

Group	**Frequency band of the amplication**	**Vs_{30} (ms^{-1})**	**Sites**
1	F ≥15 Hz	Vs_{30} ≥700	Abbar, Deyhuk, Ghaen, Jovakan, Kakhk, Naghan, Saadabad, Tabas
2	5 - 15 Hz	500 - 700	Kavar, Maku, Manjil, Vendik, Zanjiran
3	2 - 5 Hz	300 -500	Fin, Firouzabad, Ghazvin, Golbaf, Rudbar, Zarrat
4	F≤2 Hz	Vs_{30} ≤300	Abhar, Lahijan, Hosseinieh, Rudsar, Shabankareh, Tonkabon, Talesh

The measured velocity profiles corresponding to each of these classes are grouped in Fig. 3-35. The main characteristic of category 1 is that the S-wave exceeds 700 ms^{-1} at depths beyond 5 m, although the values may be much lower at very shallow depths (thin layers with resonance frequencies exceeding 15 Hz). On the opposite, the velocity profiles in category 4 exhibit low velocities at the surface (below 250 ms^{-1}) and at depth (below 500 ms^{-1}down to 30 m) except for three `exceptional' sites for which there was a clear discrepancy between velocity profile and RF curve, that we checked several times and could not interpret. Velo-city profiles for categories 2 and 3 are intermediate.

The microtremor H/V spectra corresponding to each of these 4 categories are displayed in Fig. 3-36. It clearly shows that, to the contrary of many published studies, microtre-mors could not, in our case, point out the fundamental frequency, this negative result may perhaps be related to the absence of strong impedance contrasts in velocity profiles, except for some class 4 sites. In any case, it requires further work, and probably new measurements, before it can be understood.

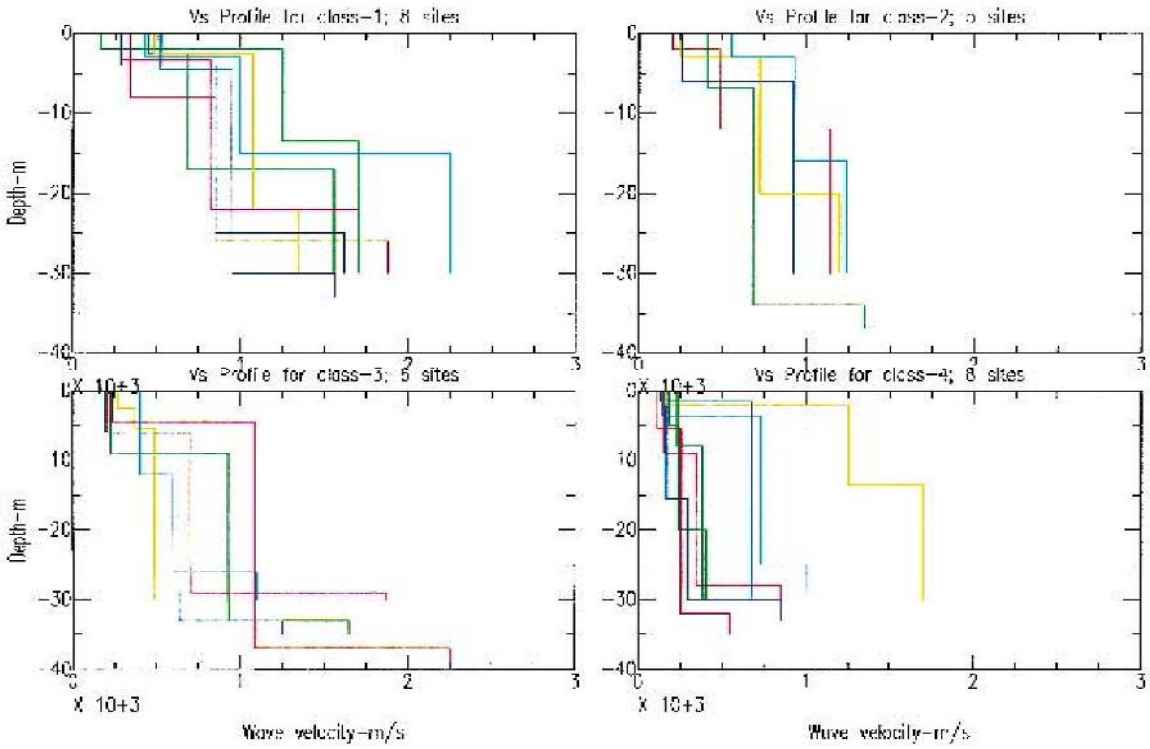

Fig. 3-35. The comparison of shear wave velocity pro®les in four site classes.

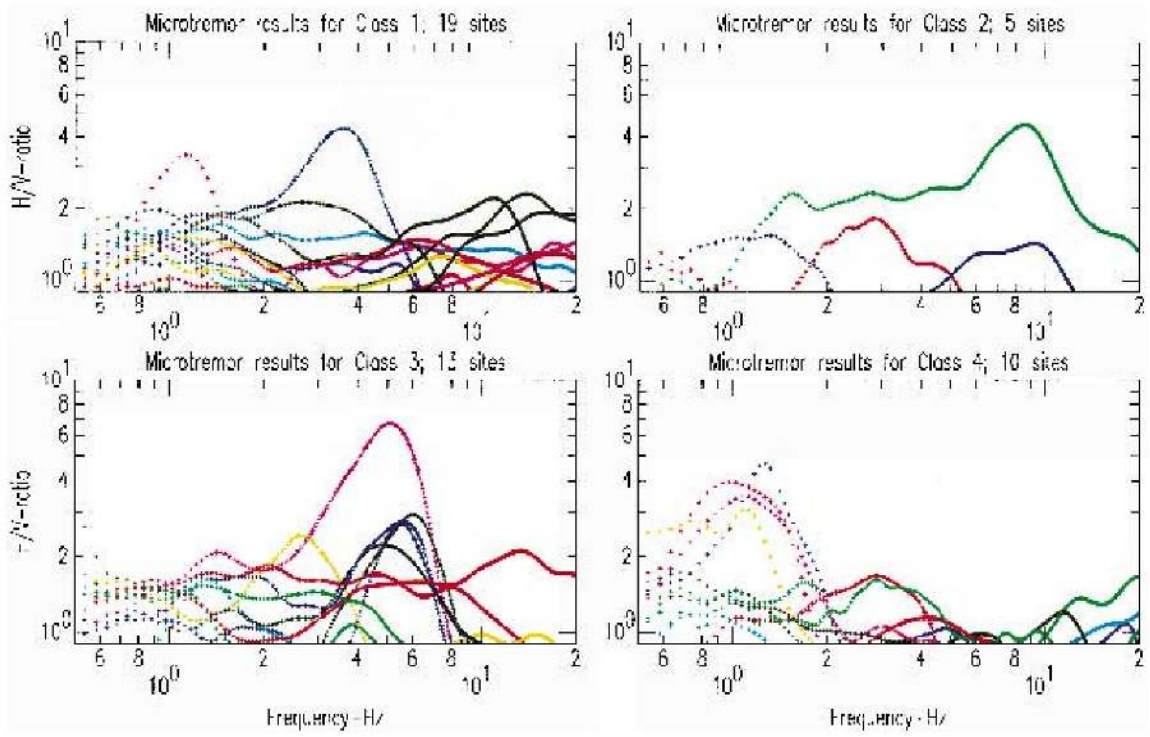

Fig. 3-36. The comparison of the H/V ratio for the microtremors in four site classes

Main articles of this chapter:

Luzi L, Puglia R, Russo E, D'Amico M, Felicetta C, Pacor F, Lanzano G, Ceken U, Clinton J, Costa G, Duni L, Farzanegan E. Guéguen P, Ionescu C, Kalogeras I, Özener H, Pesaresi D, Sleeman R, Strollo A. and **Zaré M**, (2016), "The engineering strong-motion database: A platform to access pan-European accelerometric data", *Seismological Research Letters,* 87(4): 987-997. doi: 10.1785/0220150278.

Zaré M., Kamranzad, F., and Farzanegan, E., (2016), "An Assessment of Recent Near-Field Strong Motion Data in Iran", *17th Iranian Geophysics Conference*.

Zaré M., Kamranzad F., Mona Lisa., and Rajaure, (2015), "A Seismological Overview of the 25 April 2015, Mw7.8 Nepal Earthquake", submitted.

Zaré M., and Sinaiean, F., (2014), "Site Effects and Classification of Iran Accelerographic Stations", *Geodynamics Research International Bulletin*, (Special Issue on Intra- Plate Earthquakes), Vol. (I) - No. 02, pp.15-23.

Zahedi-Khameneh A. R. Scherer A, and **Zaré M**, (2013), "A non-parametric wave type based model for real-time prediction of strong ground motion accelerogram", *Soil Dynamics and Earthquake Engineering*, DOI: 10.1016/j.soildyn.2013.01.024.

Ghasemi H, **Zaré M** and F. Sinaeian, (2009), "Smooth Spectra of Horizontal and Vertical Ground Motions For Iran", *ISET Journal of Earthquake Technology*, Paper No. 500, Vol. 46, No. 1, March 2009, pp. 1–17.

Ghasemi, H., **Zaré M**, Y. Fukushima and F. Sinaiean, (2009), "Applying empirical methods in site classification, using response spectral ratio (H/V): A case study on Iranian strong motion network (ISMN)", *Soil Dynamics and Earthquake Engineering*, Vol.29, pp.121-132.

Ansari A., A. Noorzad and **Zaré M**, (2007), "Application of wavelet multi-resolution analysis for correction of seismic acceleration records", *Journal of Geophysics and Engineering*, 4, pp. 362–377.

Zaré M., (2007), "Spectral Demand Curves Based on the Selected Strong Motion Records in Iran", *Journal of Seismology and Earthquake Engineering (JSEE)*, Vol. 7, No.3. pp.111-123.

Zaré M., and H. Hamzehloo, (2005), "Strong Motion study on Bam Earthquake of 26 December 2003", *Earthquake Spectra*, Special Issue on Bam earthquake.

Zaré M., (2004), "Strong Motion Data of the 1994-2002 Earthquakes in Iran: A Catalogue of 100 Selected Records with Higher Qualities in the Low Frequencies", *Journal of Seismology and Earthquake Engineering (JSEE)*, Vol. 6 No. 2, pp.1-17.

Zaré M., (2004), "Bam , Iran earthquake of 26 December 2003, M_W6.5: A study on the strong ground motions", *13th World Conference on Earthquake Engineering*, Vancouver, B.C., Canada August 1-6, 2004, Paper No. 8001.

Zaré M., (2002), "Doppler Effect Observed on the Recorded Strong Ground Motions in Iran and Turkey", *Journal of Seismology and Earthquake Engineering*, Vol.4, No. 2 and 3, pp.21-36.

Zaré M., and P.-Y. Bard, (2002), "Strong Motion Dataset of Turkey: Data Processing and Site Classification", *Soil Dynamics and Earthquake Engineering*, Vol. 22., No.8, Pages 703-718.

Zaré M., P.-Y. Bard and M. Ghafory-Ashtiany, (1999), "Site characterization for the Iranian Strong Motion Network", *Soil Dynamics and Earthquake Engineering*, Vol. 18, No.2, pp. 101-123.

Chapter 4: Attenuation

Selection of appropriate ground-motion attenuation relations is a key element in any probabilistic seismic hazard assessment PSHA. Where ground-motion recordings are abundant, ground-motion relations would be developed empirically based on regression analysis of previously recorded ground motions. In contrast, where recordings are inadequate, they could be often derived theoretically based on seismological models to generate synthetic accelerograms. However, in reference to Campbell (2003), in regions where real recorded data are sparse, there could be considerable uncertainty in calculating absolute values of ground motions from seismological models. In addition, in reference to several studies (e.g., Bommer et al., 2005), it has become standard practice to employ more than one ground-motion relation in the formulations of logic-tree for PSHA. Thus, the applicability of the selected attenuation relations to address the seismic hazard assessment of any region is an important issue.

In this chapter, I discuss about nine attenuation models developed empirically during my research works for Iran and other regions (e.g. Malaysia).

4-1. On the selection of ground–motion attenuation relations for seismic hazard assessment of the Peninsular Malaysia region due to distant Sumatran subduction intraslab earthquakes

** **Source Article:** Vaez Shoushtari, A., B. A. Azlan , and **Zaré M**, (2016), "On the selection of ground–motion attenuation relations for seismic hazard assessment of the Peninsular Malaysia region due to distant Sumatran subduction intraslab earthquakes", Soil Dynamics and Earthquake Engineering, 82, 123–137. DOI: 10.1016/j.soildyn.2015.11.012.*

In the following section I present the recently prepared attenuation relations for distant subduction intraslab earthquakes in Peninsular Malaysia, an analysis taken from the published article Vaez Shoushtari (2016). This study has attempted first to derive response spectral ground-motion attenuation relations for distant subduction intraslab earthquakes based on the ground-motion data recorded in Peninsular Malaysia, Japan, and Iran.

Ground-motion database for regression:

The amount of ground-motion data recorded in Peninsular Malaysia due to Sumatran subduction intraslab earthquakes is limited. In order to derive an appropriate set of spectral

ground-motion relations for distant subduction intraslab earthquakes, the response spectra database was compiled based on the ground motions due to Sumatran and Japan subduction intraslab earthquakes recorded in Peninsular Malaysia and Japan, respectively. In addition, the ground-motion recordings due to one subduction intraslab earthquake in the Java region recorded in Peninsular Malaysia as well as the recent Saravan-Iran earthquake in 2013 with M7.7, focal depth of about 51 km, and extension faulting mechanism were also included in the database (Table 4-1). These ground-motion records were from the Malaysian Meteorological Department (MMD)- Malaysia, Kyoshin network (K-NET) and Kiban Kyoshin network (KiK-net)-Japan, and the Iran Strong Motion Network (ISMN) databases. The final database included 531 sets of two horizontal components digital ground-motion records. In reference to National Earthquake Hazards Reduction Program (NEHRP, 2003) site classification, each record was assigned to a site class. The data recorded on all site classes covered relatively all the magnitude–distance ranges. The moment magnitudes are from M 5.0 to 7.7 with R_{hyp} 120 up to 1400 km.

Table 4-1. Subduction intraslab earthquakes used in the present study

No.	Location	Date (dd/mm/yy)	Time (GMT)	Longitude (°)	Latitude (°)	Focal depth (km)	Moment Magnitude	Record no.
1	Japan	26/05/2003	09:24:39	141.57	38.94	61	7	82
2	Sumatra	01/12/2006	03:58:00	99.05	3.46	208	6.3	4
3	Java	08/08/2007	17:05:00	107.58	- 6.03	305	7.5	1
4	Sumatra	30/09/2009	10:16:00	99.67	- 0.79	78	7.6	10
5	Japan	14/01/2010	18:46:28	143.1	42.17	70	5	24
6	Japan	13/03/2010	12:46:28	141.45	37.62	75	5.5	45
7	Japan	30/07/2011	18:54:00	141.16	37	53	6.4	81
8	Sumatra	05/09/2011	17:55:00	97.86	2.88	95	6.7	12
9	Japan	23/05/2012	15:02:28	142.22	41.39	54	6	65
10	Sumatra	23/06/2012	04:34:00	97.77	2.98	105	6.1	8
11	Japan	07/12/2012	08:18:35	144.09	38.01	58	7.2	86
12	Japan	02/02/2013	14:17:43	143.24	42.85	105	6.9	91
13	Iran	16/04/2013	10:44:32	62.21	27.89	51	7.7	22

Attenuation model and regression analysis:

Nonlinear regression analysis of the compiled database including the geometric mean of two horizontal components was based on the least-squares method. The attenuation model of the relation used here was selected by trial and error using different models proposed in previous studies until there was a sufficient match between the predicted and observed values based on the calculated standard deviation and R-square values. Finally, according to Fukushima and Tanaka (1990), the following form of attenuation model was selected (all log in base 10):

$$\log(Y) = aM + bR - \log(R + c*10^{aM}) + d + S_k + \varepsilon_{\log(Y)} \qquad (4\text{-}1)$$

where Y is either PGA, PGV, or 5% damped pseudo-acceleration (PSA). The acceleration values are in cm/s^2 and velocity values are in cm/s. M is moment magnitude, R is hypocentral distance in km, $\varepsilon_{\log(Y)}$ has a normal distribution that represents the random error with a mean value of zero and a standard deviation (sd) of $\sigma_{\log(Y)}$, S_k is the site class term that represents site effects, and a, b, c, and d are regression coefficients. The regression analysis was done considering all soil types (NEHRP site classes B, C, D and E). Least-squares method minimizes the sum of squared residuals, where the residual is the difference between the log(Y) observed and that predicted using Eq. (4-1). The resulted regression coefficients of various spectral periods of engineering interest are tabulated in Table 4-2.

Table 4-2. Regression coefficients.

Period (s)	a	b	c	d	S_B	S_C	S_D	S_E	$\sigma_{\log(Y)}$
PGA	0.6241	0.001623	0.01134646	0.1694	0.5930	0.1206	0.0830	0.1597	0.489
PGV	0.7905	0.001334	0.00089834	2.0851	0.6122	0.1939	0.0123	0.2026	0.332
0.10	0.5193	0.001670	0.03692850	1.0457	0.4847	0.0627	0.0953	0.0922	0.587
0.15	0.5707	0.001756	0.02070174	0.8663	0.6331	0.0964	0.0691	0.0931	0.560
0.20	0.6057	0.001703	0.01435259	0.6604	0.7030	0.1409	0.0748	0.1046	0.529
0.25	0.6532	0.001655	0.00653504	0.3528	0.7815	0.2255	0.0448	0.1135	0.492
0.30	0.6930	0.001617	0.00391245	0.0916	0.8019	0.2616	0.0365	0.1031	0.468
0.40	0.6996	0.001552	0.00361459	0.0132	0.8148	0.3233	0.0168	0.1382	0.431
0.50	0.7504	0.001471	0.00176890	0.3527	0.8440	0.3646	0.0768	0.1483	0.405
0.60	0.8153	0.001500	0.00085436	0.7250	0.8971	0.4120	0.1547	0.1307	0.394
0.70	0.9539	0.001545	0.00015722	1.4462	1.0183	0.5320	0.3018	0.0244	0.391
0.80	1.0444	0.001512	0.00004874	1.9156	1.1317	0.6609	0.4409	0.1148	0.398
0.90	1.0916	0.001479	0.00002801	2.2034	1.1657	0.6924	0.4837	0.1943	0.394
1.00	1.0904	0.001409	0.00002447	2.2878	1.1987	0.7187	0.4863	0.2240	0.390
1.20	1.0954	0.001350	0.00001908	3.0689	0.5684	0.1372	0.0864	0.3498	0.388
1.50	1.0906	0.001275	0.00001580	3.2028	0.6270	0.1830	0.0056	0.2404	0.392
2.00	1.0655	0.001199	0.00001665	3.1919	0.7151	0.2916	0.1436	0.1145	0.387
2.50	1.0392	0.001138	0.00001363	3.1805	0.8401	0.4554	0.2746	0.0419	0.381
3.00	0.9982	0.001090	0.00001713	3.0050	0.9095	0.5858	0.3989	0.1536	0.370
4.00	0.9903	0.001023	0.00001035	3.1383	0.9796	0.7178	0.5675	0.3141	0.347
5.00	0.9506	0.000909	0.00000578	3.0629	1.0477	0.8044	0.6774	0.4311	0.330

Response spectral accelerations of Sumatran/Java subduction intraslab earthquakes:

The main purpose of this study was to propose an appropriate set of empirical spectral ground-motion attenuation relations for distant subduction intraslab earthquakes to be more applicable for assessing the seismic hazard of Peninsular Malaysia. Therefore, the ground motions recorded at long distances in Peninsular Malaysia due to the five Sumatran/Java subduction intraslab earthquakes were used in order to have an evaluation of the derived

empirical ground-motion relations (Table 4-3). Geometric mean of 5% damped pseudo-acceleration response spectra of these intraslab earthquakes are plotted in Fig. 4-1 together with the predictions of the present and selected spectral global and overseas regional ground-motion relations. The estimated acceleration response spectra by the present study attenuation relations are shown by three lines; solid line with filled circle symbols indicates mean values and dashed lines with open circle symbols reflect the mean ± one standard deviation (sd).

As seen in Fig. 4-1, most of the observed acceleration response spectra have fallen relatively within the range between the mean ± one standard deviation attenuation curves by the present study equations. This shows the capability of proposed empirical attenuation relations to predict actual response spectral accelerations within an acceptable level of uncertainty. According to the figure, the spectra estimated by the LL08 model have been significantly overestimated compared to all observed spectra due to the five intraslab earthquakes. At most of the events, the BC15 model tends to predict lower spectral amplitudes than do the other models. In Fig. 4-1, it can be seen that the four AB03/08, ZAE06, BC15, and the present study ground-motion relations have produced spectra with approximately consistent shapes to that of the observed ones.

In final, the evaluation and comparison presented in Fig. 4-1 illustrate that the empirical spectral ground-motion relations derived by this study together with the AB03/08, ZEA06, and BC15 spectral models would be applicable in view of developing ground-motion logic trees for seismic hazard assessment in the regions affected by long distance subduction intraslab earthquakes such as the Peninsular Malaysia region.

Table 4-3. List of ground motions recorded at long distances in Peninsular Malaysia due to five Sumatran/Java subduction intraslab earthquakes.

No	Date	Time/UTC	Longitude	Latitude	Focal Depth	Moment Magnitude	Station	R_{hyp} (km)
1	01/12/2006	03:58:00	99.05	3.46	208	6.3	KGM	542
2	08/08/2007	17:05:00	107.58	6.03	305	7.5	IPM	1420
3	30/09/2009	10:16:00	99.67	–0.79	78	7.6	KUM	690
4	30/09/2009	10:16:00	99.67	–0.79	78	7.6	PYSM_B0	476
5	05/09/2011	17:55:00	97.86	2.88	95	6.7	KOM	683
6	23/06/2012	04:34:00	97.77	2.98	105	6.1	KGM	634

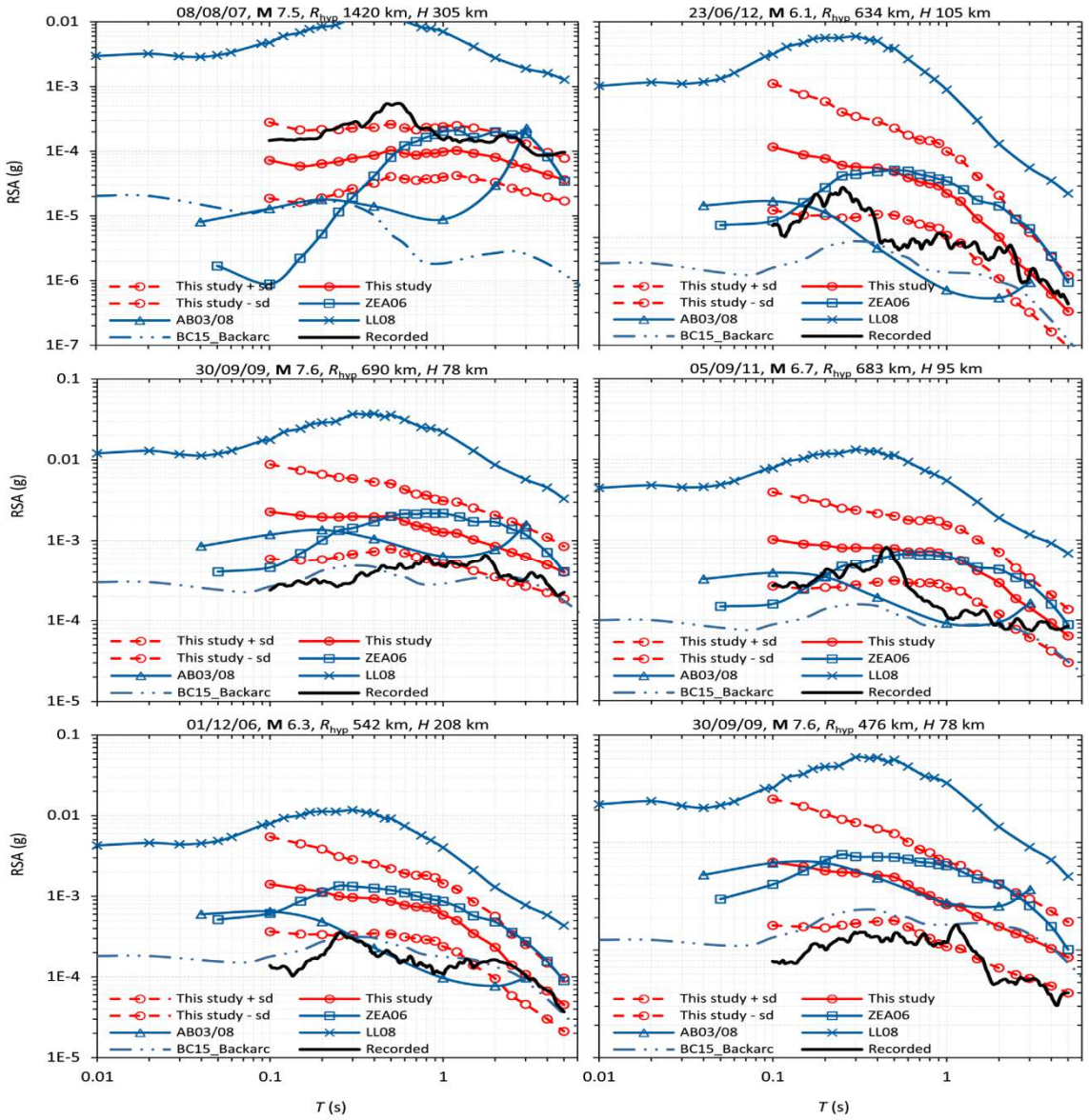

Fig. 4-1. Recorded and predicted acceleration response spectra of the five Sumatran/Java subduction intraslab earthquakes listed in Table 4-3 by the present study and selected spectral global and overseas regional ground-motion attenuation relations.

4-2. Recent development of the intensity prediction equations for Iran

** **Source Article:** **Zaré M**, (2016), " Recent development of the earthquake strong motion-intensity catalog and intensity prediction equations for Iran ", Journal of seismology, DOI: 10.1007/s10950-016-9622-4.*

In the following section I present my recent study on development of intensity prediction equations performed in 2016, In this study (Zare, 2016), two empirical relations between the "intensity" and "Ground Motion Parameters (GMPs)" were determined. At first, a relation was calculated in which the value of intensity was considered as a function of five predictive variables including Log (PGA), moment magnitude (M_w), epicentral distance, duration and site type. Then, due to the maximum correlation between the Log (PGA) and intensity, a simple regression between these two parameters was defined which can be used in rapid preliminary assessments.

Development of strong motion-intensity database:

At first, it was tried to provide a catalog of all the available GMPs and intensity data for the time span of 1975-2014 as follow:

Strong motion Database: The strong motion data of the current study was selected from processed databanks prepared by Zare (1999; 468 accelerograms of 1974-1997), Sinaiean (2006; 3268 accelerograms of 1994-2004), Zare et al., (2015; 140 accelerograms of 1974-1997; see section 3-3-2 of this manuscript) and Akkar et al., (2014; selection of records of three foreign events including the 1999 Izmit Turkey (M_w7.5), 2005 Balakot Pakistan (M_w7.5) and 2011 Van Turkey (M_w7.5) from the EMME strong motion catalog).

Intensity Database: To collect intensity database of the Iranian earthquakes, different sources were used including the database provided by Zare and Memarian (2003), as well as papers, iso-intensity maps and field reports in which intensities of important earthquakes were mostly prepared by the Iranian organizations such as the IIEES, BHRC, GSI and IGUT.

Completing the Database: Among all of the compiled strong-motion and intensity data, the data corresponding to the sites, where both strong-motion and intensity values have been simultaneously recorded, were selected and merged in the form a catalog which contains 306 data consisting of important information such as stations, record number, date, time, M_w, focal depth, PGA, PGV, PGD, duration, epicentral distance, site type and the intensity levels (Table 2 and Fig.1 of Zare, 2016).

Multiple Regression Analysis:

In this study, the effect of five available parameters consisting of "Log (PGA)", "M_w", "epicentral distance", "site type", and "duration" on the "intensity" was investigated. The parameters were tested as predictive independent variables to see whether there is a mathematical meaningful relation between the earthquake intensity and them. For this propose, 186 out of 306 existing data in GMPs-intensity catalog was considered, because this number of data covers all the calculated GMPs along with intensity, while 120 others which mostly belong to Sinaiean (2006) and Akker et al. (2014) strong-motion databases, were removed due to the lack of the parameter "duration". The correlations between the earthquake intensity and the predictive variables are presented in Table 4-4.

Table 4-4. Pearson correlation between predictors and intensity

	Intensity	**M_w**	**Epicentral Distance**	**Duration**	**Log (PHA)**	**Site Type**
Intensity	1.000	0.337	-0.558	-0.396	0.760	-0.182
M_w	*	1.000	0.198	0.179	0.272	-0.125
Epicentral Distance	*	*	1.000	0.274	-0.503	0.119
Duration	*	*	*	1.000	-0.380	0.185
Log (PHA)	*	*	*	*	1.000	-0.140
Site Type	*	*	*	*	*	1.000

There are different methods to conduct a multiple regression such as forward selection, backward removal and stepwise. In this study, the stepwise method was employed which is a combination of the two forward selection and backward removal methods. The stepwise calculates coefficient of effective independent variables in the relations and/or removes least significant variables. A stepwise regression was applied to the Iranian data and the coefficients of the PMGs-intensity relationships were obtained (Table 4-5). The stepwise regression has provided 4 models participating the predictive variables. In model 1, the predictors only contain Log (PHA); In model 2, the predictors contain Log (PHA) and M_w; In model 3, predictors contains Log (PHA), M_w and epicentral distance and finally In model 4, predictors contains Log (PHA), M_w, epicentral distance and duration. The P-value (or called significance probability) which describes the effectiveness of independent variables in a regression has adopted values less than 0.05. If the P-value is more than 0.05, the independent parameter is removed from regression. This shows that the parameter soil type is removed from the regression since it probably has no considerable effect based on the available data. Moreover, the parameter Log (PHA) is involved in all the presented models.

This indicates that intensity is more affected by Log (PHA), meanwhile they have also the highest correlation. Then, the instrumental intensities of the records were predicted by application of the Model 4. The residual values were calculated. Descriptive statistics of the residuals are represented in Table 4-6. It indicates that the residuals have a normal distribution in a range between -2.5 to 2.5 with no considerable bias in predictions.

Table 4-5. Coefficients of GMPs-intensity equation in the four models of stepwise regression

Model		Coefficients		P-value	95.0% Confidence Interval for Coefficients	
		Value	Std. Error		Lower Bound	Upper Bound
1	(Constant)	1.136	0.170	-	0.803	1.470
	Log (PHA)	2.377	0.106	0.00	2.170	2.585
2	(Constant)	-1.142	0.582	-	-2.287	0.003
	Log (PHA)	2.258	0.107	0.00	2.046	2.469
	M_w	0.390	0.096	0.00	0.202	0.578
3	(Constant)	-1.460	0.549	-	-2.539	-0.381
	Log (PHA)	1.584	0.139	0.00	1.311	1.856
	M_w	0.723	0.101	0.00	0.523	0.922
	Epic. Dist	-0.007	0.001	0.00	-0.010	-0.005
4	(Constant)	-1.448	0.521	-	-2.472	-0.423
	Log (PHA)	1.212	0.144	0.00	0.930	1.495
	M_w	0.935	0.102	0.00	0.735	1.135
	Epic. Dist	-0.008	0.001	0.00	-0.010	-0.006
	Duration	-0.033	0.005	0.00	-0.043	-0.023

Dependent Variable: Intensity

Table 4-6. Descriptive statistics of the residuals derived by multiple GMPs-intensity regression

	No. Samples	Min	Max	Mean	Standard deviation of Mean	Variance	Skewness	Kurtosis
Residual	186	-2.42	2.20	1.02E-16	0.05	0.76	-0.06	0.09

PGA-MMI Regression:

As it was mentioned, PGA correlates better with the intensity comparing to the other predictors. It is also the most available parameter to predict instrumental intensity and to generate shake maps quickly. Thus, another regression is performed to test the correlation between PGA and intensity and to calculate a proper relationship. The new regression can be directly calculated using all the PGA-intensity values (e.g. Margottini et al. 1992; Faccioli & Cauzzi 2006) or can be calculated considering the a single average value of the PGA for each intensity levels (e.g. Trifunac & Brady 1975; Wald et al. 1999a). It is noted that by using data grouped into intensity classes obviates the problems of the large scatter of the peak ground motion data for each intensity unit (Faenza and Michelini, 2010). In this study, the second

approach was chosen. Thus, average values of PGA with their standard deviations were calculated for each intensity level (Table 4-7). Subsequently, the simple Ordinary Least Squares (OLS) method was applied to the Log (PHA)-intensity data and the regression equation was obtained as the following:

$$\text{Intensity} = 4.07 \text{ Log (PHA)} - 1.726 \qquad (4\text{-}2)$$

This equation was also used to re-estimate the intensity of the existing 306 data of GMPs-intensity catalog of Iran. Residuals (observed intensity minus predicted intensity) were again calculated and descriptive statistics were obtained (Table 4-8). It demonstrates that it has a normal distribution in a range between -4.5 to 4.5 with no considerable bias in predictions.

Comparing the residuals of the multiple regression (between the "Intensity" and "Log (PHA)", "M_w", "epicentral distance" and "duration") to the residuals of the OLS regression (between the "Intensity" and "Log (PHA)") shows that the multiple regression is able to predict the intensity more accurately based on the multiple predictors. Overestimations and underestimations are more evident in the OLS regression, however the OLS regression between Intensity and Log (PHA) can be used in rapid damage assessments.

Table 4-7. Average values of Log (PHA) for each intensity level

Observed Intensity	**Avg. Log (PHA)**	
	cm/s²	**stdev***
2	1.08	0.09
2.5	1.17	0.04
3	1.15	0.21
3.5	1.50	0.29
4	1.31	0.34
4.5	1.22	0.20
5	1.51	0.31
5.5	1.86	0.40
6	1.89	0.37
6.5	2.01	0.36
7	2.11	0.27
7.5	2.34	0.51
8	2.36	0.39
8.5	2.66	0.10
9	2.54	0.30
10	2.80	0.22

stdev= standard deviation

Table 4-8. Descriptive statistics of residuals derived by OLS regression between Log (PHA) and I.

	No. Samples	Min	Max	Mean	Stdev of Mean	Variance	Skewness	Kurtosis
Residual	306	-4.43	4.49	0.2960	0.05689	1.980	-0.367	0.099

4-3. An empirical spectral ground-motion model for Iran

* ***Source Article:*** *Ghasemi H , **Zaré M**, Y. Fukushima, K. Koketsu, (2009), "An empirical spectral ground-motion model for Iran", Journal of Seismology, Volume 13, Issue 4, pp 499-515, DOI 10.1007/s10950-008-9143-x.*

A new ground-motion prediction equation for 5%-damped horizontal spectral acceleration applicable to Iran is presented. The advantages of using this model rather than those proposed previously for Iran are discussed by considering the distribution of residuals against the explanatory variables, magnitude and distance. The applicability of the proposed model, as well as those of several other models developed for shallow crustal environments, is also investigated by means of statistical tools. The results reveal the overall suitability of the new model as well as the validity of models developed using mainly Eurasian strong-motion records.

Selected strong-motion records:

We analyzed 716 triaxial accelerograms, recorded during 200 earthquakes of $M_W \geq 5$ in Iran. In addition to the Iranian data, 177 triaxial strong ground-motion records from West-Eurasia and data of the Kobe earthquake were analyzed, to augment the Iranian dataset in certain distance and magnitude intervals. All the data span 0.5–100 km in distance and M_w 5.0–7.4.

Functional form:

To identify the most appropriate functional form, several models of ground-motion prediction equations with similar explanatory variables as those for this study were examined. The functional form finally selected is:

$$\log_{10} Sa(T) = a_1 + a_2 M + a_3 \log_{10}(R + a_4 10^{a_5 M}) + a_6 S_1 + a_7 S_2 \qquad (4\text{-}5)$$

where $Sa(T)$ is the spectral acceleration with 5% damping in cm/s^2. a_1–a_7 are period-dependent coefficients that must be determined via regression analysis. The variables S_1 and S_2 take on values as: S_1=1 and S_2=0 for rock and S_1=0 and S_2 =1 for soil. In the above model, the addition of the term $a_4 10^{(a5M)}$ to R in the geometrical spreading term allows the amplitude saturation in the near-fault region to be expressed (Fukushima et al. 2003). To avoid instable results for a_5 coefficient due to the lack of data close to the fault, we ultimately fixed a_5 at 0.42 (Fukushima et al. 2000). Then, a direct search technique known as the Nelder–Meade

algorithm was used to search for values of the nonlinear parameters that minimize the norm of the residual. The estimated attenuation coefficients and the logarithmic standard deviation for 5%-damped spectral acceleration values at periods of up to 3 s are shown in Table 4-11.

Table 4-11. Empirical attenuation coefficients and logarithmic standard deviation values for 5%-damped spectral acceleration

Period (s)	a_1	a_2	a_3	a_4	a_5	a_6	a_7	σ log y
0.05	0.868	0.405	−1.424	0.014	0.420	0.859	0.836	0.319
0.06	0.906	0.398	−1.440	0.015	0.420	0.944	0.911	0.322
0.07	0.957	0.394	−1.449	0.015	0.420	0.978	0.937	0.325
0.08	0.700	0.387	−1.427	0.015	0.420	1.282	1.238	0.325
0.09	0.966	0.384	−1.413	0.016	0.420	1.046	1.005	0.326
0.1	0.904	0.380	−1.396	0.016	0.420	1.136	1.096	0.331
0.2	0.786	0.425	−1.215	0.015	0.420	0.663	0.748	0.319
0.3	0.432	0.474	−1.134	0.014	0.420	0.477	0.605	0.318
0.4	0.246	0.528	−1.080	0.011	0.420	0.135	0.289	0.327
0.5	0.003	0.571	−1.069	0.010	0.420	0.002	0.173	0.333
0.6	−0.118	0.608	−1.053	0.010	0.420	−0.209	−0.037	0.337
0.7	−0.234	0.635	−1.034	0.009	0.420	−0.361	−0.194	0.347
0.8	−0.331	0.673	−1.083	0.010	0.420	−0.450	−0.300	0.336
0.9	−0.459	0.706	−1.092	0.011	0.420	−0.570	−0.424	0.335
1	−0.567	0.727	−1.071	0.011	0.420	−0.678	−0.533	0.336
2	−1.209	0.876	−1.104	0.011	0.420	−1.291	−1.183	0.363
3	−1.436	0.920	−1.151	0.012	0.420	−1.515	−1.411	0.370

Fig. 4-3 (left) compares the predicted response spectra for the same site category and magnitude M_W7 at different distances. This figure reveals that, as expected, the spectral amplitude steadily decreases with increasing distance. It also shows decrease of ground-motion attenuation with distance at longer periods. The effect of magnitude on the predicted response spectra is illustrated in Fig. 4-3 (right). As expected, a systematic decrease in the amplitudes of the response spectra with decreasing magnitude at all periods is observed.

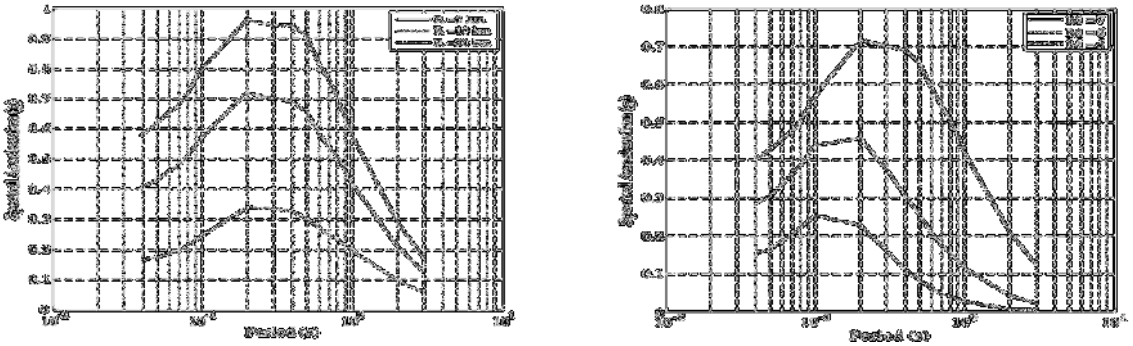

Fig. 4-3. Comparison of predicted mean acceleration spectra of the same site category (soil) at different distance ranges for M_W=7 events and *(left)* of the same site category (soil) at different magnitude ranges for distance of R=10 km *(right)*.

Comparison with other relationships:

The ground-motion models, considered in this study (i.e., Fukushima et al. 2003; Ambraseys et al. 2005; Boore and Atkinson 2008; Campbell and Bozorgnia 2008; Chiou and Youngs 2008) have each been developed based on strong ground-motion observations made in seismically active shallow crustal environments similar to that beneath the Iranian plateau. In order to evaluate the applicability of these different relationships, strong ground motions recorded during some earthquakes were considered. Supplementary detailed studies of the rupture process and causative fault geometry are available for all these events. Such information is essential in estimating the necessary inputs for the NGA ground-motion models. Since seismic hazard analysis is commonly performed for rock site conditions, only those ground motions recorded on rock sites are considered. The resulting dataset contains 69 triaxial strong motions spanning distances of 9–150 km and magnitudes of 5.6–7.3. The selected records are temporarily excluded from the prepared catalogue and the coefficients of the regression model re-calculated.

For a median LH value of at least 0.2, with the absolute value of the mean and median of the normalized residuals and their standard deviations all being smaller than 0.75, the ground-motion model is ranked as class “C”. The sample standard deviation should also be smaller than 1.5. A median LH value of at least 0.3, absolute values of the mean and median of the normalized residuals and their standard deviations all being smaller than 0.5, and a sample standard deviation of less than 1.25 constitute class “B”. For residual sets calculated at periods of up to T=2 s using the different ground-motion models, the median LH values, the maximum likelihood estimates of the central tendency parameters, and corresponding standard deviations of these parameters are tabulated in Table 4-12”.

Table 4-12. Results of the applied statistical measurements on residual sets for various ground motion models

Model	LH	Sigma	Mean	Sigma	Median	Sigma	Std	Sigma	Rank
Boore and Atkinson (2008)	0.364	0.014	−0.082	0.038	0.071	0.042	1.361	0.032	C
Campbell and Bozorgnia (2008)	0.424	0.015	0.156	0.031	0.268	0.038	1.137	0.024	B
Chiou and Youngs (2008)	0.332	0.017	−0.590	0.04	−0.434	0.045	1.506	0.032	D
Ambraseys et al. (2005)	0.414	0.013	0.186	0.031	0.324	0.042	1.148	0.023	B
Fukushima et al. (2003)	0.413	0.021	0.237	0.038	0.357	0.048	1.121	0.028	B
This study (2009)	0.46	0.014	0.041	0.028	0.2	0.033	1.004	0.02	A

4-4. Ranking of several ground-motion models for seismic hazard analysis in Iran

** **Source Article:** Ghasemi H., **Zaré M** and Y Fukushima, (2008), "Ranking of several ground-motion models for seismic hazard analysis in Iran", Journal of Geophysics and Engineering. 5, pp. 301–310.*

The main goal of our study was to rank the most repeatedly used attenuation relations for seismic hazard analysis in Iran, using a set of recent earthquake records. A review of selected earthquake characteristics and their corresponding strong-motion records is presented after a brief description of the candidate ground-motion models considered in this study. The results of statistical measurements and tests are presented afterwards. Using the ranking scheme proposed by Scherbaum et al (2004), the candidate ground-motion models are finally ranked into four different qualitative classes. Obviously, this ranking is valid in the Iranian plateau, and we will not discuss the prominence of attenuation relations itself.

To select candidate ground-motion models, published relations developed for Iran and those developed for regions with similar tectonic regime to Iran are considered. Four out of six ground-motion models considered in this study (i.e. Fukushima et al (2003); Boore and Atkinson (2007); Campbell and Bozorgnia (2007) and Chiou and Youngs (2006)) are developed based on strong motions, recorded in seismically active shallow crustal environments, and the rest (Zare´ 1999; Sinaeian 2006) are derived merely from ISMN data.

In this study, the strong motions recorded during the 2002 Avaj, 2003 Bam, 2004 Kojour and 2006 Silakhor earthquakes are considered. The supplementary studies on the rupture process and the causative fault geometry are available for all these events (ERI 2002; Jackson et al 2006; Tatar et al 2007). Such information is essential in estimating the necessary inputs of NGA ground motion models.

The first considered GOF test is the t-test which can be applied on a normalized residual set to test the hypothesis of supplying the data in the sample vector from a distribution of zero mean. The test statistic has a Student *t*-distribution if the null hypothesis (mean is zero) is true. The data are assumed to be gained from a normal distribution of unknown variance. The *t*-test *p*-values are given in Table 4-13. The *p*-value of a statistical significance test represents the probability of obtaining values of the test statistic that are equal to or greater in magnitude than the observed test statistic, and is another quantitative measure for reporting the result of

a test of a hypothesis (NIST, 2006). Generally, one rejects the null hypothesis if the *p*-value is smaller than or equal to the significance level. As can be seen from the *t*-test results, the normal distribution with zero mean at the 5% significance level can be rejected for the Campbell and Bozorgnia (2007) and Fukushima *et al* (2003) models and not for others.

Table 4-13. Results of the applied statistical tests. The rank of each model is also listed.

Model	*t*-test	lil-test	var-test	K–S	LH	Sigma	Mean	Sigma	Median	Sigma	deviation	Sigma	Rank
Boore and Atkinson (2007)	0.86	0.02	0.00	0.00	0.18	0.03	0.021	0.119	0.271	0.158	1.829	0.079	D
Campbell and Bozorgnia (2007)	0.00	0.03	0.00	0.00	0.30	0.02	0.522	0.080	0.674	0.073	1.312	0.062	C
Chiou and Youngs (2006)	0.31	0.08	0.00	0.00	0.21	0.04	0.108	0.107	0.044	0.129	1.671	0.065	D
Sinaeian (2006)	0.21	0.02	0.05	0.31	0.46	0.04	−0.088	0.072	0.054	0.067	1.089	0.050	A
Fukushima et al (2003)	0.03	0.02	0.00	0.00	0.37	0.03	0.170	0.083	0.331	0.089	1.242	0.057	B
Zare´ (1999)	0.08	0.02	0.08	0.18	0.54	0.03	−0.086	0.067	−0.004	0.059	0.988	0.086	A

The *p*-values calculated in this test are given in Table 4-13. Considering the results of the lil-test, the null hypothesis cannot be rejected at the 5% significance level only in the Chiou and Youngs (2006) model. The variance test (var-test) is applied to check the unit variance for the residual sets. It performs a chi-square test for the hypothesis of sample vector data gathered from a normal distribution with unit variance. This test is applied to the binned data and computed by finding the observed and expected counts for each bin. The calculated *p*-values of this test for residual sets considered in this study are listed in Table 4-13. It shows that the normal distribution at the 5% significance level cannot be rejected only for the Zare (1999) model. Regarding the reported *p*-values (in Table 4-13), the assumption of standard normal distribution should not be rejected for Sinaeian (2006) and Zare´ (1999) models.

The maximum likelihood estimates of the central tendency parameters and standard deviation of the residual sets are tabulated in Table 4-13. The corresponding standard deviations of these parameters are calculated using the bootstrap technique through data re-sampling. The parameters just described, as will be shown later, are used by Scherbaum *et al* (2004) to rank ground-motion models

According to the *p*-values of the *t*-test for the residual sets, the largest value is obtained for the Boore and Atkinson (2007) model, as expected considering the mean values listed in Table 4-13. On the other hand, the most suitable model based on the *p*-values of the var-test is the Zare´ (1999) model with the standard deviation close to unity. These GOF tests are used only to check one of the underlying assumptions. Hence, GOF measures that can be

used to test whether or not a residual set follows standard normal distribution, e.g. Kolmogorov–Smirnov and LH values, are more appropriate in ranking schemes. According to the Kolmogorov–Smirnov test, the largest values are determined for Sinaeian (2006) and Zare´ (1999) models, while *p*-values are almost zero in others. Considering the median LH values, it can be seen that the Zare´ (1999) and Sinaeian (2006) models provide values closest to 0.5. A median LH value for the Zare´ (1999) model is slightly higher than 0.5 due to its corresponding residual distribution standard deviation being slightly lower than 1. The smallest values are obtained for Boore and Atkinson (2007) and Chiou and Young (2006).

As indicated by Scherbaum et al (2006), and also shown by the results of this study, none of the statistical tests for significance considered, i.e. *t*-test, var-test, lil-test and K–S test, seem to be appropriate to be used in a practical ranking scheme. Indeed most of the tests only check for one hypothesis, i.e. normal distribution, zero mean or unit standard deviation, and consequently they cannot be used for the ranking because all the models would be rejected by at least one of the tests. The K–S statistical test, which checks simultaneously the entire hypothesis, also failed to rank ground-motion models, and all of the models except the Zare´ (1999) and Sinaeian (2006) models are rejected at the 5% significance level.

Recently, Scherbaum et al (2004) proposed a comprehensive data-driven ranking scheme. This scheme is based on the LH median value together with the mean, median and standard deviation of the residuals. If a median LH value of at least 0.2, with the absolute value of mean and median of the normalized residuals and their standard deviation smaller than 0.75, is determined for a normalized residual set, the ground-motion model should be ranked as class ‘C’. The sample standard deviation should also be smaller than 1.5. A median LH value of at least 0.3, with the absolute value of mean and median of the normalized residuals and their standard deviation smaller than 0.5, and sample standard deviation smaller than 1.25 give a rank ‘B’ to the model. The best rank ‘A’ is obtained with a median LH value of at least 0.4, with the absolute value of mean and median of the normalized residuals and their standard deviation smaller than 0.25, and sample standard deviation smaller than 1.125. A model that does not satisfy the mentioned criteria for any of these classes should be ranked as class ‘D’. Following this scheme, the Zare´ (1999) and Sinaeian (2006) models are assigned rank A, Fukushima *et al* (2003) rank B, Campbell and Bozorgnia (2007) rank C and the other models are ranked D or unacceptable.

4-5. Spectral attenuation of strong motions for near source data in Iran

** **Source Article:** **Zaré M**., S. Karimi-Paridari, and S. Sabzali, (2008), "Spectral Attenuation of Strong Motions for Near Source Motions in Iran", Journal of Seismology and Earthquake Engineering (JSEE), Fall 2008, Vol. 10, No. 3. Technical Note. Pp147-152.*

In this section, I present my study on the spectral attenuation of strong motions for near source data in Iran, an analysis taken from the published article by Zaré et al. (2008). This study is to investigate spectral attenuation law for Iran, using the response spectra of Iranian strong motion data in the form of different parameters. It is to establish the empirical relationships for the strong motions and to study the changes in different regions of the country, regarding attenuation law.

The Applied Approaches:

To establish the attenuation relationships for Iran, the approach presented by Joyner and Boore (1981) and Fukushma and Tanaka (1990) was followed. A one-step regression is used to fit a model to multiple independent variables (magnitude, distance, site parameters…). *"In the two-stage methods, the parameters controlling distance dependence and a set of amplitude factors, one for each earthquake, are determined in the first stage, by maximizing the likelihood of the set of observations. The parameters controlling magnitude dependence are then determined in the second stage by maximizing the likelihood of the set of amplitude factors"* (Joyner and Boore, 1993). In the one-step method, all parameters are obtained simultaneously by maximizing the likelihood of observations. This approach is used by Brillinger and Pristler (1984), yielding the results similar to the two-step method for the spectral ordinates using the north-western American data (Brillinger and Pristler, 1984).

Fundamental Form:

The genuine form of the dependence is:

$$\text{Log } A = a.M + b.R - d.\text{Log } R + ci.Si + \sigma P \qquad (4\text{-}6)$$

where, A is the strong motion parameter, a is the magnitude coefficient, M is the magnitude, b is the distance coefficient showing inelastic attenuation, R is the distance, c is the site class coefficient, S is the site class, σ is 84 percent (P=1) to be added to the mean (50 percent values; P=0), d is the coefficient for logR introduced to allow a geometrical expansion which

may be different from the body wave dependence. In this study the moment magnitude (M_w) is used for M and the hypocentral distance for X. The ci.Si expression is to show the site effects for 4 site classes that are already defined by Zaré et al (1999). In short, site classes are assigned to the sites of fundamental frequencies; over 15Hz for site class 1; 5-15Hz for site class 2; 2-5Hz for site class 3; below 2Hz for site class 4.

Ground Motion Parameters:

"The regressions were performed for various ground motion parameters for the spectral accelerations, Sa(T). The regression on Sa(T) was fulfilled for 7 different periods between 0.1 and 2sec. found for the damping of %5" (Zare, 2012). The general form of the attenuation relationship for the spectral acceleration (Sa) is;

$$\text{Log Sa(T)} = a\,(T).M + b(T).R - \text{Log } R + c_i\,(T).S_i + \sigma(T).P \qquad (4\text{-}7)$$

In the present study another form of this relation is used based on better accordance with the input data. his formula is already used by Boore et al (1997);

$$\ln \text{Sa(T)} = b_1(T).Si + b_2(T)\,(M-6) + b_3(T)\,(M-6)^2 + b_5(T).\text{Ln } R + \sigma \text{Sa}(T).P \qquad (4\text{-}8)$$

b_2 and b_3 are assumed as constant coefficients; here, only b_1 and b_5 are calculated for different site types.

The Input Database:

The database, used as the input for this study, consists of 87 three components accelerograms, recorded between 1975 and Dec. 2003 by National Iranian Strong Motion Network. The moment magnitude and hypocentral distance are estimated for these records directly by the strong motion records. The hypocentral distance is obtained by the S-P time difference, while the seismic moment is directly calculated by the level of acceleration spectra plateau and the corner frequency (Zare, 1999).

The spectral values of selected records are used to derive the empirical attenuation laws for different response spectral ordinates in different site conditions. The strong motions are selected based on their PGA values (PGA of 0.05g on at least one component) and the good signal quality in the frequency band of 0.3Hz or lower. The data are splitted into two subsets corresponding to two geographical areas: 1. central Iran and Alborz region 2. Zagros region, according to the strong earthquakes recorded at 60km distances (1975-2003). *"The results presented in this paper are the coefficients obtained for all data (89 records) selected including the data of Alborz-Central Iran and Zagros (Table 1 of Zare et al., 2008)".*

Results:

The results of the regressions are presented in Table 4-14. The coefficients are presented for 7 different periods from 0.1sec (PGA) to 2 seconds. The attenuation coefficients are used and tested giving a magnitude 7.0 and 10km hypocentral distances on the horizontal component in Fig. 4-4 for different site classes. The response spectra for a rock site (class-1) for horizontal component and different distances of 5, 10, 20 and 40 kilometers are assessed using the results presented in Table 4-14 for the magnitude M_w=7.0, see Fig. 4-5. These results show greater amplification of spectral values for the softer soil conditions. The amplification increase approaching towards the site class 4 from the site class 1.

Table 4-14. The coefficients calculated for spectral attenuation in the horizontal component.

$b_1(T).Si + b_2(T)\ (M-6) + b_3(T)\ (M-6)^2 + b_5(T).Ln\ R + \sigma Sa(T).P$								
Iran	***Constant***		***Calculated***					
Period (sec)	***b2***	***b3***	***b1.1***	***b1.2***	***b1.3***	***b1.4***	***b5***	***sigma***
0.10	*0.753*	*-0.226*	0.037	0.304	-0.480	-0.186	-0.037	0.48
0.14	*0.707*	*-0.230*	0.279	0.337	0.015	0.210	-0.054	0.47
0.20	*0.711*	*-0.207*	0.459	0.349	0.257	0.373	-0.102	0.50
0.44	*0.852*	*-0.108*	-0.431	-1.023	-0.986	-0.736	-0.093	0.67
0.70	*0.962*	*-0.053*	-0.459	-0.833	-0.778	-0.231	-0.251	0.74
1.30	*1.073*	*-0.035*	-1.710	-2.537	-2.961	-1.884	-0.178	0.84
2.00	*1.085*	*-0.085*	-1.204	-2.268	-1.154	-1.265	-0.546	0.91

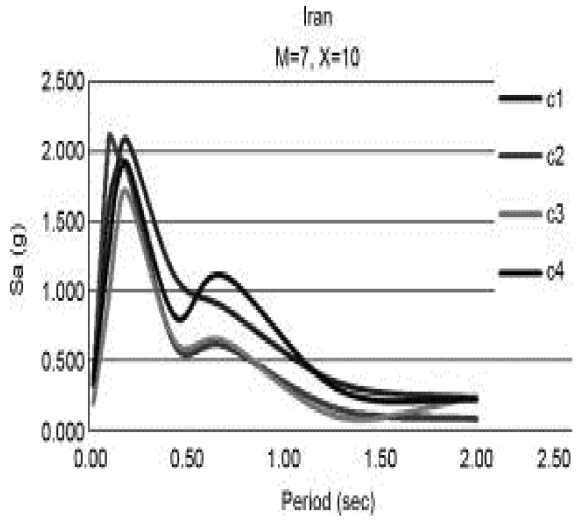

Fig. 4-4. Spectral attenuation for horizontal component, magnitude 7.0, 10km hypocentral distance in site classes 1, 2, 3 and 4.

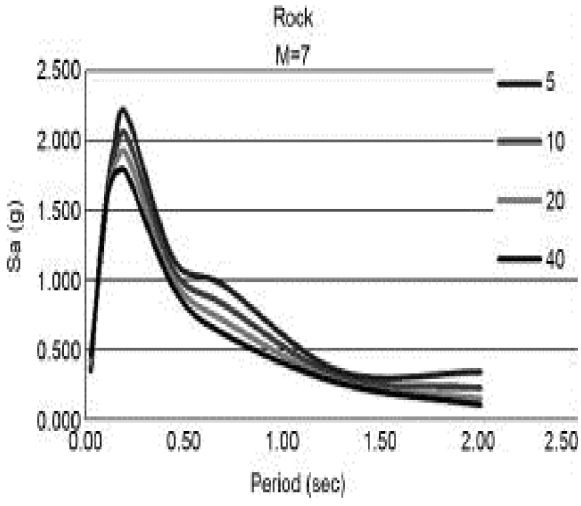

Fig. 4-5. Spectral attenuation coefficient for horizontal component, magnitude 7.0, site classes 1 (Rock) and hypocentral distances of 5, 10, 20 and 40km.

4-6. Spectral attenuation of strong motions in Iran

** **Source Article:** **Zaré, M**. S Sabzali, (2006), "Spectral attenuation of strong motions in Iran", Proceedings of the third international symposium of the effects of surface geology on seismic motion, Grenoble, France, 30 August - 1 September 2006, 10 pages.*

In this section, I present the spectral attenuation of strong motions in Iran, an analysis taken from the published article by Zaré and Sabzali (2006). The scope of this study was to investigate spectral attenuation law for the Iran, using the response spectra of the Iranian strong motion data, in form of different parameters. It was intended to establish the empirical relationships for the strong motions and to observe if any difference may be distinguished in different regions of the country in view point of the attenuation law.

In the present study, the form of a formula already used by Boore et al(1997) is considered:

$$\text{Log Sa} = a_1(T).M + a_2(T).M^2 + b(T).\text{Log R} + c_i(T).S_i + \sigma_{sa}(T).P \qquad (4\text{-}9)$$

The input data consists of 89 three components accelerograms, recorded between 1975 and December 2003 by the IRSC. The waveforms were selected based on their PGA of 0.05g on at least one component and the good signal quality in the low frequency band of 0.3Hz or lesser.

The results of the regressions (Eq. 4-9) are presented in Table 4-15 and Table 4-16 for the horizontal and vertical components, respectively. The coefficients are presented for 22 different periods from 0 sec (PGA) to 4.0 seconds. The response spectra for M_w=7.0 and distance of 10km obtained for different site classes (1 to 4) on the horizontal component is shown in Fig. 4-6-a. These results show greater amplification of spectral values for the softer soil conditions (towards the site class 4). Another response spectra is obtained in Fig. 4-6-b for different site classes (assuming M_w=7.0 and a hypocentral distance of 10km) on the vertical component. Comparing Fig. 4-6-a and b, greater spectral ordinates (of the order of about 20%) is found for the horizontal component.

Table 4-15. The coefficients of attenuation for horizontal component

Period	a_1	a_2	b	c_1	c_2	c_3	c_4	s
PGA	0.5781	-0.0317	-0.4352	-2.6224	-2.5154	-2.4654	-2.6213	0.2768
0.10	-0.1268	0.0378	-0.3554	-0.6127	-0.3864	-0.6271	-0.6789	0.3965
0.12	0.0804	0.0216	-0.3581	-1.2384	-1.0401	-1.2306	-1.2815	0.3964
0.14	0.1785	0.0164	-0.3245	-1.6669	-1.5104	-1.6197	-1.6732	0.4038
0.16	0.2050	0.0156	-0.3154	-1.8400	-1.6829	-1.7759	-1.8045	0.3998
0.18	0.2090	0.0174	-0.3272	-1.9581	-1.7999	-1.8384	-1.8702	0.3979
0.20	0.2816	0.0131	-0.3706	-2.2031	-2.0942	-2.0409	-2.0630	0.3970

0.24	0.3363	0.0093	-0.3544	-2.4600	-2.4147	-2.3231	-2.3132	0.4040
0.30	0.4995	-0.0017	-0.3241	-3.1487	-3.1373	-3.0708	-3.0349	0.4005
0.34	0.5880	-0.0076	-0.3308	-3.4829	-3.5049	-3.4664	-3.4022	0.3926
0.40	0.6728	-0.0139	-0.3166	-3.8298	-3.8950	-3.8717	-3.7706	0.3906
0.44	0.7571	-0.0198	-0.3392	-4.1494	-4.2510	-4.2190	-4.0985	0.3937
0.50	0.7427	-0.0166	-0.3510	-4.2176	-4.3455	-4.3264	-4.1991	0.3975
0.60	0.8631	-0.0239	-0.3638	-4.7556	-4.8980	-4.8942	-4.7262	0.3885
0.70	0.8915	-0.0237	-0.3957	-4.9757	-5.1107	-5.0906	-4.9026	0.3806
0.80	0.8558	-0.0182	-0.4142	-5.0398	-5.1495	-5.1394	-4.9479	0.3863
0.90	0.9180	-0.0228	-0.3836	-5.3799	-5.4849	-5.4762	-5.3091	0.3821
1.00	0.9840	-0.0271	-0.3777	-5.7144	-5.8141	-5.8119	-5.6495	0.3719
1.50	0.8706	-0.0125	-0.4196	-5.7244	-5.8760	-5.8406	-5.6622	0.3559
2.00	0.7104	0.0049	-0.4295	-5.5496	-5.7268	-5.6646	-5.5175	0.3494
3.00	0.5148	0.0227	-0.3788	-5.3979	-5.5819	-5.5157	-5.3762	0.3300
4.00	0.2006	0.0493	-0.3873	-4.6677	-4.8708	-4.7623	-4.5708	0.3172

Table 4-16. The coefficients of attenuation for vertical component.

Period	a_1	a_2	b	c_1	c_2	c_3	c_4	s
PGA	0.5593	-0.0258	-0.6119	-2.6261	-2.6667	-2.5633	-2.7346	0.2961
0.1	-0.2552	0.0561	-0.4854	-0.4866	-0.4764	-0.38	-0.579	0.4282
0.12	-0.1986	0.0535	-0.5125	-0.6966	-0.7456	-0.6132	-0.7568	0.4134
0.14	-0.1104	0.0479	-0.4364	-1.1841	-1.2004	-1.0672	-1.2107	0.4063
0.16	0.0728	0.0346	-0.4739	-1.7724	-1.7558	-1.6578	-1.7811	0.3801
0.18	0.2125	0.0247	-0.4851	-2.279	-2.2396	-2.1349	-2.2567	0.3796
0.2	0.415	0.0075	-0.516	-2.855	-2.8054	-2.7472	-2.842	0.3898
0.24	0.5045	-0.0009	-0.5084	-3.1925	-3.1596	-3.1131	-3.1826	0.3965
0.3	0.757	-0.0204	-0.495	-4.0612	-4.0382	-4.0881	-4.0895	0.4044
0.34	0.7979	-0.0216	-0.486	-4.3081	-4.2664	-4.3771	-4.3293	0.4006
0.4	0.9255	-0.032	-0.4379	-4.7837	-4.7938	-4.9261	-4.8358	0.399
0.44	0.9432	-0.0342	-0.3898	-4.9266	-5.0141	-5.1454	-5.0029	0.3946
0.5	1.158	-0.0509	-0.4054	-5.6335	-5.7361	-5.8479	-5.739	0.3918
0.6	1.0831	-0.0415	-0.3901	-5.6818	-5.8021	-5.8726	-5.7446	0.3693
0.7	1.1669	-0.0445	-0.436	-6.0706	-6.1828	-6.2552	-6.1234	0.3689
0.8	1.2803	-0.0528	-0.4834	-6.4507	-6.5458	-6.6204	-6.4759	0.3667
0.9	1.2743	-0.0502	-0.4723	-6.6025	-6.6969	-6.7364	-6.6349	0.3666
1	1.1663	-0.0379	-0.4453	-6.5341	-6.6488	-6.622	-6.5569	0.37
1.5	1.1954	-0.0382	-0.3742	-6.9971	-7.1584	-7.079	-7.0761	0.384
2	1.0394	-0.0212	-0.3457	-6.8936	-7.063	-6.8969	-6.9362	0.3713
3	0.4556	0.0315	-0.3462	-5.5778	-5.7703	-5.691	-5.6513	0.3562
4	0.3087	0.0434	-0.2749	-5.4165	-5.5875	-5.4693	-5.4951	0.3311

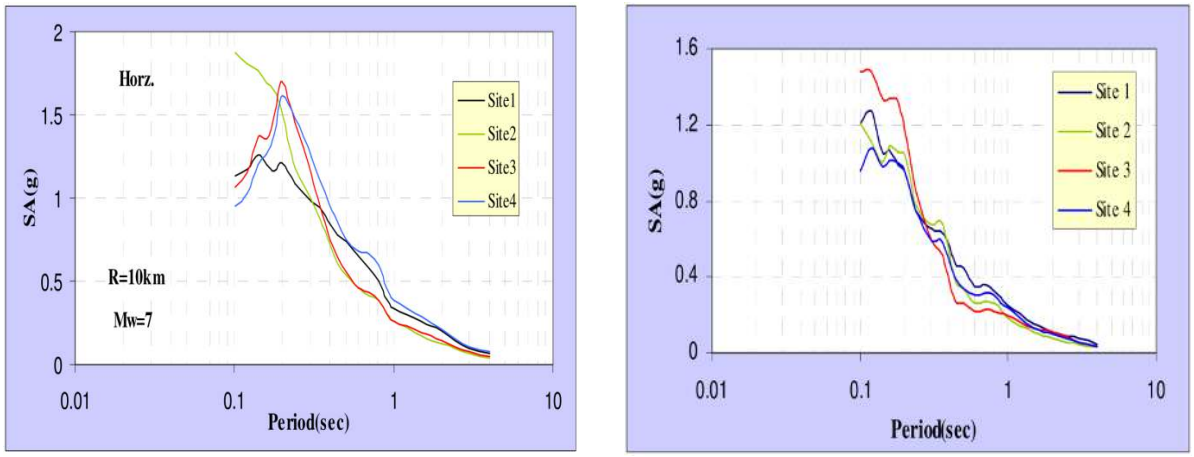

(a) (b)

Fig. 4-6. Response spectra obtained by the attenuation coefficients obtained for the horizontal (a) and vertical (b) component, for M=7.0, hypocentral distance of 10km and different site classes.

4-7. Macroseismic intensity and attenuation laws: a study on the intensities of the Iranian earthquakes of 1975-2000

** **Source Article:** **Zaré M**. and Memarian H., (2003), "Macroseismic Intensity and Attenuation laws: A Study on the Intensities of the Iranian Earthquakes of 1975-2000", 4th International Conference of Earthquake Engineering and Seismology, 12-14 May 2003 Tehran, Iran, 8 pages.*

A catalog for the earthquakes since 1975 until 2000 was prepared that comprises the 470 intensity values for which the information for the localities of reported or estimated intensity values and the earthquake source specifications could be found (see section 2-3-6, catalog developed by Zare and Memarian, 2002).

Attenuation of intensities in Iran:

At first, the regression was performed without the site condition coefficients. The regression was performed for intensity (as a dependent parameter) and magnitude (M_w) and epicentral distance (to be taken as horizontal distance to the fault/source, in km) based on the following simple model. This model considers the an-elastic attenuation geometric expansion separately, as proposed by Ambraseys (1995);

$$I=a.M -b.X - c\ln X +\sigma.P \qquad (4\text{-}10)$$

The coefficient for this attenuation formula is presented as given in Table 4-17. Another attempt is carried out for intensity (as a dependent parameter) and macroseismic intensity (I_0), and the macroseismic epicentral distance (to be taken as horizontal distance to the fault/source, in km) based on the equation 4-11. The coefficients for such equation are represented in Table 4-18.

$$I=a.I_0 -b.X - c\ln X+ \sigma.P \qquad (4\text{-}11)$$

Table 4-17. The coefficients for the equation 4-10, R is the coefficient of correlation

Region	a	b	c	σ	R (Correlation)
Alborz-C.Iran	1.207	0.0126	0.227	0.92	0.88
Zagros	1.148	0.0214	0.120	0.72	0.94
IRAN	1.175	0.0140	0.227	0.88	0.77

Table 4-18. The coefficients for the equation 4-11, R is the coefficient of correlation

Region	a	b	c	σ	R (Correlation)
Alborz-C.Iran	0.994	0.0160	0.212	0.92	0.86
Zagros	0.942	0.0152	0.188	0.88	0.77
IRAN	0.942	0.0162	0.196	0.91	0.82

To consider the site conditions the same procedure explained for equation 4-10 is taken in equation 4-12 by adding the site coefficients (to be either 1 or 2 as explained above for hard or soft soils respectively). The coefficients for such equation are given in Table 4-19. Another attempt similar to equation 4-11 is carried out for intensity (as a dependent parameter) and macroseismic intensity (I_0) as independent parameter, adding the "site" parameter, in equation 4-13. The coefficients for such equation are represented in Table 4-20.

$$I=a.M -b.X - clnX+ ci.Si +\sigma.P \quad (4\text{-}12)$$

$$I=a.I_0 -b.X - clnX+ ci.Si +\sigma.P \quad (4\text{-}13)$$

Table 4-19. The coefficients for the equation 4-12, R is the coefficient of correlation

Region	a	b	c	d_1	d_2	R (Correlation)
Alborz-C.Iran	1.268	0.0142	0.256	-1.061	-1.590	0.8
Zagros	1.107	0.0188	0.227	-0.040	0.566	0.55
IRAN	1.279	0.0125	0.270	-1.274	-1.600	0.76

Table 4-20. The coefficients for the equation 4-13, R is the coefficient of correlation

Region	a	b	c	d_1	d_2	R (Correlation)
Alborz-C.Iran	0.719	0.0146	0.221	1.806	1.524	0.84
Zagros	0.702	0.0178	0.202	1.577	1.275	0.72
IRAN	0.746	0.0142	0.226	1.422	1.280	0.79

Conclusion:

The attenuation model fit the earthquake intensities in Iran are presented considering the magnitude or macroseismic intensities and for the cases when we consider or not the site effect parameter. Based on the dispersion of the site effect estimations, it is recommended to use the attenuation laws which are developed in this study with no consideration of site effects. The general (form of the attenuation of intensities in Iran follows the attenuation model of acceleration for Iran (Zaré 1999).

4-8. Attenuation law for the strong-motions in Iran

** **Source Article:** **Zaré, M**., M Ghafory-Ashtiany, PY Bard, (1999), "Attenuation law for the strong-motions in Iran", Proceedings of the third international conference on seismology and earthquake engineering, pp. 345-354.*

The attenuation of the Iranian strong motion is studied using the Iranian strong motions database. This database comprised 468 three-component well recorded data (analog and digital) for which the teleseismic source parameters were available, or calculated from the strong motion records. The two-step used attenuation model used in this study is:

$$\log A = a.M - b.X - d.\log X + c_i.S_i + \sigma.P \quad , i = 1, 2, 3, 4 \qquad (4\text{-}14)$$

Where A is strong motion parameter, M is the moment magnitude, X is the hypocentral distance. The coefficients a, b and c_i are the coefficients of magnitude, anelastic attenuation with the distance and site effects (as c_1, c_2, c_3 and c_4 for the four-class site classification by Zare et al., 1999; see Table 3-2 in section 3-3-2) respectively. The sigma term represent the 84.1% standard deviation with P=1 to be added to the mean (50% values; P=0). The d coefficient for the logX term is introduced to allow a geometrical expansion which may be different from the body wave 1/x dependence. The regression were performed in this paper for various ground motion parameters; PGA, PGV and PGD.

Database

The database used as the input for this study consists of 468 three-component accelerograms (169 analog by SMA-1 instruments and 299 SSA-2 records) recorded between 1975 and February 1996 by the Iran Strong Motion Network. The magnitude range for the whole dataset of records was 2.7 to 7.4, and the range for hypocentral distance was 4-224 km.

Results:

The results of regressions are presented in this paper in the form of peak values. The values of the coefficients for the maximum of strong motion parameters (PGA, PGV and PGD) are estimated in Table 4-21 to 4-23 for d=1. The "b" values, which represent the anelastic attenuation, found to be the positive values in some cases in Table 4-21 to 4-23. Such condition, that does not seems to be normal, might be concerned to the fixed values of logX term in our regression, however the values of "b" are very low.

Table 4-21. Coefficients for the attenuation of PGA, for 468 cases

Region	a	b	c_1	c_2	c_3	c_4	Sigma
Alborz-C.Iran (*vertical*)	0.322	0.0003	-0.828	-0.754	-0.971	-0.788	0.352
Alborz-C.Iran (*horizontal*)	0.322	0.0004	-0.688	-0.458	-0.720	-0.585	0.394
Zagros (*vertical*)	0.406	-0.0038	-1.262	-1.333	-1.230	-1.777	0.356
Zagros (*horizontal*)	0.399	-0.0019	-1.047	-1.065	-1.020	-0.975	0.329
Iran (*vertical*)	0.362	0.0002	-1.124	-1.150	-1.139	-1.064	0.336
Iran (*horizontal*)	0.360	0.0003	-0.916	-0.862	-0.900	-0.859	0.333

Table 4-22. Coefficients for the attenuation of PGV, for 381 cases

Region	a	b	c_1	c_2	c_3	c_4	Sigma
Alborz-C.Iran (*vertical*)	0.466	0.0014	-3.108	-3.178	-3.328	-3.069	0.363
Alborz-C.Iran (*horizontal*)	0.471	0.0006	-2.865	-2.896	-2.969	-2.737	0.360
Zagros (*vertical*)	0.612	0.0028	-4.011	-4.101	-3.984	-3.917	0.319
Zagros (*horizontal*)	0.588	0.0040	-3.627	-3.651	-3.632	-3.502	0.315
Iran (*vertical*)	0.548	0.0018	-3.675	-3.761	-3.702	-3.610	0.336
Iran (*horizontal*)	0.538	0.0014	-3.335	-3.360	-3.348	-3.224	0.338

Table 4-23. Coefficients for the attenuation of PGD, for 346 cases

Region	a	b	c_1	c_2	c_3	c_4	Sigma
Alborz-C.Iran (*vertical*)	0.828	-0.0029	-5.861	-6.127	-6.023	-5.753	0.521
Alborz-C.Iran (*horizontal*)	0.828	-0.0036	-5.694	-5.837	-5.771	-5.352	0.489
Zagros (*vertical*)	0.784	0.0084	-6.043	-6.164	-6.144	-6.109	0.312
Zagros (*horizontal*)	0.797	0.0086	-5.893	-5.973	-5.954	-5.743	0.334
Iran (*vertical*)	0.830	-0.0003	-6.051	-6.213	-6.136	-6.081	0.337
Iran (*horizontal*)	0.829	-0.0010	-5.831	-5.942	-5.899	-5.645	0.388

Main articles of this chapter:

Vaez Shoushtari, A., B. A. Azlan , and **Zaré M**, (2016), "On the selection of ground–motion attenuation relations for seismic hazard assessment of the Peninsular Malaysia region due to distant Sumatran subduction intraslab earthquakes", *Soil Dynamics and Earthquake Engineering*, 82, 123–137. DOI: 10.1016/j.soildyn.2015.11.012.

Zaré M, (2016), " Recent development of the earthquake strong motion-intensity catalog and intensity prediction equations for Iran ", *Journal of seismology*, DOI: 10.1007/s10950-016-9622-4.

Vasheghani Farahani J, **Zaré M**, Cichowicz A, (2012), "Attenuation of high-frequency P and S waves in south and southeast Tehran using blast data", *Soil Dynamics and Earthquake Engineering*, Volume 40, September 2012, Pages 99–108.

Ghasemi H , **Zaré M**, Y. Fukushima, K. Koketsu, (2009), "An empirical spectral ground-motion model for Iran", *Journal of Seismology*, Volume 13, Issue 4, pp 499-515, DOI 10.1007/s10950-008-9143-x.

Ghasemi H., **Zaré M** and Y Fukushima, (2008), "Ranking of several ground-motion models for seismic hazard analysis in Iran", *Journal of Geophysics and Engineering*. 5, pp. 301–310.

Zaré M., S. Karimi-Paridari, and S. Sabzali, (2008), "Spectral Attenuation of Strong Motions for Near Source Motions in Iran", *Journal of Seismology and Earthquake Engineering (JSEE)*, Fall 2008, Vol. 10, No. 3. Technical Note. Pp147-152.

Zaré, M. S Sabzali, (2006), "Spectral attenuation of strong motions in Iran", *Proceedings of the third international symposium of the effects of surface geology on seismic motion*, Grenoble, France, 30 August - 1 September 2006, 10 pages.

Zaré, M. and Memarian., H, (2003), "Macroseismic Intensity and Attenuation laws: A Study on the Intensities of the Iranian Earthquakes of 1975-2000", *4th International Conference of Earthquake Engineering and Seismology,* 12-14 May 2003 Tehran, Iran, 8 pages.

Zaré, M., M Ghafory-Ashtiany, PY Bard, (1999), "Attenuation law for the strong-motions in Iran", *Proceedings of the third international conference on seismology and earthquake engineering*, pp. 345-354.

Chapter 5: Seismic Hazard Analysis

In the current chapter, I explain my most important studies or research collaborations on seismic hazard assessment and its related concepts. The chapter starts with the review of seismic hazard analysis in Iran and its challenges, introducing the studies on seismic sources and magnitude assessments and terminates to the seismic hazard studies which I was involved in. In this regard, at first, I review the studies of the seismic hazard analysis of Iran performed during the last 40 years in the section 5-1 and then I will point out the challenges of such studies in Iran in the section 5-2. In the sections 5-3 and 5-4, I will describe the researches on seismotectonic and source identification and earthquake magnitude evaluation, respectively; the studies which I contributed in. I then demonstrate the recent studies on the seismic hazard in Iran and some parts of Asia in the sections 5-5 and 5-6, respectively.

5-1. Seismic hazard zoning in Iran: a state-of-the-art on the studies during four decades

** **Source Article:** **Zaré M**, (2017), "Seismic hazard zoning in Iran: a state-of-the-art on the studies during four decades", JSEE, Vol 19, No 2, pp 71-101.*

It is efficient to carry out earthquake hazard analysis of seismically active regions for the earthquake resistant design of civil structures. In this respect, it is essential to have the fullest possible understanding of earthquake hazard by preparing detailed seismic zoning maps in terms of intensity, peak ground motion parameters, spectral accelerations and etc. The output of a seismic hazard zoning map depend on completeness level and accuracy of available data and analysis method. The better input for hazard analysis results in more reliable parameters and seismic hazard assessments.

Iran is considered as one of the most seismically active regions in the world faced with different earthquakes each year. Active tectonic conditions, existence of different faults and seismic sources and a large population in earthquake-prone areas, makes it necessary to perform more considerations and scientific studies in order to analyze the seismic risks.

The seismic hazard zoning maps are developing in Iran using seismicity and active tectonic data since the mid-1970s. The analysis have been expressed using different seismic parameters. The studies to determine the level of seismic hazard in Iran were established using active fault maps, iso-intensity maps of major earthquakes, seismotectonic map (e.g. Nowroozi, 1976; Berberian, 1976a; Berberian, 1976b; Nogol Sadat, 1993; Ramazi, 1995;

Tavakoli, 1996; Mirzaei et al., 1998; Zare and Memarian, 2000; Mojarab et al., 2014) as well as an earthquake catalog of Iran (Ambraseys and Melville, 1982; Berberian, 1994; Moinfar et al, 1994; Mirzaei et al., 1997; Shahvar et al., 2013; Karimiparidari et al.,2013).

Continuous improvement in providing earthquake catalogs, defining seismotectonic provinces and intensities has led to evolution of the hazard analysis. The first generation of seismic hazard maps were developed based on the deterministic approach in terms of maximum intensity levels. Then, by progress in data completion and methods, the probabilistic approaches in terms of peak ground accelerations were proposed (Cornell, 1968; Algermissen et al., 1982). Most of the probabilistic seismic hazard analysis (PSHA) involve several steps as below:

- Definition of the nature and locations of earthquake sources.
- Seismicity and frequency-magnitude relationships for the sources.
- Attenuation of ground motion with distance from the sources.
- Determination of exceedance probability at given sites.

In this section, some of the most important seismic hazard zonings in Iran during the last four decades are explained. The trend of such zoning studies started by deterministic approaches, continued by probabilistic approaches and finally is under consideration in terms of spectral zoning maps. It is tried to depict the development history of seismic hazard zoning in Iran which starts from 1977 by Neghabat and Liu and terminates to the last updated version carried out by Zare et al (2015).

Development History of the Seismic Hazard Zoning Studies in Iran

Since the mid-70's by 2015, dozens seismic hazard analysis have been carried out for the country and its regions, employing different data and methods.

In 1977, Neghabat and Liu prepared an earthquake microzonation analysis of Iran. They initially divided the geological area of Iran into four seismic regions including the Zagros folded belt, the Rezaiye-Esfandagheh orogenic belt, the central and southeast Persia and the Alborz ranges. Each of the four regions were divided into several sub-regions as earthquake source zones in order to be analyzed separately. The earthquake database of their analysis comprised of the instrumental mainshocks with Richter magnitude greater or equal to 4, recorded during 1900-1970. Then, the probability of the maximum earthquake intensity for each independent zone was determined based on different statistical and probabilistic

relationships such as Gutenberg-Richter reoccurrence relation, arrival rates and attenuation functions and the seismic hazard method developed by Cornell (1968). Finally, by synthesizing the results of the four mentioned geological regions, a general isoseismic contour map was presented for the entire country in terms of the Modified Mercalli intensity corresponding to various return periods of 20, 100, 500 and 2500 years. Neghabat and Liu (1977) concluded that the highest intensity levels occur in the northeastern section of the country which is expected according to the relatively shallow depth of earthquakes i.e. 15 kilometers in this region. A lower intensity level belong to the Persian Gulf, northwestern of Iran and the lowest risk areas occur basically in the northwest between Tehran and Tabriz and the central and southeastern part of the country.

In the same year, Berberian and Mohajer-Ashjai (1977), prepared another seismic hazard map of Iran based on the deterministic estimate of the maximum intensity, adding other available data such as historic earthquakes, effects of the major Quaternary and active faults of the country. Their paper presents a deterministic estimate of the maximum intensity levels to be expected in different parts of Iran.

Mohajer-Ashjai and Nowroozi (1978) used thirteen available isoseismal maps of Iranian major earthquakes, reports of historical damages, distribution of moderate and large earthquakes and post Quaternary faults and volcanoes to construct two intensity zoning maps for Iran. The first map was prepared on the basis of observed and calculated intensities in which 5 zones were introduced. The second map consisted of probable intensity zones which were calculated assuming seismic activity of post-Quaternary faults.

Berberian (1981) also depict a seismic hazard zoning map in terms of intensity in which the values were not expressed as the maximum possible intensities but the most probable intensities. Looking at the map reveals that the third zone with maximum intensity covers the region of Quaternary faults and the area associated with past destructive earthquakes.

Up to this time, most of the seismic hazard studies were concentrated on deterministic estimation of the intensity parameter. Since then, by progress in data collection and statistical methods, the probabilistic approach was employed to calculate the probable peak ground accelerations. The PSHA method takes all possible earthquake occurrences and ground motions into account to calculate a combined probability of exceedance that incorporates the relative frequencies of occurrence of different earthquakes and ground-motion characteristics.

The first probabilistic hazard analysis in terms of PGA versus annual risk and return period was carried out by Bozorgnia and Mohajer-Ashjai in 1982. For this purpose, they used

a catalog of 2346 recorded instrumental events during 1900-1981 in Iran. They also modeled a total number of 324 seismic sources from which 304 were fault segments and 20 were area sources. They finally presented the probable PGA in 25 major cities of Iran corresponding to 20, 50, 100, 150, 200, 500, 1000 and 10,000 years return periods.

Nowroozi and Ahmadi (1986) also conducted a PSHA for Iran using seismotectonic province model and compiled and statistically treated earthquake data of each province. They first calculated the coefficients of a log-linear and a log-quadratic magnitude frequency relationship and estimated the PGA for a set of return periods and epicentral distances and noted the substantial variations in return periods for a given earthquake magnitude.

Another important seismic hazard zoning for the country has been produced as an attachment of the Iranian seismic code for buildings (known also as the Standard No. 2800). Until now, four editions of the Standard 2800 have been published and updated in 1988, 1999, 2007 and 2012, respectively (Fig. 5-1- a, b, c). All maps have been prepared based on the study on relative seismic hazard zoning using different seismic, tectonic and geology data. To produce the seismic hazard zoning maps with relative earthquake hazard, seismic history, known Quaternary faults, seismotectonic maps and attenuation relations were applied as the main data. In addition, some important factors such as considering the socio-economic importance of different cities and possibility of unknown Quaternary faults were also usually taken into account. Last version of this map was published in 2012 for which a comprehensive study on some disciplines, or revision of some important aspects was carried out. For instance, a new fault map was compiled in the scale of 1:1,000,000 in which 700 faults with over 20 km in length were identified meanwhile magnetic basement lineaments were removed. A refined and updated catalogue of the Iranian earthquakes including historic to 2011 events was compiled with the expertise judgments. In addition other data such as tectonic condition of different parts of the country, seismic sources, recorded strong motion data, and the case studies of important structures' sites such as dams and power plants were also used. On the basis of combination of these updated data, a hazard map was produced which divides the country into four zones with design base accelerations of 0.35g, 0.30g, 0.25g, and 0.20g (Fig. 5-1-c). The defined zones are rated as very high, high, moderate, and low hazard, respectively. This map indicates that about 70% of the area in the map corresponds to 0.30g (high hazard) zone.

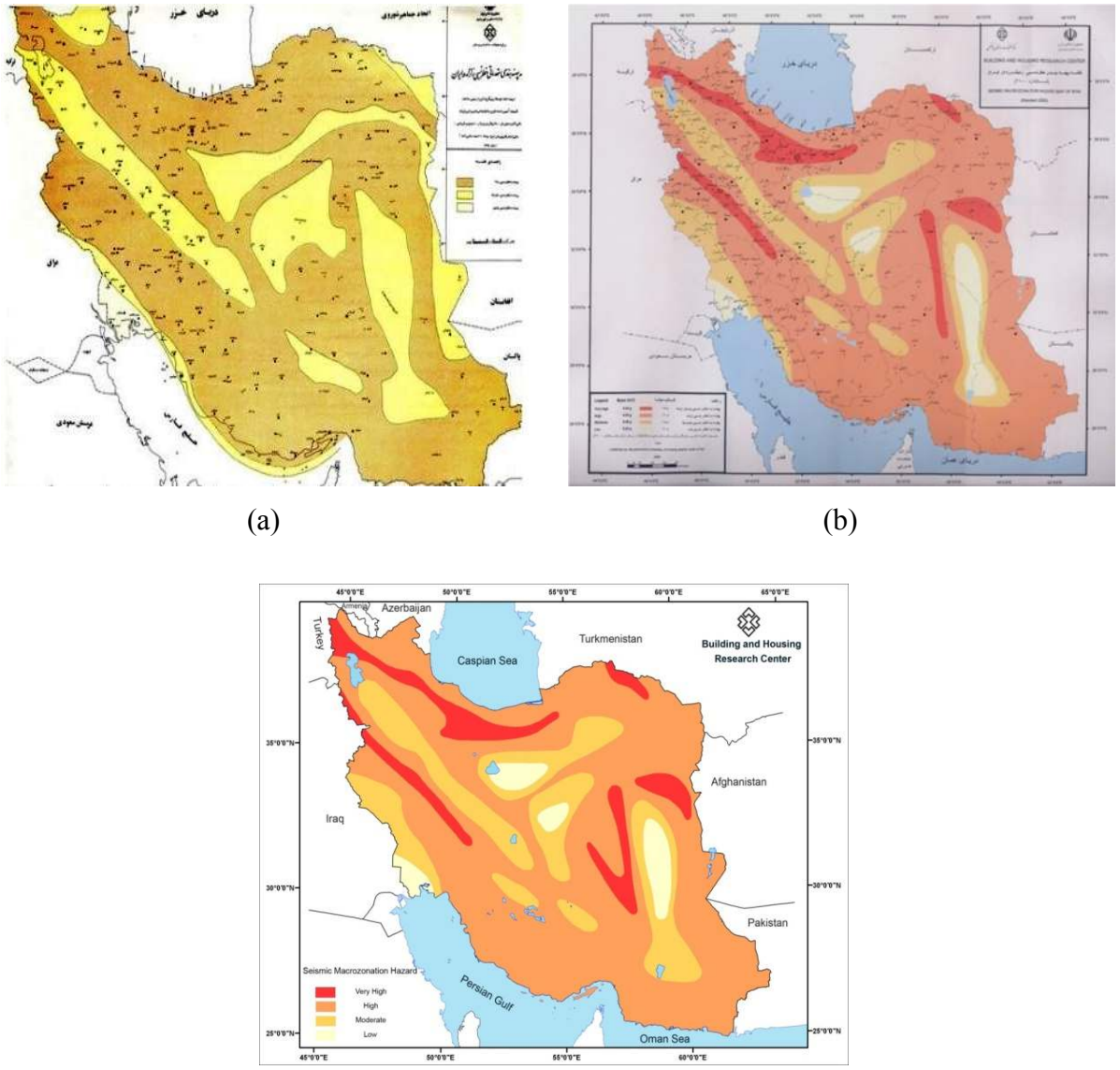

(a) (b)

(c)

Fig. 5-1. Seismic macrozonation hazard map of Iran as an attachment to the Standard 2800 published in: 1999 (a) 2007 (b) and 2012 (c).

Tavakoli and Ghafouri-Ashtiani (1999) prepared seismic hazard maps of Iran in the forms of iso-acceleration contour lines and seismic hazard zoning using PSHA method on the basis of three kinds of data: earthquake database, seismotectonic provinces and attenuation relationships. In their study, the computer program SEISRISK III was applied to calculate the PGA. Accordingly, the two mentioned maps (contour lines and zoning) were originally presented on 1:5000000 scale. These maps indicated that the minimum and maximum accelerations ranged from 15% to 48% g. The highest PGA were predicted to be 0.45g and 0.3g for return periods of 475 and 75, respectively, encompassing North Tabriz, North

Tehran and Dasht-e-Bayaz fault zones. The lowest PGA were predicted to be less than 0.35g and 0.2g for return periods of 475 and 75, respectively, for a narrow NW-SE band from Urumiyeh to Esfahan and in the Central Lut zone. It is notable that the calculated PGA is corresponding to the maximum horizontal acceleration in bedrock level and the PGA on surface soil level should be then calculated for each region using proper attenuations relations and soil profiles. Their results were then also published in the Global Seismic Hazard Assessment Program (GSHAP, 1999) (Fig 5-2).

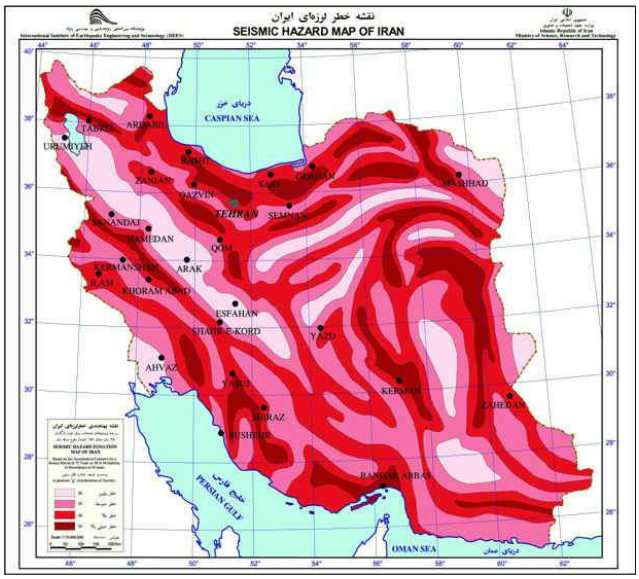

Fig. 5-2. seismic hazard zoning of Iran. four zone levels are defined, rated as: very high hazard, high hazard, moderate hazard and low hazard (GSHAP, 1999).

Mäntyniemi et al. (2007) used a new method called "parametric-historic" (Kijko and Graham, 1999) to map PGA, PGV and PGD. This method does not require any definition of seismic sources and/or seismic zones and permits the use of both incompletely reported historical and complete instrumental earthquake catalogs as input data, considering the inherent magnitude errors and uncertainties of earthquake locations. Mäntyniemi et al. (2007) used 3345 earthquake mainshocks on the M_w scale in the time span of 734-2002 which was compiled by Zare (2002). Using the data and employing the Iranian attenuation relationship given by Zare et al (1999), final seismic hazard map was prepared which specified a 10% probability of exeedence of the given horizontal PGA values for an exposure time of 50 years, corresponding to a return period of 475 years. The soil category of rock and stiff sediments was assumed. The new map does not show such strong elongation of contours as

previous works that are based on assumptions of seismotectonic units. In this new one the resulting PGA values are lower than those of previous works which can be resulted from a different methodology.

In 2008, with regard to earthquake hazard mitigation program and retrofitting of structures, infrastructures and lifelines, a new detailed seismic hazard analysis project was proposed by the President Deputy Strategic Planning and Control of Iran. The project was divided into 7 phases for which six different regions of the country containing the Greater Tehran, Alborz, northwestern Iran, eastern Iran, central Iran and south of Zagros were considered for seismic hazard analysis for which their results will be further combined to derive a unique map for the country. Up to now, the first phase of the program (the Greater Tehran) has been published under the consideration of the faculty of engineering, University of Tehran (Gholipour et al, 2008). The next two phases (Khorasan and Azarbaijan regions) are currently being done under consideration of the Geological Survey of Iran. In addition, with respect to significant importance of the plan, the responsibility of monitoring the plan was assigned to the road, housing and urban development research center. In the first phase for the Greater Tehran region, available surface/subsurface geophysical, seismological, geotechnical, geodetic and hydro geological characteristics of the project area was first evaluated. The analysis resulted in preparing a seismic hazard map in which maximum acceleration of an earthquake with a determined occurrence probability is presented. Keeping in mind the different kinds of uncertainties for earthquake size and location and future triggering, the analysis has been performed for events of 2%, 5%, 10% and 50% occurrence probabilities in 50 years and for different soil profiles including 150, 255, 525, 760 and 1070 m/s shear wave velocities. In addition, uniform seismic response spectra and simplified uniform spectra for 475-year and 2475-year return periods were also presented.

In 2012, several seismic hazard analysis were published for the country. Moinfar et al. (2012) published a paper on the subject defining the trend of preparing seismic hazard map for the Iranian seismic code for buildings. They tried to make *"a comparison between the base accelerations of the updated Iranian seismic hazard map with those of the neighbor countries. This comparison shows that there is a relatively good agreement with countries located in the west and northwest of Iran, while there are some disagreements with the northeast and eastern neighbors"* (Moinfar et al., 2012). Therefore, their finding recommends that a future collaboration between the countries in the region can aim to develop a unified seismic hazard zoning map for the region and the Middle East.

At the same time, Zare (2012) introduced a new map based on new seismic source determination. The determination of seismic source zones were performed using the up-to-date geophysical and geodetical measurements. The new data showed that the revision in seismic hazard zoning maps in local and regional (nation-wide) scale is necessary. In his study, new map was prepared according to new seismic source data and parametric method (Fig. 5-3).

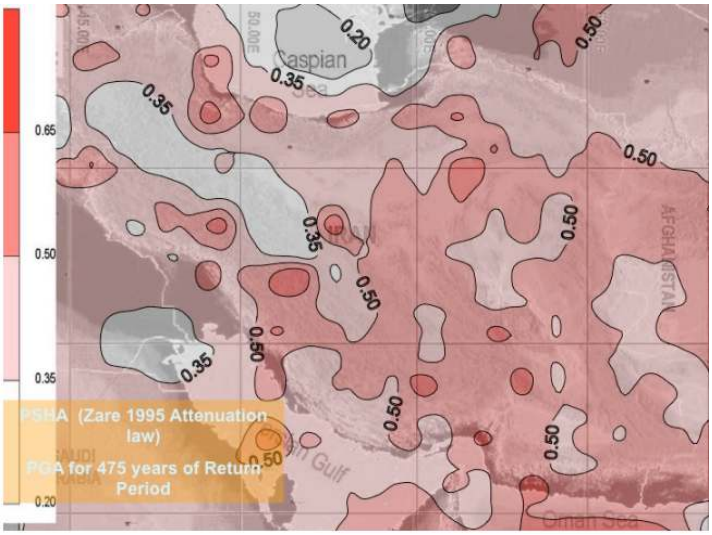

Fig. 5-3. Seismic Hazard Zoning for Iran, using parametric method and assessing PGA for 475 years of return period (Zare, 2012).

Hamzehloo et al. (2012) also developed new seismic hazard maps for Iran based on probabilistic earthquake hazard analysis. As the first step, necessary data were provided. The IIEES catalogue, which is based on the reports from International seismological institutes, and reports from Ambreseys and Melville (1982) were used, considering moment magnitude (M_w) in all calculations. In this respect, the authors estimated the seismicity parameters and the return period for different earthquake magnitudes using the Kijko (2000) method which makes it possible to combine the information of the historical part of earthquake catalog with those of the instrumental part. The method is based on assumption of the Poisson occurrence of earthquakes with the activity rate of λ and the doubly truncated Gutenberg- Richter distribution. On the basis of geological and seismological studies, Hamzehloo et al. (2012) found 25 source zones in which seismicity parameters were estimated after omitting foreshocks and aftershocks from the catalogue. In addition, four attenuation relationships (Ghasemi et al., 2009; Boore et al., 1997; Campbell and Bozorgnia, 2003; Abrahamson and

Silva, 1997) were also considered. They also presented the disaggregation and uniform hazard plots showing the contribution of hazard for major cities in Iran.

Yazdani and Kowsari (2013), for the first time, used time-independent Bayesian probability method to assess seismic hazard in Iran. The earthquake database they used in the prior estimation contained 140 historical and 495 instrumental events. *"The Bayesian approach was applied to calculate the probability that a certain cut-off magnitude would be exceeded at certain time intervals in different regions of Iran"* (Yazdani and Kowsari, 2013). The results for the cut off magnitude of 6.5 indicated that the highest probability of seismic hazard exists in the Alborz, Kopeh-Dagh, Bandar-Abas, Kerman, and Zagros regions. The seismic hazard was assessed to be lowest for the Esfahan–Sirgan region, the Arabian Platform, the Persian Gulf, and Kavir in Central Iran. Based on their results, the comparison of results between the Bayesian method and previous seismotectonic models of Iran revealed the ability of the Bayesian method to identify seismotectonic provinces based on earthquake data alone. They also explained that identification of different seismotectonic provinces with similar characteristics in a region of intensity is one of the most important goals of seismic hazard studies. This task is usually completed by subjective interpretation, based on geological and seismotectonic information. It should be emphasized that Bayesian updating is a strong tool that can be used for more reliable geological and seismological interpretation.

Recently, a comprehensive earthquake seismic hazard analysis was performed in the framework of EMME (Earthquake Model of the Middle East Region) project. The EMME Project is a regional project of the umbrella GEM (Global Earthquake Model) project. The PSHA approach and the existing source models were revised or modified by the incorporation of newly acquired data. More importantly, the most distinguishing aspect of the EMME project from the previous ones is its dynamic character. This very important characteristic is accomplished by the design of a flexible and scalable database that will permit continuous update, refinement, and analysis. In 2013, a part of the project was finished and new seismic hazard maps were released (for more details, see section 5-6-1).

In the early 2015, Mousavi Bafrouei et al. published new PGA and spectral acceleration (SA) hazard maps of Iran using a modified probabilistic seismic hazard assessment, developed by Chinese researchers. As the input data, they used a unified catalog of de-clustered earthquakes containing both historical and instrumental until late 2012 as well as an area source model which contains 238 potential seismic sources within 5 major seismotectonic provinces. For each seismotectonic provinces, seismicity parameters and

background seismicity were determined. Then seismic hazard assessment of Iran for a grid of over 40,000 points with 10 km interval was carried out using OpenQuake software by three different GMPEs (Boore and Atkinson, 2008; Chiou and Youngs, 2008; Campbell and Bozorgnia, 2008) and two models of seismicity for potential seismic sources in a logic tree. Finally, Mousavi Bafrouei et al. (2015) calculated the PGA and SA for 5% damping ratio at 0.2 and 2 seconds corresponding to 10% and 63% probability of exceedance within 50 years (475-year and 50-year mean return periods, respectively). They found the maximum and minimum PGA for 475-years return period to be 0.63g in North-East of Lorestan and 0.1g in central Iran, respectively. They also found that the comparison of their results with the last version of the seismic hazard map in Standard 2800 and showed significant differences, so that seismic hazard levels estimated in this study in southern Iran, Sistan-Baluchestan, Hormozgan and Fars provinces, indicated significantly higher values.

The most recent seismic hazard map of Iran was developed using the most recently comprehensive data and a PSHA approach by Zare et al. (2015). In this regard, a homogeneous earthquake catalog of Iran developed by Karimiparidari et al (2013) was used, which includes the Iranian events in terms of uniform moment magnitudes (M_w) with the range of M_W 3.5–7.9 from the 3rd millennium BC to April 2010. Until now, this catalog seems to be the most comprehensive data, since it covers a wide time span of earthquake history and contains of uniform scaled magnitudes. Zare et al., (2015) used new seismic source models and seismotectonic zoning map of Iran (Karimiparidari et al., 2011). This seismotectonic models were developed based on the latest data of active tectonic, topography, magnetic intensity and seismicity catalog. These new maps divide the area of Iran into 27 seismotectonic zones and demonstrate two models for linear and regional seismic sources. Modification and computation local coefficients of the space-time windows in the well-known window algorithm developed by Gardner and Knopoff (1974), was also performed in the research by Zare et al., (2015). To modify the space-time windows, the well-documented events of Iranian earthquake catalog in the time period of 1972 to 2008 were used. The data contains 21 different sequences of mainshocks and aftershocks with the magnitude of the mainshocks ranged between Mw 5.4 and 7.1. The updated temporal and spatial windows were applied to the seismic catalog in different seismotectonic zones of Iran. After declustering, the seismic catalogs were found to follow a Poisson distribution in all studied zones based on the results of the statistical Kolmogorov-Smirnov test. The same test on times between successive declustered events shows that the inter-event times of all catalogs follow

an exponential distribution. Following the removal of foreshocks and aftershocks, magnitude of completeness of each seismotectonic zone was established for the entire time span of the catalog. They also made a comparison study on available strong motion attenuation relations to select proper models and weight them in a logic tree. In this respect, six attenuation models (including Ghasemi et al., 2009; Zafarani and Soghrat, 2012; Boore and Atkinson, 2008; Akkar and Cagnan, 2010; Ambraseys, 2005) which had the best coincidence to the Iranian data were used to conduct the PSHA. In this respect, for each seismotectonic zone, very lower level of its seismicity was considered as the background seismicity. Frequency of earthquakes was attributed to each zone using the ratio of the uncovered area by sources to the total area of zone. In the following, seismicity parameters were calculated and the probabilistic source-based approach established by Cornell in 1968 was followed by different branches defined in logic tree. Accordingly, a grid network with 0.2*0.2 square kilometers cells in the area of study was taken into account and seismic hazard zoning map of Iran with 475-year return period was prepared using CRISIS2007 software and Kriging interpolate method. (For more details, see section 5-5-1).

The seismic hazard zoning maps are developing in Iran using seismicity and active tectonic data since the mid-1970s. During the first years of this four decades, studies mostly focused on deterministic earthquake intensity approaches. Developing strong motion data, attenuation relations and probabilistic methods, probabilistic maximum acceleration approaches were replaced to the deterministic intensity method. Most of the recent seismic hazard analysis studies and projects were conducted based on PSHA method, meanwhile some other mathematical/statistical algorithms were rarely used.

Although the deterministic and probabilistic PGA methods are efficient, some other modern seismic hazard analysis approaches are currently proposed in the world such as spectral analysis, neo-deterministic and realistic acceleration approaches. It is expected that the further studies to be focused on the new approaches as well as the developing of spectral zoning maps, a new focus on M_{max} assignments and incorporation of seismic historical data in hazardous region having rare instrumental seismicity data. Meanwhile some tools are provided in the 10 recent years such as defining spectral attenuation models by different researches (e.g. Khademi, 2002; Ghodrati Amiri et al., 2007; Zaré et al., 2008; Zafarani et al., 2008; Ghasemi et al., 2009; Sadeghi et al., 2010; Ghodrati Amiri et al., 2010; Bagheri et al., 2011; Saffari et al., 2012; Hamzehloo and Mahood, 2012; Soghrat et al., 2012; Zafarani and Soghrat, 2012; Kale et al., 2015) which may provide new tools for further hazard zone

mapping in Iran. There are currently published some spectral acceleration hazard maps (e.g. Hamzehloo et al., 2012; Mousavi Bafrouei et al., 2015). and a comprehensive study is under preparation by IIEES.

The future trend in hazard mapping seems to cover the intensity assessment, realistic acceleration and the neo-deterministic approaches and also the development of site specific hazard analysis for Iran based on the detailed integrated the site characteristics database.

5-2. Challenges of seismic hazard analysis in Iran

Some recent earthquake occurrences in Iran have shown that in some cases, earthquake hazard assessments have failed to correctly predict the real ground motions and intensities. As mentioned before, such condition goes back to lack of enough data and uncertainties in attenuation, maximum magnitudes and algorithms. Although there are fairly good recorded historic and instrumental data in Iran and good researches on some critical active faults of the Iranian Plateau (e.g. studies on paleoseismic, GPS and seismicity rate of North-Tehran, North Tabriz and Mosha faults; Nazari, 2006), but more investigation such as paleoseismic investigation and evaluation of seismic capacity of other active faults as well as identification of blind faults are still a matter of concern.

A fault that is likely to have another earthquake sometime in the future and has at least one of the following characteristics:

- Fault are commonly considered to be active if it has moved one or more times during the past 10,000 years (Holocene).
- The U.S. Nuclear Regulatory Commission defines a fault as capable if the fault has moved at least once in the 35,000 years or more than once in the past 500,000 years.
- Macro-seismicity instrumentally determined with records of sufficient precision to demonstrate a direct relationship with the fault.
- Micro-seismicity instrumentally determined with records of sufficient precision to demonstrate a direct relationship with the fault.
- A structural relationship to a capable fault according to characteristics such that movement on one could be reasonably expected to be accompanied by movement on the other.
- Fault has been historically active in such a way that with the available features, the location of earthquake could be determined with sufficient precision.

- The existence of fault scarp on surface that has not been eroded.
- The existence of subsurface faults that offset Quaternary deposits and geomorphic features.

Here, I point out to two important earthquakes which are good examples to show that what happened was so different of what we expected.

The first example of such incorrectly predicted situation was the September 16, 1978, M_w7.4 Tabas earthquake in which about 15,000 people were killed. The thing that I can mention as a big challenge related to this earthquake is that, before the earthquake, we did not recognize the causative fault which could generate such a great catastrophic event. According to Berberian, (2014), *"The earthquake ruptured the unmapped and unknown Tabas thrust fault at the western Neogene foothills of the Shotori Mountains. The 1978 Tabas earthquake was associated with (i) 75-km long, coseismic surface thrust faulting dipping east–northeast along a curved fault line and (ii) flexural-slip faulting in the form of bedding-plane slip with a thrust mechanism on the hanging wall of the Tabas thrust in a vast area. About 75 km of discontinuous coseismic thrust faulting, in several segments of arcuate form, was mapped at the surface along an existing but unrecognized foothill-front reverse fault, the Tabas active thrust. The majority of the slip, in at least four subevents, contributing to the strong-motion signals and the WWSSN body waves, terminated about 15 km NW of Tabas-e Golshan, giving a fault length of 90 km. Maximum coseismic surface faulting of about 75 km was observed and mapped on the surface. Since the maximum measured "single" thrust displacement at the surface was only 35 cm, the major part of the primary rupture is likely to have been blind."*

Another important example that I can mention as a challenge we faced is the December 26, 2003 (M_w6.5) Bam earthquake, indicating the failure of the Iranian seismic hazard zoning map. Before the 2003 Bam earthquake, the region was classified as a zone with an average hazard in the seismic hazard zoning map of Iran in the Iranian building code (Standard No. 2800). However, the 2003 earthquake revealed the high potential of the fault in the region as well as the unpredicted strong shaking due to the near-field effect. In the earthquake report by Eshghi and Zare (2003), we indicated that *"the trends of the main faults (including the Bam fault) in this region are North-South, and NW-SE. These two systems intersect in western Lut area. The NW-SE faults (Kuhbanan and Ravar faults) and the north-south faults (Nayband, Chahar-Farsakh, Anduhjerd, Gowk, Sarvestan and Bam faults) have determined the border of the north-south structures in the Lut area with the NW-SE structures. These intersection*

zones were some of the main sources for the disastrous earthquakes. The existing records on historical seismicity indicate no major earthquake in Bam since the historical time. It seems that the Bam earthquake of 26/12/2003 has ended a seismic gap along the Bam fault. This seismic gap could be verified with the Arg-e Bam castle, which was constructed about 2000 years ago and since then, until the 2003 earthquake of Bam.

5-3. Studies on Seismotectonic and Sources

5-3.1. Modeling of the seismotectonic provinces of Iran using the self-organizing map (SOM) algorithm

** **Source Article:** Mojarab M., Memarian H., **Zaré M**, Morshedy A.H., Pishahang M.H., (2014), "Modeling of the seismotectonic provinces of Iran using the self-organizing map algorithm", Computers & Geosciences, Vol. 67, pp. 150–162, doi: 10.1016/j.cageo.2013.12.007.*

In this section, I present the modeling of the seismotectonic provinces of Iran using the self-organizing map (SOM) algorithm, an analysis taken from the published article by Mojarab et al. (2014).

Seismotectonic modeling of Iran using the SOM smart algorithm requires a data bank of the necessary features. In all of the smart clustering methods, each input data record is defined as a point in a multi-dimensional space. Therefore, each local point in the area of study has geological, seismic, geophysical, and morphological features.

To prepare a data bank and to assign features, including seismic, fault, gravity, magnetic, and topography, to specific coordinates, the map of Iran was first covered by a regular (X,Y) network, and approximately 20,000 points were generated for thorough coverage. In the next step, the collected information was designated to each coordinate (X, Y). Then, for each (X, Y) in the thorough coverage network, along with the geographical coordinates, other information, such as topography, seismic density, fault density, gravity, and magnetism, was designated. Accordingly, the information on a 20,000-point collection with seven features was acquired for clustering. Then, the collected information layers were converted to one single layer with seven different features for clustering.

The SOM algorithm, which was first defined by Kohonen (1981), is a nonparametric, recursive regression process in which a set of input data with high dimension is mapped to a lower dimensional space. A flowchart of the various steps in the current study is presented in Fig. 5-4.

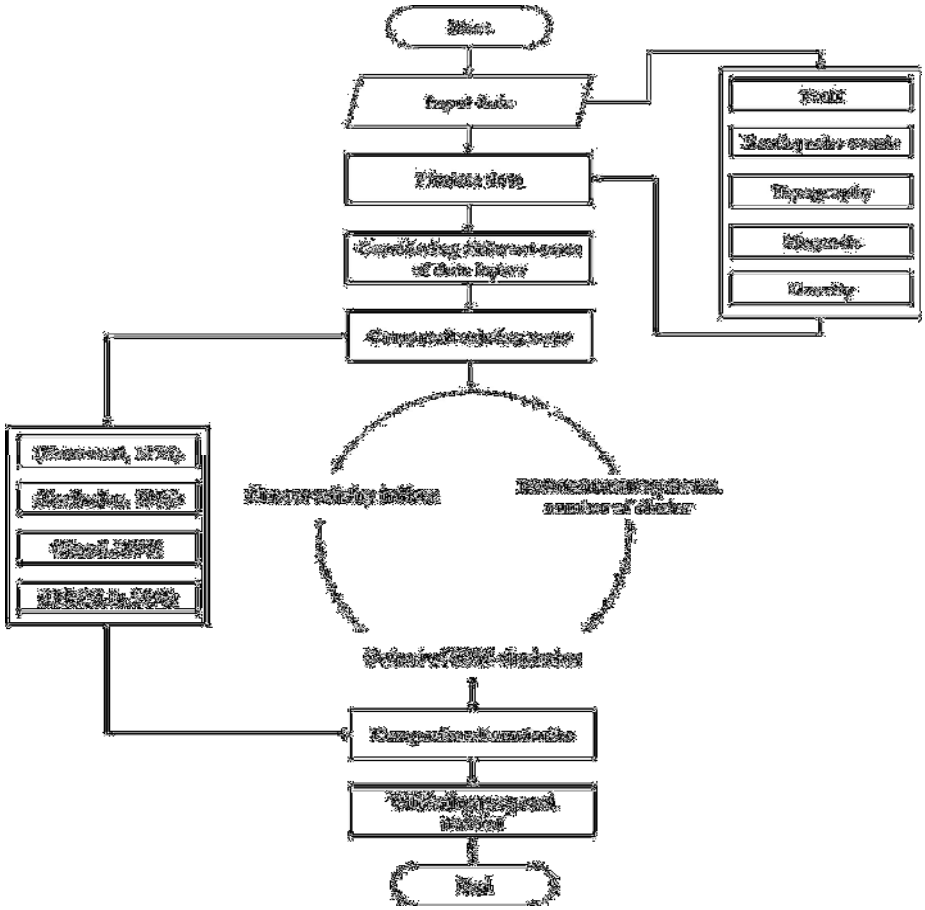

Fig. 5-4. Steps of zonation, including preparing input data, validating cluster number, applying SOM algorithm, and comparing the output of the SOM algorithm to the output of the combined model.

To verify the efficiency of the SOM algorithm, four of the most referenced seismotectonic models of Iran (Nowroozi 1976; Berberian 1976b; Nogol Sadat, 1993; and IRCOLD, 1996) were selected from the literature.

Considering that the SOM_a model has one of the best compatibilities with the combined model of the Iranian seismotectonic provinces, to assess it more precisely, we compared this model with each of the four models selected from the literature. In Fig. 5-5a, the output of SOM_a is compared with Nowroozi's model. It is observed that this model in Zagros, Makran, West Alborz, and most of Central Alborz has good compatibility with the output of the SOM network. Although in other regions of seismotectonic provinces, the two models were not

very compatible, some of the borders of the provinces, such as the southern borders of Alborz and western borders of Central Iran, have been well identified.

In Fig. 5-5b, which compares Berberian's model with the output of the SOM network, it is clear that the zones of Zagros, Makran, Alborz, and South Makran are quite compatible in both models, with dissimilarities only in Central Iran and North-West Iran. Interestingly, the borders of many of the seismotectonic provinces are the same in both models, and in some cases, the torsions and curvatures of these borders are well identified in the SOM outputs.

In Fig. 5-5d the IRCOLD model with SOM output is compatible in the Zagros, Makran, and Alborz, regions of Northern Makran and Eastern Iran, and the region of Bandar-Abbas. In addition, a comparison of the SOM outputs and Nogol's map indicates that good compatibility does not exist between these two models, except at the Zagros border, the Makran zone, and the East Iran Mountains (Fig. 5-5c).

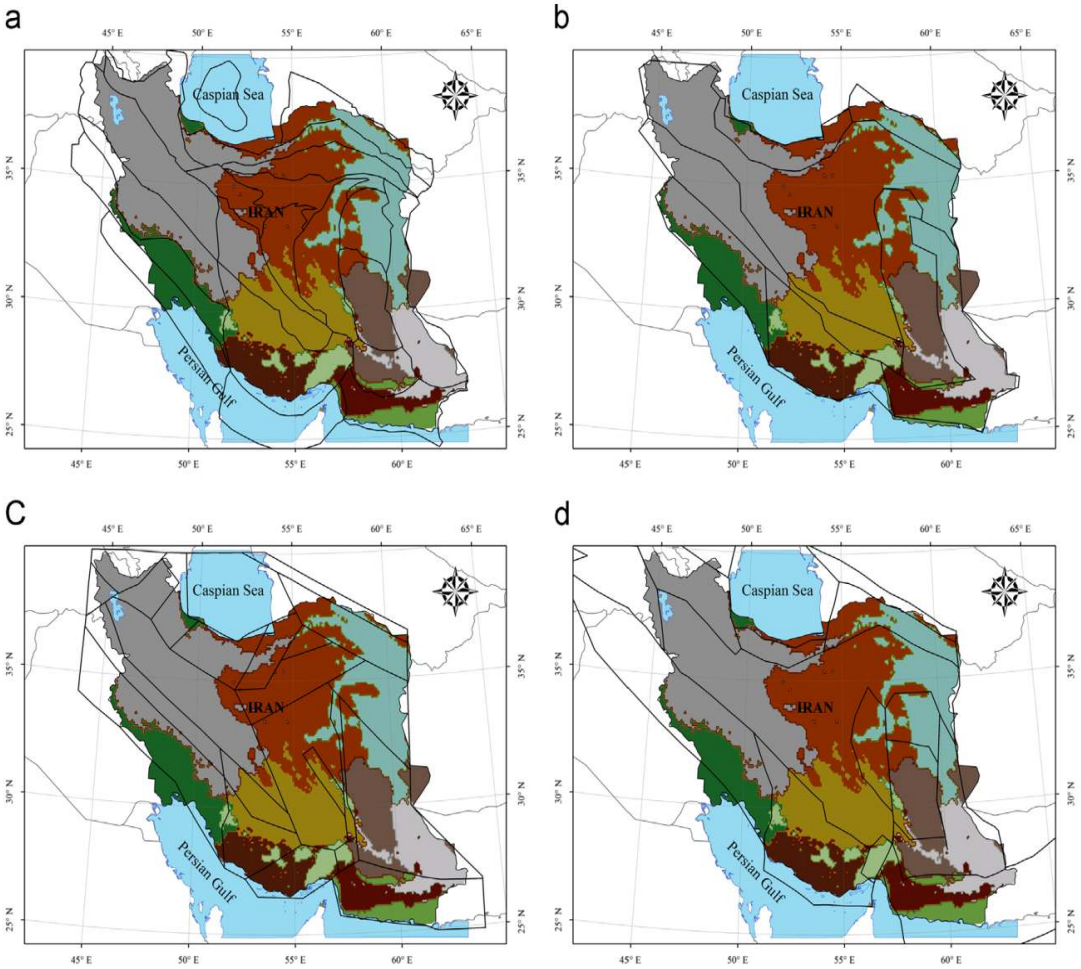

Fig. 5-5. Comparison between the SOMa model with the four presented seismotectonic models: (a) Nowroozi, (b) Berberian, (c) Nogol and (d) IRCOLD

5-3.2. New seismotectonic zoning and source maps of Iran

** **Source Article:** Karimiparidari S., **Zaré M**. and Memarian H., (2008), "New seismotectonic zoning map of Iran", 6th International Conference on Seismology and Earthquake Engineering (SEE6), Tehran, Iran.*

In this section, I present a new seismotectonic zoning and source maps of Iran, an analysis taken from the published article by Karimiparidari et al. (2014).

The new seismotectonic zoning map of Iran is developed using earthquake data, tectonic and different active fault maps, the magnetic intensity map and the topography map of Iran. Distinct characteristic of different parts helped to divide Iran into several zones. The borders defined for some zones may not be precise in some parts, as uniform information are not available for all parts of Iran. As an instant, the magnetic intensity map has some gaps in south west of Iran and also in the country's border lines. Generally, boundaries of zones follow the main active fault traces, which are in good harmony with the magnetic trends and seismicity. In central Iran, the topography map helped to make decision about some boundaries. The major seismotectonic zones such as Zagros mountain range, Alborz mountain range, Central Iran and Makran are divided into several subzones. Fig. 5-6 illustrates the newly seismotectonic zoning map of Iran which includes 29 zones, each with different seismotectonic characteristics.

In order to test the completeness of the catalogue in each zone, the dependent events should be removed. In this respect, the window algorithm, employed in the method described by Gardner and Knopoff (1974), was used. Proper diagrams were developed to estimate the magnitude of completeness. The first zone (zone No.16 in Fig. 5-6), which is selected from the north west of Zagros mountain range, shows the magnitude of completeness at or above M_w 4.2. The second one is selected from south part of Zagros mountain range (zone No. 9 in Fig. 5-6) and its magnitude of completeness is 4.0. The catalogue in Alborz mountain range (zone No. 21 in Fig. 5-6) is complete for M_w 4.0 and above. Makran coast (zone No. 27 in Fig. 5-6) has the completeness at M_w 4.5. Catalogue in zone number 6 in Fig. 5-6 as a part of Central Iran is complete at magnitude M_w 4.0 and above.

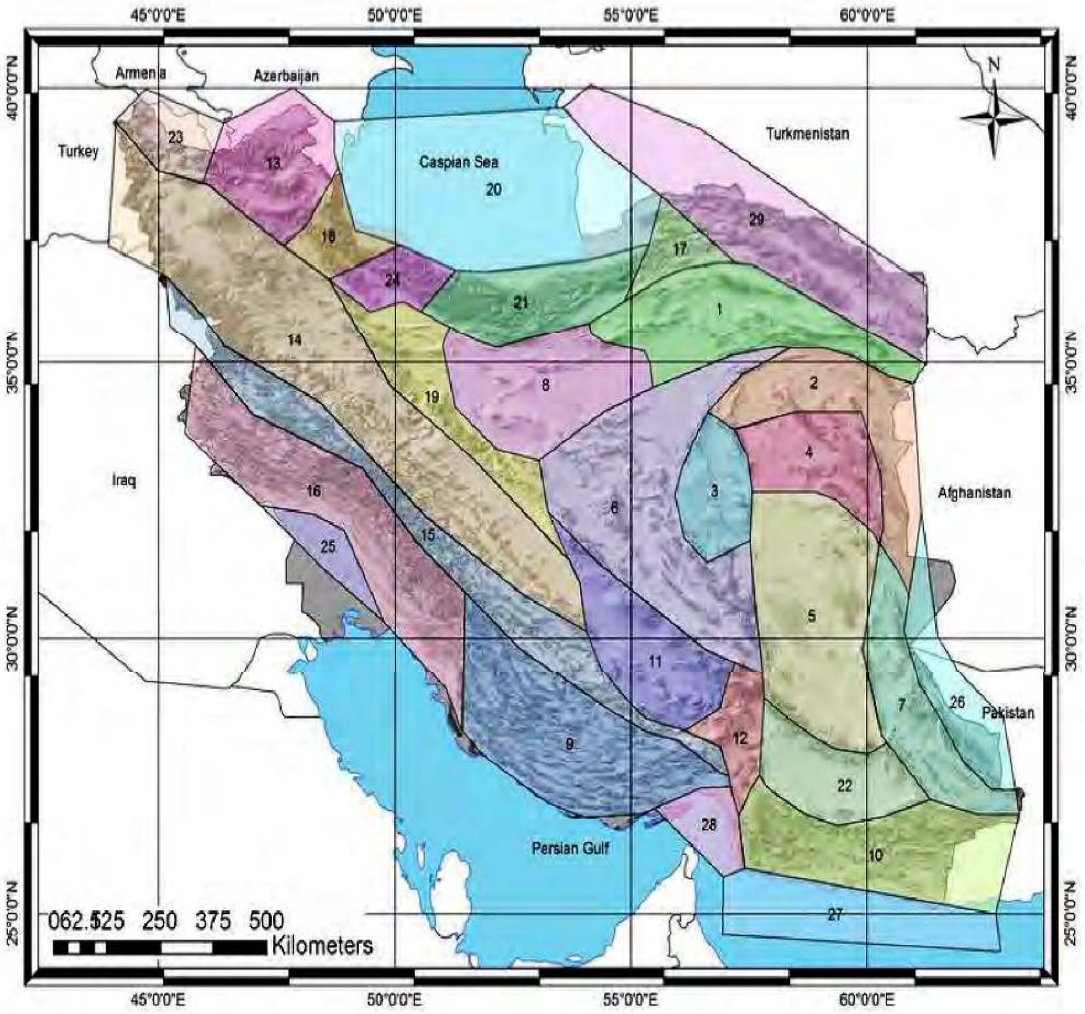

Fig. 5-6. New seismotectonic zoning map of Iran which includes 29 zones with different seismotectonic characteristics.

5-3.3. Inception of activity and slip rate on the main recent fault of Zagros mountains, Iran

** **Source Article:** Alipoor R., **Zaré M**. and Ghasemi M.R., (2012), "Inception of activity and slip rate on the Main Recent Fault of Zagros Mountains, Iran", Geomorphology, Vol. 175–176, pp. 86–97, doi: 10.1016/j.geomorph.2012.06.025.*

In this section, I present the inception of activity and slip rate on the main recent fault of Zagros Mountains, Iran, an analysis taken from the published article by Alipoor et al. (2012). *"The Main Recent Fault (MRF) is the manifestation of a major active strike-slip fault in the*

hinterland of the Zagros fold-and-thrust belt in Iran. We used geological, geomorphological markers, pull-apart basins, and drainage patterns to explore totally a new more accurate strike-slip offset on the MRF of the Zagros Mountains in SW Iran. The MRF has a NW–SE strike that is among the most important structural features within the Arabian–Iranian continental collision zone. Inception of the MRF has been suggested to be related to the slab break-off underneath the Zagros during the last 10–5 Ma. We conclude that the maximum total right-lateral offset on the MRF is about 16km, leading to a slip rate of about 1.6–3.2 mmy^{-1}. These figures for the fault inception time and slip rate are consistent according to geodetic estimates and three-dimensional mechanical modeling.

Considering, the new suggested 16-km offset on the MRF, the fault inception can be calculated by the previously estimated various slip rates. Fig. 5-7 shows the fault inception for the MRF with respect to our new 16-km offset and compares them with the previously estimated slip rates.

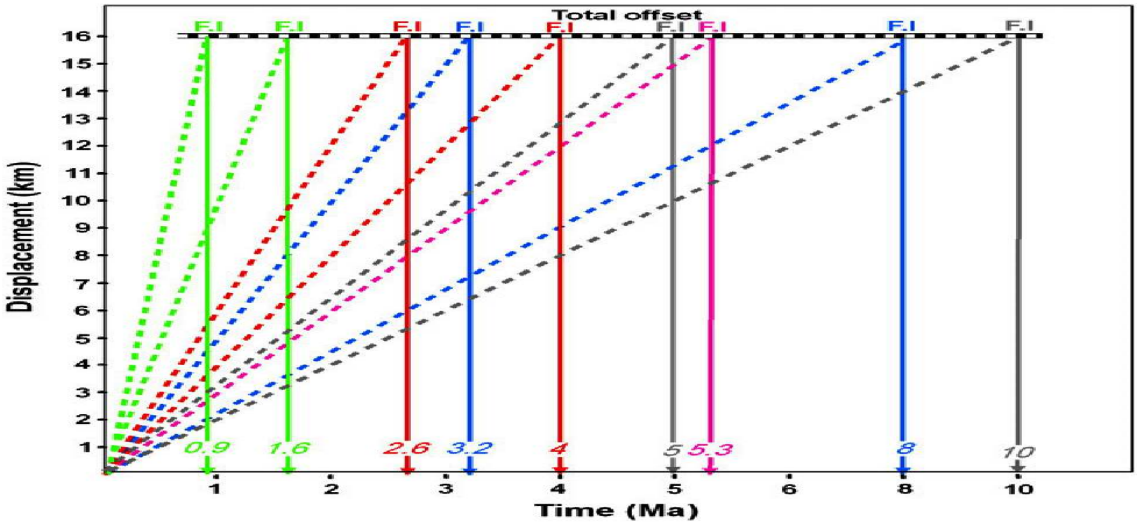

Fig. 5-7. *Fault displacement versus time. A variety of offsets allows an independent determination of inception of faulting. Total offset according to this study is 16 km; and F.I represents the various fault inception times. Grey line shows 5 –10 Ma age for inception of faulting in this study. Green and red lines show the 0.9–1.6 and 2.6–4 Ma age for inception of faulting with respect to the 10–17 and 4–6 mm/y slip rates as suggested by Talebian and Jackson (2002) and Walpersdorf et al. (2006), respectively. Blue and pink lines show the 3.2–8 and 5.3 Ma age for inception of faulting with respect to the 2–5 and 3 mm/y slip rate as suggested by Copley and Jackson (2006) and Vernant et al. (2004), respectively"* (Alipoor et al., 2012).

5-3.4. Geophysical and geological study on the West Qarchak fault and its implications in seismic hazard, Tehran, Northern Iran

** **Source Article:** Esmaeili, B. M. Almasian, **M. Zaré**, R. Alipoor, A. Alizadeh, (2014), "Geophysical and geological study on the West Qarchak fault and its implications in seismic hazard, Tehran, Northern Iran", Episodes, Vol. 37, no. 2, pp 105-110.*

In this section, I present the geophysical and geological study on the West Qarchak fault and its implications in seismic hazard, Tehran, Northern Iran, an analysis taken from the published article by Esmaeili et al. (2014).

Geo-electrical investigations:

The electrical resistivity method (29 geo-electrical measurement) were carried out based on Wenner–Schlumberger array with lengths between 360 to 490m in four sections (Profiles A, B, C and D in Fig. 5-8), across the West Qarchak Fault. The length, position and direction of the profiles were chosen to cover the scarp completely. The distance between profile A and profile D is about 4 km. In addition, to explain and discover the geological condition and displacement of sub-surface layers along the scarp, four sections were illustrated with regard to the geo-electrical tests information. As shown in Fig. 5-9, an apparent vertical displacement can be found from Northeast to Southwest direction. However, it is difficult to correlate the stratigraphical units to geo-electric sections, but about 25 to 30m total vertical displacement can be estimated along the West Qarchak Fault scarp in subsurface layers.

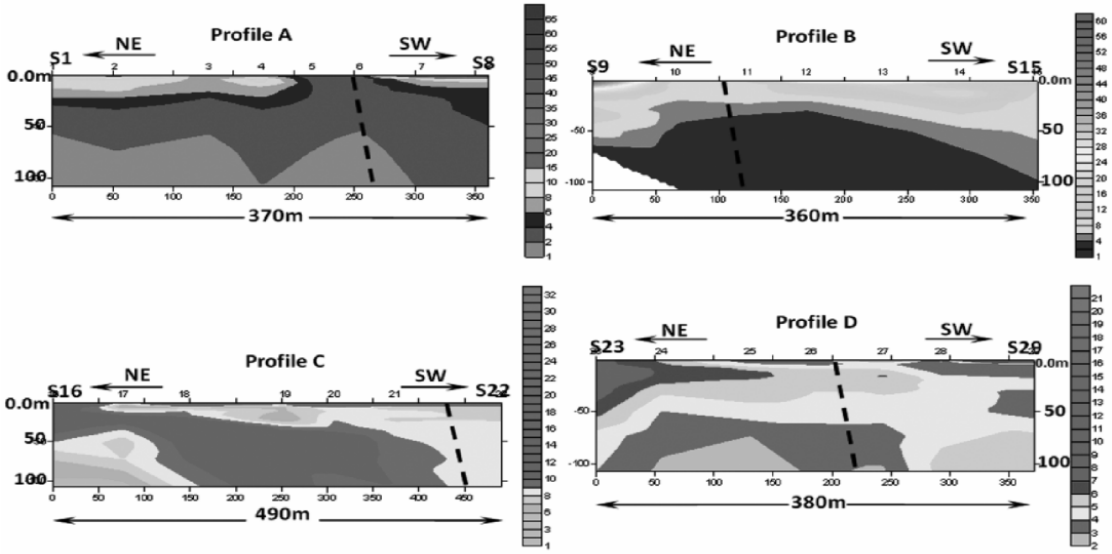

Fig. 5-8. *Iso-resistivity profiles (A, B, C and D) and apparent dip direction to south west.*

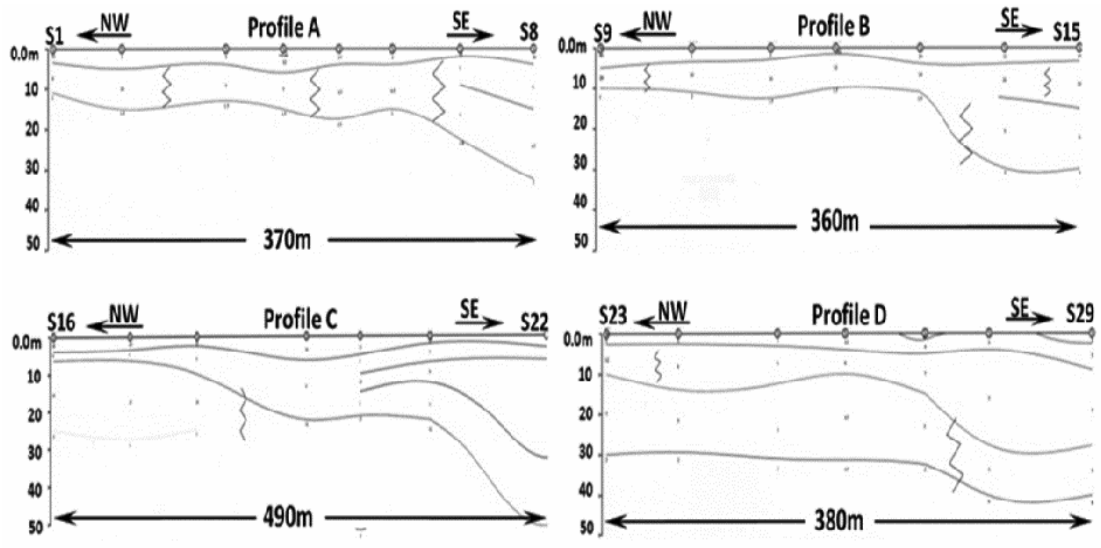

Fig. 5-9. *Electrical resistivity sections show about 25-30 total vertical displacement for WQF.*

In the present study, a segment of West Qarchak Fault with length of 4 km was investigated (Fig. 5-10) by geo-electrical method. It can be said that this fault reaches the Pishva Fault in southeast with same faulting characteristics and joints of Kahrizak Fault in Northwest (Fig. 5-10). The scarp of the West Qrchak Fault reaches the scarp of Kahrizak Fault and both of them follow contour lines, and therefore they are not ancient shorelines.

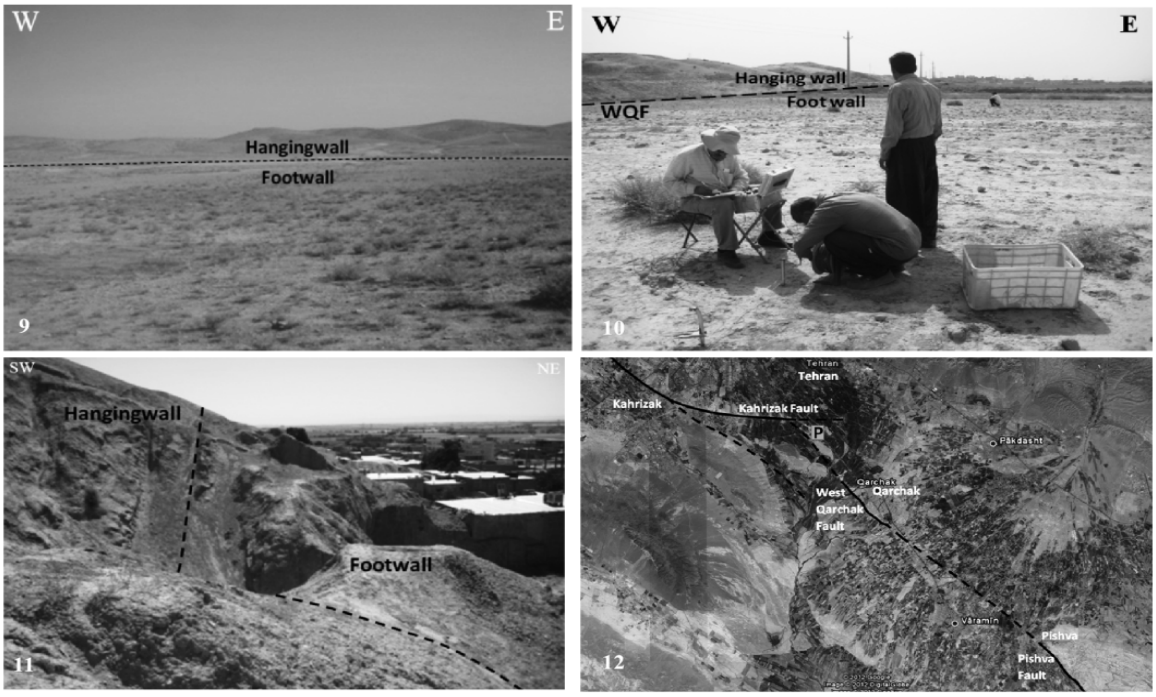

Fig. 5-10. *West Qarchak Fault and its scarp and Geo-electrical tests in the profiles"* (Esmaeili et al., 2014).

5-4. Magnitude Assessments

5-4.1. Calculation of confidence intervals for the maximum magnitude of earthquakes in different seismotectonic zones of Iran

** **Source Article:** Salamat M., **Zaré M.**, Holschneider M. and Zöller G., (2016), "Calculation of confidence intervals for the maximum magnitude of earthquakes in different seismotectonic zones of Iran", Pure and Applied Geophysics, pp 1–15, doi:10.1007/s00024-016-1418-5.*

In the current study, the upper bound of the confidence interval of the maximum possible earthquake magnitude M_{max} in different seismotectonic zones of Iran is calculated. This calculation is performed for different predefined levels of confidence based on a complete earthquake catalog. To study the confidence interval of the maximum magnitude in different seismotectonic zones of Iran, the uniform earthquake catalog between 1900 and 2015 in Iran and the surrounding area is gathered. It is divided into six sub-catalogs in six seismotectonic zones of Alborz, Azerbaijan, Central Iran, Zagros, Makran, Kopeh Dagh and both original and declustered catalogs are considered. To have independent events to a certain degree, the method of Grunthal (1985) is applied to decluster the original catalog. This allows to evaluate the influence of a possible violation of the assumption of the independence of events. It is assumed that seismic events in the studied region follow the Gutenberg–Richter relation with known magnitude of completeness m_0 and the Richter-b value calculated from Aki's formula.

Because the confidence interval is known to be unbounded in many cases, we calculate the highest confidence level with finite confidence interval $1-\alpha_c$. The critical value of the confidence level $1-\alpha_c$ is calculated for the original and a declustered version of the catalog in different magnitudes of completeness equal to 4.8, 5.0 and 5.5. Based on the calculations, it is deduced that increasing the magnitude of completeness resulted in the higher value of the confidence level but the removal of a higher percentage of data must be considered in this case. For m_0= 5.5, $1-\alpha_c$ in the original catalog is higher than the declustered catalog in all seismic zones. For m_0= 4.8 and m_0= 5.0, more significant results for $1-\alpha_c$ are shown in declustered catalog of Zagros seismotectonic zone and it seems logical based on the existence of numerous clusters with magnitude less than 5 in the mentioned zone.

After calculation of the critical value of the confidence level $1-\alpha_c$ in different seismotectonic zones of Iran for m_0= 5.5, we use three different values of the confidence

level lower than the critical one to calculate the finite confidence intervals. Tables 5-1 and 5-2 show the results of confidence intervals for different values of 1-α a in both catalogs for six seismotectonic zones. For different numbers of events, maximum observed magnitudes and the Richter-*b* values, the highest confidence level $1-\alpha_c$ in the original and the declustered catalog of each zone is calculated and the result shows the highest value in the Central Iran and the Zagros seismotectonic zones. The confidence levels in the Central Iran seismotectonic zone, for the completeness magnitude of m_0=5.5, m_0= 5.0 and m_0= 4.8 in the original and the declustered catalog are equal to 0.96, 0.72, 0.27 and 0.91, 0.81, 0.55, respectively. These values are equal to 0.94, 0.57, 0.36 and 0.81, 0.79, 0.76 for the original and the declustered catalog in Zagros seismotectonic zone for m_0=5.5, m_0= 5.0 and m_0= 4.8, respectively. It should be noted, even though, increasing the magnitude of completeness would probably result in more independency of events, but reduction of the number of events may cause high uncertainty in the estimation of M_{max}. Calculations of the confidence interval in the original catalog of the Central Iran indicate that with m_0=5.5, the confidence interval ranges are [7.4, 8.11], [7.4, 7.9], [7.4, 7.79] for 90, 85 and 80% of all cases. The same results are equal to [6.9, 7.5], [6.9, 7.29], [6.9, 7.19] for 90, 85 and 80% of all cases in the Zagros seismotectonic zone. Calculation of the confidence interval in Kopeh Dagh, Alborz and Azerbaijan seismotectonic zones are not that much promising and still too low due to the lack of sufficient data in the Makran seismotectonic zone, the seismic catalog is not qualified enough to have a good estimation in this zone and the current estimation is not meaningful.

Results of the calculated confidence interval for m_0= 5.5 in original catalogs of all seismotectonic zones of Iran are more acceptable in comparison with different values of the magnitude of completeness. Since for m_0= 5.5, declustering the catalog does not have any effect on the seismicity parameters in all seismotectonic zones; to calculate the confidence interval, it is recommended to use the original catalog without any declustering. Getting the reasonable confidence interval with the low probability of error needs qualified statistics of more events, and the current catalog with few events, high uncertainty and small number of large events especially in Makran, Kopeh Dagh, Alborz and Azerbaijan does not result in a meaningful level of confidence with finite confidence interval. Reduction in the probability of error may result in a reasonable level of confidence, but it causes the divergence of the confidence interval between the maximum observed magnitude and infinity which means unbounded confidence intervals.

Table. 5-1. Different levels of confidence and confidence intervals in original catalogs of six seismotectonic zones of Iran

Zone	Magnitude of completeness (m_0)	Level of confidence 1-α	Maximum observed magnitude	Upper bound of the confidence interval ψ(μ)
		0.5	7.3	8.66
Alborz	5.5	0.45	7.3	8.11
		0.4	7.3	7.87
		0.58	7.3	8.59
Azerbaijan	5.5	0.55	7.3	8.16
		0.5	7.3	7.88
		0.6	7.2	8.38
Kopeh Dagh	5.5	0.55	7.2	7.97
		0.5	7.2	7.77
		-	8	-
Makran	5.5	-	8	-
		-	8	-
		0.9	7.4	8.11
Central Iran	5.5	0.85	7.4	7.9
		0.8	7.4	7.79
		0.9	6.9	7.5
Zagros	5.5	0.85	6.9	7.29
		0.8	6.9	7.19

Table. 5-2. Different levels of confidence and confidence intervals in declustered catalog of six seismotectonic zones of Iran

Zone	Magnitude of completeness (m_0)	Level of confidence 1-α	Maximum observed magnitude	Upper bound of the confidence interval ψ(μ)
		0.5	7.3	8.79
Alborz	5.5	0.45	7.3	8.18
		0.4	7.3	7.93
		0.5	7.3	8.18
Azerbaijan	5.5	0.45	7.3	7.89
		0.4	7.3	7.74
		0.6	7.2	8.93
Kopeh Dagh	5.5	0.55	7.2	8.15
		0.5	7.2	7.87
		-	8	-
Makran	5.5	-	8	-
		-	8	-
		0.85	7.4	8.25
Central Iran	5.5	0.8	7.4	8
		0.75	7.4	7.87
		0.8	6.9	7.96
Zagros	5.5	0.75	6.9	7.46
		0.7	6.9	7.31

5-4.2. Estimating magnitudes of prehistoric earthquakes and seismic capability of fault from landslide data in Noor valley (Central Alborz, Iran)

** **Source Article:** Asadi Z. and **Zaré M**, (2014), "Estimating magnitudes of prehistoric earthquakes and seismic capability of fault from landslide data in Noor valley (central Alborz, Iran)", Natural Hazard, Vol. 74, Issue 2, pp. 445–461, doi: 10.1007/s11069-014-1186-4.*

In this section, I present the estimating magnitudes of prehistoric earthquakes and seismic capability of fault from landslide data in Noor valley (Central Alborz, Iran), an analysis taken from the published article by Azadi and Zaré (2014).

Giant paleolandslides in Noor valley

We have identified several giant landslides in Noor valley including Razan, Iva, Baladeh, and Vakamar. These landslides and their properties have been listed in Table 5-3.

Large size of Noor valley landslides and the location of this valley in an active tectonic region are evidence showing these giant landslides have been trigged by earthquakes. As there is no performed geotechnical analysis, it cannot be definitely concluded that the landslide has been triggered by seismic activity. Nevertheless, three or four out of six criteria, defined by Crozier (1992), have been used to explain that the origin of these giant paleolandslides is earthquake. These criteria are as follows :(1): Ongoing seismicity in central Alborz; (2): The spatial relationships between the patterns of landslides and active faults in Noor valley; (3): Large size of landslides; (4): Insufficient explanation landslide distribution only on the basis of geological and geomorphological conditions.
The presence of these four factors has been investigated in this research.

***Table. 5-3.** Giant landslides have identified in Noor valley*

Name	Size (km)	Area (km^2)	Volume (km^3)	Location		Classification	
Razan	6.74 * 24.9	~167.82	–	52.26	36.18	Duab	10.06 * 8.45
				52.19	36.22	Razan	6.27 * 6.06
				52.1	36.22	Ina	7.57 * 6.92
Baladeh	4.01 * 4.09	16.4	~0.1	51.83	36.22	–	
Iva	3.75 * 4.5	16.92	~0.08	52.04	36.18	–	
Vakamar	5.28 * 3	16.14	–	52.03	36.22	–	

Estimating magnitudes of triggering earthquakes by landslide data

The volume of giant landslides is calculated in Noor valley through Eq. (5-1), presented by Mather et al. (2003).

$$Volume = 0.1667\ \pi\ D_r\ W_r\ L_r \qquad (5\text{-}1)$$

Where D_r—depth of surface of rupture (m), W_r—equivalent surface width of surface of rupture (m), L_r—equivalent surface length of surface of rupture (m), so volume is ''m^3''.

In this study, volumes for all giant landslides have not been calculated in Noor valley. Only the volumes of Baladeh and Iva giant landslides have been estimated based on Eq. 5-1, because of measuring the depths of their rupture surfaces (D_r). In fact ''Dr'' is the height of slip scarp and is measurable only in these landslides. The measured D_r Values are 10–15 m in Iva landslide (20 m in its certain parts) and 15–20 m in Baladeh. W_r and L_r have been measured based on the satellite images and aerial photographs and presented in Table 5-3. The volumes of Baladeh and Iva giant landslides have been calculated through Eq. 5-1 as 0.08–0.17 and 0.1 km^3, respectively. As the volume in Eq. 5-2 is in the form of km^3, the volume obtained in Eq. 5-1 is converted to km^3.

The sizes and patterns of prehistoric and historic ground failures directly imply the relation between strong motions and the mass volumes of the occurred landslides (Nepop and Agatova 2008), presented in Eq. 5-2.

$$Log\ V_{Lmax} = 1.36M - 11.58\ (\pm 0.49) \qquad (5\text{-}2)$$

where V_{Lmax} is the volume of largest landslide (km^3). According to Eq. 5-2, the magnitudes (M), estimated for triggering earthquake of Baladeh and Iva giant landslides, are 7.7 ± 0.49 and 7.9 ± 0.49, respectively.

According to Keefer (1984) as well as the current study, an earthquake should have occurred around this valley for triggering its giant landslides. The North Alborz fault can probably be considered as causative fault. However, concerning the linear distribution of giant landslides along the most important fault of Noor valley (Baladeh fault) shows the effect of mentioned fault in the occurrence of landslides triggering earthquakes in this region. Besides, the linear distribution of giant landslides along Baladeh fault indicates that the eastern segment of Baladeh fault probably causes an earthquake that triggers giant landslides (Fig. 5-11).

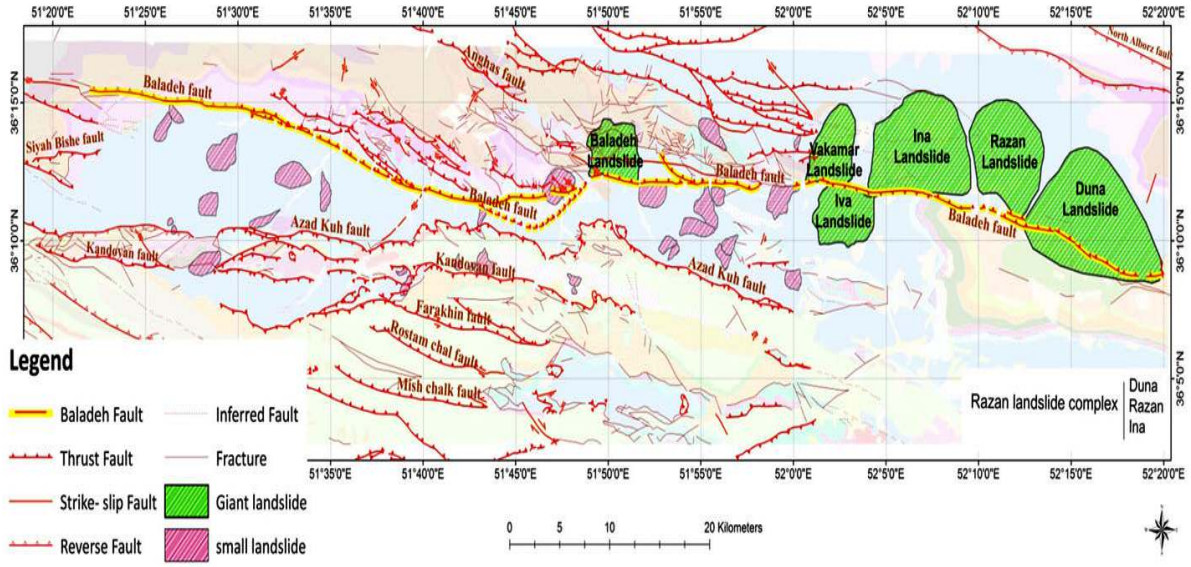

Fig. 5-11. *Baladeh fault and other faults in Noor valley"* (Asadi and Zare, 2014).

5-4.3. Aftershock decay rates in the Iranian plateau

** **Source Article:** Ommi S., Zafarani H, and **Zaré M.**, (2016), "Aftershock Decay Rates in the Iranian Plateau", Pure and Applied Geophysics, Vol. 173, Issue 7, pp. 2305–2324, doi: 10.1007/s00024-016-1285-0.*

In this section, I present the aftershock decay rates in the Iranian plateau, an analysis taken from the published article by Ommi et al. (2016).

Paying attention to the completeness period in the calculation of the modified Omori law parameters has a considerable impact. An increase in the completeness period is accompanied by a decrease in the parameters C and K, however, it has less effects on parameter P (Utsu and Ogata 1995). To be more accurate in the selection of the M_C, here, this parameter is calculated for different seismotectonic provinces using the earthquake catalogue of Iran between 1920 and 2013. To estimate M_C in each region, maximum curvature M_C (MaxC), b-value stability M_C (CAO) (Cao and Gao 2002) and Entire Magnitude Range methods (Ogata and Katsura 1993; Woessner and Wiemer 2005) have been used.

To determine the modified Omori law variables, the best way is to find them with maximizing likelihood function (Ogata, 1983). With the help of the this method, the calculation of the modified Omori law parameters for the selected earthquakes of Iran have

been done considering the occurrence time of the mainshock events (Fig. 5-12 and Table 5-4) in order to study the aftershock decay rates.

To be more precise, 1000 bootstraps have been used for this calculation. Some aftershock sequences include secondary aftershocks, which are aftershocks of a major aftershock (Utsu, 1970). In these cases, the change of the rate is seen in the aftershock catalogue which has had an influence on the trend shape and parameter amount. The reason for this change in the rate is the occurrence of a major aftershock or a cluster close to the previous cluster which can affect the seismicity rate of the region (Hamdache et al. 2013). According to the epidemic type aftershock sequence (ETAS) model that is developed by Ogata (1988) and is based on the stochastic point process theory, aftershock seismicity rate is calculated with a combination of all secondary aftershock sequences.

Table. 5-4. Sequence characteristics and resulted aftershock parameters

Date	M_N	Duration[a]	N[b]	N>C[c]	M_c	K[d]	Err	P[d]	Err	C[d]	Err	A[e]	b value[e]
06/22/2002	6.4	479	552	143	2.9	13.5	3.6	0.95	0.06	0.02	0.1	-1.62	0.81
12/26/2003	6.4	778	229	210	2.9	20	13.41	0.95	0.1	0.05	0.26	-1.32	0.77
05/28/2004	6.3	644	628	210	2.3	50	8.9	1.27	0.06	0.59	0.1	-1.3	0.77
02/22/2005	6.3	670	269	161	3.2	13.3	4	0.87	0.06	0.23	0.34	-1.58	0.9
11/27/2005	5.9	372	68	52	3.1	10	0	1.14	0.07	0.51	0.31	-1.43	0.9
02/28/2006	5.8	434	62	38	3.1	10	0.81	1.2	0.06	2.1	1.2	-0.81	0.67
03/25/2006	6	486	82	78	2.7	10	1.12	0.99	0.03	0.106	0.17	-1.2	0.71
03/31/2006	5.9	414	306	150	2.7	18.6	6.3	0.97	0.07	0.183	0.18	-1.46	0.88
08/27/2008	5.7	351	215	148	2.6	11.5	13.2	0.85	0.17	0.01	0.24	-1.79	0.95
09/10/2008	6	457	130	87	3.1	10	6.07	0.94	0.04	0.18	0.41	-1.07	0.74
09/27/2010	6.1	506	267	102	2.4	10	0.07	0.94	0.02	5	0.4	-1.84	0.79
12/20/2010	6.5	679	309	204	3.2	16	2	0.93	0.08	0.04	0.52	-1.8	0.94
10/23/2011	7.1	689	179	161	3	15.9	1.33	0.97	0.03	0.04	0.01	-2.53	0.93
08/11/2012	6.5	724	5089	2523	1.8	441.1	37.67	1.03	0.02	1.41	0.16	-0.94	0.78
04/09/2013	6.3	479	272	215	2.8	43.5	19.54	1.16	0.13	0.47	0.25	-0.78	0.71

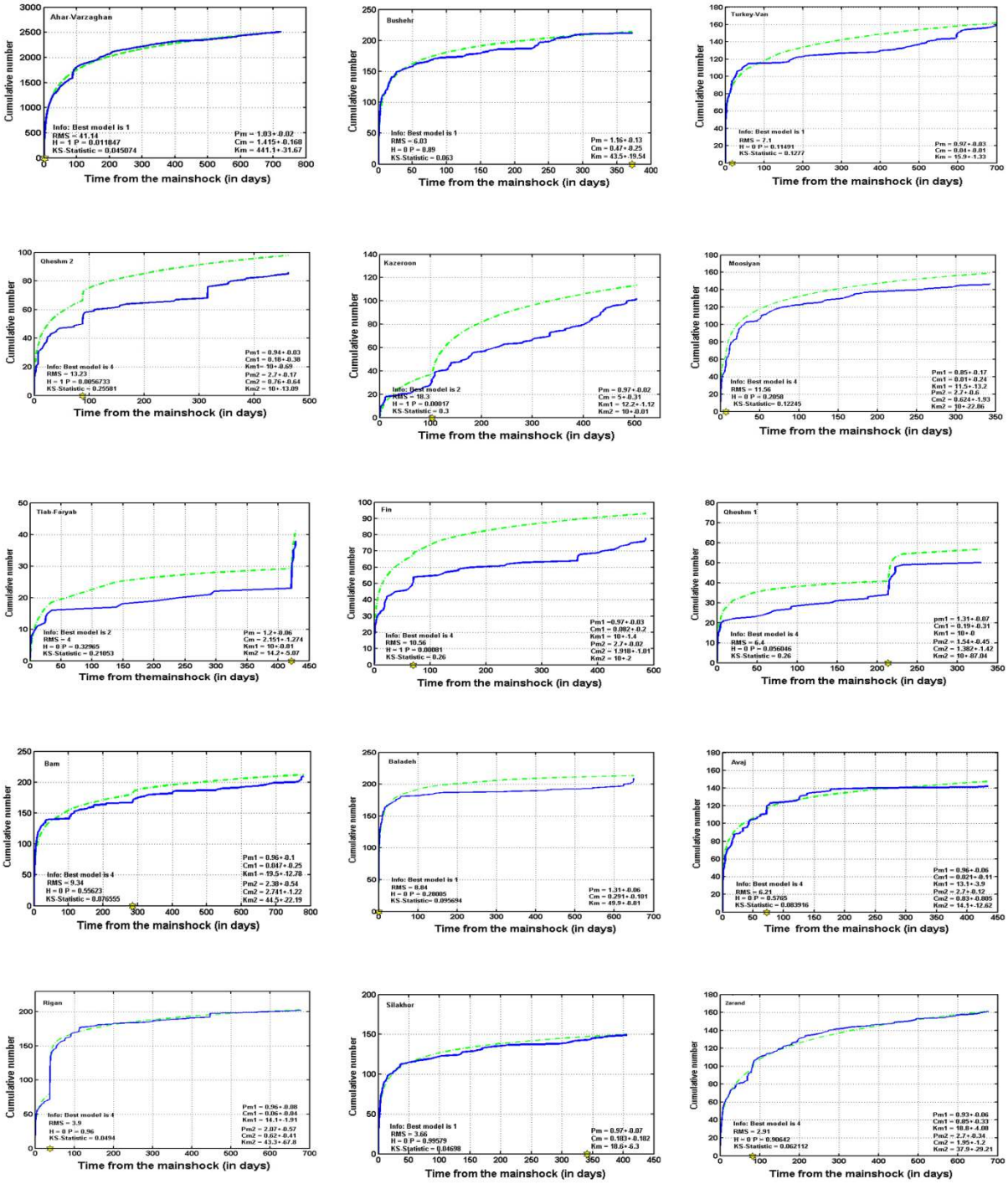

Fig. 5-12. Calculation of the revised Modified Omori law parameters (the exactness of these calculations is 1000 bootstraps). The solid line represents the plentitude of events per day and the dashed line shows the practice of the observed given inputs. The star shows the location of the secondary aftershocks, H is the result of the test of goodness of fit, RMS shows the root mean square, KS shows the amount of mean Kolmogorov-Smirnov value, parameter P is for statistical testing to make adaption with the observations, P, C, K are the coefficients of the modified Omori Law

5-5. Recent Seismic Hazard Zoning in Iran

5-5.1. Seismic hazard analysis in Iran (475 years return period)

** **Source Article:** **Zaré M.**, Karimiparidari S., Memarian H., (2015) "Seismic Hazard Analysis in Iran (475 Years Return Period)", Submitted.*

This study aims to conduct a probabilistic seismic hazard analysis for Iran using the most recently comprehensive data. For this purpose, a homogeneous earthquake catalog of Iran developed by Karimiparidari et al (2013) was used, which includes the Iranian events in terms of uniform moment magnitudes with the range of M_W 3.5–7.9 from the 3rd millennium BC to April 2010 (see section 2-3-2). Moreover, new seismic source models and seismotectonic zoning map of Iran were used which were developed based on the latest data of active tectonic, topography, magnetic intensity and seismicity catalog. These new maps divide the area of Iran into 27 seismotectonic zones and demonstrate two models for linear and regional seismic sources (Karimiparidari, 2008; see section 5-3-2). Following the removal of foreshocks and aftershocks, magnitude of completeness of each seismotectonic zone was established for the entire time span of the catalog. A comparison study also performed on available strong motion attenuation relations to select models and weight them in the logic tree. Finally, seismicity parameters were calculated and the probabilistic source-based approach established by Cornell in 1968 was followed by different branches defined in logic tree and the new probabilistic hazard map of Iran for a 475 years return period was developed.

Seismicity Parameters of Seismic Sources:

In order to calculate seismicity parameters, earthquakes related to each seismic source were determined individually. After declustering dependent events using the modified Gardner and Knopoff's (1974) space-time window (by Karimiparidari et al., 2016; see section 2-3-4), completeness threshold of the catalog for each seismic source was determined. In order to determine completeness threshold of the catalog, MAXC method (Wyss et al., 1999; Wiemer and Wyss, 2000) was applied using ZMAP software (Wiemer, 2001). In this method, maximum value of the first derivative of the magnitude-frequency curve is calculated which is coincident to the magnitude of maximum frequency of events in non-cumulative

magnitude-frequency FDM distribution. The 475 years return period was determined using Gutenberg- Richter model.

Seismicity parameters related to 27 seismotectonic zones were calculated to use in seismic hazard analysis. Events with magnitude of 3.5-7.9 were considered. Information of seismic catalog (time span, total number of events, number of independent events, percentage of removed events, magnitude of completeness (M_W) after 1900) and seismicity parameters (λ, b-value, β, observed M_{max}, date of observed M_{max}, estimated M_{max} and final M_{max}) calculated for each seismotectonic zone are presented in the Table 5-5. It is notable that the value of λ was normalized to the time span of catalog but not to the area of zones. Minimum and maximum of the final M_{max} in Shahr-e-Babak and Makran boundary were proposed 5.9±0.4 and 8±0.1 respectively.

As expected, seismic sources are sometimes defined in some regions where there are not enough earthquakes to calculate seismicity parameters. In such a condition, data of similar sources close to these sources or seismicity parameters of the related seismotectonic zones were used. Considering logic tree weighting, maximum magnitude of earthquake attributed to each source was calculated by averaging between maximum calculated magnitude based on the last edition developed method by Kijko and Sellevoll (1989 and 1992), maximum observed magnitude and calculated magnitude obtained from magnitude-fault length experimental relation (Figure 5-13).

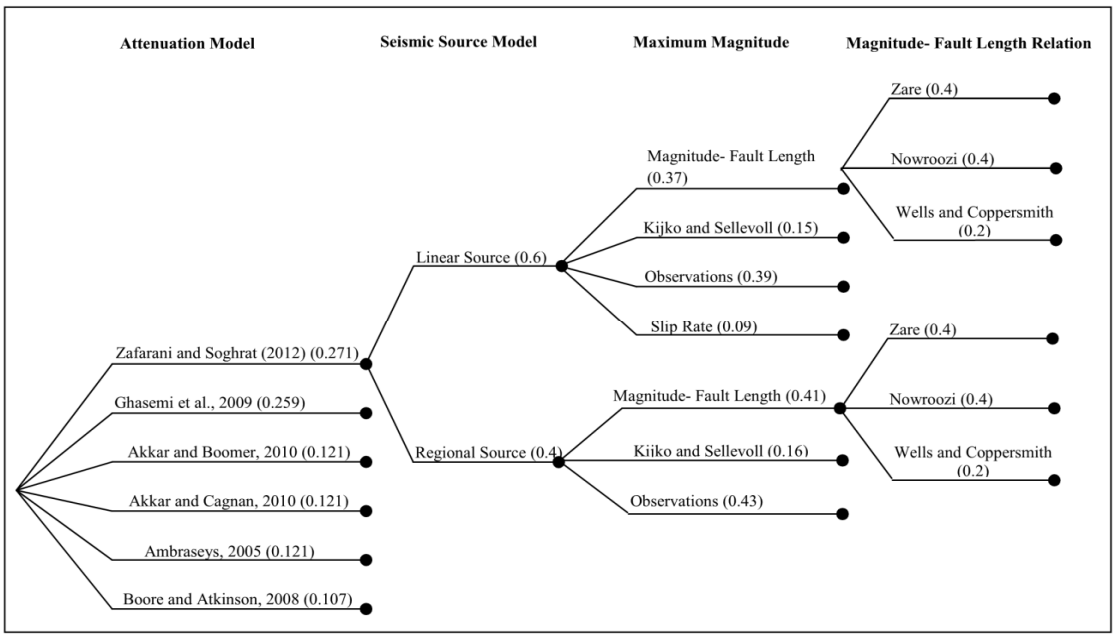

Fig. 5-13. Logic tree showing different uncertainties

Table. 5-4. Specifications of seismic catalog, completeness of magnitude and seismic parameters of 27 seismotectonic zones

No.	Name of Seismic Source	Time span	Total No. of events	No. of independent events	Percentage of removed events	Mag. of completeness (Mw)after 1900	Parameters					
							λ(4.6)	b-value	β	Obs. M_{max}	M_{max} Obs. Date	M_{max}(KS)	Final M_{max}
1	Ahvaz	840 - 2007	115	82	29%	4.2	0.57 ± 0.23	1.09 ± 0.08	2.51 ± 0.19	6.5 ±0.6	840	6.6 ± 0.6	6.6 ± 0.6
2	Alborz	4th Cen BC- 2010	365	216	41%	4.2	0.43 ± 0.12	0.70 ± 0.05	1.62 ± 0.10	7.6 ±0.5	958/2/23	7.7 ± 0.5	7.7 ± 0.5
3	Azerbaijan	200 - 2010	256	210	21%	4.0	0.67 ±0.13	0.78 ± 0.05	1.80 ± 0.11	7.6 ±0.4	1721/4/26 & 1780/1/8	7.9 ± 0.5	7.8 ± 0.5
4	Biabanak	1954 - 2010	334	170	49%	4.0	0.99 ± 0.31	0.76 ± 0.05	1.76 ± 0.11	7.2 ± 0.1	1981/7/28	7.5 ± 0.3	7.4 ± 0.2
5	Caspian	874 - 2010	237	187	21%	4.2	0.55 ± 0.23	1.09 ± 0.06	2.51 ± 0.15	7.4 ± 0.5	1895/7/8	7.7 ± 0.6	7.6 ± 0.6
6	CheshmehRostam	1939 - 2010	96	50	48%	4.6	0.37 ± 0.08	1.03 ± 0.09	2.38 ± 0.21	7.3 ± 0.1	1978/9/16	7.6 ± 0.1	7.5 ± 0.1
7	Dasht-e-Bayaz	1238 – 2009	124	87	30%	4.0	0.54 ± 0.40	1.15 ± 0.06	2.01 ± 0.15	7.5 ±0.4	1336/10/21	7.7 ± 0.6	7.6 ± 0.5
8	Jiroft	1849 - 2010	318	155	51%	4.5	1.38 ± 0.24	1.05 ± 0.08	2.43 ± 0.18	6.4 ±0.1	1999/3/4	6.9 ± 0.5	6.7 ± 0.3
9	Kashan	3rd Mil BC - 2010	51	42	18%	4.1	0.18 ± 0.10	0.96 ± 0.07	2.20 ±0.15	7.1 ±0.2	1177/5 & 1962/9/1	7.9 ± 0.8	7.5 ± 0.5
10	Khozestan	1430 - 2010	121	95	21%	4.1	0.69 ± 0.31	0.97 ± 0.07	2.24 ± 0.17	6.2 ± 0.3	1927/11/12	6.3 ± 0.3	6.3 ± 0.3
11	KopetDagh	943 - 2009	133	117	12%	4.1	0.50 ± 0.29	1.02 ± 0.06	2.35 ± 0.14	7.8 ± 0.6	943/5 & 1209 & 1389/2	7.5 ± 0.5	7.6 ± 0.6
12	Lut	1838 – 2009	117	62	47%	4.0	0.26 ± 0.14	0.90 ± 0.08	2.07 ± 0.18	7.0 ± 0.5	1838	7.3 ± 0.5	7.2 ± 0.5
13	Main_Kopet_Dagh_Fault	1st Cen BC - 2010	197	137	30%	4.0	0.78 ± 0.25	0.85 ± 0.07	1.95 ± 0.16	7.2 ± 0.3	1929/5/1	7.3 ± 0.3	7.3 ± 0.3
14	Main Zagros Reverse fault	913 - 2009	427	326	24%	4.2	1.27 ± 0.33	1.18 ± 0.04	2.71 ± 0.09	7.3 ± 0.2	1909/1/23	7.6 ± 0.4	7.5 ± 0.3
15	Makran	1919 - 2009	139	110	21%	4.5	1.18 ± 0.21	0.95 ± 0.08	2.18 ± 0.19	6.1 ± 0.2	1979/1/10	6.2 ± 0.2	6.2 ± 0.2
16	Makran coast	1483 - 2009	52	45	13%	4.5	0.39 ± 0.10	1.11 ± 0.08	2.57 ± 0.18	7.9 ± 0.1	1945/11/27	8.1± 0.1	8.0 ± 0.1
17	North Doruneh	840 - 2010	87	77	11%	3.9	0.41 ± 0.23	0.85 ± 0.05	1.96 ± 0.12	7.5 ± 0.5	1405/11/23	7.8 ± 0.6	7.7 ± 0.6
18	North Lut	763 - 2008	215	72	67%	4.4	0.66 ± 0.17	0.93 ± 0.06	2.14 ± 0.14	7.5 ± 0.5	763	7.8 ± 0.6	7.7 ± 0.6
19	NW Zagros	872 - 2010	1254	775	38%	4.5	3.01 ± 0.44	0.89 ± 0.05	2.60 ± 0.10	6.8 ± 0.5	872/6/22 & 1052 & 1130/2/27	6.9 ± 0.5	6.9 ± 0.5
20	Persian Gulf Coast	1703 - 2010	168	109	35%	3.8	0.48 ± 0.31	0.90 ± 0.06	2.07 ± 0.14	6.8 ± 0.5	1703	7.1 ± 06	7.0 ± 0.6
21	Shahr-e-Babak	1944 - 2008	41	39	5%	4.0	0.22 ± 0.17	0.98 ± 0.09	2.27 ± 0.20	5.7 ± 0.3	1944/7/23	6.1 ± 0.5	5.9 ± 0.4
22	SiahKuh	1808 - 2009	50	47	6%	4.0	0.41 ± 0.24	0.87 ± 0.07	2.00 ± 0.17	6.6 ± 0.5	1808/6/26	6.9 ± 0.6	6.8 ± 0.6
23	South Lut	1947 - 2007	55	50	9%	4.6	0.47 ± 0.10	0.95 ± 0.09	2.19 ± 0.21	6.7 ± 0.2	1969/11/7	7.0 ± 0.2	6.9 ± 0.2
24	South Zagros	857 - 2010	1806	944	48%	4.0	2.18 ± 0.50	0.97 ± 0.03	2.24 ± 0.06	7.0 ± 0.5	1440	7.1 ± 0.5	7.1 ± 0.5
25	Strait of Hormoz	1361 – 2009	159	61	62%	4.1	0.27 ± 0.13	0.96 ± 0.07	2.21 ± 0.16	6.5 ± 0.5	1497	6.7 ± 0.5	6.6 ± 0.5
26	Urumiehlsphahan	956 - 2010	185	151	18%	4.0	0.48 ± 0.23	1.04 ± 0.04	2.39 ± 0.10	7.1 ± 0.4	1930/5/6	7.4 ± 0.5	7.3 ± 0.5
27	Zahedan	734 - 2009	81	59	27%	3.8	0.45 ± 0.24	0.65 ± 0.06	1.49 ± 0.15	7.0 ± 0.4	805/12/2 & 815 & 1905/6/19	7.1 ± 0.4	7.1 ± 0.4

Results of Seismic Hazard Analysis for Iran

Seismic hazard of Iran was mapped for a 475 years return period based on seismic sources and specific seismicity parameters using CRISIS2007 software. In this software, seismic sources were defined as the regional and linear sources, maximum acceleration at period 0 was calculated and attenuation relations were defined in appropriate distances. In addition, a grid with 0.2*0.2 square kilometers cells was applied as the best result.

Six relations by Akkar and Boomer (2010), Zafarani and Soghrat (2012), Ghasemi et al. (2009), Akkar and Cagnan (2010), Ambraseys (2005) and Boore and Atkinson (2008) were used which had the best coincidence to the Iranian data. Moreover, both seismic sources and background seismicity were considered. In this regard, for each seismotectonic zone, very lower level of its seismicity was considered as the background seismicity. Frequency of earthquakes was attributed to each zone using the ratio of the uncovered area by sources to the total area of zone. Finally, seismic hazard map of Iran for a 475 years return period was produced using Kriging interpolate method and weighted average of the results of all six attenuation relations (Figure 5-14). Maximum acceleration was calculated 0.5g.

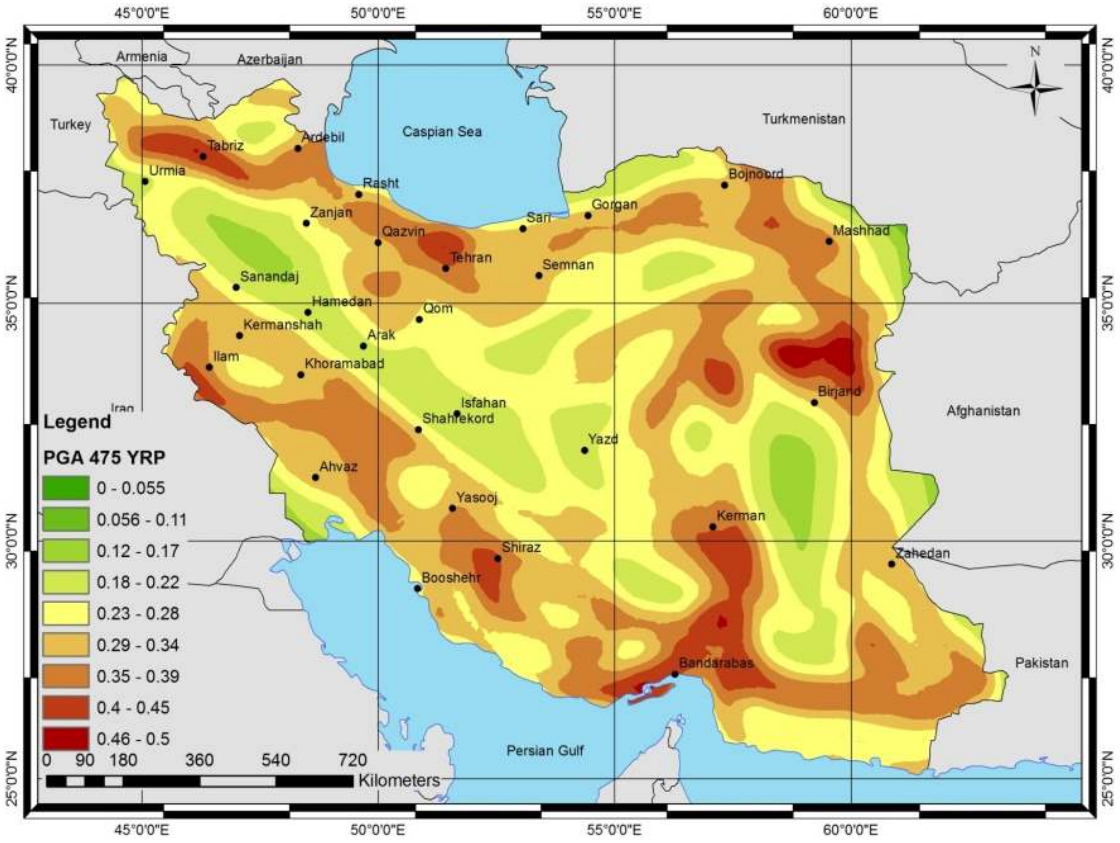

Fig. 5-14. Seismic hazard map of Iran for 475 years return period calculated averaging two models of seismic sources and six attenuation relations.

The results of this study were compared to other studies such as Iranian research center of urban Planning and architecture (1997), GSHAP (1999), Iranian code of practice for seismic resistant design of buildings (Standard No. 2800) (2005) and Hamzehloo et al. (2012) for some important and earthquake-prone cities of Iran (Table 5-5). In this study, maximum acceleration was calculated 0.5g, while it was calculated 0.5g, 0.45g, 0.35g, 0.46g in the studies by Iranian research center of urban Planning and architecture (1997), GSHAP (1999), Standard No. 2800 (2005) and Hamzehloo et al. (2012) respectively. The city of Ghaen in the current study, Standard No. 2800 (2005) and GSHAP (1999) has the highest hazard level but stands on the second level in studies by Iranian research center of urban Planning and architecture (1997) and Hamzehloo et al. (2012). In the all seismic hazard maps, the city of Tabriz has the highest acceleration. In this study, the acceleration of Tehran was calculated 0.36-0.4g for 475 years return period which is more than calculated acceleration by Iranian research center of urban Planning and architecture (1997) and Standard No. 2800 (2005), less than calculated acceleration by GSHAP (1999) and close to the calculated acceleration by Hamzehloo et al. (2012).

Table. 5-5. comparing calculated acceleration of this study to other studies such as Iranian research center of urban Planning and architecture (1997), GSHAP (1999), Standard No. 2800 (2005) and Hamzehloo et al. (2012) for some important earthquake-prone cities of Iran.

Name of City	**Acceleration (g)**				
	Iranian research center of urban Planning and architecture (1997)	**GSHAP (1999)**	**Standard No. 2800 (2005)**	**Hamzehloo et al. (2012)**	**This Study**
Tehran	0.2-0.3	0.45	0.35	0.36-0.46	0.36-0.4
Tabriz	0.5 <	0.45	0.35	0.46 <	0.46-0.5
Mashahd	0.15-0.2	0.35	0.3	0.36-0.46	0.16-0.35
Shiraz	0.2-0.3	0.4	0.3	0.36-0.46	0.41-0.45
Ghaen	0.3-0.4	0.45	0.35	0.36-0.46	0.46-0.5
Kerman	0.2-0.3	0.4	0.3	0.36-0.46	0.36-0.4

5-5.2. Seismic hazard and risk assessment in Tehran

** **Source Article:** **Zaré M**., Kamranzad F, Ostad-Taghizadeh A., (2016), "Risk Assessment of Multiple Natural Hazards in Tehran", Submitted.*

Tehran as the Capital and the most populated city in Iran is located in the "Alborz" seismotectonic region. Active tectonic conditions, potentially seismic faults, experience of historic destructive earthquakes as well as a large population in this earthquake-prone area have necessitate to perform more studies in order to analyze the seismic hazards and risks of the city. In this research, the seismic hazard map of Tehran is firstly prepared. The map is then combined with the distribution of non-resistant structures as the vulnerability factor and the population density as the exposure term to derive a seismic risk map for Tehran.

Tectonically, Tehran is in an active region with shortening velocity of about 8 ± 2mm/yr at the longitude of Tehran (Vernant et al., 2004). The active tectonic condition has caused Tehran to be surrounded by many active faults including the North Tehran, Mosha, North Rey, South Rey, Kahrizak, and Eivanekey faults. Based on existing evidences, the area of Tehran and its vicinity have been destroyed completely several times by severe earthquakes with magnitude greater than 7 (Table 5-6).

In this study, a new seismic hazard analysis for Tehran is performed and the results are presented in the form of two maps: (i): a peak ground acceleration (PGA) zoning map with 475 years return period that is calculated using the probabilistic seismic hazard analysis. This map shows probable surface PGA by consideration of site effects. (ii): a surface fault rupture hazard map which shows the surface fault rupture width for the seismic sources in Tehran.

Table. 5-6. Significant earthquakes (7≤M) around Tehran (Ambraseys and Melville, 1982).

Date	Lat. N	Lon. E	Magnitude	Region
4th BC	35.5	51.8	7.6	Rey
743	35.3	52.2	7.2	Rey
855	35.6	51.5	7.1	Rey
958/02/23	36	51.1	7.7	Rey - Taleghan
1177/05	35.7	50.7	7.2	Rey - Buin Zahra
1384	35.3	52.2	~ 7	Rey
1608/04/20	36.4	50.5	7.6	Taleghan
1830/03/27	35.7	52.5	7.1	Damavand
1962/09/01	35.63	49.87	7.1	Buin Zahra
1990/06/21	37.07	49.28	7.4	Manjil

PGA map with 475 years return period for surface deposits

To develop a new seismic hazard map of the metropolitan Tehran, the probabilistic approach (Cornell, 1968) which is the most popular method, is applied to estimate the PGA for the Tehran region. *"The assessment of values of input parameters (M_{max}, distance to the seismic source and the site conditions) and the selection of the attenuation models to evaluate the seismic hazard parameters contains different amounts of uncertainties"* (Zare, 2006). As the first step of the PSHA study, the historical and instrumental earthquake data and tectonic settings within 150 km radius of the central Tehran was considered.

The fault map introduced by Hessami et al, (2003) and the EMME declustered earthquake catalog (Zare et al., 2014) were used. Since the geometry of the faults is not precisely clear, it is useful to consider the seismic sources as area sources. Seismic area sources are usually determined based on the seismicity and the accumulation of past earthquakes, the fault rupture width maps and their trends, correspondence of the selected zones or their boundaries with the topography and geophysical aeromagnetic maps. Keeping in mind these points, nine seismic area sources are identified around Tehran (Fig. 5-15). Seismic sources were then modeled and recurrence relationship was established. For this purpose, the method proposed by Kijko and Sellevoll (1992) was employed which considers uncertainty in magnitude and incomplete earthquake catalogue to estimate seismicity parameters from incomplete data. In this way, for each area source, seismicity parameters including b-value of the Gutenberg-Richter relation, annual mean occurrence rate (λ), and maximum possible magnitude, (M_{max}) were evaluated (Table 5-7). It should be noticed that the M_{max} is estimated based on the maximum observed historical/instrumental earthquake and the assessment of maximum probable earthquake for a seismic source using empirical relationships between the magnitude and fault length. In this study, two empirical relationships were used to calculate the probable M_{max} of each area source as the follows:

$$M_w = 0.91 \ln L_R + 3.66 \quad \text{(Zare, 1999)} \qquad (5\text{-}3)$$

$$M_w = 5.08 + 1.16 \log L_R \quad \text{(Wells \& Coppersmith, 1994)} \qquad (5\text{-}4)$$

where L_R is the rupture length and equals to 37% of the fault length based on the records of the Iranian fault ruptures (Zare, 1999).

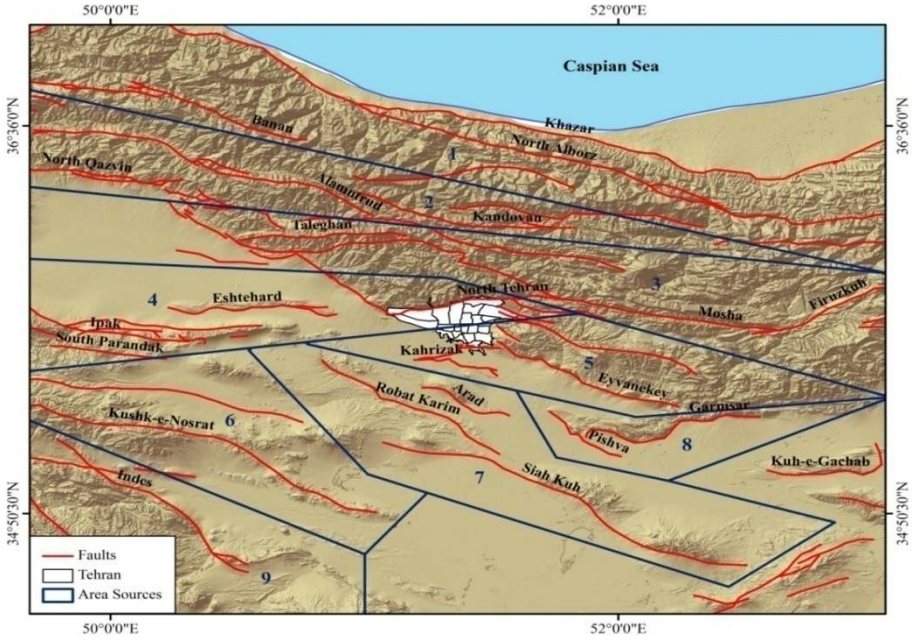

Fig. 5-15. Seismic area sources for PSHA study in Tehran

Table. 5-7. Seismicity parameters of the selected seismic area sources.

Zone	L_{fmax} (km)	L_R (km)	M_{min}	M_{max}			Selected M_{max}	β	λ_{Mmin}
				Observed	Zare (1999)	Wells & Coppersmith (1994)			
1	>150	55.5	4.5	7.4	7.3	7.1	7.4	2.06	0.22
2	120	44.4	4.5	7.6	7.1	7.0	7.6	2.07	0.07
3	200	74	4.5	7.7	7.6	7.2	7.7	2.15	0.12
4	110	40.7	4.5	7.2	7.0	6.9	7.2	2.12	0.19
5	80	29.6	4.5	7.5	6.7	6.8	7.5	2.14	0.11
6	165	61.05	4.5	5.4	7.4	7.2	7.4	2.22	0.14
7	90	33.3	4.5	6.4	6.9	6.8	6.9	2.33	0.11
8	72	26.64	4.5	7.1	6.6	6.7	7.1	2.22	0.14
9	113	41.81	4.5	6.2	7.1	7.0	7.1	2.32	0.14

Then, five attenuation relations which are consistent with the condition of the study area are used. This relations have been defined by Zare (1999), Zare and Sabzali (2006), Ambraseys et al (2005), Boore and Atinkson (2008), Akkar and Bommer (2010).

The aim is to perform PSHA and derive two PGA maps for bedrock and surface levels. In order to calculate the surface PGA, soil effect should be taken into account. The site conditions are classified mostly based on the seismic codes in 4 orders of site conditions. Here, V_{30} map in Tehran introduced by Gholipoor et al (2008) was used to consider the site effect. The area of interest has been divided by 0.01° intervals generating 1657 grid points. Finally, two PSHA maps (basement and surface) with 475 years return period were prepared for Tehran (Fig. 5-16).

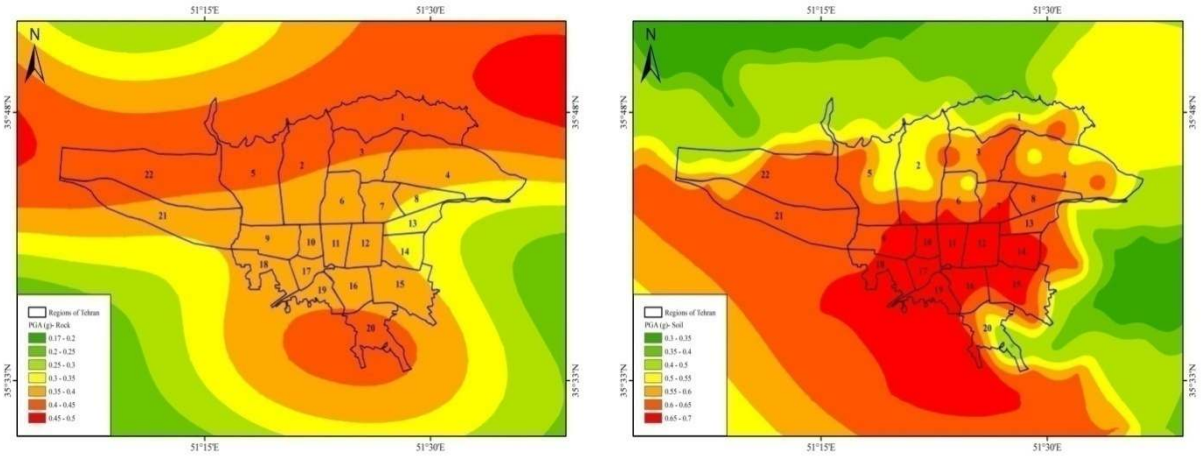

(a) (b)

Fig. 5-16. Hazard map of Tehran for 475 years return period in terms of PGA on (a): rock basement and (b): on surface soil.

The first seismic hazard map is produced using PGA evaluation on the bedrock of Tehran. This map shows a maximum PGA of 0.45-0.5g in the northern and southern parts of Tehran where are near the Mosha, North Tehran and Rey-Kahrizak faults. The second seismic hazard map is produced using PGA evaluation on surface above soil deposits of Tehran considering the average shear wave velocity in 30 meter depth of the surface (V_{30}) map. The surface hazard map shows a maximum PGA of 0.7g in the southern regions of Tehran. Comparing the two hazard maps on bedrock and surface confirms that the thick soil deposits in different parts of Tehran are able to amplify ground motions during an earthquake. Therefore, central and southern areas of the city are assigned as the highest hazardous zones which are exposed to amplified strong motions due to large earthquakes.

Fault Rupture Hazard Map

Beside evaluation of earthquake hazard in terms of maximum probable acceleration maps, probable surface fault rupture zones are subjected to a specific attentions. Severe displacements in a rupture zone due to the near field/near fault effects can lead to large damages to structures and may cause secondary hazardous phenomena such as induced landslides. Consequently, areas located in a probable rupture zones should be determined as hazardous zones in hazard/ risk assessments. In this regard, the faults within and near Tehran were considered and classified into three group: Major, Medium and Minor Faults. Major faults are those that have length of more 20 km and are the North Tehran, Sorkh Hesar-

Tarasht, Eivanekey-Rey and Kahrizak-Pishva fault zones. Mediums and Minors have 5-15 and less than 5 km length, respectively.

On the basis of reliable datasets corresponding to 23 seismic faults of the Iranian Plateau, Zare (2001) showed that the surface rupture width best fits with the rupture length as the following empirical regression:

$$W = 10^{(a+b\,logL_R)} \pm \sigma \quad \text{(Zare, 2001)} \qquad (5\text{-}5)$$

where L_R is the rupture length and the coefficient a= -0.45, b= 0.48 with standard deviation of σ=0.7. In this research, the surface rupture width of each group is estimated according to the above formula (Table 5-8). Fig. 5-17 shows the rupture width zones map which is considered as a hazard map for the seismic hazard assessment in the study area. Finally the two obtained maps in terms of the surface maximum probable acceleration as well as the surface rupture width are the results for earthquake hazard assessment in Tehran.

Table. 5-8. Surface rupture width of the faults within Tehran

Fault Zones		Length (km)	Surface Rupture Length (Km) (Zare, 1994)	Mw (Zare, 1999)	Surface Rupture Width (km) (Zare, 2001)
Major Faults	North Tehran	130	48.1	7.2	3.0
	Sorkh Hesar- Tarasht	50	18.5	6.3	2.1
	Eivanekey-Rey	100	37.0	6.9	2.7
	Kahrizak-Pishva	75	27.7	6.7	2.5
Medium Faults		5-15	3.70	4.9	1.4
Minor Faults		<5	0.92	3.5	1.0

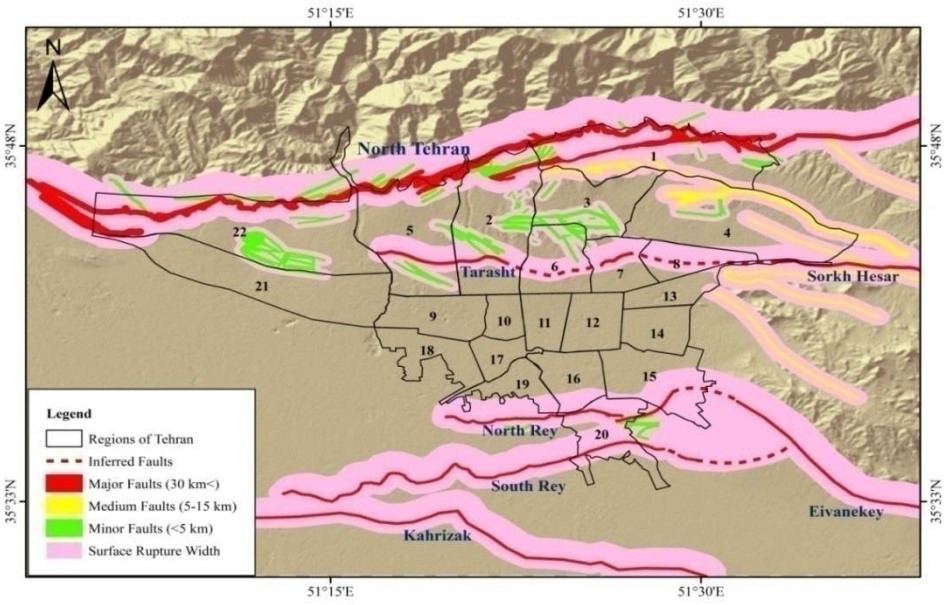

Fig. 5-17. Fault rupture width zones in the city of Tehran.

Earthquake Risk Map

The purpose of risk mapping is usually to prepare useful informative tools in order to assess disaster preparedness and to increase resiliency and safety of a society. Risk is defined as the multiplication of three factors as below:

$$\text{Risk} = \text{Hazard} * \text{Vulnerability} * \text{Exposure} \qquad (5\text{-}6)$$

in which hazard is calculated using probability and intensity of a disaster. vulnerability can be described in terms of technical-physical, organizational, Psycho-social and economic vulnerabilities and exposure is the number or amount of the target society who are considered as elements at risk such as population of a city.

Until preparing this study, there was no homogenous accurate data about the organizational, Psycho-social and economic vulnerabilities and physical vulnerability of structures in Tehran. Thus, in order to map the risk, the seismic hazard map is combined with the distribution of non-resistant structures (Fig. 5-18) as the vulnerability factor and the population density (Fig. 5-19) as the exposure term. Finally, the seismic risk map of Tehran is prepared (Fig. 5-20). This map shows that the central and southern regions of Tehran are in a higher risk of multiple hazards than other regions. Moreover, looking at the Figs. 5-18 and 5-19 reveals that most of the non-resistant and densely populated areas are located on the central and southern Tehran, intensifying the risk of natural disasters.

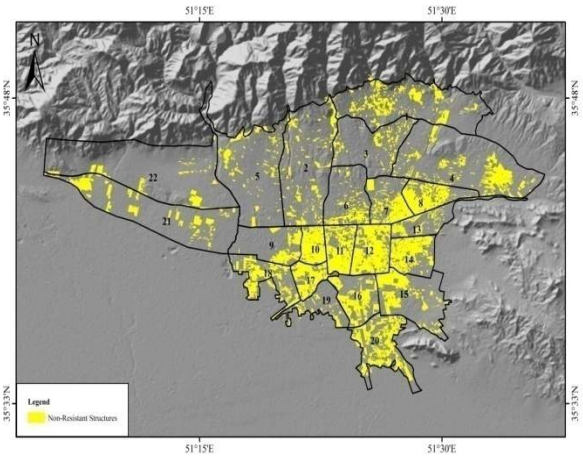

Fig. 5-18. Distribution of non-resistant structures in Tehran

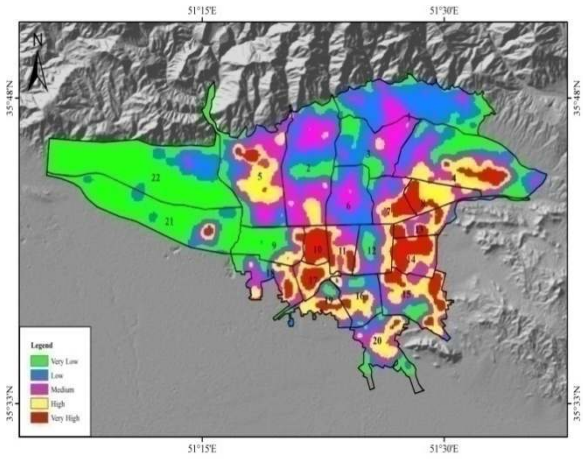

Fig. 5-19. Population density in Tehran

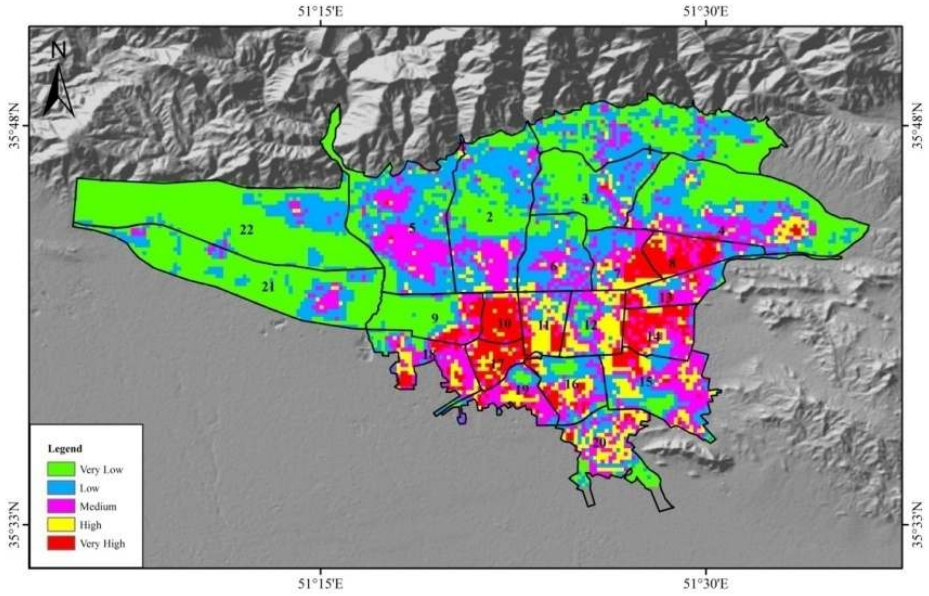

Fig. 5-20. Seismic risk Map of Tehran

Discussion

It is notable that in this study, only in-situ risks have been considered, meaning that other secondary risks and aftermaths such as post-earthquake conflagration, safety issues, problems of population displacement after great disasters, far distances to hospitals and emergency rescue services and so on were not considered.

Keeping in mind the inevitable application of data with different accuracy and resolutions (e.g. earthquake catalogs, fault maps, rupture relationships, landslide data, DEM map, rain, geology and site conditions, river flows, subsidence, exposure, vulnerabilities and so on), the inhomogeneous can be assigned as an uncertainty source which may affect the results.

In order to improve risk assessments of multiple natural hazards in Tehran, the following points are proposed for further studies:

- Data, qualitative/quantitative assessment methods and vulnerability factors should be continuously reviewed and updated.
- By improving data, it should be tried to prepare online risk maps which monitors and evaluates hazard status, rescue facilities and exposures at any moment.
- In aspect of disaster management, it is useful to approve several specific action plans for some critical probable scenarios of disasters.

5-6. Seismic Hazard Zoning in Some Parts of Asia

5-6.1. Assessment of seismic hazard in the Middle East and Caucasus: EMME (Earthquake Model of Middle-East) project

** **Source Article:** Erdik M., Şeşetyan K., Demircioğlu M.B., Tüzün C., Giardini D., Gülen L., Akkar D.S. and **Zaré M.**, (2015), "Assessment of Seismic Hazard in the Middle East and Caucasus: EMME (Earthquake Model of Middle East) Project", 15th World Conferences on Earthquake Engineering (WCEE)*

In this section, I present the EMME hazard model, an analysis taken from the published article by Erdik et al. (2015). The study on the EMME catalog was performed by Zaré et al (2014) *"to establish the new catalog of seismicity for the Middle East, using all historical (pre-1900), early and modern instrumental events up to 2006. According to different seismicity, which depends on geophysical, geological, tectonic, and seismicity data, this region was subdivided to nine subregions, consisting of Alborz–Azerbaijan, Afghanistan–Pakistan, Saudi Arabia, Caucasus, Central Iran, Kopeh–Dagh, Makran, Zagros, and Turkey (Eastern Anatolia; after 30° E)"* (Zaré et al., 2014). In this regard, a new uniform catalog of earthquakes in the Middle East region in terms of moment magnitude (M_w) was developed in order to prepare a reliable and most complete collection of available information of seismicity in this region. In addition, some of the seismicity information, i.e., number of events, range of magnitudes, and magnitude completeness (Mc) and seismicity depths of this region were also determined (for more details, see section 2-3-1).

According to Erdik et al. (2015), *"Active faults are the places where earthquakes occur, so the delineation of the active fault zones and the parameterization of their characteristics is the first step in seismic hazard assessment. A digital active tectonic map of the Middle East region was generated in ArcGIS format. A total of 3,397 active fault sections were defined and faults with a total length of 91,551 km were parameterized for the EMME Project (Fig. 5-21). The areal source zonation model developed for the EMME region is presented in Fig. 5-22.*

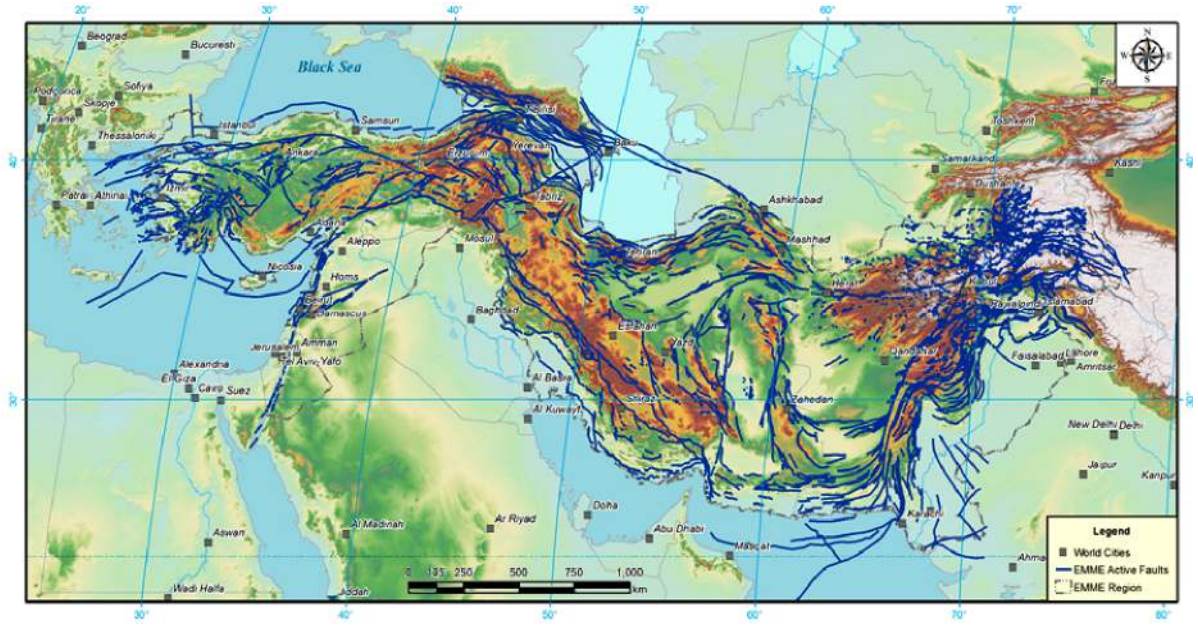

Fig. 5-21. Active fault map of the EMME Project region.

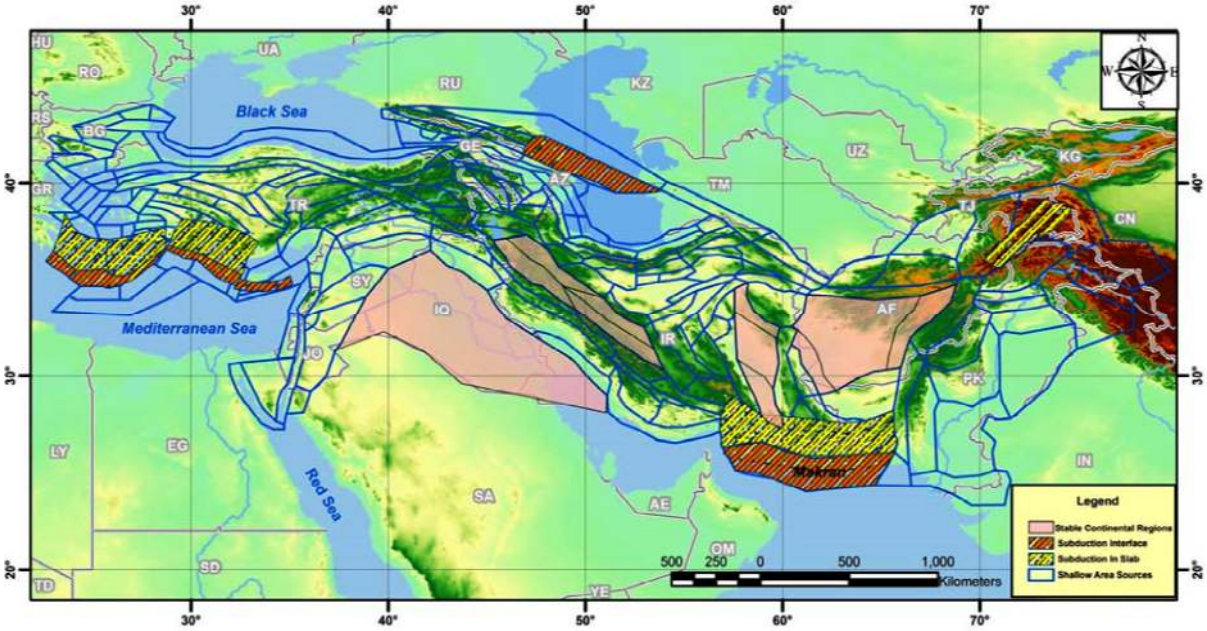

Fig. 5-22. The seismic source zonation map of the EMME region.

Table 5-9 lists the ground-motion models selected for GMPE logic tree for the EMME project and Fig. 5-23 shows the hazard maps for selected return periods for the median (from the logic tree) of PGA (), PGV, PGD and spectral ordinates at a reference bedrock level.

Table. 5-9. GMPE logic-tree in EMME (bold numbers denote suggested logic-tree weights).

GMPEs for SACRs	GMPEs for SRs
Akkar and Bommer (2010) 0.25	Boore and Atkinson (2003) 0.20
Akkar and Cagnan (2010) 0.25	Lin and Lee (2008) 0.20
Chiou and Youngs (2008) 0.25	Youngs et al. (1997) 0.20
Zhao et al. (2006) 0.25	Zhao et al. (2006) 0.40

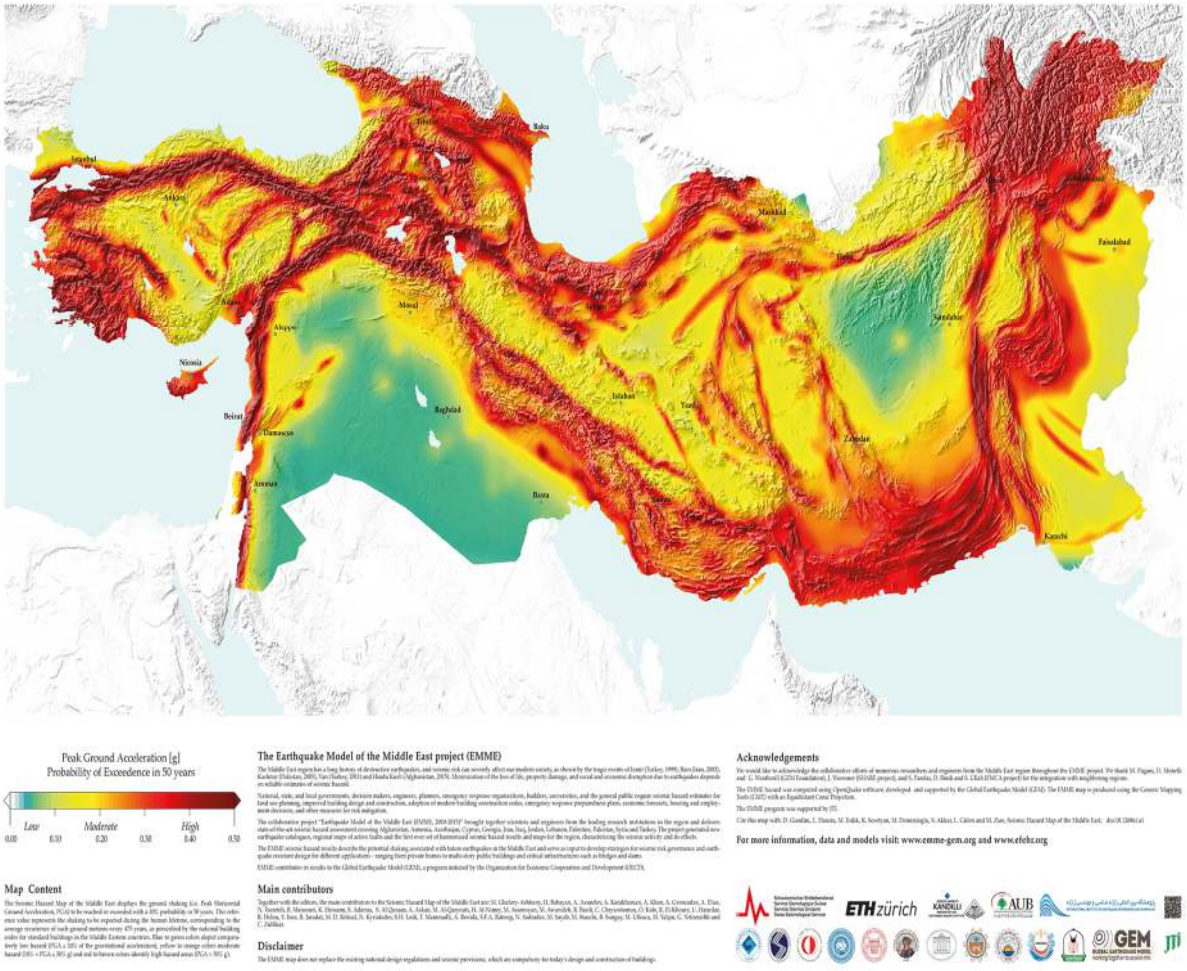

Fig. 5-23. The seismic hazard map of the Middle East displays the ground shaking (i.e. Peak Horizontal Ground Acceleration, PGA) to be reached or exceeded with a 10% probability in 50 years. This reference value represents the shaking to be expected during the human lifetime, corresponding to the averages recurrence of such ground motion every 475 years, as prescribed by the national building codes for standard building in the Middle Eastern countries. Blue to green colors depict comparatively low hazard (PGA ≤ 10%g of the gravitational acceleration), yellow to orange colors moderate hazard (10% < PGA ≤ 30%g) and red to brown colors identify high hazard areas (PGA>30%g).

5-6.2. Estimation of the maximum credible hazard in Kuala Lumpur and Singapore due to gigantic Sumatran mega thrust earthquakes: based on a comparative study on attenuation laws

* ***Source Article:*** *Vaez Shoushtari A., Azlan B.A and* ***Zaré M****, Harith NSH, (2015), "Estimation of the maximum credible hazard in Kuala Lumpur and Singapore due to gigantic Sumatran megathrust earthquakes: based on a comparative study on attenuation laws", Natural Hazards, Vol.78, pp. 725-751, doi: 10.1007/s11069-015-1742-6.*

In this section, I present a comparative study on attenuation laws for estimation of the maximum credible hazard in Kuala Lumpur and Singapore, an analysis taken from the published article by Vaez Shoushtari et al. (2015). In this paper, nine attenuation laws (including Nabilah and Balendra 2012; Zhao et al. 2006; Fukushima and Tanaka 1992; Petersen et al. 2004; Adnan et al. 2005; Megawati and Pan 2010; Atkinson and Boore 2003; Lin and Lee 2008 and Skarlatoudis et al. 2013) for subduction interface earthquakes in Sumatra as well as other regions with different limitations in the moment magnitude and source-to-site distance range were classified using PGAs recorded in Peninsular Malaysia and Singapore to identify which were the most compatible with the region.

In this study, only the peak ground accelerations of events recorded in Peninsular Malaysia and Singapore were collected and the attenuation law proposed by Zhao et al. (2006) was the most compatible spectral attenuation relationship with the region. Thus, in order to estimate the maximum credible hazard in Kuala Lumpur and Singapore, the predicted acceleration response spectra (geometric mean of two horizontal components—μ) due to the three worst possible earthquake scenarios were calculated based on the spectral attenuation law for three soil site classes (NEHRP site classes A, B, and C) for both cities. The results are shown in Figs. 5-24 and 5-25.

British Standard building design code (BS) 8110 (BS 8110-1:1997), being used in Peninsular Malaysia and Singapore, does not account for seismic loads. However, to ensure structural robustness, the design code does require that all buildings should be capable of resisting a notional ultimate horizontal design load that is equal to 1.5 % of the characteristic dead weight of the structure and applied at each floor level simultaneously. The design wind load should not be less than this value. Given the moderate design wind speed of about 30 m/s in Singapore (Megawati et al. 2005) and Kuala Lumpur, the notional horizontal load is generally greater than the wind loading for most medium-rise buildings. As a result, the

minimum design level of buildings across the entire natural period range is a constant at 1.5 % g (~0.15 m/s2) (Megawati and Pan 2010). This lateral design load is shown as a horizontal solid line in Figs. 5-24 and 5-25.

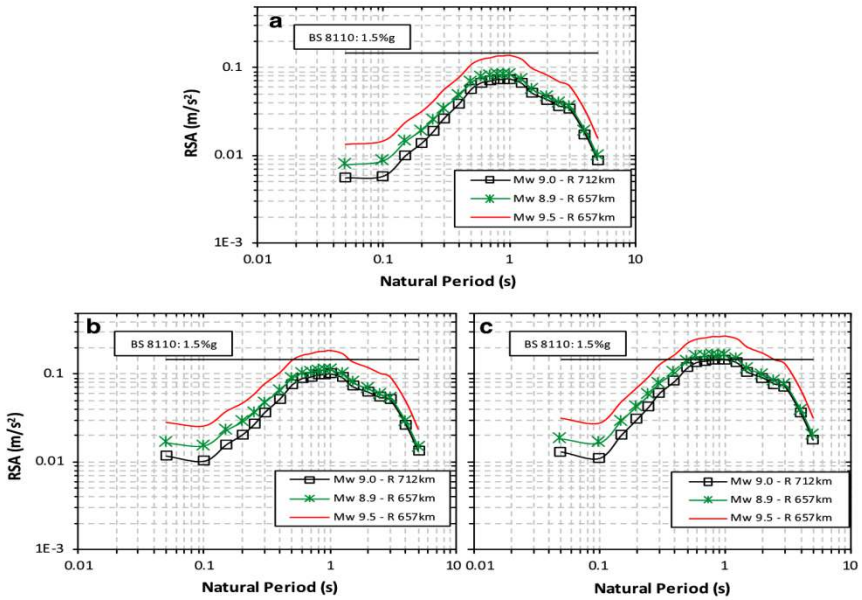

Fig. 5-24. Acceleration response spectra (μ—5 % damping ratio) in Kuala Lumpur on three soil site classes: a NEHRP site class A, b NEHRP site class B, and c NEHRP site class C, resulting from the three worst possible earthquake scenarios using Zhao et al. (2006) spectral attenuation law

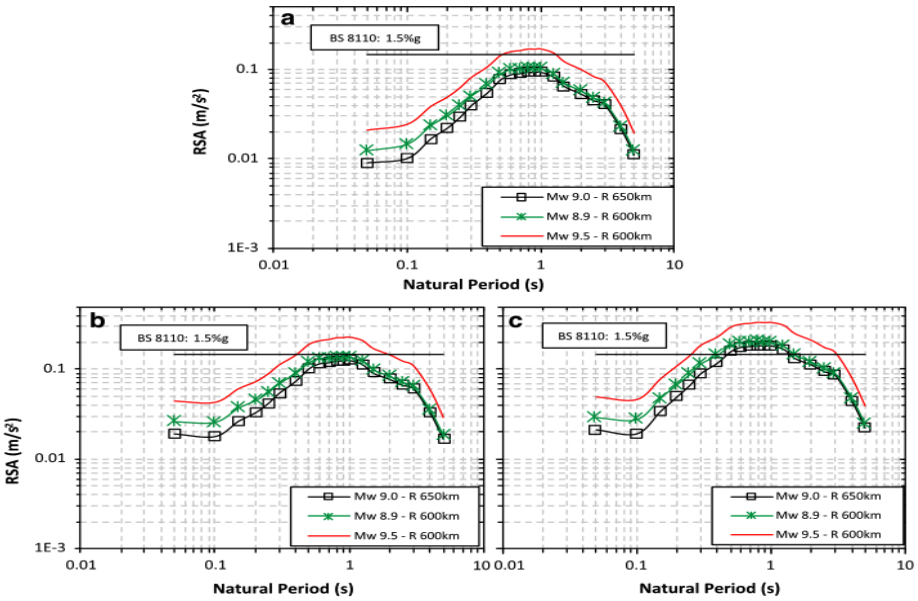

Fig. 5-25. Acceleration response spectra (μ—5 % damping ratio) in Singapore on three soil site classes: a NEHRP site class A, b NEHRP site class B, and c NEHRP site class C, resulting from the three worst possible earthquake scenarios using Zhao et al. (2006) spectral attenuation law

Fig. 5-24 shows that the design level of buildings in Kuala Lumpur with the entire natural period range located on hard rock sites (NEHRP site class A) was higher than the demand spectra caused by all the three worst possible earthquake scenarios. Fig. 5-24 shows that the risk level for typical buildings in Kuala Lumpur with natural periods ranging from 0.5 to 1.5 s on rock sites (NEHRP site class B) is low as the demand spectrum due to the worst possible earthquake scenario with M_W 9.5 and an estimated epicentral distance of 657 km is larger than the design level with a maximum value of 0.187 m/s2 at T_n=1s, corresponding to buildings with ten stories. Fig. 5-24 also shows that the risk level for buildings in Kuala Lumpur located on hard soil sites (NEHRP site class C) with the periods ranging from 0.5 to 2 s and subjected to the same earthquake scenario was relatively high as the demand spectrum was higher than the design level of the buildings. For instance, the response spectral acceleration values based on the demand spectrum for buildings with natural periods of one and one and half seconds (T_n= 1 and 1.5 s), corresponding to buildings with 10 and 15 stories, as are commonly found in Kuala Lumpur, were about 0.27 and 0.20 m/s^2 which means that they are 1.8 and 1.33 times larger than their 0.15 m/s^2 design level.

Fig. 5-25 shows higher values than Fig. 5-24 as the epicenters of the worst possible earthquake scenarios were closer to Singapore than to Kuala Lumpur. It is understood from Fig. 5-25 that the risk level for typical buildings in Singapore with natural periods ranging from 0.5 to 1.5 s on hard rock sites (NEHRP site class A) is very low as the demand spectrum due to the third worst possible earthquake scenario with M_W 9.5 and an epicentral distance of 600 km away from the city is larger than the design level with a maximum value of 0.17 m/s^2 at T_n=1 s, corresponding to 10-story buildings. Fig. 5-25 shows that although there is no risk to Singapore structures with T_n=1 s, located on NEHRP class B sites exposed to the first and second worst possible earthquake scenarios, the structures built on the same soil sites would be at risk during the third worst possible earthquake scenario as the demand spectrum based on Zhao et al. (2006) spectral attenuation relation is remarkably higher than the capacity of these structures. In Fig. 5-25, from the demand spectrum due to the same worst possible earthquake scenario (M_W 9.5—R_{epi} 600 km), it is shown that the risk level for buildings in Singapore located on hard soil sites (NEHRP site class C) with natural periods ranging from 0.5 to 2 s is very high as the demand is higher than the design level of the buildings. For example, at T_n= 1 and 1.5 s which corresponds to 10- and 15-story buildings that are frequently constructed in Singapore, the response spectrum acceleration values are about 0.33 and 0.25 m/s^2, which are about 120 and 67 % larger than the approved value of 1.5 % g. Fig.

5-25 shows that any future earthquakes similar to the first and second worst possible earthquake scenarios identified by Megawati and Pan (2002) and Balendra et al. (2002) would be able to put the buildings in Singapore with natural periods ranging from 0.5 to 1.25 s built on NEHRP class C sites at risk, as the demand spectrum values due to such earthquakes exceed their design level. As shown in Figs. 5-24 and 5-25, the peaks of the spectral acceleration based on Zhao et al. (2006) spectral attenuation law for distant gigantic Sumatran megathrust earthquakes (R_{epi}~600–712 km) have been occurred between 0.8 and 1s.

In this study, the normalized acceleration response spectra of all the three worst possible earthquake scenarios, on hard soil sites (NEHRP site class C) in Kuala Lumpur and Singapore, using the most compatible spectral attenuation law with the Peninsular Malaysia and Singapore region [i.e., Zhao et al. (2006) spectral relation], were compared to IBC 2012 (International Code Council 2011) and Eurocode 8 (BS EN 1998-1:2004) (type 2) design spectra. The normalized design spectra from IBC 2012 and EC8 (type 2) and the normalized acceleration response spectra due to the three worst possible earthquake scenarios are plotted together in Fig. 5-26.

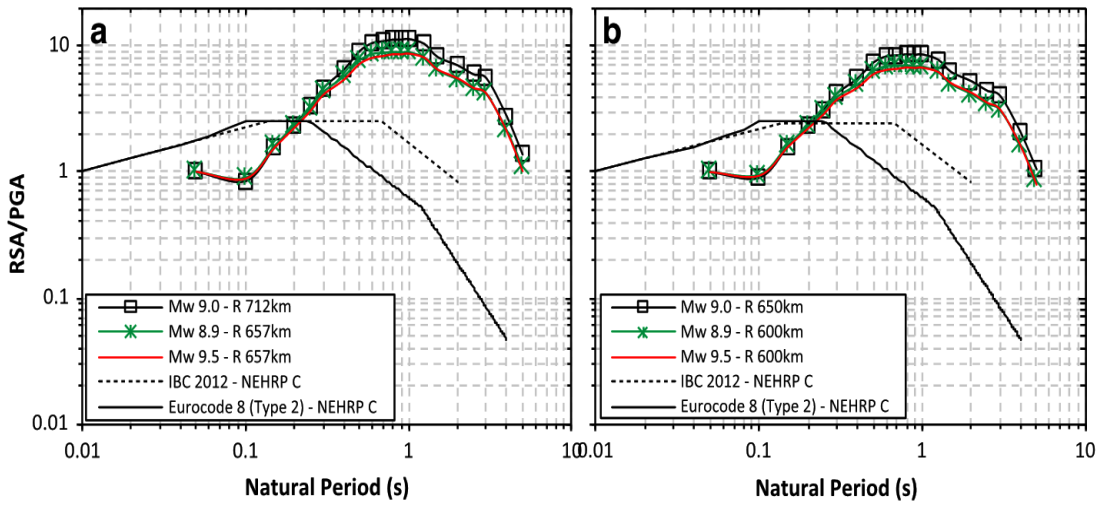

Fig. 5-26. Normalized acceleration response spectra from IBC 2012 and Eurocode 8 (Type 2) on NEHRP soil site class C and the three gigantic Sumatran megathrust earthquakes using Zhao et al. (2006) spectral attenuation law in a Kuala Lumpur and b Singapore

5-6.3. A case study of seismic hazard analysis at al-Tajiat and al-Zawraa stadiums in Baghdad/Iraq region

** **Source Article:** Norouzi N., Mojarab M, Asadi Z and **Zaré M**, (2014), "A Case Study of Seismic Hazard Analysis at Al-Tajiat and Al-Zawraa Stadiums in Baghdad/Iraq Region", Arabian Journal for Science and Engineering, Vol. 40, Issue 7, pp. 1987–2002, doi: 10.1007/s13369-014-1559-8.*

In this section, I present a case study of seismic hazard analysis at al-Tajiat and al-Zawraa stadiums in Baghdad/Iraq region, an analysis taken from the published article by Nourouzi et al. (2014).

Seismic Sources:

By means of all available geological, tectonic, and seismic data, five area seismic sources were identified (Fig. 5-27). Delineations of the source boundaries, especially for seismic source A_1, were chosen based on the topography of the region. The seismic source A_1 is placed in the Zagros continental collision zone, which is one of the youngest and most active tectonic regions on Earth.

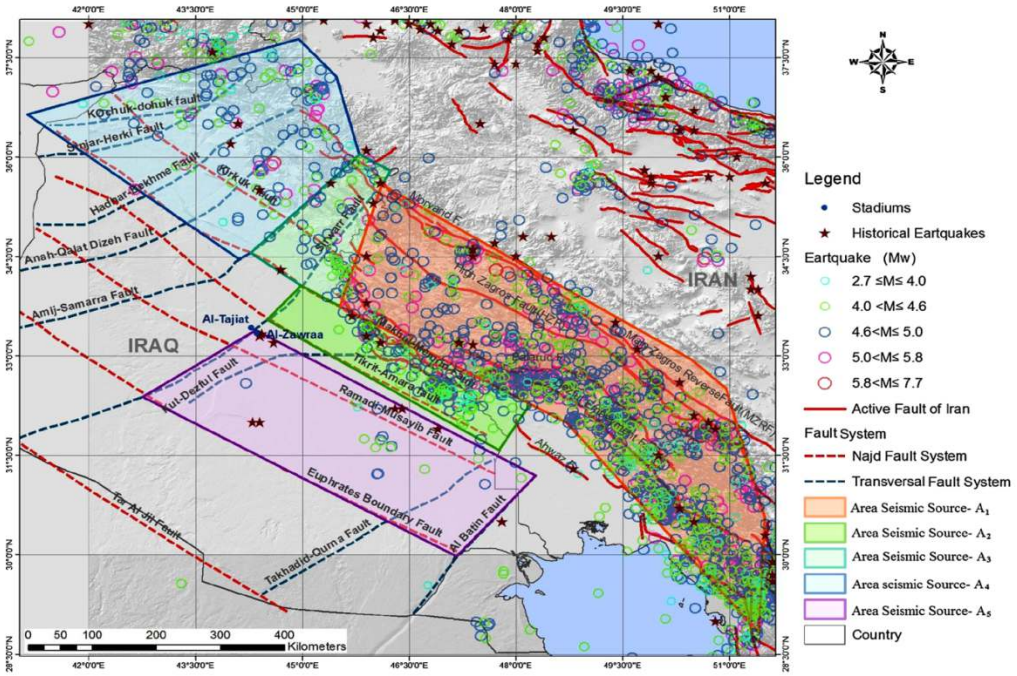

Fig. 5-27. Showing the seismic sources map

Seismicity Parameters:

A key issue in the seismic hazard analysis is the estimation of the seismicity parameters. The main parameters include the rate of occurrence (λ), the b (β)-value (slope of the Gutenberg–Richter magnitude–frequency curve; Gutenberg and Richter, 1956), and the maximum probable magnitude (M_{max}). In this study, the seismicity parameters were calculated by Matlab code using the latest extension of the procedure developed by Kijko and Sellevoll (1992).

The knowledge of the largest magnitude which may occur within a potential seismic source is of practical importance. The current study uses two main approaches to estimate M_{max}. The first approach was based on the observed earthquakes occurred in each seismic source assuming that major earthquakes happen preferentially near the sites of previous events. The second approach was based on a study done by Kijko and Sellevoll (1992) to estimate M_{max} in Kijko program. Practically, in order to select the assigned M_{max} for each seismic source, the maximum value of the obtained data was considered (Table 5-10).

Table. 5-10. Seismicity parameters of seismic sources

Area source	M_{min}	λ	β	*M* observed		Kijko program	Final *M*
				M_w	Date	M_{max}	
A1	4.1	4.73	1.24	7	1008	6.8	7
A2	4.8	1.9	3.15	6.5	1226/11/18	6	6.5
A3	4.8	0.36	2.9	6.6	1179/4/29	6.1	6.6
A4	4.8	1.09	2.78	6.8	1130/2/27	6.4	6.8
A5	4.8	0.33	1.66	6.1	1457	5.2	6.1

Seismic Hazard Analysis in Iraq:

According to the results of PSHA, differences between the two mentioned sites can be neglected. Therefore, the results obtained from seismic analysis of both sites are shown in Tables 5-11 and 5-12. The result of seismic hazard assessment based on DSHA method is shown in Table 5-13. As is obvious, the controlling source is A_5.

Table. 5-11. Horizontal PGA value based on different attenuation relationships in PSHA method

Return period	Abrahamson and Silva (2008)	Boore and Atkinson (2008)	Campbell and Bozorgnia (2008)	Chiou and Youngs (2008)	Zare et al. (1999)	Mean
75	0.06	0.06	0.04	0.05	0.04	0.06
475	0.12	0.09	0.08	0.17	0.06	0.12
2,475	0.19	0.14	0.13	0.29	0.09	0.21

Table. 5-12. Vertical PGA value based on different attenuation relationships in PSHA method

Return period	Campbell and Bozorgnia (2003)	Zare et al. (1999)	Mean
75	0.04	0.03	0.03
475	0.08	0.05	0.07
2,475	0.12	0.08	0.10

Table. 5-13. Horizontal and vertical PGA value based on DSHA method

Return period	Mw	PGAH	PGAV
A_5	6.1	0.31	0.16
A_2	6.5	0.13	0.07
A_1	7.0	0.04	0.01
A_3	6.6	0.03	0.01
A_4	6.8	0.03	0.01

Main articles of this chapter:

Mojarab M., Memarian H., **Zaré M**, Morshedy A.H., Pishahang M.H., (2014), "Modeling of the seismotectonic provinces of Iran using the self-organizing map algorithm", *Computers & Geosciences*, Vol. 67, pp. 150–162, doi: 10.1016/j.cageo.2013.12.007.

Karimiparidari S., **Zaré M**. and Memarian H., (2008), "New seismotectonic zoning map of Iran", *6th International Conference on Seismology and Earthquake Engineering (SEE6)*, Tehran, Iran.

Alipoor R., **Zaré M**. and Ghasemi M.R., (2012), "Inception of activity and slip rate on the Main Recent Fault of Zagros Mountains, Iran", *Geomorphology*, Vol. 175–176, pp. 86–97, doi: 10.1016/j.geomorph.2012.06.025.

Esmaeili, B. M. Almasian, **M. Zaré**, R. Alipoor, A. Alizadeh, (2014), "Geophysical and geological study on the West Qarchak fault and its implications in seismic hazard, Tehran, Northern Iran", *Episodes*, Vol. 37, no. 2, pp 105-110.

Salamat M., **Zaré M**., Holschneider M. and Zöller G., (2016), "Calculation of confidence intervals for the maximum magnitude of earthquakes in different seismotectonic zones of Iran", *Pure and Applied Geophysics*, pp 1–15, doi:10.1007/s00024-016-1418-5.

Asadi Z. and **Zaré M**, (2014), "Estimating magnitudes of prehistoric earthquakes and seismic capability of fault from landslide data in Noor valley (central Alborz, Iran)", *Natural Hazard*, Vol. 74, Issue 2, pp. 445–461, doi: 10.1007/s11069-014-1186-4.

Ommi S., Zafarani H, and **Zaré M**., (2016), "Aftershock Decay Rates in the Iranian Plateau", *Pure and Applied Geophysics*, Vol. 173, Issue 7, pp. 2305–2324, doi: 10.1007/s00024-016-1285-0.

Zaré M., Karimiparidari S., Memarian H., (2015) "Seismic Hazard Analysis in Iran (475 Years Return Period)", Submitted.

Zaré M., (2015), "Seismic Hazard Zoning in Iran: A State-of-the-Art on the Studies During Four Decades", Submitted.

Zaré M., Kamranzad F, Ostad-Taghizadeh A., (2016), "Risk Assessment of Multiple Natural Hazards in Tehran", Submitted.

Erdik M., Şeşetyan K., Demircioğlu M.B., Tüzün C., Giardini D., Gülen L., Akkar D.S. and **Zaré M**., (2015), "Assessment of Seismic Hazard in the Middle East and Caucasus: EMME (Earthquake Model of Middle East) Project", *15th World Conferences on Earthquake Engineering (WCEE)*

Vaez Shoushtari A., Azlan B.A and **Zaré M**, Harith NSH, (2015), "Estimation of the maximum credible hazard in Kuala Lumpur and Singapore due to gigantic Sumatran megathrust earthquakes: based on a comparative study on attenuation laws", *Natural Hazards*, Vol.78, pp. 725-751, doi: 10.1007/s11069-015-1742-6.

Norouzi N., Mojarab M, Asadi Z and **Zaré M**, (2014), "A Case Study of Seismic Hazard Analysis at Al-Tajiat and Al-Zawraa Stadiums in Baghdad/Iraq Region", *Arabian Journal for Science and Engineering*, Vol. 40, Issue 7, pp. 1987–2002, doi: 10.1007/s13369-014-1559-8.

Chapter 6: Lessons Learned from Earthquakes (Reconnaissance Studies of Earthquakes)

6-1. Introduction

Moderate to large magnitude earthquakes may lead to large damages. Field observations performed after many earthquakes in Iran indicate that there has been a major difference between the *observed* and the *expected* ground motions and intensities. A large part this difference about ground motions goes back to the lack of enough data or hypothesis (e.g. source geometry, faulting probabilities, etc...) as it was mentioned in chapters 1 and 5. In many cases, expected intensities are intensified by the unknown site effects such as soil amplifications as well as topography conditions.

In this chapter, a combination of lessons learned from in-situ earthquakes damages and subsequent phenomena observed during reconnaissance studies in different earthquake-affected areas are presented. In this regard, selected topics such as the data acquisition in earthquake recognitions, the analysis of recorded strong motions, the determination of physical damage, the near-field effects associated with directivity and fling-step, and the importance of these analysis in hazard zoning provide some insights into the seismic hazard assessment. These studies are the results of field investigations that I performed following the fourteen important recent earthquakes in Iran and other countries in the Middle East. The field studies by the author start from the 2003 Bam (Iran) earthquake, continue with the 2003 Boumerdès-Zemmouri (Algeria), 2005 Balakot (Pakistan), 2009 Padang (Indonesia), 2009 Southeastern Tehran (Iran), 2010 Kuh-Zar (Iran), 2011 Tohoku (Japan), 2011 Van (Turkey), 2012 Varzeghan (Iran) twin events, 2013 Shonbeh (Iran), 2013 Saravan (Iran), 2013 Bashagard (Iran), 2014 Mormori (Iran) earthquakes and finally ends to the 2015 Gorkha (Nepal) earthquake. The thesis shows a synthesis of the main observations and comparison of local SHA and scenarios between the different regions.

6-2. Earthquake intensity and damage distribution

In Table 6-1, a summary of the visited earthquakes is shown.

Table 6-1. List of the visited earthquakes by the author

No	Earthquake	Date	M_w	Depth (km)	I_0	No. Death	No. Injured
1	Manjil, Iran	1990/06/21	7.3	19	X	35,000	60,000
2	Boumerdès, Algeria	2003/05/21	6.8	12	X	2,266	10,261
3	Bam, Iran	2003/12/26	6.5	8	IX	33,000	50,000
4	Balakot, Pakistan	2005/10/08	7.6	15	VIII	87,000	70,000
5	Padang, Indonesia	2009/09/30	7.6	90	VII	1,115	2,902
6	Kuh-Zar, Iran	2010/08/27	5.7	15	VII	4	40
7	Tohoku, Japan	2011/03/11	9.1	29	IX	15,894	6,152
8	Van, Turkey	2011/10/23	7.1	7	VIII	644	4,412
9	Varzeghan, Iran	2012/08/11	6.3	12	VIII+	306	3,037
10	Shonbeh, Iran	2013/04/09	6.3	10	VII	37	850
11	Saravan, Iran	2013/04/16	7.7	82	VI	35	117
12	Bashagard, Iran	2013/05/11	6.2	25	VI+	1	-
13	Mormori, Iran	2014/08/18	6.2	10	VII	0	250
14	Gorkha, Nepal	2015/04/25	7.8	8	IX	8,964	21,952

The April 25, 2015 Nepal earthquake was practically the most recent destructive event, with widespread damages to many buildings, infrastructures and historic monuments mostly within the central part of the country. In all the visited areas, there were many low-resilient multi-storey masonry or concrete buildings which were fully collapsed, tilted or severely damaged. Most of the destructions had occurred in mountainous villages especially in Barpak, Laprak and Saurpani villages in Gorkha District as well as Langtang village in a 60 kilometer distance northeast of Kathmandu. In Kathmandu, violent damages were mostly observed in the central and western parts of the city. Around the Dhading New Bus Park in Gongabu ring road northwest of Kathmandu, business and shopping centers and residential complexes sustained major damages (Fig. 6-1). Based on our observations, the earthquake intensity was estimated to be about VIII, VII and V on the EMS98 intensity scale for the epicentral region, Kathmandu as well as Bhaktapur and Pokhara, respectively.

Fig. 6-1. Sever damages to the building in the Dhading New Bus Park in Gongabu Ring Road northwest of Kathmandu.

In 2014, M_w 6.2 earthquake happened in Mormori (Ilam) SW Iran. Based on the fields investigations (Zare et al., 2014), the most damages were observed in Mormori (a population of about 4000) and the villages of Abanar (Fig. 6-2) and Siahgel and there were also partial damages to historical and archaeological buildings. There were also some damages to the residential complexes of "Maskan-e Mehr" (social apartments built in the last decade in Iran for low-income people) in Abdanan (Fig. 6-3). The shake maps were developed for this event in which a maximum intensity of VII-VIII (EMS98) are estimated for the epicenter. The Maximum acceleration between 100 to 200 gals are estimated for the epicenter.

Fig. 6-2. Damage to the buildings in Abanar: collapse of walls, figures and object and plaster fall.

Fig. 6-3. Fissures created in "Mehr" Apartments (Maskan-e Mehr) in Abdanan (38km to the epicenter); constructed about one year ago and suffer extensive damages due to an intensity VI (EMS98) in the 18 Aug 2014 Mormori earthquake.

In 16 April 2013, Saravan earthquake of Mw 7.7 occurred in a *sparsely populated area* with about 35 km distance to the city of Gosht (Fig 6-4). *The shock was felt strongly in Gosht (assessed VI+, 35 km southwest of epicenter), Saravan (VI, 60 km S) and Zahedan (VI, 190 km NW) and less strongly in Masqat (IV, 650 km S) and Persian gulf Islands (IV, >700 km W) as well as the strong shaking felt in the high rise buildings of Dubai, Doha, Manama and even in Kuwait"* (Zare et al., 2013).

Fig. 6-4. The damages in the epicentral region of Gosht, Saravan Earthquake, 16 April 2013, Mw7.8 earthquake (Photo by AFP).

The M_w6.4 Shonbeh (Bushehr) earthquake was the next important event that happened the 2013. In Zare et al. (2013) we show that *"Most of the buildings damaged in the 2013 M_w6.4 Shonbeh (Bushehr), Iran earthquake were adobe buildings, made of heavy material and constructed in the last 50 years (Fig. 6-5). The walls collapsed mostly in east-west or NNW-SSE directions. The shock was felt strongly in Shonbeh (assessed at VII), 18 km SW of the epicenter; Khormoj (assessed at VI+), 22 km NE; and Bushehr (assessed at V), 86 km NW. The maximum recorded acceleration in this event was obtained in Khormoj (70 gals); the mainshock was recorded in Khormoj (the records are available at the BHRC web site: https://www.bhrc.ac.ir). In Bushehr (80 km NW of the epicenter), where the maximum acceleration was estimated at around 50 gals, there was no damage reported to a nuclear power plant"*.

Fig. 6-5. Buildings damaged in the 2013 Mw6.4 Shonbeh (Bushehr), Iran earthquake

On 11 August 2012, two relatively large shallow that struck Varzeghan region in NW Iran, causing about 306 deaths, 3037 injuries and 30000 homeless people. Following the earthquakes, reconnaissance team was dispatched to the area by IIEES (Zaré et al, 2012). According to Vasheghani Farahani and Zare, (2014), *"the maximum intensity was estimated to be VIII+ on the EMS98 scale in Varzeghan and affected villages, VII+ in Ahar city and VI+ in Heris city. The intensity of the earthquake in Tabriz was V.*

Based on observations in the region, the main failure mode was the collapse of heavy roofs. Masonry buildings, for example in Fig. 6-6-a, b (very weak mortar), suffered very heavy structural damage with a damage grade (based on Grunthal, 1998) of five (destruction), total or near total collapse. In Baj e Baj, most of the buildings were made of bricks and arched wood beam roofs, adobe and low-quality masonry materials. In types of structure with simple stone masonry such as in Fig. 6-6-c, d, some parts of the bearing walls collapse of the roof and floor slabs. This kind of heavy structural damage is of damage grade is 4. In Heris city, a hospital was built on a hill slope one year before the 11 August 2012 earthquakes. Although, the city was located about 20 km away from the earthquake epicenter, the hospital was rendered out of service. This hospital (the main health center near the epicentral zone) was located 73 kilometers east of Tabriz, the capital city of the east Azerbaijan province (Fig. 6-7- a, b). Moreover, there were some structures with large diagonal cracks in the walls or some cracks in the exterior wall in the twin Varzeghan earthquakes region. Fig. 6-7-c shows an example of these buildings that exhibited moderate structure damage of grade is 3. In type of structure with many vertical cracks, such as Fig. 6-7-d, slight structural damage resulted and the damage was of grade two".

Fig. 6-6. (a and b) Examples of total collapse in very weak buildings, (c and d). Examples of demolished buildings in Varzeghan (left-c) and Baj e Baj (right-d) (Zaré et al, 2012).

Fig. 6-7. (a and b). Examples of Heris Hospital, (c and d). Example of diagonal cracks in walls, and of slight structural damage in the region, respectively (Zaré, 2012).

By the occurrence of the 27 August 2010 Mw 5.7 Kuh-Zar earthquake (Iran), More than 80% of the rural houses in Iran are composed of adobe or stone masonry and are constructed using only local materials and unskilled labor (Maheri et al. 2005). In the Kuh-Zar region, the greatest intensity of damage was due to the traditional construction, very poor clay materials, single-story houses of weak masonry, non-reinforced adobe (Fig. 6-8-d), overloaded construction, and flat wooden and steel-beamed roofs (Fig. 6-8-e), a number of which were damaged in the earthquake (Shahvar and Zare., 2012).

Fig. 6-8. Field photographs: a Coseismic fracture near the epicenter (Foroutan et al. 2010). b Crack from the 2010 Kuh-Zar earthquake (near the epicenter), cracks strike E to W. c Fissuring in Kelu village, 5 kilometers from the epicenter, crack strike is N70. d Typical adobe-brick house at Kelu; the non-load-bearing walls collapse in an earthquake first. e Collapse started in the corner, where it was easier to initiate instability.

An M_w7.6 earthquake hit the western Sumatra and Padang city on September 30th 2009. A reconnaissance team was dispatched to the area by IIEES. There was no ground motion record available to estimate the earthquake PGA or the response spectra. The damage observation covers building and houses, water supply network and transportation system. A quick survey of hospitals was also performed during the reconnaissance trip. The buildings in the region can be categorized mainly as masonry and RC buildings. Low quality material and incorrect construction methods were identified as the main reasons of damage as shown in the following pictures. Soft storey effect was observed in several RC buildings in the Padang city. Considerable damage to historical buildings was observed (Fig. 6-9).

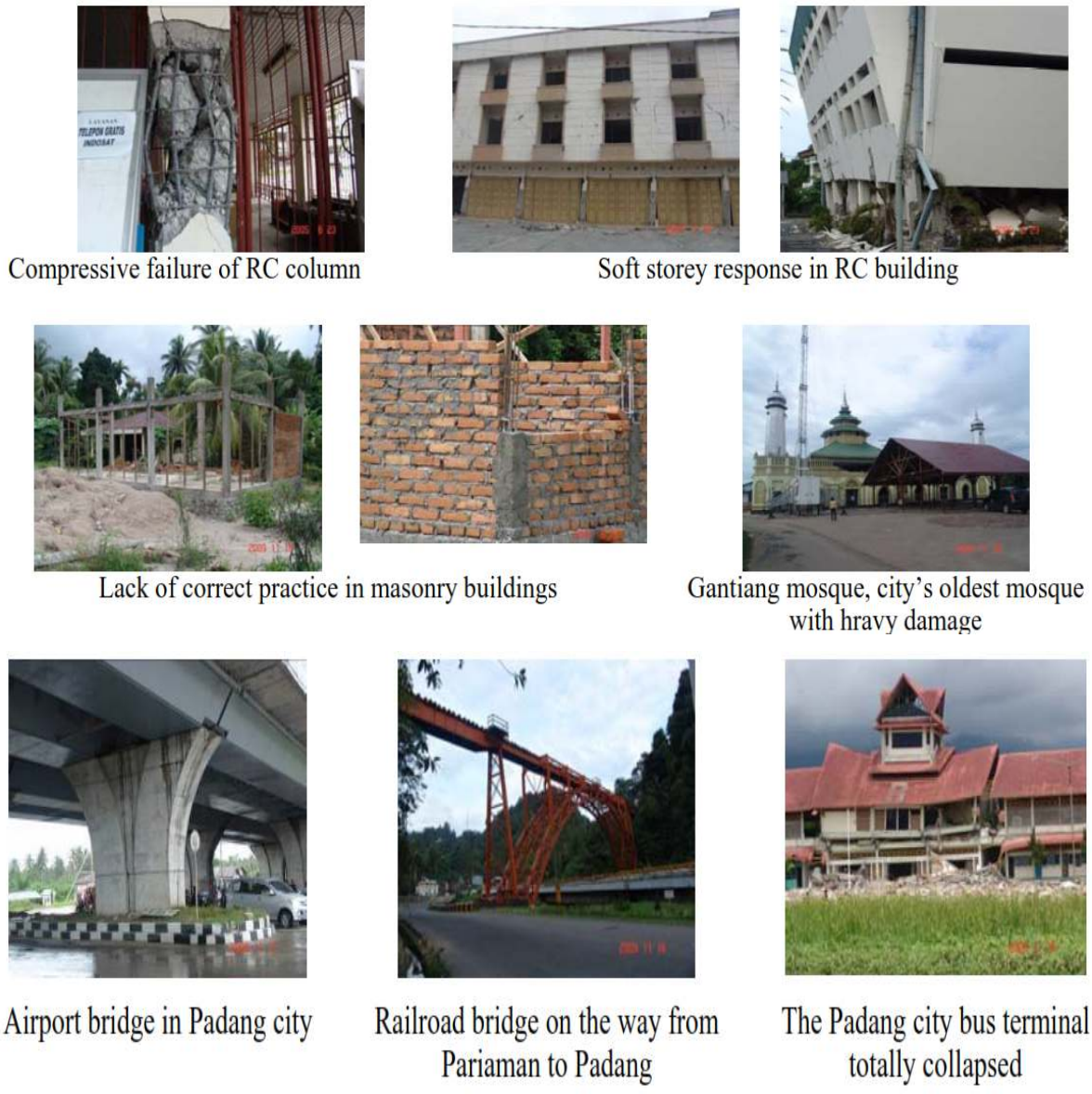

Fig. 6-9. Different examples of damages to buildings and transportation facilities

Following the 8 October 2005 Pakistan earthquake, a visit to the earthquake area was performed by the author. *"The visits took place less than 3 weeks after the epicentral mainshock. The maximum intensity was estimated to be around Balakot and along Muzaffarabad fault, with a width of 10–15 km around the fault. The greatest damage was observed in Balakot representing complete destruction (i.e., more than 1 m dislocation of the concrete bridge over Balakot River; Fig. 6-10). Balakot region is as-signed intensity X [according to The European Macroseismic Scale (EMS-98) scale]. All buildings in this valley city were destroyed totally. The city of Muzaffarabad is located on a river terrace. Based on damages seen in Ijaz Golab military hospital, an intensity of IX on EMS-98 scale is estimated. The retaining walls were collapsed in some roads (Fig. 6-11). In Ijaz Golab hospital, the northern block fell down due to the first floor collapse (soft story), but other parts of the hospital show less damage. The daily life had returned to normal 18 days after the event when IIEES reconnaissance team visited the epicentral region. Intensity in Abbottabad was estimated to be VIII (EMS-98 scale) derived from a hotel col-lapse. Due to the observed damage of residential buildings, VIII intensity is assigned to Mansehra (Fig. 6-12). No damage was observed on the dam and the facilities upon the inspection of Tarbela earth-rock fill dam. To the SW of the epicenter, the landslides were observed in the region between Punjab and Jammu and Kashmir (India). This region is assigned an intensity of about VI. While there was not as much damage in Islamabad, a Margala tower collapsed in the north-west of Islamabad (Fig. 6-13) because of its struc-tural engineering and also the type of soil (grain alluvium with clay matrix)"* (Zare and Karimiparidari, 2008).

Fig. 6-10. About 1 m displacement in the abutment of Balakot southern bridge due to the earthquake mainshock on 8 Oct. 2005

Fig. 6-11. Muzaffarabad: the retaining wall collapse due to Balakot earthquake mainshock on 8 Oct. 2005

Fig. 6-12. Destruction at Mansehra

Fig. 6-13. Margala Tower collapse in Islamabad (Associated Press, Oct. 2005)

Another destructive earthquake during last decades in Iran was the Bam (SE Iran) earthquake of 26 December 2003, Mw6.5 which was explained previously in Chapter 5. The macroseismic intensity of the earthquake is estimated to be I0=IX (in the EMS98 scale), where the strong motions and damaging effects seems to be attenuated very fast especially in the fault-normal direction. The intensity levels are estimated to be VIII in Baravat, VII in New-Arg (Arg-e Jadid) and the airport area. The intensity level was estimated to be around IV-V in Kerman and Mahan.

In the 2009, M_w7.6, Padang, Sumatra, Indonesia, site effect might had an essential role in amplifying the ground shaking in the epicentral area, especially in the city of Padang. This idea come from the most sever damages observed to the engineered constructed building in this city, while the epicentral distances for this city is greater than the central part of the Pariaman, for example. A preliminary Vs30 map prepared by Petresen (2007) based on assigning a shear wave velocity to geological units. The soils in Padang city consist mainly from Quaternary alluvium (includes some swamps, bay and estuary mud) and have a very low shear wave velocity in upper 30 meters (180- 360 m/s). Regarding this range of velocity we can expected the ground motion amplification for the frequencies ranges from 1.5 to 4 Hz.

6-3. Earthquake-induced landslides

Earthquake-induced landslides are common events that occur after large earthquakes, moving medium to huge debris and blocking roads and lifelines. Based on the performed reconnaissance surveys by the author, large earthquake-induced landslides were observed in mountainous areas during the 1990 Manjil-Iran, 2005 Balakot-Pakistan, 2009 Padang-Indonesia, 2013 Goharan-Iran and 2015 Gorkha-Nepal earthquakes some of which are pointed out briefly in the following.

In Zare et al. (2008), we show that *"The 2005 Balakot, Pakistan earthquake occurrence accompanied by landslides made a lot of dust especially in Darebagh, Muzaffarabad, and Balakot. Such phenomena with huge stones falling destroyed the roads in different places (Fig. 6-15) and blocked the traffic, leading to extreme congestion. Numerous landslides occurred in the meisoseismal region, and most of them were associated with the fault scarp where the rupture reached the surface. The landslides mostly occurred from the eastern parts of Darebagh to Muzaffarabad and Balakot (Fig. 6-16) which damaged or blocked roads and also induced some damages to the transport facilities such as tunnels, having no halter or cover, and bridges in the south of Muzaffarabad. Some vertical and horizontal cracks and fissures have been observed on the south Muzaffarabad Bridge. The bridge was barricaded, and the road was closed in the first days after the event. By reopening this tunnel, the connection between Islamabad and Muzaffarabad was resumed"*.

Fig. 6-15. Islamabad–Muzaffarabad road destroyed by Balakot earthquake on 8 Oct. 2005

Fig. 6-16. An example of landslide south of Balakot along the earthquake fault rupture

Relief Web reported that over 1000 landslides were triggered by the 2009 Padang, Indonesia earthquake. Based on the reports 400-600 death of the total of more than 1200 death caused by earthquake were killed by landslides. Three villages were completely demolished by landslide and many others were damaged (Fig. 6-17). Many roads were damaged or blocked by landslides and result in difficulties in rescue efforts. The most destructive landslides happened during this earthquake are concentrated in the Tandikat regency.

Fig. 6-17. Two giant landslides happened on Tandikat regency along the Lembah Tiga valley. Upper part of the photo: Cumanak landslide wiped and buried the village of Cumanak and killed near 200-300 peoples gathered for a wedding ceremony. Lower part of the photo: a landslide adjacent to the Lubuk Laweh landslide cut a road.

Such phenomenon was also observed as a major rock slide about 5km north of Goharan during 11 May 2013 Bashagard earthquake of Iran (Fig. 6-18).

Fig. 6-18. A rock slide in the Goharan to Irar road, during the 11 May 2013 earthquake.

Following the 2015 Gorkha Nepal earthquake, many landslides, avalanches, ground fissures and fault ruptures happened. Based on our observations, the earthquake triggered some new landslides in the form of debris falls and rock slides along the intercity road from Kathmandu westward to Gorkha and Pokhara. At about 62 km west of Kathmandu, a relatively large landslide could be observed with an approximate size of 100m width * 50m length (Fig. 6-19). Because of the continued aftershocks occurred throughout Nepal in the first weeks, the country also had a continued risk of landslides. The earthquake also sparked an avalanche on Mount Everest and a huge avalanche in the Langtang valley, blocking mountain routes, killing several individuals and missing hundreds. In Pokhara city, there were some structure damages mostly due to earthquake-induced landslides. It is notable that the city of Pokhara is located aside the Phewa Lake in 207 km west of Kathmandu. Evidently, the Phewa lake seems to be formed by a landslide dam (possibly triggered by the 1833 or 1934 earthquakes) (Fig. 6-20).

Fig. 6-19. Observed debris slide with about 100m width and 50m length 62 km west of Kathmandu.

Fig. 6-20. The Phewa Lake that seems to be formed by a landslide dam (possibly triggered by a previous earthquakes). Red arrow shows the direction of the probable earthquake-induced landslide blocking the lake.

6-4. Fault ruptures, surface fissures and geotechnical features

One of the superficial phenomenon caused by the earthquake are surface fissures anf cracks as well as fault rupture. In the following, some of the observed fault ruptures and surface fissures are pointed out briefly.

A typical ground fissure was observed at a distance about 9 km southeast of Kathmandu toward Bhaktapur with a NE-SW direction and 2 meter vertical displacement (Fig. 6-21) as an aftermath of the 2015 Gorkha, Nepal earthquake.

Fig. 6-21. Ground surface fissures with azimuth of 196-208° and 2m vertical displacement occurred in the road between Bhaktapour and Kathmandu.

Such surface fissures were found nearby Gosht and in the Village of Gol-Pichak during the 2013, Mw7.8, Gosht (Saravan) earthquake (Fig. 6-22).

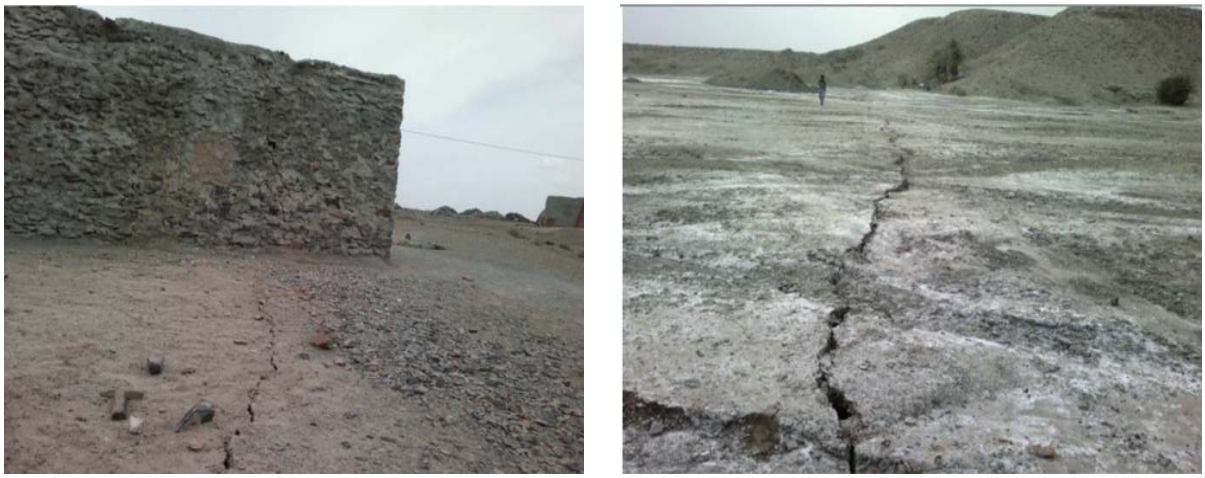

Fig. 6-22. The surface fissure in Gol-Pichak village (nearby Gosht) created during the mainshock of 16 April 2013 Mw7.8 earthquake.

In Zare et al. (2013) we show that *"according to the existing faults in the region of the 2013 Bashagard, SE of Iran, the Manujan fault with a right lateral strike-slip movement and a NW-SE trend having a slip towards east was expected to be the causative fault. The location of the epicenter and the fault slip towards east might be a justification for a depth between 20 to 25km for this earthquake. The Surface fissures, is observed around the road from Goharan to Irar (kilometer 5, north of Goharan, and just at the end of this road (Fig. 6-23). However it does not present the systematic evidences of surface fault rupturing, it continues in an enechelon NE-SW direction near Irar (Fig. 6-24), along about 5kms, and the fissure segments has mostly the azimuths of N320 to N330"*.

Fig. 6-23. The tension cracks in the Goharan to Irar road, created during the mainshock of the 11 May 2013 earthquake.

Fig. 6-24. Surface fissures in the epicenter of 11 May 2013, Mw6.2 Iran earthquake (in the village of Irar).

The 2012 Varzeghan earthquakes caused ground surface rupture. The causative fault was assessed to be the South Ahar fault, having an east-west trend and a length of about 60 km. The surface rupture of the Varzeghan fault was surveyed along about 4 km of ground surface by the investigating team and is located 13 km south of Varzeghan. Its Azimuth is N 245-260 degrees, as shown on Fig. 6-25.

Fig. 6-25. Surface rupture on the Varzeghan twin earthquakes fault (Zaré, 2012).

Such a situation was also observed in the 2003 Bam earthquake in which according to Eshghi and Zare. (2003), *"The Bam fault with a near north-south direction passes from the vicinity of the city of Bam (less that 1km distance to the east of Bam, and between the cities of Bam and Baravat. The surface fissures created after the Bam earthquake are observed around the Bam fault between the cities on Bam and Baravat (Fig. 6-26). The fissures are created in the form of the sinkholes in the city of Baravat (Fig. 6-27)"*.

Figure 6-26. The surface fissures along the Bam fault (near Baravat) in the prone area of the 26/12/2003 earthquake). a) The fissures nearby Baravat, b) the fissure that ruptured the road from Bam to Baravat, and c) the fissures in the foot of the fault scarp of the Bam fault.

Figure 6-27. The sinkholes created during the 26/12/2006 Bam earthquake in Baravat.

The 2014 Mormori (Ilam) SW Iran's earthquake caused road blocks, fissures and subsidence in the road (kilometer of 32 from Darreh-Shahr; Fig. 6-28 and 6-29), and followed up by the debris slides during the aftershocks.

Fig. 6-28. Darreh-Shahr to Abdanan Road (20km from Darreh-Shahr) caused the road block (about 52km to the epicenter.)

Fig. 6-29. Road from Darreh-Shahr to Abdanan (32km from Darreh-Shahr): Fissures and land subsidence caused by the 18 August 2014 earthquake (about 42km distance to epicenter).

In Zare et al. (2013) we show that *"the 2013, Mw 6.4 Shonbeh earthquake had some geotechnical features. Near Shonbeh (4km southeast of the city) there is clear evidence of liquefaction along the Mond River in the Dashte-Zaal ("white plain"), (Fig. 6-30). Some*

surface tension cracks were induced by liquefaction in the Mond River terrace (Fig. 6-31). These features could be seen along about 3 km of the terrace. Surface fissures along the reported causative fault could be observed south of Shonbeh, on the road to Baghan and Bandar-Daiyer (Fig. 6-32 and 6-33). These en-echelon, non-continuous segmented fissures do not show the displacement consistent with the fault mechanism (compressional with a strike slip movement); however, it is mostly a vertical displacement in most of segment, with some surface strike slip movements (not systematic in the same direction). The segments were located about 1 km distant from the Jashak Salt Diapir and it may be that the salt layers are effective in conducting the rupture to the alluvium surface".

Fig. 6-30. Close-up view of liquefaction in the Dashte Zaal area.

Fig. 6-31. Extension cracks and joints in young alluvium river bank deposit in the Dashte Zaal.

Fig. 6-32. Surface fissure (N300-320) in young alluvium deposit, east area of Jashk Salt-Diapir 8 km of this fissure could be seen in the field.

Fig. 6-33. Closer view of surface fissure (N300-320) in young deposits.

Main articles of this chapter:

Talebi M, **Zaré M**., A. R. Madahi-zadeh and Bali-Lashak, (2015), "Spatial-temporal analysis of seismicity before the 2012 Varzeghan, Iran, Mw 6.5 earthquake", *Turkish Journal of Earth Sciences*, Vol24, 24: TÜBİTAK doi:10.3906/yer-1410-13, pp.1-13.

Zaré M, (2015), "Le séisme de Gorkha, Népal, 2015; Rapport de Reconnaissance et distribution des dégâts", *9ème Colloque National AFPS 2007* – Ecole Centrale Paris, 8 pages.

Zaré M., Saeedi M., Kamranzad F. and Pishnamazi P., (2015), "An overview of disaster management during the April 25, 2015 Mw7.8 Nepal earthquake", subimtted.

Vasheghani-Farhani J. and **Zaré M**, (2014), "Seismological aspects of the Varzeghan twin Earthquakes on 11 August 2012 (Mw 6.3 and Mw 6.1), in East Azerbaijan province, NW Iran", *Episodes* Vol. 37, no. 2, pp. 96-104.

Zaré M., Farzanegan E., Shahvar M., Kamali E. and Saeidi A., (2014), "Mormori (Ilam) SW Iran's Earthquake of 18 August 2014, Mw6.2: A Preliminary Reconnaissance Report ", published by *EERRI*, 22 pages.

Shahvar , M. P. and **Zaré M**, (2013), The 27 August 2010 Mw 5.7 Kuh-Zar earthquake (Iran): field investigation and strong-motion evidence, *Natural Hazards*, DOI 10.1007/s11069-012-0507-8.

Zaré M., and B. Nazmazar, (2013), Van, Turkey Earthquake of 23 October 2011, Mw 7.2; An Overview on Disaster Management, *Iranian Journal of Public Health*, Vol. 42, No.2, Feb 2013, pp. 134-144.

Zaré M., Ansari A., Ashkpour-Motlagh SH., Esmaeili B. and Shahvar M., (2013), "The Mw6.4 Shonbeh (Bushehr), Iran Earthquake, April 2013 ", published by *EERRI*, 7 pages.

Zaré M., Ansari A., Heydari H., Shahvar M., Daneshdust M., Mahdian M., Sinaiean F., Farzanegan E and Mirzaei-Alavijeh H., (2013), "A Reconnaissance Report on two Iran, Makran Earthquakes: Iran, Makran Earthquakes ; 16 April 2013, Mw7.8, Gosht (Saravan) and 11 May 2013 Irar (Goharan), Bashagard, SE of Iran", report published by *EERI*, 12 pages.

Zaré M. and , S Ghaychi Afrouz, (2012), Crisis Management of Tohoku; Japan Earthquake and Tsunami, 11 March 2011, *Iranian Journal of Public Health*, Vol. 41, No.6, Jun 2012, pp.12-20.

Vasheghani Farahani J and **Zaré M**, (2011), The Southeastern Tehran Earthquake of 17 October 2009 (Mw = 4.0), doi: 10.1785/gssrl.82.3.404, *Seismological Research Letters* May/June 2011 v. 82 no. 3 p. 404-412.

Zaré M., Haghshenas E.and Kalantari A., (2009), "Earthquake of 30 September 2009, Mw7.6, Padang, Sumatra, Indonesia: A Preliminary Reconnaissance Report ", published by IIEES and the collaboration ofCenter of Technology for Natural Resources Inventory (PTISDA), Jakarta – Indonesia, 6 pages.

Zaré M., S. Karimiparidari, MonaLisa, (2009), An investigation on Balakot, Muzaffarabad (Pakistan) earthquake, 8 Oct. 2005, Mw 7.6; geological aspects and intensity distribution, *Journal of Seismology*, DOI 10.1007/s10950-008-9120-4.

Zaré M., (2003), "A preliminary reconnaissance report on the Algeria earthquake of 21 May 2003, Mw6. 8", http://www. iiees.ac.ir.

Eshghi S. and **Zaré M** (2003), "Bam (SE Iran) earthquake of 26 December 2003, Mw6. 5: A preliminary reconnaissance report", 7 pages, available on *IIEES*, http://www. iiees.ac.ir.

Chapter 7: Research Proposal: A Regional Seismic Database (Earthquake Catalog and Strong Motion Database) for the South Asia Region

7-1. Earthquake Hazard in the South Asia

The South Asia region is located in the Alpine-Himalayan chain where the tectonic plates collide with high rates of deformation. In tectonic terms, the Asia is on four large tectonic plates that are: (i) Eurasian plate (include Europe and almost all Asia); (ii) Arabian Plate; (iii) India plate (or Indo-Australian plate in old books); and (iv) a small part of North American plate. More important tectonic feature that are regional sources of earthquakes are: (a) continental collision between Indo-Australian plate and Asian plate; (b) many offshore subduction zones in Pacific and Indic ocean and (c) collision between the Eurasian and Arabian plates in the Middle-East and the Iranian Plateau.

In the past century, several destructive earthquakes have occurred in the region such as the October 26, 2015 Afghanistan-Pakistan (M_w7.5), April 25, 2015 Gorkha Nepal (M_w7.8), September 24, 2013 Balochistan Pakistan (M_w7.7) October 8, 2005 Balakot Pakistan (M_w7.6), December 26, 2004 Sumatra (M_w9.3), January 26, 2001 Gujarat India (M_w7.9), September 29, 1993 Latur-Killari, India (M_w6.2), August 15, 1950 Assam–Tibet (M_w8.7), January 15, 1934 Nepal–Bihar (M_w8.3) and June 12, 1897 Assam India (M_w8.3).

With respect to the high seismicity and experience of destructive large-magnitude earthquakes, it reminds that several metropolis in the South Asia, such as Dhaka in Bangladesh, Kolkata, Mumbai and Delhi in India, Karachi in Pakistan, Kabul in Afghanistan and etc, are exposed to high seismic hazards and risks. The cities are almost taken into account as metropolises of developing or less-developed countries where more efforts for data provisions, seismic hazard investigations and risk assessments are necessary in order to reduce life and property losses.

As an example, on April 25, 2015, an intense M_w7.8 earthquake struck the central Nepal, causing large damages to the structures and infrastructures of the Nepal's society and claiming more than 8000 lives and 22,000 injuries. It is believed that the 25 April 2015 Nepal’s earthquake is the first major earthquake in a third world country where the following damages is not determined by the number of dead people (which was not relatively high comparing to the vulnerability of such a major quake), but by the damages to its key infrastructures (in the form of damages that will make the future of this poor country harder and more complicated). The 2015 Nepal’s earthquake is a symbol of the vulnerability and resiliency in densely populated areas of the third world, underdeveloped and developing countries facing natural disasters, particularly earthquakes in the twenty-first century.

On the other hand, seismic designs have not been considered in low-seismic regions of Southeast Asia, as these regions have never experienced disasters due to earthquakes. Kuala Lumpur, the capital of Malaysia, and Singapore are good examples of these regions. Even though they are both located in a low-seismic region, they may be vulnerable to distant earthquakes generated by the active seismic zones located more than 300 km away, along and off the western coast of Sumatra Island. These seismic zones have generated numerous earthquakes some of which have shaken high-rise structures in Kuala Lumpur and Singapore. The number of felt events is increasing due to the rapid construction of high-rise buildings in these two cities (Pan 1997). Even though earthquakes have never caused any structural damage in Kuala Lumpur or Singapore, the effects of even a moderate level of ground motion may be enormous because of the large population and many commercial activities taking place in structures that have not been designed for earthquake loads (Megawati et al. 2005).

Important available prepared seismic hazard maps for the region of interest, are those developed by the Global Seismic Hazard Assessment Program (GSHAP, 1999) (Fig. 7-1a) and some parts of interest (e.g. Afghanistan and Pakistan) in the EMME hazard map (Giardini et al, 2016) performed under the framework of Global Earthquake Model (GEM) (Fig. 7-1b).

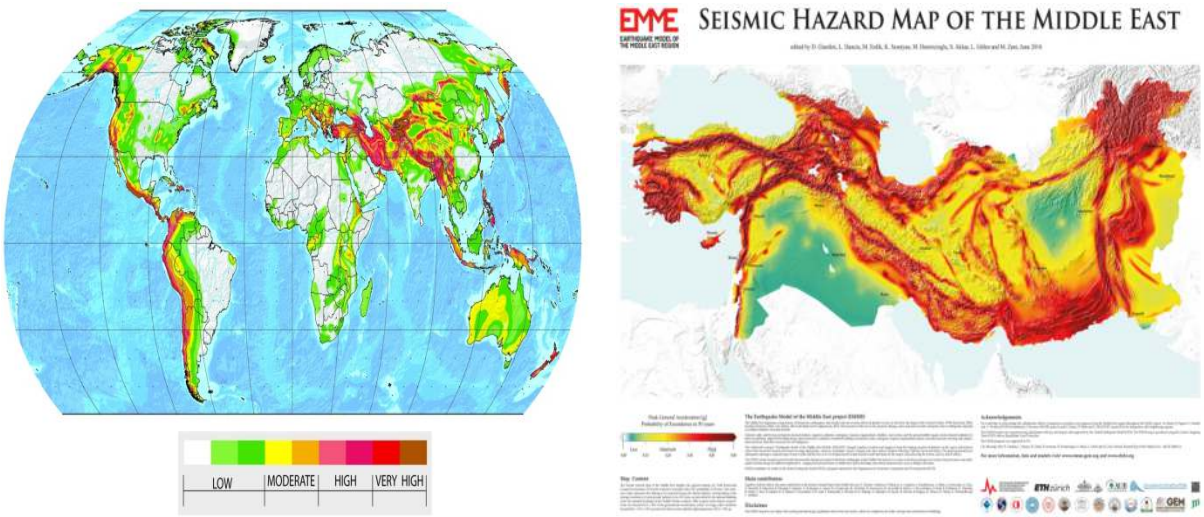

(a) (b)

Fig. 7-1. (a): Global seismic hazard by (GSHAP, 1999) and (b) seismic hazard map of the Middle-East region (Giardini et al, 2016).

Although there have been several studies about seismicity and earthquake hazard of the South Asia region, more attempts are needed in dataset collection including seismicity catalog and strong motion databases which can improve future researches and give more insights and less uncertainties in seismic hazard assessments.

7-2. Scope of the Project

- Undertake and in-depth analysis of the existing studies conducted in Asia Pacific countries related to seismic hazard and risk mapping, geophysical and geological tectonics of the region, seismic risk management policies and analyzing its institutions and their roles, legal and organizational frameworks.
- Contribute to the improvement of seismic risk reduction through providing the government and other actors with up-to date data and systemic analysis of seismic risk management delivery systems at city, national and international level;
- Dialogue with decision-makers and sensitization among them about importance of seismic risk vs. seismic hazard;
- Updating and/or preparation of earthquake catalogue, seismic sources and ground motion prediction equations for model building;
- Verification of existing seismic, geological and geotechnical studies, comprehensive interaction between the existing projects;
- Capacity building among experts and decision-makers of the South Asia countries, integrating local expertise in a sub-regional context and communicating earthquake risk clearly, accurately and transparently to all users;

7-3. Working Packages

Task 1: Compilation of existing catalogs

The current historical earthquake catalog will be culled from various catalogs, both global and local, that are developed since the first catalogs. Early global catalogs made simple mention of earthquakes. Meanwhile, catalogs that mainly focused on the region give more explicit descriptions of earthquake accounts and adopted descriptions by local historians. Over the years, various historians and seismologists kept on building their own catalogs whose contents varied depending on each author's perspective and purpose. For example,

some authors make simple listings of earthquakes while some would include detailed descriptions. Others give their own intensity estimates as well as draw their own isoseismal maps.

1: *Global earthquake catalogs*

The existing historical earthquake data of the South Asia region (in the global catalogs) starts since prehistoric earthquakes and mainly related to last 15 centuries, when the earthquakes affecting the region started to be noticed and documented. These earthquake citations may be grouped into those cited in global catalogs while the other group belongs to the country-specific catalogs. The redetermination of the magnitudes covering pre-1900 to early 20th century period will help to improve the earthquake data in the South Asia region.

2: *Country-focused historical earthquake catalogs*

These sources included various European travelers who wrote books, chronicles or accounts of their travels. Despite exaggerations and misquoted names of places, works became one of the most referred to earthquake catalog for the region.

Task 2: Reevaluating the historical earthquake catalogs

After determining the epicenters of historical events, we evaluate the completeness of the resulting historical catalog. We plot the typical yearly number of earthquakes with M 6.5 and above for the region for both the historical and recent periods. A substantial number of earthquakes will be reviewed and located.

Task 3: Incorporating the new sources of information

Inaccuracies, exaggerations and biases sometimes creep into interpretation of historical accounts. Thus, it is always better to go back to the primary source of information. The search for new sources of information starts from the original list of references by previous authors. The original list has since more than doubled and potential new sources of information will be considered.

7-4. Strong Motion Database

- To derive region specific ground-motion prediction equations for the South Asia and Caucuses by considering various ground-motion parameters that involve spectral acceleration, displacement and peak ground-motion values.

- To develop region specific tools useful for mapping local site conditions based on Vs_{30} proxies, which are derived from the compilations of shallow geology and topography maps.

7-5. Steps of the project

Step 1: Assembly of Ground-motion database

We will assemble an extended ground-motion database for the South Asia and Caucuses region, to serve for model selection and adjustments, to test for regional patterns and for the evaluation of site amplification factors. The database will be principally composed of the accelerograms of Turkey and Iran that are the two important accelerometric data providers in the region. Additional data with reliable seismological information (magnitude, distance, faulting style, site class etc.) from the other project participants will also be considered as part of the project's strong-motion database.

High-quality digital strong motions recorded at sites with known velocity profiles (Vs30) will be ranked in priority during the collection and compilation of the regional dataset.

Step 2: Predictive model for peak ground motion and spectral values

Existing ground motion models (recent global and regional models as well as those from the NGA project) will be selected and compiled using the approach presented in Cotton et al. (2006). The region-specific ground-motion model(s) will then be derived systematically by following the steps indicated below:

1. The strong-motion database of the project will be used to explore how the pre-selected GMPEs to characterize the seismotectonic variations in level-I regions. Residuals analysis, estimation of minimum-misfit stochastic models from empirical GMPEs and expert discussions will help to define uncertainty bounds of the selected predictive models. Selected models will tried to be adjusted for common magnitude, distance, style-of-faulting, horizontal component definitions, and will then be combined with appropriate weighting in a logic tree approach (both for the median and aleatory variability), to cover a broad spectrum of expert opinions. During the evaluation of GMPEs, specific emphasis will be put on the events with smaller magnitudes (M<5), to test scaling issues in the compatibility of small-magnitude records from the region of interest with large-

magnitude global patterns. The predictive model(s) with the highest credentials will be adjusted for a better representation of the seismicity in Level-I regions.

2. The most appropriate global and/or regional models will be adjusted to the regions of low seismicity or regions lacking strong-motion data (target regions) through the host-to-target scaling factors that are derived from the synthetics generated for the target and host regions (Campbell, 2003). The point-source (or finite-fault as long as the seismic information is sufficient for its application) stochastic method will be used for the synthetics. Weak-motion data and other geophysical source information from Level II and III regions will be used to derive the synthetics in the target regions. The models will be calibrated on small-to-moderate earthquakes and host-to-target scaling will consider this fact while transforming the host predictive models to target regions (Akinci et al., 2006; Malagnini et al., 2006). The spectra for target regions are evaluated on the basis of available seismological, seismotectonic and geological information (e.g. Chandler et al., 2006). Extrapolations to larger magnitude events for the host region adjustments will be obtained through the calibration of the stress parameter of the region specific source spectrum.

Step 3: Site amplification and soil linear and nonlinear behavior

Goal of this task is to make appropriate calibrations for the application of ground motion prediction equations to specific soil and rock conditions, along two directions:

1. Keeping the well-accepted site classification criteria unchanged and proposing the "optimal" spectral shapes and/or amplification factors for the region that are applicable to sites where Vs_{30} velocities are known or can be predicted with reasonable accuracy. The work will first consist in compiling the site amplification functions used in the recent GMPEs for their comparison in view of the quality of the background geotechnical information that is very diverse in the region of interest. In the second stage, the strong-motion dataset built will be used to evaluate the consistency of these functional forms (and essentially improve them in case if it is required) for their reliable estimations of soil behavior depending on certain ground-motion levels (usually characterized by PGA or some strain level).
2. Exploring "proxies" to site conditions and Vs_{30} velocities, such as surface topography slope that can be inferred from satellite images (e.g. the Global Vs_{30} model of Wald and Allen on http://earthquake.usss.gov/research/hazmaps/interactive/vs30A) for mapping site

conditions with appropriate density and coverage for regions that lack useful information on Vs_{30} velocities, and proposing site amplification factors accordingly. Statistical tests will be performed to check the relevance of such proxies for their application in the regional scale and their compatibility with the proposed Vs_{30} classification schemes.

Chapter 8: Research Formation

8-1. Introduction

My researches were mainly concentrated on subjects such as the study of seismicity parameters, strong ground motion, development of attenuation models, and seismic hazard analysis in Iran and other active zones of the Middle East and south Asia. The most emphasis was to represent the important controlling factors in seismic source determinations, seismicity parameters and ground motion models. These studies were carried out in the framework of research work at the IIEES as well as in collaboration with the universities and research institutes.

8-2. Supervised Ph.D. Thesis

Over the past 25 years, when I started my research works at the IIEES, I supervised or co-supervised several M.Sc and Ph.D thesis in the field of seismology, engineering seismology, seismic hazard analysis, earthquake prediction, geotechnical earthquake engineering and etc in the IIEES as well as other universities of Iran. Until now, I was supervisor of approximately 80 M.Sc thesis and advisor of about 50 M.Sc thesis in different universities of Iran such as IIEES, University of Tehran (college of engineering and college of geography), K.N. Toosi University of Technology, Shahid Beheshti University, Islamic Azad University in Iran and so on.

My first Ph.D student (now Dr. Fereidoon Sinaiean) defended of his thesis in November 2006. Since then, during the last 10 years, I supervised or co-supervised nine other Ph.D thesis in the IIEES, University of Tehran and University of Technology Malaysia.

In the following, the abstract of the researches in form of supervision or co-supervision of doctoral thesis of my former Ph.D students are presented.

8-2-1. Studies on the Strong Ground Motions in Iran; Source Parameters and Attenuation laws

- *By: Fereidoon Sinaiean*
- *Thesis defense date: November 2006*
- *Affiliation: IIEES*

The Iranian strong ground motions data are used to derive the empirical attenuation laws for different strong motion parameters: peak acceleration, peak velocity, peak displacement, response spectral ordinates. The empirical relationships are established for the strong motion

parameters as a function of the moment magnitude, the epicentral and hypocentral distances, and a constant parameter representing the site conditions. The one and two step approaches for the regressions will be applied. The dataset consists of 3500 three component accelerograms, all recorded during 1994-2003 in Iran. These dataset will complete a previous research by (Zaré and Bard; 1999). It is split in two subsets corresponding to two geographical areas: during the period of observation, stronger earthquakes occurred in central Iran and Alborz region and were recorded at distances as far as 220km, whereas the Zagros belt experienced only the intermediate events (M4-6) recorded at distances up to about 60km. This difference, and a probable difference in attenuation between these two main regions, cause different coefficients for the attenuation relationships. The site effects are studied in 50 stations, using the seismic refraction and microtremors tests. The soil effects will be considered in the regressions: the resulting site dependence is not very large, but it does agree with our previous site classification for Iran.

The attenuation relationships in Iran are studied in 1999 by M. Zaré, in his thesis in LGIT lab in Grenoble University, France. The present study is a continuation of the mentioned research. The purpose of this study is therefore to fill the gap of the studies for the data recorded after 1994. A cleaned catalog is established in this study, that keeps only the data for which the magnitude and epicentral distance are known, and for which the signal to noise ratio was acceptable. The studies on the attenuation relationships for Iran ware previously started using only the strong and representative earthquakes of each region (Zaré 1995a) and for the strong motions recorded during 1974-1994 in Iran. The conditions were devoted special attention and measurements, which led to a new categorization in four different site classes, on the basis of H/V ratio for the strong motion records.

The scope of this study is to investigate attenuation law for the strong motions in Iran, using the Iranian data, in form of different parameters. It was intended to establish the empirical relationships for the strong motions and to observe if any difference may be distinguished in different regions of the country in view point of the attenuation law. Another scope was to provide the design spectra for the sample sites in different regions in Iran. These regions will be designated using the measured kappa and Q (attenuation) parameters.

The results of the study will be presented in form of the different parameters. The coefficients of the regression will be presented not only for the spectral values but also for the parameters such as peak ground acceleration (PGA), peak ground velocity (PGV) and peak ground velocity (PGD). All coefficients are presented for horizontal and vertical components

and separated for different determined regions in the Iranian plateau, and finally for the entire of the Iranian data.

8-2-2. Seismic hazard analysis, a case study from eastern Iran: Tabas region

- *By: Mohammad Aryamanesh*
- *Thesis defense date: February 2007*
- *Affiliation: IIEES*

Landsat TM data were used in the study of neotectonics of the Tabas region in eastern Iran and the eastern great Iranian desert through assessment of the drainage pattern and migration patterns of rivers. Evaluation and inspection of active tectonic processes and their effects such as earthquakes is of great importance in earthquake hazard analysis in any area. The city of Tabas was previously classified as a low seismic risk area before the M_w7.3 earthquake of September 16, 1978, but this earthquake justified the necessity of revising the studies of active tectonics in this area. Since most processes directly related to seismic risk are not expressed in ways measurable from ground or satellite observations, utilizing morphotectonic indicators of active tectonics may be useful for identifying these events. In this study, we examine the Tabas area of eastern Iran and evaluate the response of the Tabas to the 1978 earthquake, using field studies, and Satellite Image Processing. We focus our studies on the changes in the drainage network and the migration of rivers to get a clear understating from active tectonics in the area. These channels belong to the main rivers which originate from Shotori Mountain to the east of the city of Tabas. The relief in the area is remarkable due to its sharp contrasts and the multitude and variability of the morphological elements: high rugged mountains, basins, and wide hilly areas composed of loose sands, gravels and boulders. In an area such as this, where the morphology of the terrain responds to tectonic changes, where erosion is slow, fault ruptures cutting pediment surfaces are well preserved. Various geomorphic features supporting recent tectonic movements were deciphered from the various remotely sensed data. These include: strike-slip faults, fault line scarps, triangular facets, uphill facing scarps, pressure-ridges, and abrupt changes in topographic slope angles along fault traces, offset drainage, truncated fans and beheaded drainage channels. Most of these features were examined in the field and revealed movements that have occurred during the Holocene (past 10,000 years).Subsequently the locus of active deformation seems to have

shifted northwest, and more precisely in an anti-clockwise direction, to where the most active zone of deformation is now buried in the desert of the Tabas plain.

Phenomena such as sedimentation displacement and horizontal excavation of the river have emerged in many rivers of the Tabas plain. Morphotectonic studies in the studied region indicate that tectonics has a direct effect on occurrence and evolution of the regional morphology; and the consistency between the structural pattern and mountains and fields, rivers, and complexity of the areas around the faults, indicate the direct role of tectonic motions. Studying the morphotectonic elements including streams, alluvial deposits, meanders, rivers, shapes, streams asymmetry, channel patterns, tectonic sag ponds in mountain front, V-shape valleys, and triangular facets in mountain fronts, all indicate the strong activity of the studied region. Seismic actions are not limited to the 1965 earthquake fractured zone, and generally these regions have the potential of seismic hazard. Our observations show that the Shotori Mountain front fault zone is a major and active structural element accommodating shear in the area. Because the fault shows principally strike-slip motion on the Tabas plain, we can use the strike of the fault (N 25_W) to locally define the azimuth of maximum shear accommodation. The azimuth is significantly more westerly than other major strike-slip faults within the area.

Mapping in the Tabas plain clarifies the Holocene and right-lateral nature of slip along the Shotori Mountain fault zone and left lateral nature for the Tabas plain, especially associated with the younger movements. Within Shotori Mountain, the fault shows primarily right-lateral motions within an intermountain valley. The range front fault traverses northwestward and majority of the faults acquire a component of reverse motion in addition to the right lateral strike-slip. However, the similarity of the values is consistent with the idea that the slip rate has been relatively constant since inception of the fault. The occurrence of displacement of Holocene deposits shows the recent nature of deformation and is suggestive of a relatively frequent earthquake recurrence time. An approximate estimate of the average recurrence time of earthquakes can be made if we use the displacements recorded on single-event scarps.

The recent estimations indicate that the most of the activity is related to the immediate parts of the mountain front and the Sardar river bed has been strongly affected by the activities. What is important is the changes that exist along the meanders, in a manner that a new front is rising and the existing meanders are in back thrusting with a reverse grade.

We conclude that all the major parts of this interpretation can be inferred directly from the landscape, illustrating that if we know what signs to look for, we can identify zones of active thrust faulting even if they have not experienced recent earthquake activity, and even if no discrete fault scarps are reported at the surface. Long-term folding and uplift produce a simple and self-consistent picture of the faulting at Tabas. Indications of active faulting and folding and drainage incision are present in the landscape across the entire plain of Tabas. Modern satellite imagery enhances our ability to see the sometimes subtle patterns of uplift and drainage incision.

8-2-3. Response Spectra of Iranian earthquakes recorded strong ground motions

- *By: Hadi Ghasemi*
- *Thesis defense date: March 2009*
- *Affiliation: IIEES*

A Case-history is developed on the response spectral studies on the Iranian strong ground motions. The Iranian plateau lies on one of the most seismically active belts in the world called as Alpine-Himalaya. Almost all parts of the territory have been struck by destructive earthquakes. In some cases the observed destructions to buildings fault-related directionality and localized site effect are among the major effective factors.

In this study recorded strong motions during the main shock of well-known earthquakes in Iran have been used to investigate the reasons of observed damage due to each of them. Seismic movement anisotropy method is used to study the directionality effect while the response spectral ratio method is used to study the latter one. Furthermore, the derived response spectra of the recorded time series are compared with the given design spectra at Iranian building code and the results are given.

The main characteristics of strong ground motion will significantly affects the performance of Buildings and structures during an earthquake shaking. Generally, such characteristics can be classified as: earthquake magnitude, source-to-site distance, and site conditions. In order to examine the effects of the mentioned factors on response spectra, a catalogue based on strong motions, recorded during Iran large earthquakes, since 1975 to 2003, have been prepared. The included records are processed and combined together based on simplified assumptions made. Then they grouped in different magnitude, distance and site classes. Comparisons were made between obtained mean response spectra for different

groups and results given and discussed. It is revealed that the general behaviors of response spectra with source-site distance are almost similar; therefore the shapes of response spectra show weak distance dependency. Larger earthquakes have more low frequency energy and less high frequency energy relative to smaller ones which significantly affects the shape as well as the spectral values at different periods. Regarding the site effect it is shown that the soil site condition will have effects on response spectra at distances more than 50 km; while its effects on the shape and values of response spectra are still ambiguous due to mentioned restrictions. The determined normalized response spectra are also compared with standard spectra given at Iran building code (Iran 2800). It is shown that on average the standard spectra can be applied only in the case of the mean response spectra on hard sites, while for other sites, it needs modifications.

In the present study, we have studied the effects of source-site distance, local site and magnitude, on the averaged acceleration response spectra. We prepared a catalogue based on recorded strong motions in Iran during recent large earthquakes, since 1975 to 2003. The available records in the catalogue are processed to remove baseline offset as well as high frequency noise; then the 5% elastic response spectra calculated. Based on simplified assumption made about the main earthquake characteristics in Iran, the derived acceleration response spectra are grouped and averaged for different distance, site and magnitude classes. In this case, the final derived standard deviation would be the summation of inter and intra earthquake term. While the latter one seems to be small, it will significantly restrict us to have only general concludes about the results. Regarding the source-site distance, it is revealed that the behaviors of the averaged response spectra of the same site and magnitude category at different distance ranges are more or less same. In addition, clear spectral attenuation with distance, observed. It is worth to mention that although the hypocentral distance is used as a definition for source-site distance, but generally, it is poor measure for this purpose especially for stations close to the source of the large earthquakes. In these cases other definitions like closest distance to the surface projection of the fault plane, etc. are recommended. Unfortunately, our knowledge about geometry of causative fault planes, for most of the earthquakes used, is poor; so the hypocentral distance is used to keep the homogeneity of the catalogue for source-site distance term.

According to the local site effect on response spectra, it is necessary to go back to the method used to determine site class at each station and its main drawbacks. Site classification is done for most of the stations based on the correlation between the average shear wave

velocity over the top 30 m and place of the fundamental frequency determined using strong motion or microtremor measurements. This kind of classification can be effectively used to separate the hard sites from the general soil sites. Thus, in the present study, records in each assumed class might be contaminated by records from other site classes, especially in the case of soil sites. Regarding this, the average behavior of the given response curves at different site classes must be considered in each distance and magnitude ranges. Based on the given comparisons in figure 9, it is revealed that local site has significance influence on the amplitude of response spectra at distances greater than 50 km, in addition it has not significance influence on the shape of response spectra, although some shifts in the place of higher values of acceleration response can be observed.

It is shown that the magnitude will considerably affects the spectral values as well as the shape of the response spectra. It suggests considering magnitude dependent design response spectra in Iran 2800, but to do so, more detail studies on magnitude effect on response spectra especially at longer periods, as well as developing and modifying the available network to obtain more high quality data are vital. Finally given results based on the comparisons between the standard spectra (Iran 2800) and derived spectra in this study, suggest: 1) In the case of mean response spectra for hard sites, well agreement can be observed between the derived curves and proposed one in Iran 2800, but for soil sites, the proposed standard response spectra suggest overestimated values in whole period range. 2) In the case of mean plus one standard deviation, significant increase observed at higher spectral values (~40%) causes the standard response spectra to be underestimating.

8-2-4. "Probabilistic earthquake prediction model based on the earthquake catalog of Iran"

- *By: Aref Bali-Lashak*
- *Thesis defense date: October 2010*
- *Affiliation: IIEES*

Due to the high risk of earthquakes in densely populated areas of the Iran, in this study, it is attempted to investigate the short-term, medium-term and long-term earthquake prediction in country, based on logical and meaningful methods. At first, some concepts in earthquake predictions including the prediction and decision trees, deterministic time series, stochastic,

chaotic, periodic as well as quasi-periodic processes, predictability and different attitudes to earthquake prediction according to earthquake precursors and statistical - probabilistic approaches are presented. Then, using the coefficient of time variations between successive earthquakes in Iran, the country is divided into four zones in terms of seismicity rate, so that based on the quantity of this parameter in each zone, random distribution patterns, slow-change or fast-change can be applied for probabilistic earthquake predictions. In addition, by introducing an innovative method called BZEFM, and by optimizing the concept of earthquakes clustering as well as defining the seismic dual areas, a new model for the statistical-probabilistic medium-term and short-term earthquake prediction methods are presented. In this study, it is proved that long-term clustering exists in both the primary catalog and the residual catalog. Then, the probabilistic long-term prediction model proposed by Kagan is implemented for the earthquakes catalog of Iran and adjustable parameters and the required regional coefficients of this method are calculated and optimized with regard to Iranian seismic data and application of the genetic algorithm. The moment tensor calculation for some major earthquakes in Iran is considered too. Finally, prediction probability density maps for different time periods and different regional coefficients are depicted.
According to the obtained results, the best performance corresponds to the period when catalog is divided into two equal intervals. Validation shows that the presented short-term, medium-term and long-term prediction methods are acceptable in Iran.

8-2-5. Tehran Seismic network (TDMMO): Micro-Earthquake, Microtremor and Quarry Blast Data

- *By: Jamileh Vasheghani Farahani*
- *Thesis defense date: August 2012*
- *Affiliation: IIEES*

The microseismicity of Tehran region bounded 34.43°-36.87° N and 49.07°-53.13° E which is investigated by the network of Tehran Disaster Mitigation and Management Organization (TDMMO) Tehran from 2004 to 2010/04. The main purpose of this study was to substantiate the current tectonic activity of the region; we checked whether the observed faults in the region are active or not.

We could find some active trend in the region which the strongest level of their activity is related to eastern part of the region especially the North Tehran, Parchin, Pishva, Mosha

and the Garmsar faults. Also, we observed strong historical earthquakes in this zone. Historical earthquakes showed that the east of Tehran is more active that the west. The distribution of micro earthquakes in the E, NE and SE is in a local magnitude 2. Major faults crisscross Tehran are located at the foot of the Alborz mountains. Released seismic energy map of the region showed the main active zones with high energy values for micro earthquakes data in the east of the region.

The extended coda normalization method was applied in south and southeast Tehran. It was found that Q_p^{-1} and Q_s^{-1} show frequency dependence by a power law function. The attenuation parameters for average of three components can be expressed as:

$$Q_p^{-1} = (100 \pm 6) \times 10^{-3}(f^{(1\pm0.07)}) \text{ and } Q_s^{-1} = (73 \pm 2) \times 10^{-3}(f^{(1.06\pm0.03)})$$

The results show stronger attenuation for P waves than for S waves in the 1-12 Hz frequency band. The unknown value of γ for south and southeast Tehran for the P and S waves were determined by assuming γ to be a constant for distances less than 25 km. The changes in γ ranged from 0.55 to 0.85 for distances greater than 25 km. Finally, $\gamma_2 = 0.90$ was obtained for body waves for distances greater than 25 km by comparing all results.

The results from the blast data show higher attenuation for the body wave than for attenuation obtained from earthquake data in Iran. The attenuation relationship (Q^{-1}) can be used for discriminating quarry blasts. The ratio $Q_p^{-1}/Q_s^{-1}>1$ and <2, which is similar to results obtained by other studies. Also, this study indicates the possibility of discrimination of small explosions (e.g., quarry blasts) from tectonic events (e.g., micro earthquakes).

"We did a Study of Horizontal-to-Vertical Component Spectral Ratio in the Tehran Seismic Zone. Micro-earthquakes, microtremors and quarry blasts data were used as an estimation of the site response in the Tehran zone. Site effects were studied based on horizontal to vertical ratios by Nakamura's technique. Also, we used the spectra of the signals for three components with the lowest noise levels for spectral slope studies. The analysis used seismic events from a network of 13 seismic stations by the permanent local seismological network of the Tehran Disaster Mitigation and Management Organization (TDMMO) from 2004 to 2007. The number of events used was different for each station. Quarry blast events were with $1.2 \leq M_L \leq 2.2$ and Micro-earthquakes were with $1.1 \leq M_L \leq 4.1$.

By comparing results for earthquake, microtremor and quarry blast, we could see that there is a significant difference between them. The data showed clear observations, especially in high-frequencies. The H/V spectral ratios indicate dominant frequency for rock/soft site

with a higher ratio level for quarry blast ratios, which are comparable to the earthquake results due to their difference sources. The results derived by spectral H/V ratios and spectral analysis may be used to distinguish between local earthquakes and quarry blasts" (Vasheghani and Zare, 2014).

8-2-6. Analysis and Development of ShakeMaps for earthquakes in Iran

- *By: Mohammad Shahvar*
- *Thesis defense date: April 2013*
- *Affiliation: IIEES*

In this study, our research has progressed from focusing on intermediate and large earthquakes (Mw ≥ 4) and creates a unified, homogeneous catalogue by merging data from 2 local (national) catalogs and 7 international agencies.

The catalog is provided in a declustered (for time-independent earthquake hazard studies) and non-declustered (for time-dependent earthquake hazard studies) form accompanied by the style-of-faulting and estimated uncertainty for the events with original magnitude of Mw. Also, for ShakeMap generation in cases where an output in terms of intensity is desired, empirical relationships between instrumental ground motion parameters and observed macroseismic intensity have been developed for Iran region.

Moreover, the catalog of strong motions has been provided by correcting for baseline shifts, high-frequency noise, and long-period impacts. Consequently, the strong motion parameters such as Peak ground parameters and spectral amplitudes together with macroseismic intensities were included in the earthquake catalog. The fault parameters (Strike, Dip, Rake, rjb, and rrup) for significant earthquakes were determined and included in the catalog.

Finally, to check the consistency of ground motion prediction equations against the observed data, we used some statistical test and an information theoretic approach to use the best GMPE and GMIPE in ShakeMap generation for Iran region and the Atlas of ShakeMaps have been provided for significant Iranian earthquakes

8-2-7. Seismic Hazard Analysis in Iran (475 Years Return Period)

- *By: Sepideh Karimi-Paridari*
- *Thesis defense date: October 2013*

- *Affiliation: IIEES*

The seismic hazard analyse of Iran was the subject of this thesis. The documented seismic history of Iran reports many catastrophic events, due to earthquakes. There are reports of heavy life and property losses due to historical events. The active tectonic of Iran and its earthquakes hazards necessitate more detailed seismic hazard studies for Iran.

A homogeneous earthquake catalogue is an essential tool in any seismic hazard analysis. In this study a seismic catalogue of Iran and adjacent areas was compiled, using international and national databanks. Different priorities were applied in selecting magnitude and earthquake location: a) local catalogues were given higher priority for establishing the location of an earthquake; and b) global catalogues were preferred for determining earthquake magnitudes. Earthquakes that have occurred within an area 23–42°N and 42–65°E, with magnitude range MW 3.5–7.9, from the 3rd millennium BC until April 2010 were included. In an effort to avoid the 'boundary effect', since the newly compiled catalogue will be mainly used for seismic hazard assessment, the study area includes the areas adjacent to Iran. The standardization of the catalogue in terms of magnitude was achieved by the conversion of all types of magnitude into moment magnitude, MWusing orthogonal regression method.

According to Zare et al., (2016), *"Modification and computation local coefficients of the space-time windows in the well-known window algorithm developed by Gardner and Knopoff in 1974, was also performed in this research. To modify the space-time windows, the well-documented events of Iranian earthquake catalogue in the time period of 1972 to 2008 were used. The data contains 21 different sequences of mainshocks and aftershocks with the magnitude of the mainshocks ranged between Mw 5.4 and 7.1. The updated temporal and spatial windows were applied to the seismic catalogue in different seismotectonic zones of Iran. After de-clustering, the seismic catalogues were found to follow a Poisson distribution in all studied zones based on the results of the Kolmogorov-Smirnov test. The same test on times between successive de-clustered events shows that the inter-event times of all catalogues follow an exponential distribution.*

This study also reports a new seismic source zoning map for Iran, which was developed based on the latest data on active tectonic, topography, magnetic intensity and seismicity catalogue. To specify different seismic sources, two different active fault maps (Hessami et al., 2003 and Berberian, 1976) were used. The active fault traces and magnetic intensity data have significant role in defining the intersections and final boundaries of some zones. New

map divides Iran into 27 zones with different seismotectonic characteristics. Following removal of foreshocks and aftershocks, magnitude of completeness of each zone was established for the entire time span of the catalogue.

The attenuation of strong motions was also studied using Iranian strong motions database. The data set consists of 89 three component accelerograms, all recorded in 1975-2003. The one-step regression method was used and the empirical relationship was established for the spectral acceleration as the function of moment magnitude, hypocentral distances, and constant parameter representing the site conditions. A comparison study also performed on available attenuation models to select models and weight them in the logic tree accordingly.

Developing the new probabilistic hazard map of Iran was the main goal of this study. The probabilistic source-based approach established by Cornell in 1968 was followed with different branches defined in the logic tree. The final seismic hazard map of Iran is developed for 475 years return period".

8-2-8. Study of Earthquake Prediction in Iran by M8 Algorithm

- *By: Masoud Mojarab*
- *Thesis defense date: June 2014*
- *Affiliation: University of Tehran*

Iranian Plateau, located along the Alpine-Himalayan seismic belt, is one of the world's most seismically active countries. In the recent centuries, several destructive earthquakes have occurred in this region. Although seismic hazard maps provide valuable information about these events, it is impossible to specify the time of occurrence of these events by these maps. In such situation, organizing crisis management centers, short term planning for seismic retrofit, and prioritization of area in term of vulnerability are impossible. To achieve these goals, it is necessary to monitor the high-risk seismic zones, in medium-term scales.

In the recent years, so much effort has been made for predicting earthquakes. Two principal methods for earthquake prediction are precursory and pattern-recognition-based,. Precursory monitoring is expensive and needs special equipments. Hence, in the present research, the statistical methods based on pattern recognition were applied.

Various algorithms presented so far for predicting earthquakes, among them the M8 successfully predicted several major events. The acceptable results of the global application

of the M8 algorithm, between 1984 and 2013, encourage the use of this algorithm for prediction of great earthquakes within the Iranian plateau. Reviewing the seismicity of the Iranian plateau indicates that this region experienced numerous earthquake of 7+ magnitude. Since earthquake prediction is considered as a tool for decreasing the seismic hazard risks, the present dissertation used the M8 algorithm to predict the time and location window for the next major earthquake of Iran.

Considering the seismological conditions of the Iranian plateau, the M8 algorithm was modified by changing the circle of investigation (CI) radius and lowering its magnitude cutoff. To evaluate the performance of the modified algorithms, nine great earthquakes occurred in the Iranian plateau, between 1988 and 2013, were studied using two different approaches. In total, 60 modified algorithms were produced and compared to each other using Molchan and ROC curves in order to find the best prediction algorithm. The modified algorithms were applied to the regions with a high frequency of occurrences of faults and earthquakes, over successive half-year intervals. The evaluation of results, before the next update of the seismic catalog, leads to the selection of an algorithm with a CI's radius of 393 km, a lower magnitude cutoff of 2- 4, and a confidence level of 99.4% for forward prediction in the Iranian plateau. The selected algorithm named $M8_{Ir}$ as it was developed to be used in the Iranian plateau. Finally, two earthquakes in Makran region, Saravan (2013) and Avaran (2013), were successfully predicted with forward approach.

Due to the existence of significant uncertainty in alarm areas, to decrease the spatial uncertainty of M7+ events, data fusion and multi criteria decision making methods were used. To achieve this goal, a geological database of Iran was prepared. This Database includes several layers such as gravity, magnetism, earthquake density, fault density and topography.

In the data fusion approach, the map of areas prone to the M7+ earthquake occurrence was prepared using a fuzzy analytical hierarchy process. The map of seismic potential anomaly was divided into high (%43) and low (%57) potential parts. The high potential part covered %90 of M7+ instrumental earthquakes. Combination of seismic prone and alarm areas leads to decrease the area of alarm, significantly.

Subsequently, the low seismicity Sialk region, as an area prone to M7+ events was studied. As a M7+ event is proven in that region, the reliability of the prepared map was successfully confirmed. Proving an event with magnitude 7+ in this region, emphasized the reliability of prone to earthquake 7+ zonation map.

The present research developed a medium-term prediction algorithm and modeled major earthquakes in the Iranian plateau with %99.4 confidence level. It also successfully predicted, the Saravan and Avaran events by the suggested algorithm.

By developing a new software, now it is possible to automatically run the algorithm for the updated catalog. In addition, new M8 algorithm was executed on seismotectonic provinces of Iran. Furthermore, the spatial uncertainty of major earthquakes decreased significantly by data-fusion-based approach

8-2-9. Study of Earthquake Prediction in Zagros by CN Algorithm

- *By: Majid Maybodian*
- *Thesis defense date: October 2014*
- *Affiliation: IIEES*

"This study illustrates the application of CN algorithm for the analysis of precursory seismicity patterns in the Zagros region (Iran), an area characterized by a complex seismotectonic setting and by a remarkable seismic activity. CN is a formally defined and widely tested algorithm for intermediate-term middle-range earthquake prediction, based on the analysis of routinely compiled earthquake catalogs. To allow its application, the global and regional catalogs available for the territory of Iran have been analyzed, so as to compile a data set sufficiently complete and homogeneous over a time span of about three decades, as required for CN application. A number of tests have been performed with respect to changes in the input catalogs, assuming different magnitude completeness level, as well considering different magnitude thresholds for the selection of target earthquakes. Different variants of the regionalization have been outlined according to the seismotectonic model, and it is concluded that precursory seismicity patterns for the largest events need to be searched in the whole Zagros tectonic domain" (Maybidian et al., 2013). Accordingly, an experiment has been set up aimed at validation of intermediate-term middle-range prediction of earthquakes with magnitude M ≥ 6.2 in the Zagros region. Starting on March 2012, CN prediction results are routinely updated, based on the events with M ≥ Mc=4.0 as they are reported in the IIIEES catalog.

8-2-10. Seismic hazard assessment of Peninsular Malaysia based on new ground-motion prediction equations for subduction earthquakes

- *By: Abdollah Vaez Shoushtari*
- *Thesis defense date: January 15, 2015*
- *Affiliation: University of Technology, Malaysia*

On the basis of regional economic growth, most cities in Southeast Asia have seen rapid development over the past forty years. In general, seismic design has not been taken into account in Southeast Asia regions with low to moderate seismicity, as these areas have not experienced disaster caused by earthquakes. Peninsular Malaysia is an example of these regions. Although the main cities of this region are located in a low seismicity area, they may be vulnerable to distant earthquakes generated by active seismic sources located more than 300 km along and off the west coast of Sumatra Island. Since 2007, several earthquakes due to the local faults within the Peninsular Malaysia region with maximum moment magnitude (M_{max}) of 4.4 have occurred. Even though the local earthquakes were small in size, the epicenters were as close as 20 km to Kuala Lumpur, which could have remarkable effects on seismic hazard of the region. After understanding this fact that Peninsular Malaysia could be affected by either the large magnitude, distant Sumatran earthquakes or the local earthquakes, appropriate seismic hazard maps and a set of desirable elastic response spectral acceleration for seismic design purposes would be required. Despite the earlier seismic hazard studies for this region, which were proposed based on only the far-field Sumatran earthquakes, this study has presented new maps and elastic response spectra using the combination of the local and Sumatran seismic sources. Ground-Motion Prediction Equations (GMPEs) are the main input in any seismic hazard assessment. This study has attempted first to derive new empirical spectral GMPEs for distant subduction earthquakes (the both interface and intraslab events). The proposed GMPEs are for peak ground acceleration (PGA), peak ground velocity (PGV), and 5% damped pseudo-acceleration for four site classes (i.e. National Earthquake Hazard Reduction Program (NEHRP) site class B, C, D and E, corresponding to rock, stiff soil, medium soil, and soft soil site conditions). The response spectra database has been compiled from hundreds of ground-motion recordings from subduction earthquakes of moment magnitude (M) 5.0 to 9.1, hypocentral distance (R_{hyp}) of 120 to 1300 km and (M) 5.0 to 7.7, R_{hyp} of 120 to 1400 km for interface and intraslab events, respectively. The probabilistic seismic hazard maps for PGA are presented over a 12.5 km

grid for 10% and 2% Probabilities of Exceedance (PE) in 50 years corresponding to 475 and 2,475 years return periods, respectively. The proposed new hazard maps give the expected ground motions based on the extended earthquake catalog, consideration of the both Sumatran and local seismic sources, upgraded seismic source parameters, and more compatible GMPEs. The maximum estimated PGAs on rock site condition across the Peninsular Malaysia region for 10% and 2% PE in 50-year are 11%g and 20%g, respectively. In final, the horizontal elastic and design acceleration response spectra following the principles of Eurocode 8, on four soil site conditions with soil factors of 1, 1.45, 2 and 2.35 for rock, stiff soil, medium soil and soft soil ground types, respectively, have been presented for the Peninsular Malaysia region based on the computed uniform hazard spectra with 475 and 2,475 years return period.

Bibliography

Abrahamson, N. A., Silva, W. J. (1997). 'Empirical spectral attenuation relations for shallow crustal earthquakes'. Seismological Research letter, 68, 94-127.

Abrahamson, N.; Silva, W.: (2008), Summary of the Abrahamson & Silva NGA ground motion relations. Earthq. Spectra 24(1), 67–97

Abrahamson, N.A., and J.J. Bommer (2005).Opinion Paper: Probability and Uncertainty in Seismic Hazard Analysis," Earthquake Spectra, Vol. 21, No. 2, pp. 1-5.

Adnan A, Hendriyawan H, Marto A, Irsyam M (2005) Selection and development of appropriate attenuation relationship for Peninsular Malaysia., Malaysian Science and Technology Congress (MSTC), Cititel Hotel, Midvalley, Kuala Lumpur

Aki K, Chouet B., (1975), "Origin of coda waves: source, attenuation and scattering effects", Journal of Geophysical Research, 80:3322–42.

Aki K, Richards PG., (2002), "Quantitative Seismology". Sausalito: University Science Books.

Aki, K., and Richards, P. G., (1980). Quantitative Seismology: Theory and Methods, W. H. Freeman, San Francisco, Vol. 1, 558 pp.

Akkar, S., & Bommer, J. J. (2010), "Empirical equations for the prediction of PGA, PGV and spectral accelerations in Europe, the Mediterranean region and the Middle East". Seismological Research Letters, 81(2), 195–206.

Akkar, S., Cagnan, Z., (2010). 'A local ground-motion predictive model for Turkey and its comparison with other regional and global ground-motion models'. Bull. Seismol. Soc. Am. 100, 2978–2995.

Akkar, S., M. A. Sandıkkaya, M. Şenyurt, A. Azari Sisi, B. Ö. Ay, P. Traversa, J. Douglas, F. Cotton, L. Luzi, B. Hernandez, et al. (2013). Reference database for seismic ground-motion in Europe (RESORCE), Bull. Earthq. Eng. 12, no. 1, 311–339, doi: 10.1007/ s10518-013-9506-8.

Akkar, S., Z. Çağnan, E. Yenier, Ö. Erdoğan, M. A. Sandıkkaya, and P. Gülkan (2010). The recently compiled Turkish strong-motion database: Preliminary investigation for seismological parameters, J. Seismol. 14, no. 3, 457–479, doi: 10.1007/s10950-009-9176-9.

Algermissen, S.T., Perkins, D.M., Thenhaus, P.C., Hanson, S.L., and Bender, B.L., (1982), 'Probabilistic estimates of maximum acceleration and velocity in rock in the contiguous

United States' U.S. Geological Survey Open- Report 82-1033.

Alipoor R., Zaré M. and Ghasemi M.R., (2012), "Inception of activity and slip rate on the Main Recent Fault of Zagros Mountains, Iran", Geomorphology, Vol. 175–176, pp. 86–97, doi: 10.1016/j.geomorph.2012.06.025.

Alizadeh, H., (2010), "Geo-Electrical study of West Qarchak region", Kavir Sang Ab Company, Kayson Company.

Ambraseys N.N (1995). "The Prediction of Earthquake Peak Ground Acceleration in Europe", Earthquake Eng. Struct. Dyn. Vol.24, pp.467-490.

Ambraseys N.N., Melville C.P., (1982). "A History of Persian Earthquakes", Cambrige Earth Science Ser.

Ambraseys NN (2001) Reassessment of earthquakes 1900–1999, in the Eastern Mediterranean and the Middle East. Geophys J Int 145(2):471–485

Ambraseys NN (2009) Earthquakes in the Mediterranean and Middle East, a multidisciplinary study of seismicity up to 1900. Cambridge University Press, Cambridge

Ambraseys NN, Jackson JA, Melville CP (2002) Historical seis-micity and tectonics: the case of the Eastern Mediterranean and the Middle East, international handbook of earthquake and engineering seismology, V.81A, Copyright~2002 by the Int'l Assoc. Seismol. & Phys. Earth's Interior, Committee on Education. ISBN: 0-12-440652-1

Ambraseys NN, Melville CP, Adams RD (2005) The seismicity of Egypt, Arabia and the Red Sea: a historical review. Cambridge University Press, Cambridge

Ambraseys, N. N., (2005), 'The prediction of earthquake peak ground acceleration in Europe'. Earthquake Engng. Struct. Dyn., 24: 467–490. doi: 10.1002/eqe.4290240402.

Ambraseys, N. N., Douglas, J., Sarma S. K. and Smit, P. M., (2005), "Equations for the Estimation of Strong Ground Motions from Shallow Crustal Earthquakes Using Data from Europe and the Middle East: Horizontal Peak Ground Acceleration and Spectral Acceleration", Bulletin of Earthquake Engineering, 3:1–53.

Ambraseys, N. N., J. Douglas, R. Sigbjörnsson, C. Berge-Thierry, P. Su-hadolc, G. Costa, and P. M. Smit (2004). Dissemination of Euro-pean strong-motion data, Proc. of Thirteenth World Conf. on Earthquake Engineering, Vol. 2, Vancouver, British Columbia, Can-ada, 1–6

August 2004, Paper Number 32.

Ambraseys, N. N., P. Smit, J. Douglas, B. Margaris, R. Sigbjornsson, S. Olafsson, P. Suhadolc, and G. Costa (2004). Internet-site for European strong-motion data, Bollettino di Geofisica Teorica ed Ap-plicata 45, no. 3, 113–129; also available at http://www.isesd.hi.is (last accessed March 2016).

Ambraseys, N.N. (2001) Reassessment of earthquakes, 1900–1999, in the Eastern, Mediterranean and the Middle East, Geophys. J. Int., 145, 471–485

Ameer, A.S., Sharma, M.L., Wason, H.R., Alsinawi, S.A.: (2005)m Probabilistic seismic hazard assessment for Iraq using complete earth-quake catalogue files. Pure Appl. Geophys. 162. doi:10. 1007/s00024-004-2650-y

Amini H., Zaré M. and Gasperini P., (2016), "Catalogue of the earthquakes with maximum intensities (Imax) in Iran", Submitted.

Ansari A., A. Noorzad and Zaré M, (2007), "Application of wavelet multi-resolution analysis for correction of seismic acceleration records", Journal of Geophysics and Engineering, 4, pp. 362–377.

Asadi Z. and Zaré M, (2014), "Estimating magnitudes of prehistoric earthquakes and seismic capability of fault from landslide data in Noor valley (central Alborz, Iran)", Natural Hazard, Vol. 74, Issue 2, pp. 445–461, doi: 10.1007/s11069-014-1186-4.

Ashtari M, Hatzfeld D, Kamalian. N., (2005), "Microseismicity in the region of Tehran", Tectonophysics, 395:193–208.

Atkinson G.M., (2004), "An overview of developments in seismic hazard analysis", 13th World Conference on Earthquake Engineering, Vancouver, B.C., Canada, August 1-6, 2004, Paper No. 5001.

Atkinson GM, Boore DM (2003) Empirical ground-motion relations for subduction-zone earthquakes and their application to Cascadia and other regions. Bull Seismol Soc Ame 93:1703–1729

Azadi, A., Hessami, Kh., Javan-Doloei, (2010), "Integrated geophysical methods for determining geometry of the Kahrizak Fault:Tehran", Natural Hazards DOI 10.1007/S11069-010-9506-9.

Bagheri, A., Ghodrati Amiri, G., Khorasani, M. and Haghdoust, J., (2011), 'Determination of attenuation relationships using an optimization problem', international journal of optimization in civil engineering, 4, pp. 597-607.

Baker J.W. (2008). "An Introduction to Probabilistic Seismic Hazard Analysis (PSHA)," White Paper, Version 1.3, 72 pp.

Bard P.-Y., Zaré, M., and Ghafory-Ashtiany, M. (1998). "The Iranian Accelerometric Data Bank, A Revision and Data Correction", *Journal of Seismology and Earthquake Engineering*, **1**(1), 1-22.

Berberian, M., (2014) "Earthquakes and coseismic surface faulting on the Iranian Plateau; a historical, social, and physical approach", Elsevier, Developments in Earth Surface Processes, 17, 714 p. ISBN: 978-0-444-63292-0. First Edition.

Berberian M (1994) Natural hazards and the first earthquake catalogue of Iran, historical hazard in Iran prior to 1900. International Institute of Earthquake Engineering and Seismology (IIEES) 1:620

Berberian, M. (1977) Contribution of the seismotectonics of Iran (Part III), Geological and mining survey of Iran, Report No. 40.

Berberian, M. Qorashi, J.C.P. Jakson (1992). "The Rudbar-Tarom Earthquake of 20 June 1990 in NW Persia: Preliminary field and Seismological Observations, and its Tectonic Significance", Bul. of Seismological Soc. of America, Vol.82, No.4, pp.1726-1755.

Berberian, M., (1976). "Contribution to the Seismotectonics of Iran (Part II)". Geological Survey of Iran, Report No. 39, p. 517

Berberian, M., (1976b), "Seismotectonic map of Iran (1:2 500 000)", Geological Survey of Iran Report No. 39.

Berberian, M., (1981), 'Active faulting and tectonics of Iran', Zagros- Hindu Kush- Himalaya Geodynamic Evolution, AGU, Geodynamics Series, vol. 3, pp. 33-69.

Berberian, M., and Mohajer-Ashjai, A., (1977)A- 'Seismic Risk Map of Iran, A Proposal'. In: Contribution to the Seismotectonics of Iran, Part III (ed. M. Berberian). Geol. Min. Surv. Iran, 40, 121-150.

Berberian, M., Ghorashi, M., Arzhangravash, B., Mohajer Ashjai, A., (1993), "Seismotectonic and Earthquack-Fault Hazard Investigations in the Tehran Region", Geological Survey of Iran, Report No. 56.

Berberian, M., Qorashi, M., Arzhangravesh, B., and Mohajer-Ashjai, A., (1985), 'Recent tectonics, seismotectonics, and earthquake-fault hazard study of the Greater Tehran region'. Geol. Surv. Iran, 56, 316p. (in Persian).

Berberian, M.: (1995), Master blind thrust faults hidden under the Zagros Folds: active basement tectonics and surface morphotec-tonics. Tectonophysics 241, 193–224

BHRC (2010) Building and Housing Research Centre, Iran Strong Motion Network. Tehran, Iran. Available at http:// www.bhrc.ac.ir/portal/Default.aspx?tabid=519

Bindi, D., D. Spallarossa, C. Eva, and M. Cattaneo (2005). Local and duration magnitude in northwestern Italy and seismic moment versus magnitude relationships, Bull. Seismol. Soc. Am. 95, no. 2, 592–604.

Bommer JJ, Scherbaum F, Bungum H, Cotton F, Sabetta F, Abrahamson NA, (2005), "On the use of logic trees for ground-motion prediction equations in seismic-hazard analysis", Bulletin of the Seismological Society of America, 95:377–89. http://dx.doi.org/ 10.1785/0120040073.

Bommer, J.J., Douglas, J., Scherbaum, F., Cotton, F., Bungum, H., Donat Fah, D.: (2010), On the selection of ground motion prediction equations for seismic hazard analysis. Seismol. Res. Lett. 81(5). doi:10.1785/gssrl.81.5.783

Bondár, I. and D. Storchak (2011). Improved location procedures at the International Seismological Centre, Geophys. J. Int., 186, 1220-1244.

Boore D M and Atkinson G (2007), "Boore–Atkinson NGA ground motion relations for the geometric mean horizontal component of peak and spectral ground motion parameters", PEER Report 2007/01

Boore, D. M. (2005). On pads and filters: Processing strong-motion data, Bull. Seismol. Soc. Am. 95, no. 2, 745–750.

Boore, D. M., and S. Akkar (2003). Effect of causal and acausal filters on elastic and inelastic response spectra, Earthq. Eng. Struct. Dyn. 32, no. 11, 1729–1748, doi: 10.1002/eqe.299.

Boore, D. M., Joyner, W.B., Fumal,T.E. (1997). 'Equations for estimating horizontal response spectra and peak acceleration from western north American earthquakes': A summary of rcent work. Seismological Research letter, 68, 128-153.

Boore, D.M., and Atkinson G. M. (2008), "Ground-Motion Prediction Equations for the Average Horizontal Component of PGA, PGV, and 5%-Damped PSA at Spectral Periods between 0.01 s and 10.0 s", Earthquake Spectra, Volume 24, No. 1, pages 99–138.

Boore, D.M., Joyner, W.B., and Fumal, T.E. (1997). "Equations for Estimating Horizontal Response Spectra and Peak Acceleration from Western North American Earthquakes: A Summary of Recent Work", Seismological Research Letters, 68, 128-153.

Boore, D.M.; Atkinson, G.M.: (2008), Ground motion prediction equa-tions for the average horizontal component of PGA, PGV, and 5%-damped PSA at spectral periods between 0.01 s and 10.0 s. Earthq. Spectra 24(1), 99–138

Bozorgnia, Y. and Mohajer-Ashjai, A., (1982), 'Seismic risk investigation of major cities of Iran', J. Earth Space Phys., 11, pp. 15–38.

Braunmiller, J., N. Deichmann, D. Giardini, and S. Wiemerthe SED Magnitude Working Group (2005). Homogeneous moment– magnitude calibration in Switzerland, Bull. Seismol. Soc. Am. 95, no. 1, 58–74.

Brillinger, D.R. and Pristler, H.K. (1984). "An Exploratory Analysis of the Joyner-Boore Attenuation Data", Bull. of Seismological Soc. of America, 74(4), 1441-1450.

Campbell K and Bozorgnia Y (2007), "Campbell–Bozorgnia NGA ground motion relations for the geometric mean horizontal component of peak and spectral ground motion parameters", PEER Report 2007/02

Campbell KW., (2003), "Prediction of strong ground motion using the hybrid empirical method and its use in the development of ground-motion (attenuation) relations in Eastern North America".Bulletin of the Seismological Society of America, 93:1012–33.

Campbell, K. W. and Bozorgnia, Y., (2008), 'NGA ground motion model for the geometric mean horizontal component of PGA, PGV, PGD and 5% damped linear elastic response spectra for periods ranging from 0.01 to 10 s', Earthquake Spectra, 24,139-171.

Campbell, K.W., Bozorgnia, Y., (2003), 'Updated near source ground motion (attenuation)

relations for the horizontal and vertical components of peak ground acceleration and acceleration response spectra', B.S.S.A., 93, 314-331.

Campos, J., Madariaga, R., Nabelek, J., Bukchin, B. G., and Deschamps, A., 1994. Faulting process of the 1990 June 20 Iran earthquake from broad-band records, *Geophys. J. Int.* **118**, 31Ð46.

Cao, A., and Gao, S. S. (2002). "Temporal Variation of Seismic B-Values beneath Northeastern Japan Island Arc", Geophysical research letters. 29 48-41-48-43.

Castellaro, S., and P. Bormann (2007). Performance of different regression procedures on the magnitude conversion problem, Bull. Seismol. Soc. Am. 97, 1167–1175.

Castellaro, S., F. Mulargia, and Y. Y. Kagan (2006). Regression problems for magnitudes, Geophys. J. Int. 165, 913–930.

Cauzzi, C., and E. Faccioli (2008). Broadband (0.05 to 20 s) prediction of displacement response spectra based on worldwide digital records, J. Seismol. 12, no. 4, 453–475, doi: 10.1007/s10950-008-9098-y.

Cauzzi, C., R. Sleeman, J. Clinton, J. Domingo Ballesta, O. Galanis, and P. Kästli (2016). Introducing the European rapid raw strong-motion database, Seismol. Res. Lett. 87, no. 4, doi: 10.1785/0220150271.

Chen, K. P., and T. B. Tsai (2008). A catalog of Taiwan earthquakes (1900–2006) with homogenized Mw magnitudes, Bull. Seismol. Soc. Am. 98, 483–489.

Chiou Y and Youngs R (2006), "Chiou–Youngs NGA ground motion relations for the geometric mean horizontal component of peak and spectral ground motion parameters", PEER Interim Report for USGS Review

Chiou, B. S. J. and Youngs, R. R., (2008), 'An NGA model for the average horizontal component of peak ground motion and response spectra', Earthquake Spectra, 24, 173-215.

Chung TW, Sato H., (2001), "Attenuation of high-frequency P and S waves in the crust of the southeastern Korea", Bulletin of the Seismological Society of America, 91:1867–74.

Cichowicz A, Birch D., (2011), "Attenuation model for mining districts in South Africa" optimal geometrical spreading. Council for Geoscience. Report No. 2011-0020 2011.

Colman-Sadd, S.: (1978), Fold development in Zagros simply folded belt, southwest Iran. Am. Assoc. Petrol. Geol. Bull. 62, 984– 1003

Copley, A., Jackson, J., (2006), "Active tectonics of the Turkish–Iranian plateau", Tectonics 25, 1–19.

Cornell, C.A., (1968), 'Engineering seismic risk analysis', Bulletin of the Seismological Society of America (BSSA)., Vol. 58, No. 5, pp. 1583-1606.

Crozier MJ (1992), "Determination of palaeoseismicity from landslides In: Bell DH (ed) Landslides (Glissements de terrain)", International Symposium, Christchurch, New Zealand. Balkema, Rotterdam, pp 1173–1180

Cruden DM, Varnes DJ (1996), "Landslide types and processes. In: Turner AK, Schuster RL (eds) Landslides, investigation and mitigation", Transportation Research Board Special Report, vol 247. National Academy Press, Washington, pp 36–76

Davis S D, Frohlich C (1991): Single-link cluster analysis, synthetic earthquake catalogues, and aftershock identication. *Geophysical Journal International*, 104: 289-306.

DeMets, C., R.G. Gordon, D.F. Argus, and S. Stein, (1994), Effects of recent revisions to the geomagnetic reversal time scale on estimates of current plate motions, Geophysical Research Letters, 21, 2191-2194.

Dixon JP, Stihler SD, Power JA, Tytgat G, Estes S, McNutt SR Catalog of earthquake hypocenters at Alaskan volcanoes: January 1 through December 31, (2005), USGS science for a changing world

Draper, N. R., and H. Smith (1998). Applied Regression Analysis, Third Ed., Wiley, New York, 79–83.

Drouet S, Scherbaum F, Cotton F, Souriau A (2007) Selec-tion and ranking of ground motion models for seismic hazard analysis in the Pyrenees. J Seismol 11:87–100. doi:10.1007/s10950-006-9039-6

Earthquake Research Institute (ERI) (2002) http://www.eic.eri.u-tokyo.ac.jp

Engdahl, E.R., R. van der Hilst, and R. Buland (1998). Global teleseismic earthquake relocation with improved travel times and procedures for depth determination, Bull. Seism. Soc. Am.

88, 722-743.

Erdik M., Şeşetyan K., Demircioğlu M.B., Tüzün C., Giardini D., Gülen L., Akkar D.S. and Zaré M., (2015), "Assessment of Seismic Hazard in the Middle East and Caucasus: EMME (Earthquake Model of Middle East) Project", 15th World Conferences on Earthquake Engineering (WCEE)

Eshghi S. and M. Zaré (2003), "Bam (SE Iran) earthquake of 26 December 2003, Mw6. 5: A preliminary reconnaissance report", 7 pages, available on IIEES, http://www. iiees.ac.ir.

Esmaeili, B. M. Almasian, M. Zaré, R. Alipoor, A. Alizadeh, (2014), "Geophysical and geological study on the West Qarchak fault and its implications in seismic hazard, Tehran, Northern Iran", Episodes Vol. 37, no. 2, pp 105-110.

Eurocode 8 (2002). Design Provisions for Earthquake Resistance of Structures. Seismic Actions and General Requirements of Structures, ENV 1998-1-1, European Committee for Standardization (CEN), CEN/TC 250, Draft.

Faccioli, E. & Cauzzi, C., 2006. Macroseismic intensities for seismic scenarios, estimated from instrumentally based correlations, in Abstract Book 1st ECEES, http://www.ecees.org/abstracts_book.pdf, p. 125.

Faenza, L. and Michelini, L., (2010), "Regression analysis of MCS intensity and ground motion parameters in Italy and its application in ShakeMap", *Geophys. J. Int.,* 180, 1138–1152, doi: 10.1111/j.1365-246X.2009.04467.x.

Falcon, N.: (1974),Southern Iran: Zagros mountains in Mesozoic– Cenozoic orogenic belts. Spec. Publ. Geol. Soc. Lond. 4, 199– 211

Freedman, D., Stark, P., (2003). What is the chance of an earthquake? Mulargia, F., Geller, R.J. (Eds.), Earthquake Science and Seismic Risk Reduction, NATO Science Series IV: Earth and Environmental Sciences, 32. Kluwer, Dordrecht, The Netherlands, pp. 201–213.

Frohlich C, Davis S D (1990): Single-link cluster analysis as a method to evaluate spatial and temporal properties of earthquake catalogues. *Geophysical Journal International,*100: 19-32.

Fukushima Y, Berge-Thierry C, Volant P, Pommera D and Cotton F (2003), "Attenuation relation for west Eurasia determined with recent near-fault records from California, Japan and

Turkey", J. Earthq. Eng. 7 573–98

Fukushima Y, Irikura K, Uetake T, Matsumoto H (2000) Characteristics of observed peak amplitude for strong ground motion from the 1995 Hyogo-ken Nanbu (Kobe) earthquake. Bull Seismol Soc Am 90:545–565. doi:10.1785/0119990066

Fukushima Y, Tanaka T (1992) Revised attenuation relation of peak horizontal acceleration by using a new data base. Programme Abstr Seismol Soc Jpn 2:116 (in Japanese)

Fukushima Y. and Tanaka, T. (1990). "A New Attenuation Relation for Peak Horizontal Acceleration of Strong Earthquake Ground Motion in Japan", Bull. of Seismological Soc. of America, 80(4), 757-783.

Galetzka,J., Melgar, D., Genrich, J.F., Geng, J., Owen, S., Xu, X., Bock, Y., Avouac, J.P., Adhikari, L.B., Upreti, B.N., Pratt-Sitaula, B., Bhattarai, T.N., Sitaula, B., Moore, A., Hudnut, K.W., Lindsey, E.O., Szeliga, W., Normandeau, J., Fend, M., Flouzat, M., Bollinger, L., Shrestha, P., Koirala, B., Gautam, U., Bhatterai, M., Gupta, R., Kandel, T., Timsina, C., Sapkota, S.N., Rajaure, S. and Maharjan, N., (2015), Slip pulse and resonance of Kathmandu basin during the 2015 Mw 7.8, Gorkha earthquake, Nepal imaged with space geodesy, Science., Vol. 349 no. 6252 pp. 1091-1095 , DOI: 10.1126/science.aac6383

Gardner J.K, Knopoff L (1974) Is the sequence of earthquakes in Southern California, with aftershocks removed, Poissonian?. Bulletin of the Seismological Society of America 64 (5): pp 1363–1367.

Gasperini P., Bernardini F., Valensise G. and Boschi E. (1999) Defining seismogenic sources from historical felt reports, Bull. Seismol. Soc. Am., 89, 94-110.

Geller, R.J., (2011). Shake-up time for Japanese seismology. Nature 472, 407–409.

Geological Survey of Iran. (1998). "Total airborne magnetic intensity maps of Iran (flight line spacing of 7.5 km, in three colors)". 1:250,000, Tehran, Geological Survey of Iran.

Ghasemi H , Zaré M, Y. Fukushima, K. Koketsu, (2009), "An empirical spectral ground-motion model for Iran", Journal of Seismology, Volume 13, Issue 4, pp 499-515, DOI 10.1007/s10950-008-9143-x.

Ghasemi H, Zare M, Fukushima Y (2008b) Ranking of several ground motion models for seismic hazard analysis in Iran. J Geophys Eng 5:301–310. doi:10. 1088/1742-2132/5/3/006

Ghodrati Amiri, G., Khorasani, M., Mirza Hessabi, M. and Razavian Amrei, S. A., (2010), 'Ground motion prediction equations of spectral ordinates and Arias intensity for Iran', Journal of Earthquake Engineering, 14, 1-29.

Ghodrati Amiri, G., Mahdavian, A. and Dana, F. M., (2007), 'Attenuation relationships for Iran', Journal of Earthquake Engineering, 11, 469492.

Gholipour, Y., Bozorgnia, Y., Berberian, M., Rahnama, M., Qorashi, M., Talebian, Nazari, Shoja-Taaheri, J. and Shafiei, A., (2008), "Probabilistic seismic hazard analyses, Phase 1 Greater Tehran Regions , final report", President Deputy Strategic Planning and Control, college of engineering university of Tehran, available at http://iranhazard.mporg.ir/files/report/Final%20Report%20I.pdf.

Giardini, D., Grünthal, G., Shedlock, K. M. and Zhang, P., (1999), 'The GSHAP Global Seismic Hazard Map'. Annali di Geofisica 42 (6), 1225-1228.

Goda, K., Kiyota, T., Mohan Pokhrel, R., Chiaro, G., Katagiri, T., Sharma,K., & Wilkinson, S. (2015). The 2015 Gorkha Nepal Earthquake: Insights from Earthquake Damage Survey. Frontiers in Built Environment, 1(8), 1 15.10.3389/fbuil.2015.00008.

Godinho J., (2007), "Probabilistic seismic hazard analysis – an introduction to theoretical basis and applied methodology", M.Sc thesis at University of Patras, Greece.

Gru¨nthal, G. (1985). "The Up-dated earthquake catalog for the German Democratic Republic and adjacent areas", proc, of the 3rd int. symp. On the Analysis of Seismicity and Seismic. Risk, 1(1), 19–25.

Grunthal G. (Editor), (1998). European Macroseismic Scale 1998, Conseil de l'Europe, Cahiers du Centre Européen de Géodynamique et de Séismologie, vol. 15, 99.

Gutdeutsch, R., S. Castellaro, and D. Kaiser (2011). The magnitude conversion problem: further insights, Bull. Seismol. Soc. Am. 101, 379–384.

Gutenberg B, Richter CF (1944) Frequency of earthquakes in California. Bull Seismol Soc Am 34:185–188

Gutenberg, B.; Richter, C.F.: (1956), Earthquake magnitude, intensity, energy and acceleration. Bull. Seismol. Soc. Am. 46, 2105145

Haddadi H, Shakal A, Huang M & Parrish J., (2012), "Report on Progress at the Center for Engineering Strong Motion Data (CESMD)", 15th World Conferences on Earthquake Engineering (15WCEE).

Hamdache, M., Pelaez, J., and Talebi, A. (2013). "Analysis of aftershock sequences in South and Southeastern Spain". Physics and Chemistry of the Earth, Parts A/B/C, 63, 55–76.

Hamzehloo, H., Alikhanzadeh, A., Rahmani, M. and Ansari, A., (2012), 'Seismic hazard maps of Iran', 15th World Conferences on Earthquake Engineering (WCEE), 8 pages.

Hamzehloo, H., Mahood, M., (2012), 'Ground-Motion Attenuation Relationship for East Central Iran', Bulletin of the Seismological Society of America, Vol. 102, No. 6, pp. 1-8, doi: 10.1785/0120110249.

Hanks, T.C. and Kanamori, H. (1979). "A Moment Magnitude Scale", *J. of Geoph. Res.* , **84**(B5), 2348-2350.

Harvard CMT Catalog (2010) Harvard Centroid Moment Tensor Catalog. Harvard University, Cambridge. Available at http://www.globalcmt.org/CMTsearch.html

Haskell, N. A., 1960. Crustal reßection of plane SH waves, *J. Geophys. Res.* **65**, 4147Ð4150.

Hessami, K., Jamali, F. and Tabasi H. (2003). "Major active fault of Iran". 1:2,500,000, Tehran, International Institute of Earthquake Engineering and Seismology.

Hessami, K.; Nilforoushan, F.; Talbot, C.J.: (2006), Active deformation within the Zagros Mountains deduced from GPS measurements. J. Geol. Soc. 163, 43–148

Hessami, Kh. and Jamali, F. (2006). "Explanatory notes to the map of Major Active Faults of Iran". Journal of Seismology and Earthquake Engineering 8 (1), 1–11.

Holschneider, M., Zo¨ller, G., & Hainzl, S. (2011). "Estimation of the maximum possible magnitude in the framework of a doubly truncated Gutenberg Richter model". Bulletin of the Seismological Society of America, 101(4), 1649–1659.

http://www.seismo.ethz.ch/static/GSHAP/

Iervolino, I., C. Galasso, and E. Cosenza (2009). REXEL: Computer aided record selection for code-based seismic structural analysis, Bull. Earthq. Eng. 8, no. 2, 339–362, doi:

10.1007/s10518-009-9146-1.

Iervolino, I., C. Galasso, R. Paolucci, and F. Pacor (2011). Engineering ground motion record selection in the ITalian ACcelerometric Archive, Bull. Earthq. Eng. 9, no. 6, 1761–1778.

IIEES (2010) International Institute of Earthquake Engineering and Seismology. Tehran, Iran Available at http:// www.iiees.ac.ir/iiees/EQsearch/%28rgiauxmiwbwmba 55uqakes45%29/EventQuery.aspx

Iranian code of practice for seismic resistant design of buildings (Standard No. 2800) (First edition)", (1988), Building and Housing Research Center (BHRC).

Iranian code of practice for seismic resistant design of buildings (Standard No. 2800) (Fourth edition)", (2012), Building and Housing Research Center (BHRC).

Iranian code of practice for seismic resistant design of buildings (Standard No. 2800) (Second edition)", (1999), Building and Housing Research Center (BHRC).

Iranian code of practice for seismic resistant design of buildings (Standard No. 2800) (Third edition)", (2007), Building and Housing Research Center (BHRC).

Iranian Code of Practice for Seismic Resistant Design of Build-ings Standard No. 2800-05 (ISIRI 2800): (2005), Building and Housing Research Center (BHRC). 3rd edition, Iran, Tehran

IRCOLD (Iranian National Committee on Large Dams), (1996), "Seismotectonic pro-vince of Iran", Report No. 12, 50 pp. (in Persian).

IRSC (2010) Iranian Seismological Centre, University of Tehran, Tehran, Iran. Available at http://irsc.ut.ac.ir/bulletin.php

ISC (2010) International Seismological Centre, EHB bulletin. International Seismological Centre, Thatcham, UK. Available at http://www.isc.ac.uk

Jackson J et al (2006), "Seismotectonic, rupture-process, and earthquake-hazard aspects of the 26 December 2003 Bam, Iran", earthquake Geophys. J. Int. 166 1270–92

Jackson, J.A.; McKenzie, D.P.: (1984), Active tectonics of the Alpine– Himalayan belt between Turkey and Pakistan. Geophys. J. R. Astron. Soc. 77(1), 185–264

Japan Working Group for TC4 Committee (1992). Seismic Zoning on Geotechnical Hazard, Draft,

114p. Harvard University, Seismology Dept., Web page, (2001) http://www.harvard.seismology.edu/.

JICA (2002), The Study on Earthquake Disaster Mitigation in the Kathmandu Valley Kingdom of Nepal,Japan International Cooperation Agency (JICA) and Ministry of Home Affairs His Majesty's Government of Nepal, Volume I 2002, Summary p. 110, Volume III, Main Report 2/2, Earthquake Disaster Assessment and Data Base System, pp. 76.

Jones A, Michael A, Simpson B, Jacob S, Oppenheimer D (2000) Rapid distribution of earthquake information for everybody. Seis Res Lett 71:355–358

Joyner, W.B. and Boore, D.M. (1981). "Peak Horizontal Acceleration and Velocity from Strong Motion Records from the 1979 Imperial Valley, California, Earthquake", Bull. of Seismological Soc. of America, 71(6), 2011-2038.

Joyner, W.B. and Boore, D.M. (1993). "Methods for Regression Analysis of Strong Motion Data", Bull. of Seismological Soc. of America, 83(2), 469-487.

Kagan, Y.Y., (1996). Comment on "The Gutenberg–Richter or characteristic earthquake distribution, which is it?" by S. Wesnousky. Bulletin of the Seismological Society of America 86, 274–285.

Kagan, Y.Y., Jackson, D.D., (1991). Seismic gap hypothesis: ten years after. Journal of Geophysical Research 96, 21,419–21,431.

Kagan, Y.Y., Jackson, D.D., (1995). New seismic gap hypothesis: five years after. Journal of Geophysical Research 99, 3943–3959.

Kale, O., Akkar, S., Ansari, A and Hamzehloo, H., (2015), 'A Ground-Motion Predictive Model for Iran and Turkey for Horizontal PGA, PGV, and 5% Damped Response Spectrum: Investigation of Possible Regional Effects', Bulletin of the Seismological Society of America, Vol. 105, No. 2A, pp. 963–980, doi: 10.1785/0120140134.

Kanamori, H. (1977). The energy release in great earthquakes, J. Geophys. Res. 82, 2981–2987.

Karimiparidari S., Zaré M. and Memarian H., (2008), "New seismotectonic zoning map of Iran", 6th International Conference on Seismology and Earthquake Engineering (SEE6), Tehran, Iran.

Karimiparidari S., Zaré M., Memarian H. and Kijko A., (2013), “Iranian earthquakes, a uniform catalog with moment magnitudes”, Journal of Seismology, Vol.17, pp.897–911. DOI:10.1007/s10950-013-9360-9.

Karimiparidari. S., Zaré. M , Memarian, M., (2011), 'New Seismotectonic Zoning Map of Iran', Proceeding of the 6th International Conference on Seismology and Earthquake Engineering (SEE6). CD-ROM. 8p.

Keefer D (1984), "Landslides caused by earthquakes", Geol Soc Am Bull 95:406–421

Kennett BLN, Engdahl ER, Buland R (1995) Constraints on seismic velocities in the Earth from travel times. Geophys J Int 122:108–124

Khademi, M. H., (2002), 'Attenuation of peak and spectral accelerations in the Persian plateau', Proceedings of 10th European Conference on Earthquake Engineering, 330.

Kijko A (2010) Seismic hazard assessment for selected area. Description of MATLAB code HA2, ver. 2.05. University of Pretoria, Pretoria, 12 pp

Kijko, A. and Graham, G., (1998), 'Parametric-historic procedure for probabilistic seismic hazard analysis', Part I: Estimation of maximum regional magnitude mmax, Pure Appl. Geophys. 152, 413-442.

Kijko, A. and Graham, G., (1999), 'Parametric-historic procedure for probabilistic seismic hazard analysis', Part II: Assessment of seismic hazard at specified site, Pure Appl. Geophys. 154, 1-22.

Kijko, A. and Sellevoll, M. A. (1992) Estimation of earthquake hazard parameters from incomplete data files, Part II: Incorporation magnitude heterogeneity, B. Seismol. Soc. Am., 82, 120–134.

Kijko, A., (2000), 'Statistical estimation of maximum regional earthquake magnitude M', Workshop : seismicity modeling in seismic hazard mapping project Solvenia, May 22-24.

Kijko, A.; Sellevoll, M.A.: (1989), Estimation of earthquake hazard para-meters from incomplete data files, part I, utilization of extreme and complete catalogues with different threshold magnitudes. Bull. Seismol. Soc. Am. 79, 645–654

Kim KD, Chung TW, Kyung JB., (2004), "Attenuation of high frequency P and S waves in the crust of Choongchung provinces, central South Korea", Bulletin of the Seismological

Society of America, 94:1070–8.

Knopoff L (1964): The Statistics of Earthquakes in Sourthern California. *Bulletin of the Seismological Society of America* 54(6): 1871-1873.

Kohonen, T., (1981), "Automatic formation of topological maps of patterns in a self-organizing system". In: Proceedings of the 2nd Scandinavian conference on image analysis, pp. 214–220.

Konno K, Ohmachi T., (1998), "Ground motion characteristic estimated from spectral ratio between horizontal and vertical components of microtremors", Bull Seismol Soc Am, 68(1): 228 – 41.

Kossobokov, V.G., Nekrasova, A.K., (2012). "Global Seismic Hazard Assessment Program maps are erroneous". Seismic instruments 48, 162–170.

Kramer, C. Y. (1956). Extension of multiple range tests to group means with unequal numbers of replications, Biometrics 12, 307–310.

Lay, T., and Wallace, C., 1995. *Modern Global Seismology*, Academic Press, San Diego, CA.

Lin PS, Lee CT (2008) Ground-motion attenuation relationships for subduction-zone earthquakes in Northeastern Taiwan. Bull Seismol Soc Am 98:220–240

Luen B, Stark P. B (2012): Poisson tests of de-clustered catalogues. *Geophysical Journal International,* 189: 691–700. doi: 10.1111/j.1365-246X.2012.05400.x.

Luo, G., Liu, M., (2010). Stress evolution and fault interactions before and after the 2008 Great Wenchuan earthquake. Tectonophysics 491 (1–4), 127–140. http:// dx.doi.org/10.1016/j.tecto.2009.12.019.

Luzi L, Puglia R, Russo E, D'Amico M, Felicetta C, Pacor F, Lanzano G, Ceken U, Clinton J, Costa G, Duni L, Farzanegan E. Guéguen P, Ionescu C, Kalogeras I, Özener H, Pesaresi D, Sleeman R, Strollo A. and Zaré M, (2016), "The engineering strong-motion database: A platform to access pan-European accelerometric data", Seismological Research Letters, 87(4): 987-997. doi: 10.1785/0220150278.

Luzi, L., S. Hailemikael, D. Bindi, F. Pacor, F. Mele, and F. Sabetta (2008). ITACA (ITalian ACcelerometric Archive): A web portal for the dissemination of Italian strong-motion data,

Seismol. Res. Lett. 79, no. 5, 716–722, doi: 10.1785/gssrl.79.5.716.

Ma'hood M, Hamzehloo H, Doloei GJ., (2009), "Attenuation of high frequency P and S waves in the crust of the east-central Iran", Geophysical Journal International, 179:1669–78.

Maggi A, Priestley K, Jackson J (2002) Focal depths of moderate and large size earthquakes in Iran. J Seismol Earthq Eng JSEE 4(No. 2&3):1–2

Mak S and Schorlemmer D, "A Comparison between the Forecast by the United States National Seismic Hazard Maps with Recent Ground-Motion Records", Bulletin of the Seismological Society of America August 2016 vol. 106 no. 4 1817-1831. 10.1785/0120150323.

Mäntyniemi, P., Zaré, M., Singh, M. and Kijko A., (2007), 'Probabilistic Seismic Hazard Maps for Ground Motions in Iran based on Historical and Instrumental Earthquake Data', Proceedings of the 5th Int. Conf. on Seismology and Earthquake Engineering (SEE5), 6 pages.

Margottini, C.,Molin, D.&Serva, L., (1992), "Intensity versus ground motion: a new approach using Italian data", Eng. Geol., 33(1), 45–58.

Marsan D, Lengline O (2008): Extending Earthquakes' Reach Through Cascading, *Science*. 319(5866): 1076-1079. doi:10.1126/science.1148783.

Mather AE, Griffiths JS, Stokes M (2003), A"natomy of a 'fossil' landslide from the Pleistocene of SE Spain", Geomorphology 50:135–149

McCloskey, J., Nalbant, S.S., Steacy, S., (2005). Indonesian earthquake: earthquake risk from co-seismic stress. Nature 434, 291.

McClusky, S., S. Balassanian, A. Barka, C. Demir, S. Ergintav, I. Georgiev, O. Gurkan, M. Hamburger, K. Hurst, H. Kahle, K. Kasten, G. Kekelidze, R.W. King, V. Kotzev, O. Lenk, S. Mahmoud, A. Mishin, M. Nadariya, A. Ouzoumis, D. Paradissis, Y. Peter, M. Prilepin, R. Reilinger, I. Sanli, H. Seeger, A. Tealeb, M.N. Toksöz, and G. Veis, (2000), GPS constraints on plate motions and deformations in eastern Mediterranean and Caucasus, J. Geophys. Res., 105, 5695-5719.

Megawati K (2010) Seismic hazard assessment. World bank-global development learning network session on conducting multi-hazard assessments

Megawati K, Pan TC (2002) Prediction of the maximum credible ground motion in Singapore due to a great Sumatran subduction earthquake: the worst-case scenario. Earthq Eng Struct Dyn 31:1501–1523

Megawati K, Pan TC (2010) Ground-motion attenuation relationship for the Sumatran megathrust earthquakes. Earthq Eng Struct Dyn 39:827–845

Megawati K, Pan TC, Koketsu K (2003) Response spectral attenuation relationships for Singapore and the Malay Peninsula due to distant Sumatran-fault earthquakes. Earthq Eng Struct Dyn 32:2241–2265

Michel, C., B. Edwards, V. Poggi, J. Burjanek, D. Roten, C. Cauzzi, and D. Fah (2014). Assessment of site effects in alpine regions through systematic site characterization of seismic stations, Bull. Seismol. Soc. Am. 104, doi: 10.1785/0120140097.

Mignan A, Woessner J (2012) Estimating the magnitude of completeness for earthquake catalogs. Community Online Resource for Statistical Seismicity Analysis. doi:10.5078/ corssa-00180805. Available at http://www.corssa.org

Milkereit C., Zunbul, S., Karakisa, S., Iravul, Y., and Zschau, J. (SABO Group) and Baumbach, M.,Grosser, H., Gunther, E., Umutlu, N., Kuru, T., Erkul, E., Kling, K., Ibsvon Sebt, M., and Karahan, A. (Task Force) (2000). "Preliminary Aftershock Analysis of the Mw =7.4 Izmit and Mw7.1 Duzce Earthquake in Western Turkey, in A. Baraka, O. Kozaci, E. Altunel (Eds.); The 1999 Izmit and Duzce Earthquakes: Preliminary Results", Istanbul Technical Univ. Press, Turkey.

Mirzaei N, Gao MT, Chen YT, Jian W., (1997), 'A uniform catalog of earthquakes for seismic hazard assessment in Iran'. Acta Seismologica Sinica 10(6):713–726. doi:10.1007/s11589997-0003-5.

Mirzaei, N., Gao, M., Chen, Y. T. (1998). "Seismic source regionalization for seismic zoning of Iran: major seismotectonic provinces". J. Earthquake prediction Research, 7, pp. 465-495.

Mirzaei N., Shabani E., and Mousavi Bafrouei S.H., (2014), "Comment on "A Unified Seismic Catalog for the Iranian Plateau (1900–2011)" by Mohammad P. Shahvar, Mehdi Zare, and Silvia Castellaro", Seismological Research Letters Volume 85, pp. 179-183.

Mohajer, A. A. and A.A. Nowroozi, (1978), 'observed and Probable intensity zoning of Iran',

Tectonophysics, Vol. 49. pp 149-160.

Moinfar A.A., M. Naderzadeh A. (1990). "An Immediate and Preliminary Report on the Manjil Iran Earthquake of 20 June 1990", Building and Housing Research Center, Rep. No#119, 68p.

Moinfar, A., Mahdavian, A., Maleki, E., (1994), 'Historical and instrumental earthquake data collection of Iran'. Iranian Cultural Fairs Institute, Tehran, 446 pp.

Moinfar, A.A., Naderzadeh, A. and Nabavi, M.H., (2012), 'New Iranian seismic hazard zoning map for new edition of seismic code and its comparison with neighbor countries', 15th World Conferences on Earthquake Engineering (WCEE), 10 pages.

Mojarab M., Memarian H., Zaré M, Morshedy A.H., Pishahang M.H., (2014), "Modeling of the seismotectonic provinces of Iran using the self-organizing map algorithm", Computers & Geosciences, Vol. 67, pp. 150–162, doi: 10.1016/j.cageo.2013.12.007.

Moribayashi, S. and Maruo, Y. (1980). Basement topography of the Kathmandu valley Nepal: an application of gravitational method to the survey of a tectonic basin in Himalayas. J. Jap. Soc. Eng. Geol. 21, 30-37.

MOS (2010) Institution of the Russian Academy of Sciences Geophysical Centre of RAS Moscow, Russia. Available at http://www.gcras.ru/index_e.html

Mousavi Bafrouei, S.H., Mirzaei, N., Shabani, E. and Eskandari-Ghadi, M., (2015), 'Seismic hazard zoning in Iran and estimating peak ground acceleration in provincial capitals', journal of earth and space physics, 40 (4), pp. 15-38.

Mousavi, S.M, (2016), Comment on “Recent developments of the Middle East catalog” by Zare et al., Journal of Seismology.

Myers SC, Shultz CA (2001) Statistical characterization of refer-ence event accuracy. Seismol Res Lett 72:244

Nabilah AB, Balendra T (2012) Seismic hazard analysis for Kuala Lumpur, Malaysia. Earthq Eng 16:1076–1094

National Cartographic Center of Iran. “Digital Elevation Model”. 1:2,500,000 Tehran, National Cartographic Center of Iran

Neghabat, F., and Liu, S.C., (1977), 'Earthquake regionalization of Iran', Six World Conf. Earthq. Eng., New Delhi, pp. 859-865.

NEHRP recommended seismic provisions for new buildings and other structures, (2003) Edition:Part I (Provisions) and Part II (Commentary), FEMA 450. Building Seismic Safety Council. Washington: Federal Emergency Management Agency.

NEIC Bulletins US (2010) National Earthquake Information Centre bulletin. US Geological Survey, World Data Center A for Seismology, Boulder, CO, USA. Available at http://neic.usgs.gov/neis/epic

Nepop RK, Agatova AR (2008), "Estimating magnitudes of prehistoric earthquakes from landslide data: first experience in southeastern Altai", Russ Geol Geophys 49:144–151

NIST/SEMATECH (2006) e-Handbook of Statistical Methods http://www.itl.nist.gov/div898/handbook

Nogol Sadat, M.A.A., (1993), "Seismotectonic map of Iran (scale 1:1 000 000)", Geological Survey of Iran.

Nogol-Sadat, M. A. A. (1994). “Seismotectonic Map of Iran”. Teritise on the Geology of Iran, 1:1000,000 Scale

Norouzi N., Mojarab M, Asadi Z and Zaré M, (2014), "A Case Study of Seismic Hazard Analysis at Al-Tajiat and Al-Zawraa Stadiums in Baghdad/Iraq Region", Arab J Sci Eng, Vol. 40, Issue 7, pp. 1987–2002, doi: 10.1007/s13369-014-1559-8.

Nowroozi, A. A. (1976). “Seismotectonic provinces of Iran”. Bull. Seism. Soc. Am. 66, pp. 1249-1276.

Nowroozi, A.A and Ahmadi, G, (1986), 'Analysis of earthquake risk in Iran based on seismotectonic provinces', Tectonophysics, 122, pp. 89-114.

Nowroozi, A.A.: (1972), Focal mechanism of earthquakes in Persia, Turkey, west Pakistan and Afghanistan and plate tectonics of the Middle East. Bull. Seismol. Soc. Am. 62(3), 832–850

Nowroozi, G., (2006), "Seismological constraints on the crustal structure of NE Iran", PhD thesis. International Institute of Earthquake Engineering and Seismology, Tehran; 2006.

Nuttli, O. W. (1973). Seismic wave attenuation relations for eastern North America, J. Geophys.

Res. 78, 855–876.

NW Persia: Preliminary field and Seismological Observations, and its Tectonic Significance, Bul. of Seismological Soc. of America, Vol.82, No.4, pp.1726-1755.

Ogata, Y. (1983). "Estimation of the Parameters in the Modified Omori Formula for Aftershock Frequencies by the Maximum Likelihood Procedure", Journal of Physics of the Earth. 31 115–124.

Ogata, Y. (1988). "Statistical models for earthquake occurrences and residual analysis for point processes", J. Am. Stat. Assoc. Applic. 83 (401) 9–27.

Ogata, Y., and Katsura, K. (1993). "Analysis of Temporal and Spatial Heterogeneity of Magnitude Frequency Distribution Inferred from Earthquake Catalogues", Geophysical Journal International. 113 727–738.

Ommi S., Zafarani H, and Zaré M., (2016), "Aftershock Decay Rates in the Iranian Plateau", Pure Appl. Geophys, Vol. 173, Issue 7, pp. 2305–2324, doi: 10.1007/s00024-016-1285-0.

Pacor, F., R. Paolucci, G. Ameri, M. Massa, and R. Puglia (2011). Italian strong motion records in ITACA: Overview and record processing, Bull. Earthq. Eng. 9, no. 6, 1741–1759, doi: 10.1007/s10518-011-9295-x.

Pacor, F., R. Paolucci, L. Luzi, F. Sabetta, A. Spinelli, A. Gorini, M. Nicoletti, S. Marcucci, L. Filippi, and M. Dolce (2011). Overview of the Italian strong-motion database ITACA 1.0, Bull. Earthq. Eng. 9, no. 6, 1723–1739, doi: 10.1007/s10518-011-9327-6.

Pan TC, Megawati K., (2002), "Estimation of peak ground accelerations of the Malay Peninsula due to distant Sumatra earthquakes", Bulletin of the Seismological Society of America,92:1082–94. http://dx.doi.org/10.1785/0120010123.

Panza, G.F., Romanelli, F., Vaccari, F. (2001), "Seismic wave propagation in laterally heterogeneus anelastic media: theory and applications to seismic zonation", Advances in Geophysics, 43, 1-95.

Paolucci, R., F. Pacor, R. Puglia, G. Ameri, C. Cauzzi, and M. Massa (2011). Record processing in ITACA, the new Italian strong-motion database, in Earthquake Data in Engineering Seismology—Predictive Models, Data Management and Networks, S. Akkar, P. Gülkan, and T. van Eck (Editors), Springer, Dordrecht, Netherlands, 99–113, ISBN: 978-94-007-

0151-9 (printed version) 978-94-007-0152-6 (e-book version).

Paudyal, Y. R., Yatabe, R., Bhandary, N. P., Dahal, R. K., (2012), A study of local amplification effect of soil layers on ground motion in the Kathmandu Valley using microtremor analysis. Earthquake Engineering and Engineering Vibration 11, 257-268, (10.1007/s11803-012-0115-3).

Petersen MD, Dewey J, Hartzell S, Mueller C, Harmsen S, Frankel A, Rukstales K (2004) Probabilistic seismic hazard analysis for Sumatra, Indonesia and across the Southern Malaysian Peninsula. Tectonophys 390:141–158

Philip, H., Meghraui, M., Feb. (1983), "Structural Analysis and Interpretation of the surface Deformations of the El ASNAM Earthqauke of October, 10, 1980", Tectonics, v. 2, No. 1, pp. 17-49.

Press WH, Teukolsky SA, Vetterling WT, Flannery BP. (2001), Numerical recipes in FORTRAN 77: the art of scientific computing. second ed. Cambridge: Cambridge University Press.

Puri N and Jain A, (2016), "Deterministic Seismic Hazard Analysis for the State of Haryana, India", Indian Geotechnical Journal June 2016, Volume 46, Issue 2, pp 164–174. DOI: 10.1007/s40098-015-0167-1.

Ramazi, H. (1995), 'Seismotectonic map of Iran, 1/2500000 scale'. Ph.D Dissertation. Engineering Geophysics, Charles University, Prague, Czech Republic, 100 pp.

Reasenberg P (1985): Second-order moment of central California seismicity, 1969-82. *Journal of Geophysical Research,* 90: 5479-5495.

Régnier, J., A. Laurendeau, A. M. Duval, and P. Guéguen (2010). From heterogeneous set of soil data to V_S profile: Application on the French permanent accelerometric network (RAP) sites, Proc. of the 14th European Conference on Earthquake Engineering, Ohrid, Republic of Macedonia, 30 August–3 September 2010.

Reiter, L. (1990). "Earthquake Hazard Analysis- Issues and Insights", Columbia University Press, New York, 254 pp.

Rezapour, M. (2005). Magnitude scale in the Tabriz seismic network, J. Earth Space Phys. 31, no. 1, 13–21.

Richter CF (1958) Elementary seismology, Freeman, 768 pp Rydelek PA, Sacks IS (1989) Testing the completeness of earthquake catalogs and the hypothesis of self-similarity. Nature 337:251–253

Roca, A., P. Guéguen, S. Godey, X. Goula, T. Susagna, C. Péquegnat, C. S. Oliveira, J. Clinton, C. Pappaioanou, and C. Zülfikar (2011). The European–Mediterranean distributed accelerometric data-base, in Earthquake Data in Engineering Seismology—Predictive Models, Data Management and Networks, S. Akkar, P. Gülkan, and T. van Eck (Editors), Springer, Dordrecht, Netherlands, 115–128, ISBN: 978-94-007-0151-9 (printed version) and 978-94-007-0152-6 (e-book version).

Sadeghi, H., Shooshtari, A. and Jaladat, M., (2010), 'prediction of horizontal response spectra of strong ground motions in Iran and its regions', Proceedings of the 9th U.S. National and 10th Canadian Conference on Earthquake Engineering, July 25-29, 2010, Toronto, Ontario, Canada • Paper No 861, 10 pages.

Saffari, H., Kuwata, K., Takada, H. and Mahdavian A., (2012), 'Updated PGA, PGV, and Spectral Acceleration Attenuation Relations for Iran', Earthquake Spectra, Volume 28, No. 1, pp. 257–276.

Sakai, H., Fujii, R., and Kuwahara, Y. (2002). Changes in the depositional system of the Paleo-Kathmandu Lake caused by uplift of the Nepal Lesser Himalayas. J. Asian Earth Sci. 20, 267–276. doi:10.1016/S1367-9120(01)00046-3.

Salamat M., Zaré M., Holschneider M. and Zöller G., (2016), "Calculation of confidence intervals for the maximum magnitude of earthquakes in different seismotectonic zones of Iran", Pure and Applied Geophysics, pp 1–15, doi:10.1007/s00024-016-1418-5.

Sarkar, I., Hamzehloo, H., and Khattri, K. N., 2003. Estimation of causative fault parameters of the Rudbar earthquake of June 20, 1990 from near Þeld SH-wave data, *Tectonophysics* **364**, 55Ð70.

Savage, J.C., (1991). Criticism of some forecasts of the national earthquake prediction council. Bulletin of the Seismological Society of America 81, 862–881.

Scherbaum F, Cotton F and Smit P (2004), "On the use of response spectral reference data for the selection and ranking of ground-motion models for seismic hazard analysis in regions of moderate seismicity: the case of rock motion", Bull. Seismol. Soc. Am. 94 1–22

Scherbaum, F., E. Delavaud, and C. Riggelsen (2009). Model selection in seismic hazard analysis: an information-theoretic perspective, Bull. Seismol. Soc. Am. 99, 3234–3247.

Scordilis, E. M. (2006). Empirical global relations converting MS and mb to moment magnitude, J. Seismol. 10, 225–236.

Seismic hazard zoning of Iran and 1:250,000 map, (1997), Iranian research center of urban Planning and architecture (First Edition).

Shah M.A., Qaisar M., Iqbal J. and Ahmed S., (2012), "Deterministic Seismic Hazard Assessment of Quetta, Pakistan ", 15th World Conferences on Earthquake Engineering (WCEE), September 24-28, 2012, in Lisbon, Portugal.

Shahvar M. P. and M. Zaré, (2013), The 27 August 2010 Mw 5.7 Kuh-Zar earthquake (Iran): field investigation and strong-motion evidence, Nat Hazards, DOI 10.1007/s11069-012-0507-8.

Shahvar M, M. Zaré, and Castellaro S, (2013), "A unified seismic catalogue for the Iranian plateau (1900-2011)", Seismological Research Letter, doi: 10.1785/0220120144.

Shahvar M.P., Zaré M., and Castellaro S., (2014), "Reply to "Comment on 'A Unified Seismic Catalog for the Iranian Plateau (1900–2011)' by Mohammad P. Shahvar, Mehdi Zaré, and Silvia Castellaro" by Noorbakhsh Mirzaei, Elham Shabani, and Seyed Hasan Mousavi Bafrouei", Seismological Research Letters Volume 85, pp. 184-185. doi: 10.1785/0220130144

Sharma B, Gupta AK, Devi DK, Kumar D, Teotia SS, Rastogi BK., (2008), "Attenuation of high-frequency seismic waves in Kachchh region, Gujarat, India", Bulletin of the Seismological Society of America, 98:2325–40.

Shortlink: http://www.gfz-potsdam.de/GSHAP.

Shoushtari AV, Adnan A, Zare M, Harith NSH., (2015), "Estimation of the maximum credible hazard in Kuala Lumpur and Singapore due to gigantic Sumatran megathrust earthquakes: based on a comparative study on attenuation laws", Nat Hazards, 78:725–51. http://dx.doi.org/10.1007/s11069-015-1742-6.

Sinaeian F (2006), "Study on Iran strong motion records", PhD Thesis International Institute of Earthquake Engineering and Seismology, Tehran, Iran

Sinaiean, F., (2006), Research on strong ground movement in Iran (the catalog attenuation relations), Ph.D Thesis, International Institute of Earthquake Engineering and Seismology.

Sipkin SA, Person WJ, Presgrave BW (2000) Earthquake bulletins and catalogs at the USGS National Earthquake Information Center, U.S. Geological Survey National Earthquake Information Center

Skarlatoudis AA et al (2013) Ground-motion prediction equations of intermediate-depth earthquakes in the Hellenic Arc, Southern Aegean Subduction Area. Bull Seismol Soc Am 103:1952–1968

Soghrat, M. R., Khaji, N. and Zafarani, H., (2012), 'Simulation of strong ground motion in northern Iran using the specific barrier model', Geophys. J. Int., 188, 645-679.

Stein S, Geller R.J, Liu M, (2012), "Why earthquake hazard maps often fail and what to do about it", Tectonophysics 562–563 (2012) 1–25.

Stein, R., (1999). The role of stress transfer in earthquake occurrence. Nature 402, 605–609.

Stein, R., Yates, R.S., (1989). Hidden earthquakes. Scientific American 260, 48–57 (January).

Stocklin, J. (1968). “Structural history and tectonics of Iran”. Bull. Am. Assoc. Petol. Geologists 52, pp. 1229-1258.

Stucchi M, Rovida A, Gomez Capera AA, Alexandre P, Camelbeeck T, Demircioglu MB, Gasperini P, Kouskouna V, Musson RMW. Radulian M, Sesetyan K, Vilanova S, Baumont D, Bungum H, Fäh D, Lenhardt W, Makropoulos K, Martinez Solares JM, Scotti O, Živčić M, Albini P, Batllo J, Papaioannou C, Tatevossian R, Locati M, Meletti C, Viganò D, Giardini D, springer, publish online, (2012), The SHARE European Earthquake Catalogue (SHEEC) 1000– 1899, J Seismol. doi:10.1007/s10950-012-9335-2

Sweeney JJ (1998) Criteria for selecting accurate event locations from NEIC and ISC bulletins, Lawrence Livermore National Laboratory, UCRL-JC-130655

Sweeney, J.J., 1996, Accuracy of teleseismic event locations in the Middle East and North Africa, Lawrence Livermore National Laboratory, UCRL- ID-125868.

Takin, M. (1972). “Iranian geology and continental drift in the Middle East”. Nature, 235, (5334), pp. 147- 150

Taleb, N.N., (2007). The Black Swan: The Impact of the Highly Improbable. Random House, New York.

Talebi M, M. Zaré, A. R. Madahi-zadeh and Bali-Lashak, (2015), "Spatial-temporal analysis of seismicity before the 2012 Varzeghan, Iran, Mw 6.5 earthquake", Turkish Journal of Earth Sciences, Vol24, 24: © TÜBİTAK doi:10.3906/yer-1410-13, pp.1-13.

Talebian, M., Jackson, J., (2002), "Offset on the main recent fault of NW Iran and implications on the late Cenozoic tectonics of the Arabia–Eurasia collision zone", Geophysical Journal International 150, 422–439.

Tatar M, Jackson J, Hatzfeld D and Bergman E (2007), "The 2004 May 28 Baladeh earthquake (Mw 6.2) in the Alborz, Iran: overthrusting the South Caspian basin margin, partitioning of oblique convergence and the seismic hazard of Tehran", Geophys. J. Int. 170 249–61

Tavakoli, B. (1996). "Major Seismotectonic Provinces of Iran", International Institute of Earthquake Engineering and Seismology (IIEES), (in Persian), Tehran, Iran

Tavakoli, B. and Ghafory-Ashtiany, M. (1999). "Seismic Hazard Assessment of Iran", Annali DiGeofisica, Vol. 42, pp. 1013-1021.

Theodulidis, N. and Bard, P.-Y. (1995). "(H/V) Spectral Ratio and Geological Condition; An Analysis of Strong Motion Data from Greece and Taiwan, (SMART-1)", *Soil Dynamics and Earthquake Engineering*, **14**, 177-197.

Theodulidis, N., I. Kalogeras, C. Papazachos, V. Karastathis, B. M. Margaris, C. Papaioannu, and A. Skarlatoudis (2004). HEAD 1.0: A Unified HEllenic Accelerogram Database, Seismol. Res. Lett. 75, no. 1, 36–45.

Tibi, R., Bock, G., Xia, Y., Baumbach, M., Grosse, H., Milkereit, C., Karakisa, S., Zunbul, Z., Kind, R., and Zschau, J. (2001). "Rupture Process of the 1999 August 17 Izmit and November 12 Duzce (Turkey) Earthquakes", Geophys. J. Int., F1-F7.

Trifunac, M.D. & Brady, A.G., (1975), "On the correlation of seismic intensity scales with the peaks of recorded strong ground motion", Bull. seism. Soc. Am., 65(1), 139–162.

Uhrhammer R (1986) Characteristics of northern and southern California seismicity. Earthq Notes 57:21

Uniform Building Code (UBC 1997): (1997), International Council of Building Officials. vol. 2

Urkhard, M., and Grunthal, G. (2009). "Seismic Source Zone Characterization for the Seismic Hazard Assessment Project Pegasos by the Expert Group 2 (Eg1b)", Swiss Journal of Geosciences. 102 149–188.

Utsu, T., (1970). "Aftershocks and earthquake statistics (II)—further investigation of aftershock and earthquake sequences based on new classification of earthquake sequences". J. Fac. Sci. Hokkaido Univ. Ser. VII 3, 197–266.

Utsu, T., and Ogata, Y. (1995). "The centenary of the Omori formula for a decay law of aftershock activity". Journal of Physics of the Earth, 43(1), 1–33.

Vaez Shoushtari A., Azlan B.A and Zaré M, Harith NSH, (2015), "Estimation of the maximum credible hazard in Kuala Lumpur and Singapore due to gigantic Sumatran megathrust earthquakes: based on a comparative study on attenuation laws", Natural Hazards, Vol.78, pp. 725-751, doi: 10.1007/s11069-015-1742-6.

Vaez Shoushtari, A., B. A. Azlan , and Zaré M, (2016), "On the selection of ground–motion attenuation relations for seismic hazard assessment of the Peninsular Malaysia region due to distant Sumatran subduction intraslab earthquakes", Soil Dynamics and Earthquake Engineering, 82, 123–137. DOI: 10.1016/j.soildyn.2015.11.012.

Valensise, G., Pantosti, D., (2001). Investigation of potential earthquake sources in penin-sular Italy: a review. Journal of Seismology 5, 287–306.

Van Stiphout T, Zhuang J, and Marsan D (2012): Seismicity declustering, Community Online Resource for Statistical Seismicity Analysis, doi:10.5078/corssa- 52382934. Available at http://www.corssa.org.

Vasheghani Farahani J and M. Zaré, (2011), The Southeastern Tehran Earthquake of 17 October 2009 (Mw = 4.0), doi: 10.1785/gssrl.82.3.404, Seismological Research Letters May/June 2011 v. 82 no. 3 p. 404-412.

Vasheghani Farahani J, Zaré M, Cichowicz A, (2012), "Attenuation of high-frequency P and S waves in south and southeast Tehran using blast data", Soil Dynamics and Earthquake Engineering, Volume 40, September 2012, Pages 99–108.

Vasheghani-Farahani J, Zare´ M, Lucas C., (2012), "Adaptive neuro-fuzzy inference systems for

semi-automatic discrimination between seismic events: a study in Tehran region", Journal of Seismology, http://dx.doi.org/10.1007/ s10950-011-9270-7.

Vasheghani-Farhani J. and M. Zaré, (2014), "Seismological aspects of the Varzeghan twin Earthquakes on 11 August 2012 (Mw 6.3 and Mw 6.1), in East Azerbaijan province, NW Iran", Episodes Vol. 37, no. 2, pp. 96-104.

Vere-Jones D (1970): Stochastic models for earthquake occurrence. *Journal of the Royal Statistical Society*, Ser B 32:1-62.

Vernant, P., Nilforoushan, F., Chéry, J., Bayer, R., Djamour, Y., Masson, F., Nankali, F., Ritz, J.F., Sedighi, M., and Tavakoli, F. (2004). "Deciphering oblique shortening of central Alborz in Iran using geodetic data". Earth and Planetary Science Letters 223, 177– 185.

Vernant, P., Nilforoushan, F., Hatzfeld, D., Abbassi, M., Vigny, C., Masson, F., Nankali, H., Martinod, J., Ashtiani, A., Bayer, R., Tavakoli, F., Chéry, J., (2004), "Present-day crustal deformation and plate kinematics in the Middle East constrained by GPS measure-ments in Iran and northern Oman", Geophysical Journal International 157, 381–398.

Wald, D. J., V. Quitoriano, T. H. Heaton, and H. Kanamori., (1999a), "Relationship between peak ground acceleration, peak ground velocity, and Modified Mercalli Intensity for earthquakes in California", Earthquake Spectra 15, 557–564.

Wald, D. J., V. Quitoriano, T. H. Heaton, H. Kanamori, C. W. Scrivner, and C. B. Worden, (1999b). TriNet ShakeMaps: Rapid Generation of Instrumental Ground Motion and Intensity Maps for Earthquakes in Southern California, Earthquake Spectra, 15, 537-556.

Walker, R., Jackson, J., (2002), "Offset and evolution of the Gowk fault, S.E. Iran: a major intra-continental strike-slip system", Journal of Structural Geology 24, 1677–1698.

Walpersdorf, A., Hatzfeld, D., Nankali, H.R., Tavakoli, F., Nilforoushan, F., Tatar, M., Vernant, P., Chery, J., Masson, F., (2006), "Difference in the GPS deformation pattern of North and Central Zagros (Iran)", Geophysical Journal International 167, 1077–1088.

Wang Q, Jackson DD, Kagan YY (2009) California earth-quakes, 1800–2007: a unified catalog with moment mag-nitudes, uncertainties, and focal mechanisms. Seismol Res Lett 80:446–457

Wang, Q., P.Z. Zhang, J.T. Freymueller, R. Bilham, K.M. Larson, X. Lai, X. You, Z. Niu, J. Wu,

Y. Li, J. Liu, Z. Yang, and Q. Chen, (2001), Present-day crustal deformation in China by Global Positioning System measurements, Science, 294, 574-577.

Wells, D. L., and Coppersmith, K. J. (1994). "New Empirical Relationships among Magnitude, Rupture Length, Rupture Width, Rupture Area, and Surface Displacement", Bulletin of the Seismological Society of America. 84 974–1002.

Wells. D. L. & Coppersmith. K. J., (1994), "New Empirical Relationships among Magnitude, Rupture Length, Rupture Width, Rupture Area, and Surface Displacement", Bulletin of the Seismological Society of America, Vol. 84, No. 4, Pp. 974-1002.

Wiemer S (2001) A software package to analyze seismicity: ZMAP. Seismol Res Lett 72:373–382

Wiemer, S., Wyss, M., (2000). Minimum magnitude of complete reporting in earthquake catalogs: examples from alaska, the western united states, and japan, Bull. Seismol. Soc. Am., 90: pp 859-869.

Wyss M, Hasegawa A, Wiemer S, Umino N (1999) Quantitative mapping of precursory seismic quiescence before the 1989, m7.1 off-sanriku earthquake, japan, Annali Di Geofisica, 42: pp 851-869.

Wyss M, Wiemer S, Zuniga R (2001) ZMAP a tool for analyses of seismicity patterns, typical applications and uses: a cookbook

Yazdani, A. and Kowsari, M., (2013), 'Bayesian estimation of seismic hazards in Iran', Scientica Iranica, Volume 20, Issue 3, , pp. 422–430, doi:10.1016/j.scient.2012.12.032.

Yenier, E., M. A. Sandikkaya, and S. Akkar (2010). Update strong-ground motion database, deliverable 4.1 of Seismic Hazard Harmonization in Europe (SHARE), Grant Agreement 226967, 34 pp.

Yoshida, M and Gautam, P., (1988), Magnetostratigraphy of Plio-Pleistocene lacustrine deposites in the Kathmandu valley, central Nepal, Proc. Indian. Nat. Sci. Acad., v,54A, pp.410-417.

Yoshimoto K, Sato H, Ohtake M., (1993), "Frequency-dependent attenuation of P and S waves in the Kanto area, Japan, based on the coda-normalization method", Geophysical Journal International, 11:165–74.

Yunatci AA (2010) GIS Based seismic hazard mapping of Turkey. Thesis submitted to the

graduate school of natural and applied sciences of Middle East technical university

Zafarani, H. and Soghrat, M., (2012), 'Simulation of ground motion in the Zagros region of Iran using the specific barrier model and the stochastic method', Bull. Seism. Soc. Am., 102, 2031-2045.

Zafarani, H., Mousavi, M., Noorzad, A. S. and Ansari, A., (2008), 'Calibration of the specific barrier model to Iranian plateau earthquakes and development of physically based attenuation relationships for Iran', Soil Dynam. Earthquake Eng., 28, 550-576.

Zahedi-Khameneh A. R. Scherer A, and Zaré M, (2013), "A non-parametric wave type based model for real-time prediction of strong ground motion accelerogram", Soil Dynamics and Earthquake Engineering, DOI: 10.1016/j.soildyn.2013.01.024.

Zaré M (1999). "Contribution à l'études des Mouvements forts en Iran : du Catalogue aux lois d'Atténuation", Thèse de Doctorat , Université Joseph Fourier , 237p.

Zaré M and Bard P-Y., (2002), "Strong motion dataset of Turkey: data processing and site classification", Soil Dynamics and Earthquake Engineering, Vol. 22, Issue 8, pp. 703–718, doi: 10.1016/S0267-7261(02)00028-3.

Zaré M and Memarian M (2002). "The Iranian Earthquake Intensity Database: 1975-2000", 12 International Association of Engineering Geology Congress, South Africa, Proceedings (published on the CD-ROM).

Zaré M, H. Amini, P. Yazdi, K. Sesetyan, M. B. Demircioglu, D. Kalafat, M. Erdik, D. Giardini, M.A. Khan, N. Tseriteli, (2014), "Recent developments of the Middle East catalogue", Journal of Seismology, DOI 10.1007/s10950-014-9444-1.

Zaré M, (2015), "Le séisme de Gorkha, Népal, 2015; Rapport de Reconnaissance et distribution des dégâts", 9ème Colloque National AFPS 2007 – Ecole Centrale Paris, 8 pages.

Zaré M, (2016), " Recent development of the earthquake strong motion-intensity catalog and intensity prediction equations for Iran ", Journal of seismology, DOI: 10.1007/s10950-016-9622-4.

Zaré M, Bard P-Y, Ghafory-Ashtinany M. (1998), The Iranian accelerometric data bank, a revision and data correction. Journal of Seismology and Earthquake Engineering 1(1):1±22.

Zaré M, Bard P-Y, Ghafory-Ashtiany M (1999), "Site Characterizations for the Iranian Strong Motion network", Journal of Soil Dynamics and Earthquake Engineering, Vol.18, no.2, pp.101-123.

Zare M, Karimi-Paridari S, Lisa M (2009), "An investigation on Balakot, Muzaffarabad (Pakistan) earth-quake, 8 Oct. 2005, Mw 7.6; geological aspects and intensity distribution", J Seismol 13:327–337

Zaré M. and , S Ghaychi Afrouz, (2012), Crisis Management of Tohoku; Japan Earthquake and Tsunami, 11 March 2011, Iranian J Publ Health, Vol. 41, No.6, Jun 2012, pp.12-20.

Zaré M. and Memarian H., (2002), "The Iranian earthquake intensity database: 1975-2000", 9th International Congress of the International Association of Engineering Geology and the Environment, pp.2894-2903.

Zaré M. and Memarian, H. (2003) Macroseismic Intensity and Attenuation laws: A Study on the Intensities of the Iranian Earthquakes of 1975-2000, Fourth International Conference of Earthquake Engineering and Seismology, 12-14 May 2003 Tehran, Islamic Republic of Iran.

Zaré M., Haghshenas E.and Kalantari A., (2009), "Earthquake of 30 September 2009, Mw7.6, Padang, Sumatra, Indonesia: A Preliminary Reconnaissance Report ", published by IIEES and the collaboration ofCenter of Technology for Natural Resources Inventory (PTISDA), Jakarta – Indonesia, 6 pages.

Zaré M., Saeedi M., Kamranzad F. and Pishnamazi P., (2015), "An overview of disaster management during the April 25, 2015 Mw7.8 Nepal earthquake", subimtted.

Zaré M., (2002), "Doppler Effect Observed on the Recorded Strong Ground Motions in Iran and Turkey", Journal of Seismology and Earthquake Engineering, Vol.4, No. 2 and 3, pp.21-36.

Zaré M., (2003), "A preliminary reconnaissance report on the Algeria earthquake of 21 May 2003, Mw6. 8", http://www. iiees.ac.ir.

Zaré M., (2004), "Bam , Iran earthquake of 26 December 2003, MW6.5: A study on the strong ground motions", 13th World Conference on Earthquake Engineering, Vancouver, B.C., Canada August 1-6, 2004, Paper No. 8001.

Zare M., (2004), "Strong Motion Data of the 1994-2002 Earthquakes in Iran: A Catalogue of 100 Selected Records with Higher Qualities in the Low Frequencies", JSEE: Summer 2004, Vol.

6 No. 2, pp.1-17.

Zaré M., (2007), "Spectral Demand Curves Based on the Selected Strong Motion Records in Iran", Journal of Seismology and Earthquake Engineering (JSEE), Vol. 7, No.3. pp.111-123.

Zaré M., (2015), "Seismic Hazard Zoning in Iran: A State-of-the-Art on the Studies During Four Decades", Submitted.

Zaré M., Amini H., Yazdi P., Sesetyan K., Demircioglu M.B., Kalafat D., Erdik M., Giardini D., Asif Khan M. and Tsereteli N., (2014), "Recent developments of the Middle East catalog", Journal of Seismology, Vol 18., pp.749–772, DOI: 10.1007/s10950-014-9444-1.

Zaré M., and B. Nazmazar, (2013), Van, Turkey Earthquake of 23 October 2011, Mw 7.2; An Overview on Disaster Management, Iranian J Publ Health, Vol. 42, No.2, Feb 2013, pp. 134-144.

Zaré M., and H. Hamzehloo, (2005), "Strong Motion study on Bam Earthquake of 26 December 2003", Earthquake Spectra, Special Issue on Bam earthquake.

Zaré M., and P.-Y. Bard, (2002), "Strong Motion Dataset of Turkey: Data Processing and Site Classification", Soil Dynamics and Earthquake Engineering, Vol. 22., No.8, Pages 703-718.

Zaré M., and Sinaiean, F., (2014), "Site Effects and Classification of Iran Accelerographic Stations", Geodynamics Research International Bulletin, (Special Issue on Intra- Plate Earthquakes), Vol. (I) - No. 02, pp.15-23.

Zaré M., Ansari A., Ashkpour-Motlagh SH., Esmaeili B. and Shahvar M., (2013), "The Mw6.4 Shonbeh (Bushehr), Iran Earthquake, April 2013 ", published by EERRI, 7 pages.

Zaré M., Ansari A., Heydari H., Shahvar M., Daneshdust M., Mahdian M., Sinaiean F., Farzanegan E and Mirzaei-Alavijeh H., (2013), "A Reconnaissance Report on two Iran, Makran Earthquakes: Iran, Makran Earthquakes ; 16 April 2013, Mw7.8, Gosht (Saravan) and 11 May 2013 Irar (Goharan), Bashagard, SE of Iran", report published by EERI, 12 pages.

Zaré M., Bard P.-Y., Ghafory-Ashtiany M., (1999), Site Characterizations for the Iranian Strong Motion network, Journal of Soil Dynamics and Earthquake Engineering, Vol.18, no.2, pp.101-123.

Zaré M., Farzanegan E., Shahvar M., Kamali E. and Saeidi A., (2014), "Mormori (Ilam) SW Iran's Earthquake of 18 August 2014, Mw6.2: A Preliminary Reconnaissance Report ", published by EERRI, 22 pages.

Zaré M., Kamranzad F, Ostad-Taghizadeh A., (2016), "Risk Assessment of Multiple Natural Hazards in Tehran", Submitted.

Zaré M., Kamranzad F., Mona Lisa., and Rajaure, (2015), "A Seismological Overview of the 25 April 2015, Mw7.8 Nepal Earthquake", submitted.

Zaré M., Kamranzad, F., and Farzanegan, E., (2016), "An Assessment of Recent Near-Field Strong Motion Data in Iran", 17th Iranian Geophysics Conference.

Zaré M., Karimiparidari S., Memarian H., (2015) "Seismic Hazard Analysis in Iran (475 Years Return Period)", Submitted.

Zaré M., Karimiparidari S., Memarian H., (2015), "On the Poisson distribution of the Iranian de-clustered earthquake catalogue", 7th International Conference on Seismology & Earthquake Engineering (SEE7), Tehran, Iran.

Zaré M., Karimiparidari, S. Sabzali S., (2008), 'Spectral Attenuation of Strong Motions for Near Source Motions in Iran', Journal of Seismology and Earthquake Engineering (JSEE), Technical Note, Fall 2008, Vol. 10, No. 3, 147-152.

Zaré M., P.-Y. Bard and M. Ghafory-Ashtiany, (1999), "Site characterization for the Iranian Strong Motion Network", Soil Dynamics and Earthquake Engineering, Vol. 18, No.2, pp. 101-123.

Zaré M., S. Karimiparidari, MonaLisa, (2009), An investigation on Balakot, Muzaffarabad (Pakistan) earthquake, 8 Oct. 2005, Mw 7.6; geological aspects and intensity distribution, J of Seismology, DOI 10.1007/s10950-008-9120-4.

Zare, M. (2010). "Fundamental of Seismic Hazard Analyses" International Institute of Earthquake Engineering and Seismology (IIEES), (in Persian), Tehran, Iran, p 142

Zare, M. and Memarian, H., (2003), "Macroseismic Intensity and Attenuation Laws: A Study on the Intensities of the Iranian Earthquakes of 1975- 2000", 4th International Conf. on Seismology and Earthquake Engineering, IIEES, I.R. Iran.

Zare, M. and Sabzali, S., (2006), "Spectral attenuation of strong motions in iran", Third International Symposium on the Effects of Surface Geology on Seismic Motion Grenoble,

France, 30 August - 1 September 2006.

Zare, M., (2001), "Construction and Earthquake hazard in North Tabriz Fault and earthquake fault width in Iran", Journal of Seismology and Earthquake Engineering, 4th year, No. 2, 3, pp. 46-57.

Zare, M., (2002), 'Iranian earthquake catalogue, unpublished compilation of Iranian seismicity data', IIEES, mzare@iiees.ac.ir.

Zare, M., (2012), 'Development of Seismic Hazard Zoning Map for Iran, Based on New Seismic Source Determination', 15th World Conferences on Earthquake Engineering (WCEE), 9 pages.

Zare, M., Amini, H., Yazdi, P., Sesetyan, K., Betul Demircioglu, M., Kalafat, D., Erdik, M., Giardini, D., Asif Khan, M. and Tsereteli, N., (2014), "Recent developments of the Middle East catalog", Journal of seismology, DOI 10.1007/s10950-014-9444-1.

Zare, M., Bard, P.Y. and Ghafory-Ashtiany, M., (1999), 'Attenuation law for the strong motions in Iran', 3rd Int. Conf. on Seismology and Earthquake Engineering (SEE3), Proc. Vol. 1, pp.345-354.

Zare, M., Karimiparidari, S. and Memarian, H., (2015), 'Seismic Hazard Analysis in Iran (475 Years Return Period)', Submitted.

Zare, M., Memarian, H., (2000). 'Simulation of earthquakes intensity in Iran', research report of Iranian Red Crescent. Tehran, Iran. 150 pp [in Persian].

Zare M., Amini H., Yazdi P, Sesetyan K, Demircioglu M.B., Kalafat D., Erdik M., Giardini D., Asif Khan M. and Tsereteli N., (2016), Reply to "comment on 'recent developments of the Middle East catalog'", Journal of Seismology, pp 1–3, doi:10.1007/s10950-016-9626-0

Zarean A, Farrokhi M, Chaychizadeh S., (2008), "Attenuation of high frequency P and S waves on Qeshm Island, Iran", Presented at: 14th world conference on earthquake engineering. Beijing, China; October 12–17, 2008.

Zhao JX, Irikura K, Zhang J, Fukushima Y, Somerville PG, Asano A, et al. (2006), "An empirical site-classification method for strong-motion stations in Japan using H/V response spectral ratio", Bull Seismol Soc Am 2006;96:914–25.

Zhao JX et al (2006) Attenuation relations of strong ground motion in Japan using site classification based on predominant period. Bull Seismol Soc Am 96:898–913

Zhuang J, Ogata Y, Vere-Jones D (2002): Stochastic de-clustering of space-time earthquake occurrences. *Journal of the American Statistical Association,* 97(458): 369-380.

Zuccolo E, Vaccari F, Peresan A and Panza G. F. (2011), "Neo-Deterministic and Probabilistic Seismic Hazard Assessments: a Comparison over the Italian Territory", Pure and Applied Geophysics January 2011, Volume 168, Issue 1, pp 69–83, doi: 10.1007/s00024-010-0151-8.

Curriculum Vitae

A Brief Introduction:

Dr. Mehdi ZARE is a full professor in engineering seismology (IIEES, Tehran, IRAN) and a senior researcher in earthquake hazard and risk analysis and engaged since 1991 in the field of earthquake hazard studies and risk reduction in his country and in the region. He is an internationally known scientist in his field of expertise.

There are about 50 articles authored or co-authored by Dr. Mehdi ZARE on the seismicity and seismic hazard and risk of Iran and the region, published in the highly cited scientific international journals. Meanwhile, he has published 13 books in Persian on the earthquake hazard analysis and seismicity of Iran (including 5 text books and 8 public scientific books for non-specialist readers). He is the first author of a book (in English) which is published by IIEES on the reconnaissance study on the Padanag, Indonesia, 30 September 2009 earthquake (co-authored by 2 IIEES colleagues and 3 Indonesian scientist from BPPT, Jakarta).

He had a long career of international collaboration with LGIT, Grenoble (since he started his PhD there in 1995), EOST Strasbourg (Since 2002), Kandilli Observatory and Earthquake Research Institute in Istanbul, Turkey (Since 1999, after the Izmit earthquake), and the Dept of Earthquake Engineering in UTM, Johur, Malaysia (Since 2010).

He has a long career in popularizing the concepts of earthquake hazard and risk and safety in the public media (Iranian State Radio and TV), through participations in the live and recorded broad casts since 1999. There are about monthly seminars on disaster risk management in Iran organized or cooperated by him.

Dr. Mehdi ZARE is an associate member of the division of geology in department of basic sciences of the Academy of Sciences, I.R. of Iran (Since Feb 2016). He is the senior advisor to the National Disaster Management Organization of Iran (NDMO; official organization for Disaster management in Iran; under the ministry of Interior) and the Tehran Disaster Management and Mitigation Organization (TDMMO; under the municipality of Tehran) as well as the senior advisor to the Iran Strong-Motion Network (ISMN; under the Road, Housing and Development Research Center). He is also a permanent member of the technical supervisor committee of the "Iranian Code of Practice for Seismic Resistant Design of Buildings" (Standard No. 2800), since 1999.

Personal Profile:

- *Name:* Mehdi Zare
- *Nationality:* Iranian
- *Date of Birth:* 09 September 1968
- *Gender:* Male
- *E-mail:* mzare@iiees.ac.ir, mehdi.zare.iran@gmail.com
- *Phone:* +98 21 22830830
- *Cell phone:* +98 9121007813
- Address: International Institute of Earthquake Engineering and Seismology, No. 21, Arghavan St., North Dibajee, Farmanieh, Tehran, IRAN. P.O.Box: 19537-14453.

Education:

- March 1999 **Ph.D.,** Engineering Seismology, Joseph-Fourier (Grenoble I) University, Grenoble, France.
- March 1994 **M.Sc.,** Engineering Geology, Tarbiat-Modarres University, Tehran, Iran.
- June 1990 **B.Sc.**, Geology (degree with Honor), University of Tehran, Tehran, Iran,

Professional Experiences:

- Since February 2016: Associate member of Geology Division, Department of Basic Sciences; Academy of Sciences of the I.R. Iran. (Started collaboration with the Academy of Sciences since June 2014 as an invited member)
- Since October 2015: Full Professor of Engineering Seismology, International Institute of Earthquake Engineering and Seismology (IIEES), Tehran.
- Since June 2014; Director of Engineering Seismology Department, IIEES.
- Since September 2013; Adjacent Professor; Faculty of Geography, University of Tehran, Tehran, IRAN.
- Since November 2008; Adjacent Professor; Disaster & Emergency Health Academy, I.R. Iran National Institute of Health Research, Tehran University of Medical Sciences, Tehran, IRAN.
- November 2007- June 2014: Director of National Center for Earthquake Prediction.
- November 2007-Oct 2013: IIEES Vice-President for Research and Technology.

- February 2005-November 2007: Director of Seismology Research Center of IIEES.
- November 2005: Associate Professor of Engineering Seismology, International Institute of Earthquake Engineering and Seismology, Tehran.
- Since March 2000: Adjacent Professor; Mining Engineering Department, Faculty of Engineering, University of Tehran, Tehran, IRAN.
- May 2000-May 2005; Technical Advisor to the Dez-Ab Consulting Engineers.
- Since March 1999: Assistant Professor: International Institute of Earthquake Engineering and Seismology, Tehran.
- October 1995 to March 1999: Research Student in the "Laboratoire de Géophysique Interne et Tectonophysique LGIT, IRIGM, Université Joseph Fourier, Grenoble, France. (Meanwhile: Faculty member and Head of Earthquake Reconnaissance Dept., International Institute of Earthquake Engineering and Seismology, Tehran.)
- December 1992 to October 1995: Research Associate in the In International Institute of Earthquake Engineering and Seismology, Tehran.
- September 1990 to December 1992: Engineering Geologist and Geotechnical expert, Mahab-Ghods Consulting Engineers, Tehran.
- Since June 1992: Freelance Engineering Seismologist, Seismic Hazard and Risk Assessment for the Engineering Projects (Dams, Power Plants, Urbanism, etc) in Iran (45 projects studied).
- Expert to Control the Seismic Hazard Studies on the Bushehr Nuclear Power Plant.

Supervised PhD Thesis:

1. Dr Fereidoun Sinaiean; November 2006, "Strong Motion Studies in Iran, Analysis and Attenuation Relationships". IIEES (1st Finalized PhD in Geophysics in an Iranian Academic center; i.e. inside Iran)
2. Dr Mohammad Aryamanesh; (co-supervised with Dr M.R Zolfaghari); April 2007, Seismic Hazard Studies in Tabas Region, East Iran, IIEES
3. Dr Hadi Ghasemi, February 2009; Spectral Attenuation of Strong motion Studies in Iran, IIEES.
4. Dr Aref Bali-Lashak, September 2010; Earthquake Forecast in Iran, IIEES
5. Dr Arezu Dorostian, February 2011; Strong Motion Data Modelling in the Near-Field, IAU, Tehran

6. Dr Deynaz Iranbodi, September 2011; Earthquake Rupture Hazard Zone in South Tehran Region; IAU, Tehran
7. Dr Jamileh Vasheghani-Farahani, August 2012; Attenuation of Explosion Seismic Motions, IIEES.
8. Dr Mohammad Poumohammad-Shahvar; April 2013; Developing the ShakeMaps for Earthquakes in Iran, IIEES
9. Dr Sepideh Karimiparidari (co-supervised with Prof H. Memarian); September 2013; Probabilistic Seismic Hazard Zoning in Iran for 475 years return period, IIEES
10. Dr Masoud Mojarab, June 2014, (co-supervised with Prof H. Memarian), Earthquake Prediction in Iran; M8 Method for mid-term predictions, College of Engineering, University of Tehran.
11. Dr Majid Maybodian; October 2014; Earthquake Forecast Using CN Method in Zagros Belt, Iran, IIEES
12. Abdolah Vaez-Shushtari, December 2015 University Technology Malaysia (UTM), Attenuation of Strong Ground motions in SE Asia; (co-supervisor with Prof Adnan B. Azlan.

Under Supervision PhD Thesis:

1. Farnaz Kamranzad; "Development of seismic hazard analysis in Iran based on new data and methods"; University of Tehran, (Started October 2016).
2. Mona Salamat; "M_{max} assessment and analysis for Iranian seismic source zones; IIEES, (Started Nov 2012).
3. Zoya Farajpour; "Next generation attenuation (GMPE) for Iran"; IIEES, (Started Nov 2012).
4. Hamideh Amini; "Uncertainties on the seismic hazard zoning in Iran", IIEES (Started in 2011).

Scientific Activities:

- Since May 1999: Seismic Regulations for the Nuclear Power Plants.
- Since May 1992: member of editorial board and founding the “Engineering Geology Group” in the Omran Magazine; Faculty of Civil Engineering, Sharif University of Technology, Tehran.

Teaching Courses:

- Seismic Hazard Analysis and Zoning
- Applied Geophysics
- Seismology
- Strong Ground Motion Seismology
- Seismic Risk Analysis
- Seismotectonic
- Disaster Risk Management and Uncertainties
- Aftermaths of Natural Disasters

  (in BSc, MSc and PhD levels for Geophysics, Earthquake Engineering, Civil and Mining Engineering) in Tehran University, Petroleum Industry University, K.N. Toosi University of Technology, IAU University.

Languages:

● Persian (Native)
● English (Reading, Writing and Speaking)
● Arabic and German (Reading only)
● French (Reading, Writing and Speaking)

Scientific Stages:

- September 1998: Commissariat d'Enérgie Atomique (CEA), Fontenay-aux-roses, Attenuation of Strong Ground Motions, France.
- June-September 2000: LGIT-IRIGM, Grenoble France.

Fields of Interest:

Engineering Seismology, Seismic Hazard and Risk Analysis, Strong Ground Motion, Earthquake Prediction

Citation indices (by Google scholar)	All	Since 2011
Citations	603	363
h-index	12	10
i10-index	17	10

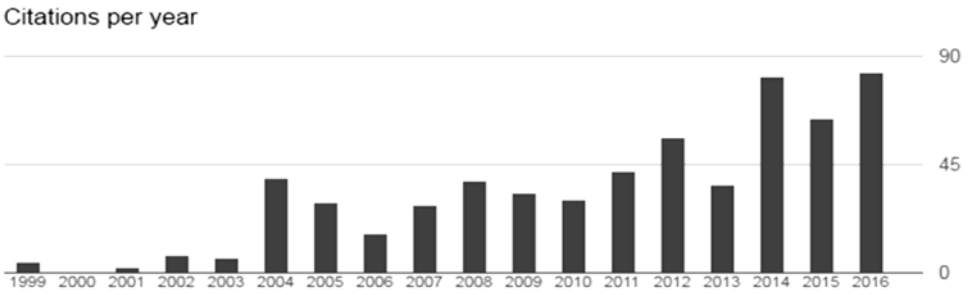

Number of published articles in cited international journals: over 50

Some Recent Major International Journal Papers:

1. **Zaré M**, (2016), "Recent development of the earthquake strong motion-intensity catalog and intensity prediction equations for Iran", Journal of Seismology, pp 1–23, doi:10.1007/s10950-016-9622-4.
2. **Zaré M**, Karimiparidari S., Memarian H. and Kamranzad F., (2016), "Poisson distribution of the Iranian declustered earthquake catalog", Arabian Journal of Geosciences, doi:10.1007/s12517-016-2765-3.
3. Salamat M., **Zaré M**., Holschneider M. and Zoller G., (2016), "Calculation of Confidence Intervals for the Maximum Magnitude of Earthquakes in Different Seismotectonic Zones of Iran", Pure and Applied Geophysics, doi:10.1007/s00024-016-1418-5.
4. uzi L., Puglia R., Russo E., D'Amico M., Felicetta C., Pacor F., Lanzano G., Çeken U., Clinton H., Costa G., Duni L., Farzanegan E., Gueguen Ph, Ionescu C., Kalogeras I., Özener H., Pesaresi D., Sleeman R., Strollo A. and **Zaré M**., (2016), "The Engineering Strong-Motion Database: A Platform to Access Pan-European Accelerometric Data", *Seismological Research Letters*, Vol 87, No. 4, pp. 1-11, doi: 10.1785/0220150278.
5. Ommi S., Zafarani H, and **Zaré M**, (2016), "Aftershock Decay Rates in the Iranian Plateau", *Pure Appl. Geophys*, Vol. 173, Issue 7, pp. 2305–2324, doi: 10.1007/s00024-016-1285-0.
6. Vaez Shoushtari A., Azlan B.A and **Zaré M**, (2016), "On the selection of ground–motion attenuation relations for seismic hazard assessment of the Peninsular Malaysia

region due to distant Sumatran subduction intraslab earthquakes", *Soil Dynamics and Earthquake Engineering*, Vol. 82, pp. 123–137, doi: 10.1016/j.soildyn.2015.11.012.

7. Vaez Shoushtari A., Azlan B.A and **Zaré M**, Harith NSH, (2015), "Estimation of the maximum credible hazard in Kuala Lumpur and Singapore due to gigantic Sumatran megathrust earthquakes: based on a comparative study on attenuation laws", *Natural Hazards*, Vol.78, pp. 725-751, doi: 10.1007/s11069-015-1742-6.

8. Ramezani Besheli P., **Zaré M.**, Ramazani Umali R. and Nakhaeezadeh G., (2015), "Zoning Iran based on earthquake precursor importance and introducing a main zone using a data-mining process", *Natural Hazards*, Vol. 78, Issue 2, pp. 821–835, doi: 10.1007/s11069-015-1745-3.

9. Talebi M., **Zaré M**, Madahi-zadeh A.R. and Bali-Lashak A., (2015), "Spatial-temporal analysis of seismicity before the 2012 Varzeghan, Iran, Mw 6.5 earthquake", *Turkish Journal of Earth Sciences*, Vol. 24, pp.289-301, doi:10.3906/yer-1410-13.

10. Norouzi N., Mojarab M, Asadi Z and **Zaré M**, (2014), "A Case Study of Seismic Hazard Analysis at Al-Tajiat and Al-Zawraa Stadiums in Baghdad/Iraq Region", *Arab J Sci Eng*, Vol. 40, Issue 7, pp. 1987–2002, doi: 10.1007/s13369-014-1559-8.

11. **Zaré M**., Amini H., Yazdi P., Sesetyan K., Demircioglu M.B., Kalafat D., Erdik M., Giardini D., Khan M.A. and Tseriteli N., (2014), "Recent developments of the Middle East catalog", *Journal of Seismology*, Vol. 18, Issue 4, pp. 749–772, doi: 10.1007/s10950-014-9444-1.

12. Vasheghani-Farhani J. and **Zaré M**, (2014), "Site characterizations for the Tehran network (TDMMO) in Tehran region using micro-earthquake, microtremor and quarry blast data", *Soil Dynamics and Earthquake Engineering*, Vol. 63, pp. 235–247, doi: 10.1016/j.soildyn.2014.03.013

13. Vasheghani-Farhani J., **Zaré M**, and Cichowicz A. (2014), "Microseismicity of the Tehran region based on the data recorded in a local monitoring network: 2004-2010", *Episodes,* Vol. 37, No. 3, pp. 206-217.

14. Vasheghani-Farhani J. and **Zaré M**, (2014), "Seismological aspects of the Varzeghan twin Earthquakes on 11 August 2012 (Mw 6.3 and Mw 6.1), in East Azerbaijan Province, NW Iran", *Episodes*, Vol. 37, No. 2, pp. 96-104.

15. Esmaeili B., Almasian M., **Zaré M**, Alipoor R. and Alizadeh A., (2014), "0Geophysical and geological study on the West Qarchak fault and its implications in seismic hazard, Tehran, Northern Iran", *Episodes,* Vol. 37, No. 2, pp. 105-110.

16. Asadi Z. and **Zaré M**, (2014), "Estimating magnitudes of prehistoric earthquakes and seismic capability of fault from landslide data in Noor valley (central Alborz, Iran)", *Natural Hazard*, Vol. 74, Issue 2, pp. 445–461, doi: 10.1007/s11069-014-1186-4.

17. Mojarab M., Memarian H., **Zaré M**, Morshedy A.H., Pishahang M.H., (2014), "Modeling of the seismotectonic provinces of Iran using the self-organizing map algorithm", *Computers & Geosciences*, Vol. 67, pp. 150–162, doi: 10.1016/j.cageo.2013.12.007.

18. Mojarab M., Memarian H. and **Zaré M**, (2014), "Performance evaluation of the M8 algorithm to predict M7+ earthquakes in Turkey", *Arab Journal of Earth Sciences*, Vol. 8, Issue 8, pp. 5921–5934, doi: 10.1007/s12517-014-1624-3.

19. Zahedi-Khameneh A., Scherer R.J, and **Zaré M**, (2013), "Non-parametric wave type based model for real-time prediction of strong ground motion accelerogram", *Soil Dynamics and Earthquake Engineering*, Vol. 49, pp.181–196, doi: 10.1016/j.soildyn.2013.01.024

20. Maybodian M., **Zaré M**, Hamzehloo H., Peresan A., Ansari A. and Panza G., (2013), "Analysis of precursory seismicity patterns in Zagros (Iran) by CN algorithm", *Turkish J Earth Sci,* Vol. 23, pp.91-99, doi:10.3906/yer-1212-6, pp1-9.

21. Karimiparidari S. **Zaré M**, Memarian H. and Kijko A., (2013), "Iranian earthquakes; A Uniformed Catalog with Moment Magnitude". *Journal of seismology*, Vol. 17, Issue 3, pp. 897–911, doi: 10.1007/s10950-013-9360-9.

22. Radan M.Y., Hamzehloo H., Peresan A., **Zaré M**. and Zafarani H., (2013), "Assessing performances of pattern informatics method: a retrospective analysis for Iran and Italy", *Natural Hazard*, Vol. 68, Issue 2, pp. 855–881, doi: 10.1007/s11069-013-0660-8.

23. Shahvar M.P, **Zaré M**, and Castellaro S., (2013), "A unified seismic catalog for the Iranian plateau (1900-2011)"; *Seismological Research Letter*, Vol.84, No. 2, pp. 233-249, doi: 10.1785/0220120144.

24. **Zaré M**., Hashemi A., Ebadi R., Amirnejad-Mojdehi S., Rahmani R. and Sardar A., (2013), "Tsunami hazard in the shorelines of Khark island (Persian Gulf), Iran", *Earthquake Science*, Vol. 25, Issue 4, pp. 299–305, doi:10.1007/s11589-012-0855-1.

25. **Zaré M**, and Nazmazar B., (2013), "Van, Turkey Earthquake of 23 October 2011, Mw 7.2; An Overview on Disaster Management", *Iranian J Publ Health*, Vol. 42, No.2, pp. 134-144.

26. Maybodian M., **Zaré M**, Hamzehloo H., Peresan A., Ansari A. and Panza G., (2013), "Scaling of Long-Term Seismicity in Zagros, Iran", *Journal of Seismology and Earthquake Engineering*, Vol.15, No.2, pp. 91-99.

27. Shahvar M.P. and **Zaré M**, (2012), "The 27 August 2010 Mw 5.7 Kuh-Zar earthquake (Iran): field investigation and strong-motion evidence", *Nat Hazards*, Vol. 66, Issue 2, pp. 689–706, doi: 10.1007/s11069-012-0507-8.

28. Alipoor R., **Zaré M**. and Ghassemi M.R, (2012), "Inception of activity and slip rate on the Main Recent Fault of Zagros Mountains, Iran", *J of Geomorphology*, Vol.175–176, pp. 86–97, doi: 10.1016/j.geomorph.2012.06.025.

29. Vasheghani Farahani J., **Zaré M** and Lucas C., (2012), "Adaptive neuro-fuzzy inference systems for semi-automatic discrimination between seismic events: a study in Tehran region", *Journal of seismology,* Vol.16, Issue 2, pp. 291–303, doi: 10.1007/s10950-011-9270-7.

30. Vasheghani Farahani J, **Zaré M**, and Cichowicz A., (2012), "Attenuation of high-frequency P and S waves in south and southeast Tehran using blast data", *Soil Dynamics and Earthquake Engineering*, Vol. 40, pp. 99–108, doi: 10.1016/j.soildyn.2012.03.005.

31. **Zaré M.** and Ghaychi-Afrouz S., (2012), "Crisis Management of Tohoku; Japan Earthquake and Tsunami, 11 March 2011", *Iranian J Publ Health*, Vol. 41, No. 6, pp. 12-20.

32. Naghavi M, Shomali Z.H, and **Zaré M**, (2012), "Lg Coda Variations in North-Central Iran", *International Journal of Geophysics*, Vol. 2012, Article ID 673506, 7 pages, doi: 10.1155/2012/673506.

33. Bali-Lashak A., **Zaré M**, Andalib A., Poubeyramvand K. and Radan Y., (2012), "A Novel Method for Detection of Seismic Dual-Zones with Application to Earthquake Forecasting", *Journal of Seismology and Earthquake Engineering*, Vol 14, No.1, pp. 1-12.

34. Alipoor R., **Zaré M**. and Ghasemi M.R., (2012), "Inception of activity and slip rate on the Main Recent Fault of Zagros Mountains, Iran", *Geomorphology*, Vol. 175–176, pp. 86–97, doi: 10.1016/j.geomorph.2012.06.025.

35. Vasheghani Farahani J and **Zaré M**, (2011), "The Southeastern Tehran Earthquake of 17 October 2009 (M_w=4.0)", *Seismological Research Letters*, Vol. 82, No. 3, pp. 404-412, doi: 10.1785/gssrl.82.3.404.

36. Alipoor, R. Poorkermani M., **Zaré M.**, and Hamdouni R.E., (2011), "Active Tectonic Assessment around Rudbar Lorestan Dam Site, High Zagros Belt (SW of Iran)", *Journal of Geomorphology*, Vol. 128, Issues 1–2, pp.1–14, doi: 10.1016/j.geomorph.2010.10.014.

37. Bali-Lashak A., **Zaré M**, Mortezanejad Gh. and Poubeyranvand Sh., (2010), "Moment tensor inversion of nine events in Iran using INSN data", *Journal of Seismology*, Vol. 14, Issue 4, pp. 751-760, doi: 10.1007/s10950-010-9197-4.

38. Ghasemi H., **Zaré M** and Sinaeian F., (2009), "Smooth Spectra of Horizontal and Vertical Ground Motions For Iran", *ISET Journal of Earthquake Technology,* Paper No. 500, Vol. 46, No. 1, March 2009, pp. 1–17.

39. Ghasemi H., **Zaré M**, Fukushima Y. and Sinaiean F., (2009), Applying empirical methods in site classification, using response spectral ratio (H/V): A case study on Iranian strong motion network (ISMN), *Journal of Soil Dynamics and Earthquake Engineering*, Vol. 29, Issue 1, pp. 121–132, doi: 10.1016/j.soildyn.2008.01.007.

40. Ghasemi H., **Zaré M**, Fukushima Y. and Koketsu K., (2008), "An empirical spectral ground-motion model for Iran", *Journal of Seismology*, Vol. 13, Issue 4, pp. 499–515, doi:10.1007/s10950-008-9143-x.

41. Ghasemi H., **Zaré M** and Fukushima Y., (2008), "Ranking of several ground-motion models for seismic hazard analysis in Iran", *J. Geophys. Eng*, Vol. 5, No. 3, pp. 301–310.

42. **Zaré M**, Karimiparidari S., and Sabzali S., (2008), "Spectral Attenuation of Strong Motions for Near Source Motions in Iran", *Journal of Seismology and Earthquake Engineering (JSEE)*, Technical Note, Vol. 10, No.3, pp. 147-152.

43. **Zaré M**, Karimiparidari S. and MonaLisa, (2008), "An investigation on Balakot, Muzaffarabad (Pakistan) earthquake, 8 Oct. 2005, Mw 7.6; geological aspects and intensity distribution", *Journal of Seismology*, Vol. 13, Issue 3, pp. 327–337, doi:10.1007/s10950-008-9120-4.

44. **Zaré M**, (2007), "Spectral Demand Curves Based on the Selected Strong Motion Records in Iran", *Journal of Seismology and Earthquake Engineering (JSEE),* Vol. 7, No. 3, pp. 111-123.

45. Ansari A., Noorzad A. and **Zaré M**, (2007), "Application of wavelet multi-resolution analysis for correction of seismic acceleration records", *Journal of Geophysics and Engineering*, Vol. 4, pp. 362–377.

46. **Zaré M**. and Hamzehloo H., (2005), "Strong Motion study on Bam Earthquake of 26 December 2003", *Earthquake Spectra*, Vol. 21, No. S1, pp. S165–S179.

47. **Zaré M**. and Bard P.-Y., (2002), "Strong Motion Dataset of Turkey: Data Processing and Site Classification", *Journal of Soil Dynamics and Earthquake Engineering*, Vol. 22., No.8, pp. 703-718, doi: 10.1016/S0267-7261(02)00028-3.

48. **Zaré M**, (2002), "Doppler Effect Observed on the Recorded Strong Ground Motions in Iran and Turkey", *Journal of Seismology and Earthquake Engineering (JSEE),* Vol. 4, No. 2 and pp.21-36.

49. **Zaré M**., Bard P.-Y. and Ghafory-Ashtiany M., (1999), "Site characterization for the Iranian Strong Motion Network", *Soil Dynamics and Earthquake Engineering*, Vol. 18, No.2, pp. 101-123, doi: 10.1016/S0267-7261(98)00040-2.

50. **Zaré M**., Bard P.-Y. and Ghafory-Ashtiany M., (1999), "The Iranian Strong Motion Data Bank; A Revision and Data Correction", *Journal of Seismology and Earthquake Engineering (JSEE),* Vol.1, No.1, pp.1-23.

51. **Zaré M**., (1998), "An Overview on the Ardebil Iran (23 February 1997) Earthquake", *Seismological Research Letters*.

52. **Zaré M**. and Moinfar A.A., (1994), "Comment on the “Rudbar-Tarom Earthquake of

20 June 1990 in NW Persia, a Preliminary Field and Seismological Observations", by: M.Berberian, M.Qorashi, J.A.Jackson, and T.Wallace", *Bulletin of the Seismological Society of America (BSSA),* Vol. 84, pp. 484-485.

Attachments

#1. Zaré M., Amini H., Yazdi P., Sesetyan K., Demircioglu M.B., Kalafat D., Erdik M., Giardini D., Khan M.A. and Tseriteli N., (2014), "Recent developments of the Middle East catalog", Journal of Seismology, vol. 18, issue 4, pp. 749–772, doi: 10.1007/s10950-014-9444-1.

J Seismol (2014) 18:749–772
DOI 10.1007/s10950-014-9444-1

ORIGINAL ARTICLE

Recent developments of the Middle East catalog

Mehdi Zare · Hamideh Amini · Pouye Yazdi · Karin Sesetyan · Mine Betul Demircioglu · Dogan Kalafat · Mustafa Erdik · Domenico Giardini · M. Asif Khan · Nino Tsereteli

Received: 9 July 2013 / Accepted: 27 May 2014 / Published online: 13 June 2014

Abstract This article summarizes a recent study in the framework of the Global Earth model (GEM) and the Earthquake Model of the Middle East (EMME) project to establish the new catalog of seismicity for the Middle East, using all historical (pre-1900), early and modern instrumental events up to 2006. According to different seismicity, which depends on geophysical, geological, tectonic, and seismicity data, this region is subdivided to nine subregions, consisting of Alborz–Azerbaijan, Afghanistan–Pakistan, Saudi Arabia, Caucasus, Central Iran, Kopeh–Dagh, Makran, Zagros, and Turkey (Eastern Anatolia; after 30° E). After omitting the duplicate events, aftershocks, and foreshocks by using the Gruenthal method, and uniform all magnitude to *Mw* scale, 28,244 main events remain for the new catalog of Middle East from 1250 B.C. through 2006. The magnitude of completeness (*Mc*) was determined as 4.9 for five out of nine subregions, where the least values of *Mc* were found to be 4.2. The threshold of Mc is around 5.5, 5.0, 4.5, and 4.0, for the time after 1950, 1963, 1975, and 2000, respectively. The average of teleseismic depths in all regions is less than 15 km. Totally, majority of depth for Kopeh–Dagh and Central Iran, Zagros, and Alborz–Azerbaijan, approximately, is 15, 13, and 11 km and for Afghanistan–Pakistan, Caucasus, Makran, Turkey (after 30° E), and Saudi Arabia is about 9 km.

Keywords Seismicity · Catalog · Middle East · Depth · Historical · Instrumental · Magnitude

Electronic supplementary material The online version of this article (doi:10.1007/s10950-014-9444-1) contains supplementary material, which is available to authorized users.

M. Zare (✉) · H. Amini · P. Yazdi
International Institute of Earthquake Engineering and Seismology (IIEES), Tehran, Iran
e-mail: mzare@iiees.ac.ir

K. Sesetyan · M. B. Demircioglu · D. Kalafat · M. Erdik
Kandili Observatory and Earthquake Research Institute, Bogazici University, Istanbul, Turkey

D. Giardini
Institute for Geophysics, ETH Zürich, Zürich, Switzerland
e-mail: domenico.giardini@sed.ethz.ch

M. A. Khan
National Centre of Excellence in Geology, University of Peshawar, Peshawar, Pakistan
e-mail: masifk@upesh.edu.pk

N. Tsereteli
Department of Seismology and Experimental Geophysics, Institute of Geophysics, Tbilisi, Georgia
e-mail: nino66_ts@yahoo.com

1 Introduction

According to Global Position System (GPS) measurements, there are high seismic activities in the Middle East region; it is partially influenced by the continental convergence and active crustal shortening between the African, Arabian, and the Indian plate northwards with respect to the Eurasian plate (Fig. 1). According to Ambraseys et al. 2002, the historical record confirms

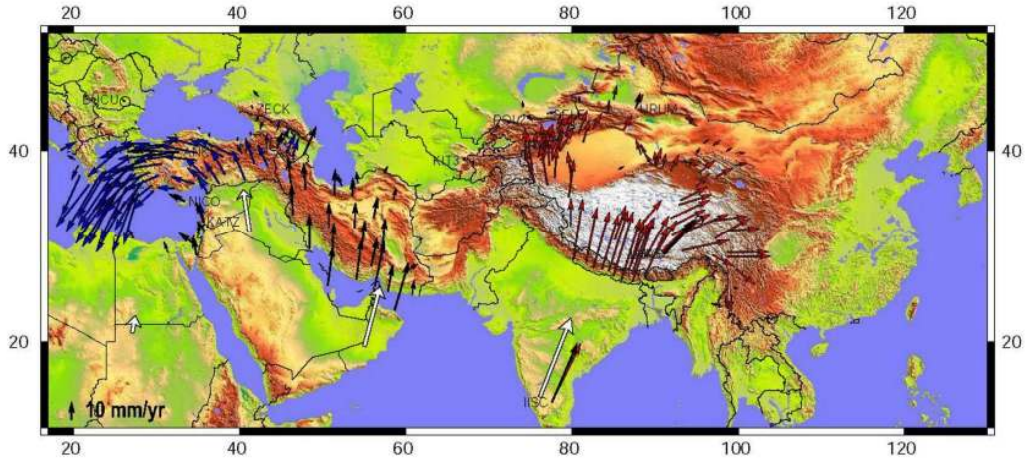

Fig. 1 Horizontal velocity field for a major part of the Alpine–Himalayan chain. The *blue vectors* are by McClusky et al. (2000) and the *red vectors* are by Wang et al. (2001). The *black vectors* are by Vernant et al. (2004). The *white vectors* are the Nuvel1-A plate velocity model by DeMets et al. (1994) (According to Tavakoli 2007)

that some regions that are active today (e.g., the North Anatolian fault zone) were also active 2,500 years ago, demonstrating the long-term nature of their seismicity. It also shows that some regions that are, at present, quiescent (such as the Jordan Rift Valley), are capable of generating relatively large earthquakes. For some of these events, this is consistent with their known active tectonic environment. In historical period, many moderate and almost all of the small events were missed out; however, after installation of the World Wide Seismic Standard Network (WWSSN) seismograms in the Middle East and around the world; and by improving the seismograms in this time, we have fairly good information for earthquake events now.

Using a complete uniform catalog is most important to determine the seismic hazard analysis in each region. In this investigation for arranging lists of earthquakes in a catalog for the Middle East region; all historical and instrumental events were compiled in a new established catalog.

"A History of Persian Earthquakes" (Ambrasys and Melville 1982), "The seismicity of Egypt, Arabia and the Red Sea" (Ambraseys et al. 2005), "Earthquakes in the Mediterranean and Middle East" (Ambraseys 2009), and "The SHARE European Earthquake Catalogue (SHEEC) 1,000–1,899" (Stucchi et al. 2012) are contained main resources of historical earthquake information on this region.

Many researchers estimated some information about different features, subregions, and their specifications for different parts of the Middle East region. For the Middle East region, the published studies are GPS constraints on plate motions, crustal deformation, and plate kinematics, i.e., by Vernant et al. (2004), Tavakoli (2007), and McClusky et al. (2000); focal mechanisms and active shortening and tectonics, i.e., by Talebian and Jackson (2004) and Tatar et al. (2004); relocation and assessment of seismicity, i.e., by Engdahl et al. (2006), earthquake focal depths by Maggi et al. (2000); completeness for earthquake catalogs, i.e., by Mignan and Woessner (2012); and Seismicity declustering, i.e., by Van Stiphout et al. (2012).

Different subregions are studied in previous special researches, for example, the Middle East, i.e., by Vernant et al. (2004) and Tavakoli (2007); Iran, i.e., by Engdahl et al. (2006), Tavakoli (2007), and Maggi et al. (2000); Tibetan plateau, i.e., by Molnar and Lyon-Caen (1989); Tien Shan and Central Asia, i.e., by Nelson et al. (1987); Pakistan, Azad Jammu, and Kashmir, i.e., by Pakistan Meteorological Department and Norwegian Seismic Array (NORSAR), Norway, (2007) were considered by their researchers.

In this article, by unifying all of the records and using ZMAP software (Wiemer 2001; Wyss et al. 2001), some seismicity information for this region will be estimated. We describe the development of a new catalog for the Middle East and determine some of the seismicity information, i.e., number of events, range of magnitudes, and magnitude completeness (*Mc*) and seismicity depths of this region.

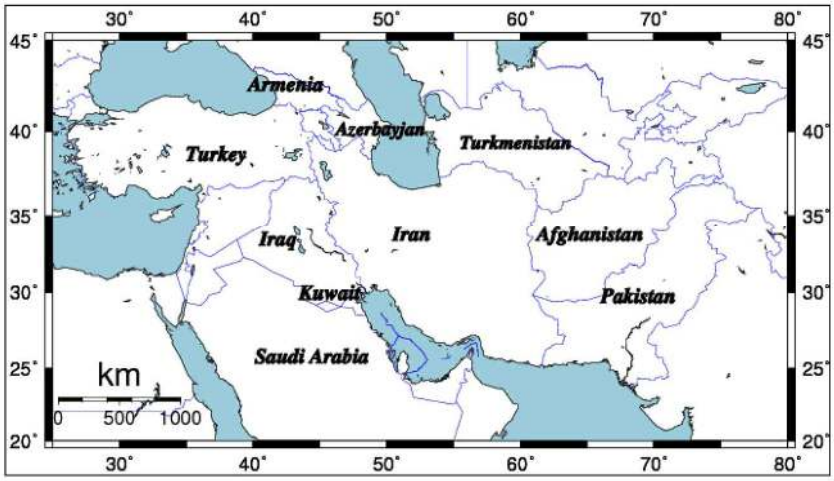

Fig. 2 Boundaries of the Middle East and its countries

2 Developed catalog

2.1 Database used (earthquake database)

The first step for calculating seismic hazard in an area is preparing a uniform catalog, consisting of all historical and instrumental events. The considered region in this investigation covers a quadrangle limited by 11° to 44° N and 30° to 75° E and includes 21 countries compiled from both local and global sources (Fig. 2). The Middle East region is in the continental convergence between the African, Arabian, and the Indian plate northwards with respect to the Eurasian plate; then, there are high seismic activities in this region.

For making a good catalog, we used both global sources, such as important international agencies the same as the National Earthquake Information Center (NEIC), International Seismological Center (ISC), and EHB Bulletin, and local networks and local area such as the International Institute of Earthquake Engineering and Seismology (IIEES) and Iranian Seismological Center (IRSC). In addition to this information, some published earthquake catalogs, the same as "A History of Persian Earthquakes" (Ambrasys and Melville 1982), "The seismicity of Egypt, Arabia and the Red Sea" (Ambraseys et al. 2005), and "Earthquakes in the Mediterranean and Middle East" (Ambraseys 2009) were considered.

In this catalog, there were 28,244 events caused of combination all of references with summary of origin times, longitude, latitude, magnitudes, and depth for each event. A list of important source data with number

Table 1 List of all sources which were used in the new catalog

Original source of data	The number of events	Time period	Included magnitude values
Ambraseys	543	400 B.C.–1999	*Ms, mb*
BHRC	431	1503–2005	*Ms, mb*
EDIG	1,400	1250 B.C.–2003	*Ms, mb*
EHB	2,686	1960–2006	*Ms, mb*
IIEES	1,013	2000–2006	*Ms, mb, ML*
IRSC	37	2006	*MN*
ISC	13,758	1901–2006	*Ms, mb, ML*
ISK	1,521	1901–2006	*mb*
KOERI	1,817	1901–2006	*mb*
Jordan	52	1990–2006	*Ms, mb*
Mak	5,459	1901–2006	*mb*
NC	265	50–1969	*Ms, mb*
NCUSSR	189	1900–1976	*mb*
NEIC	95	1963–2002	*Ms, mb*
NOAA	61	31 B.C.–1970	*mb*
PDE	77	1973–2006	*mb, Ms*
PLN	987	1976–2006	*Ms, mb*
NOW	54	1924–1964	*Ms, mb*
PAPA003	336	1010–1899	*mb*
SHE	231	1900–1999	*mb*
SMCG	535	1991–2006	*Ms, mb*
SOYAL981	239	1003–1998	*mb*
Sul	269	1905–1999	*mb*
TARMAN	221	1970–2002	*Ms, mb*
USGS	199	1903–2006	*Ms, mb*

Table 1 Relationship between Ms, Ml, mb, and Mw in Middle East region by comparing the recorded magnitude of the events

Type of magnitude	Conversion relation	Boundary	R^2	Number	σ	
mb, *Mw*	*Mw*=0.87*mb*+0.83	3.5≤*mb*≤6.0	0.89	16,752	0.3	This study
	Mw=0.85 (±0.04)*mb*+1.03 (±0.23)	3.5≤*mb*≤6.2	0.52	39,784	0.29	Scordilis
Ms, *Mw*	*Mw*=0.76*Ms*+2.11 *Mw*=0.93*Ms*+0.45	2.8≤*Ms*≤6.1 6.2≤*Ms*≤8.2	0.94 0.88	4,103 139	0.28	This study
	Mw=0.67 (±0.005)*Ms*+2.07 (±0.03) *Mw*=0.99 (±0.02)*Ms*+0.08 (±0.13)	3.0≤*Ms*≤6.1 6.2≤*Ms*≤8.2	0.77 0.81	23,921 2,382	0.17 0.2	Scordilis
Ml, *Mw*	*Mw*=1.01*Ml*−0.05	4.0≤*Ml*≤8.3	0.98	2,271	0.25	This study

of events from them used in the final version of this catalog is summarized in Table 1 and explanation of dataset for countries is summarized in Appendix (1).

2.2 Uniform catalog

Ambraseys and Jackson (1998) investigated the earthquakes from Eastern Mediterranean from 464 B.C. up to 1995. For 62 of the 150 earthquakes which have both well-determined surface–wave magnitudes (*Ms*) from instrumentation data and reasonably reliable rupture lengths from field observations; almost 55, 30, and 15 % of the data came from strike–slip, normal, and thrust faults, respectively.

To preparing a unified catalog, we need to uniform all of the magnitudes to one scale. For this purpose, all events with two magnitudes from *mb*, *ML*, *Ms*, and *Mw* were considered. After finding relations between them (Appendix (2)), the magnitude of all events were converted to *Mw*. The result of the derived relationship was represented in Table 2.

Now, in this catalog, all of the magnitude scales were unified by using regional conversion equations between *mb*, *Ms*, *ML*, and *Mw* and convert to magnitude in *Mw* scale. After omitting events with zero magnitudes and erroneously large depth (Wyss et al. 2001), there will be a catalog with 28,244 events from all of historical and instrumental events, in *Mw* magnitude scale (Fig. 3). This catalog contains events with magnitudes 4.0–8.1 between 1250 B.C. and 2006 of which 22,427 events occurred between 1976 and 2006 in the last 10 years.

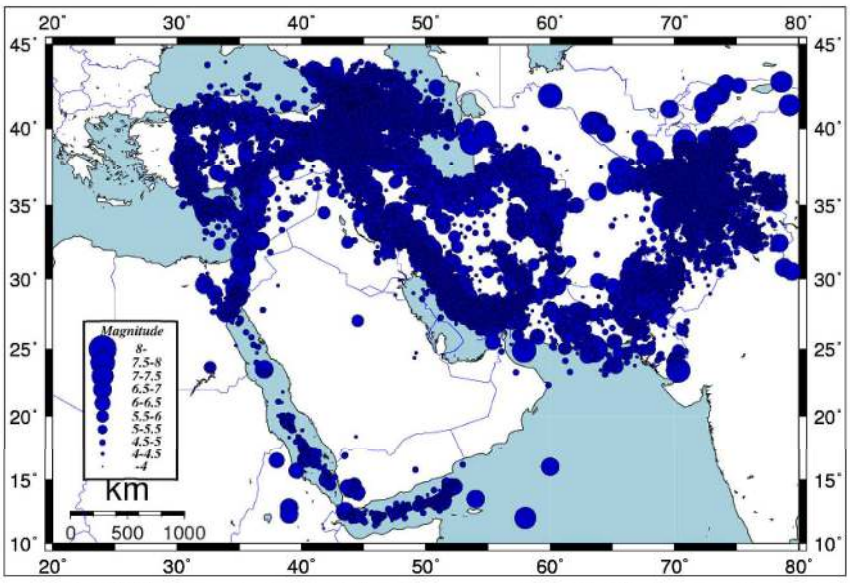

Fig. 3 Seismic map of the Middle East region before declustering represented by 28,244 epicenters of earthquakes occurred during historical and instrumental period

2.3 Declustering catalog

Each catalog needs to omit duplicate events, aftershocks, and foreshocks; on the other hand, main shocks should be separated for use in the final catalog. We study the most common declustering methods, mainshock-window and linked-window declustering. Linked-window declustering replaces each cluster with a single event, for instance, the first, largest, or an "equivalent event" (Luen and Stark 2012).

Windowing techniques are a simple way of identifying mainshocks and aftershocks. For each earthquake in the catalog with magnitude M, the subsequent shocks are identified as aftershocks if they occur within a specified time interval $T(M)$, and within a distance interval $L(M)$. Foreshocks are treated in the same way as aftershocks. The time–space windows are reset according to the magnitude of the largest shock in a sequence and usually, these algorithms do not distinguish between direct and indirect aftershocks. Catalogs declustered with windowing methods have a minimum spacing between events: if a catalog contains two events that are very close in space and time, the later event will fall within the window of the former, and one or both of them will be deleted (Van Stiphout et al. 2012).

In this article, the ZMAP Software (Wiemer 2001) was used for declustering these events. There are four algorithms for doing decluster in this software. Each algorithm considers different time and distance ranges for declustering. Reasenberg (1985) is the most widely used linked-window method and Reasenberg's windows are larger in space but shorter in time the larger the shock. Reasenberg's algorithm (1985) spatial interaction relationship is defined by the threshold $\log d(km)=0.4M0–1.943+k$ (Molchan and Dmitrieva 1992), where k is 1 for the distance to the largest earthquake and 0 for the distance to the last one. The temporal extension of the interaction zone is based on Omori's law. All linked events define a cluster, for which, the largest earthquake is considered the mainshock and smaller earthquakes are divided into foreshocks and aftershocks (Van Stiphout et al. 2012). Default standard parameter values of Reasenberg's algorithm (1985) are represented in Table 3. An approximation of the windows' sizes according to Gardner and Knopoff (1974), Gruenthal (pers. comm.) and Uhrhammer (1986) is shown in Table 4.

Table 3 The standard input parameters for declustering algorithm by Reasenberg (1985)

Parameter	Standard	Simulation range	
		Min	Max
τ_{min} [days]	1	0.5	2.5
τ_{max} [days]	10	3	15
P	0.95	0.9	0.99
x_{meff}	4.0	0	1
x_k	0.5	1.6	1.8
r_{fact}	10	5	20

τ_{min} is the minimum value of the look-ahead time for building clusters when the first event is not clustered, τ_{max} is the maximum value of the look-ahead time for building clusters, $P1$ is the probability of detecting the next clustered event used to compute the look-ahead time, τ and x_k is the increase of the lower cut-off magnitude during clusters: $x_{meff}=x_{meff}+x_kM$, where M is the magnitude of the largest event in the cluster, x_{meff} is the effective lower magnitude cutoff for catalog, and r_{fact} is the number of crack radii surrounding each earthquake within new events considered to be part of the cluster (Stiphout, 2012)

The Middle East catalog was declustered with the Gardner and Knopoff (1974), Gruenthal (pers. comm.), Uhrhammer (1986), and Reasenberg (1985) algorithms. These declustered catalogs contain 10,131; 7,272; 16,569; and 24,530 events, respectively (Table 5). The frequency–magnitude distributions of each algorithm for this catalog are presented in Fig. 4.

Finally, we use the merged declustered catalog with omitting foreshocks and aftershocks by Stefan Wiemer's ZMAP package for MATLAB to apply Gruenthal's algorithm, resulting in a minimum number of events in the catalog after declustering, in order to be

Table 4 An approximation of the windows sizes which is considered by Gardner and Knopoff (1974), Gruenthal (pers. comm.), and Uhrhammer (1986)

Method	Distance (km)	Time (days)
Gardner and Knopoff (1974)	$10^{0.1238M+0.983}$	$10^{0.032M+2.7389}$, if $M\geq 6.5$ $10^{0.5409M-0.547}$, else
Gruenthal (pers.comm.)	$10^{1.77+(0.037+1.02M)^2}$	$\left\lvert e^{-3.95+(0.62+17.32M)^2}\right\rvert$, if $M\geq 6.5$ $10^{2.8+0.024M}$, else
Uhrhammer (1986)	$e^{-1.024+0.804M}$	$e^{-2.87+1.235M}$

Table 5 Number of events in different method in ZMAP Software; by using each method, we can have different number of events in final catalog

Type of method	Number of events	Number of clusters	Number of event in final catalog	Number of event out of catalog
Gardner and Knopoff 1974	28,244	3,042	10,131	17,933
Uhrhammer 1986		2,398	16,569	11,495
Reasenberg 1985		1,041	24,530	3,534
Gruenthal, pers. comm.		2,960	7,272	20,792

sure that the dependent events are eliminated from the catalog of the mainshocks.

By using ZMAP software for declustering to apply Gruenthal algorithm, 7,272 mainshocks remain. There are 378; 1,058; and 5,837 events in the period before 1900 (historical earthquake), 1901–1963 (early instrumental earthquake), and 1964–2006 (modern instrumental earthquake) (Fig. 5).

3 Seismicity

3.1 Number of events

The assessment seismicity of each region may be strongly inferred from the recorded events as database. The database of the Middle East region after declustering present a set of uniform information for

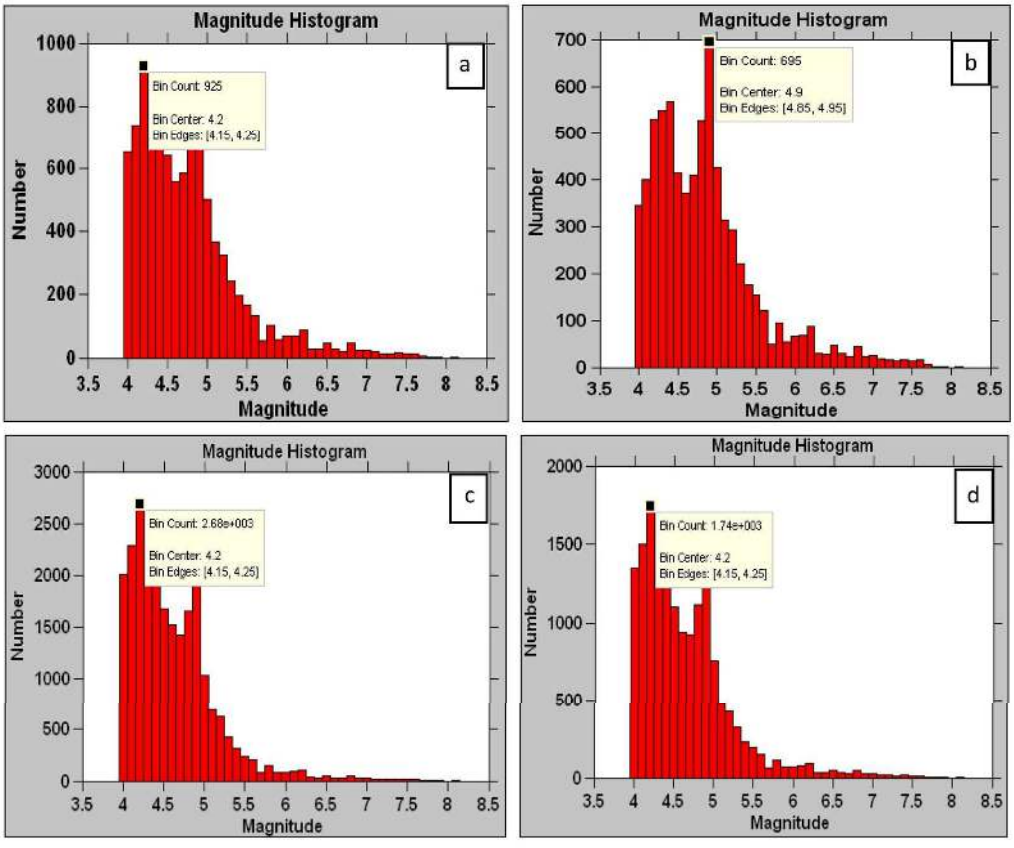

Fig. 4 Calculated frequency–magnitude distributions plots after declustering using each of the methods; **a** Gardner and Knopoff method, **b** Grunthal method, **c** Reseanberg method, and **d** Uhrhammer method

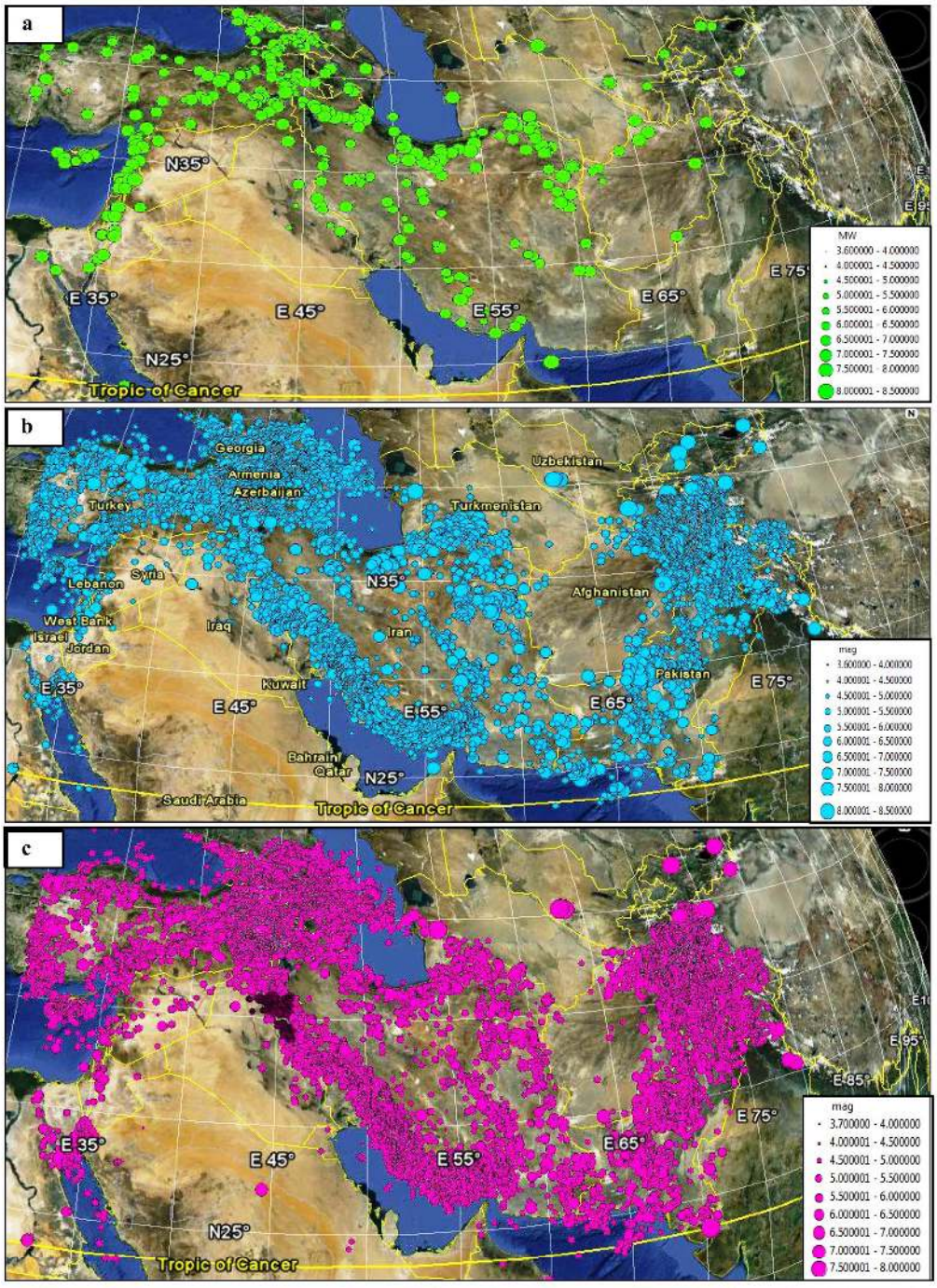

Fig. 5 Distribution of the earthquake magnitudes of the events of the Middle East region after declustering. **a** Historical events from before 1900. **b** Primary instrumental events from 1901–1963, and **c** modern instrumental events from 1964–2006

7,272 earthquakes including historical and instrumental recorded events from 1250 B.C. through 2006.

The seismotectonic map of Iran prepared by Mirzaei et al. (1998) was used to divide the entire

region to nine subregions; five major seismotectonic provinces in Iran delineated, based on all available geophysical, geological, tectonic, and earthquake data, as the main subregions and another remained part of the region are the other subregions in this investigation. These subregions consist of Alborz–Azerbaijan, Central Iran, Kopeh–Dogh, Makran, Zagros, Afghanistan–Pakistan, Saudi Arabia, Caucasus, and Turkey (Eastern Anatolia; after 30° E)) (Fig. 6).

It is observed that in the historical period, many moderate and almost all of small events were missed out. However, there are at least two sharp growth period in the detectability of events and data survival at the early 1960s in consequence of the installation of WWSSN exist and in the twentieth century following the installation of seismographic instruments around the world; and it will be better in the future because of the large number of seismographs with more accuracy than last time. Moreover, the plot of events in each period of 5 years confirms that the number and accuracy of events were increased in length of time until now (Fig. 7). Number of events in each subregion of Middle East region for full duration of the catalog is represented in Table 6.

3.2 Range of magnitudes

Magnitude determination is highly affected on the quality of dataset and different parameters used in relations. From 28,244 events of this catalog after declustering, there is only one event with more than 8 magnitudes in this region, this is in the Makran subregion with M_w=8.1 (1945). Moreover, number of events between 7–8, 6–7, and 5–6 are 125, 444, and 1,897 using Gruenthal algorithm. M=4.0 is selected to be the minimum magnitude in adding data from different catalogs for the Earthquake Model of the Middle East (EMME) catalog. Then, maximum and minimum magnitudes in this catalog would be 4 and 8.1, respectively (Fig. 8). Frequency of magnitudes in each subregion of this area is presented in Fig. 9.

3.3 Range of magnitude completeness

The magnitude of completeness, *Mc*, is theoretically defined as the lowest magnitude at which 100 % of the earthquakes in a space–time volume are detected (Rydelek and Sacks 1989) which might be studied in the specific time windows. Determination Mc of instrumental earthquake catalogs is an essential and compulsory step for any seismicity analysis (Mignan and Woessner 2012).

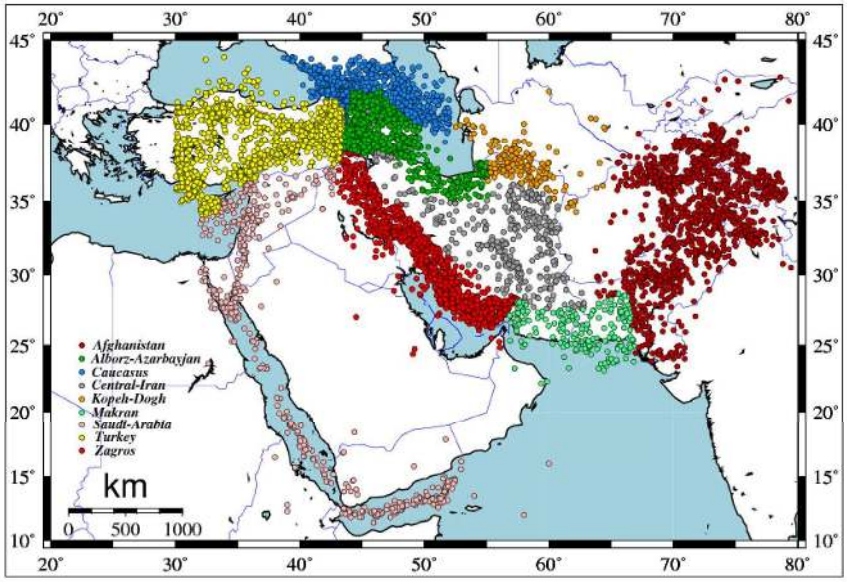

Fig. 6 Map of epicenters with nine sections of the Middle East catalog, which was determined in this research

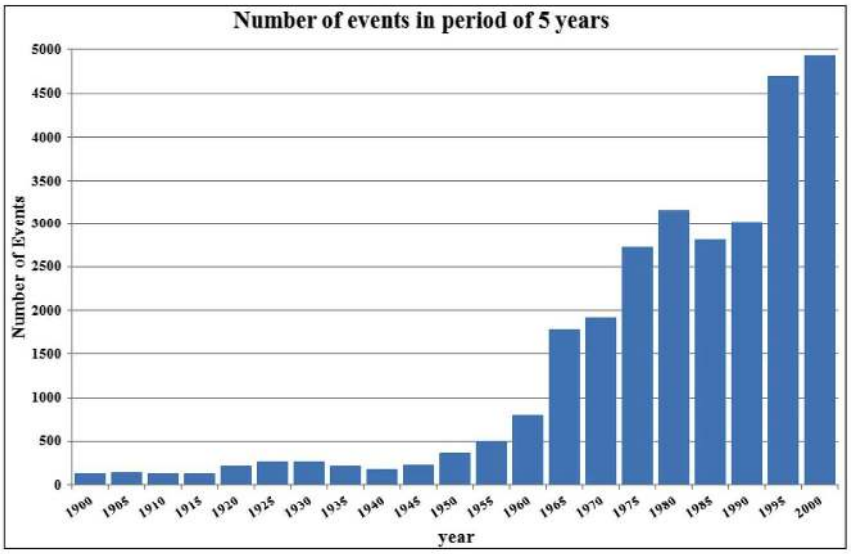

Fig. 7 Number of events for periods of 5 years; plot show that the number of events increase in period of time until now

Ambraseys (2001) explained that it is unlikely that all small and perhaps a few moderate shocks in the early part of the twentieth century in Afghanistan, Africa, and offshore would have been recorded, the available twentieth-century data for the whole region are almost complete only for moderate earthquakes or greater (Ambraseys 2001).

There are several methods to determine the *Mc*. In this investigation for the Middle East region and each subregion (defined in this article), *Mc* was calculated by using two main methods. The traditional and common method for estimating completeness of a catalog is using the cumulative frequency–magnitude distribution of Gutenberg and Richter (1944) and Richter (1958) (i.e., $\log N = a - bM$, where N counts the number of earthquakes with magnitude greater than or equal to magnitude M; and a and b are seismicity and zone-dependent constants (Bayliss and Burton 2007)). Moreover, the *Mc* can be determined by using the frequency magnitude distribution to apply the seismological analysis in software ZMAP (Wiemer 2001) (Dixon et al. 2005). Then, *Mc* was determined for each subregion of the Middle

Table 6 All of the 7,272 records in this area split in nine parts that in this table we can see the number of events in each part for each period of events record

[illegible]	[illegible]	[illegible]			
		[illegible]	[illegible]	[illegible]	[illegible]
1	[illegible]	[illegible]	[illegible]	[illegible]	[illegible]
2	[illegible]	[illegible]	[illegible]	[illegible]	[illegible]
3	[illegible]	[illegible]	[illegible]	[illegible]	[illegible]
4	[illegible]	[illegible]	[illegible]	[illegible]	[illegible]
5	[illegible]	[illegible]	[illegible]	[illegible]	[illegible]
6	[illegible]	[illegible]	[illegible]	[illegible]	[illegible]
7	[illegible]	[illegible]	[illegible]	[illegible]	[illegible]
8	[illegible]	[illegible]	[illegible]	[illegible]	[illegible]
9	[illegible]	[illegible]	[illegible]	[illegible]	[illegible]
10	[illegible]	[illegible]	[illegible]	[illegible]	[illegible]

[illegible]

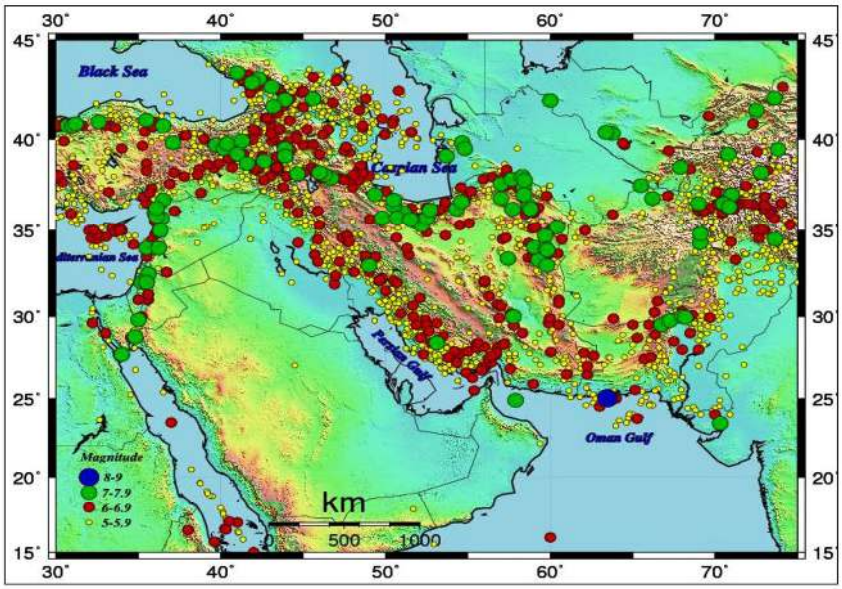

Fig. 8 Earthquake catalog of the Middle East region from 1220 B.C. to 2006, with $Mw \geq 5.0$ in Google Earth map. Magnitudes between 5–6, 6–7, 7–8, and more than 8 are shown in *yellow*, *blue*, *green*, and *red*, respectively

East. These methods confirm the results of each other (Tables 7 and 8) (Figs. 10, 11, and 12).

As felt by humans, the magnitude of completeness for historical period of time is around 6 and 7. For instrumental earthquakes, depending on the region and accuracy of seismogram recorded, *Mc* can be presented by recorded events which have different value. The *Mc* for each subregion of Middle East is presented in Tables 7 and 8 and Figs. 10 and 11. Magnitude of completeness map for this region is shown in Fig. 12. The total threshold of magnitude based on all Middle East earthquake data was calculated as 5.5, 5.0, 4.5, and 4 (or less than 4) for the time periods before 1950, 1963, 1975, and 2000, respectively.

3.4 Range of seismicity depths

Accuracy of focal depths for earthquakes is important in understanding tectonics of a region and for evaluating earthquake hazards (Maggi et al. 2002). There is no complete reliable evidence of intermediate focal depth of earthquakes. The assessment of depth is a controversial issue, even for modern instrumental earthquakes.

In a study of continental gravity and topography, McKenzie and Fairhead (1997) concluded that the effective elastic thickness (*Te*) on the continents is usually close to the thickness of the seismogenic crust (Ts) allowing the simple interpretation that the strength of the lithosphere resides in that layer, although they were unable to estimate the depth to the top of any elastic layer. The concentration of seismicity depth in the continental crust in all areas, and their ranges, is shallower than 20 km in most of areas; with correlation of maximum focal depth with surface heat flow, suggests that temperature has also the main control on the continents (e.g., Chen and Molnar 1983).

In several parts of Africa, Asia, and North America, seismicity continues throughout the crust to Moho depths. In East Africa, the Tien Shan, and the Indian shield, some of the deepest earthquakes in the crust occur so close to the Moho that uncertainties in their depth and crustal thickness allow them to be in the uppermost mantle (Fig. 13) (Maggi et al. 2000).

The starting depth is usually a fixed parameter and set to the most likely depth for the region. For local earthquakes that are usually in the range of 10–20 km, distant events are often set to 33 km (Havskov 2000).

Fig. 9 Frequency of magnitude in each section of the Middle East ▶ region; **a** Zagros (from 859), **b** Makran (from 1483), **c** Kopeh–Dagh (from 10), **d** Central Iran (from 734), **e** Alborz–Azerbaijan (from 550 B.C.), **f** Turkey (after 30 E) (from 995), **g** Caucasus (from 1250 B.C.), and **h** Afghanistan–Pakistan (from 818)

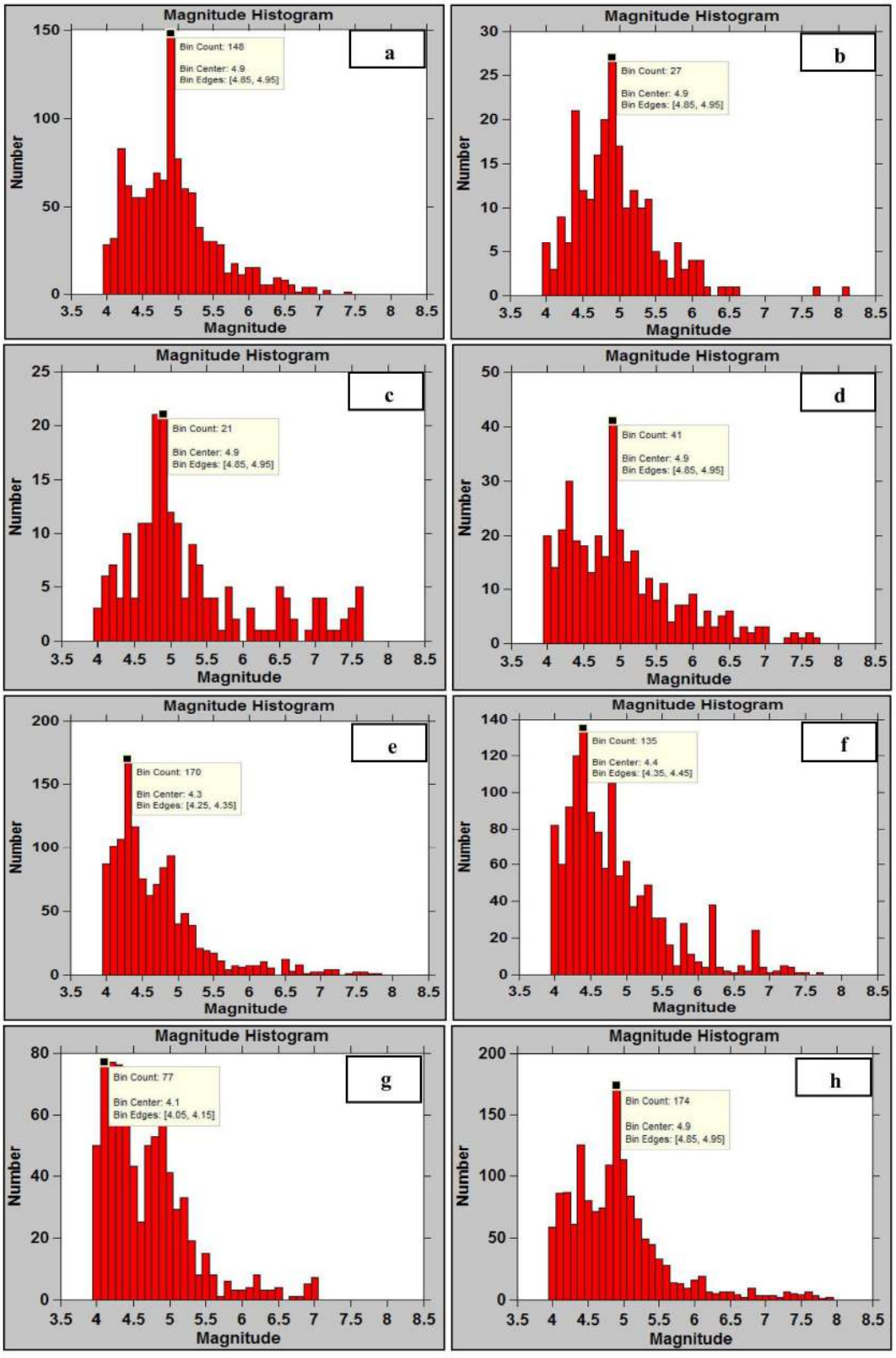
Magnitude Histogram
a
Bin Count: 148
Bin Center: 4.9
Bin Edges: [4.85, 4.95]
Number
Magnitude
Magnitude Histogram
b
Bin Count: 27
Bin Center: 4.9
Bin Edges: [4.85, 4.95]
Number
Magnitude
Magnitude Histogram
c
Bin Count: 21
Bin Center: 4.9
Bin Edges: [4.85, 4.95]
Number
Magnitude
Magnitude Histogram
d
Bin Count: 41
Bin Center: 4.9
Bin Edges: [4.85, 4.95]
Number
Magnitude
Magnitude Histogram
e
Bin Count: 170
Bin Center: 4.3
Bin Edges: [4.25, 4.35]
Number
Magnitude
Magnitude Histogram
f
Bin Count: 135
Bin Center: 4.4
Bin Edges: [4.35, 4.45]
Number
Magnitude
Magnitude Histogram
g
Bin Count: 77
Bin Center: 4.1
Bin Edges: [4.05, 4.15]
Number
Magnitude
Magnitude Histogram
h
Bin Count: 174
Bin Center: 4.9
Bin Edges: [4.85, 4.95]
Number
Magnitude

Table 7 Some of the information on seismicity for each section, Magnitude (minimum, maximum and Mc), Depth (maximum and with depth of zero)

Number	Name of section	Magnitude		Depth		Average of depth	Start year	Depth reported by Mirzaei et al.(1997)
		Mc	M_{max}	Max	= 0			
1	Afghanistan–Pakistan	4.9	7.9	300	184	9	818	
2	Kopeh–Dagh	4.9	7.6	46	80	15	10	7~35
3	Central Iran	4.9	7.7	106	91	15	734	8~20
4	Makran	4.8	8.1	164	19	9	1483	Up to 60
5	Zagros	4.9	7.4	185	147	13	859	8~15
6	Alborz–Azerbaijan	4.3	7.8	92	419	11	550 B.C.	7~35
7	Caucasus	4.2	7.0	165	67	9	1,250 B.C.	
8	Turkey (after 33° E)	4.4	7.7	169	375	9	995	
9	Saudi Arabia	4.9	7.5	101	109	8	31 B.C.	

According to Engdahl et al. (2006), earthquakes in the Central Caspian occur over a wide range of depths with a median depth of 40±15 km, in the Alborz region and other southern Caspian basin, active border regions to the SW and E occur at all depths in the crust with a median depth of 20±8 km. Nearly all earthquakes in the Zagros are less than 30 km in depth and the median depth in this region is 15±7 km. The deepest earthquakes are in a depth of ~30 km. The Makran region has earthquakes both at upper crustal depths and at depths almost excess of 40 km with a median depth of 25±19 km. In Eastern Iran, earthquakes have a median depth of 12±5 km (Fig. 14).

Results of waveform modeling and micro-earthquake studies show that the majority of earthquakes in Iran occur in depths of ~8–15 km in Zagros, ~7–35 km in northern Iran and southern Caspian, and ~8–20 km in the east and southeast of the country. From the Makran coast of southeastern Iran to the Makran coast of southwestern Pakistan, focal depths increase up to about 60 km (Mirzaei et al. 1997).

In a research by the Pakistan Meteorological Department and NORSAR (2007), focal depths of earthquakes for Pakistan vary from the shallow to deep. It is seen that most of the seismicity (80 %) is shallow, i.e., below 40 km, while between 40- and 320-km depths occur in nearly 20 % of the events.

For recent investigation in Middle East region, the events with erroneously large depth and with magnitude zero were omitted. Moreover, we omitted the events with depth of 33, because this is an assumption that depth for the events do not determine in an exact value. Plot of region depth imply that the location discrepancies for larger earthquakes are considerably less than discrepancies for smaller events and there is no significant

Table 8 Beginning year of complete reporting of earthquakes in each section of Middle East region

Sections	$Mw \leq 4.0$	$4.0 < Mw \leq 4.5$	$4.5 < Mw \leq 5.0$	$5.0 < Mw \leq 5.5$	$5.5 < Mw$
Afghanistan–Pakistan	1980	1963	1960	1925	1900
Kopeh–Dagh	2000	1925	1910	1900	1880
Central Iran	1950	1930	1910	1250	850
Makran	1970	1975	1963	1950	1920
Zagros	1980	1950	1925	1850	1820
Alborz–Azerbaijan	1955	1800	1680	1440	850
Caucasus	1930	1910	1870	1845	1780
Turkey (after 33° E)	1963	1955	1925	1845	1820

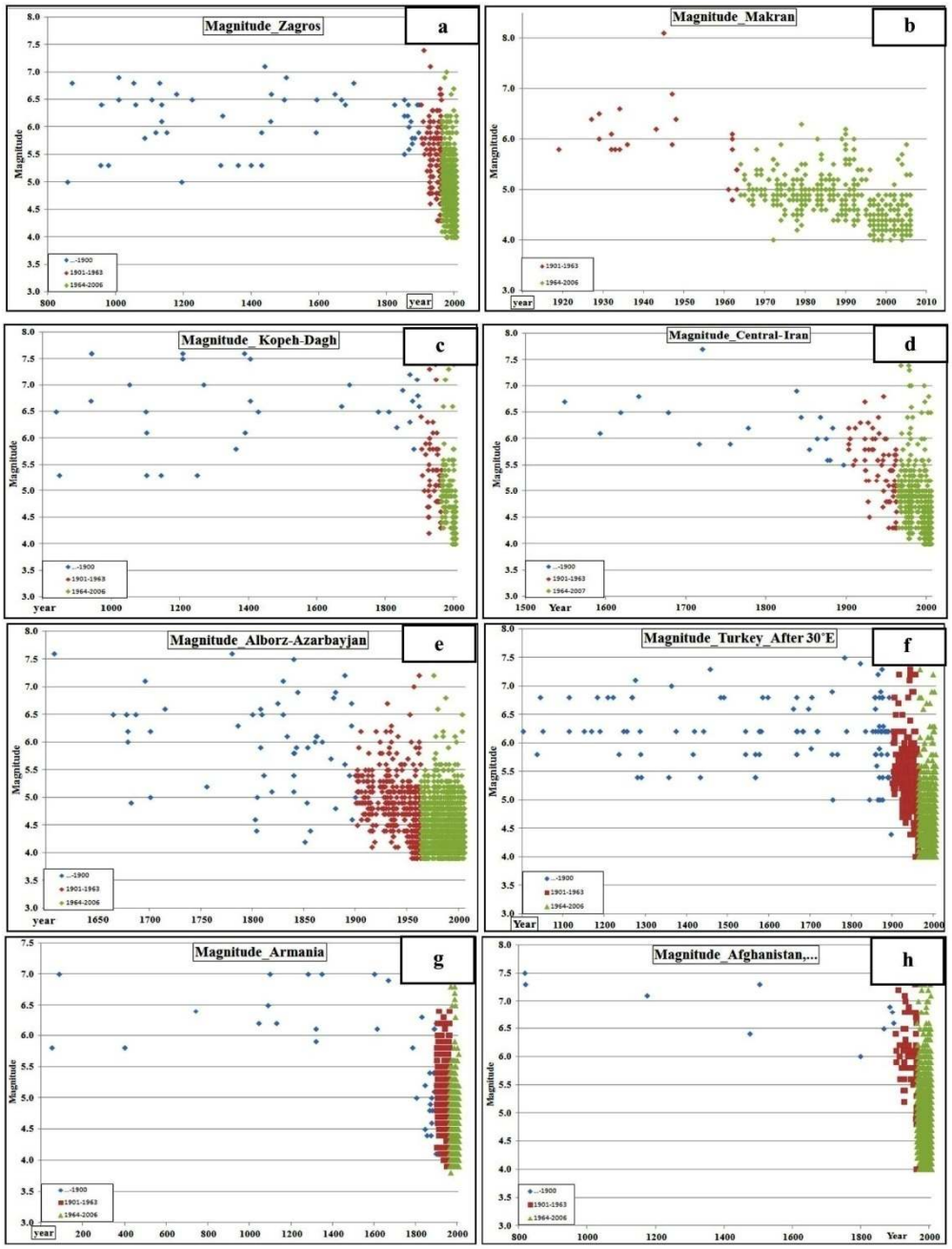

Fig. 10 Plot of magnitude of completeness of sections of the Middle East region. The *blue*, *red*, *and green color* is for periods of before 1900, 1901–1963, and 1964–2006, respectively; **a** Zagros (from 859), **b** Makran (from 1483), **c** Kopeh–Dagh (from 10), **d** Central Iran (from 734), **e** Alborz–Azerbaijan (from 550 B.C.), **f** Turkey (after 30° E) (from 995), **g** Caucasus (from 1250 B.C.), and **h** Afghanistan–Pakistan (from 818)

improvement in location determination with respect to the occurrence time of earthquakes in the period of 1800 to 2006 in this region (Fig. 15). Figure 16 shows the situation of depth of events in different

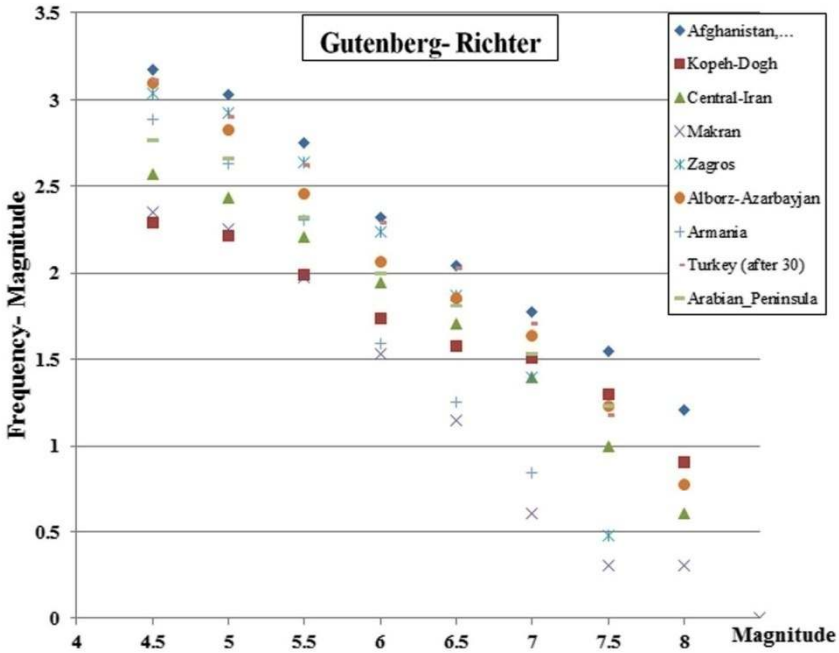

Fig. 11 The cumulative number of earthquakes in each section of Middle East region by using Gutenberg-Richter method

places in the Middle East region. Averages of depth for each subregion are estimated by using software ZMAP (Wiemer 2001) (Table 7) (Fig. 17) and by plotting all of the events in their depth (Fig. 18).

Majority of depth for Kopeh–Dogh and Central Iran; Zagros; and Alborz–Azarbayjan are 15, 13, and 11 km, respectively; all of them have depths with more than 10 km. Majority of depth for Afghanistan–Pakistan, Caucasus, Makran, and Turkey (after 30° E) is 9 km and Saudi Arabia has depth with 9 km (Table 7) (Figs. 18 and 17).

4 Uncertainty

For a catalog, a clear description and evaluation of uncertainty of earthquake parameters is effective. Based on a number of local and regional seismographic stations, station distribution, and velocity models, there is apparent uncertainty in different earthquake parameters. Value of uncertainty is decreased during the time until now. By comparing some of the location, depth, and magnitude, which are reported by different seismological centers, we can assess uncertainties for each earthquake and center.

The feasibility of selecting "reference events" (events where the hypocenters can be considered known to high accuracy) was investigated by Sweeney (1996) in continental regions from global bulletins such as those published by the ISC and NEIC that contains predominantly teleseismic arrival time data. Sweeney (1996) suggested when the largest azimuthal gap between stations surrounding the epicenter is less than 200 ° and at least 50 first-arriving P phases are used, locations from these catalogs have an accuracy of 10–15 km. Sweeney (1998) revised these selection criteria for teleseismic networks with an azimuthal gap of less than 90 ° and with at least 50 first-arriving P phases that were used in the location he found 15 km (or better) epicenter accuracy.

Analysis of events with independently known coordinates indicates that most Preliminary Determination of Epicenters (PDE) determinations are accurate to a few tenths of a degree in epicentral position and 25 km in depth. Because of these uncertainties, verbal descriptions of locations in news releases are rounded to the nearest 5 miles and/or 10 km (Sipkin et al. 2000).

Engdahl et al. 1998, by using travel–time tables (Kennett et al. 1995), produced a "groomed" ISC catalog. Myers and Shultz (2001), when the largest

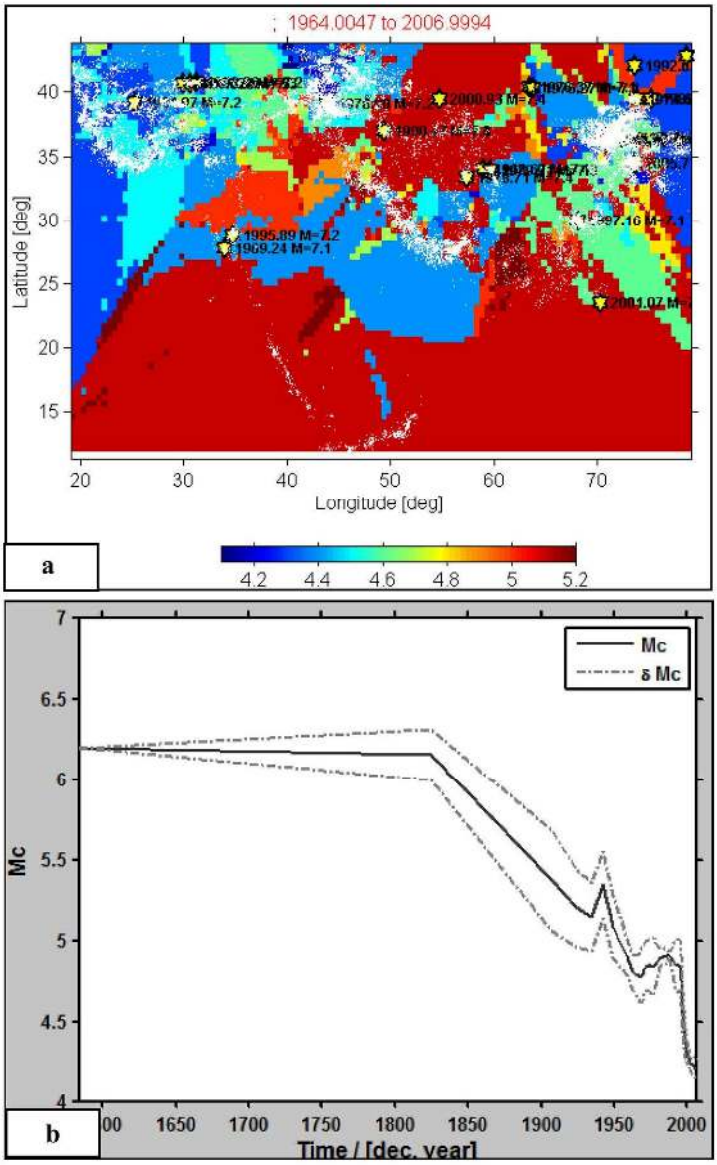

Fig. 12 Magnitude of completeness map for Middle East region by using ZMAP Software (from 1220 B.C. to 2006); **a** Map of *Mc*. **b** Variations of *Mc* with time

azimuthal gap is less than 90 °, estimated the epicenter accuracy in the EHB catalog which is 15 km or better at the 95 % confidence level for events not in subduction zones. Ambraseys (2001) claimed for the eastern Mediterranean (Middle East) region that the instrumental locations before the early 1970s had low accuracy. International Seismological Summary (ISS)/ISC locations are systematically shifted by 10–30 km to the N or NE from their macroseismic epicenters, a bias which is unlikely to be due to systematic errors in the macroseismic positions. According to Yunatci (2010), the macroseismicity catalog for Turkey has revealed that the location uncertainty of focal points of events can reach over 10 km. Due to moment magnitude estimates, the average value of magnitude being equal to 0.17 magnitude units assigned as the constant value of parameter uncertainty in the current GMPE model. Then, we will have at least 20 km and 0.17 uncertainty for location and magnitude.

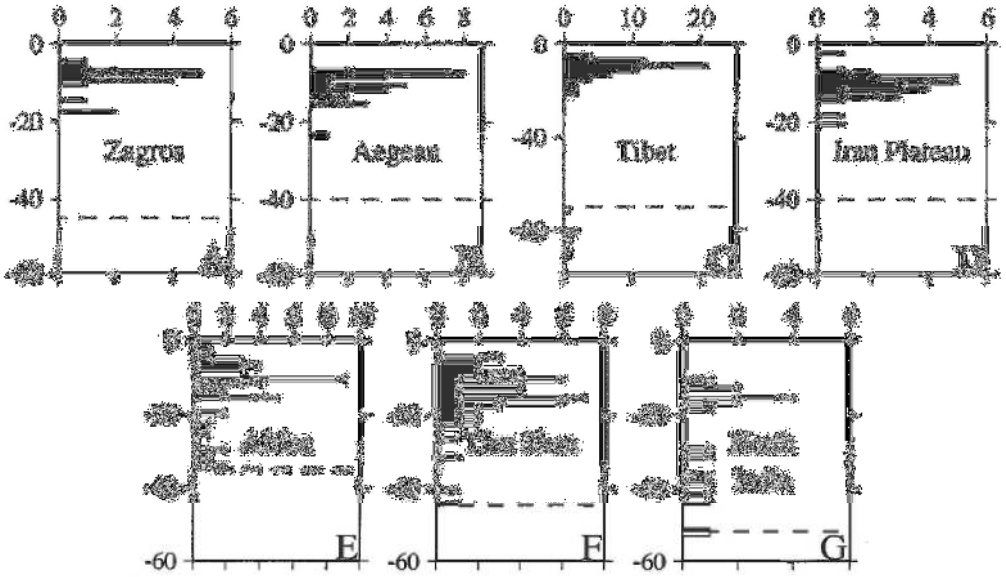

Fig. 13 Histograms of earthquake focal depths determined by modeling of long-period teleseismic P (primary) and SH (secondary horizontal) seismograms (*solid bars*). *White bar* in North India (**g**) is depth determined from short-period depth phases in Shillong Plateau by Chen and Molnar (1990). *White bars* in Tibet (**c**) are subcrustal earthquakes, but not necessarily in mantle of continental origin. Approximate Moho depths are indicated by *dashed lines*. Focal depth and Moho data are from various sources, including Nelson et al. (1987), Molnar and Lyon-Caen (1989), Mangino et al. (1999), and Maggi et al. (2000). Focal depths based on arrival times recorded at local seismic networks have also found seismicity throughout crust in several parts of North America (according to Maggi et al. 2000)

Mirzaei et al. 1997, based on the quality and quantity of available information, determined uncertainty of earthquake parameter for Iran in three periods of time: for the historical period (pre 1900) uncertainty in depth, location, and magnitude represent in 30 and 100 km and 0.4 to 0.8, respectively; for the early instrumental period (1900–1963), 20 km and 0.3 to 0.5 was calculated for location and magnitude; and for the modern instrumental period (1964–1994), location errors for moderate and

converting them to magnitude in *Mw* scale, there was a catalog with 28,244 events. In this primary catalog, summary of origin times, longitude, latitude, magnitudes, and depth for each event is presented.

Wiemer's ZMAP package (2001) to apply Gruenthal algorithm was used to omit duplicate events, aftershocks, and foreshocks; finally, 7,272 main events remain for this region in this catalog from 1250 B.C. through 2006. Events of this region

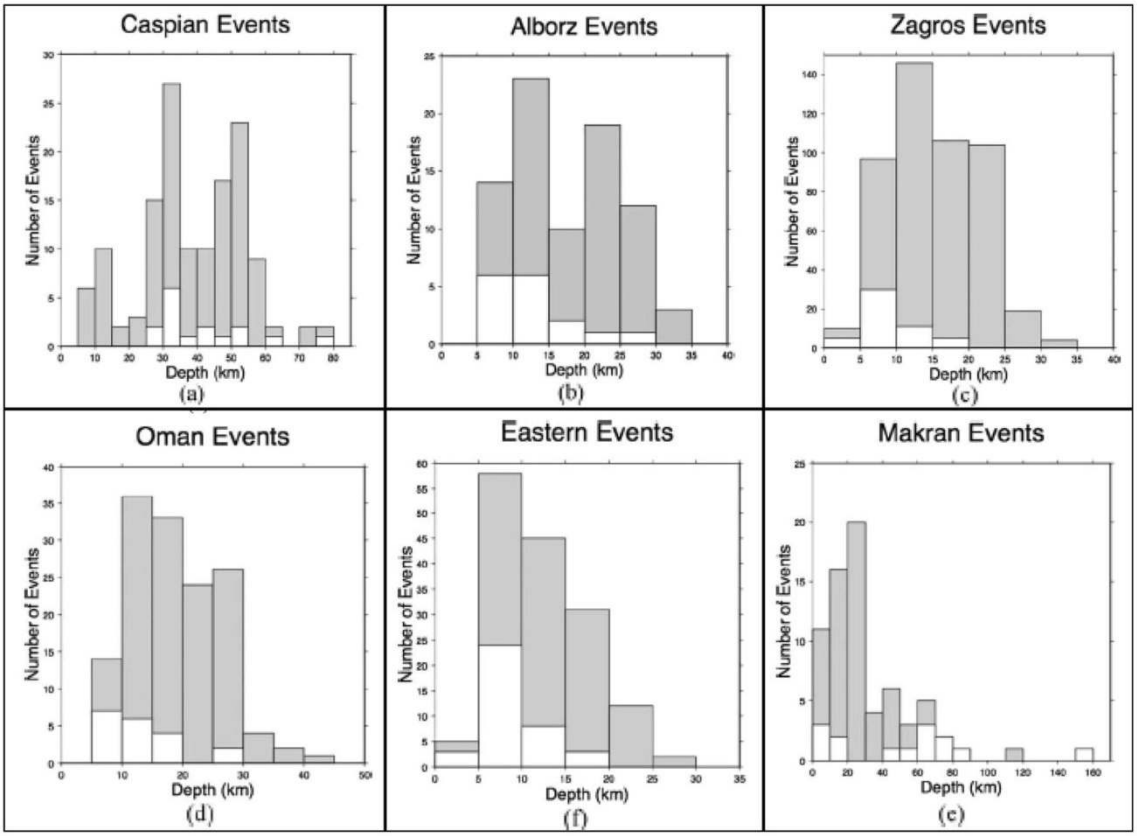

Fig. 14 Earthquake depth distribution by region (depths determined by waveform modeling are not shaded). **a** Caspian, **b** Alborz, **c** Zagros, **d** Oman Line, **e** Makran, and (**f**) (Engdahl et al. 2006)

The magnitude of completeness was determined by cumulative frequency–magnitude distribution of Gutenberg and Richter (1944) and seismological analysis in software ZMAP (Wiemer 2001) for total of the Middle East. The threshold of magnitude is different for each subregions of the Middle East. Considering all subregions, maximum year for 5.5, 5.0, 4.5, and 4 (or less than 4) magnitude was determined for the time periods before 1950, 1963, 1975, and 2000, respectively.

According to this investigation in the Middle East region, average of depths for each subregion are estimated by using software ZMAP (Wiemer 2001) and plotting all of events in their depth for each subregion. Average of depth for Kopeh–Dogh and Central Iran; Zagros; Alborz–Azerbaijan; Afghanistan–Pakistan, Caucasus, Makran, and Turkey (after 30° E); and Saudi Arabia are approximately 15, 13, 11, 9, and 8 km, respectively. In total, events of earthquake occurred in depths of less than 15 km in Middle East region.

Acknowledgement This article was a result of the Global Earth Model (GEM); and the Earthquake Model of the Middle East (EMME) project and was performed in IIEES as a partner of EMME project, as of (Work package-1-WP1) based on an internal research project of IIEES (No;IIEES/EMME:2010) conducted by the first (corresponding) author of this project. The support of the IIEES president (Prof Tasnimi) and Dr A. Ansari, are strongly appreciated. These thanks go to all partners of the project in the region.

Appendices

Appendix 1 The main sources of data for the Middle East Earthquakes

International sources

Generally, the information and database of the international catalogs are available on their internet websites. Here, we are going to briefly introduce those international sources which we used in this project;

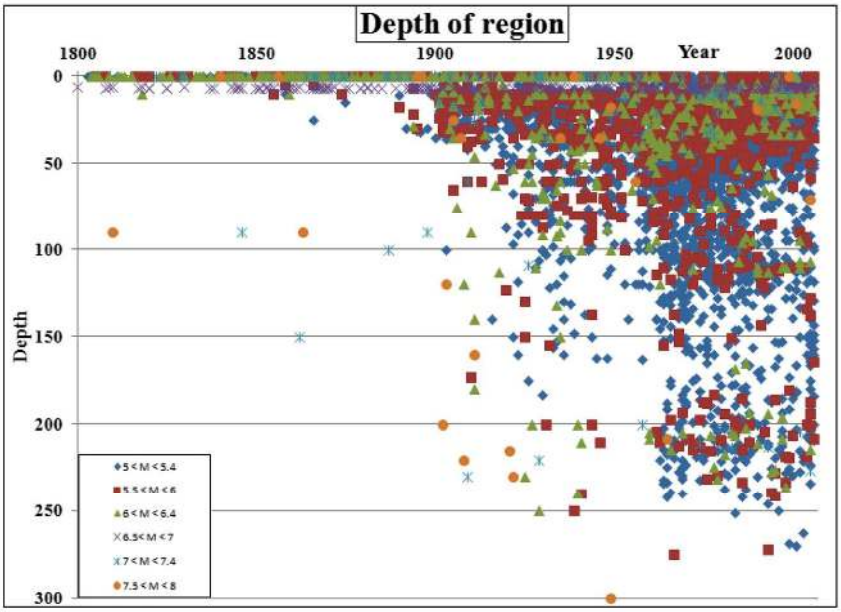

Fig. 15 Plot of depth of all events in the Middle East region; there is no significant improvement in location determination with respect to the time of occurrence of earthquakes in period of 1800 to 2007 in this region

The mission of the National Earthquake Information Center (NEIC) is to determine rapidly the location and size of all destructive earthquakes worldwide. This center was established in 1966 by the Environmental Science Services Administration (ESSA). In 1940, the first Preliminary Determination of Epicenters (PDE) was published. In 1970, NEIC transferred to the National Oceanic and Atmospheric Administration (NOAA), and in 1973, transferred to the US Geological Survey (USGS).

The International Seismological Center (ISC) was formed in Edinburgh in 1964, to continue the work of

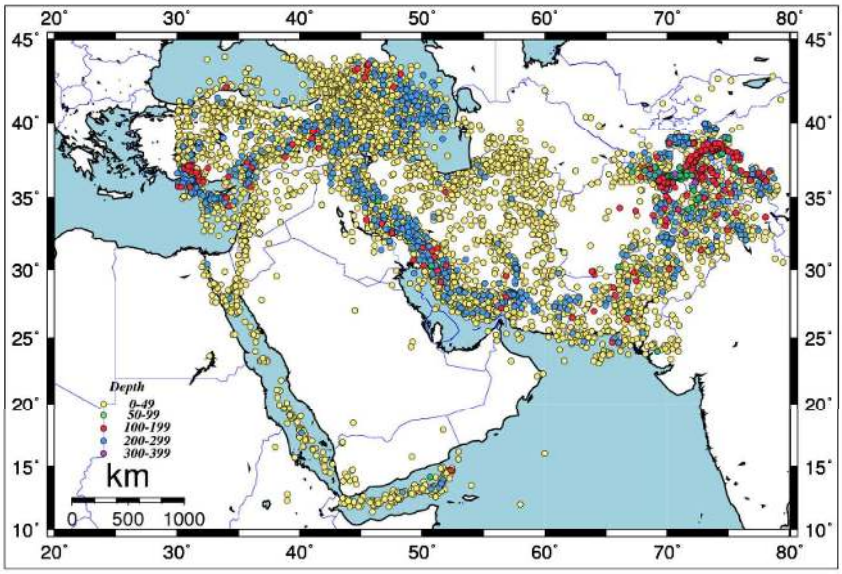

Fig. 16 Range of depth in different parts of the Middle East Region; maximum depth in this region is in the east of it (in east of Afghanistan)

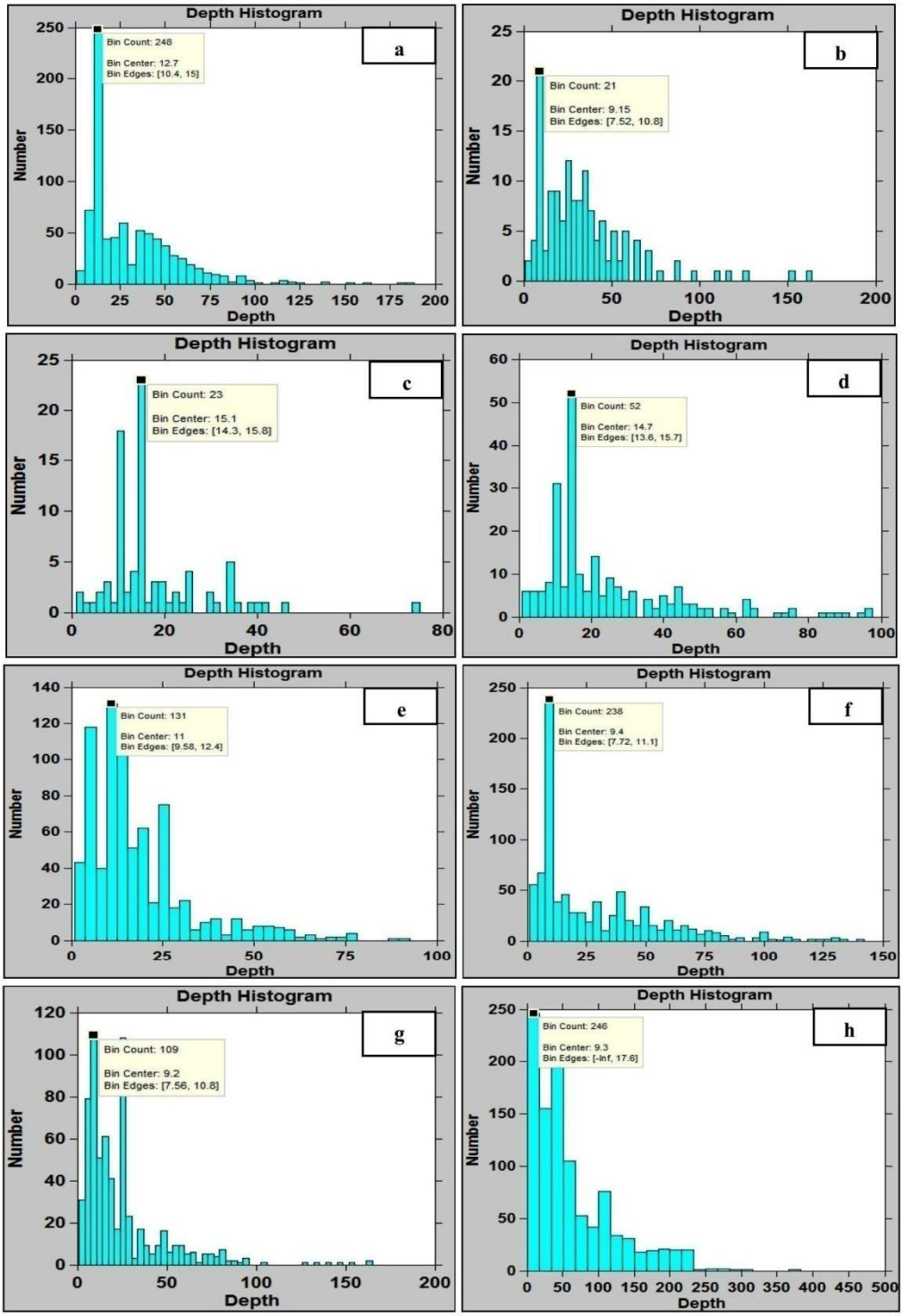

Fig. 17 Frequency of depth in each sections of Middle East region after omitting the 0 and 33 magnitudes; **a** Zagros, **b** Makran, **c** Kopeh–Dagh, **d** Central Iran, **e** Alborz–Azerbaijan, **f** Turkey (after 30° E), **g** Caucasus, and **h** Afghanistan–Pakistan

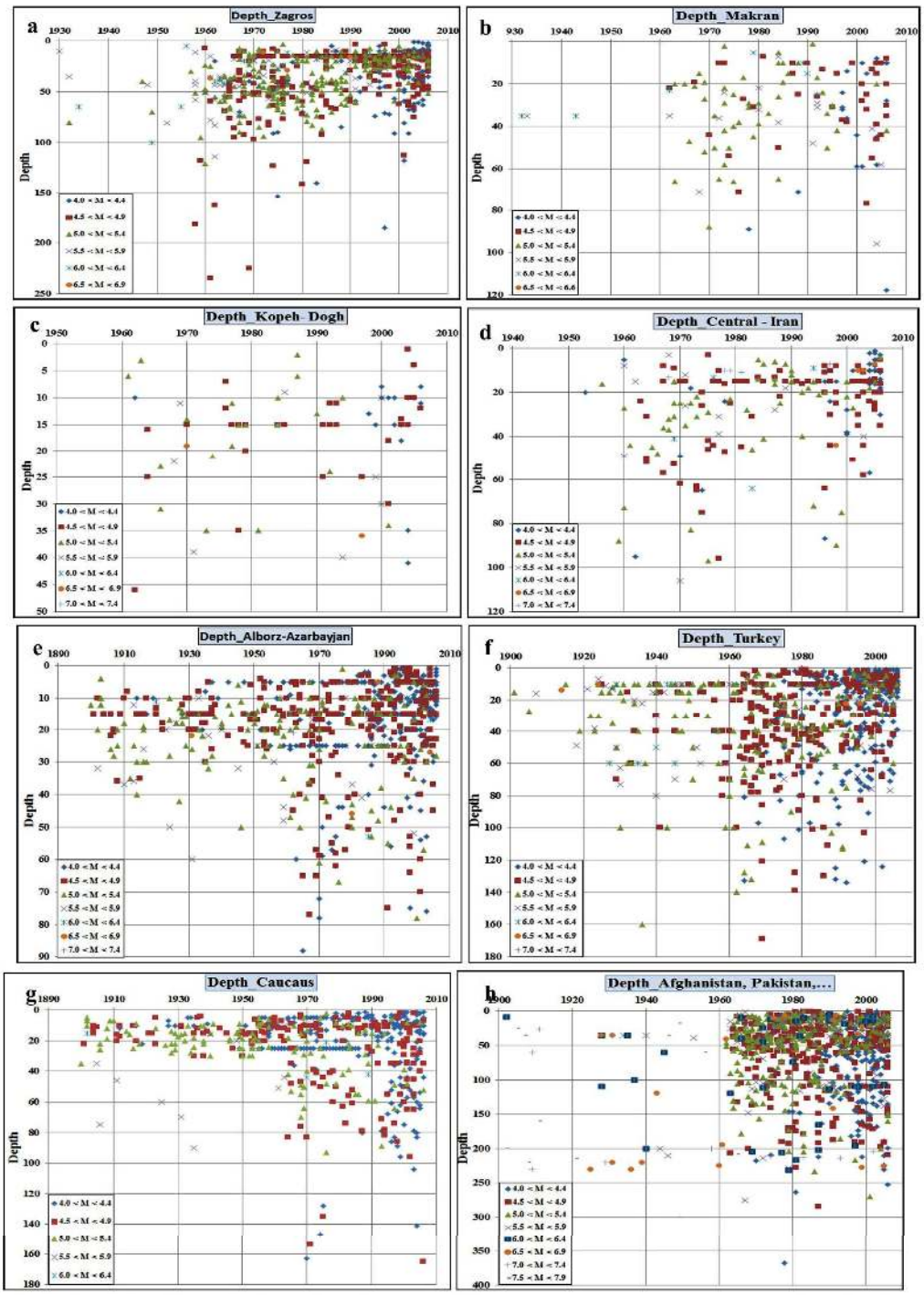

Fig. 18 Distribution of all earthquake depth in each section of the Middle East region; **a** Zagros, **b** Makran, **c** Kopeh–Dagh, **d** Central Iran, **e** Alborz–Azerbaijan, **f** Turkey (after 30° E), **g** Caucasus, and **h** Afghanistan–Pakistan

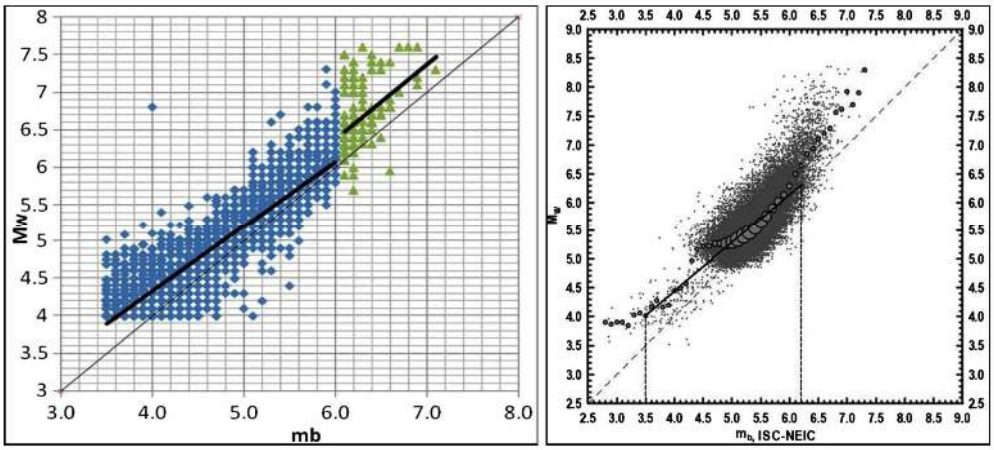

Fig. 19 The correlation between *mb* and *Mw*. *Left* The earthquake catalog of this project for the Middle East (1900–2010). *Right* the earthquake catalog of NEIC and ISC for the World (1965–2003)

the International Seismological Summary (ISS), which was the first gathering of all observations of earthquakes worldwide.

The Engdahl et al. (1998; EHB) algorithm has been used to significantly improve routine hypocenter determinations made by the ISS, ISC and PDE.

Regional sources

Beside the international sources we used for collecting the earthquake data, there are some local and regional catalogs which were given through the meetings for this project.

The Armenian catalogs are reporting only mb as the magnitude value. The chosen name for the source of these data in our final catalog in "Armenia."

Regarding their report, they had used the data from the new catalog of strong earthquake in USSR (NCUS SR) for the events up to 1975. The other source of data is the Russian Space System Cooperation (RSSC) catalog.

The main mentioned sources for Georgia data are GMCS and EDNS which were kept intact in our final catalog.

Iran, with three different sources of data, improved the catalog within its area. The International Institute of

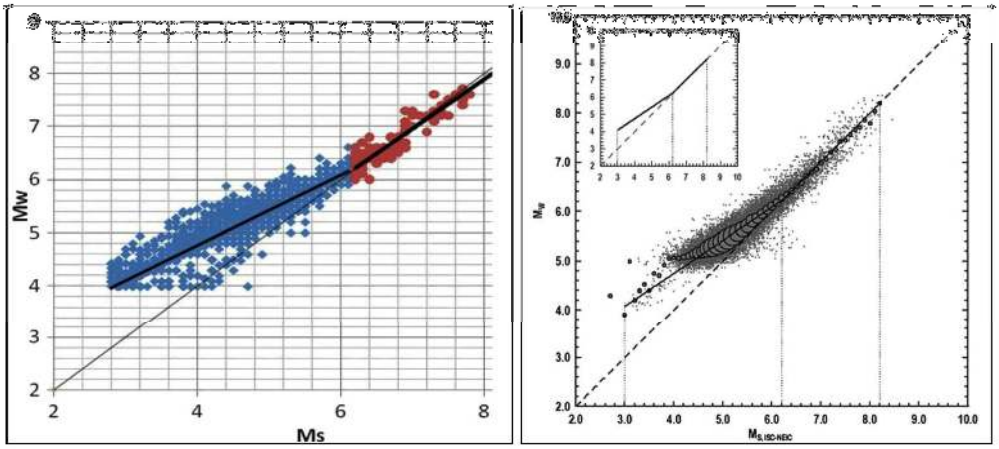

Fig. 20 The correlation between *Ms* and *Mw*. *Left* The earthquake catalog of this project for the Middle East (1900–2009). *Right* the earthquake catalog of NEIC and ISC for the world (1978–2003)

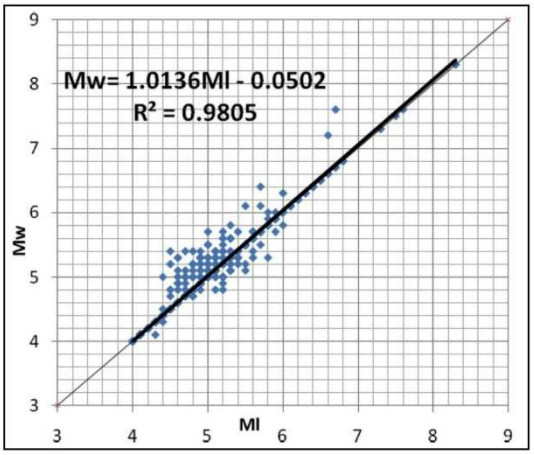

Fig. 21 The correlation between *Ml* and *Mw* in the earthquake catalog of this project for the Middle East

Earthquake Engineering and Seismology (IIEES), by enhancing the Iranian National Seismic Network (INSN), developed a catalog for the twenty-first century. The Iranian Seismological Center (IRSC), whose seismological network in Iran is the largest one, started to work in 1995 via the Geophysical Institute of Tehran University. The other organization who publish earthquake catalog for Iran is The Building and Housing Research of Iran (BHRC).

The National Center of Geophysical Research (NCGR) was established in 1975 by the National Council of Scientific Research (CNRS) in Lebanon. Nowadays, the seismic national network of this country with title of "Geophysical Research Arrays of Lebanon (GRAL)" is expanding.

The main source of all Turkey's records is "ISK."

More than 20 short period digital stations which account as the Syrian National Seismological Network (SNSN) were established in 1995.

Egyptian National Seismograph Network (ENSN) has started its work in 2003.

Kuwait National Seismic Network (KNSN) was established in 1996 and has started to monitor the seismicity of this small country.

In this project, just one of his books' parametric historical catalogs; "The seismicity of Egypt, Arabia and the Red sea" had been transferred to an Excel file format. This catalog is referenced by the term "Amb" in our final historical catalog.

Appendix 2 Relationship between different magnitudes in this region

Relations were derived from earthquakes recorded in the Middle East region. Results of this relations present in equations from Eqs. (1) to (7) and Figs. 19, 20, and 21, total information collect in Table 9. These comparisons made us to believe in the correlation between different magnitudes in our catalog's records and use it for further conversions instead of any other formula from other authors.

Conversion relation between mb and Mw

A relation was derived from those records that had both mb and Mw. Figure 19 shows this relation and its trend line in comparison to what was obtained by Scordilis in 2006 for the correlation of about 39,000 global records from NEIC and ISC (1965–2003).

Table 9 Relationship between *Ms*, *Ml*, *mb*, and *Mw* in the Middle East region by comparing the recorded magnitude of the events

Type of magnitude	Conversion relation	Boundary	R^2	Number	σ	
mb, *Mw*	$Mw=0.8744mb+0.8277$	$3.5\leq mb\leq 6.0$	0.8803	16,752		This study
	$Mw=0.85\ (\pm 0.04)mb+1.03\ (\pm 0.23)$	$3.5\leq mb\leq 6.2$	0.53	39,784	0.29	Scordilis
Ms, *Mw*	$Mw=0.6633Ms+2.1117$	$2.8\leq Ms\leq 6.1$	0.9425	4,123		This study
	$Mw=0.9307Ms+0.4491$	$6.2\leq Ms\leq 8.2$	0.88	129		
	$Mw=0.67\ (\pm 0.005)Ms+2.07\ (\pm 0.03)$	$3.0\leq Ms\leq 6.1$	0.77	23,921	0.17	Scordilis
	$Mw=0.99\ (\pm 0.02)Ms+0.08\ (\pm 0.13)$	$6.2\leq Ms\leq 8.2$	0.81	2,382	0.2	
Ml, *Mw*	$Mw=1.0136Ml-0.0502$	$4.0\leq Ml\leq 8.3$	0.9805	2,271		This study

This correlation was obtained as below;

$$Mw = 0.8744mb + 0.8277;\ 3.5 \le mb \le 6.0 \text{ and } R^2 = 0.8803 \text{ and } n = 16752 \quad (1)$$

While the Scordilis relation is:

$$Mw = 0.85(\pm 0.04)mb + 1.03(\pm 0.23);\ 3.5 \le mb \le 6.2 \text{ and } R^2 = 0.53 \text{ and } n = 39784 \text{ and } \sigma = 0.29 \quad (2)$$

Conversion relation between *Ms* and *Mw*

For determining *Mw* from *Ms*, a relation was derived from those records that had both *Ms* and *Mw*. Figure 20 shows this relation and its trend line in comparison to what was obtained by Scordilis in 2006 for the correlation of about 26,000 global records from NEIC and ISC with depth of ≤70 km (1978–2003). This correlation shows a dual behavior with the turning point on about *Ms*=6.1, therefore, we are facing with two formulas. (note: in our case, the depth of the events is not considered);

$$Mw = 0.6633Ms + 2.1117;\ 2.8 \le Ms \le 6.1\ \&\ R^2 = 0.9425 \text{ and } n = 4123 \quad (3)$$

$$Mw = 0.9307Ms + 0.4491;\ 6.1 \le Ms \le 8.2 \text{ and } R^2 = 0.88 \text{ and } n = 129 \quad (4)$$

While the Scordilis relations are:

$$Mw = 0.67(\pm 0.005)Ms + 2.07(\pm 0.03);\ 3.0 \le Ms \le 6.1 \text{ and } R^2 = 0.77 \text{ and } \sigma = 17\ n = 23921 \quad (5)$$

$$Mw = 0.99(\pm 0.02)Ms + 0.08(\pm 0.13);\ 6.2 \le Ms \le 8.2 \text{ and } R^2 = 0.81 \text{ and } \sigma = 2 \text{ and } n = 2382 \quad (6)$$

Conversion relation between *Ml* and *Mw*

Many authors have studied the correlation between *Ml* and *Mw* but their ideas do not converge, partly due to the different effective magnification of Wood-Anderson Seismographs and distance corrections. As Scordilis (2006) says, it is not possible to define unique global relations connecting *Ml* to *Mw* or to other magnitude scales. Therefore, we could only trust the internal correlation which exists in about 2,000 records with both *Mw* and *Ml*. This correlation for 2,271 records and for the time period of 1975 to 2010 is shown in Fig. 21. The divergence or distribution of the points is minimum and the R^2=0.98 is also convincing to pick up this relation at this stage.

$$Mw = 1.0136Ml - 0.0502;\ 4.0 \le Ml \le 8.3 \text{ and } R^2 = 0.9805 \text{ and } n = 2271 \quad (7)$$

References

Ambraseys NN (2001) Reassessment of earthquakes 1900–1999, in the Eastern Mediterranean and the Middle East. Geophys J Int 145(2):471–485

Ambraseys NN (2009) Earthquakes in the Mediterranean and Middle East, a multidisciplinary study of seismicity up to 1900. Cambridge University Press, Cambridge

Ambraseys NN, Jackson JA (1998) Faulting associated with historical and recent earthquakes in the Eastern Mediterranean region. Geophys J Int 133:390–406

Ambraseys NN, Jackson JA, Melville CP (2002) Historical seismicity and tectonics: the case of the Eastern Mediterranean and the Middle East, international handbook of earthquake and engineering seismology, V.81A, Copyright~2002 by the Int'l Assoc. Seismol. & Phys. Earth's Interior, Committee on Education. ISBN: 0-12-440652-1

Ambraseys NN, Melville CP, Adams RD (2005) The seismicity of Egypt, Arabia and the Red Sea: a historical review. Cambridge University Press, Cambridge

Ambrasys NN, Melville CP (1982) A history of Persian earthquake. Cambridge University Press, Cambridge

Bayliss TJ, Burton PW (2007) A new earthquake catalogue for Bulgaria and the conterminous Balkan high hazard region. Nat Hazards Earth Syst Sci 7:345–359

Chen WP, Molnar P (1983) Focal depths of intracontinental and intraplate earthquakes and their implications for the thermal and mechanical properties of the lithosphere. J Geophys Res 88:4183–4214

Chen WP, Molnar P (1990) Source parameters of earthquakes and intraplate deformation beneath the Shilhong Plateau and northern Indoburman ranges. J Geophys Res 95:12, 527–12,552

DeMets C, Gordon RG, Argus DF, Stein S (1994) Effects of recent revisions to the geomagnetic reversal time scale on estimates of current plate motions. Geophys Res Lett 21:2191–2194

Dixon JP, Stihler SD, Power JA, Tytgat G, Estes S, McNutt SR Catalog of earthquake hypocenters at Alaskan volcanoes: January 1 through December 31, 2005, USGS science for a changing world

Engdahl ER, van der Hilst R, Buland R (1998) Global teleseismic earthquake relocation with improved travel times and procedures for depth determination. Bull Seismol Soc Am 88:722–743

Engdahl ER, Jackson JA, Myers SC, Bergman EA, Priestley K (2006) Relocation and assessment of seismicity in the Iran region. Geophys J Int 167:761–778. doi:10.1111/j.1365-246X.2006.03127.x, GJI

Gardner JK, Knopoff L (1974) Is the sequence of earthquakes in southern California, with aftershocks removed, Poissonian? Bull Seismol Soc Am 64(5):1363–1367

Gutenberg B, Richter CF (1944) Frequency of earthquakes in California. Bull Seismol Soc Am 34:185–188

Havskov J (2000) Earthquake location, Institute of Solid Earth Physics. University of Bergen, Norway

Kennett BLN, Engdahl ER, Buland R (1995) Constraints on seismic velocities in the Earth from travel times. Geophys J Int 122:108–124

Luen B, Stark PB (2012) Poisson tests of declustered catalogs. Geophys J Int 189(1):691–700

Maggi A, Jackson JA, McKenzie D, Priestley K (2000) Earthquake focal depths, effective elastic thickness, and the strength of the continental lithosphere. Geology 28(6): 495–498

Maggi A, Priestley K, Jackson J (2002) Focal depths of moderate and large size earthquakes in Iran. J Seismol Earthq Eng JSEE 4(No. 2&3):1–2

Mangino S, Priestley K, Ebel J (1999) The receiver structure beneath the China digital seismograph network stations. Bull Seismol Soc Am 89:1053–1076

McClusky S, Balassanian S, Barka A, Demir C, Ergintav S, Georgiev I, Gurkan O, Hamburger M, Hurst K, Kahle H, Kasten K, Kekelidze G, King RW, Kotzev V, Lenk O, Mahmoud S, Mishin A, Nadariya M, Ouzoumis A, Paradissis D, Peter Y, Prilepin M, Reilinger R, Sanli I, Seeger H, Tealeb A, Toksöz MN, Veis G (2000) GPS constraints on plate motions and deformations in eastern Mediterranean and Caucasus. J Geophys Res 105: 5695–5719

McKenzie D, Fairhead D (1997) Estimates of the effective elastic thickness of the continental lithosphere from Bouguer and free air gravity anomalies. J Geophys Res 102:27 523–27 552

Mignan A, Woessner J (2012) Estimating the magnitude of completeness for earthquake catalogs. Estimating the magnitude of completeness for earthquake catalogs. CORSSA. doi:10.5078/corssa-00180805, Available at http://www.corssa.org

Mirzaei N, Mengtan G, Yantai C, Wangi J (1997) A uniform catalog of earthquakes for hazard assessment in Iran seismic. Acta Seismol Sin 10(No. 6):713–726

Mirzaei N, Mengtan G, Yantai C (1998) Seismic source regionalization for seismic zoning of Iran: major seismotectonic provinces. J Earthq Prediction Res 7:465–495

Molchan G, Dmitrieva O (1992) Aftershock identification: methods and new approaches. Geophys J Int 109:501–516, 6, 9, 11

Molnar P, Lyon-Caen H (1989) Fault plane solutions of earthquakes and active tectonics of the Tiebetan plateau and its margins. Geophys J Int 99:123–153

Reasenberg P (1985) Second-order moment of central California seismicity, 1969–82. J Geophys Res 90(5479–5495):3–18

Richter CF (1958) Elementary seismology, Freeman, 768 pp

Rydelek PA, Sacks IS (1989) Testing the completeness of earthquake catalogs and the hypothesis of self-similarity. Nature 337:251–253

Scordilis EM (2006) Empirical global relations converting Ms and mb to moment magnitude. J Seismol 10:225–236. doi:10.1007/s10950-006-9012-4

Sipkin SA, Person WJ, Presgrave BW (2000) Earthquake bulletins and catalogs at the USGS National Earthquake Information Center, U.S. Geological Survey National Earthquake Information Center

Stucchi M, Rovida A, Gomez Capera AA, Alexandre P, Camelbeeck T, Demircioglu MB, Gasperini P, Kouskouna V, Musson RMW. Radulian M, Sesetyan K, Vilanova S, Baumont D, Bungum H, Fäh D, Lenhardt W, Makropoulos K, Martinez Solares JM, Scotti O, Živčić M, Albini P, Batllo J, Papaioannou C, Tatevossian R, Locati M, Meletti C, Viganò D, Giardini D, springer, publish online, 2012, The SHARE European Earthquake Catalogue (SHEEC) 1000–1899, J Seismol. doi:10.1007/s10950-012-9335-2

Sweeney, J.J., 1996, Accuracy of teleseismic event locations in the Middle East and North Africa, *Lawrence Livermore National Laboratory*, UCRL- ID-125868.

Sweeney JJ (1998) Criteria for selecting accurate event locations from NEIC and ISC bulletins, *Lawrence Livermore National Laboratory*, UCRL-JC-130655

Talebian M, Jackson J (2004) A reappraisal of earthquake focal mechanisms and active shortening in the Zagros mountains of Iran. Geophys J Int 156:506–526

Tatar M, Hatzfeld D, Ghafory-Ashtiany M (2004) Tectonis of the central Zagros (Iran) deduced from microearthquake seismicity. Geophys J Int 156:255–266

Tavakoli F (2007) Present-day deformation and kinematics of the active faults observed by GPS in the Zagros and east of Iran, PHD Thesis

Uhrhammer R (1986) Characteristics of northern and southern California seismicity. Earthq Notes 57:21

Van Stiphout T, Zhuang J, Marsan D (2012) Seismicity declustering. CORSSA. doi:10.5078/corssa- 52382934, Available at http://www.corssa.org

Vernant P, Nilforoushan F, Hatzfeld D, Abbassi MR, Vigny C, Masson F, Nankali H, Martinod J, Ashtiani A, Bayer R, Tavakoli F, Chéry J (2004) Present-day crustal deformation and plate kinematics in the Middle East constrained by GPS measurements in Iran and northern Oman. Geophys J Int 157: 381–398. doi:10.1111/j.1365-246X.2004.02222.x

Wang Q, Zhang PZ, Freymueller JT, Bilham R, Larson KM, Lai X, You X, Niu Z, Wu J, Li Y, Liu J, Yang Z, Chen Q (2001) Present-day crustal deformation in China by Global Positioning System measurements. Science 294:574–577

Wiemer S (2001) A software package to analyze seismicity:

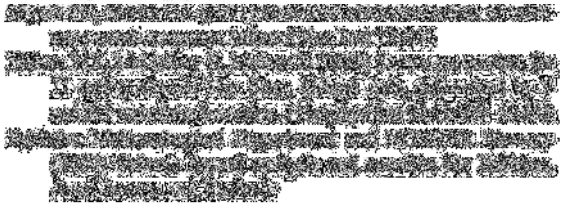

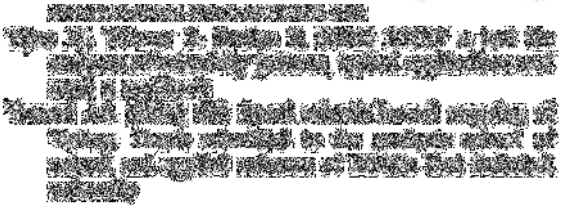

#2. Vasheghani-Farhani J. and Zaré M, (2014), "Site characterizations for the Tehran network (TDMMO) in Tehran region using micro-earthquake, microtremor and quarry blast data", Soil Dynamics and Earthquake Engineering, vol. 63, pp. 235–247, doi: 10.1016/j.soildyn.2014.03.013.

Soil Dynamics and Earthquake Engineering 63 (2014) 235–247

Contents lists available at ScienceDirect

Soil Dynamics and Earthquake Engineering

journal homepage: www.elsevier.com/locate/soildyn

Site characterizations for the Tehran network (TDMMO) in Tehran region using micro-earthquake, microtremor and quarry blast data

Jamileh Vasheghani Farahani [1], Mehdi Zaré *

International Institute of Earthquake Engineering and Seismology, Tehran, Iran

ARTICLE INFO

Article history:
Received 21 April 2012
Accepted 15 March 2014

Keywords:
H/V
Amplification
Site effects
Quarry blast
Earthquake
Microtremor
Tehran

ABSTRACT

We did a Study of Horizontal-to-Vertical Component Spectral Ratio in the Tehran seismic zone. Micro-earthquakes, microtremors and quarry blasts data were used as an estimation of the site response in the Tehran zone. Site effects were studied based on horizontal to vertical ratios by the Nakamura's technique. Also, we used the spectra of signals for three components with the lowest noise levels for spectral slope studies. The analysis used seismic events from a network of 13 seismic stations by the permanent local seismological network of the Tehran Disaster Mitigation and Management Organization (TDMMO) from 2004 to 2007. The number of events used were different for each station. Quarry blast events were with $1.2 \leq M_L \leq 2.2$ and micro-earthquakes were with $1.1 \leq M_L \leq 4.1$.

By comparing results for earthquake, microtremor and quarry blast, we could see that there is a significant difference between them. The data showed clear observations, especially in high-frequencies. The H/V spectral ratios indicate dominant frequency for rock/soft site with a higher ratio level for quarry blast ratios, which are comparable to the earthquake results due to their difference sources. The results derived by spectral H/V ratios and spectral analysis may be used to distinguish between local earthquakes and quarry blasts.

1. Introduction

Local site conditions may affect meaningfully the amplitude of earthquake ground motions known as site effects [1].

Site effect studies were recognized in the Japan earthquake in 1891 [2], the 1906 San Francisco earthquake [3], and the Long Beach earthquake of 1933 [4]. Gutenberg [5] studied sediment amplification in southern California for the first time [6].

Non-linearity of soil response and topographical effects are effective in ground motion parameters [7]. For instance, in the earthquake occurred on September 26, 1997 (Umbria – Marche, Italy), site amplification observed even at large distances from the epicenter [8].

Assessing seismic hazard is very important for Tehran. It is the most populated city in Iran. Some researchers have studied the local site conditions (using microtremors) and site effects in earthquakes recorded in strong motion stations and local temporary network/profiles in Tehran [9–11]. Others have worked on the realistic strong motion modeling, paying attention to site effects [12]. Local site condition analysis is an important issue of seismic hazard, since damages observed for earthquakes are related to geologic conditions and local site effect or site response [13–16]. Site response study is a strong input for microzonation, which has an important role to modify old buildings or to construct new ones [16].

In this study, we assessed site response based on an analysis of seismograms from three kinds of data in Tehran region. We try to estimate the amplification effects for earthquakes, microtremors and small explosions. We concentrate on the weak ground motions including micro-earthquakes, microtremors and quarry blasts in Tehran.

There is a long history of using microtremors to describe site characteristics. In Japan, Kanai et al. in 1950s and 1960s have suggested different methods based on the microtremor data in Tokyo [17]. Spectral ratio of the horizontal component to the vertical component (H/V) was suggested by Nakamura [18]. For engineering purposes, microtremor studies are applied to determine the predominate frequency of surface layers (14).

Records of earthquakes can help us understand the site effects and response of structures. So, we can use H/V spectral ratio not only for microtremor, but also for earthquake. Earthquake records are able to estimate predominant frequency and the amplification factor too. In our region, Tehran city, we do not have strong ground motion records. However, we tried to overcome this lack of data by using weak motions like microtremors, micro-earthquakes or effects due to explosions in order to assess the site effects. Udwadia and Trifunac [19] indicated that the differences might be due to recorded waves related to strong and weak motion. Such differences might be about their different types and their different propagation paths [20].

* Corresponding author.
[1] Present address: Institute of Geophysics, University of Tehran, Tehran, Iran.

http://dx.doi.org/10.1016/j.soildyn.2014.03.013
0267-7261/

In this research, we will show that H/V spectral ratios of microtremor and earthquake usually are the same, especially for rock sites. We observed a special characteristic in H/V spectral ratio for quarry blasts that they generally are different from earthquakes. First, we will discuss about the general tectonic of the region, and then the methodology is described. We present our results and discuss about them afterwards. The concluding remarks are presented finally.

2. General tectonic settings

The Iranian plateau is located on the Alpine-Himalayan seismic belt at the convergence of the Eurasian and Arabian plates. Most deformation in Iran is concentrated in the Zagros, Alborz and Kopeh Dagh mountains and eastern Iran [21]. Alborz is an active mountain trend belonging to the Alpine-Hymalian seismic belt, connecting the Talesh and the Lesser Caucasus ranges to the West, and the Eastern Alborz structures to the East. Central Alborz is subdivided into two main bordering structures: The Qazvin, North Tehran, Parchin and Garmsar southwards thrusting fault zone to the South, and the Khazar fault northwards thrusting fault to the North. Inside Alborz, the Taleghan, Mosha, Firouzkuh and Astaneh faults define a main left-lateral strike-slip corridor attesting of the partitioning of the deformation in Alborz [22].

The Alborz Mountains Belt is an active E–W trend with 100 km width and 600 km length, which was formed when Gondwana collided with Eurasia in the Late Triassic [23]. The Alborz range comprises several sedimentary and volcanic layers from the Cambrian to Eocene ages that were deformed during the late Cenozoic collision [24–26]. Its total shortening since the early Pliocene has been evaluated to be 30 km at the longitude of Tehran [27]. The mean elevation in the Alborz drops sharply from 3000 m in the inner belt to −28 m at the Caspian shoreline to the North. Alborz was affected by several successive tectonic events, from the Eo-Cimmerian orogeny to Late Tertiary-Quaternary intracontinental transpression [27], and is still strongly seismically active [28].

Tehran is situated in an enlargement along Alborz mountain front filled with alluvial materials originating from the rise of the Alborz range. The abrupt change of 2750 m in elevation between

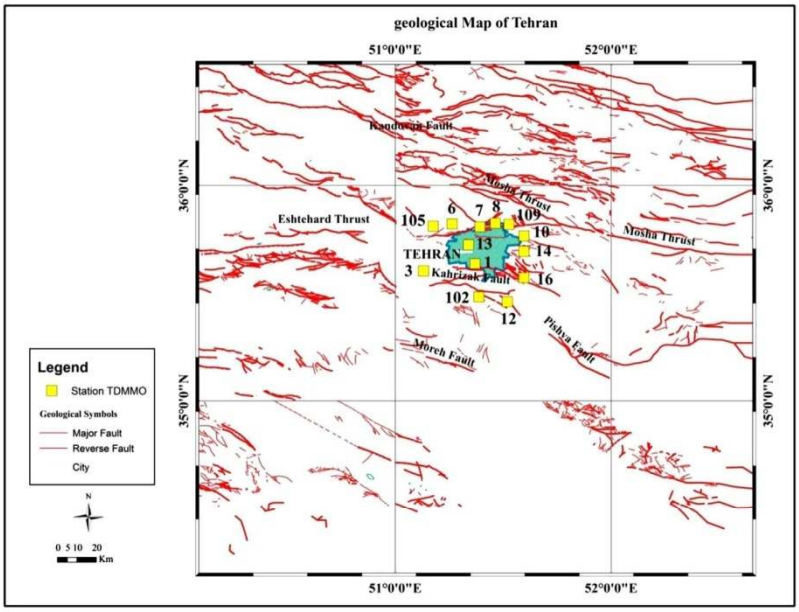

Fig. 1. Location of the seismic stations for Tehran network (TDMMO).

Table 1
Location of seismic stations for Tehran network (TDMMO).

Station no.	Latitude	Longitude	Altitude (m)	Geographic location
1	N 38.24' 35°	E 22.18' 51°	1100	Shariati park
102	N 29.00' 35°	E 23.26' 51°	983	Ghasem abaad
3	N 36.20' 35°	E 7.84' 51°	1090	Saba shahr
105	N48.69' 35°	E 10.51' 51°	1864	Vardyj
6	N 49.34' 35°	E 15.82' 51°	1680	Sulaqan
7	N 48.53' 35°	E 23.55' 51°	1820	Velenjak
8	N 49.52' 35°	E 27.84' 51°	1851	Jamshidieh park
109	N 49.15' 35°	E 31.62' 51°	2110	Shahrak area
10	N 45.93' 35°	E 35.80' 51°	1676	North of Tehran pars
12	N 27.59' 35°	E 31.17' 51°	967	Eshgh abaad
13	N 43.50' 35°	E 20.37' 51°	1274	Tehran disaster mitigation and management organization
14	N 41.69' 35°	E 35.78' 51°	1666	Hameh sin
16	N 34.30' 35°	E 35.79' 51°	1231	Lapeh zanak

the city and the nearest summit of the northern range is a striking topographic feature which is mainly the consequence of vertical movement along the major mountain-bordering reverse fault, the North Tehran Fault, as reported by Tchalenko et al. [29].

The northern areas of Tehran province form part of the central Alborz mountain range. South Tehran is a part of the low-altitude plains of central Iran. The geomorphic and geological features of the province are closely connected to its geographical components [30].

Quaternary faulting is the basic tectonic activity in the region. Most of the faults in the area are longitudinal and follow the Alborz fold-thrust mountain belt [31]. Faults located in southern Tehran are the Eyvanekey fault (75–80 km in length) with a compressive mechanism and strike slip component, and the Kahrizak fault (40 km in length) with a compressive mechanism [32].

2.1. Methodology: H/V spectral ratio technique

Nogoshi and Igarashi [33] showed a ratio of Horizontal and vertical component of the motion having a relationship to the ellipticity curve of Rayleigh wave, and took advantage of the

Table 2
Site amplification using earthquake records (mean value by H/V ratios).

Site location.	**Amplification in frequency range**			Peak amplification (level of factor)
	0.5–2 Hz	2–4 Hz	4–7.5 Hz	
Site-001	1.9–2.3	1.6–2.0	1.5–2.0	2.3
Site-102	1.0–2.0	1.1–1.3	1.3–1.8	2.0
Site-105	0.8–1.0	1.0–1.4	1.3–1.5	1.5
Site-006	1.0–1.5	1.4–2.6	1.6–2.6	2.6
Site-007	1.3–1.7	1.5–1.8	1.6–2.2	2.2
Site-008	1.0–1.7	1.8–2.0	1.5–1.9	2.0
Site-109	1.2–1.5	1.4–2.0	1.6–1.8	2.0
Site-010	1.1–1.4	0.9–1.5	0.9–1.3	1.5
Site-012	1.2–1.6	1.2–1.7	1.7–1.9	1.9
Site-014	1.1–1.3	1.2–1.7	1.5–1.9	1.9
Site-016	0.8–1.8	1.8–2.1	1.8–2.2	2.2

Table 3
Site amplification using microtremor records (mean value by H/V ratios).

Site location.	**Amplification in frequency range**			Peak amplification
	0.5–2 Hz	2–4 Hz	4–7.5 Hz	
Site-001	1.0–2.1	1.2–1.6	1.4–1.6	2.1
Site-102	1.6–3.2	0.8–1.5	1.5–3.1	3.2
Site-105	0.8–1.1	1.2–1.4	1.3–1.4	1.4
Site-006	0.7–1.7	1.4–1.8	1.4–2.1	2.1
Site-007	1.5–2.0	1.5–1.8	1.8–2.8	2.8
Site-008	1.0–1.5	1.4–1.7	1.2–1.7	1.7
Site-109	1.2–1.7	1.2–1.8	1.2–1.7	1.8
Site-010	0.8–1.1	0.7–0.8	0.8–0.9	1.1
Site-012	1.3–1.8	1.1–1.5	1.3–2.1	2.1
Site-014	1.0–1.3	1.1–1.3	1.3–1.5	1.5
Site-016	0.7–1.8	1.4–1.8	1.7–2.2	2.2

Table 4
Site amplification using quarry blast records (mean value by H/V ratios).

Site location.	**Amplification in frequency range**			Peak amplification
	0.5–2 Hz	2–4 Hz	4–7.5 Hz	
Site-001	1.3–2.7	1.8–4.0	1.6–2.4	4.0
Site-102	1.5–2.7	1.1–1.4	1.3–2.4	2.7
Site-105	0.7–1.1	0.9–1.8	1.4–1.9	1.9
Site-006	1.1–1.8	1.5–3.0	1.5–3.0	3.0
Site-007	1.3–1.7	1.4–2.1	1.6–2.9	2.9
Site-008	0.7–1.8	1.5–2.4	0.8–2.9	2.9
Site-109	1.0–2.0	1.7–3.1	0.8–1.6	3.1
Site-010	0.8–1.5	0.9–1.5	0.8–1.6	1.6
Site-012	1.0–1.4	1.0–1.8	1.4–2.0	2.0
Site-014	1.2–2.0	0.9–2.5	1.2–2.5	2.5
Site-016	0.8–1.6	1.0–1.8	1.8–4.3	4.3

coincidence between the lowest frequency maximum of this H/V curve with the fundamental resonance frequency, to use it as a parameter of amplification due to underground soil condition. The method was later revised by Nakamura [18] so that the ratio to be a reliable estimation of the site transfer function for S waves (which led him to use the name "Quasi-Transfer Spectrum") [34].

Nakamura [18] suggested a technique for obtaining site amplification factors using microtremor H/V spectral ratios. Many researchers have used this method. We used this procedure for our research in Tehran region. In the present study, first, the recorded time series data were gathered from eleven stations of TDMMO network. Then the Fourier spectra were calculated for using the Fast Fourier Transform (FFT) algorithm and the Fourier spectra were smoothed.

The Fourier amplitude ratio for two horizontal Fourier spectra and vertical Fourier spectrum calculated. The calculation is shown by the following equation.

$$H/V_{\text{Spectral ratio}} = \{(S_{NS}(f)^2 + S_{EW}(f)^2)/2\}^{1/2}/S_V(f)$$

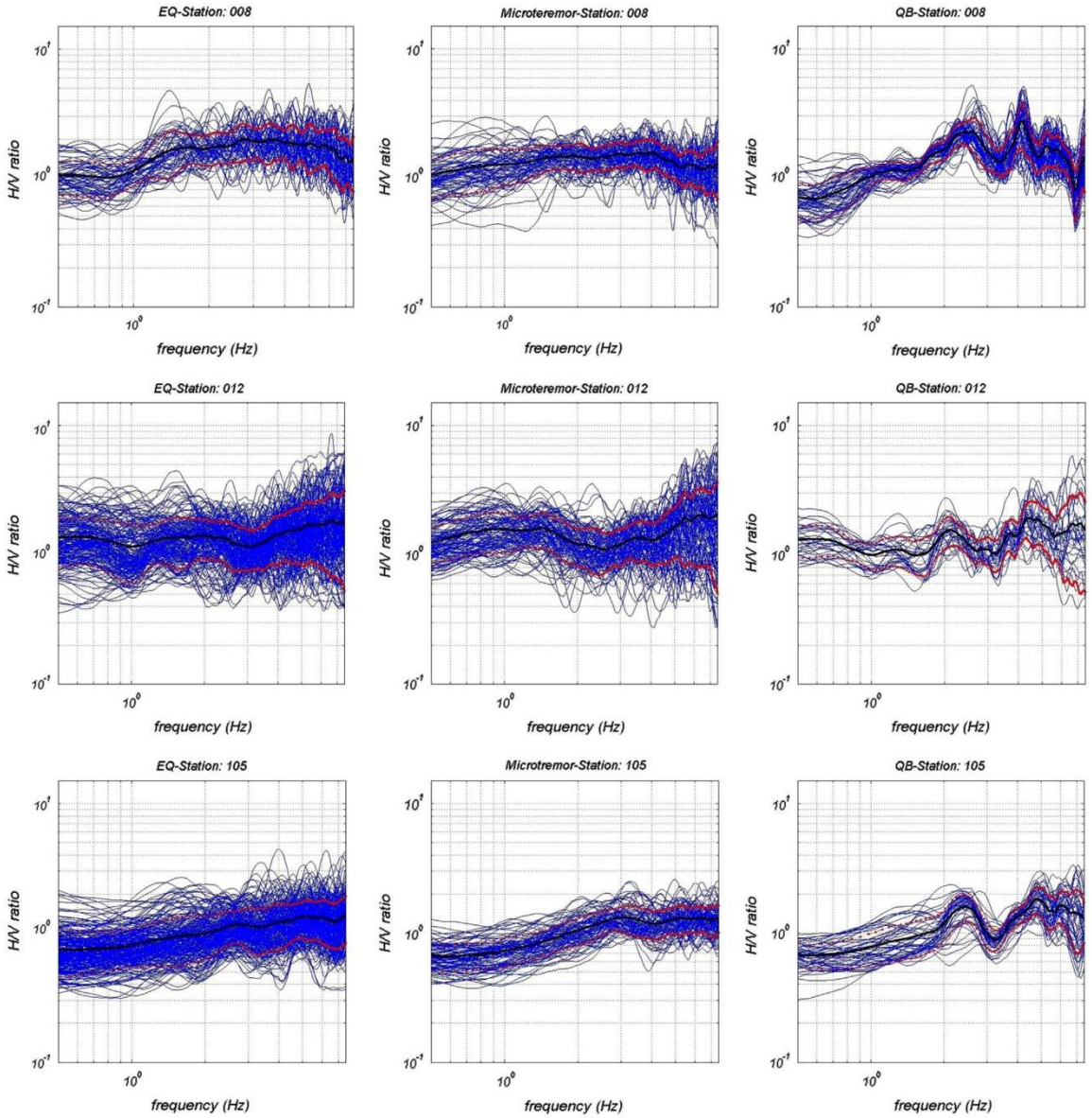

Fig. 2. Site amplification (H/V curves) computed by the Nakamura method using earthquake, microtremor and quarry blast records at eleven sites in Tehran region. The dark line denotes the average curve estimation for all events and the upper and lower light lines shows standard deviation.

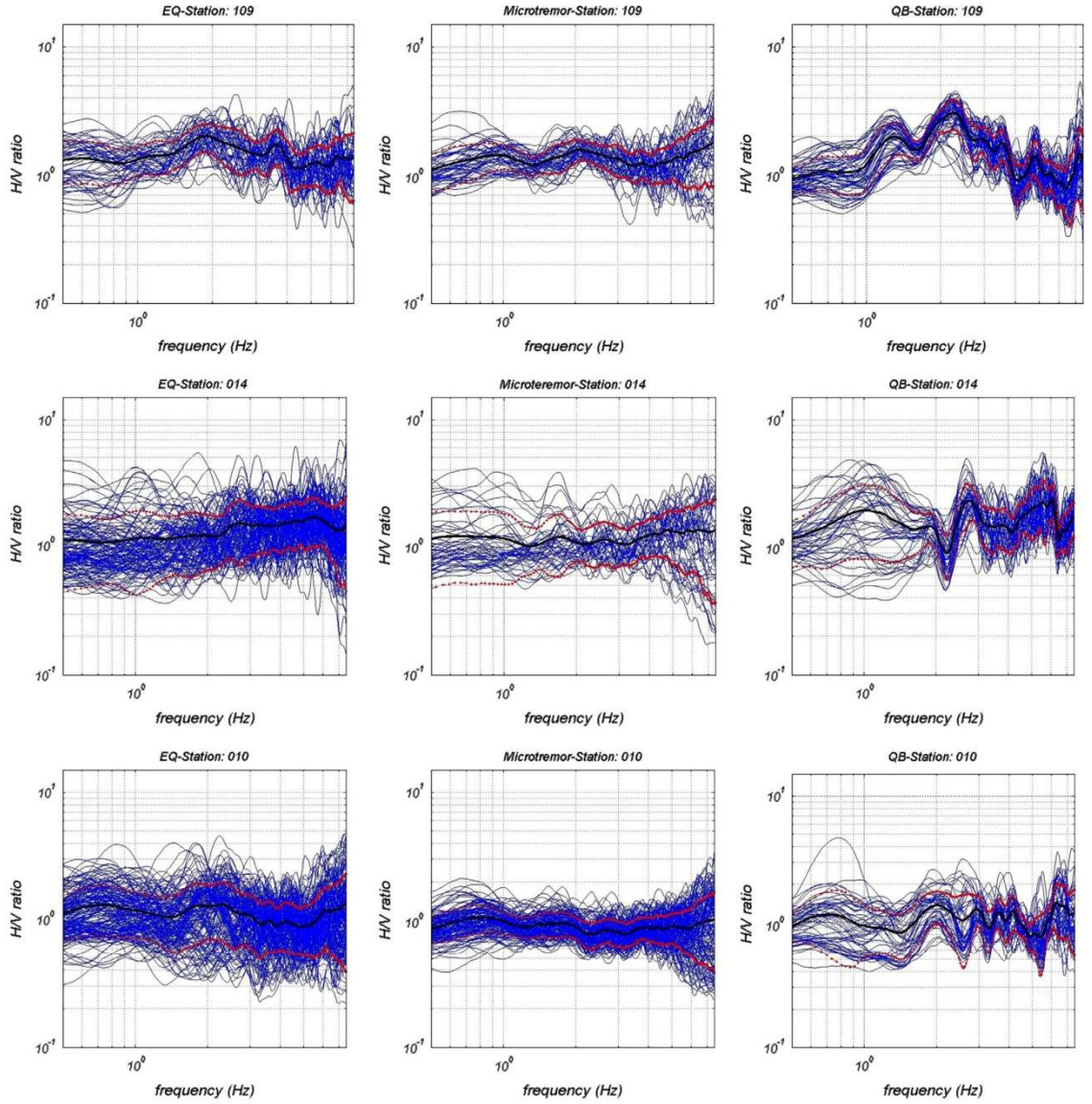

Fig. 2. (*continued*)

where H/V is the horizontal to vertical spectrum ratio, S_{NS}, S_{EW} and S_V are the Fourier amplitude spectra in the NS, EW and UD directions, respectively.

The average of the spectra and standard deviations obtained for sites. The peak frequency of the H/V spectrum shows the predominant frequency of the site. The H/V spectra for all sites were calculated, and the predominant frequencies of ground motion were determined.

Zaré et al. [35] believe that there is a relatively good relationship between the *S*-wave velocity profiles and the fundamental frequency results, so we used their class site categorization.

Based on site category determined by Zaré et al. [35] we have decided to classify our data for site conditions according to the frequency band of the fundamental frequency based on our results for H/V spectral ratio.

3. Database and data processing

3.1. Local network

The amplification effects were analyzed for eleven stations that their location is shown in Fig. 1. Seismic stations equipped with CK-1П seismometers (Russia) deployed in the Tehran region with natural frequency 1 Hz, between 2004 and 2007 by the permanent local seismological network of Tehran Disaster Mitigation and

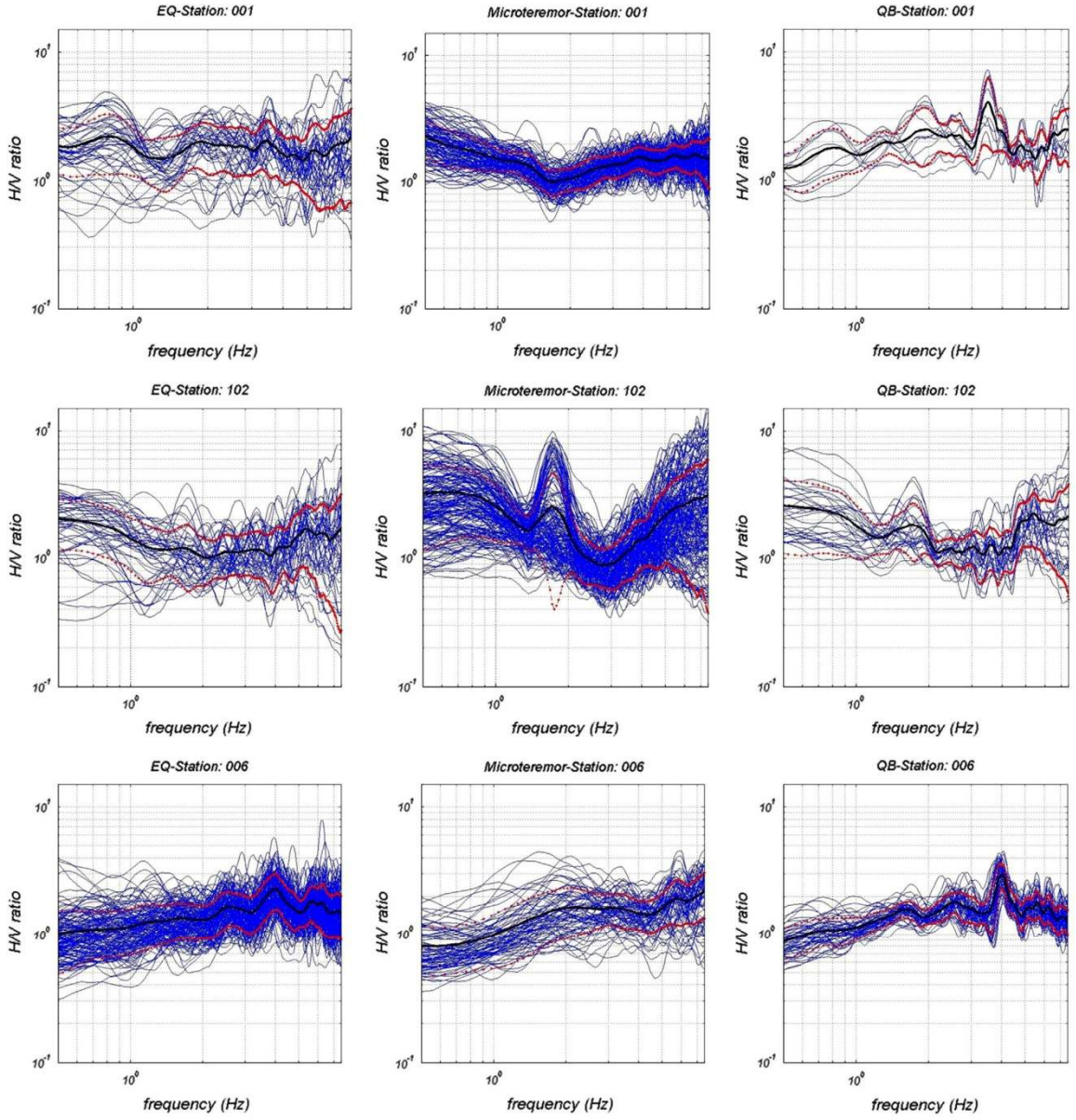

Fig. 2. (*continued*)

Management Organization (TDMMO). These stations recorded data in continuous mode and in all stations. The seismograms used with sampling rate 35.71 with 24-bit resolution, from 2004 to 2007.

Vasheghani et al. [32] in 2012 organized a dataset of quarry blasts by TDMMO network. There is no separate network for recording of data mining in Tehran city. TDMMO network records all of events including earthquakes and quarry blasts. They decided to discriminate these events by Adaptive neuro-fuzzy inference systems for semi-automatic discrimination between seismic events. ANFIS classifiers were used to detect seismic events using some inputs that defined the seismic events like weak earthquakes and quarry blasts. This method could successfully train to recognize seismic events based on seismic parameters [36].

3.2. Data processing

In this study, for computing the H/V ratios, we processed a data set which was recorded in 11 stations. The number of events used were different for each station. To determine the H/V ratios, first, we converted data to SAC format. We calculated the signal-to-noise

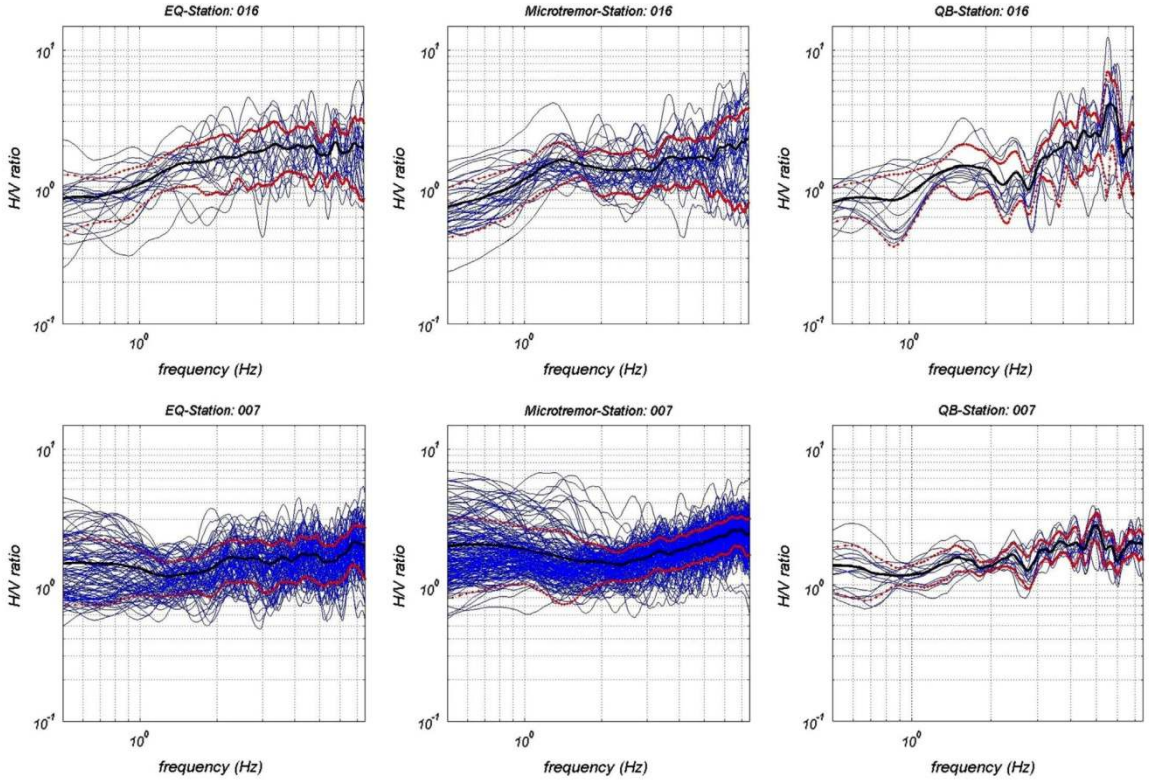

Fig. 2. (*continued*)

ratio, H/V ratios and spectral amplitudes for all data with SAC format using the Matlab software in this study. Spectral amplitudes for three components (NS, EW, and Z) are calculated using a four-pole Butterworth band pass filter. Also, calculated Fourier spectra of three components that were smoothed with software mentioned above. The horizontal components were merged by geometric mean. Then, the H/V ratios were calculated by dividing the spectra of the merged horizontal components to the spectra of the vertical component. Finally, the mean and standard deviations of H/V ratios were obtained for all results of stations.

Bard [34] believes that it is not reasonable for concentration only on microtremor data for studying site effects. Earthquake data are preferable at least for a local "calibration" of noise results. The best method for estimation of the soil fundamental frequency is the H/V technique, especially with the quality improvement for the determination of H/V peak frequency in sites with low impedance contrast. The noise difference at long period, $T > 1$s and short period, $T < 1$s (For example: human activity) relates to difference between " microseisms" with a natural origin and "microtremors" with an artificial origin. In urban areas that they described by low frequency, high impedance contrast subsoils, and artificial microtremors may be more energetic than natural microseisms [34].

Quarry blasts ($1.2 \leq M_L \leq 2.2$) and earthquakes selected ($1.1 \leq M_L \leq 4.1$) with signal-to-noise ratio greater than two.

We selected the whole recorded signals including P and S wave windows as used by Theodulidis and Bard [37] to keep and apply the available data as much as possible.

4. Results

The Nakamura technique (H/V amplification function) used essentially the accelerometric data. Monika [40] showed that there is not visible difference between velocity seismograms and accelerograms. Therefore, we used velocity records for our study.

Site response ranges are shown in Tables 1 and 2 (earthquake), Table 3 (microtremor) and Table 4 (quarry blast) for the frequency ranges 0.5–2 Hz, 2–4 Hz and 4–7.5 Hz. These frequency ranges are reasonable due to natural frequencies of multistory buildings. For example, the frequency range between 0.5 and 2 Hz is the natural frequency of more than five storey buildings or for frequency range between 2 and 4 Hz, the natural frequency is more than 2.5 storey buildings.

Site amplification has been shown in Tables 2–4 and Fig. 2 using earthquake, microtremor and quarry blast data for comparison at eleven sites in the Tehran region. Generally, comparison results of site amplification (Fig. 2) for earthquake and microtremor show that amplification for earthquake data is similar to the site amplification for microtremor data. If we want to compare details of them, we can observe that site amplification for earthquake data slightly is more than microtremor data, because most of the site conditions correspond to hard alluvium or rock outcrops.

Generally, comparison results of site amplification (Fig. 3a, b and c) for earthquake, microtremor and quarry blast records show that amplification level for quarry blast is more than that obtained from earthquake and microtremor waves. We believe that site amplifications assessed using quarry blast waves are more

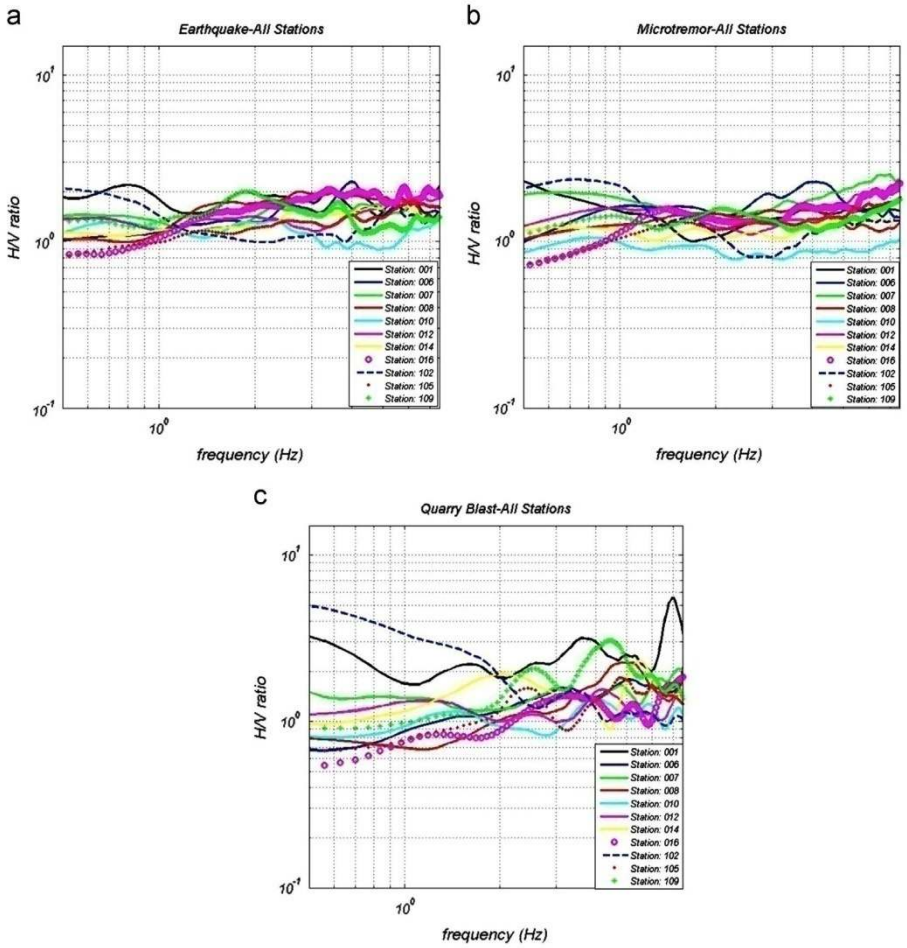

Fig. 3. Comparison of average of H/V curves for earthquake, microtremor and quarry blast records for "total" of stations.

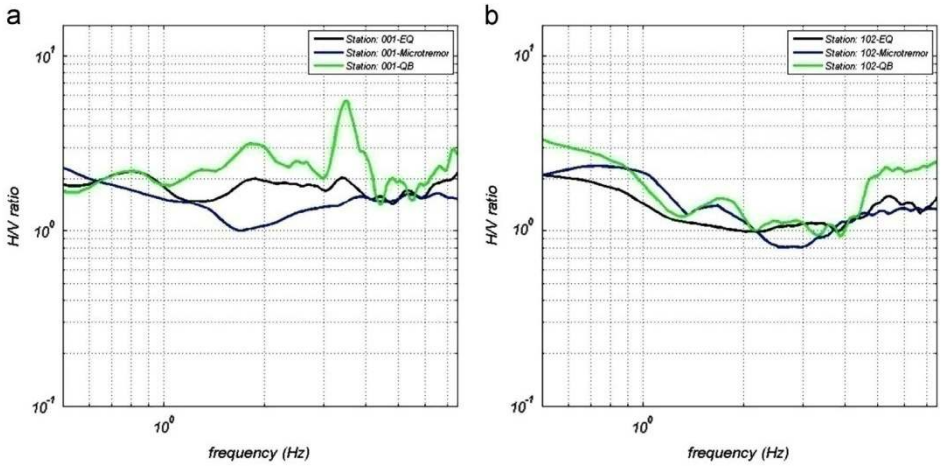

Fig. 4. Comparison results of site amplification for earthquake, microtremor and quarry blast records by 001 (Shariati Park) and 102 (Ghasem Abaad) stations.

reliable than those obtained from earthquake and microtremor data for f < 2 Hz in site of soft soil (Fig. 4a for station:102 and 4b for station:001), because they produce from shallow shots that may contribute significantly for the generation of surface wave motion. Quarry blasts records show that they are an important source of surface waves energy in low frequency for soft soil in this study. Our results by quarry blast records (Fig. 3c) from TDMMO network from 2004 to 2007 for study of site amplification shows that H/V spectral ratios recognized higher amplification due to body waves trapped in lower velocity layers, especially for $f > 2$ Hz.

5. Discussion

5.1. Reliability of method

We have shown that the H/V ratio and spectral amplitudes can be used to site studies by three kinds of data with different sources.

Bard [34] indicated that based on the experimental results demonstrated, H/V ratio does point out the fundamental frequency of soft soils. He emphasized that the assessment of the fundamental frequency is easier on the H/V ratio than on absolute spectra or site to reference spectral ratios, especially in the case of moderate impedance contrast. Bard [34] showed that the preferred theoretical explanation is the ellipticity ratio of Rayleigh waves.

We considered some steps for testing the reliability of H/V peak assessed by this research. These steps are expressed herein:

1. Our criterion for H/V peak amplitude is equal or greater than 2.
2. We considered a reliable estimation for fundamental resonance frequency to the lowest frequency maximum in H/V curves.
3. The peak appears at the same frequency (within ± 5%) on the H/V curves similar to mean ± standard deviation.
4. The site classification is based on the amplitude and level of the highest peak on the fundamental frequency curve.

5.2. Comparison of H/V amplifications in microtremors, micro-earthquakes and quarry blasts

H/V spectral ratios from microtremors, micro-earthquakes and quarry blasts helped us to understand about the soil type in Tehran region. Our results showed that six sites of TDMMO network are

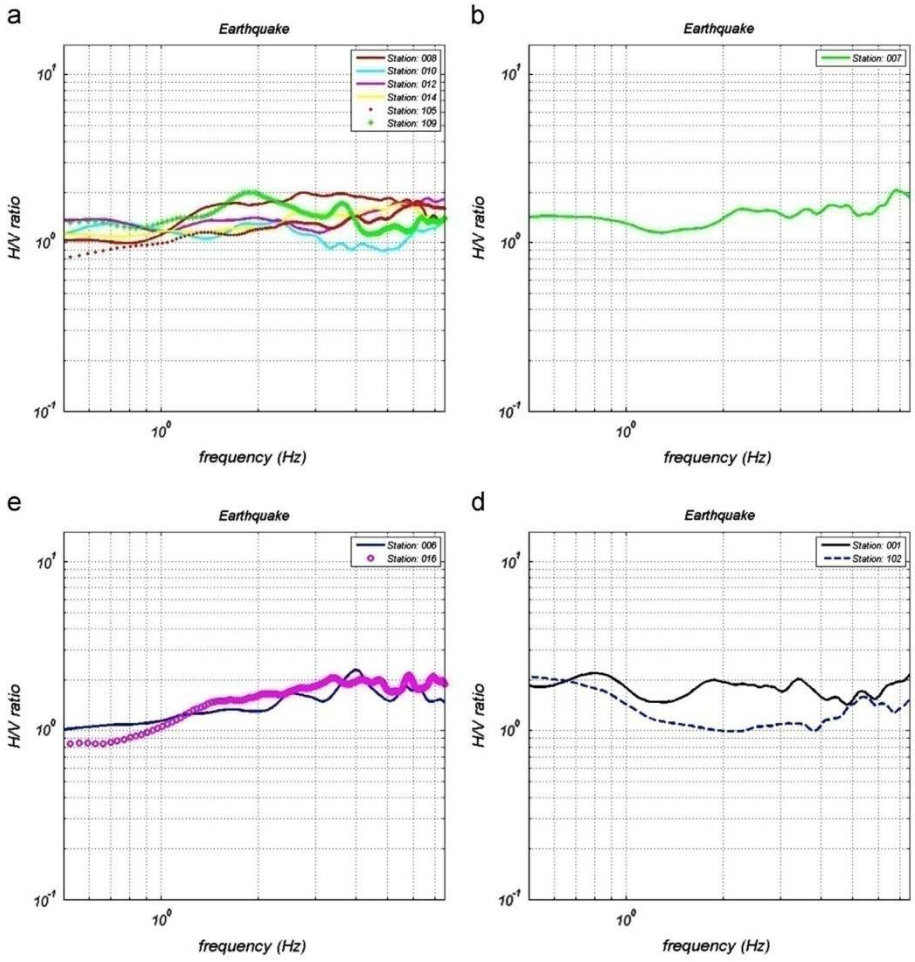

Fig. 5. Site classification: a(class I)- b(site class II))-c(site class III)- d(site class IV).

rock sites (Fig. 5a). Others are soft soil (Fig. 5b) and alluvial sites (5c and 5d), (deep cohesionless soil and hard alluvium). We try to discuss about their results with the method that is mentioned above.

We know that frequency band between 0.5 and 4 Hz is very important and interesting in engineering [38]. We attempted to concentrate on this band, too. For three kinds of data, we calculated H/V ratio and spectral amplitudes. Comparison of the mean H/V ratio, standard deviations and spectral amplitudes showed that there is a significant difference between earthquakes and quarry blasts. The spectrum of quarry blast is decreasing with increasing frequency more quickly than earthquake (Fig. 6). Different shapes for these data should be due to the difference between the two sources. In velocity spectrum of earthquake source, for instance in site 008 (Jamshidiyeh Park, North Tehran, rock site, Fig.6a) higher amplitude spectral velocity ($\sim 10^9$) occurs in the frequency of about 1 Hz, but the spectrum of blast source (Fig. 6b) in the maximum spectral velocity ($\sim 10^8$) occurs in the frequency range of about 2–3 Hz. So, the earthquake spectrum shows the higher energy in velocity spectral ordinates (frequency range of 0.1– 7 Hz).

In our previous studies, we studied about Q-value for blast data, and we could obtain high Q_p^{-1} and Q_s^{-1} values for blast data in Tehran region. The attenuation parameters were: $Q_p^{-1}=(100\pm 6)\times 10^{-3}$ ($f^{-1\pm 0.07}$) and $Q_s^{-1}=(73\pm 2)\times 10^{-3}$ ($f^{-1.06\pm 0.03}$) indicating that the strong frequency dependency of Q_p^{-1} and Q_s^{-1} can propose heterogeneity of the medium. We saw that quarry blast source has a lack of energy in high frequencies as compared to earthquake source [39].

Quarry blasts are shot at highly shallow depths, so we can see that blast attenuation is strong. Since quarry blasts and earthquakes have different source properties or different propagation path effect, especially when their location is not close together, therefore, the H/V amplification functions show important differences in stations like Jamshidiyeh, Vardyj, and Hameh sin.

Spectral amplitude results display spectrum of earthquake, and microtremors are smoother than quarry blast.

5.3. Classification of studies seismic stations using H/V ratio

The earthquake and microtremor spectral H/V ratios are similar in some stations (Fig. 7), especially in stations: 008 (Jamshidiyeh), 105 (Vardyj), 014 (Hameh Sin) and 016 (Lapeh Zanak) (Tables 2 and 3). About the earthquake and quarry blast spectral H/V ratios, we observed difference of the amplification level in $f>$ 4.0 Hz (to be stronger than other frequency ranges), the most important peak at 4.2 Hz for quarry blast in station 008, about 4.5 Hz in station 105, about 5.9 Hz in station 014, 6 Hz in station 016 and about 5 Hz in station 007 (Fig. 7). We may observe amplification of the level almost near 3 for blast results in station 008, near 2.0 for blast in station 105, near 2.5 for station 014 and 2.9 for station 007 (Table 4). These differences in high frequency might be due to the energy carried by body waves where they are trapped in the low-velocity layer [38].

Meanwhile, we did not find any significant variation of the amplitude level in the low-frequency band, especially for $f<2.0$ Hz in stations mentioned above. The H/V amplification functions at sites (109; Shahrak and 010; North of Tehran Pars) show peaks at 2.3 and 2 Hz for quarry blasts, respectively (Fig. 2, Table 4). This behavior shows that in low frequencies, surface waves for small explosions contribute more than earthquake data for stations that we discussed above.

The site effects are not exactly the same for earthquakes, microtremors and blast in the stations like Kahrizak (102) and Shariati Park (001), i.e. soft soil sites.

We did the comparison of spectral H/V ratios for earthquake, microtremor and quarry blast in Shariati Park station (001). For microtremor, we cannot see significant variations in high frequency (>2 Hz), but in less than 1 Hz, we have amplification of level about a factor of 2. In this station, we have a peak of H/V spectral ratio for quarry blast in 3.5 Hz with a factor of 4 (Fig. 4a).

For station 001, in the low-frequency band (between $f=0.5$ and 2 Hz), the comparison of mean H/V ratios for earthquake and small explosion show a well-defined peak at about 0.8 Hz for

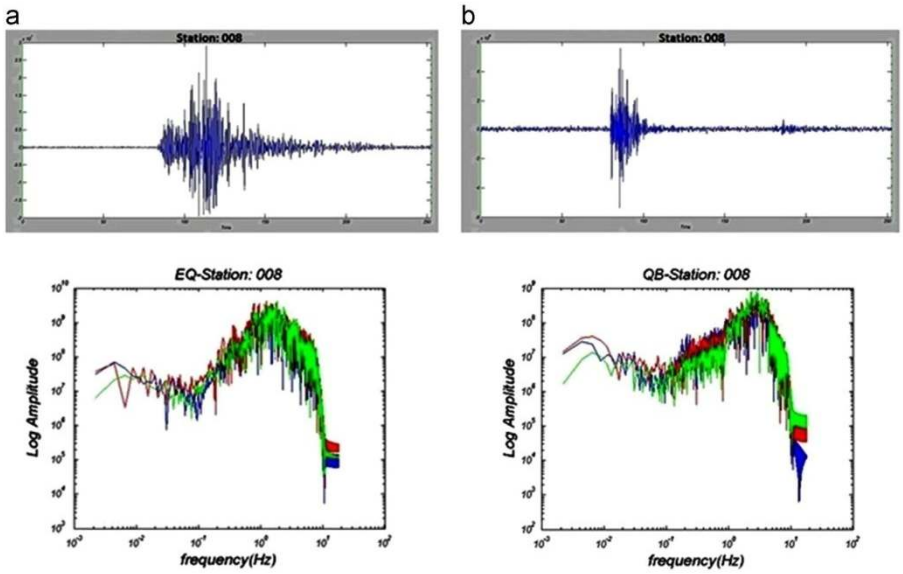

Fig. 6. Typical example of seismograms recorded at station 008 (Jamshidieh Park) for vertical component (top) and the spectral amplitude of all three components (bottom), (a) Earthquake with M_L 2.0 at a distance of 28.9 km. (b) Quarry blast with M_L 4.1 at a distance of 161 km.

earthquake where the amplification level is greater than 2 (Fig. 4a). For the frequency band of 1–2.0 Hz, we observe a difference between quarry blast, earthquake and microtremors in spectral ratios. This is due to surface waves generated efficiently in shallow small explosions comparing to earthquakes and microtremors [38].

Our investigation for soft soil site station Ghasem Abad (102), south of Kahrizak, Fig. 4b) showed that in $f=0.6$ Hz, we may see

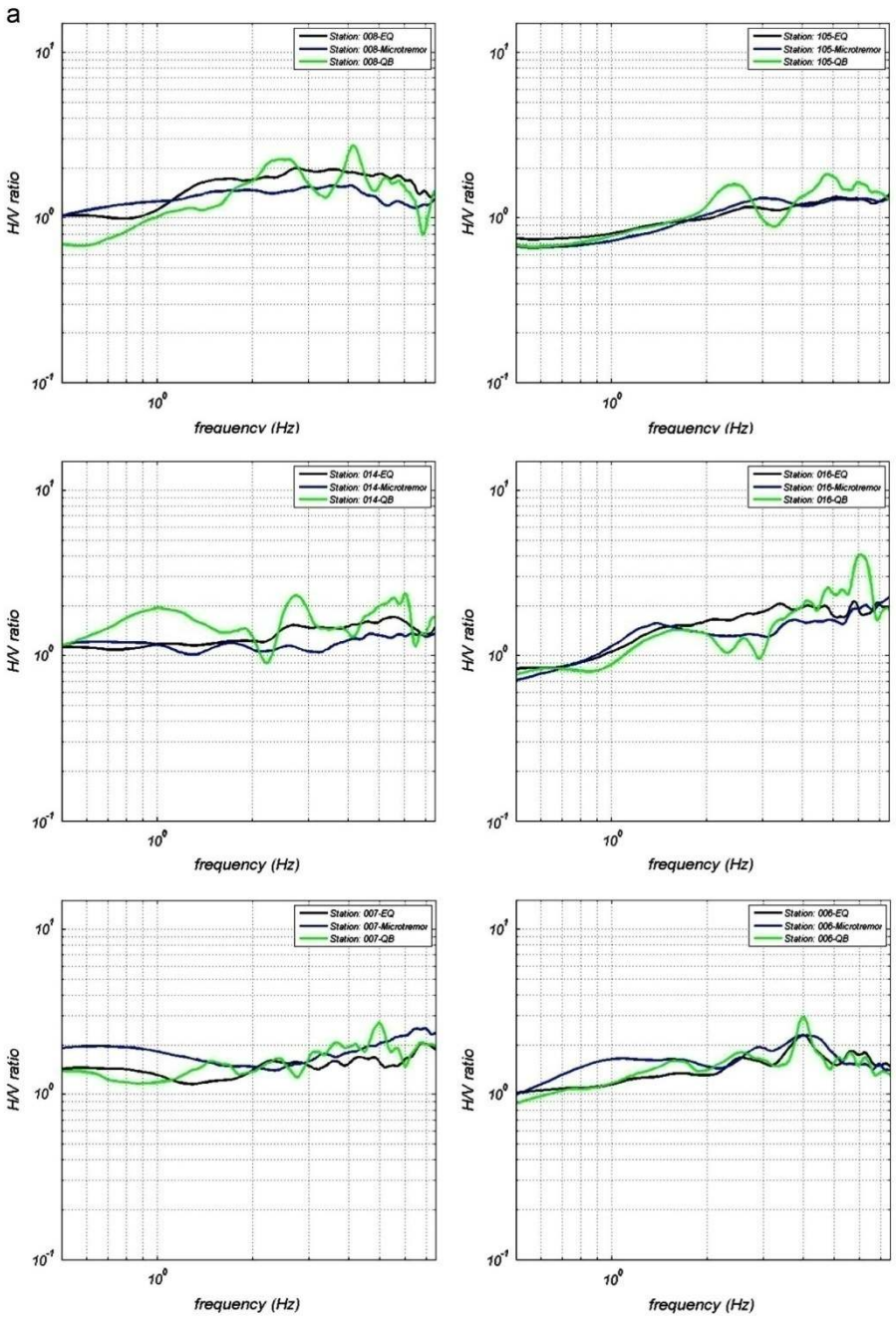

Fig. 7. Comparison results of site amplification for earthquake, microtremor and quarry blast records by 008 (Jamshidieh park),105 (Vardyj), 014 (Hameh sin), 016 (Lapeh zanak), 007 (Velenjak) and 006 (Sulaqan) stations.

Table 5
The results of site classification.

No.	Station name	Fundamental frequency (Hz)	Peak amplification (level of H/V factor)	Site classification
1	001- Shariati park	0.8	2.3	IV
2	102- Ghasem abaad	0.5–0.6	2.0	IV
3	105- Vardyj	0.5–7.5	<2.0	I
4	006- Sulaqan	4.0	2.6	III
5	007- Velenjak	6.7	2.2	II
6	008- Jamshidieh park	0.5–7.5	<2.0	I
7	109- Shahrak Area	0.5–7.5	<2.0	I
8	010- North of Tehran pars	0.5–7.5	<2.0	I
9	012- Eshgh abaad	0.5–7.5	<2.0	I
10	014- Hameh sin	0.5–7.5	<2.0	I
11	016- Lapeh zanak	3.2	2.2	III

dominant frequency for three kinds of our data. However, the amplification levels are significant in low frequencies ($f < 1.0$ Hz,) to be 3.0 for quarry blast, about 2.2 for microtremors (between 0.5 to 0.9 Hz and 1.5 Hz) and about 2 for earthquake (about less than 0.6 Hz).

This significant amplification for earthquake, microtremors and quarry blast in $f < 2$ Hz, giving higher ratios for quarry blasts, may show the importance of surface waves' amplification of quarry blasts on this soft soil site.

In station Soulaqan (006) (Fig. 7), the amplification function for earthquakes shows a peak at 4.0 Hz, which might be representative for soft alluvium site. The H/V amplification for quarry blasts shows the same peak for 4.0 Hz.

For station 016 (Lapeh Zanak, Fig. 7), the amplification function for earthquakes displays a peak at 3.5 Hz, which might be representative for soft alluvium site. We have a peak of H/V spectral ratio for quarry blast in 6.0 Hz with a factor of 4.

As far as it was evident from our study, the amplification function of H/V for quarry blast data may not be a representative of site classification, since the amplification function for blast data is contaminated evidently by surface wave predominant motions, especially in the low frequencies (≤ 4.0 Hz), except for the soft soil site in which the amplification ratios are dominant (even in Blast data) in low frequencies.

6. Conclusion

We did a comparison of H/V amplification functions for three kinds of seismic sources (micro-earthquakes, microtremors and quarry blasts) in Tehran region using data recorded in TDMMO network. This study presented results of an analysis of amplification factors for stations in this network. The results in the soft soil stations, i.e. Kahrizak (102), Shariati Park (001) indicated some amplification in low frequencies. A comparison between micro-earthquakes, microtremors and quarry blasts in $1.0 < f < 2.0$ Hz showed higher ratios in quarry blasts that is due to importance of surface waves that is much more effective for shallow quarry blasts than for earthquakes and microtremors.

In the case of rock sites; i.e. Jamshidiyeh (008), Vardyj (105), Hameh Sin (014), Shahrak (109), Eshgh Abaad (012) and North of Tehran Pars (010) stations, the H/V earthquake and microtremor plots showed no amplification greater than 2 in frequencies $f < 7.0$ Hz. Amplification of level was different in frequencies between 2.0 and 7.0 Hz for earthquakes, microtremors and quarry blasts. The results of site classification in Table 5 show that these six sites of TDMMO network are rock sites. Others are Velenjak (007; hard alluvium), Lapeh Zanak (016) and Soulaqan (006) to be on deep cohesionless soil condition.

Our results indicated that the spectral H/V ratio method and spectral analysis may be applied as a discrimination tool between local earthquakes and quarry blasts.

Acknowledgments

The authors appreciate the collaboration of Dr. Farzam Yaminifard at IIEES in a portion of the data studies. The data used in this study recorded by The Network of Tehran Disaster Mitigation and Management Organization (IIEES86913), which is greatly appreciated.

References

[1] Elnashai AS, Di Sarno L. Fundam Earthq Eng 2008:347.
[2] Milne J. Seismology. first Ed.. . Trench, Trube, London: Kegan Paul; 1898.
[3] Wood HD. Distribution of apparent intensity in San Francisco, in the California earthquake of April 18, 1906. ; 1908; 220–45 (Report of the State Earthquake Investigation Commission, Carnegie Institute).
[4] Wood HD. Preliminary report on the Long Beach earthquake. Bull Seismol Soc Am 1933;23:42–56.
[5] Gutenberg B. Effects of ground on earthquake motion. Bull Seismol Soc Am 1957;47:221–50.
[6] Field EH. Accounting for site effects in probabilistic seismic hazard analyses of Southern California. ; 2000; S1–31 (Overview of the SCEC phase III report 6B).
[7] Silva, WJ. Soil response to earthquake ground motion. Electric power research institute, Report No. EPRI - NP - 5747, Palo Alto, CA, USA.
[8] Sano, T and Pugliese, A. Parametric study on topographic effects in seismic soil amplification. In: Proceedings of the Advances in Earthquake Engineering , Earthquake Resistant Engineering Structures II 1999, 4, 321–330.
[9] Haghshenas E. Condition Géotechnique et alea sismique a Téhéran. [These de Doctorat]. LGIT, UJF, Grenoble, France, 2005.
[10] Haghshenas E, Bard P-Y, Jafari MK, Hatzfeld D, Ravanfar O., Preliminary results of site effects assessment in the city of Tehran (Iran) Using Earthquake and Microtremor recording In: Proceedings of the Fourth International Conference of Earthquake Engineering and Seismology, 2003.
[11] Jafari M.K, Kamalian M., Razmkhah A, Sohrabi A., North of Tehran site effect microzonation In: Proceedings of the 13th World Conference on Earthquake Engineering Vancouver, B.C., Canada, 2004; 3423.
[12] Hamzehloo H, Vaccari F, Panza GF. Toward a reliable seismic microzonation in Tehran, Iran. Eng Geol 2007;93:1–16.
[13] Aki, K. Local site effects on strong ground motion. In: Proceedings of the. Earthquake Engineering. Soil Dynamics. 1988. 103-155.
[14] Field EH, Jacob KH, Hough SH. Earthquake site response estimation: a week motion case study. Bull Seism Soc Am 1992;82:2283–307.
[15] Field EH, Jacob KH. A comparison and test of various site response estimation techniques, including three that are not reference site dependent. Bull Seism Soc Am 1995;1995(85):1127–43.
[16] Kayal JR. Microearthq Seismol Seism South Asia 2008:503.
[17] Kanai K, Osada T, Tanaka T. An investigation into the nature of microtremors. Bull Earthq Res Inst 1954;32:199–209.
[18] Nakamura Y. A method for dynamic characteristics estimation of subsurface using microtremor on the ground surface. ; 1989; 25–33 (Quarterly Report of Railway Technical Research Institute (RTRI) No 1).
[19] Udwadia FE, Trifunac MD. Comparison of earthquake and microtremor ground motions in El Centro, California. Bull Seism Soc Am 1973;63:1227–53.
[20] Sanchez-Sesma FJ, Palencia VJ, Luzo'n F. Estimation of local site effects during earthquakes: an overview. ISET J Earthq Technol 2002:167–93.
[21] Jackson J, McKenzie D. Active tectonics of the Alpine-Himalayan belt between western Turkey and Pakistan. Geophys J Roy Astron Soc 1984;77(1):185–264.
[22] Nazari, H, Ritz, JF, Salamati, R, Solaymani, S, Balescu, S, Michelot, JL, et al. Paleoseismological analysis in central Alborz, Iran. In: Proceedings of The Anniversary Earthquake Conference Commemorating the 1957 Gobi-Altay Earthquake (July–August 2007, Ulaanbaatar-Mongolia). 1-6.
[23] Sengor AMC, Altiner D, Ustaomer D, Hsu KJ. Origin and assembly of the Tehyside orogenic collage at the expense of Gondwana Land. Geol Soc Lond Spec Publ 1988;37:119–81, http://dx.doi.org/10.1144/GSL.SP.1988.037.01.09.
[24] Stocklin J. Possible ancient continental margin in Iran. In: Burke C, Drake C, editors. Geology of Continental Margins. New York: Springer-Verlag; 1974. p. 873–7.
[25] Berberian M. The southern Caspian: a compressional depression floored by a trapped, modified oceanic crust. Can J Earth Sci 1983;20:163–83.
[26] Alavi M. Tectonostratigraphic synthesis and structural style of the Alborz mountain system in northern Iran. J Geodyn 1996;21:1–33.
[27] Allen MB, Ghassemi MR, Sharabi M, Qoraishi M. Accommodation of late Cenozoic oblique shortening in the Alborz range, northern Iran. J Struct Geol 2003;25:659–72.

[28] Ritz J-F, Nazari H, Ghassemi A, Salamati R, Shafei A, Solaymani S, et al. Active transtention inside central Alborz: a new insight into the northern Iran-southern Caspian geodynamics. Geology 2006;34(6):477–80.
[29] Tchalenko JS, Braud BJ, Berberian M. Discovery of three earthquake faults in Iran. Nature 1974;248:661–3.
[30] Vasheghani-Farahani J, Zare´ M. The southeastern Tehran earthquake of 17 October 2009 (Mw=4.0). Seismol Res Lett 2011;82(3):404–12.
[31] Abbassi MR, Shabanian E. Evolution of the stress field in Tehran region during the quaternary. Tehran: International Institute of Earthquake Engineering and Seismology; 2004 (Research Report).
[32] Zaré M. Seismic Hazard Analysis for the Tehran Metropolitan Area. Tehran, Iran: International Institute of Earthquake Engineering and Seismology [Farsi]; 2004 (Research Report).
[33] Nogoshi M, Igarashi T. On the amplitude characteristics of microtremor (Part 2). J Seism Soc Jpn 1971;1971(24):26–40 (in Japanese with English abstract).
[34] Bard, P-Y. Microtremor measurements: a tool for site effect estimation?. In: Proceedings of the Second International Symposium on the Effects of Surface Geology on Seismic Motion, Yokohama, Japan, December 1998, 1999;1251-1279.
[35] Zaré M, Bard P-Y, Ghafory-Ashtiany M. Site characterizations for the Iranian strong motion network. Soil Dyn Earthq Eng 1999;18(2):101–23.
[36] Vasheghani-Farahani J, Zaré M, Lucas C. Adaptive neuro-fuzzy inference systems for semi-automatic discrimination between seismic events: a study in Tehran region. J Seismol 2012:s10950 (011-9270-7).
[37] Theodulidis N, Bard PY, Archuleta R, Bouchon M. Horizontal-to-vertical spectral ratio and geological conditions: The case of Garner valley downhole array in southern California. Bull Seism Soc Am 1996;86:306–19.
[38] Malagnini L, Tricarico P, Rovelli A, Herrmann RB, Opice S, Biella G, et al. Explosion, earthquake, and ambient noise recordings in a Pliocene sediment-filled valley: inferences on seismic response properties by reference- and non-reference- site techniques. Bull Seism Soc Am 1996;86:670–82.
[39] Vasheghani-Farahani J, Zaré M, Cichowicz A. Attenuation of high- frequency P and S waves in south and southeast Tehran using blast data. Soil Dyn Earthq Eng 2012;10:1016 (/j.soildyn.2012.03.005).
[40] Monika D. An analysis of amplification effects at selected polish seismic stations. Chapter 5. In: Idziak AF, Dubiel R, editors. Geophysics in Mining and Environmental Protection, Geoplanet, 2. Springer Verlag Berlin, Heidelberg: Earth and Planetary Sciences; 2011, http://dx.doi.org/10.1007/978-3-642-19097-1_5.

#3. Asadi Z. and Zaré M, (2014), "Estimating magnitudes of prehistoric earthquakes and seismic capability of fault from landslide data in Noor valley (central Alborz, Iran)", Natural Hazard, vol. 74, issue 2, pp. 445–461, doi: 10.1007/s11069-014-1186-4.

Nat Hazards
DOI 10.1007/s11069-014-1186-4

ORIGINAL PAPER

Estimating magnitudes of prehistoric earthquakes and seismic capability of fault from landslide data in Noor valley (central Alborz, Iran)

Zeynab Asadi · Mehdi Zare

Received: 17 August 2013 / Accepted: 12 April 2014

Abstract Detecting the paleoseismological specifications as well as seismic capability of faults has specific importance in estimating the earthquake hazard in any region. The geomorphic indices are used as indirect procedures in the mountainous area. They are appropriate and applicable methods in recognizing the specifications of active tectonics and evaluating fault seismicity in the mountainous areas. In this regard, giant landslides can be pointed out as proper indices. These landslides are usually related to tectonics and triggered by earthquakes in many cases. In this research, giant landslides existed in Noor valley (central Alborz) have been considered as geomorphological indices for recognizing the seismicity of the region and the seismic capability of its faults. There are four giant landslides in this region [illegible]

Keywords Giant landslides · Earthquake-triggered landslides · Prehistoric earthquakes · Magnitude · Noor valley · Iran

Z. Asadi (✉)
Department of Geology, Faculty of Geology, Shahid Beheshti University, Tehran, Iran
e-mail: [illegible]

M. Zare
Seismology Research Center, International Institute of Earthquake Engineering and Seismology (IIEES), Tehran, Iran
e-mail: [illegible]

Published online: 26 April 2014

1 Introduction

Estimating the seismic capability of faults as well as their governing seismicity specifications is an important factor in determining the active tectonics. Keller and Pinter (2002) have defined active tectonics as "those tectonic processes that produce deformation of the Earth's crust on a timescale of significance to human society." Therefore, the processes, related to the disruption of society within several decades to hundreds of years, are studied.

However, they should be surveyed over a much longer period (at least several thousands to tens of thousands of years) in order to study and predict the tectonic events. Accordingly, methods and evidences should be applied, which can identify the mentioned period.

Giant paleolandslides, triggered by earthquakes, as the evidences of geomorphology and paleoseismology can indirectly offer effective information of the region. They are also used as a powerful method in assessing the seismic capability of faults. Giant landslides are mostly located in the mountain ranges with high seismic potential and active tectonic specifications. As they are related to the quaternary fault zones and their relevant earthquakes, giant landslides can indicate the seismicity of the region.

In active mountain ranges, landslides in general and giant landslides in particular are important erosion processes (Pinto et al. 2008). In tectonically active regions, the created uplift along with existed joints and faults can provide critical conditions for occurring landslides. On the other hand, earthquakes that are the aftermath of active tectonics can also trigger giant landslides. Therefore, giant landslides can be used as the indicator of seismicity and tectonic activity of the region. They are triggered by earthquakes and most probably occurred because of structural reasons. These giant landslides can be considered as the prerequisites for finding active faults and their seismic capabilities.

Giant landslides usually are of high volumes up to tens of km^3 (Pinto et al. 2008), the different samples of which have been reported in the world. Saidmarreh landslide with 20–30 km^3 volume in the southwest of Iran occurred in prehistoric times (Harrison and Falcon 1938); Tsergo Ri landslide (100 km^3) in the Langthang valley of northcentral Nepal, about 40 ka ago (Ibetsberger1996); and Bogd giant paleolandslides (20 $\times$ 15 km^2) in Mongolia (Philip and Ritz 1999). Korup et al. (2007) compiled regional and global lists of existed landslides in their studies and presented a file including over 300 landslides happened on the ground. The inventory of Korup et al. (2007) includes particularly the giant and terrestrial landslides in kilometer-scale, having the areas of 10^0–10^3 km^2 and minimum volumes of 0.1 km^3. Moreover, their giant landslides are mostly located in the deep incised and glaciated valleys, that is, in the average height. Other regions in which these landslides are probably occurred are flanks of volcanoes, escarpments, fault-bounded mountains, and around active major faults (Korup et al. 2007). Locating in the mentioned regions indicates close and effective relationship between giant landslides and tectonics. About 75 % of giant landslides, presented in the Korup et al. (2007) inventory, have occurred in the major orogenic belts such as European Alps, Caucasus, Himalayas, Pamir, Tien Shan, American Cordilleras, Papua New Guinea, and Southern Alps of New Zealand. In this research, the relation between giant landslides and structural conditions of the region is shown better than ever.

In this regard, it is very important to determine earthquake-triggered giant landslides. Crozier (1992) listed six criteria for detecting the seismic sources triggering these landslides:

1. Ongoing seismicity in the region
2. Coincidence of landslide pattern with an active fault or seismic zone

3. Geotechnical analysis of slope stability showing the necessity of earthquake in triggering the slope failure
4. Large sizes of landslides
5. Liquefaction aftermath associated with the landslides
6. Insufficiency in explaining the landslide distribution only based on geological and geomorphological conditions.

These six criteria, or the least three of them, have been used to define the seismic originality of landslides, Crozier (1992). For example, Philip and Ritz (1999) and Pinto et al. (2008) have followed these criteria in their investigation, regarding the mentioned objective.

Noor valley is located in central Alborz in the north of Iran (Fig. 1a) with the coordinates are from 36°05′N to 36°15′N in latitude and from 51°20′E to 52°20′E in longitude (Vahdati Daneshmand 2000) (Fig. 1b). The Alborz mountain chain extends for several hundreds of kilometers between the Caspian Sea and the Iranian Plateau. The tectonic activity in the Alborz mountain range, northern Iran, is due both to the northward convergence of central Iran toward Eurasia and to the northwestward motion of the South Caspian Basin with respect to Eurasia inducing a left-lateral wrenching along this range. These two mechanisms give rise to an NNE–SSW transpressional regime, which is believed to have affected the entire range for the last 5 ± 2 m.y. (Ritz et al. 2006). Therefore, Noor valley have special tectonic situation in this regime. For example, Noor valley is a long straight valley surrounded with the major central Alborz faults and in the middle of this valley, its straight shape is deviated into S-shaped curve. In fact, in the large scale, changing the direct trend in the central part of valley gives the S-shape to the valley, which indicates the changing trend in the middle of valley. In this scope, the regime performance of the region has made such changing trend in the valley. In addition to the presence of numerous intensive faults in this valley can show one of the marks of transpressional regimes in the central Alborz. Therefore, historical giant paleolandslides in Noor valley can be used as indirect geomorphic indices for the identification of paleoseismicity of this area.

Considering this issue will be more important when no research with this perspective has been conducted in the crucial scope of Noor valley. This research attempts to create a relation between paleoseismology and geomorphic indices of the region. Therefore, the large old landslides which have been triggered by earthquake have been used for identifying the causative earthquakes in this region.

3 Methodology

Noor valley has a unique position in geology for its giant landslides. The straight and active valley in central Alborz and in the vicinity of several faults has provided the appropriate situation for occurring such landslides. Therefore, giant paleolandslides can be considered as geomorphic indices in Noor valley.

Geomorphic indices are useful tools in the evaluation of active tectonics because they can provide rapid insight concerning specific areas (Keller 1986). The earthquake hazard for particular area problems associated with deriving rates of faulting and study of prehistoric earthquake for the Pleistocene and Holocene (Keller and Rockwell 1984). In fact, geomorphic indices are capable of detecting landform responses to tectonics and therefore have been broadly used to investigate tectonic geomorphology (e.g., Brookfield 1998; Keller and Pinter 2002; Chen et al. 2003; Kobor and Roering 2004; El Hamdouni et al.

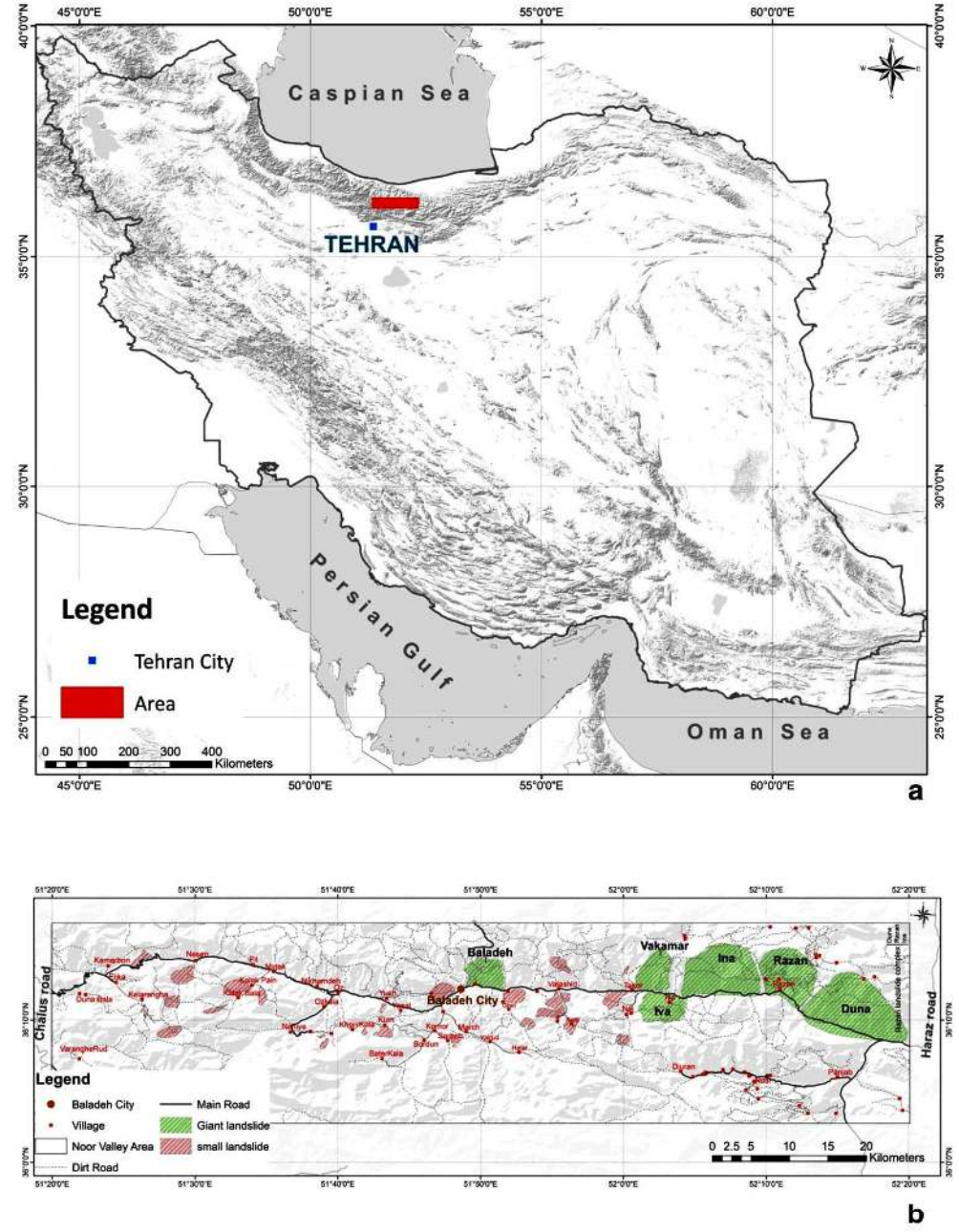

Fig. 1 **a** Map of Iran showing the location of Noor valley. **b** Noor valley and giant landslides

2008), and some indices are particularly useful for identifying relative tectonic activity (Gao et al. 2013). Therefore, it provides an indirect scale for tectonic studying of the region, which is used in this research.

We identified, traced, and described giant paleolandslides in Noor valley through field observations and remote sensing. In this research, we used aerial photograph (1:50,000 scale) and satellite images such as LANDSAT 7 Enhanced Thematic Mapper Plus (ETM^{+}), PAN band of IRS satellite.

Satellite images and remote sensing are devices that can be used in the large and mountainous regions to provide appropriate views about their conditions. In this research, satellite images (ETM+) with regional perspective have been considered as the most appropriate and accessible ones. For preparedness of images, their geo-references have been done in a degree system and geometric correction has been conducted in the next stage. Then, these satellite images have been reviewed for identifying large landslides. In order to control the obtained results, landslides, identified by satellite images and aerial photographs, have been reviewed in field studies. It should be mentioned that these studies have been continued and repeated up to total identification of the large landslides in the region.

The giant landslides, in the occurrence of which the tectonical elements have played significant roles, are used to identify the seismicity and paleoseismicity of Noor valley. The triggering earthquake magnitude has been determined based on empirical correlation with the volume of associated landslides (Nepop and Agatova 2008). The causative fault, probably triggered the earthquake, has also been identify concerning the distribution of giant landslides (Zare et al. 2009).

3 Geological setting

The Alborz range of northern Iran is a region of active deformation within the broad Arabia–Eurasia collision zone (Allen et al. 2003; Alavi 1996; Ritz et al. 2006). Noor valley is located in north of Iran in the geographical coordinates of 36°05′N–36°15′N and 51°20′E–52°20′E. This valley, locating in the northwest of Damavand volcano between Haraz and Chalus roads, is one of the largest central Alborz valleys (Fig. 1b). This is a straight valley with east–west trend that is S-shaped in its middle. There are also several intrusive units in the middle of the valley such as Golpir and Sefid-Kuh units (Fig. 2). These properties (intrusive units and S-shaped curvature) show the transtension regime of central Alborz. According to Ritz et al. (2006), transpressional regime of central Alborz is young and has been formed since 1–1.5 m.y, simultaneously with the last activity of Damavand volcano (700,000 years to 1.8 m.y ago). In Noor valley, the lithological compositions of quaternary volcanic rocks are varied with their ages. These rocks are of two age categories: (1) the trachytes are mainly contemporary with the late trachyandesite–trachyte lava of Damavand volcano; (2) the rhyolites are significantly younger, comparing with trachytes, and their chemical compositions are similar to acidic dykes of Taleghan region. Concerning their identified ages, the intrusive units can be used as proper tools for computing the relative ages of landslides.

Fig. 2 **a** The Golpir trachyte unit in the Mazid village. **b** The Sefid-Kuh rhyolite unit in the Baladeh city

3.1 Stratigraphic frameworks

This valley has diverse positions from point of stratigraphic view (Fig. 3). In the regional scales, Paleozoic units are bounded between Angas and Zanus thrust faults in the north of Noor valley. In a wider perspective, the Palaeozoic units have an outcrop, confined between Engas and Zanoos thrusts, in the north of Noor valley. A part of this outcrop is shown in Fig. 3. The north of this valley is a part of central Alborz in which the expansion of stratigraphic units is outstanding (Saidi and Ghasemi 2002).

The stratigraphic expansion of the valley mostly belongs to Mesozoic era. In other words, Noor valley has been incised in Shemshak formation by Noorrud River. In all, the deposits of Shemshak formation consist of relatively homogeneous shale and sandstone with having coals as one of their features (Aghanabati 2000). Shemshak formation has different facies in Noor valley zone. These units cannot be distinguished due to their lithological differences, and therefore, they are generally referred as Shemshak formation. In the south of Noor valley, stratigraphic units are related to Cenozoic era (Karaj formation) and are the most widespread units there (Fig. 3).

3.2 Faults

This valley is bounded by faults of North Alborz and Khazar with the dip direction toward south in the north, Mosha and Kandovan faults with the dip direction toward north in the south (Fig. 4). Thrust faults are the most important structural active in Noor valley region like other parts of central Alborz (Saidi and Ghasemi 2002). Thrust faults with dip direction toward south are of more importance thrusts comparing to others. However, normal and right-lateral faults are subordinately seen along with other fault thrusts in the region (Saidi and Ghasemi 2002). Baladeh thrust fault, which is spread all over valley, has the approximate east–west trend with the dip direction toward north. Also, there are several thrusts in the south of Baladeh thrust fault such as Azadkooh, Kandovan, and Frakhin with the dip direction toward south and Mishchalak and Varangerood with the dip direction

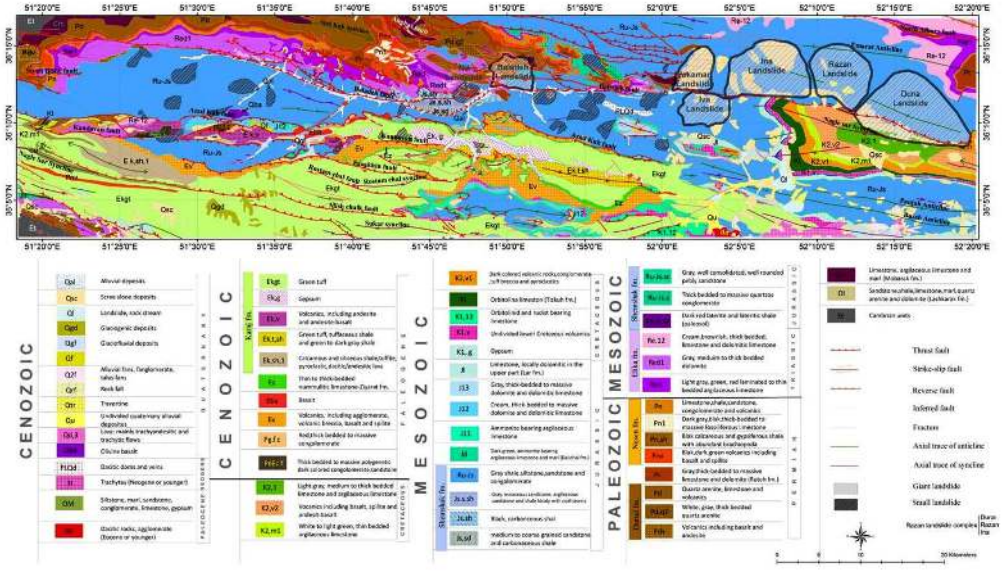

Fig. 3 Geological map of study area

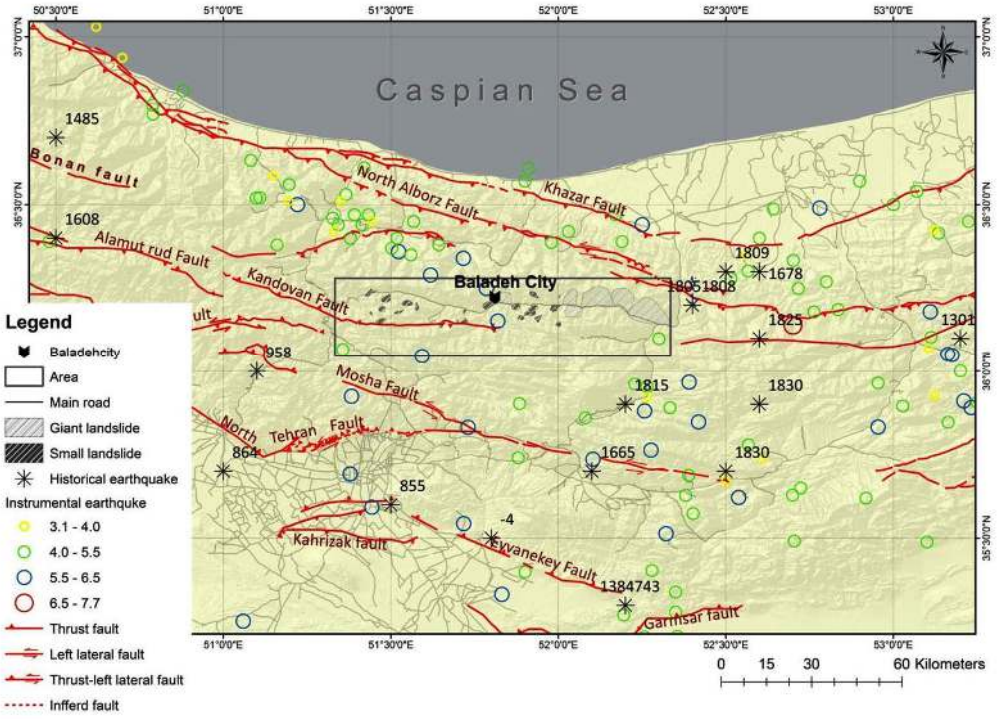

Fig. 4 Map of central Alborz with major faults and earthquakes showing the location of giant landslides in the study area

toward north. There are also several thrusts in the north of Baladeh fault thrust such as Zanoos fault with the dip direction toward south and Angas fault with the direction toward north (Fig. 3) (Saidi and Ghasemi 2002).

3.3 Seismicity

The Alborz Mountains represent a composite orogenic belt that underwent shortening and uplift during the Tertiary (Alavi 1996). Roughly 50 % of the $\sim$20 mm year^{-1} N–S convergence between Arabia and Iran (Vernant et al. 2004) is accommodated in the Alborz region, between the southern Caspian and central Iran. Noor valley is the central part of the central Alborz.

Central Alborz has experienced several earthquakes during the years (Fig. 4). Based on the distribution of historical earthquakes, no important historical event has been reported around Noor valley (Fig. 4) (Ambraseys and Melville 1982; Berberian and Yeats 2001). Nevertheless, the distribution of instrumental earthquakes indicates the high seismicity of central Alborz.

However, the crucial importance of this valley is referred to its approximately 70 km north distance from Tehran, the capital of Iran. Tehran, with about 12 million inhabitants, is widely considered as one of the most vulnerable region on the earth (Ebrahimi and Hassan 2013; Capital Cities of the World 2012).

4 Giant paleolandslides in Noor valley

Landslides are of ordinary in the mountain ranges (Pinto et al. 2008). We have identified several giant landslides in Noor valley including Razan, Iva, Baladeh, and Vakamar. These landslides and their properties have been listed in Table 1.

Table 1 Giant landslides were identified in Noor valley

Name	Size (km)	Area (km²)	Volume (km³)	Location		Classification	
Razan	6.74 × 20.9	≈ 167.82	–	52.26	36.18	Doab	10.06 × 8.45
				52.19	36.13	Razan	8.27 × 4.06
				52.1	36.23	Ina	7.51 × 6.82
Baladeh	4.01 × 4.05	16.4	≈ 0.1	51.89	36.14	–	
Iva	3.75 × 4.5	16.93	≈ 0.08	52.04	36.19	–	
Vakamar	3.25 × 5	16.14	–	52.03	36.22	–	

Razan landslide complex is located in the east of Noor valley at the beginning of Baladeh road (Fig. 1b, 8) and is divided into three landslides, Doab, Razan, and Ina landslides (Table 1; Fig. 1 b). This complex is strongly eroded (Fig. 5a) and probably had blocked the river in the past.

Iva landslide is younger comparing to Razan and other giant landslides identified in Noor valley. This landslide is located in southern hillside of the valley (Fig. 1b). One of the most important characteristics of Iva landslide is the existence of widespread slip scarp in different levels (Fig. 6).

Baladeh landslide is located in northern hillside of Noor valley and north of Baladeh city (Fig. 1b), in a complex tectonic region. As mentioned earlier, the linear trend of the valley with east–west direction is diverted to S-shape in Baladeh city, in the middle of the valley, showing a complex tectonic condition (Fig. 3).Sharp slip scarp can be identified in the Baladeh landslide as well (Fig. 7). Another giant landslide in northern hillside of Noor valley is called Vakamar (Fig. 1b), which is as old as Razan complex.

According to the large landslides and active tectonics of Noor valley, the earthquakes are the most important probable reasons, which trigger giant landslides in this region. The distribution of landslides between fractures and thrusts shows the correlation between landslides and tectonics in this valley.

North Alborz fault is one of the important faults in central Alborz. The nearest distance between its strike and Noor valley is seen in the east of the valley (Fig. 4). Furthermore, the distribution of giant landslides along the most important fault in Noor valley, Baladeh fault, shows the importance of this fault. Vakamar, Iva, and Razan landslides are located between Baladeh thrust and North Alborz fault. Iva landslide is placed between Baladeh fault and Azadkuh fault strike (Fig. 3). According to the dip direction of Baladeh fault toward north and that of North Alborz fault toward south, the mentioned giant landslides are located in hanging wall of Baladeh fault, which is very important.

In general, giant paleolandslides are eroded, and therefore, their recognition is difficult in the field. In Noor valley, giant landslides are ancient and eroded; that is, evidences have mostly been disappeared. Nevertheless, the ancient giant landslides have been recognized in Noor valley. They have been categorized into three groups according to the classification presented by Mather et al. (2003) (Table 2) as follows:

1. Iva landslide that would be described as "dormant–young" with the age of 100–500 years (Late Holocene);
2. Baladeh landslide that would be defined as "dormant–mature" with the age of 5,000–10,000 years (Early Holocene);
3. Razan landslide complex and Vakamar landslide would be mentioned as "dormant–old" with the age of 10,000–100,000 years (Late Pleistocene).

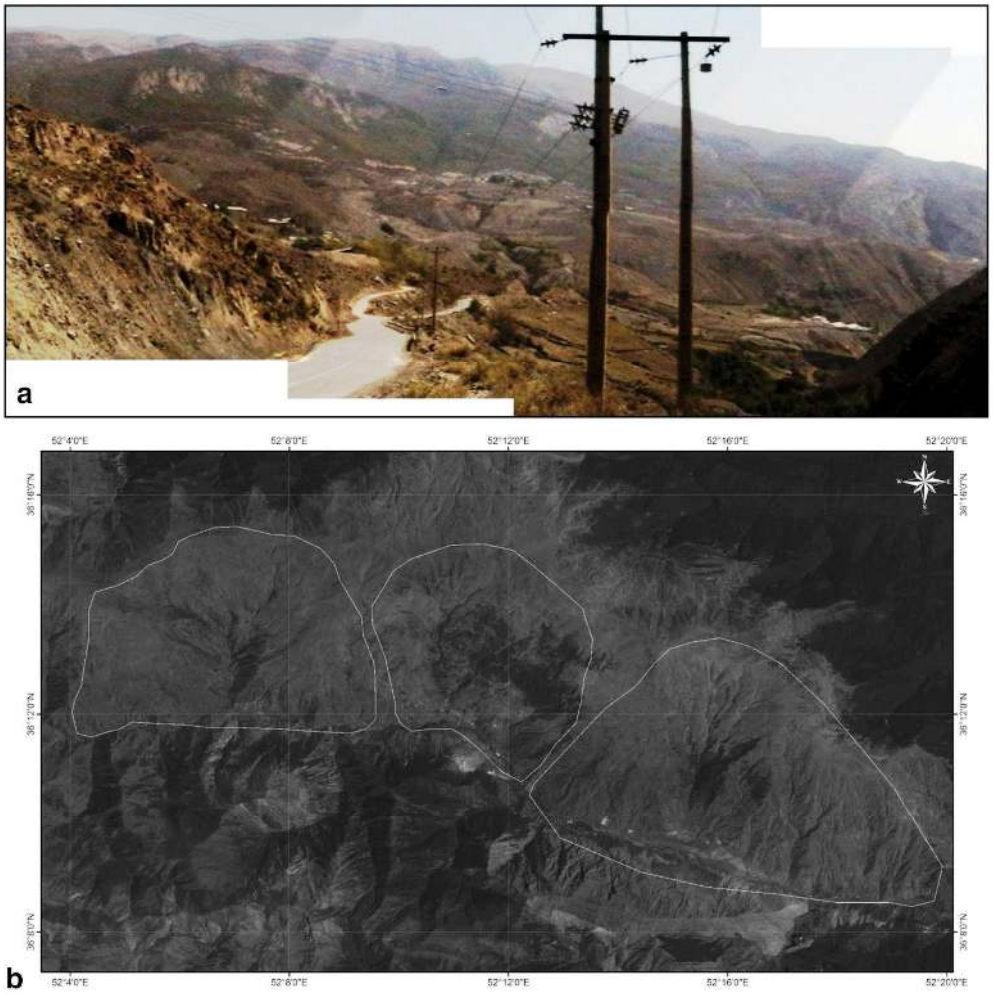

Fig. 5 **a** Part of Razan landslide complex in the field. **b** Razan landslide complex divided into three landslides, Doab, Razan, and Ina landslides in Band 7 ETM^{+}

In addition to the above classification, the determined relative ages can be controlled by using the intrusive units, explained earlier in this paper. The relatively large Nif landslide, listed in the small landslides of the valley (Asadi et al. 2009), is located in the west of Baladeh landslide (Fig. 3). The outcrop intrusive unit of Sefid-Kuh is observed in this landslide. Nif and Baladeh landslides are of the same age. The existence of pyroclastic pieces of rhyolitic tuff of Sefid-Kuh in the Nif landslide shows both slides were occurred after Nif landslide.

5 The application of these landslides in paleoseismology

Large size of these valley landslides and the location of this valley in an active tectonic region are evidence showing these giant landslides have been triggered by earthquakes. In order to do paleoseismological analysis, it seems to be highly necessary that the landslides have been triggered by seismic activity. Nevertheless, there are four out of six

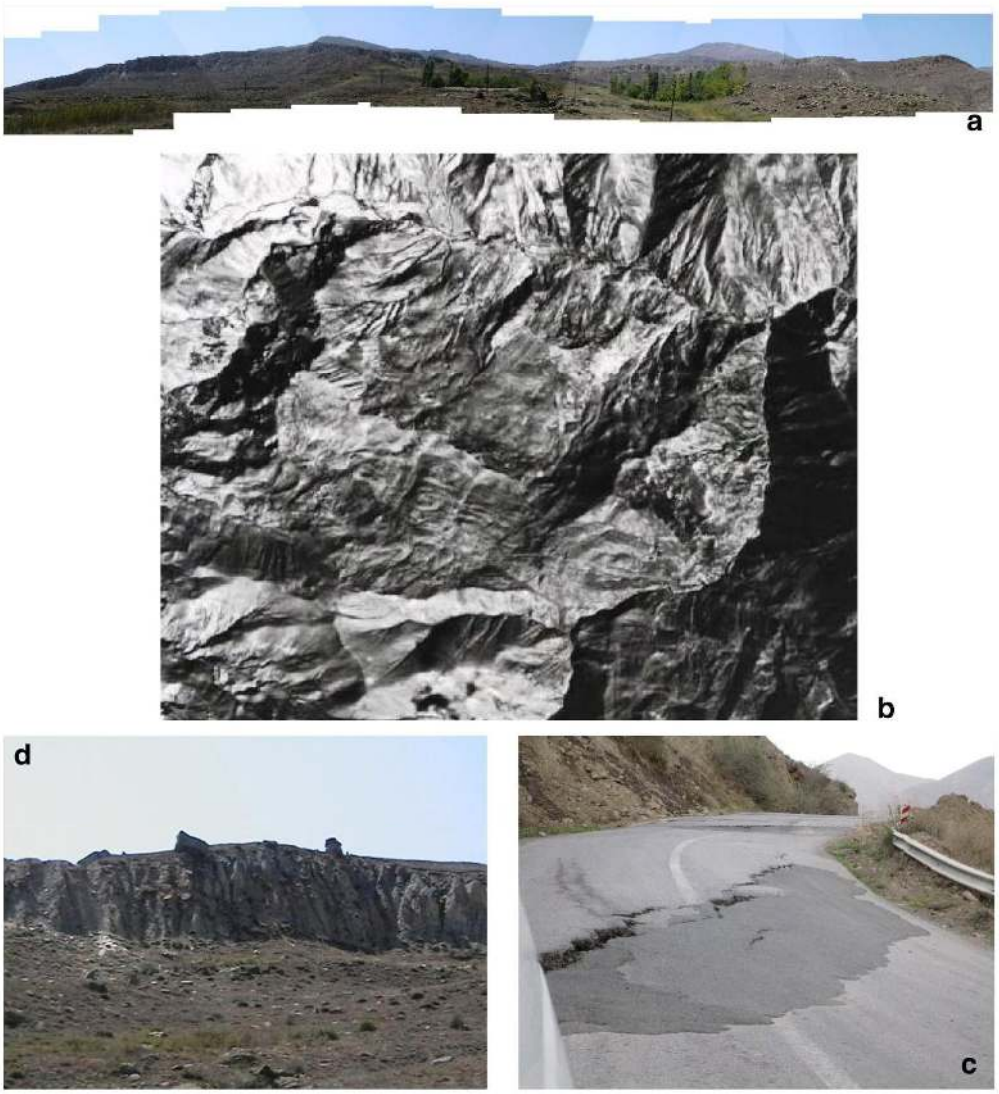

Fig. 6 **a** Widespread slip scarp in different levels in Iva landslide. **b** The Iva landslide in aerial photograph (1:50,000 scale). **c** A close-up of slip scarp in Iva landslide. **d** Iva landslide is younger comparing to other giant landslides identified in Noor valley and influence in Baladeh road

criteria, defined by Crozier (1992), have been used to explain that the origin of these giant paleolandslides is earthquake. These criteria are as follows:

1. Ongoing seismicity in central Alborz;
2. The spatial relationships between the patterns of landslides and active faults in Noor valley;
3. Large size of landslides;
4. Insufficient explanation landslide distribution only on the basis of geological and geomorphological conditions.

The presence of these four factors has been presented in this research previously. For example, the seismicity of the region has been represented in Fig. 4. The Figs. 3 and 8

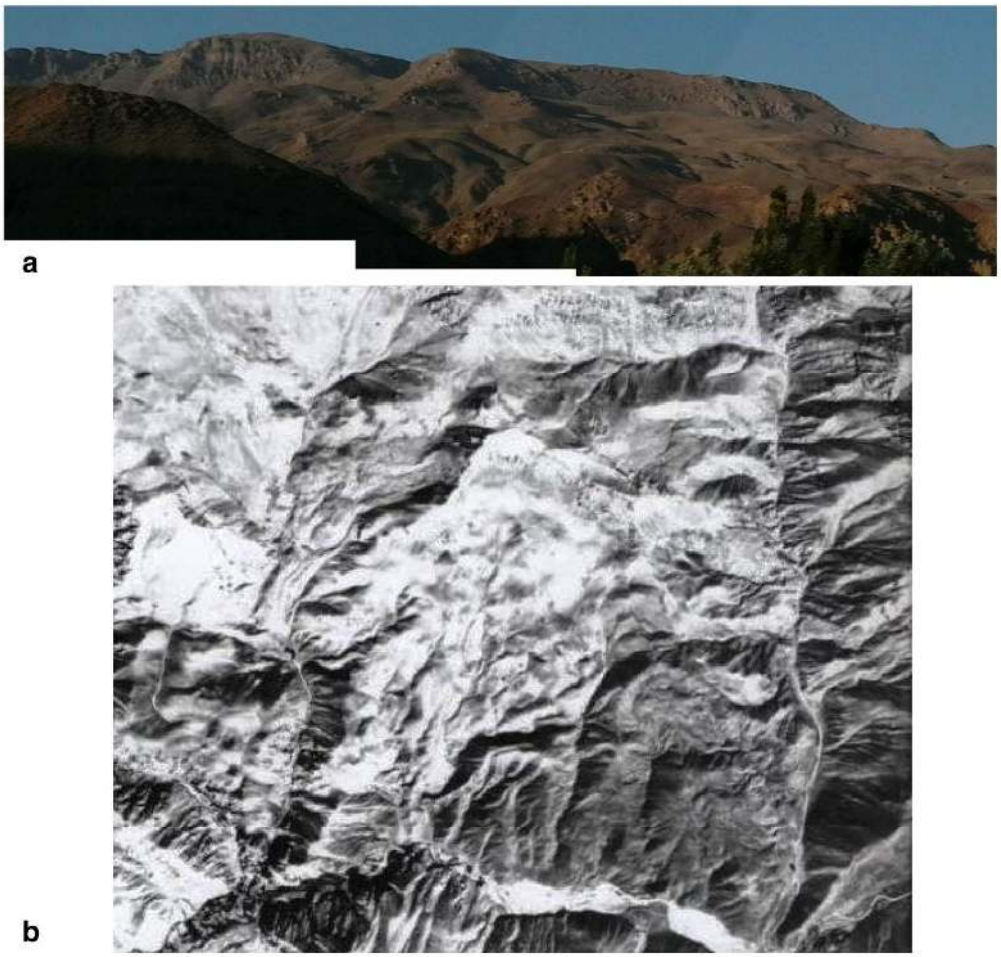

Fig. 7 **a** Slip scarp in Baladeh landslide. **b** The Baladeh landslide in aerial photograph (1:50,000 scale)

show the close relation between the structures of the region and these large landslides. The dimensions of large landslides are shown in Table 1. Geological map (Fig. 3) and slope specifications have been shown that the occurrence of the slides is not a slope unstable and therefore the structural reasons are effective in its happening.

Therefore, large size of landslides as well as the faults existed in the region would be sufficient to claim that the mentioned landslides have triggered by earthquakes. Therefore, the giant landslides of Noor valley, triggered by earthquake, have been used as the indices of geomorphology for identifying the seismicity of the region.

Keefer (1984) investigated the distribution of landslides as well as the magnitude of triggering earthquakes. According to his study, the landslide distribution (small landslides) is as they move away from epicenter. The earthquakes have probably occurred in the vicinity of Noor valley. Regarding the very large sizes of landslides, high energy is need for triggering them. However, most importantly, the giant landslides of Noor valley are probably very older than prehistoric and historic earthquakes of the central Alborz. The ages of Noor valley landslides have been mentioned earlier in this paper.

Based on the available data in the current study, it suggests that probably one or more earthquakes have occurred, but not recorded in the earthquake catalog of the central

ndslides (Mather et al. 2003)

	of causes of	Condition of main scarp			
	ement and active	Sharp; unvegetated	Sharp at e		
	ement and likely to	Sharp; unvegetated	Sharp at e		
	ement still and could re-	Relatively sharp; partially vegetated	Relati veg fed by flow of the		
	ement still but not likely	Smooth; vegetated	Smoo stre flow of th		
	ement may but associated nt climatic or gical	Dissected; vegetated	Vagu late		
	ement t associated nt climatic or gical	May not be identifiable; likely to be at least partially if not completely removed by erosion	May to be com ero		

covered by subsequent deposits

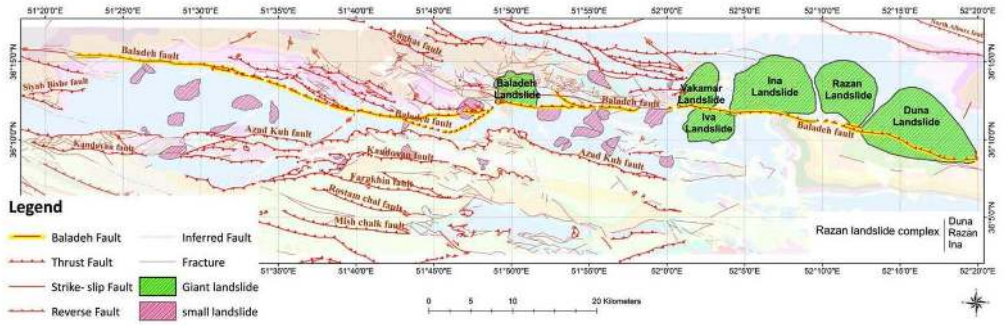

Fig. 8 Baladeh fault and other faults in Noor valley

Alborz. These earthquakes have been out of the age range of prehistoric and historic earthquakes of central Alborz and triggered the giant landslides of the valley.

5.1 Estimating magnitudes of triggering earthquakes by landslide data

Evaluating the volume of landslides is essential for estimating the magnitude of triggering earthquake in Noor valley. Old and giant landslides are not the ones that would happen in any region as mentioned in the introduction section according to Korup et al. 2007. Their giant landslides are mostly located in the deep incised and glaciated valleys, that is, in the average height. Other regions in which these landslides are probably occurred are flanks of volcanoes, escarpments, fault-bounded mountains, and around active major faults (Korup et al. 2007).

Area, Gorny Altai, that Nepop and Agatova 2008 have been offered an empirical correlation is tectonically active. Gorny Altai is the northern part of the Altai neotectonic uplift that belongs to the central Asian mountain belt. The Altai region is an active seismic area, and its seismicity has been largely studied (e.g., Chernov 1978; Masarsky and Moiseenko 1962; Moiseenko 1969a, b; Muchnaya 1975).Most of the area is located at elevations higher than 2,000 m. Axial parts of the ranges often exceed 3,500 m. (Lunina et al. 2008).The average height of Alborz mountain is 3,000 m, and the Alborz mountain range shows strong tectonic activity with several destructive earthquakes in the past (Berberian and Yeats 2001). Therefore, the occurrence of large landslides in the mountainous regions with high height and active tectonic can present similarity minimum to use the formula for both regions.

It is generally difficult to estimate the volume of active contemporary landslide. Therefore, while its remnants have been eroded, evaluating the total volume of a very old landslide is hypothetic and probabilistic (Mather et al. 2003). Cruden and Varnes (1996) suggested that in many rotational landslides, the surface of rupture is mid-ellipsoid shape. The volume of giant landslides is calculated in Noor valley through Eq. (1), presented by Mather et al. (2003).

$$\text{Volume} = 0.1667\ \pi D_r W_r L_r. \tag{1}$$

where D_r—depth of surface of rupture (m), W_r—equivalent surface width of surface of rupture (m), L_r—equivalent surface length of surface of rupture (m), so volume is "m^3."

In this study, volumes for all giant landslides have not been calculated in Noor valley. Only the volumes of Baladeh and Iva giant landslides have been estimated based on Eq. (1), because of measuring the depths of their rupture surfaces (D_r). In fact "D_r" is the

height of slip scarp and is measurable only in these landslides. The measured D_r values are 10–15 m in Iva landslide (20 m in its certain parts) and 15–20 m in Baladeh. W_r and L_r have been measured based on the satellite images and aerial photographs and presented in Table 1. The volumes of Baladeh and Iva giant landslides have been calculated through Eq. (1) as 0.08–0.17 and 0.1 km^3, respectively. As the volume in Eq. (2) is in the form of km^3, the volume obtained in Eq. (1) is converted to km^3.

Nepop and Agatova (2008) have been offered an empirical correlation between the earthquake magnitude and the volume of associated landslides. The applicability of this relationship in the Altai region has been controlled with the data of Chuya earthquake (2003), with the magnitude of $M = 7.5$. The magnitudes of paleoearthquake, derived from landslide volumes, have minimum values (Nepop and Agatova 2008). The key point of the method is geomorphic analysis of expressed surface displacement (slope failure or fault scarps) of evidently seismic origin. The sizes and patterns of prehistoric and historic ground failures directly imply the relation between strong motions and the mass volumes of the occurred landslides (Nepop and Agatova 2008), presented in Eq. (2).

$$\mathrm{Log}V_{\mathrm{Lmax}} = 1.36M - 11.58(\pm 0.49) \tag{2}$$

where V_{Lmax} is the volume of largest landslide (km^3). According to Eq. (2), the magnitudes (M), estimated for triggering earthquake of Baladeh and Iva giant landslides, are 7.7 ± 0.49 and 7.9 ± 0.49, respectively.

The estimated earthquake magnitude confirms the seismicity of central Alborz as this value has been recorded previously there. Tchalenko (1974) identified seismotectonic units in central Alborz based on its seismicity in the twentieth century. Tchalenko (1974) has pointed out that the occurrence of the earthquake is in a zone coincided with calmness in another region.

Concerning the Tchalenko's seismotectonic units, Noor valley is located in the northern hillside of northwest of Alborz and a small part of this valley is in the southern hillside of southwest part. Manjil earthquake (1990) with $M = 7.7$ in the northern hillside of northwest part and Gumes earthquake (856) with $M = 7.9$ in the eastern Alborz have occurred previously in Alborz. Therefore, it is probable that such earthquakes have happened in Noor valley as well.

5.2 Causing earthquake faults

According to Keefer (1984) as well as the current study, an earthquake should have occurred around this valley for triggering its giant landslides. As mentioned above, the nearest distance between strike of North Alborz fault and Noor valley is shown in the east of the valley. Therefore, this fault can probably be considered as causative fault. However, concerning the linear distribution of giant landslides along the most important fault of Noor valley (Baladeh fault) shows the effect of mentioned fault in the occurrence of landslides triggering earthquakes in this region.

Triggering earthquakes may occur along the faults not located around of Noor valley, as well. However, the available evidences confirm the more significant roles of the faults placed in the valley. Concerning their large sizes, these landslides need high energy to be triggered. Besides, the linear distribution of giant landslides along Baladeh fault indicates that the eastern segment of Baladeh fault probably causes an earthquake that triggers giant landslides (Fig. 8).

One of the most pressing issues is identifying causative fault in paleoearthquakes. According to the geological evidences, the eastern segment of Baladeh fault is probably the source of an earthquake that triggers the giant landslides in Noor valley. However, other faults such as North Alborz fault and the others in central Alborz should not be ignored in triggering giant landslides.

Estimating this magnitude for Baladeh fault can deform the analysis of probable maximum magnitudes of the region faults. The magnitude is estimated as 7 for a fault with 100 km length, based on the empirical relation between length–magnitude. Similarly, the probable maximum magnitudes have been estimated as 7 for the faults of Mozafarabad region concerning the length–magnitude relation. The occurrence of largest earthquake with 7.8 magnitude in the region (Zare et al. 2009) has confirmed the insufficiency of length–magnitude relation in the determination of magnitude. Therefore, using other approaches, which present new analyses, is necessary and applicable. The method, applied in this research, can estimate the probable earthquake magnitudes of the region using the geomorphic indices (giant landslides). This can be very effective in identifying the faults of the region.

6 Conclusion

In this research, giant landslides, geomorphic indices, have been used as paleoseismology indirect method in Noor valley. They have been trigged probably by one or more earthquakes in Noor valley. These landslides are located in the tectonically active region with active faults and ongoing seismicity in the central Alborz. According to the classification of Mather et al. (2003) and relative age dating, the ages of landslides have been determined as Late Holocene, Early Holocene, and Late Pleistocene. Based on an empirical correlation between the earthquake magnitude and the volume of associated landslides, the estimated earthquake magnitude of Baladeh and Iva giant landslides is measured as 7.7 ± 0.49 and $0.7.9 \pm 0.49$, respectively. Finally, the distribution of giant landslides along Baladeh fault shows that probably the eastern segment of Baladeh fault triggered giant landslides in this valley (Fig. 8).

References

Aghanabati A (2000) Geology of Iran. Geological survey of Iran, Tehran

Alavi M (1996) Tectonostratigraphic synthesis and structural style of the Alborz mountain system in Northern Iran. J Geodyn 21(1):1–33

Allen MB, Ghassemi MR, Shahrabi M, Qorashi M (2003) Accommodation of late Cenozoic oblique shortening in the Alborz range, northern Iran. J Struct Geol 25:659–672

Ambraseys NN, Melville CP (1982) A history of Persian earthquakes. Cambridge University Press, London

Asadi Z, Poorkermani M, Zare M (2009) Active tectonics of Noor valley (central Alborz). Dissertation, University of Shahid Beheshti, Iran

Berberian M, Yeats R (2001) Contribution of archaeological data to studies of earthquakes history in the Iranian plateau. J Struct Geol 23:563–584

Brookfield ME (1998) The evolution of the great river systems of southern Asia during the Cenozoic India-Asia collision: rivers draining southwards. Geomorphology 22:285–312

Capital Cities of the World—with population. http://www.worldatlas.com/capcitys.htm#.UtzUAdLLaMZ [Online]

Chen YC, Sung Q, Cheng KY (2003) Along-strike variations of morphotectonic features in the Western Foothills of Taiwan: tectonic implications based on stream gradient and hypsometric analysis. Geomorphology 56:109–137

Chernov GA (1978) Seismogeological and neotectonic studies in the Altai-Sayan area. In: Solonenko VP, Nikolaev VA (eds) Seismogeology of the Eastern Altai-Sayan Area. Nauka, Novosibirsk, pp 6–27 (in Russian)

Crozier MJ (1992) Determination of palaeoseismicity from landslides. In: Bell DH (ed) Landslides (Glissements de terrain). International Symposium, Christchurch, New Zealand. Balkema, Rotterdam, pp 1173–1180

Cruden DM, Varnes DJ (1996) Landslide types and processes. In: Turner AK, Schuster RL (eds) Landslides, investigation and mitigation. Transportation Research Board Special Report, vol 247. National Academy Press, Washington, pp 36–76

Ebrahimi S, Hassan M (2013) Whatever happened to urban knowledge in downtown Tehran? Effects of rural domination of urban society. http://www.worldcapitalinstitute.org/makciplatform/2013-tehran-iran [Online]

El Hamdouni R, Irigaray C, Fernández T, Chacón J, Keller EA (2008) Assessment of relative active

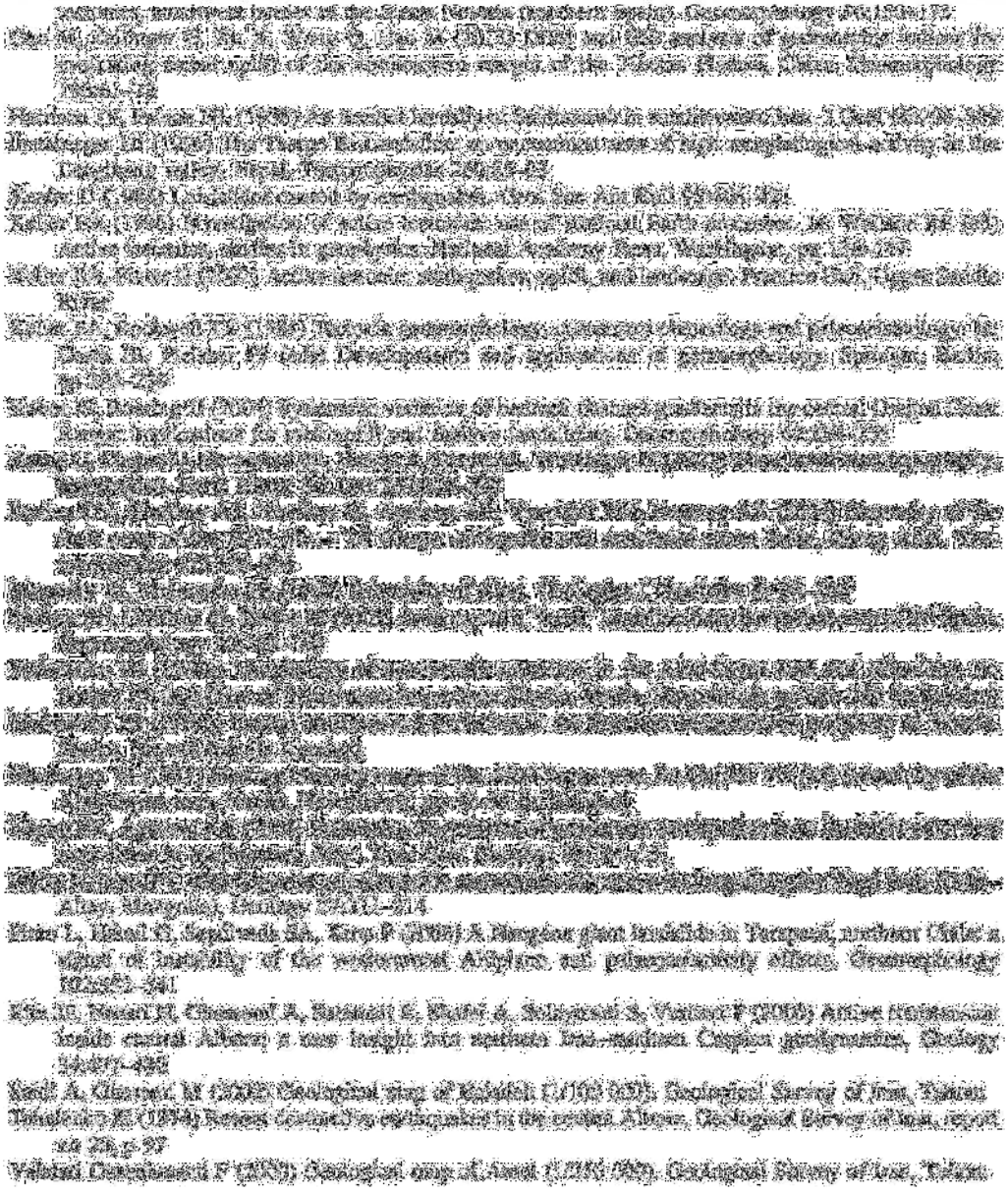

Vernant Ph, Nilforoushan F, Chéry J, Bayer R, Djamour Y, Masson F, Nankali H, Ritz JF, Sedighi M, Tavakoli F (2004) Deciphering oblique shortening of central Alborz in Iran using geodetic data. Earth Planet Sci Lett 223:177–185

Zare M, Karimi-Paridari S, Lisa M (2009) An investigation on Balakot, Muzaffarabad (Pakistan) earthquake, 8 Oct. 2005, Mw 7.6; geological aspects and intensity distribution. J Seismol 13:327–337

#4. Zaré M. and Hamzehloo H., (2005), "Strong motion study on bam earthquake of 26 December 2003", Earthquake Sspectra, vol. 21, no. s1, pp. s165–s179.

Strong Ground-Motion Measurements During the 2003 Bam, Iran, Earthquake

Mehdi Zar ,[a] M.EERI, and Hossein Hamzehloo[a]

The Bam earthquake of 26 December 2003 (M_w 6.5) occurred at 01:56:56 (GMT, 05:26:56 local time) near the city of Bam in the southeast of Iran. Two strong phases of energy are seen on the accelerograms. The first comprises a starting subevent with right-lateral strike-slip mechanism located south of Bam. The mechanism of the second subevent was a reverse mechanism. [DOI: 10.1193/1.2098307]

RECORDED STRONG GROUND MOTIONS

The strong motions of this event were recorded at 23 stations of the national Iranian Strong Motion Network (according to Building and Housing Research Center, BHRC web site, 2004; Figure 1a). The strong motion records were studied and processed and these preliminary results are presented based primarily on the main shock and aftershock records obtained at Bam station (Figure 1b). All of the strong motion data obtained during the Bam earthquake were recorded by digital Kinemetrics SSA-2 accelerographs. The attenuation of the strong motion was studied based on the records with good signal-to-noise ratio at six stations. The isoseismal map of the region is presented based on the site visits.

STRONG MOTION DATA PROCESSING

The record obtained at Bam station (Figure 2)—after band-pass filtering between 0.11 and 40 Hz—shows a PGA of 775 and 623 cm/sec2 for the east-west and north-south horizontal components, respectively, and 992 cm/sec2 for the vertical component. This processing was performed based on the estimation of the signal-to-noise ratio (Figure 3). The Fast Fourier transformation (Figure 4) shows more energy at longer periods for the fault-normal horizontal component.

A comparison of the H/V ratio obtained at Bam station during the main shock and 13 aftershocks, which occurred in the first 24 hours after the earthquake (Figure 4) shows very low-frequency amplification between 0.1 and 0.2 Hz, which is evident in the main shock, but not evident in the aftershocks. This may be taken as evidence for the vertical directivity effect (Lay and Wallace 1995). This vertical directivity might be explained in the Bam earthquake by rupture propagation from depth to the surface, with an inclination towards the north. A strong fault-normal (east-west) motion was created during the main shock as well. The demolished walls and buildings of Bam are representative of such effects in the up-down (vertical) and east-west directions (fault-normal). The Bam residents that survived the earthquake told reconnaissance team members that

[a] IIEES, 26 Arghavan Farmanieh, Tehran 19395, Iran; e-mail: mzare@iiees.ac.ir

Earthquake Spectra, Volume 21, No. S1, pages S165–S179, December 2005; © 2005, Earthquake Engineering Research Institute

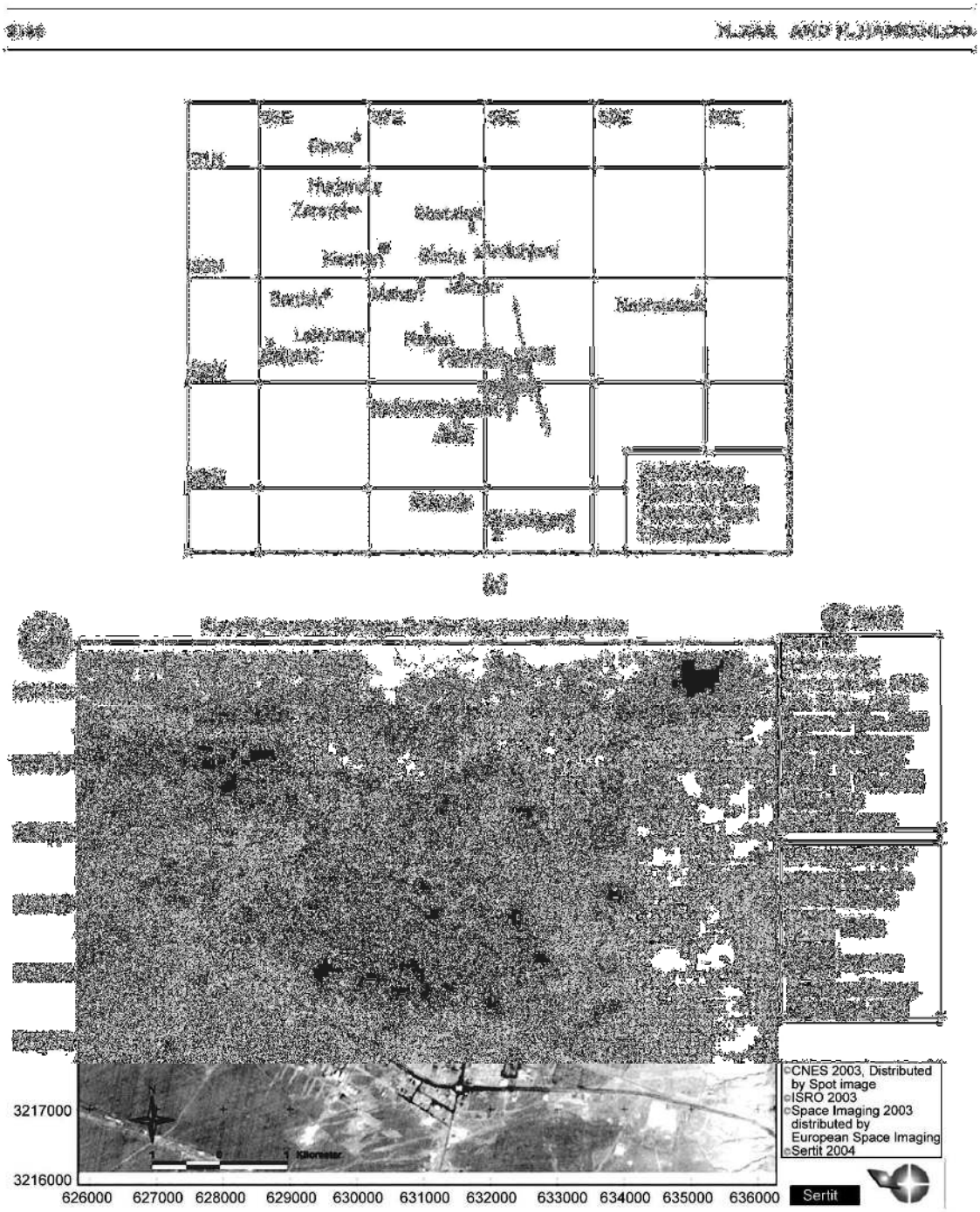

(b)

Figure 1. a. BHRC strong motion stations that recorded the Bam earthquake (BHRC 2004). b. Location of the Bam strong motion station in Bam and the location of the earthquake caused surface fissures. The trace of the Bam fault scarp is shown.

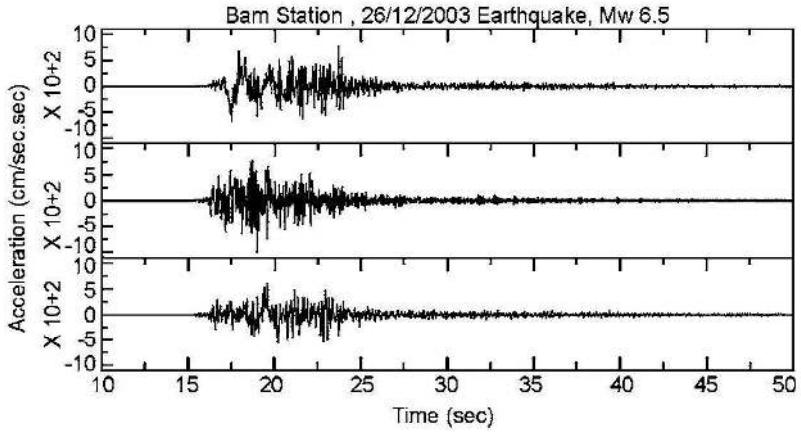

Figure 2. Bam accelerogram after filtering (between 0.11 and 40 Hz).

they felt strong up-down displacements during the main shock. The site class, however, may be taken for Class 3 since the site fundamental frequency was about 2 to5 Hz (equal to a site condition having the average shear wave velocity of about 300 to 500 m/sec in the first 30 meters of the deposits, Zar et al. 1999).

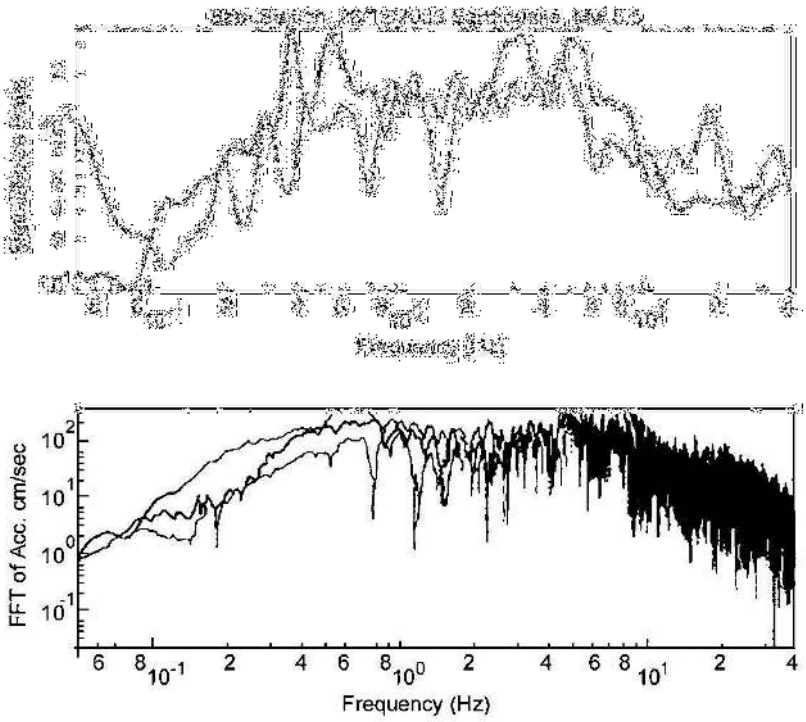

Figure 3. Signal-to-noise ratio (up) and the FFT of acceleration (down) for the three-components record of Bam.

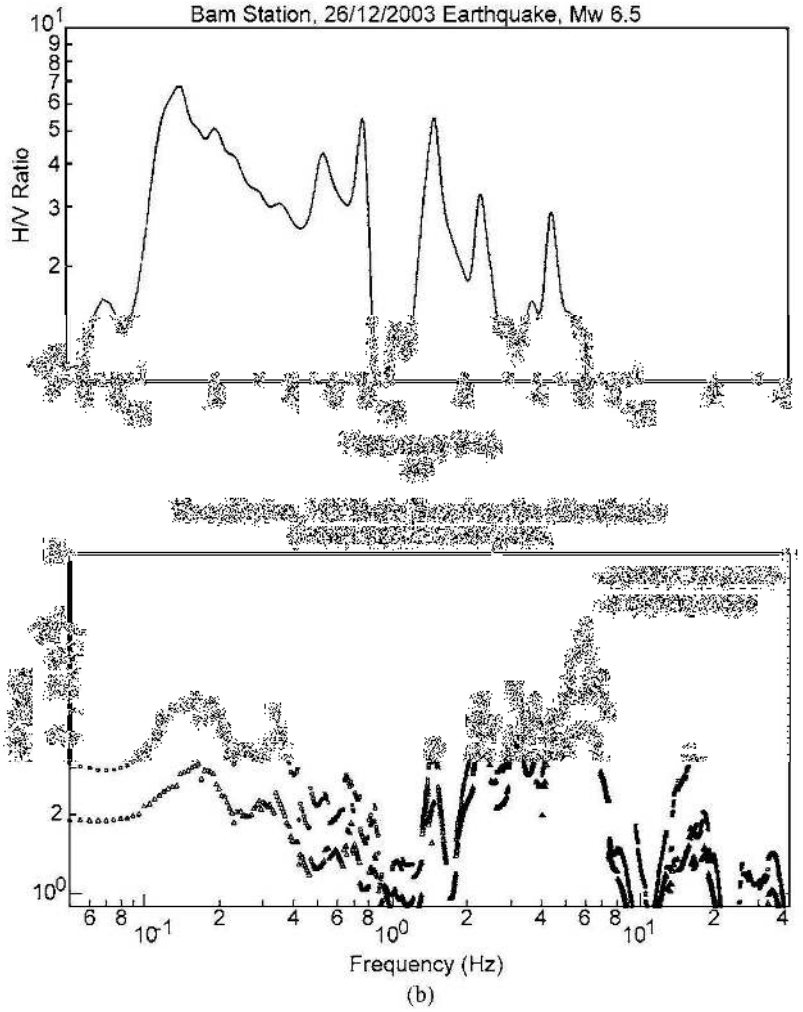

Figure 4. H/V ratio for (a) the main shock, and (b) aftershocks recorded at Bam strong motion station.

The velocity and displacement time histories of the Bam record were obtained based on single and double integration of the Bam accelerogram are shown in Figures 5 and 6. These time histories show a great pulse, especially in the fault-normal component (east-west direction).

The spectral accelerations for 5% damping are shown in Figure 7 for the three-component acceleration recorded at Bam station. The predominant period is the period corresponding to the highest peak in a response spectrum. The response spectrum in Figure 7 shows predominant periods of 0.1 second for vertical and 0.2 second for 2 horizontal components. Figure 7 also shows higher spectral ordinates for the vertical and for the fault-normal components of motion.

The spectral accelerations for 5% damping are shown in Figure 7 for the three-

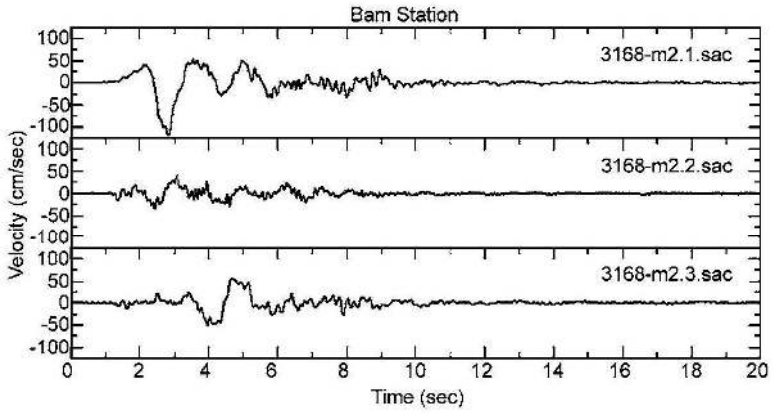

Figure 5. Velocity time history based on single integration of the accelerogram recorded in Bam.

component acceleration recorded at Bam station. The records obtained at the BHRC stations around the epicenter (Figure 1) were processed and the acceleration time histories obtained at Bam (Figure 2), Abaragh (Figure 8), Mohammadabad-e-Maskun (Figure 9), Jiroft (Figure 10), Golbaf (Figure 11), and Sirch (Figure 12) were selected for the detained strong motion studies. These records were filtered according to their corresponding signal-to-noise ratio, and the band-pass filters selected are shown in Table 1. Strong motion records obtained at the stations Anduhjerd, Cheshmehsabz, Balvard, Mahan, Bardsir, Hurjand, Joshan, Kahnuj, Kerman-Maskan, Kerman-Farmandari, Lalehzar, Zarand, Nosratabad, Ghalehganj, Shahdad, Rayan, and Ravar—for which the signal-to-noise ratios were small—were excluded from the detailed studies of the strong motion.

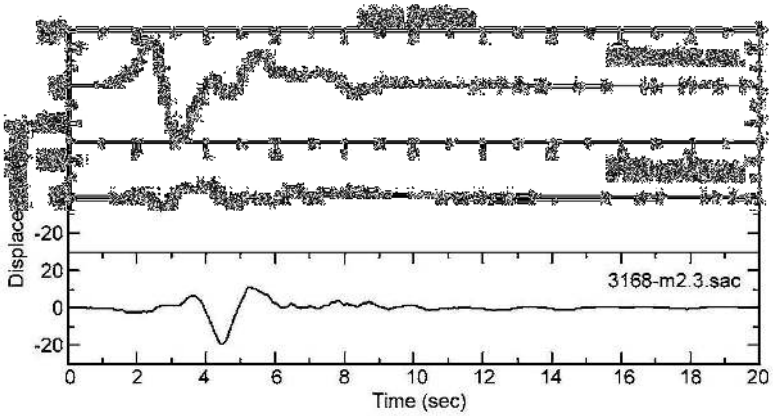

Figure 6. Displacement time history based on double integration of the accelerogram recorded in Bam.

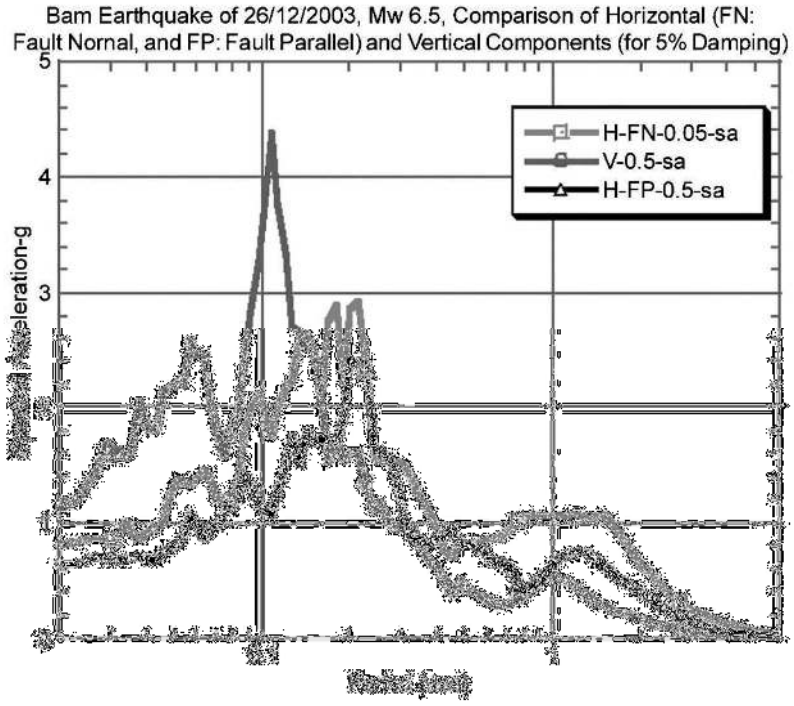

Figure 7. Response spectra for the damping value of 5% are compared for horizontal (fault normal) vertical and horizontal (fault parallel) components.

STRONG MOTION PARAMETERS

The strong motion parameters estimated for five selected strong motion records are presented in Tables 1 and 2. The spectrum intensity values reported in Table 2 are defined as the area under the pseudo-velocity response spectrum (PSV) between periods of 0.1 second and 2.5 seconds (Housner 1959). The duration values given in Table 2 are defined as the time interval between the points at which 5% and 95% of the energy in a ground motion have been delivered (Trifunac and Brady 1975).

SH-WAVE ANALYSIS

The analyses of teleseismic and strong ground motion data have been used by different investigators to infer and identify the complex rupture process and subevents (Campos et al. 1994; Sarkar et al. 2003). It is expected that the energy releases from these subevents will be identifiable in the near field strong motion data and an attempt can be made to study their properties. For this purpose, a method of Sarkar et al. (2003) has been used to estimate fault plane parameters using strong ground motion data pertaining to SH-wave only. This method is based on a point source representation and nonlinear least-square formulation that estimates the strike, dip, and rake of the causative fault and a grid search technique that provides separate estimates of the strike, dip, and rake. The analysis confines to SH-waves because these are minimally affected by crustal heterogeneity (Haskell 1960). Further, use of SH-waves minimizes the need for correc-

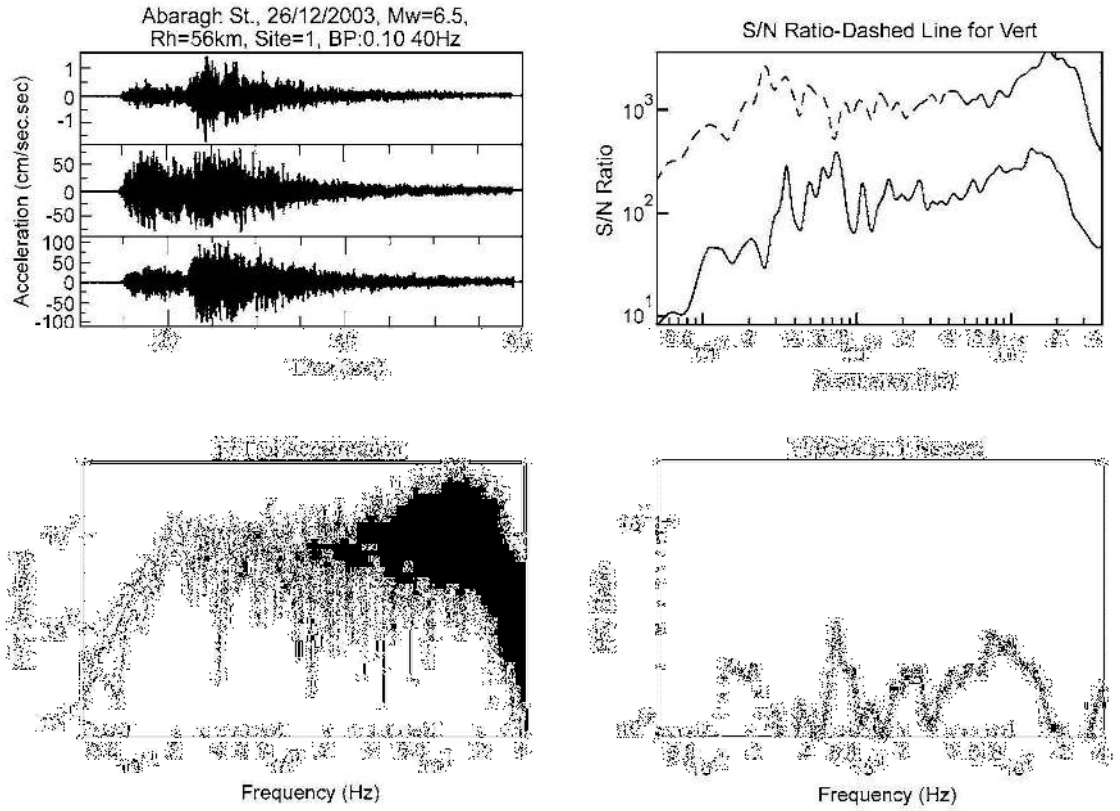

Figure 8. Processing of the record obtained at Abaragh station (56 km hypocentral distance): filtered acceleration time history (above left); the signal to noise ratio (above right); the FFT of acceleration before filtering (below left); and the H/V ratio (below right).

tions for the mode conversion at the free surface and other heterogeneities disregarded in the model used here. The spectral amplitudes at various stations were measured at the longest wavelength (lowest frequency) permitted by the data (Sarkar et al. 2003). This was done in order that the point source approximation could be as appropriate as possible.

The observed spectral amplitudes of the acceleration were picked at a common frequency, f, on all stations for a particular event, which lies in the flat portions of the spectra, and were then converted into the corresponding values of the spectral displacements. The values were then corrected for geometrical divergence. The corresponding theoretical estimates of SH-wave amplitudes of displacement were obtained from the formulae for the radiation pattern of SH-waves in a full space (Aki and Richards 1980; Lay and Wallace 1995). The error function E (strike, dip, rake) is written as:

$$\mathrm{E}\ (\text{strike},\ \text{dip},\ \text{rake}) = \Sigma_i (A_{oi} - A_{ti})^2 \qquad (1)$$

Here A_{oi} and A_{ti} denote the observed and theoretical amplitudes of the near field SH-wave displacement at the selected frequency at the ith station. The summation is over all

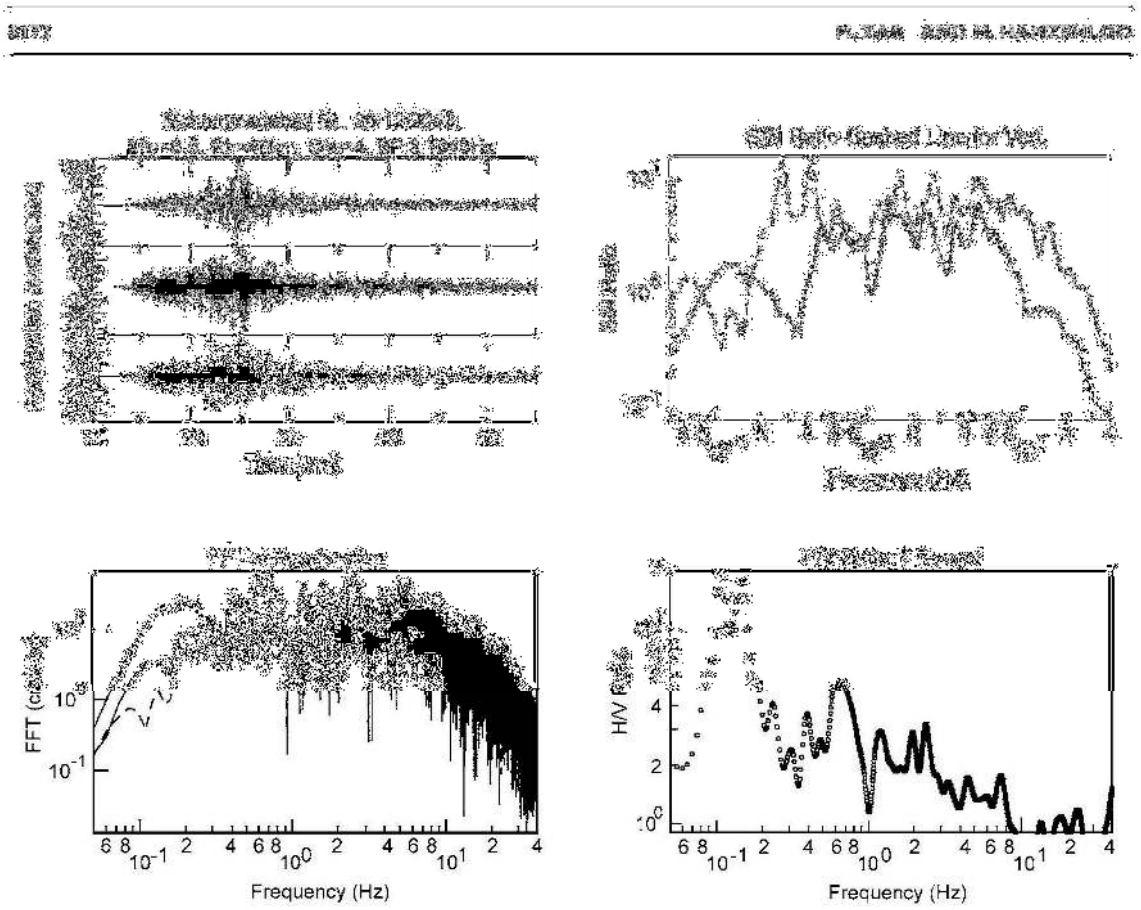

Figure 9. Processing of the record obtained at Mohammadabad-e-Maskun station (48 km hypocentral distance): filtered acceleration time history (above left); the signal-to-noise ratio (above right); the FFT of acceleration before filtering (below left); and the H/V ratio (below right).

stations that recorded the particular subevent. The nonlinear Newton technique has been used to simultaneously obtain those values of strike, dip, and rake that minimize E (strike, dip, rake) in the least square sense.

For appropriate selection of SH-wave components of the recorded data the radial (L) and transverse (T) components of recorded acceleration and displacement are suitably rotated so that corresponding estimates along and perpendicular to the azimuth direction are obtained. The rotated transverse components provide acceleration and displacement data of SH-waves, recorded at each station. The SH-wave accelerogram records for the 2003 Bam earthquake are shown in Figure 13.

In the absence of a common time code, it was not feasible to locate independently the hypocenters of the two subevents on the basis of the accelerogram data. However, a master event technique was employed to estimate the hypocentral location of the subevent from where the S1 phase of energy possibly radiated. Generally, a value of two-thirds is assumed for the ratio between vertical and horizontal peak accelerations. In recent earthquakes, however, it has been observed that in the near field there is often a

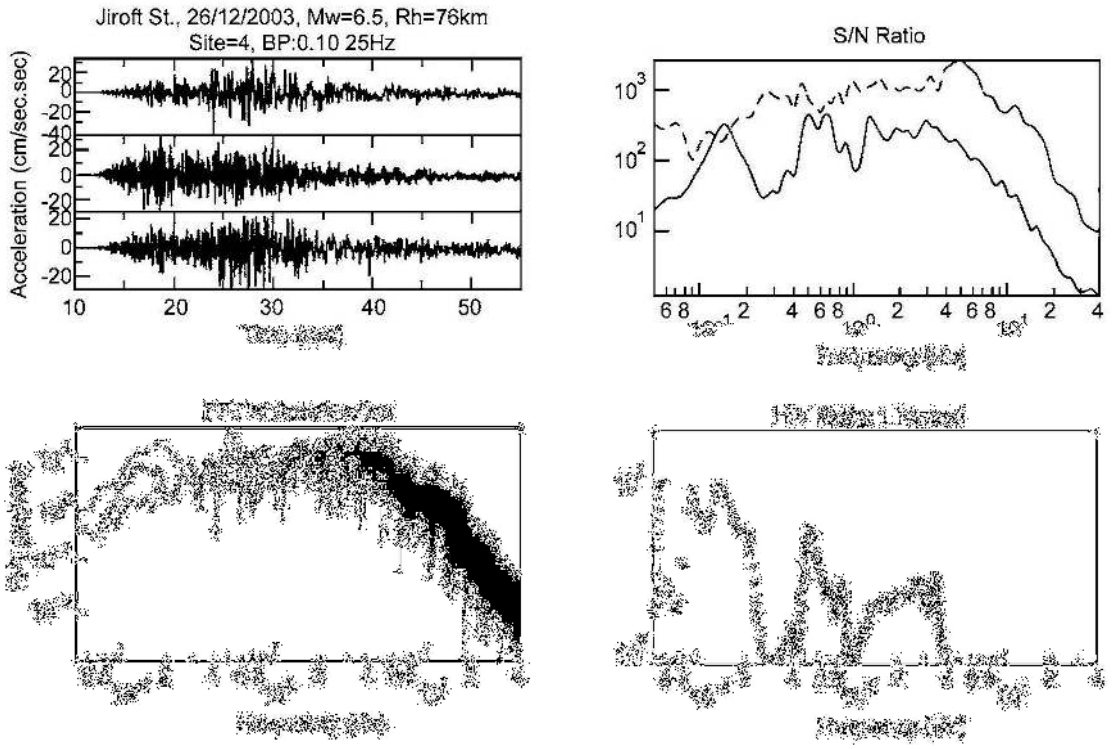

Figure 10. Processing of the record obtained at Jiroft station (76 km hypocentral distance): filtered acceleration time history (above left); the signal to noise ratio (above right); the FFT of acceleration before filtering (below left); and the H/V ratio (below right).

potential for a significant vertical component of ground shaking. The Bam station recorded vertical peak acceleration of 956 cm/sec_2, which is larger than for the two horizontal components. It seems that at Bam station, a strong up-down motion occurred. This strong up-down motion was also reported by the observers.

At the time of an earthquake, damage is maximum in the epicentral region, where the ground experiences intense shaking. Therefore, it is assumed here that the chosen master event, namely the subevent corresponding to the release of the S2 phase was located near 58.35° and 29.09° at depth of 8 km (below the Bam strong motion station). Considering this as location of S2 phases, acceleration time histories from the four stations viz. Bam, Abaragh, Mohammadbad, and Jiroft (Table 3) have been used to estimate that the S1 phase of energy was released from 29.02°N, 58.30°E, at a depth of 8 km depth, about 8 second before the release of the S2 phase of energy.

The acceleration spectra were obtained for each of the S1 and S2 phases using relevant time windows on the appropriately rotated transverse component accelerograms. These spectra were obtained using Fast Fourier Transform (FFT) along with a Hamming-Turkey window so as to reduce the effect of data truncation. Several varia-

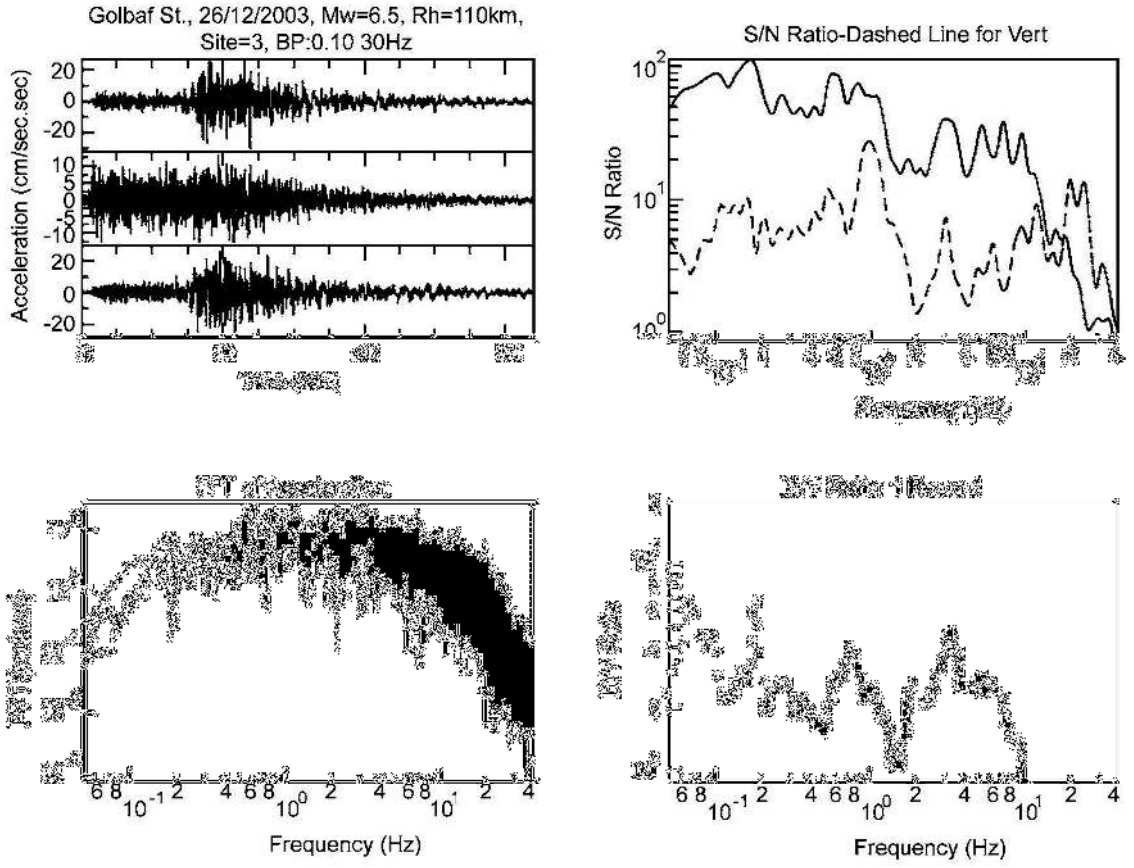

Figure 11. Processing of the record obtained at Golbaf station (110 km hypocentral distance): filtered acceleration time history (above left); the signal-to-noise ratio (above right); the FFT of acceleration before filtering (below left); and the H/V ratio (below right).

tions were performed on the window sizes and placement to confirm the stability of these spectra in terms of their general structure and frequency content. The spectra for S1 and S2 are shown in Figures 14 and 15.

The fault plane solution corresponding to the S1 subevent estimated using spectra at four stations is as follows: strike=174°N, dip=85°, rake=170°. The standard error of estimate is 0.50. This event was surmized to have occurred at 29.02 N, 58.30 E, 10.0 km.

For the causative fault of the S2 subevent, spectral data from four stations have been used to estimate the following parameters: strike=172°N, dip=65°, rake=110°. The standard error of estimate is 0.18. It was estimated earlier that the epicenter of this event was located at 29.09°N, 58.34°E km and occurred about 8 seconds after the event S1.

The total fault plane parameters, considering the SH-wave spectra including both S1 and S2, are as follows: strike=172°, dip=72°, rake=156°. The standard error of estimate is 0.32.

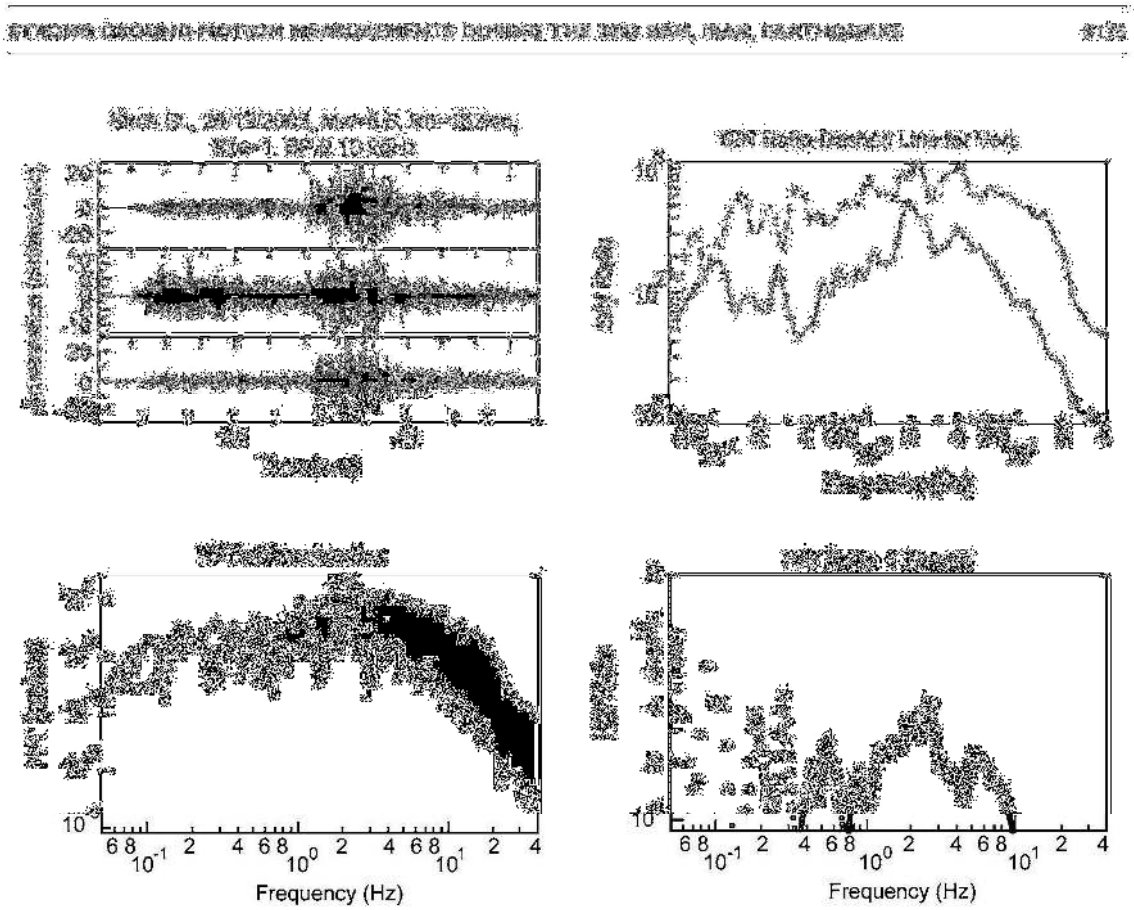

Figure 12. Processing of the record obtained at Abaragh station (152 km hypocentral distance): filtered acceleration time history (above left); the signal-to-noise ratio (above right); the FFT of acceleration before filtering (below left); and the H/V ratio (below right).

CONCLUSIONS

The strong motions records observed in the Bam earthquake are representative of a very strong, but short, earthquake that had large vertical and fault-normal near-fault effects. The following conclusions have emerged from the analysis of strong ground motion data for the Bam earthquake:

- The Bam earthquake was a complex earthquake. The SH-wave accelerograms exhibited distinct phases corresponding to the energy released from two separate events.
- Two strong phases of energy are seen on the accelerograms. The first was interpreted to represent a starting subevent with right-lateral strike slip mechanism and located south of Bam. The event corresponding to the second release of energy was interpreted to be released 8 seconds after the first subevent. The mechanism of the second subevent was a reverse mechanism.

Table 1. Strong motion parameters estimated for five selected records

No. of total	Rec.	Station	Lat.N	Long.E	Site	BP Filter (Hz)	HPGA1 (cm/sec2)	VPGA (cm/sec)	HPGA2 (cm/sec2)	HPGV1 (cm/sec)	VPGV (cm/sec)	HPGV2 (cm/sec)	HPGD1 (cm)	VPGD (cm)	HPGD2 (cm)	Fc (Hz)	Fmax-H	Fmax-V	Hypocentral Dist. (km)
1	3161	Sirch	30.24N	57.57E	1	0.1–25	30.2	14	29.2	2.4	1	2.3	0.4	0.2	0.3	0.4	8	15	152
2	3162-1	Mohammadabad	29.97N	57.88E	4	0.1–40	120.1	69.2	71	10.4	3.1	3.3	2.1	0.6	0.8	0.4	6	8	48
3	3168-2	Bam	29.12N	58.38E	3	0.11–40	992	775	623	92.3	32.3	72.6	26.4	6.3	15.5	0.3	9	18	12
4	3170-2	Jiroft	28.68N	57.76E	4	0.1–25	39.6	30.5	27.3	3.6	1.3	2.1	0.9	0.4	5.1	0.45	3.5	5	76
5	3176-1	Abaragh	29.38N	57.97E	1	0.1–40	162.6	83.2	107.7	8.2	8.1	10.2	2.8	2.6	2.2	0.25	18	25	56

BP=Bandpass HPGA=Horizontal Peak Ground Acceleration HPGV=Horizontal Peak Ground Velocity HPGD=Horizontal Peak Ground Displacement

Table 2. Additional Strong motion parameters estimated for five selected records

No. of total	Rec.	Station	Arms-H1 (cm/sec2)	Arms-V (cm/sec2)	Arms-H2 (cm/sec2)	Arias-Int H1 (cm/sec)	Arias-Int V (cm/sec)	Arias-Int H2 (cm/sec)	Vel Spectral Int. H1 (cm/sec)	Vel Spectral Int. V (cm/sec)	Vel Spectral Int. H2 (cm/sec)	Duration H1-sec	Duration V-sec	Duration H2-sec
1	3161	Sirch	5.6	3	5.2	2.4	0.7	2	8.2	4.2	8.6	17.5	30.9	17.1
2	3162-1	Mohammadabad	11.3	7.3	7.1	16.8	7	6.6	44.8	13.4	16.9	13.9	20.7	22.8
3	3168-2	Bam	140.6	133.9	110	79.1	71.8	48.4	394.3	480	515.9	7.7	7.2	8.3
4	3170-2	Jiroft	6.1	5.6	5.7	3.2	2.8	2.9	16.5	6.7	11.4	23.6	23.6	26
5	3176-1	Abaragh	19.5	15.3	16.9	36.2	22.1	27	33.2	33.7	35	15	18.4	19.1

Arms=Root mean square (RMS) acceleration Arias-Int=Arias intensity (Arias 1970)

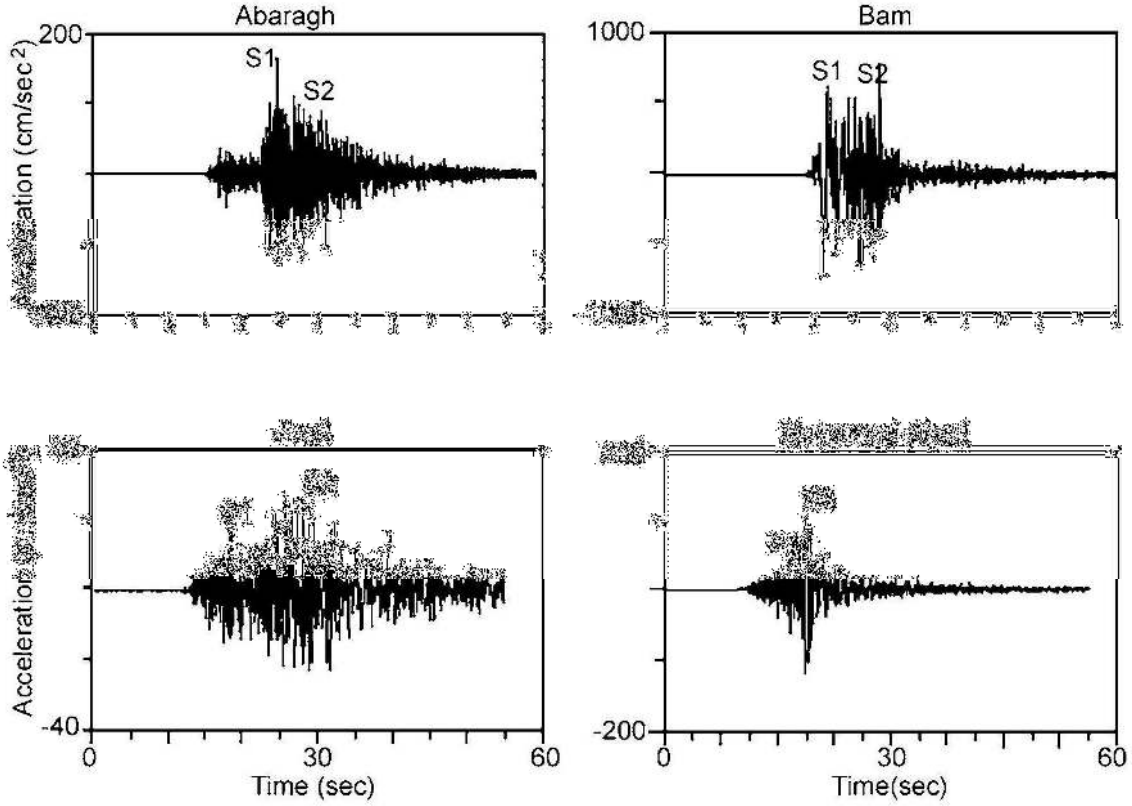

Figure 13. SH-wave accelerogram records from the four stations of strong motion array.

Table 3. Salient features of recording stations

Station	Lat.	Long.	Elev.	L/T direction
Abaragh	29.34	57.94	1644	72/162
Bam	29.09	58.35	1094	278/8
Jiroft	28.67	57.74	275	240/330
Mohammadabad	28.90	57.89	1961	350/80

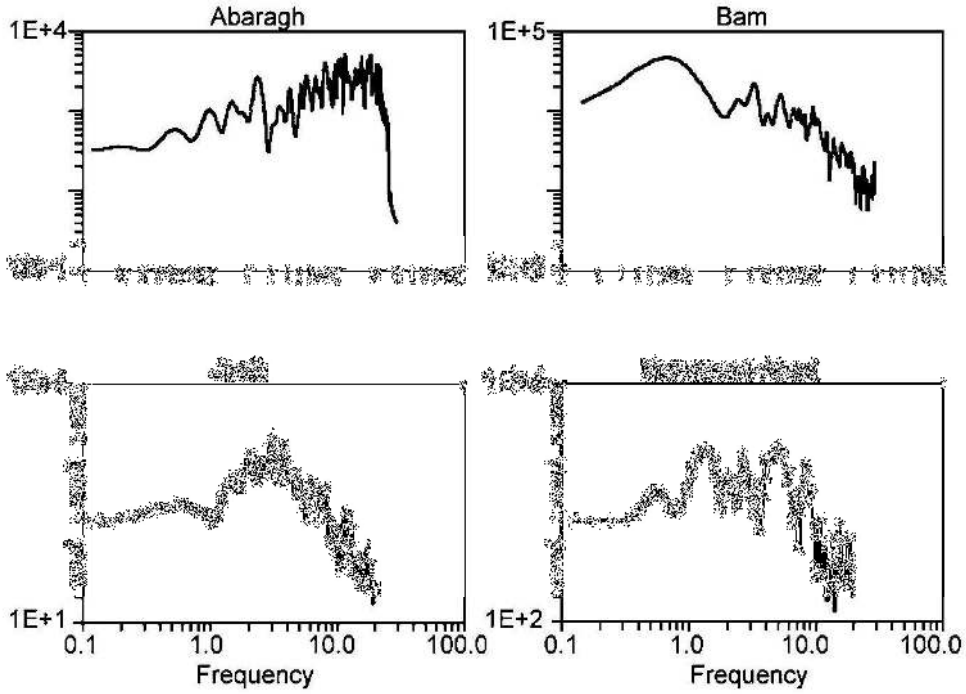

Figure 14. Observed acceleration spectra for S1 subevent.

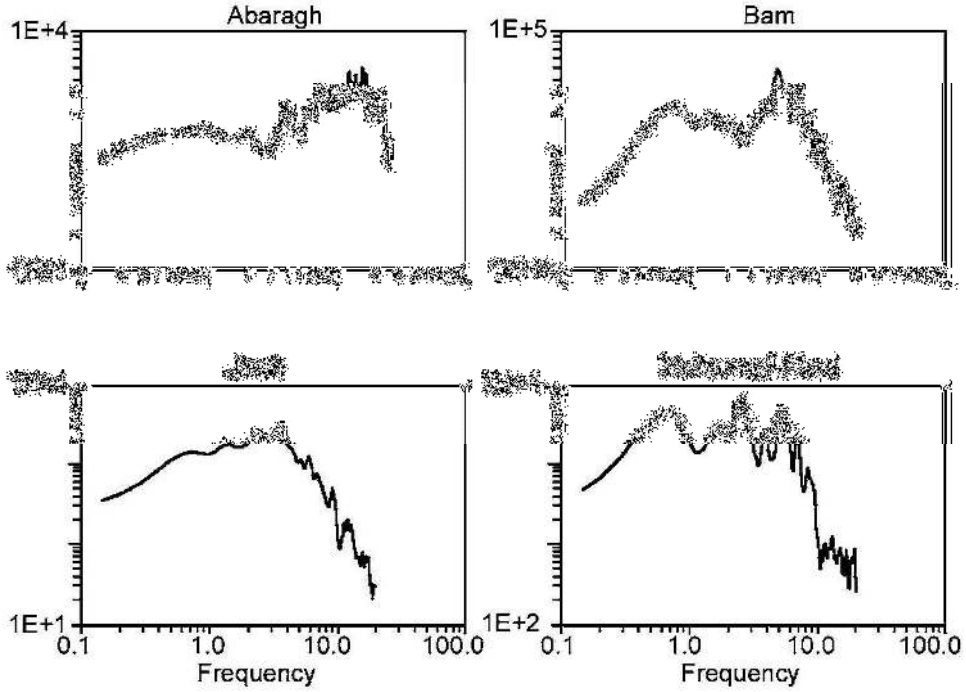

Figure 15. Observed acceleration spectra for S2 subevent.

REFERENCES[1]

Aki, K., and Richards, P. G., 1980. *Quantitative Seismology: Theory and Methods*, W. H. Freeman, San Francisco, Vol. 1, 558 pp.

Arias, A., 1970. *A Measure of Earthquake Intensity in Seismic Design of Nuclear Power Plants*, edited by R. J. Hansen, M. I. T. Press.

Building and Housing Research Center (BHRC), 2004. http://www.bhrc.gov.ir/; January.

Campos, J., Madariaga, R., Nabelek, J., Bukchin, B. G., and Deschamps, A., 1994. Faulting process of the 1990 June 20 Iran earthquake from broad-band records, *Geophys. J. Int.* **118**, 31–46.

Haskell, N. A., 1960. Crustal reflection of plane SH waves, *J. Geophys. Res.* **65**, 4147–4150.

Lay, T., and Wallace, C., 1995. *Modern Global Seismology*, Academic Press, San Diego, CA.

Housner, G. W., 1959. Behavior of structures during earthquakes, *J. Eng. Mech. Div., Am. Soc. Civ. Eng.* **85**, No. EM14, 109–129.

Sarkar, I., Hamzehloo, H., and Khattri, K. N., 2003. Estimation of causative fault parameters of the Rudbar earthquake of June 20, 1990 from near field SH-wave data, *Tectonophysics* **364**, 55–70.

Trifunac, M. D., and Brady, A. G., 1975. A study on the duration of the strong earthquake ground motions, *Bull. Seismol. Soc. Am.* **65** (3), 581–626.

Zar , M., Bard, P. Y., and Ghafory-Ashtiany, M., 1999. Site characterizations for the Iranian strong motion network, *J. Soil Dyn. Earthquake Eng.* **18** (2), 101–121.

(Received 9 October 2004; accepted 29 April 2005)

[1] Publication of this special issue on the Bam, Iran, earthquake was supported by the Learning from Earthquakes Program of the Earthquake Engineering Research Institute, with funding from the National Science Foundation under grant CMS-0131895. Any opinions, findings, conclusions, or recommendations expressed herein are the authors' and do not necessarily reflect the views of the National Science Foundation, the Earthquake Engineering Research Institute, or the authors' organizations.

#5. Zaré M. and Bard P.-Y., (2002), "Strong motion dataset of Turkey: data processing and site classification", Soil Dynamics and Earthquake Engineering, vol. 22., no.8, pp. 703-718, doi: 10.1016/s0267-7261(02)00028-3.

ELSEVIER

Soil Dynamics and Earthquake Engineering 22 (2002) 703–718

SOIL DYNAMICS AND EARTHQUAKE ENGINEERING

www.elsevier.com/locate/soildyn

Strong motion dataset of Turkey: data processing and site classification

Mehdi Zaré[a,b,*], Pierre-Yves Bard[b,c]

[a]*International Institute of Earthquake Engineering and Seismology (IIEES), P.O. Box 19395/3913, Tehran, Iran*
[b]*Laboratoire de Géophysique Interne et Tectonophysique (LGIT), IRIGM, BP53X, 38041 Grenoble Cedex, France*
[c]*Laboratoire Central des Ponts et Chaussées, 58 Bd Lefèbvre, 75732 Paris Cedex 15, France*

Accepted 30 March 2002

Abstract

Strong motion records of Turkey are studied in order to prepare a catalog to be used as a database for further studies (for instance empirical attenuation laws). The network started to be installed in 1973, and the first record was obtained in 1976. The instruments are of SMA-1 analog recorders and SIG SM-2 and GeoSys GSR-16 digital types. Out of a total of 426 records released on the web sites of the General Directorate of the Disaster Affairs and of Kandili Observatory, a set of 210 records was selected with a satisfactory quality, for which it was possible to associate correctly determined source parameters (source magnitudes and epicentral distances). Most of the records are obtained from around North and East Anatolian Fault zones, as well as from western and southwestern parts of Turkey. The main outcome of this paper is a strong motion catalog of Turkey, with the indication of site conditions, of the frequency band of the reliability of the records, peak values of acceleration, velocity and displacements, source parameters (magnitude, epicentral and macroseismic distances), intensity and finally the fault plane solutions whenever possible. The aim is to have, with other regional dataset, a homogenous and good quality dataset.

Keywords: Strong motion dataset; Turkey; Catalog; H/V ratio; PGA; Iran; Data processing; Site classification

1. Introduction

The first Turkish strong motion instruments were installed in 1973. Since that date, the strong motion network has grown considerably. Instruments first used were of Kinemetrics SMA-1 type and the first recording in the epicentral region of an earthquake was obtained in Denizli during the 19 August 1976 earthquake (mb5.0, SW Turkey) [1]. These data are presented on the Internet since 1998 by the 'General Directorate of Disaster Affairs, GDDA, (http://angora.deprem.gov.tr)'. Most of the data used in this paper are downloaded from this site. These records belong to the National Strong Motion Network that is the largest network operator in Turkey. The aim was to install one station in each of the great cities of Turkey located in earthquake zones [2]. Other records used, which are available from the Internet, are those of the Bogazici University (Kandili Observatory, Istanbul) associated with the Izmit (Kocaeli) earthquake of 17 August 1999 (Mw7.4). The total number of records which are available for this study are 426 three-component accelerograms, mostly obtained from around the North and East Anatolian fault zones, between 1976 and 30 June 2000.

The data have already provided the basis of several publications [1–6], dedicated to studies of individual earthquakes. A bibliography on the seismotectonic and fault mechanisms in Turkey [7–11] shows that the North and East Anatolian fault systems in Turkey are the main neotectonic features in this plateau. The geotechnical conditions in the earthquake prone areas and strong motion stations of Turkey are investigated as well in some published work [5,12,13].

The scope of this study is to sort and select accelerograms within this large dataset, so as to complete our strong motion dataset for the eastern Mediterranean region. The first step in this way is to work on the strong motion dataset of Iran [14,15]. During the present study, we have tried to compile a catalog of strong motion data in Turkey with appropriate source parameters and site conditions. The catalog comprises the source and site parameters as well as the maximum values of acceleration, velocity and displacement for each record. A quality index is also defined to indicate the level of reliability of each record.

* Corresponding author. Address: International Institute of Earthquake Engineering and Seismology (IIEES), P.O. Box 19395/3913, Tehran, Iran.
E-mail address: mzare@dena.iiees.ac.in (M. Zaré).

0267-7261/02/$ - see front matter
PII: S0267-7261(02)00028-3

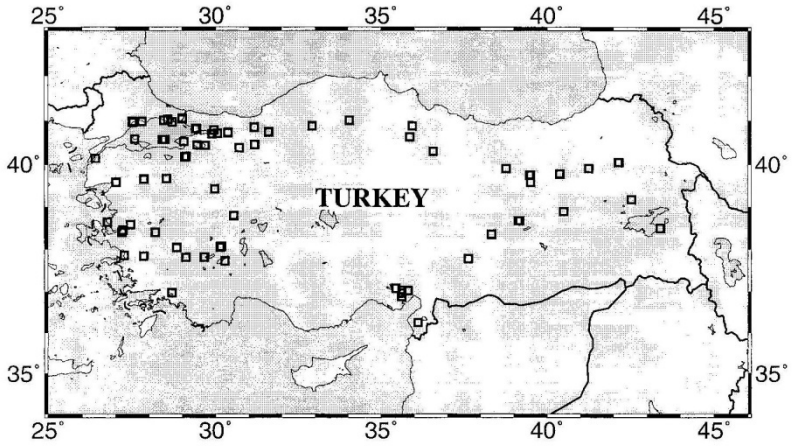

Fig. 1. Locations of the accelerometric sites in Turkey corresponding to the data selected in this study.

In this paper first we will present how we have determined the source parameters for each record. The method to select the best quality records is explained afterwards, followed by our methodology to process the accelerograms. The uncertainties are also discussed.

2. Determination of the source data for each record

Among the 426 three-component accessible records, 210 three-component records were selected. (Table 1, Fig. 1). These records obtained from earthquakes between 1976 and 30 June 2000 occurred mostly along the North and East Anatolian Fault zones as well as in southwestern Turkey (Fig. 2). Table 1 presented herein is a summarized version of the catalog prepared by the authors. Those who are interested to receive more details on the peak acceleration values of each component, different reported and estimated magnitudes, focal depths, values of the macroseismic epicentral- and hypocentral distances, intensities and focal mechanisms should contact the first author.

Most of the accelerometric data, which are available on the Internet, do not include corresponding earthquake characteristics (location and magnitude). In order to use the recordings for regression studies, we looked for the corresponding earthquake specifications, and identified the causing earthquake. Based on the existing data for each record (station location, peak accelerations, date and arrival times of the records). The epicentral coordinates determined by Turkish national seismic network are used in most of the cases. Reports by the national and international seismic networks and the macroseismic information are checked whenever possible for well recorded data. Also hypocentral distances are estimated directly from the S−P arrival time

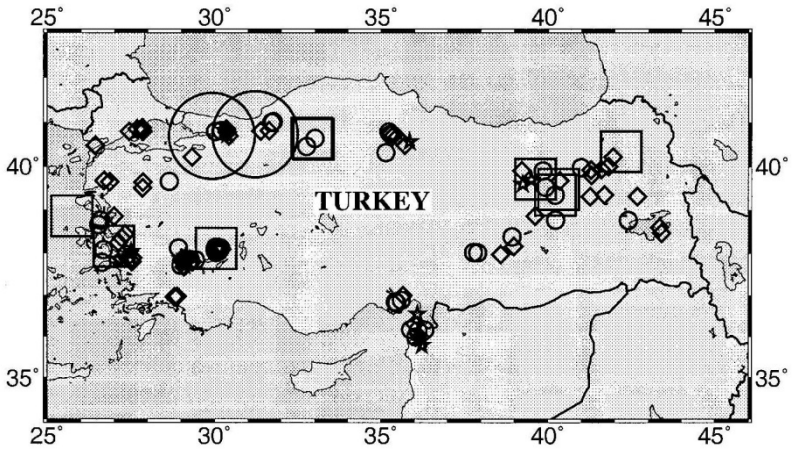

Fig. 2. The location of the epicenters of the selected events, which are recorded in the strong motion stations in Turkey. The symbols are stars for $3 \leq M < 4$; diamonds for $4 \leq M < 5$; little circles for $5 \leq M < 6$; squares for $6 \leq M < 7$ and great circles for $M \geq 7$.

Table 1
The catalog of the accelerometric data of Turkey (the published data since the beginning of its installation until the end of June 2000). See Refs. [1,4–7,13,18, 28–30] and Web site of NEIC [31] Web site of the GDDA, 5: Refs. [19,24]

No	Station	Coordinates		Code	Site	Filters applied (Hz)		PGA (m/s^2)	Earthquake (date)	Epicenter (coordinate)		Mw	Dist. epi (km)
						HP	LP						
1	DNZ (Denizli-Meteo)	37.81N	29.11E	000986A.DNZ	4	0.9	32	3.417	19/08/1976	37.71N	29.00E	5.4	9
2	IZM (Izmit-meteo)	38.40N	28.19E	024315A.IZM	1	3	25	2.520	09/12/1977	38.35N	27.23E	4.8	84
3	MLT (Malatya-meteo)	38.35N	38.34E	042421A.MLT	1	3	22	0.309	21/09/1978	37.97N	38.59E	4.5	46
4	DUR (Dursunbey)	39.67N	28.53E	072869A.DUR	4	1	22	2.673	18/07/1979	39.66N	28.65E	5.3	11
5	HTY (Hatay-Bayindirlik)	36.25N	36.11E	082756A.HTY	2	0.6	20	1.305	30/06/1981	36.17N	35.89E	5.4	20
6	HRS (Horasan)	40.04N	42.14E	0A4986A.HRS	1	0.9	22	1.482	30/10/1983	40.35N	42.18E	5.5	34
7	BLK (Balikesir-Meteo)	39.66N	27.86E	0B2422A.BLK	2	2	27	2.468	29/03/1984	39.64N	27.86E	4.7	2
8	KOY (Koycegiz-Meteo)	36.97N	28.69E	0E4996A.KOY	2	3.5	33	1.144	06/12/1985	36.95N	28.85E	4.2	18
9	GOL (Golbasi-Devlet)	37.78N	37.64E	0F1202A.GOL	3	1.5	15	0.971	05/05/1986	38.02N	37.79E	6.0	35
10	KUS (Kusadasi)	37.86N	27.26E	0G0992A.KUS	2	1d.5	18	0.843	01/06/1986	37.96N	27.39E	4.0	16
11	GOL (Golbasi-Devlet)	37.78N	37.64E	0H1202A.GOL	3	1	15	0.512	06/06/1986	38.01N	37.91E	5.8	34
12	FOC (Foca)	38.64N	26.77E	0J6165A.FOC	3	1.5	21	0.379	04/08/1988	38.86N	27.00E	4.5	30
13	ERC (Erzincan-Meteo)	39.75N	39.48E	0M2418A.ERC	1	0.5	18	5.229	13/03/1992	39.72N	39.63E	6.6	15
14	REF (Refahiyeh)	39.90N	38.77E	0M2870A.REF	1	0.7	9	0.727	13/03/1992	39.72N	39.63E	6.6	76
15	ERC (Erzincan-Meteo)	39.75N	39.48E	0N0054A.ERC	1	0.5	15	0.381	15/03/1992	39.53N	39.93E	5.9	45
16	IZR (Izmir)	38.40N	27.19E	0O6165A.IZM	1	0.7	18	0.297	06/11/1992	38.16N	26.99E	6.0	31
17	KUS (Kusadasi-Meteo)	37.86N	27.26E	0O0992A.KUS	2	0.6	28	0.814	06/11/1992	38.16N	26.99E	6.0	43
18	ERC (Erzincan-Bayindirlik)	39.74N	39.51E	0P0624A.ERC	3	1.5	26	0.995	20/01/1993	39.70N	39.50E	3.2	11
19	BUR (Bursa-Bayindirlik)	40.17N	29.08E	0T0294A.BRS	1	1.5	12	0.066	21/02/1994	40.22N	29.32E	3.9	22
20	DNZ (Denizli-Bayindirlik)	37.81N	29.11E	0U0285A.DNZ	4	1.5	40	0.124	09/04/1994	37.70N	29.11E	3.4	19
21	BLK (Balikesir-Bayindirlik)	39.66N	27.86E	0V0283A.BLK	2	2	15	0.064	07/05/1994	39.51N	27.85E	4.4	13
22	BLK (Balikesir-Bayindirlik)	39.66N	27.86E	0W0283.BLK	2	1.1	12	0.053	24/05/1994	38.66N	26.54E	5.5	158
23	FOC (Foca-Gumruk)	38.64N	26.77E	0W4984A.FOC	3	1.5	10	0.450	24/05/1994	38.66N	26.54E	5.5	22
24	FOC (Foca-Gumruk)	38.64N	26.77E	0X4984A.FOC	3	1	15	0.560	24/05/1994	38.76N	26.60E	5.0	22
25	IZR (Izmir-Bayindirlik)	38.40N	27.19E	0X0278A.IZM	1	0.5	19	0.062	24/05/1994	38.76N	26.60E	5.5	66
26	MLT (Malatya-Bayindirlik)	38.35N	38.34E	110292A.MLT	1	0.6	20	0.102	01/07/1994	38.16N	38.98E	4.8	57
27	KOY (Koycegiz-Meteo)	36.97N	28.69E	1B4996A.KOY	2	1.5	15	0.515	13/11/1994	36.96N	28.80E	4.6	12
28	KOY (Koycegiz-Meteo)	36.97N	28.69E	194996A.KOY	2	3.5	15	0.865	13/11/1994	36.97N	28.89E	4.5	16
29	ELZ (Elazig-Bayindirlik)	38.67N	39.19E	1E0280A.ELZ	4	1	20	0.066	15/12/1994	38.87N	39.63E	4.0	44
30	TER (Tercan-Meteo)	39.77N	40.39E	1J2876A.TER	1	0.8	18	0.474	29/01/1995	39.98N	40.99E	5.2	54
31	IZR (Izmir-Bayindirlik)	38.40N	27.19E	1K0278A.IZM	1	0.8	20	0.059	01/02/1995	38.44N	27.32E	4.5	14
32	VAN (Van)	38.50N	43.40E	1N0281A.VAN	3	0.5	20	0.270	26/02/1995	38.60N	43.33E	4.8	12
33	DNZ (Denizli-Bayindirlik)	37.81N	29.11E	1Q0285A.DNZ	4	0.6	38	0.178	12/03/1995	37.85N	29.06E	3.8	5
34	DNZ (Denizli-Bayindirlik)	37.81N	29.11E	1W0285A.DNZ	4	0.8	34	0.358	14/03/1995	37.82N	29.15E	3.9	4
35	DNZ (Denizli-Bayindirlik)	37.81N	29.11E	1Y0285A.DNZ	4	1.5	35	0.486	14/03/1995	37.87N	29.03E	4.1	9
36	DNZ (Denizli-Bayindirlik)	37.81N	29.11E	1Z0285A.DNZ	4	1	15	0.124	14/03/1995	37.85N	29.09E	3.6	4
37	DNZ (Denizli-Bayindirlik)	37.81N	29.11E	1U0285A.DNZ	4	0.6	35	2.597	14/03/1995	37.84N	29.09E	4.2	2
38	TKR (Tekirdag-Bayindirlik)	40.96N	27.53E	210289A.TKR	3	1.5	15	0.104	28/03/1995	40.88N	27.83E	4.2	25
39	TKR (Tekirdag-Bayindirlik)	40.96N	27.53E	220289A.TKR	3	0.4	20	0.433	13/04/1995	40.85N	27.67E	4.7	17
40	TKR (Tekirdag-Bayindirlik)	40.96N	27.53E	240289A.TKR	3	0.6	18	0.335	18/04/1995	40.80N	27.84E	4.4	30
41	ERZ (Erzerum-Bayindirlik)	39.90N	41.26E	250286A.ERZ	1	0.5	18	0.165	23/05/1995	39.92N	41.28E	4.4	2
42	ERZ (Erzincan-Bayindirlik)	39.57N	39.51E	280624A.ERZ	3	0.8	12	0.064	18/06/1995	39.90N	39.85E	5.0	47
43	ERZ (Erzerum-Bayindirlik)	39.90N	41.26E	290286A.ERZ	1	0.8	16	0.059	05/07/1995	39.93N	41.59E	4.2	28
44	DNZ (Denizli-Meteo)	37.81N	29.11E	2B0285A.DNZ	4	0.2	20	0.118	18/08/1995	37.84N	29.43E	5.6	31
45	DIN (Dinar-Meteo)	38.06N	30.15E	2F2873A.DIN	3	0.6	25	1.857	26/09/1995	38.04N	30.03E	5.3	12
46	DIN (Dinar-Meteo)	38.06N	30.15E	2G2873A.DIN	3	0.5	19	0.795	26/09/1995	38.09N	30.01E	5.1	12
47	DIN (Dinar-Meteo)	38.06N	30.15E	2H2873A.DIN	3	0.4	18	1.763	27/09/1995	38.11N	30.02E	5.7	13
48	DIN (Dinar-Meteo)	38.06N	30.15E	2L2873A.DIN	3	0.8	15	0.875	01/10/1995	38.09N	30.12E	4.8	5
49	DIN (Dinar-Meteo)	38.06N	30.15E	2N2873A.DIN	3	0.4	15	1.631	01/10/1995	38.04N	30.09E	5.5	6
50	CRD (Cardak-Sagli)	37.82N	29.66E	2M1200A.CRD	1	1.5	15	0.224	01/10/1995	38.10N	30.02E	5.0	86
51	DIN (Dinar-Meteo)	38.06N	30.15E	2M2873A.DIN	3	0.4	15	2.056	01/10/1995	38.10N	30.02E	5.8	12
52	BRD (Burdur)	37.72N	30.29E	2K2421A.BRD	1	0.35	11	0.379	01/10/1995	38.11N	30.05E	6.4	53
53	CRD (Cardak-Sagli)	37.82N	29.66E	2K12800A.CRD	1	0.4	15	0.891	01/10/1995	38.11N	30.05E	6.4	46
54	DIN (Dinar-Meteo)	38.06N	30.15E	2K2873A.DIN	3	0.2	20	3.141	01/10/1995	38.11N	30.05E	6.4	10
55	DNZ (Denizli-Bayindirlik)	37.81N	29.11E	2K0285A.DNZ	4	0.15	19	0.152	01/10/1995	38.11N	30.05E	6.4	117
56	DIN (Dinar-Meteo)	38.06N	30.15E	2O2873A.DIN	3	0.6	20	1.141	03/10/1995	38.01N	30.05E	5.1	11

(continued on next page)

Table 1 (*continued*)

No	Station	Coordinates		Code	Site	Filters applied (Hz)		PGA (m/s^2)	Earthquake (date)	Epicenter (coordinate)		Mw	Dist. epi (km)
						HP	LP						
57	DIN (Dinar-Meteo)	38.06N	30.15E	2P2873A.DIN	3	0.6	15	0.564	04/10/1995	38.08N	30.11E	4.6	5
58	DIN (Dinar-Meteo)	38.06N	30.15E	2Q2873A.DIN	3	0.2	20	1.252	05/10/1995	38.04N	30.10E	5.3	6
59	DIN (Dinar-Meteo)	38.06N	30.15E	2S2873A.DIN	3	0.3	12	1.632	06/10/1995	38.03N	30.09E	5.5	8
60	DKH (Dinar Koy)	38.05N	30.14E	420177A.DKH	3	0.6	20	0.215	10/10/1995	38.10N	30.16E	4.0	6
61	DKH (Dinar Koy)	38.05N	30.14E	410177A.DKH	3	0.5	30	0.152	10/10/1995	38.10N	30.16E	4.0	6
62	DCE (Dinar Cezaevi)	38.07N	30.16E	3Q0179A.DCE	4	0.4	20	0.443	10/10/1995	38.04N	30.12E	5.2	5
63	DJK (Dinar Jandarma)	38.07N	30.16E	3Q0178A.DJK	4	0.5	22	0.181	10/10/1995	38.04N	30.12E	4.5	5
64	DKH (Dinar Koy)	38.05N	30.14E	3Q0177A.DKH	3	0.5	35	0.365	10/10/1995	38.04N	30.12E	4.4	1
65	DKH (Dinar Koy)	38.05N	30.14E	410177A.DKH	3	0.5	30	0.152	10/10/1995	38.11N	30.21E	4.0	8
66	DKH (Dinar Koy)	38.05N	30.14E	460177A.DKH	3	0.8	40	0.076	11/10/1995	38.12N	30.13E	3.6	9
67	DSI (Dinar Devlet-Su)	38.07N	30.18E	490183A.DSI	1	0.4	30	0.152	11/10/1995	38.12N	30.18E	4.9	6
68	DDH (Dinar Devlet-Hasta)	38.07N	30.17E	490180A.DDH	1	0.2	30	0.399	11/10/1995	38.12N	30.18E	5.1	6
69	DCE (Dinar Cezaevi)	38.07N	30.16E	490179A.DCE	4	0.4	20	0.443	11/10/1995	38.12N	30.18E	5.2	9
70	DKH (Dinar Koy)	38.05N	30.14E	4D0177A.DKH	3	0.5	35	0.132	12/10/1995	38.09N	30.22E	4.1	9
71	DJK (Dinar Jandarma)	38.07N	30.16E	4F0178A.DJK	4	0.4	28	0.133	12/10/1995	38.11N	30.17E	4.6	4
72	DDH (Dinar Devlet-Hasta)	38.07N	30.17E	4F0180A.DDH	1	0.5	30	0.272	12/10/1995	38.11N	30.17E	4.3	4
73	DSI (Dinar Devlet Su)	38.07N	30.18E	4F0183A.DSI	1	0.6	28	0.091	12/10/1995	38.11N	30.17E	3.8	4
74	DKH (Dinar Koy)	38.05N	30.14E	4F0177A.DKH	3	0.4	35	0.403	12/11/1995	38.11N	30.17E	4.7	8
75	ERC (Erzincan-Bayindirlik)	39.74N	39.51E	4I0624A.ERC	3	0.2	19	0.269	05/12/1995	39.48N	40.32E	6.2	74
76	ELZ (Elazig-Bayindirlik)	38.67N	39.14E	4I0280A.ELZ	4	0.3	27	0.101	05/12/1995	39.48N	40.32E	6.1	134
77	ELZ (Elazig-Bayindirlik)	38.67N	39.14E	4H0280A.ELZ	4	0.3	30	0.083	05/12/1995	39.35N	40.22E	5.8	117
78	ERC (Erzincan-Bayindirlik)	39.74N	39.51E	4H0624A.ERC	3	0.25	20	0.274	05/12/1995	39.35N	40.22E	5.8	74
79	ERC (Erzincan-Bayindirlik)	39.74N	39.51E	4P0624A.ERC	3	0.7	28	0.467	14/02/1996	39.91N	39.23E	3.8	32
80	KUS (Kusadasi-Meteo)	37.86N	27.26E	4S0992A.KUS	2	1	18	0.209	20/02/1996	38.25N	27.13E	4.0	44
81	AMS (Amasya-Bayindirlik)	40.63N	35.87E	4U0277A.AMS	3	0.8	18	0.098	17/03/1996	40.71N	35.38E	4.5	41
82	IZR (Izmir-Ziraat)	38.40N	27.19E	4V0278A.IZM	1	0.4	15	0.182	02/04/1996	37.78N	26.64E	5.6	90
83	KUS (Kusadasi-Meteo)	37.86N	27.26E	4V0992A.KUS	2	1.5	18	0.316	02/04/1996	37.78N	26.64E	5.4	56
84	TKR (Tekirdag)	40.96N	27.53E	510289A.TKR	3	0.6	15	0.215	14/04/1996	40.80N	27.45E	4.6	16
85	HTY (Hatay-Bayindirlik)	36.25N	36.11E	560284A.HTY	2	0.5	20	0.055	19/06/1996	35.99N	36.05E	5.0	24
86	DIN (Dinar-Meteo)	38.06N	30.15E	5B2873A.DIN	3	0.2	9	0.915	29/06/1996	38.05N	30.11E	5.9	5
87	AMS (Amasya-Bayindirlik)	40.63N	35.87E	5K0277A.AMS	3	0.4	18	0.111	14/08/1996	40.32N	35.14E	5.5	70
88	AMS (Amasya-Bayindirlik)	40.63N	35.87E	5J0277A.AMS	3	0.35	20	0.328	14/08/1996	40.79N	35.23E	5.7	57
89	MRZ (Merzifon)	40.88N	35.94E	5J1186A.MRZ	3	0.4	20	0.976	14/08/1996	40.79N	35.23E	5.7	59
90	TKT (Tokat-Bayindirlik)	40.30N	36.57E	5J0291A.TKT	4	0.7	12	0.149	14/08/1996	40.79N	35.23E	5.7	126
91	AMS (Amasya-Bayindirlik)	40.63N	35.87E	5G0277A.AMS	3	0.35	15	0.529	14/08/1996	40.74N	35.29E	5.8	50
92	TKT (Tokat-Bayindirlik)	40.30N	36.57E	5G0291A.TKT	4	0.32	11	0.102	14/08/1996	40.74N	35.29E	5.8	118
93	AMS (Amasya-Bayindirlik)	40.63N	35.87E	5V0277A.AMS	3	0.9	15	0.074	20/08/1996	40.68N	35.34E	4.4	19
94	AMS (Amasya-Bayindirlik)	40.63N	35.87E	5Y0277A.AMS	3	1.5	12	0.079	06/09/1996	40.57N	35.86E	3.7	6
95	ERC (Erzincan-Bayindirlik)	39.74N	39.51E	610624A.ERC	3	1	22	0.346	18/09/1996	39.60N	39.25E	3.8	27
96	BLD (Buldan-Kayma)	38.04N	28.83E	734996A.BLD	1	0.45	20	0.393	21/01/1997	38.12N	28.92E	5.2	12
97	HTY (Hatay-Bayindirlik)	36.25N	36.11E	6N0284A.HTY	2	0.3	25	1.489	22/01/1997	36.14N	36.12E	5.7	22.5
98	HTY (Hatay-Bayindirlik)	36.25N	36.11E	6X0284A.HTY	2	0.4	18	0.132	23/01/1997	35.98N	36.19E	4.8	25
99	HTY (Hatay-Bayindirlik)	36.25N	36.11E	6T0284A.HTY	2	0.4	28	0.283	30/01/1997	36.16N	36.33E	5.2	21.5
100	AMS (Amasya-Bayindirlik)	40.63N	35.87E	790277A.AMS	3	1.5	15	0.206	28/02/1997	40.68N	35.50E	4.9	31
101	HTY (Hatay-Bayindirlik)	36.25N	36.11E	7P0284A.HTY	2	0.8	25	0.112	13/04/1997	36.31N	36.02E	4.5	20
102	KUS (Kusadasi-Meteo)	37.86N	27.26E	800992A.KUS	2	4	18	0.487	27/05/1997	37.98N	27.47E	3.3	18
103	KUS (Kusadasi-Meteo)	37.86N	27.26E	7Z0992A.KUS	2	2	18	0.377	27/05/1997	37.86N	27.12E	3.4	13
104	KUS (Kusadasi-Meteo)	37.86N	27.26E	810992A.KUS	2	4	27	0.428	29/05/1997	38.04N	27.51E	3.3	30
105	KUS (Kusadasi-Meteo)	37.86N	27.26E	820992A.KUS	2	3.5	18	0.215	29/05/1997	37.89N	27.31E	3.8	7
106	HRS (Horasan-Tarim)	40.04N	42.17E	7X0282A.HRS	4	0.25	15	0.161	01/06/1997	39.35N	41.68E	4.5	90
107	SKR (Sakaraya-Bayindirlik)	40.73N	30.38E	9B0246A.SKR	3	3	45	0.107	22/08/1997	40.73N	30.37E	3.9	1
108	HTY (Hatay-Bayindirlik)	36.25N	36.11E	8K0284A.HTY	2	1	22	0.079	12/09/1997	35.94N	36.21E	3.9	21.5
109	ERZ (Erzerum-Bayindirlik)	39.90N	41.26E	8L0286A.ERZ	1	0.7	20	0.062	15/09/1997	39.31N	41.26E	4.4	69
110	DNZ (Denizli-Bayindirlik)	37.81N	29.11E	8R0241A.DNZ	4	1	40	0.249	24/09/1997	37.81N	29.06E	3.6	4
111	DNZ (Denizli-Bayindirlik)	37.81N	29.11E	8S0241A.DNZ	4	0.8	19	0.220	24/09/1997	37.87N	29.00E	3.7	10
112	HTY (Hatay-Bayindirlik)	36.25N	36.11E	980284A.HTY	2	2	18	0.050	02/10/1997	35.79N	36.23E	3.8	24
113	VAN (Van)	38.50N	43.40E	9F0233A.VAN	3	0.4	25	0.214	12/10/1997	38.47N	43.39E	4.7	4
114	SKR (Sakaraya-Bayindirlik)	40.73N	30.38E	9K0246A.SKR	3	3	45	0.107	21/10/1997	40.70N	30.42E	3.9	6
115	CNK (Canakkale-Meteo)	40.14N	26.40E	9P0244A.CNK	4	0.5	20	0.133	25/10/1997	40.49N	26.43E	4.6	37

Table 1 (*continued*)

No	Station	Coordinates		Code	Site	Filters applied (Hz)		PGA (m/s^2)	Earthquake (date)	Epicenter (coordinate)		Mw	Dist. epi (km)
						HP	LP						
116	MLZ (Malazgirt-Meteo)	39.17N	42.54E	A10278A.MLZ	4	0.3	15	0.101	03/11/1997	39.31N	42.66E	4.6	22
117	MLZ (Malazgirt-Meteo)	39.17N	42.54E	9Z0278A.MLZ	4	0.4	12	0.169	03/11/1997	38.76N	42.40E	5.0	59
118	CNK (Canakkale-Meteo)	40.14N	26.40E	A30244A.CNK	4	0.2	18	0.102	14/11/1997	38.86N	25.74E	6.1	165
119	HTY (Hatay-Bayindirlik)	36.25N	36.11E	A70284A.HTY	2	2.2	19	0.051	04/12/1997	36.55N	36.10E	3.9	19.2
120	SKR (Sakaraya-Bayindirlik)	40.74N	30.38E	B10246A.SKR	3	0.25	33	0.696	20/02/1998	40.78N	30.37E	4.6	6
121	ERZ (Erzerum-Bayindirlik)	39.90N	41.26E	AQ0449A.ERZ	1	0.4	20	0.066	24/02/1998	39.80N	41.30E	4.5	13
122	BLK (Balikesir-Huzur)	39.66N	27.86E	AY0243A.BLK	1	0.7	18	0.092	05/03/1998	39.65N	26.86E	4.9	86
123	EDR (Edremit)	39.58N	27.02E	AX2876A.EDR	1	1.5	15	0.247	05/03/1998	39.65N	26.86E	4.1	15
124	EDR (Edremit)	39.58N	27.02E	AY2876A.EDR	1	1.5	11	0.129	05/03/1998	39.68N	26.70E	4.5	29
125	CRD (Cardak-Sagli)	37.82N	29.67E	B42418A.CRD	1	0.9	21	0.231	04/04/1998	38.14N	30.04E	5.3	50
126	DIN (Dinar-Meteo)	38.06N	30.16E	B42411A.DIN	3	0.4	10	1.342	04/04/1998	38.14N	30.04E	5.3	49
127	AYD (Aydin-Hayvan)	37.84N	27.84E	BF0453A.AYD	4	0.4	10	0.054	07/04/1998	37.80N	27.53E	4.4	28
128	HRS (Horasan-Tarim)	40.04N	42.17E	BC0282A.HRS	4	0.8	18	0.124	13/04/1998	40.00N	41.80E	4.4	30
129	TER (Tercan-Meteo)	39.78N	40.39E	BP0444A.TER	1	0.4	20	0.101	27/04/1998	39.68N	40.35E	4.6	14
130	HRS (Horasan-Tarim)	40.04N	42.17E	BR0282A.HRS	4	0.8	18	0.124	01/05/1998	40.22N	41.94E	4.4	27
131	ELZ (Elazig-Bayindirlik)	38.67N	39.19E	BT0280A.ELZ	4	0.4	18	0.257	09/05/1998	38.38N	38.94E	5.1	39
132	MLT (Malatya-Bayindirlik)	38.35N	38.34E	BT0245A.MLT	1	0.4	30	0.091	09/05/1998	38.38N	38.94E	5.1	52
133	AMS (Amasya-Bayindirlik)	40.63N	35.87E	BW0277A.AMS	3	1.5	20	0.190	31/05/1998	40.49N	35.73E	4.0	21
134	BKL (Baklali-Koyu)	37.03N	35.63E	CR0222A.BKL	4	0.2	25	0.234	04/07/1998	36.88N	35.62E	5.4	89
135	KIL (Kilicli-Koyu)	37.08N	35.45E	CR0333A.KIL	4	0.2	25	0.903	04/07/1998	36.88N	35.62E	5.4	107
136	NAC (Nacarli-Koyu)	36.87N	35.61E	CR0111A.NAC	1	0.3	20	0.302	04/07/1998	36.88N	35.62E	5.4	90
137	BKL (Baklali-Koyu)	37.03N	35.63E	CO0222A.BKL	4	0.2	25	0.280	04/07/1998	36.84N	35.44E	5.6	28
138	CYH (Ceyhan-PTT)	37.02N	35.81E	CO0247A.CYH	4	0.18	20	0.100	04/07/1998	36.84N	35.44E	5.6	39
139	KIL (Kilicli-Koyu)	37.08N	35.45E	CO0333A.KIL	4	0.5	20	0.902	04/07/1998	36.84N	35.44E	5.4	30
140	NAC (Nacarli-Koyu)	36.87N	35.61E	CO0111A.NAC	1	0.3	20	0.237	04/07/1998	36.84N	35.44E	5.4	16
141	BRN (Bornova-Ziraat)	38.45N	27.23E	D30237A.BRN	4	0.25	20	0.266	09/07/1998	38.08N	26.68E	5.6	62
142	GEC (Gecitli-Koyu)	36.96N	35.63E	DL0205A.GEC	4	0.3	30	0.076	17/07/1998	37.00N	35.67E	4.0	7
143	BNG (Bingol-Bayindirlik)	38.89N	40.50E	F30241A.BNG	1	0.2	30	0.186	08/10/1998	38.77N	40.23E	5.1	27
144	BOL (Bolu-Bayindirlik)	40.75N	31.61E	FB0240A.BOL	4	0.4	15	0.233	22/10/1998	41.00N	31.71E	5.2	29
145	CYH (Ceyhan-PTT)	37.02N	35.81E	G30283A.CYH	4	0.5	15	0.089	15/01/1999	36.81N	35.49E	5.6	37
146	ARC (Arcelik)	40.83N	29.41E	ARC22900.ASC	1	0.35	28	2.032	17/08/1999	40.70N	29.91E	7.4	68
147	ATS (Ambarlik Ter. Cent)	40.58N	28.41E	ATS22900.ASC	4	0.11	15	2.573	17/08/1999	40.70N	29.91E	7.4	127
148	BTS (Botras)	40.59N	27.58E	BTS22900.ASC	3	0.1	18	0.968	17/08/1999	40.70N	29.91E	7.4	197
149	CNAA (Cekmek Nuclear)	41.01N	28.45E	CNA22900.ASC	3	0.1	25	1.711	17/08/1999	40.70N	29.91E	7.4	129
150	DHM (Havaalani)	40.58N	28.49E	DHM22900.ASC	1	0.15	21	0.859	17/08/1999	40.70N	29.91E	7.4	120
151	BUR (Bursa)	40.18N	29.13E	BUR22900.ASC	4	0.12	18	0.996	17/08/1999	40.70N	29.91E	7.4	104
152	FAT (Fatih-Istanbul)	41.03N	28.57E	FAT22900.ASC	4	0.25	18	1.745	17/08/1999	40.70N	29.91E	7.4	119
153	HAS (Heybelida-Hospital)	40.52N	29.05E	HAS22900.ASC	1	0.17	9	0.947	17/08/1999	40.70N	29.91E	7.4	74
154	YPT (Yarimca)	40.45N	29.45E	YPT22900.ASC	1	0.15	15	3.094	17/08/1999	40.70N	29.91E	7.4	46
155	YKP (Yapi Kredi Plaza)	41.04N	29.00E	YKP22900.ASC	1	0.1	10	0.382	17/08/1999	40.70N	29.91E	7.4	86
156	IST (Istanbul-Bayindirlik)	41.06N	29.01E	I30236A.IST	3	0.1	15	0.083	17/08/1999	40.70N	29.91E	7.4	86
157	BRN (Bornova-Ziraat)	38.45N	27.23E	I30237A.BRN	4	0.2	15	0.106	17/08/1999	40.70N	29.91E	7.4	340
158	BLK (Balikesir-Huzur)	39.65N	27.85E	I30243A.BLK	1	0.15	20	0.168	17/08/1999	40.70N	29.91E	7.4	210
159	CNK (Canakkale-Meteo)	40.14N	26.40E	I30244A.CNK	4	0.2	20	0.285	17/08/1999	40.70N	29.91E	7.2	304
160	TKR (Tekirdag-Hokumat)	40.97N	27.51E	I30247A.TKR	4	0.1	20	0.329	17/08/1999	40.70N	29.91E	7.2	204
161	AFY (Afyon Bay.)	38.79N	30.56E	I30284A.AFY	4	0.15	7	0.145	17/08/1999	40.70N	29.91E	7.3	212
162	MNS (Manisa-Bayindirlik)	38.58N	27.45E	I30291A.MNS	1	0.15	4	0.118	17/08/1999	40.70N	29.91E	7.4	315
163	DZC (Duzce-Meteo)	40.85N	31.17E	I30420A.DZC	4	0.17	17	3.516	17/08/1999	40.70N	29.91E	7.4	111
164	TOS (Tosya-Meteo)	41.01N	34.04E	I32293A.TOS	1	0.12	7	0.102	17/08/1999	40.70N	29.91E	7.2	348
165	AYD (Aydin-Hayvan)	37.84N	27.84E	I32296A.AYD	4	0.15	7	0.058	17/08/1999	40.70N	29.91E	7.2	364
166	BRS (Bursa)	40.18N	29.13E	I32298A.BRS	4	0.12	18	0.996	17/08/1999	40.70N	29.91E	7.4	86
167	DNZ (Denizli-Bay.)	37.81N	29.11E	I32300A.DNZ	4	0.22	7	0.077	17/08/1999	40.70N	29.91E	7.4	326
168	KUT (Kutahya)	39.42N	29.99E	I32302A.KUT	4	0.15	12	0.574	17/08/1999	40.70N	29.91E	7.4	135
169	GYN (Goynuk-Devlet)	40.38N	30.73E	I32419A.GYN	1	0.77	21	1.361	17/08/1999	40.70N	29.91E	7.4	77
170	IZT (Izmit-Meteo)	40.79N	29.96E	I32755A.IZT	3	0.12	20	2.259	17/08/1999	40.70N	29.91E	7.4	13
171	ERG (Eregli-Kaymakamlik)	40.98N	27.79E	I32867A.ERG	1	0.5	15	1.037	17/08/1999	40.70N	29.91E	7.4	181
172	GBZ (Gebzeh-tubitak-Mar.)	40.82N	29.44E	I32878A.GBZ	4	0.38	20	2.047	17/08/1999	40.70N	29.91E	7.4	46
173	CEK (Cekmek Nuclear C.)	40.97N	28.70E	I34984A.CEK	3	0.8	12	1.213	17/08/1999	40.70N	29.91E	7.4	107

(*continued on next page*)

Table 1 (*continued*)

No	Station	Coordinates		Code	Site	Filters applied (Hz)		PGA (m/s^2)	Earthquake (date)	Epicenter (coordinate)		Mw	Dist. epi (km)
						HP	LP						
174	IZN (Iznik-Karayollari)	40.44N	29.69E	I34995A.IZN	1	0.28	20	1.263	17/08/1999	40.70N	29.91E	7.4	35
175	BLK (Balikesir-Huzur)	39.65N	27.85E	IQ0243A.BLK	1	0.5	20	0.213	17/08/1999	40.85N	30.35E	4.1	16
176	TPT (Kocaeli)	40.72N	30.07E	5H0111A.TPT	4	0.15	20	6.004	13/09/1999	40.80N	30.03E	5.9	14
177	IST (Istanbul-Bay.)	41.05N	29.01E	5H0236A.IST	3	0.15	20	0.151	13/09/1999	40.80N	30.03E	5.9	89
178	CNK (Canakkale-Meteo)	40.14N	26.40E	5H0244A.CNK	4	0.1	7	0.058	13/09/1999	40.80N	30.03E	5.9	300
179	SKR (Sakaraya)	40.73N	30.38E	5H0246A.SKR	3	0.15	30	0.511	13/09/1999	40.80N	30.03E	5.9	31
180	BAH (Ceftlikoy-Emniyat)	40.71N	29.90E	5H0713A.BAH	4	0.18	25	3.830	13/09/1999	40.80N	30.03E	5.9	19
181	KUT (Kutahya-Bay.)	39.42N	29.99E	5H2302A.KUT	4	0.2	12	0.133	13/09/1999	40.80N	30.03E	5.9	156
182	IZT (Izmit-Meteo)	40.79N	29.96E	5H2755A.IZT	3	0.8	18	3.030	13/09/1999	40.80N	30.03E	5.9	7
183	SKR (Sakaraya-Bay.)	40.74N	30.38E	7E0246A.SKR	3	0.25	25	3.334	11/11/1999	40.82N	30.20E	5.7	20
184	KUT (Kutahya-Bay.)	39.42N	29.99	7E2302A.KUT	4	0.18	12	0.099	11/11/1999	40.82N	30.20E	5.7	158
185	BOL (Bolu-Bay.)	40.74N	31.61E	0000000.BOL	4	0.2	30	7.959	12/11/1999	40.74N	31.21E	7.1	38
186	IST (Istanbul-Bay.)	41.06N	29.01E	000236A.IST	3	0.1	15	0.083	12/11/1999	40.74N	31.21E	7.1	184
187	SKR (Sakaraya-Bay.)	40.73N	30.38E	000246A.SKR	3	0.2	18	0.228	12/11/1999	40.74N	31.21E	7.1	71
188	TKR (Tekirdag-Hokumat)	40.98N	27.51E	000247A.TKR	4	0.2	15	0.059	12/11/1999	40.74N	31.21E	7.1	309
189	AFY (Afyon Bay.)	38.79N	30.56E	000284A.AFY	4	0.1	4	0.078	12/11/1999	40.74N	31.21E	7.1	238
190	TOS (Tosya-Meteo)	41.01N	34.04E	002293A.TOS	1	0.1	8	0.073	12/11/1999	40.74N	31.21E	7.1	238
191	BRS (Bursa-Sivil-Savunma)	40.18N	29.13E	002298A.BRS	4	0.12	12	0.088	12/11/1999	40.74N	31.21E	7.1	191
192	KUT (Kutahya-Bayindirlik)	39.42N	29.99E	002302A.KUT	4	0.1	10	0.203	12/11/1999	40.74N	31.21E	7.1	190
193	GYN (Goynuk-Devlet)	40.38N	30.73E	002419A.GYN	1	0.4	11	0.240	12/11/1999	40.74N	31.21E	7.1	67
194	MDR (Mudurno)	40.46N	31.18E	004959A.MDR	1	0.23	15	1.118	12/11/1999	40.74N	31.21E	7.1	48
195	DZC (Duzce-Meteo)	40.85N	31.17E	004990A.DZC	4	0.28	20	5.213	12/11/1999	40.74N	31.21E	7.1	13
196	DZC (Duzce-Meteo)	40.85N	31.17E	DUZ04500.ASC	4	0.5	15	0.363	14/02/2000	41.02N	31.76E	5.7	55
197	DNZ (Denizli-Bay.)	37.81N	29.11E	DNZ11100.ASC	4	0.2	30	0.268	21/04/2000	37.85N	29.27.E	5.3	16
198	AYD (Aydin-Hayvan)	37.84N	27.84E	AYD11300.ASC	4	0.18	25	0.168	23/04/2000	37.89N	27.55E	4.9	20
199	BOL (Bolu-Bay.)	40.75N	31.61E	BOL12900.ASC	4	0.25	25	0.093	09/05/2000	40.81N	31.38E	4.7	32
200	SKR (Sakaraya-Bay.)	40.73N	30.38E	SKR14200.ASC	3	4.0	40	0.114	22/05/2000	40.82N	30.31E	3.7	12
201	DNZ (Denizli-Bay.)	37.81N	29.11E	DNZ15501.ASC	4	0.9	20	0.057	04/06/2000	37.93N	29.14E	3.9	12
202	DNZ (Denizli-Bay.)	37.81N	29.11E	DNZ15506.ASC	4	0.35	25	0.142	04/06/2000	37.83N	29.02E	4.1	12
203	DNZ (Denizli-Bay.)	37.81N	29.11E	DNZ1550I.ASC	4	0.25	25	0.401	04/06/2000	37.79N	29.33E	4.4	12
204	DNZ (Denizli-Bay.)	37.81N	29.11E	DNZ15600.ASC	4	0.3	30	0.272	05/06/2000	37.84N	29.16E	4.4	12
205	CER (Cerkes-Meteo)	40.88N	32.91E	CER15700.ASC	1	0.15	25	0.616	06/06/2000	40.65N	32.92E	6.0	40
206	TOS (Tosya-Meteo)	41.01N	34.04E	TOS15700.ASC	1	0.2	18	0.118	06/06/2000	40.46N	32.76E	5.9	80
207	BOL (Bolu-Bay.)	40.75N	31.61E	BOL15900.ASC	4	0.4	12	0.158	08/06/2000	40.82N	31.64E	4.5	26
208	CER (Cerkes-Meteo)	40.88N	32.91E	CER15901.ASC	1	0.2	30	0.146	08/06/2000	40.64N	33.01E	5.8	36
209	CER (Cerkes-Meteo)	40.88N	32.91E	CER16000.ASC	1	0.15	20	0.185	09/06/2000	40.63N	32.97E	6.2	36
210	DNZ (Denizli-Bay.)	37.81N	29.11E	DNZ17601.ASC	4	0.8	25	0.074	25/06/2000	37.67N	29.09E	4.0	12

differences for well-recorded data as explained later in this paper.

The magnitudes of the events are presented as available; body wave, surface wave and moment magnitudes (mb, Ms and Mw, as reported by NEIC) are included, whilst the local magnitudes are those given by the Turkish National Seismic Network (catalog presented by the GDDA web site). We have decided to derive a moment magnitude for all records, to provide a uniform and reliable scale for further studies (for instance to establish the attenuation laws). Moment magnitude (Mw) is systematically calculated for well-recorded earthquakes (i.e. with large signal/noise ratio below the corner frequency). When it was not possible to calculate the Mw precisely because of the high noise level, other magnitudes were converted to Mw using a correlation. Ambraseys and Free [16] showed that such correlation exists between Ms and Mw [17] for an European database. This approach which has already been applied for the Iranian strong motion data [14] is found to be stable using the Turkish data. The Iranian strong motion derived Mw, that are already calculated using a database of 468 three-components dataset [14], where included in Fig. 3 to compare with the Turkish data and to show the consistency of the estimated Mw values. For the reported ML values, we have observed that they are systematically lower than the calculated Mw values (Fig. 3). Based on the Turkish dataset, we observe a linear relationship between the ML values reported by the Turkish national seismic network and the estimated Mw values based on the strong motion records, as

$$\mathrm{Mw} = 0.76\mathrm{ML} + 1.13$$

$$\sigma = 1.26$$

$$R = 0.75$$

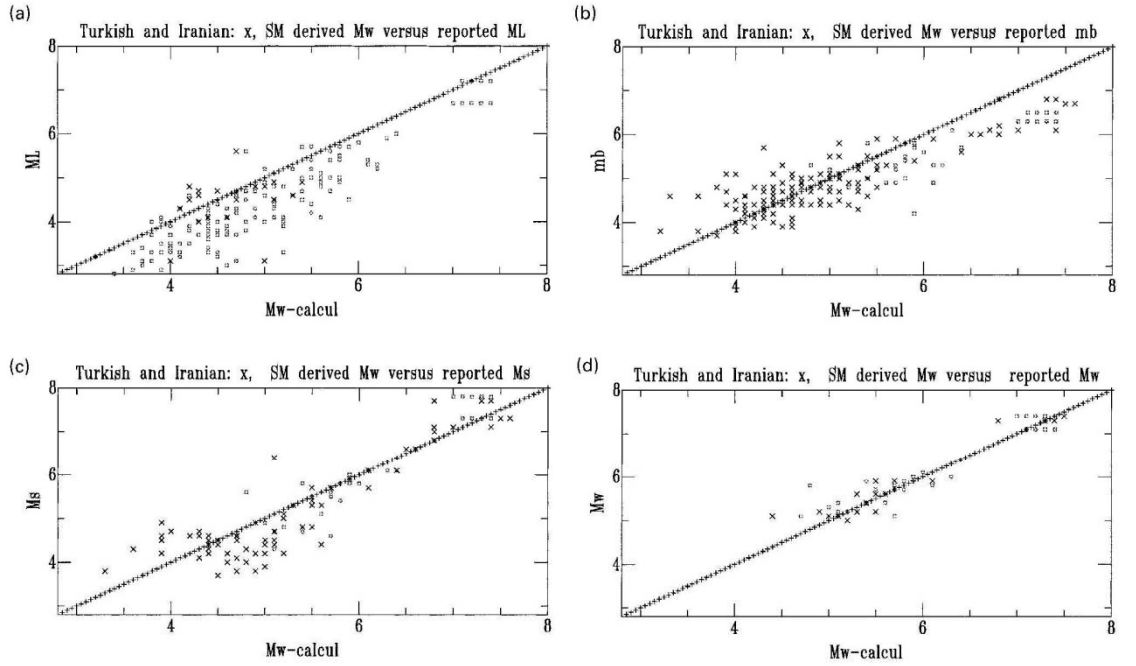

Fig. 3. The correlation between the calculated Mw and the reported ML, mb, Ms and Mw values. Open circles correspond to the Turkish data, crosses to the Iranian data.

where σ is the standard deviation and R is the correlation coefficient. The focal depths from NEIC reports show that most of the recorded events in the Anatolian plateau were superficial. Almost all of the data in Table 1 (all but one) had focal depths between 0 and 35 km (including the default values of '33 km'). There is just one event with a much larger depth (30/06/1981, ML4.7, focal depth = 63 km, epicenter located in southern Turkey near the Syrian border). For events, corresponding to 33 records, no depth was reported by any agency.

The earthquake intensities are based on published isoseismal maps or damage reports [1,5,6,18,19]. The intensity gives an idea on the degree of damage during an event in an inhabited region. In some cases the landslide reports (as geotechnical evidence) are also used to estimate the intensity; a previous study on the Manjil, Iran, earthquake [20], for example, showed that landslides in the form of rock-block slides occurred only in areas with intensities of at least VI MSK (~VI EMS98).

The focal mechanisms of the studied events are based on the NEIC catalog and Harvard CMT estimations available on the Internet. The deformation of the Anatolian plateau is accommodated through strike-slip, normal and reverse/-thrust faults. Jackson and McKenzie, Barka, Nalbant et al., Stein et al., and Straub and Kahle [7–11,21] have shown and discussed the details of stress and deformation features within the Anatolian plateau. The prevalent characteristics of this plateau relate to the strike-slip faulting along the North Anatolian Fault (NAF) system. This right-lateral fault system is one of the longest strike-slip structures in the world elongating for more than 1000 km. The east Anatolian fault system dominates southeastern and eastern parts of the plateau with a general left-lateral strike-slip movement. The Aegean Sea extensional system is partly controlling the tectonics of western Turkey and its intersection with the NAF system induces pull-apart en echelon and extensional faults. Such situation results in a variety of source mechanisms for events taking place in Turkey.

3. Extracting the most reliable records

Among the 420 records available as of June 2000 on the web sites, we selected our database according to the following criteria:

knowledge of magnitude and source location. The existence of the minimum required source parameters (magnitude and epicentral distance) is necessary to develop the attenuation laws.

signal to noise ratio greater than 3–4. Many SMA-1 records have significant level of long period noises, and it was not possible to distinguish real signal from the noise

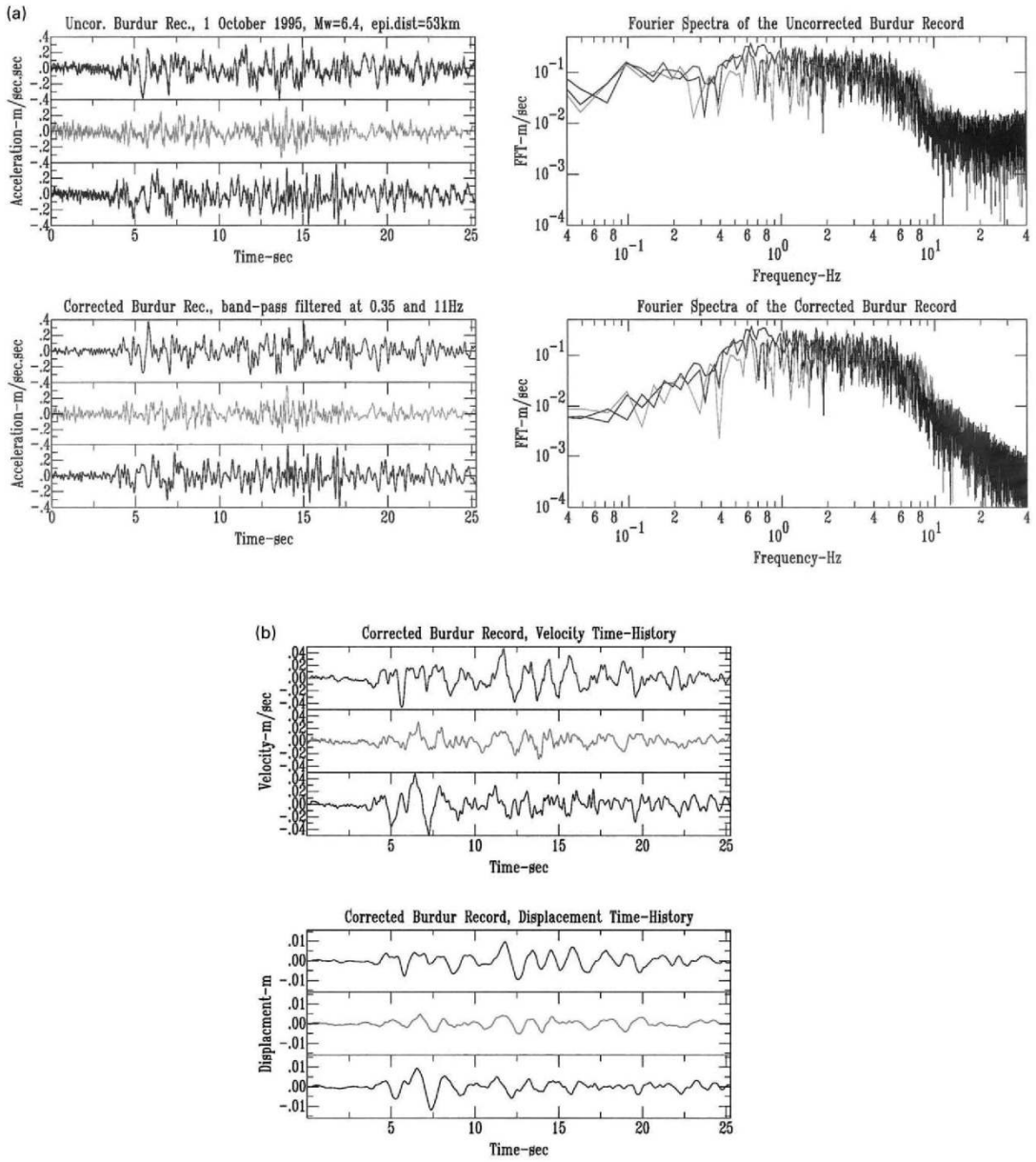

Fig. 4. (a) Three-component acceleration time history recorded in Burdur for the Dinar earthquake of 1 October 1995, Mw = 6.4, (up: uncorrected record and its Fourier spectra; down: the band-passed filtered record between 0.35 and 11 Hz and the corresponding Fourier spectra). The middle trace is the vertical and the two others (NS and EW, up and down, respectively) are the horizontal components. (b) The velocity and displacement time-histories of Burdur record after integration; the vertical component is placed in the middle and horizontal (NS and EW, up and down, respectively) components are the others.

(especially in the case of records corresponding to low magnitude events or records that were obtained in far distances from the epicenters).

peak ground acceleration (PGA) larger than 0.05 m/s^2. Only accelerograms with a PGA level in excess of 0.05 m/s^2 are selected. The PGA values presented in Table 1 are the largest peak among the three-components.

The amount of low and high frequency noise was checked for all records, as explained later.

4. Data correction

The data correction (after base-line correction) is carried out through the following steps:

4.1. Determination of the appropriate frequency band

For each record, a 'signal' window, $s(t)$, is selected as well as a 'noise' window, $n(t)$. The latter one is preferably chosen in the pre-event memory, but this is possible only in digital recordings. The Fourier transform of the signal is computed ($S(f)$) over a length t_s, and the Fourier transform of the noise $N(f)$ is computed over a length of t_n. The normalized signal to noise ratio (R_{sn}) is then derived at each frequency by

$$R_{sn}(f) = \frac{S(f)/\sqrt{t_s}}{N(f)/\sqrt{t_n}}$$

A threshold level of 3 for R_{sn} is selected to delimitate the frequency band $[f_{HP}, f_{LP}]$, where the information is meaningful, so as to obtain

$$\forall f \in [f_{HP}, f_{LP}], R_{sn}(f) \geq 3$$

This procedure is applied on smoothed Fourier spectrum. The smoothing function is the Konno and Ohmachi one [22] which keeps correct amplitudes whatever the frequency.

4.2. Spectrum shape

To be sure that the selected frequency band is the dominant signal band, the Fast Fourier Transform (FFT) is calculated for all of the records. According to the theoretical shape of the far field Fourier spectrum of acceleration, an ω^2 increase is expected in the region below the 'corner frequency' (f_c) and a decaying shape at high frequencies beyond the 'maximum frequency' (f_{max}) with a plateau in between. A more or less constant amplitude of the FFT spectrum at frequencies lower than f_c or at frequencies beyond f_{max} is generally an indication of large low or high frequency noise, respectively. The Fourier spectra of the record obtained in Burdur station during the 1 October, 1995, Dinar earthquake, (Mw6.4) is shown in Fig. 4a before and after filtering. In this figure, the parts of the spectra below 0.35 Hz and beyond 11 Hz are abnormally high. Therefore these parts may be thought of as noises and the reliable part of the signal limits between the two frequencies.

4.3. Filtering and integration

Once the reliable frequency band is determined through both signal to noise ratio (R_{sn}) and checking of the spectrum shape, the signal window is band pass filtered with a butterworth filter of order 2. Butterworth filter is chosen since it has a fairly sharp transition from pass band to stop band, and it has a moderate group delay response. The result of the use of band-pass filtering is shown in the lower part of Fig. 4a, in the case of Burdur accelerograms during the Dinar earthquake. The FFT for this three-component record after the filtering (using a band-pass filter with cutoff filters 0.35 and 11 Hz) is presented in this figure. The velocity and displacement time-histories of this record after filtering and integration are shown in Fig. 4b.

5. The site effects

The records are obtained on different soil conditions. No information can be gathered from the Internet regarding the soil condition at the strong motion stations. Based on our experience with the Iranian data, we have decided to classify the records for site conditions according to the frequency band of the fundamental frequency based on their H/V ratio. This ratio is chosen based on the location of the broadened H/V spectral ratios and the value of its amplitude [24]. In brief, site category 1 corresponds to rock and hard alluvial sites, with Vs $>$ 800 m/s over the uppermost 30 m and fundamental frequency (f_0) larger than 15 Hz. Site category 2 relates to alluvial sites; thin soft alluviums, with $500 <$ Vs < 700 over the uppermost 30 m and $5 < f_0 <$ 15 Hz. Site category 3 corresponds to soft gravel and sandy sites, with $300 <$ Vs < 500 over the uppermost 30 m and $2 < f_0 < 5$ Hz. Finally site category 4 relates to soft soil sites; thick soft alluviums with Vs < 300 m/s over the uppermost 35 m and $f_0 < 2$ Hz. This preliminary ranking is based on studies at 50 sites where geotechnical measurements were performed (compressional and shear wave velocity and microtremor measurements), as well as on three-component accelerograms, which were used to calculate the receiver function for the strong motions [24].

This method of site categorization was recently given further support by the well constrained Japanese strong motion (K-NET) dataset [23] and Yamazaki and Ansary [27]. This is the only method that may reveal the site response, in the absence of any reliable geological and geotechnical data. The velocity profiles that we measured for Iran [24] by seismic refraction techniques were limited to the first 30–35 m; the microtremors showed important amplifications just in the soft soil sites, and the geoelectric tests did not give precise results to distinguish different sites. Meanwhile, if there are thick alluvial layers on the surface (with a thickness of more than 30 m) on a very high velocity layer at greater depths, the H/V spectrum (receiver function) of strong motion is the only way to detect the low frequency effects.

We have first detected the stability of the H/V ratio for the few stations where several records were available. We observe that the number of stations is 33, 4, 14 and 30 for site classes 1, 2, 3, and 4, respectively. The stability of results is investigated and confirmed, for instance, in Dinar-Devlet-Hastanesi (site class 1; 3 records), Hatay-Bayindirlik (site class 2; 9 records), Dinar-Meteorology Station (site

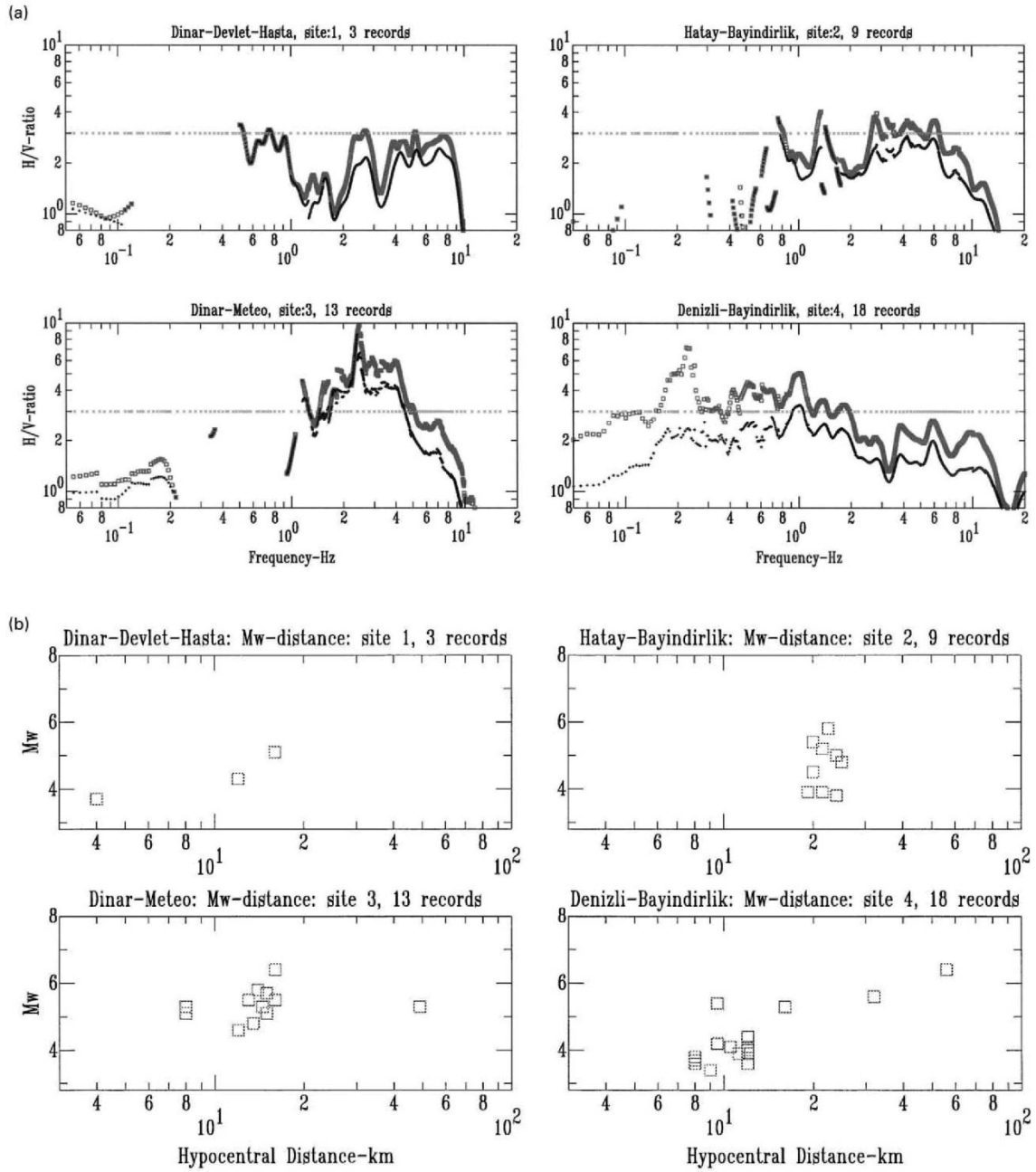

Fig. 5. Checks on the stability of the H/V ratio; (a) The H/V ratio (mean and $M - \sigma$) in: Dinar-Devlet Hasta station, site class 1, 3 records; Hatay-Bayindirlik station, site class 2, 9 records; Dinar-Meteorology station, site class 3, 13 records and Denizli-Bayindirlik station, site class 4, 18 records. (b) Distance–magnitude distributions of records in each stations.

class3; 13 records) and Denizli-Bayindirlik (site class 4; 18 records) (Fig. 5a). The magnitude–distance distributions for these sites are shown in Fig. 5b. The results of our H/V study for the Turkish strong motion stations are shown in Fig. 6 for site classes 1–4.

Site conditions derived from the H/V spectra were compared with the results from published studies on some earthquakes in Turkey. The Dinar-Devlet-Hastanesi (DDH) station in the foothill zone in the town of Dinar is interpreted to be a rock site and is used as a reference

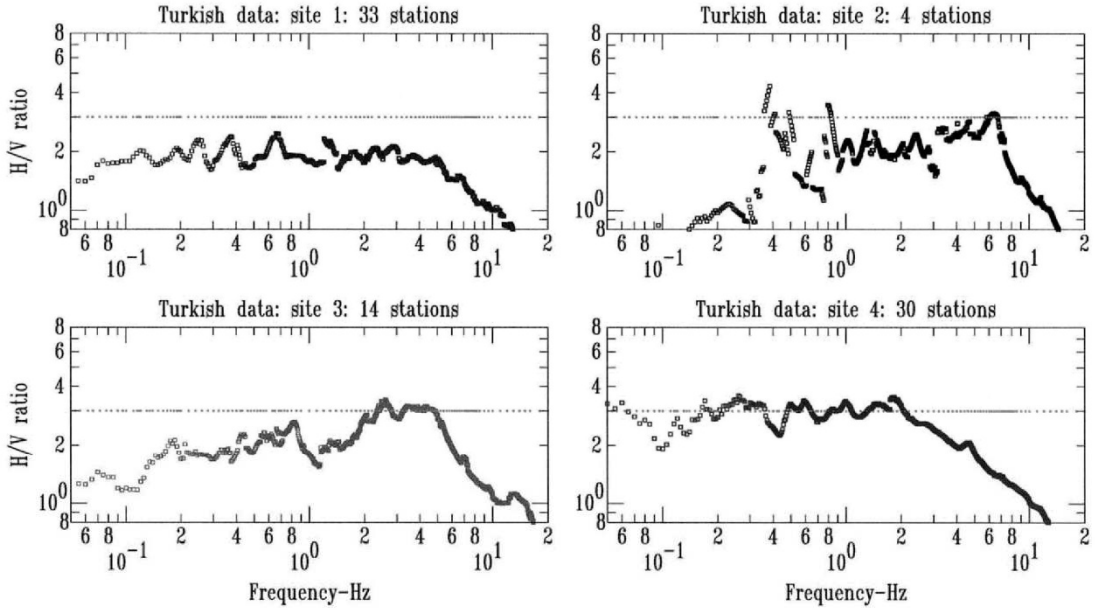

Fig. 6. The mean H/V ratio for the 4 site categories, site class 1, 33 stations; site class 2, 4 station; site class 3, 14 stations and site class 4, 30 stations.

site to estimate soil amplifications in other stations in Dinar by Durukal et al. [5]. The assignment of site class 1 in the present study, as shown in Fig. 5 (based on the record obtained during the Dinar earthquake of 1 October, 1995, Mw = 6.4, mainshock), seems to be reasonable. A site effect study on the mainshock and aftershock records of the Erzincan earthquake of 13 March, 1992 [13] showed the soft soil site conditions in the site of the Sugar factory to the south of Erzincan. Another report by Ansal and Lav [12] has shown the superficial low velocity layers to the east of Erzincan and higher velocity surface deposites in the central parts of the town. None of these papers report on the shear wave velocity measurements in the first 30 m. We have found site class 1 for the Erzincan-meteorology station (in the foothill area of Erzincan), and class 3 for the Erzincan-Bayindirlik station (located towards the east of the meteorology station) (Fig. 7a and b).

Site classes assigned to each station using the approach explained earlier can be found in Table 1.

6. Assigning a quality label to each record

A four-class categorization is used to grade the quality of each record; 'A' corresponds to the best quality and 'D' to the worst. The existence of the following four criteria are taken into account in this categorization:

1. quality of digitization of the analog records (corresponding generally to low PGA records); such that the good quality signals exist in the frequency band of 0.1–10 Hz
2. focal depth (should be determined by the seismologist, without considering the teleseismic and default values)
3. macroseismic epicentral distance (the distance to region with the maximum damage)
4. source mechanism

If all of these indications are available for one record, then its label is assigned 'A_2', and in the absence of one, two, three of these cases, the qualify factor diminishes to 'A_1', 'B', 'C'. For instance, if three of these indications exist for a record, 'A_1' is assigned, and in the presence of two indications, we have assigned 'B' to the record, and so on. The worst records that have none of these indications but have at least the earthquake 'magnitude' and the instrumental epicentral distance are referred to as 'D'.

7. The sources of uncertainties

Some sources of uncertainties during this study may originate from the following.

7.1. The instrumental and macroseismic epicentral distances

According to the international and/or Turkish agencies, the teleseismic epicenter determinations include uncertainties varying from about 0.01° (approximately about 1 km in regions like Turkey) for the great earthquakes with magnitudes more than M7, to about 0.15° (approximately

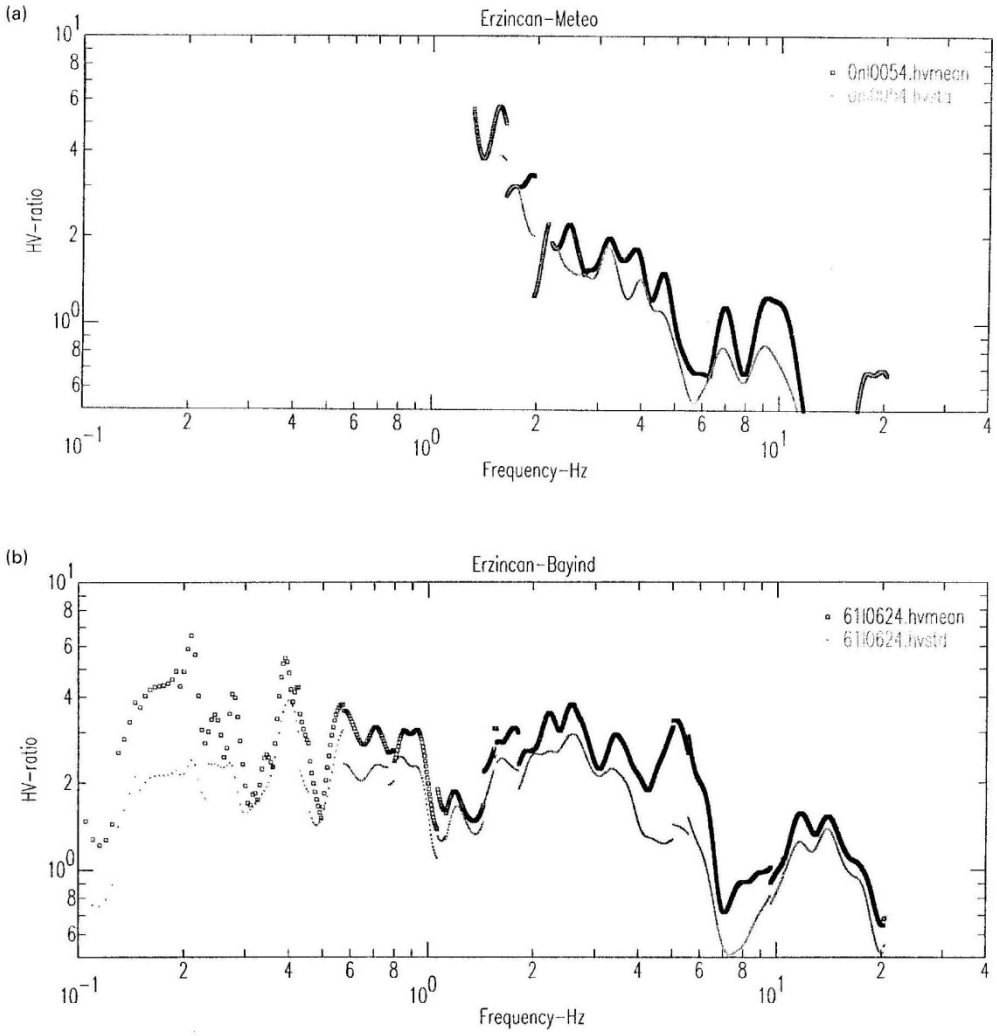

Fig. 7. The H/V ratio for the (a) Erzincan meteorology and (b) Erzincan-Bayindirlik strong motion stations.

about 15 km for such a region) for earthquakes with magnitudes about M4. We feel however that these precision estimates are very optimistic and should at least be doubled.

The macroseismic epicenters are based on damage reports, whenever available (which is only possible when damaging earthquakes occurs in inhabited areas), as well as reported surface fault ruptures, if there are any. Therefore distance estimations to macroseismic epicenters depend greatly on the presence (or absence) of damage reports, geographic distribution of the inhabited regions and finally on the presence of the surface ruptures and also on hypocentral depth. Since this information is the only available information, in most cases, the macroseismic distances are very uncertain. From this point of view, large earthquakes are exceptions (for instance the Erzincan earthquake of 13 March 1992, the Dinar earthquake of 1 October 1995, Adana-Ceyhan earthquake of 4 July 1998, and Izmit, Kocaeli earthquake of 17 August 1999), with detailed damage reports and descriptions of causative faults.

For 175 of the records (mainly the ones from SSA-2 instruments with a pre-event memory) it was possible to estimate the hypocentral distance using the well-known formula

$$D_{\text{hypo}} = 8(t_s - t_p)$$

where t_p and t_s are the arrivals of P and S waves, respectively. This formula was compared with the epicentral distances and focal depths inferred from the Turkish national network, ISC and/or NEIC locations. This distance was not computed for the near-source records of large

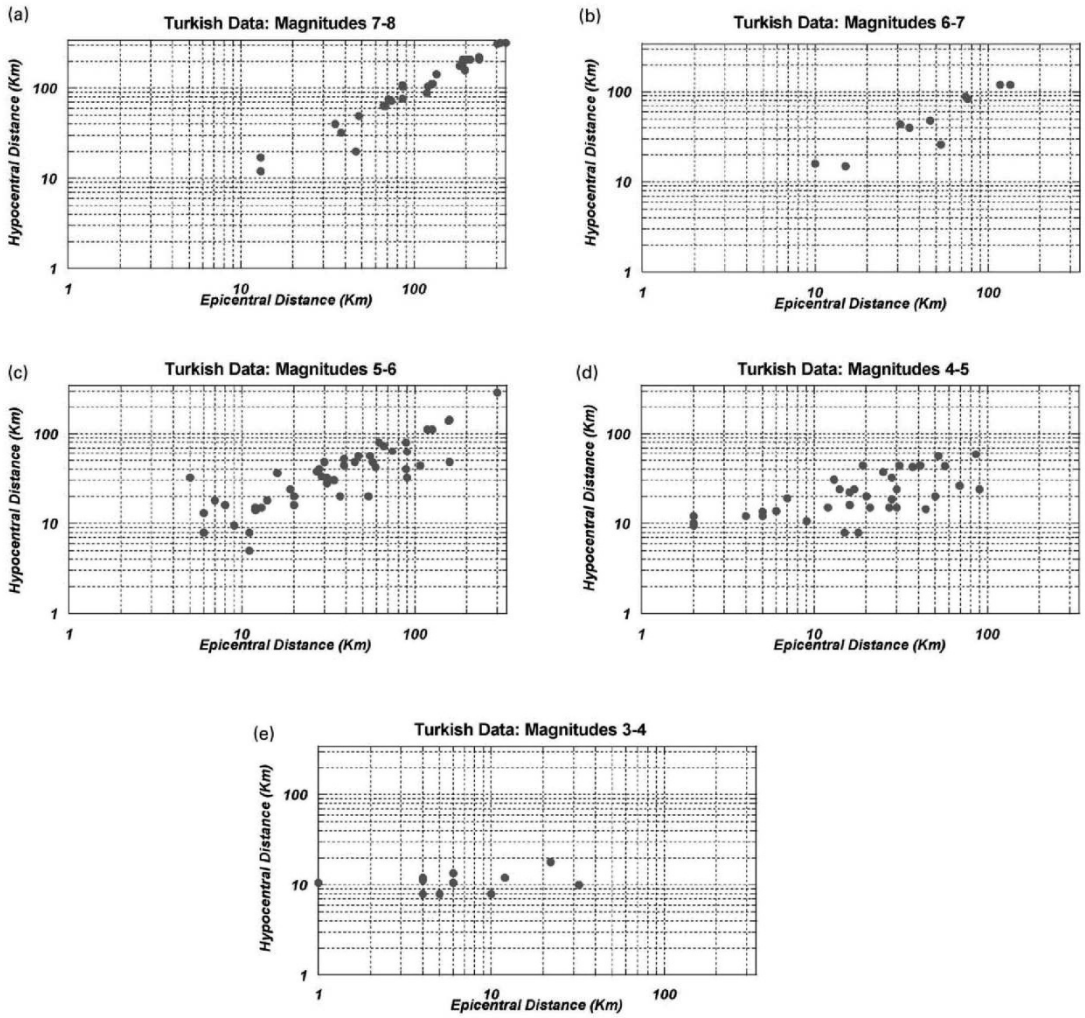

Fig. 8. The relationship between the hypocentral and epicentral distances for different magnitude ranges: (a) M7–8, (b) M6–7, (c) M5–6, (d) M4–5, (e) M3–4.

events, because it was not possible in many cases to identify clearly the P and S waves. Inferred hypocentral distances are plotted against the epicentral distances (based on the teleseismic epicenter locations) for different magnitude intervals (Fig. 8). It is evident that the epicentral distances for the lower magnitudes ($3 < M < 6$) are reported with more discrepancies (where the hypocentral distances are found to be less than the epicentral distances) when compared with the estimations for magnitudes larger than 6. Meanwhile, the estimated hypocentral distances are compared with the teleseismic hypocentral distances in Fig. 9 (the square root of the squared values of epicentral distances plus focal depths are found to be the teleseismic hypocentral distance). The greatest discrepancies could be again seen in the M3–5.5 magnitude ranges. These results hint that epicenter locations in Turkey are not very precise.

7.2. Focal depths

The earthquakes in the Anatolian plateau are mostly of the crustal type and, as mentioned earlier, most of those considered in this study are superficial with depths less than 35 km. According to the ISC monthly bulletins, the precision on focal depths varies from ±4 km for the well determined superficial earthquakes (generally the events with the magnitudes more than M6) to ±30 km for the poorly determined events (generally small earthquakes with the magnitudes less than about M4). Therefore, it may be

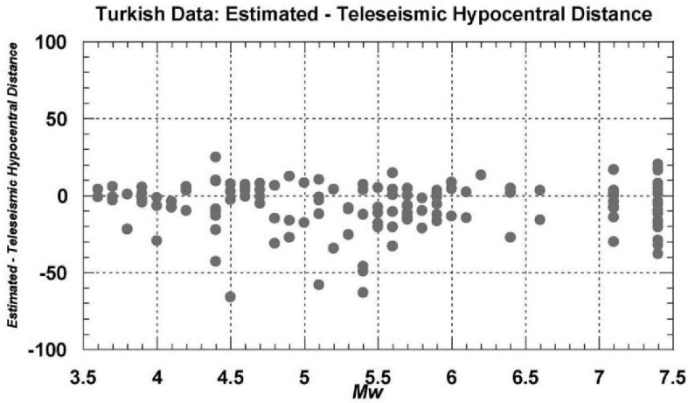

Fig. 9. The residual of the estimated and teleseismic (calculated based on the epicentral distance and focal depth) distances against magnitude.

concluded that the precision of the focal depths is even less than the precision involved in the location of the epicenters.

7.3. The integration of the filtered records

The integration to obtain the velocity and displacement time-histories may cause some long period discrepancies especially for the analog recordings, since the presence of even small low frequency noises may result in large differences in the peak values. The high-pass filtering that we applied was intended to eliminate this low frequency noise. This low frequency cut off certainly removes some real signals as well, so that the peak velocity and peak displacement values may be biased (underestimated) in some cases.

7.4. The earthquake intensities

According to the qualitative nature of intensity, different values of intensity may be assigned to the same earthquake by different investigators. On the other hand, in order to compare different damaged areas with earthquakes with

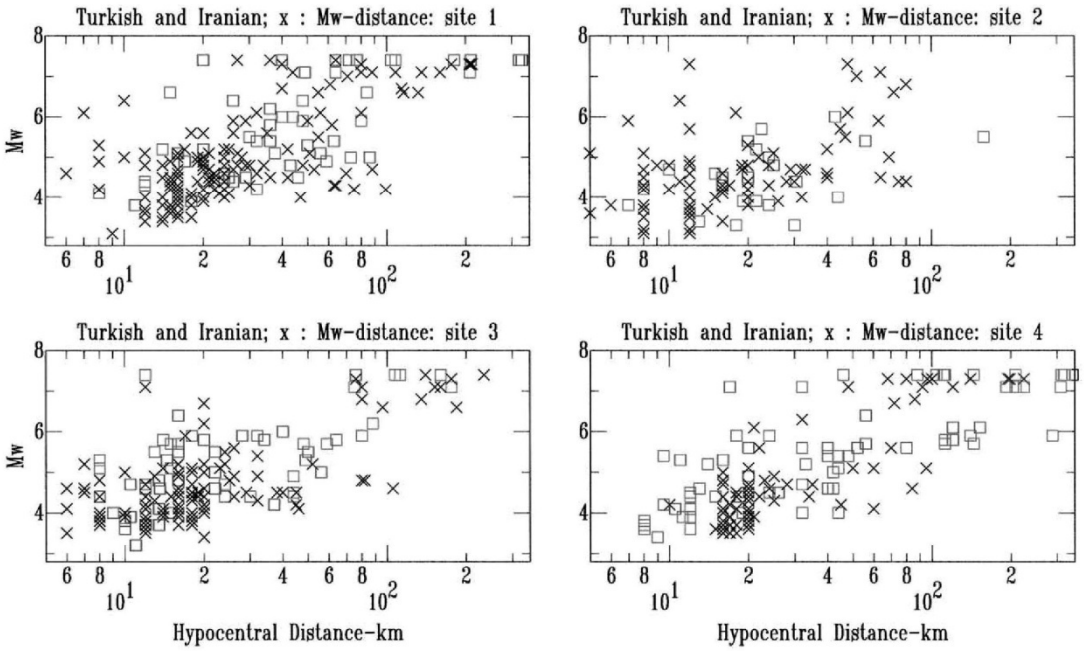

Fig. 10. The diagram showing the magnitude against hypocentral distance to sources of selected records for different site categories in the present study; the Iranian data (squares) are superimposed to show the general tendency of such distribution in these two countries.

same magnitudes and epicentral distances, we have endeavored to present all the intensities on a single scale (MSK, which is not much different from the EMS98 scale [26]). In this regard, previously reported intensities on other scales are converted to the MSK scale using the chart as presented in Japan TC-4 report [25], to correlate different intensity scales. The nature of the intensity measurements, the quality of the reports as well as the conversion of the intensities to MSK scale, may be the origin of many uncertainties.

8. Conclusion

This procedure allowed us to compile an Anatolian strong motion catalog (Table 1) consisting of 210 records. In addition to peak ground acceleration, peak ground velocity and peak ground displacement etc, this catalog includes source and site information for each selected three-component record as well as the maximum values of the acceleration, velocity and displacements. The catalog also contains intensities and focal mechanisms of the causative events (whenever available). The North Anatolian Fault was the seismically most active tectonic entity during the last 25 years in the Anatolian plateau. The most important earthquakes in this catalog are the Erzincan earthquake of 13 March 1992, the Dinar earthquake of 1 October 1995; Adana-Ceyhan earthquake of 4 July 1998; Izmit, Kocaeli earthquake of 17 August 1999, and the Duzce earthquake of 12 November 1999.

It must be noted that there are other good quality three-component records from Turkey in the WWW but they could not be included in Table 1, because they could not be assigned to any particular earthquake due to the lack of timing on SMA-1 instruments or they were associated with small acceleration levels (lower than 0.05 m/s^2).

The Anatolian strong motion data (Fig. 10) are recorded mostly in the vicinity of the northern and eastern Anatolian fault zones. The amplitude–distance distribution of the records is depicted in Fig. 10, along with the similar distribution for the Iranian strong motion data. The general distribution of the Iranian and Turkish strong motion data seems to be similar (Fig. 10). Most of the records are obtained at distances between 10 and 100 km on the soil types of 1 and 4. Therefore, it seems that the attenuation relationships that may be developed using these data will be most reliable in the magnitude range of 3–7.4 and distance range of 10–100 km. The digital data, which will be obtained in the future, may fill in the gaps between the mentioned ranges. On the other hand, it is still necessary to obtain more data in the near source regions especially for M6–7 events, in order to develop reliable analyses in the near field and to perform detailed studies on the source and/or site effects.

We hope that the present work will help in building a regional strong motion catalog that may be used by all regional countries (Iran, Iraq, Syria, Armenia, as well as with the central Asian and Caucasus republics, as well as the European countries).

Acknowledgments

Our thanks go to the Earthquake Research Department, Directorate for Disaster Affairs, who provides online access to the Turkish strong motion records on Internet, as well as to the Kandili Observatory and Earthquake Research Institute for the records of the 1999 Izmit, earthquake. The financial support in France (for the first author) was provided by a French scholarship (Ministère Français des Affaires Etrangères). Our thanks also go to an anonymous referee who gave useful comments on this article.

References

[1] Can Ates RN, Bayulke N. The 19 August 1976 Denizli, Turkey, earthquake: evaluation of the strong motion accelerograph record. Bull Seismol Soc Am 1982;72(5):1635–49.
[2] Celebi M, Toprak S, Holzer T. Strong motion, site-effects and hazard issues in rebuilding Turkey: in light of the 17 August, 1999 earthquake and its aftershocks. USGS web site: http://www.usgs.gov/, 2000.
[3] Bernard P, Gariel J-C, Dobrath L. Fault location and rupture kinematics of the magnitude 6.8, 1992 Erzincan earthquake, Turkey, from Strong ground motion and regional records. Bull Seismol Soc Am 1997;87(5):1230–43.
[4] Celebi M. The Adana-Ceyhan earthquake of June 27, 1998. EERI Special Earthquake Report, Learning from Earthquakes Program. Earthquake Engineering Research Institute web site: http://www.eeri.org/Reconn/, 1998.
[5] Durukal E, Erdik M, Avci J, Yuzugulu O, Alpay Y, Avar B, Zulfikar C, Biro T, Mert A. Analysis of the strong motion data of the 1995 Dinar, Turkey earthquake. J Soil Dyn Earthquake Engng 1998;7,8:557–78.
[6] Gulkan P et al. Dinar aftershock tests retrofitted buildings. EERI Special Earthquake Report, Learning from Earthquakes Program. Earthquake Engineering Research Institute web site: http://www.eeri.org/Reconn/, 1998.
[7] Barka AA. The North Anatolian Fault zone. Ann Tectonica 1992;(Suppl. VI):164–95.
[8] Jackson J, McKenzie DP. Active tectonics of the Alpine Himalayan belt between western Turkey and Pakistan. Geophys J R Astr Soc 1984;77:185–264.
[9] Nalbant SS, Hurbert A, King GCP. Stress coupling between earthquakes in Northwest Turkey and North Aegean Sea. J Geophys Res 1998;103(B10):24469–86.
[10] Stein RS, Barka AA, Dietrich JH. Progressive failure on the North Anatolian Fault since 1939 by earthquake stress triggering. Geophys J Int 1997;128:594–604.
[11] Straub C, Kahle H-G. Active crustal deformation in the Marmara Sea Region, NW Anatolia, inferred from GPS measurements. Geophys Res Lett 1995;22(18):2533–6.
[12] Ansal A, Lav MA. Effects of geotechnical factors in 1992 Erzincan earthquake. Proceedings of the Fifth International Conference on Seismic Zonation, Nice, Ouest Editions, Vol. 1.; 1995. p. 667–674.
[13] Celebi M, Erdik M, Avci J. Observations on the effects of surface geology on ground motion: Erzincan (Turkey) Earthquake of March 13, 1992. In: Duma G, editor. Proceedings Of the Tenth European

Conference on Earthquake Engineering, Vol. 4. Amsterdam: A.A. Balkema; 1995. p. 2599–605.
[14] Zaré M. Contribution à l'étude des mouvements forts en Iran: du Catalogue aux lois d'atténuation. PhD Thesis, Université Joseph Fourier, Grenoble, France, 1999, 237p.
[15] Bard P-Y, Zaré M, Ghafory-Ashtiany M. The Iranian accelerometric data bank, a revision and data correction. J Seismol Earthquake Engng 1998;1(1):1–22.
[16] Ambraseys NN, Free MW. Surface wave magnitude calibration for European region earthquakes. J Earthquake Engng 1997;1(1):1–22.
[17] Hanks TC, Kanamori H. A moment magnitude scale. J Geophys Res 1979;84(B5):2348–50.
[18] Malley JO. Erzincan, Turkey, of March 13, 1992 Reconnaissance Report 1993; Earthquake Engineering Research Institute EERI, supplement to Vol. 9, p. 210.
[19] Kandili Observatory web site. Kocaeli earthquake. Earthquake Engineering Department, http://www.koeri.boun.edu.tr/earthqk/earthquake.html/, 1999.
[20] Zaré M. Macrozonation of the landslides for the Manjil Iran 1990 earthquake. Proceedings of the Third International Conference on Case-histories in Geotechnical Engineering, Vol. 1. St Louis: University of Missouri-Rola; 1993.
[21] Jackson J, McKenzie DP. The Relationship between the plate motions and seismic moment tensors, and the rates of the active deformation in the Mediterranean and Middle East. Geophys J R Astr Soc 1988;93:45–73.
[22] Konno K, Ohmachi T. Ground motion characteristic estimated from spectral ratio between horizontal and vertical components of microtremors. Bull Seismol Soc Am 1998;68(1):228–41.
[23] Lusso P, Fukushima Y, Bard P-Y, Cotton F. Seismic design regulation codes: contribution of KNET data to site effect evaluation. J Earthquake Engng, Imperial College, London 2002;.
[24] Zaré M, Bard P-Y, Ghafory-Ashtiany M. Site characterizations for the Iranian strong motion network. J Soil Dyn Earthquake Engng 1999; 18(2):101–23.
[25] Japan Working Group for TC-4 Committee. Seismic Zoning on Geotechnical Hazards, Draft; 1992, 114P.
[26] Grunthal G, editor. European macroseismic scale (EMS98), Vol. 15. Luxembourg: Conseil de l'europe; 1998. 99p.
[27] Yamazaki F, Ansary MA. Horizontal-to-vertical spectrum ratio of earthquake ground motion for site characterization. Earthquake Engng Struct Dyn 1997;26:671–9.
[28] Ambraseys NN. Engineering seismology. Earthquake Engng Struct Dyn 1988;17(1):1–105.
[29] Caridis PG et al. The Dinar, Turkey earthquake of October 1, 1995. EERI Special Earthquake Report, Learning from Earthquakes Program. Earthquake Engineering Research Institute web site: http://www.eeri.org/Reconn/, 1995.
[30] Harvard University web site, CMT estimations: http://www.harvard.seismology.edu/, 2000.
[31] National Earthquake Information Center (USGS). Web site: http://www.neic.cr.usgs.gov/, June 2000.

#6. Zaré M., Bard P.-Y. and Ghafory-Ashtiany M., (1999), "Site characterization for the Iranian strong motion network", Soil Dynamics and Earthquake Engineering, vol. 18, no.2, pp. 101-123, doi: 10.1016/s0267-7261(98)00040-2.

ELSEVIER

Soil Dynamics and Earthquake Engineering 18 (1999) 101–123

SOIL DYNAMICS AND EARTHQUAKE ENGINEERING

Site characterizations for the Iranian strong motion network

M. Zaré[a,b,*], P.-Y. Bard[b,c], M. Ghafory-Ashtiany[a]

[a]*International Institute of Earthquake Engineering and Seismology, P.O. Box: 19395-3913, Tehran, Iran*
[b]*LGIT-IRIGM, Observatoire de Grenoble, Université Joseph Fourier, BP. 53X, 38041 Grenoble Cedex, France*
[c]*Laboratoire Central des Ponts-et-Chaussées, 58, Bd Lefèbvre, 75732 Paris Cedex 15, France*

Received 20 August 1998; accepted 25 August 1998

Abstract

Twenty-six sites of the Iranian strong motion network, having provided numerous records of good quality, were selected for a site effect study with the objective of obtaining a reliable site categorization for later statistical work on Iranian strong motion data. For each site, superficial Vp and Vs profiles were measured with refraction techniques, microtremor recordings were obtained and analysed with the H/V technique and the available three-component accelerograms by the receiver function technique. The aggregation of these results allows the proposition of a four-class categorization based on the H/V spectral ratio of strong ground motions, which demonstrate a satisfactory correlation with the S-wave velocity profile. Iran has a particular geological and meteorological situation compared to other seismic countries such as Japan or California, a mountainous country with dry weather conditions and a low water table in most areas. These conditions result in a relatively small number of sites with low frequency amplification, while many sites exhibit moderate amplifications in the intermediate and high frequency range.

Keywords: Iran; Site effects; H/V method; Strong motions; Seismic hazard; Site response

1. Introduction

The strong motion accelerometric network in Iran is installed throughout the country in different site conditions. The Kinemetrics SMA-1 analog instruments were initially installed in 1975, and then they were gradually expanded by the SSA-2 digital instruments since the Manjil earthquake of 1990; Mw7.4, in NW Iran [5]. The number of the instruments in this network is 1000 stations (by the end of 1997). The stations were mainly chosen within the cities or villages for an easy maintenance. However, there are no double stations (functioning as a local network on a soil site and its corresponding rock outcrop) to compare easily the soil and rock motions in different earthquakes. Meanwhile, there is no down-hole array, yet, to compare the motions on the surface and on the base rock.

The previous studies on site effects on the strong ground motions in Iran were limited to some, recent, studies on the soil effects on strong motion records during the great earthquakes [14–17]. On the other hand, some microzonation case studies were also performed in some great cities in Iran [8,9].

The scope of this study was to investigate the site effects on the strong ground motions in Iran. It also tried to select a variety of different soil and geologic conditions in such a way that at the end of this study, it will be possible to present a site categorization to be used in the seismic hazard studies and the attenuation models for Iran. Meanwhile, we hoped to determine a site categorization adaptable to the geological and meteorological situations of Iran. We intended to develop a method that would not be limited by the depth of the surface deposits. Finally, a site classification that was reliable and easily applicable was suggested (i.e. the site categorization in the United States is based on Vs_{30} which, in our opinion is not optimal [2]).

In this article the results of a study on the site characterizations of some selected sites of the network are presented. We explain, first, the methodology of the study. Then an overview on the general situations of the sites and the different performed methods are described. The results of the different tests are presented afterward. Finally a four class site categorization is introduced.

2. The methodology

Fifty sites were studied. These sites were chosen from a database of 279 records (already processed and developed [18]). The sites were chosen on the basis of the number and

* Corresponding author. Fax: + 33-476828101; e-mail: mzare@obs.ujf-grenoble.fr or mzare@dena.iiees.ac.it.

0267-7261/99/$ - see front matter
PII: S0267-7261(98)00040-2

Table 1
The results of the site effect studies, and the site classification for 137 strong motion stations in Iran.

No	Station	Site categorization	Number of records	Site geology	Vs over 1st 30 m (m s^{-1})	Amplification of H/V on microtremorts	Amplification of H/V on strong motions	Site based on surface geology (BHRC)	Electric resistivities (ohmm)	Q
1	Abbar	1	5	Stiff alluvium	621	1–2(0.2–20 Hz)	< 4 (2–5 Hz)	3	5–17 (1st 30 m)	A1
2	Abhar	4	1	Silt–clay in surface	263	> 2 (0.2–2 Hz)	> 4 (0.2–0.3 and 1–4 Hz)	4	3–25 (1st 25 m)	A1
3	Aghajari	2	1				> 4 (4–6 Hz)	1		C
4	Ahar	1	1				1–2 (3–10 Hz)	4		D
5	Ammarloo (Jirandeh)	3	6				> 4(3-5 Hz)			C
6	Andimeshk	1	3				2–3 (3–7 Hz)	2		C
7	Ardal	3	4				> 4 (2.5–3.5 Hz)	2		C
8	Ardebil	4	1				> 4(1–2.5 and 4–5 Hz)	3		C
9	Astaneh	4	1				> 4(0.7–2 Hz)	3		C
10	Avaj	1	2				3(4–7 Hz)	4		D
11	Babakalan (Gachsaran)	2	1				> 4(7–11 Hz)	2		C
12	Baba-Monir	4	1				> 4(0.9–1.7 Hz)			C
13	Babanar	2	1				> 4(5–6 Hz)			C
14	Bajestan	3	3	Silt–clay in surface		> 2(2–7 Hz)	> 4(3–6 Hz)	2		D
15	Bam	1	1				1–2(0.7–10 Hz)	4		C
16	Bandarabbas (S)	2	3	Sand beach of the Persian Gulf		1–2(1–8 Hz)	> 4(6–10 Hz)	3		B
17	Bandar-Deylam	4	1				> 4(0.3–3 Hz)			C
18	Bandar-lengeh	3	1				> 4(3–5 Hz)			C
19	Bandar-Torkman	4	1				> 4(0.9–3.5 Hz)	3		C
20	Birjand	1	4	Stiff alluvium		1(0.2–20 Hz)	1–3(0.7–7 Hz)	2		B
21	Boroujerd	3	1				> 4(2.5–3.5 Hz)	4		C
22	Boshruyeh	1	1				1–2(1–5 Hz)	2		C
23	Bostanabad	4	1				> 4(1–2.5 Hz)	2		C
24	Dalin (SE Sepidan-Fars)	2	1				> 4(5.5–6.5 Hz)			D
25	Darreh-Shahr Ilam	1	1				2–3(2–6 Hz)			C
26	Dastgerd	2	1				> 4(8–11 Hz)	2		C
27	Deh-Balla - N. Farrashband	2	1				> 4(7–11 Hz)			C
28	Delvar	2	1				> 4(9.5–10 Hz)			C
29	Deyhuk	1	3	Stiff alluvium	826	1–2(0.4–20 Hz)	2–4(2–15 Hz)	2	3–5 (1st 12 m)	A2
30	Dez Dam	1	3	Hard conglomerate			1–2(1–15 Hz)	1		C
31	Doab (Pol-e Sefid)	3	5				> 4(2.5–4 and 6.5–8 Hz)	2		C
32	Dorahun	3	1				> 4(3.5–7 Hz)			C
33	Doroud	4	1				> 4(1.5–2.5 Hz)	3		B
34	Eshtehard	4	1	Silt–clay in surface		1(0.4–20 Hz)	4(0.5–0.65 Hz)	4	20–80 (1st 25 m)	B
35	Estalkh-Posht	2	1				> 4(5–10 Hz)	1		C
36	Farrashband	1	1				1–3(5–11 Hz)			D
37	Farsan	1	1				1–2(5–8 Hz)	3		D
38	Ferdows	1	1	Stiff alluvium		1(0.4–15 Hz)	2–3(0.3–5 Hz)	2		B
39	Fin (N.Bandar-Abbas)	3	31	Soft alluvium	480	2–4(4–8 Hz)	> 4(2.5–5 Hz)	2		A1
40	Firouzabad	3	11	Soft alluvium	478	2–3(4–9 Hz)	> 4(1.5–4.5 Hz)	3	14–90 (1st 33 m)	A1
41	Gachsar	3	1				> 4(2.5–4.5 Hz)	2		C
42	Ghaemiyeh (Chenar-Shahijan)	3	1				> 4(2.5–4.5 Hz)	1		C
43	Ghaen	1	3	Stiff alluvium	867	1(0.6–25 Hz)	2–3(0.4–0.6 and 3–7 Hz)	2	1.5–100 (1st 21 m)	A2
44	Gavbandi	3	1				> 4(3–6 Hz)			C
45	Ghaleh-Ganj	1	1				2–3(2–11 Hz)			C
46	Ghazvin	3	1	Cohesionless gravel	424	1–2 (4–20 Hz)	3–4(1–5 Hz)	2	10–50 (1st 20 m)	A2
47	Gheshm-Island	1	1				1–2(1.5–8 Hz)	2		C

Table 1 (*continued*)

No	Station	Site categorization	Number of records	Site geology	Vs over 1st 30 m (m s^{-1})	Amplification of H/V on microtremorts	Amplification of H/V on strong motions	Site based on surface geology (BHRC)	Electric resistivities (ohmm)	Q
48	Ghir	3	1	Gravel		1(4–15 Hz)	3–4(4.5–5.5 Hz)	1		B
49	Gilvan	1	2				2–3(4–7 Hz)	2		D
50	Golbaf	3	13	Soft alluvium	439	1(4–8 Hz)	> 4(3–5 Hz)	3	4–8 (1st 19 m)	A2
51	Gonabad	4	3	Soft alluvium		1(0.2–40 Hz)	3–4(0.8–1.5 Hz)	3		B
52	Hajiabad	3	1				> 4(3.5–4.5 Hz)	1		C
53	Hassan-Keif	3	1				> 4(2.5–3.5 Hz)			C
54	Hosseiniyeh- Olia Andimeshk	4	11	Soft alluvium	563	1–2(0.2–6 Hz)	> 4(0.3–1 Hz)	1		A2
55	Jovakan	1	30	Soft alluvium in surface	1017	1–2(0.6–9 Hz)	2–3(5–8 Hz)	2	5–30 (1st 25 m)	A1
56	Kahrizak	4	1	Clay and marl		1–2(0.6–2 Hz)	3–4(0.4–2 Hz)	4		B
57	Kakhk	1	1	Sandstone	2200	2–4(0.8–10 Hz)	2–3(1.5–6 Hz)	1		A2
58	Karaj	1	1	Course grain gravels		1(0.4–25 Hz)	1–3(0.5–10 Hz)	2		B
59	Karkheh Dam	1	1				1–3(1–10 Hz)	1		C
60	Kashmar	3	2				3–4(2--3.5 Hz)	2		C
61	Kavar	2	13	Hard conglomerate	946	1(1–10 Hz)	2–4(1–9 Hz)	1	6–120 (1st 35 m)	A2
62	Kavar Dam	2	4				> 4(4–8 Hz)	1		C
63	Kazerun	2	2				> 4(5–11 Hz)	4		C
64	Kerman	4	2	Soft alluvium		> 3(0.2–1.1 Hz)	> 4(1.5–3 Hz)	3		B
65	Khaf	2	6				> 4(5–8 Hz)	2		C
66	Khanzanun	1	3				2–3(2–7 Hz)			C
67	Khezri	1	2	Hard conglomerate		1(0.2–25 Hz)	2–3(0.4–4 Hz)	3		B
68	Khonj	1	1				2–3(3–7 Hz)	3		C
69	Khorramabad	2	3				3–4(4–7 Hz)	2		C
70	Khoy	3	1				> 4(4--4.5 Hz)	2		C
71	Khurmodj	1	1				2–3(3.5–20 Hz)			C
72	Kiasar	2	1				> 4(6–7 Hz)	2		C
73	Kolur	1	1				> 4(15 Hz)			C
74	Kuhbanan	3	1	Soft alluvium		1–2(0.3–9 Hz)	3–4(2–6 Hz)	4		B
75	Kuhestak	3	1				> 4(2.5–6 Hz)	2		C
76	Kushk-Nosrat	4	1				> 4(0.7–1.5 Hz)	1		C
77	Lahijan	4	1	Clay and silt	264	2–4(0.8–2 Hz)	3–4(0.8–1.5 Hz)	4	4–10 (1st 10 m)	A1
78	Lali	3	8				> 4(3–5 Hz)	2		C
79	Lamerd	1	1				2–3(0.8–10 Hz)			C
80	Lar -Fars	1	2				1–2(4–15 Hz)			C
81	Lendeh	1	1				2–3(1.5–2 Hz)	2		C
82	Mahan	4	1				> 4(0.1–1.5 Hz)	2		C
83	Maharloo (PTT)	1	1				2–3(1.5–6 Hz)	1		C
84	Maku	2	4	Soft alluvium in surface	652		3–4(4–8 Hz)	2		B
85	Manjil	2	7	Fine gravel in surface	589	2–3(6–11 Hz)	> 4(5–7 Hz)	3	13–60 (1st 22 m)	A1
86	Maraveh-Tappeh	3	1				> 4(3–6 Hz)	2		C
87	Masal	3	3				3–4(2.5–7 Hz)	2		C
88	Mashad (Sakht-Azma)	4	1				3–4(0.5–2.5 Hz)	3		C
89	Masjed-Soleyman	3	1				> 4(2.5–5 Hz)	1		C
90	Minab	1	2				2–3(1.5–5 Hz)	3		C
91	Musian	3	2				> 4(2.5–6.5 Hz)			C
92	Naghan	1	16	Soft alluvium in surface	768	1–2(0.2–25 Hz)	1–2(1–20 Hz)	2	6–200 (1st 25 m)	A1
93	Namin	3	2				> 4(3.5–7 Hz)	1		C
94	Nir (Ardebil)	3	2				3–4(2–6 Hz)			C
95	Noorabad-Mamassani	3	5				> 4(3.5–5 Hz)	4		C

Table 1 (*continued*)

No	Station	Site categorization	Number of records	Site geology	Vs over 1st 30 m (m s^{-1})	Amplification of H/V on microtremorts	Amplification of H/V on strong motions	Site based on surface geology (BHRC)	Electric resistivities (ohmm)	Q
96	Old Lar	1	1				1–2(3–10 Hz)	2		C
97	Pol-Sefid	4	3				> 4(0.2–3 Hz)			C
98	Rasht (Housing Bureau)	3	2	Cohesionless gravel		1–2(0.6–3 Hz)	> 4(2–4 Hz)	3		B
99	Rasht (University)	3	1	Thick fine gravel		1–2(0.2–5 Hz)	> 4(2--2.5 Hz)	2		B
100	Ravar	3	1	Soft soil in surface		1–3(0.2–3 Hz)	3–4(1.5–3.5 Hz)			B
101	Rayen	1	1	Soft soil in surface		1–2(0.6–20 Hz)	1–2(0.2–7 Hz)	2		B
102	Robat-Karim	1	1	Coarse grain gravels		1–3(0.6–1.5 Hz)	1–2(0.2–2 Hz)	2		B
103	Roshtkhar	1	2				1–3(0.8–5 Hz)	4		C
104	Rudbar	3	22	Cohesionless river gravels	339	1–3(3–7 Hz)	> 4(3.4–5.5 Hz)	3		A1
105	Rudsar	4	1	Sand beach of Caspian sea	215	1–2(0.4–25 Hz)	> 4(0.25--0.7 Hz)	3	4–20 (1st 16 m)	A2
106	Rudshur	4	1	Silt and clay in surface			3–4(7--1.5 Hz)	3		C
107	Saadabad (Borazjan)	1	7	Fine gravel in surface	958	1–2(0.2–2 Hz)	3–4(2.5–9 Hz)	1		A2
108	Saman	2	1				> 4(5–11 Hz)			C
109	Sarbaz	2	1				> 4(4.5–6 Hz)			C
110	Sedeh	3	4	Silt and clay in surface		2–3(4–7 Hz)	3–4(3–4 Hz)	4		B
111	Sefidabeh (School)	2	1	Hard gravels			> 4(5.5–8 Hz)	2		C
112	Sefidabeh (Microwave)	1	1	Sandstone and shale			2–3(1.5–7 Hz)	1		C
113	Seifabad (S. Kazerun)	1	1				1–2(0.8–1 Hz)	1		C
114	Selseleh	3	1				> 4(3–5 Hz)			C
115	Shabankareh (Borazjan)	4	37	Silty sand in surface	337		3–4(3–6 Hz)	3		B
116	Shabastar	1	3				2–3(2–9 Hz)			C
117	Shahid Yaaghubi Dam (S. Mashhad)	3	1				> 4(3--7.5 Hz)			C
118	Shalamzar	3	2				> 4(3–5 Hz)	4		C
119	Shiraz	4	1	Silt and clay in surface		2–4(0.5–1 Hz)	> 4(0.2–1.1 Hz)	2		B
120	Siah-Cheshmeh	1	3				2–3(4–8 Hz)	4		C
121	Silvaneh	4	1				> 4(0.7–3 Hz)			C
122	Sirch	1	1	Fine gravel in surface		1–2(0.8–6 Hz)	2–3(0.2–15 Hz)	3		B
123	Sisakht	1	4				2–3(7--10.5 Hz)			C
124	Tabas	1	9	Fine gravel in surface	715	1–2(0.2–25 Hz)	2–3(1–15 Hz)	2	10–130 (1st 21 m)	A1
125	Talesh	3	5	Clay–silty gravel	514	2–3(0.6–2 Hz)	3–4(0.8–4.5 Hz)	4	10–100 (1st 28 m)	A2
126	Tasuj	2	1				> 4(6.5–8 Hz)			C
127	Taybad	4	1				> 4(0.3–0.5 Hz)	3		C
128	Tehran (BHRC)	1	1	Coarse grain gravels		1–2(0.6–15 Hz)	2–3(2–3 Hz)	2		D
129	Tehran (Chizar)	1	1	Coarse grain gravels		1–3(1–4 Hz)	1–3(0.3–5 Hz)	3		C
130	Tehran (Sharif University)	1	1	Fine gravel in surface		1–2(0.6–7 Hz)	1–2(2–3 Hz)	2		D
131	Tonkabon	4	1	Artificial soil	209		> 4(1.5–2.5 Hz)	3	4–21 (1st 25 m)	A2
132	Torbat-Heydarieh (SH)	3	1				> 4(2–4 Hz)	2		C
133	Torbat-Jam	1	2				1–2(3.5–9 Hz)	4		C
134	Vendik	2	10	Fine gravel in surface	597	1–2(0.2–20 Hz)	> 4(8–15 Hz)	3	2.5–100 (1st 27 m)	A2
135	Zanjan	1	1				2–3(1.5–5 Hz)	3		C
136	Zanjiran	2	36	Fine gravel in surface	672	1--1.5(0.3–10 Hz)	3–4(7–11 Hz)	1	10–140 (1st 15 m)	A2
137	Zarrat (school)	1	30	Fine gravel in surface	704	1–3(0.2–8 z)	3–4(3–7 Hz)	1	5–30 (1st 7.5 m)	C
138	Ziaratali -N. BandarAbbas	1	1				2–3(3–10 Hz)			C

Fig. 1. The locations of the stations which are studied and presented in this paper.

quality of corresponding records, as well as on the amplitude of the recorded motion and its dependence with a great earthquake (to compare cases of the same events). The site studies were carried out with different methods: geoseismic tests to determine the compressional and shear waves in a profile under the station, microtremor studies (with SS-1 instruments and SSR-1 sensors) and geoelectric studies. Finally, the geological site observations were performed to understand the geologic frame in each locality (type of the superficial layers, the depth of the water table, etc…). Among the fifty aforementioned sites, in 24 sites microtremor tests were applied, the geoseismic tests were performed in the 26 more important sites (the names of the sites and the results of the performed test are summarized in Table 1). In all of the sites, the obtained strong motion records are studied to obtain their horizontal to vertical spectral ratio (receiver function for the strong motions; RF SMS). Calculating the same ratio for microtremors (H/V ratio for the microtremors; H/V MTS), we were able to compare the H/V ratio for noises and earthquakes. No geotechnical boring was done through this study and no data of this type was found in the location of the stations.

Here we have tried to determine the degree of coincidence between different methods of site characterizations. This comparison and likely coincidence were possible especially in sites where we had results from all methods. We describe the factors that may have some affections on site amplifications (besides site geology) which could alter our site characterization results.

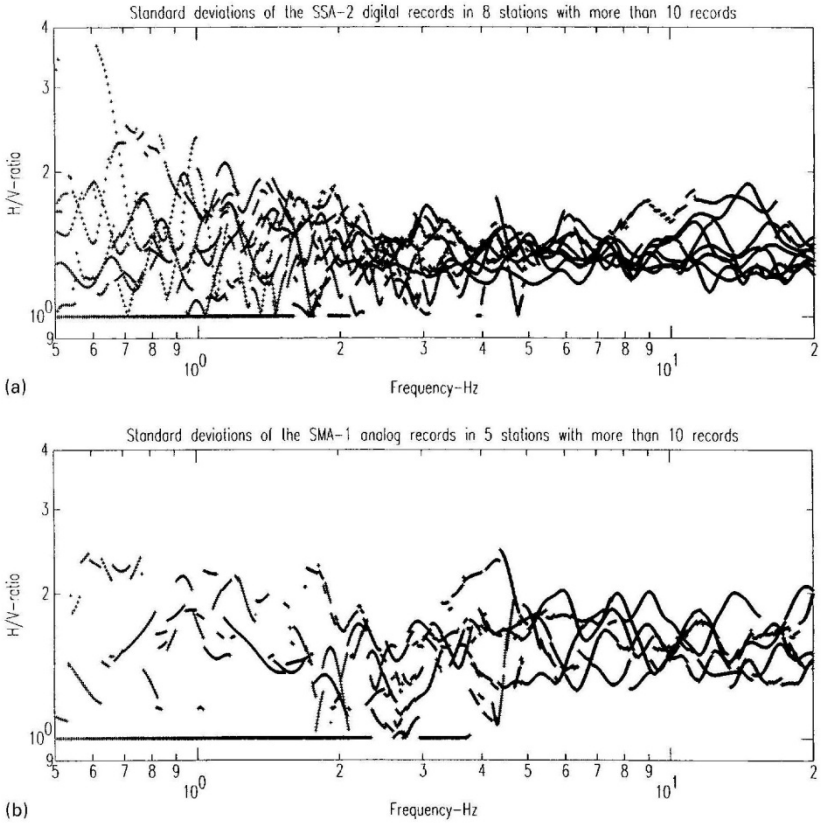

Fig. 2. The comparison of the standard deviations for the digital (SSA-2; a) and analog (SMA-1; b) recorders in the sites with more than 10 records.

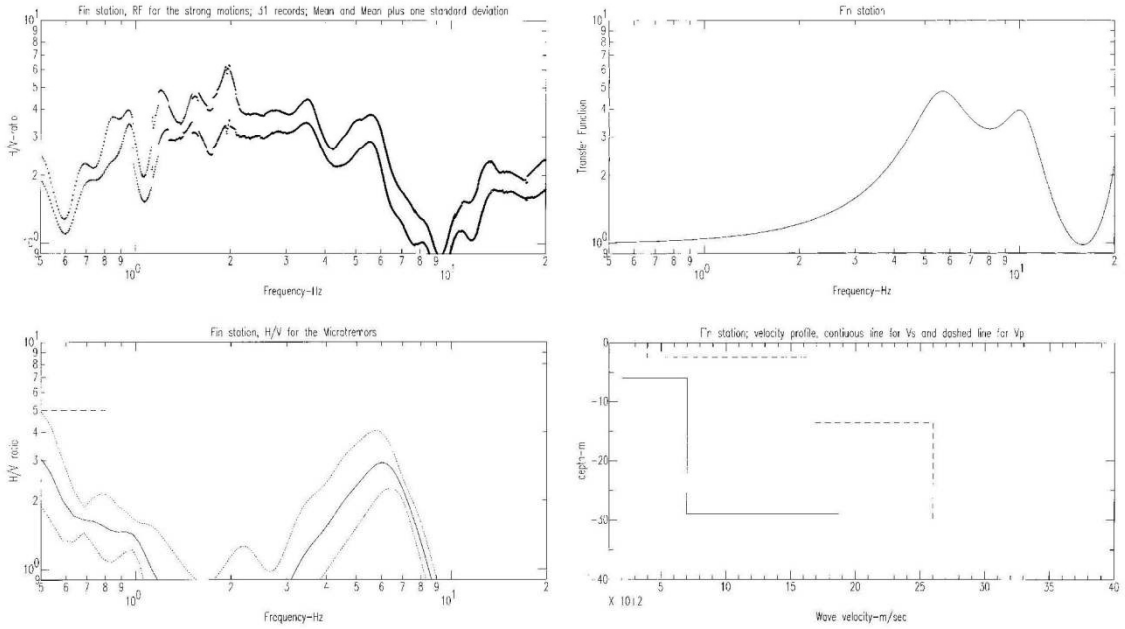

Fig. 3. The results of the site tests in Fin (North Bandarabbas) station (RF SMS, H/V MTS, transfer function and velocity profile).

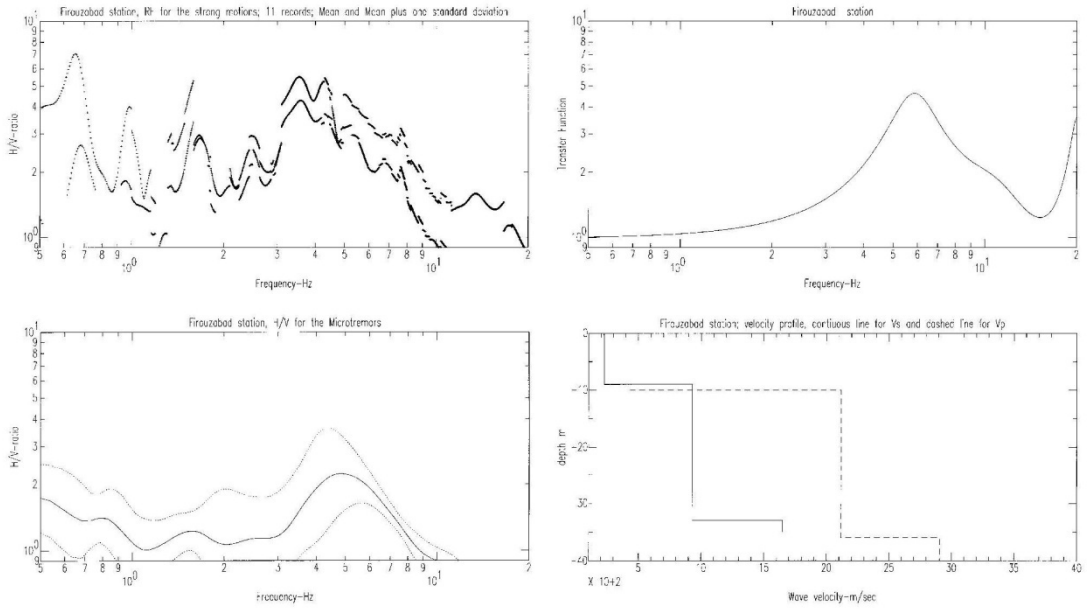

Fig. 4. The results of the site tests in Firouzabad station (RF SMS, H/V MTS, transfer function and velocity profile).

3. An overview on the general situation of the sites and the tests

The locations of each selected site are shown in Fig. 1. The sites are mostly located in the western and northern Lut area (in central-eastern Iran), the western Alborz Mountains and the central Zagros region, which correspond to areas hit by the largest events over the last 22 years.

The shear wave velocities in deep layers can not be found by the geoseismic tests, the effective investigation depth for

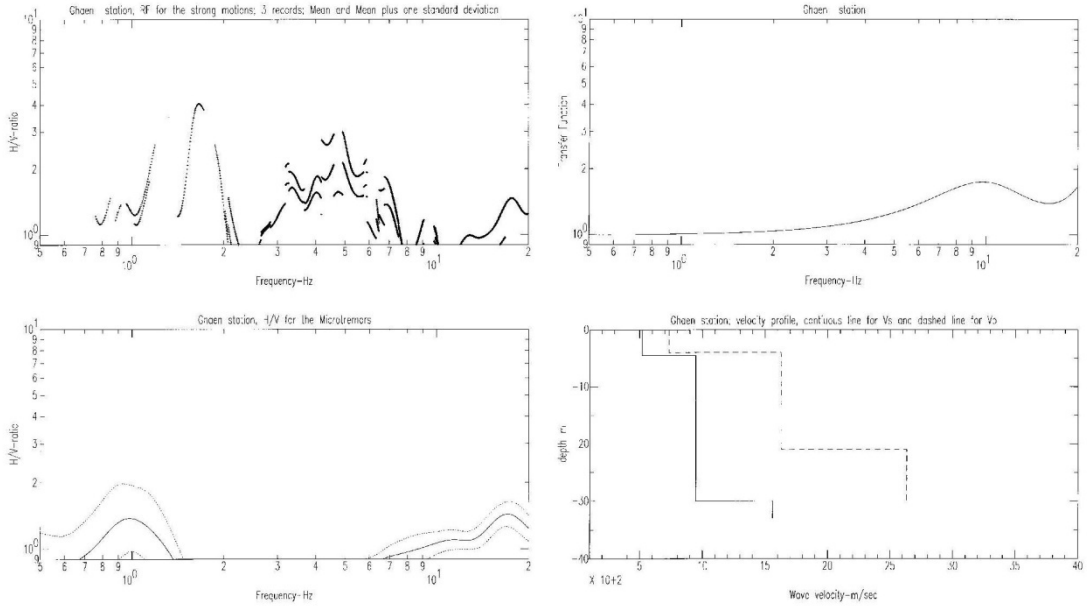

Fig. 5. The results of the site tests in Ghaen station (RF SMS, H/V MTS, transfer function and velocity profile).

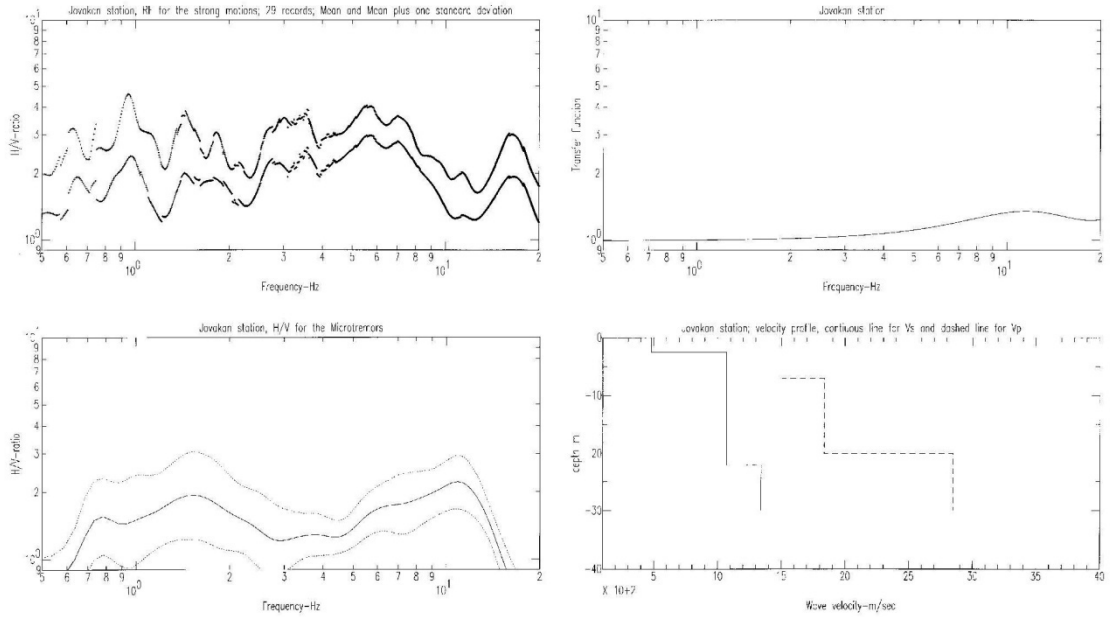

Fig. 6. The results of the site tests in Jovakan station (RF SMS, H/V MTS, transfer function and velocity profile).

the geoseismic tests is about 30–35 m. The microtremor tests were proposed, mainly in Japan, to provide some information on site conditions since seismic noise contains surface and body waves which are filtered by surface layers. The geoelectric tests may distinguish very grossly between rock and soil types within a depth of a few tens of metres. The results from the geoelectric tests give a range of electric resistivities depending on the ionization of the soil particles. The characteristic resistivities for fine and coarse grain alluviums may juxtapose a lot. It is therefore very difficult to

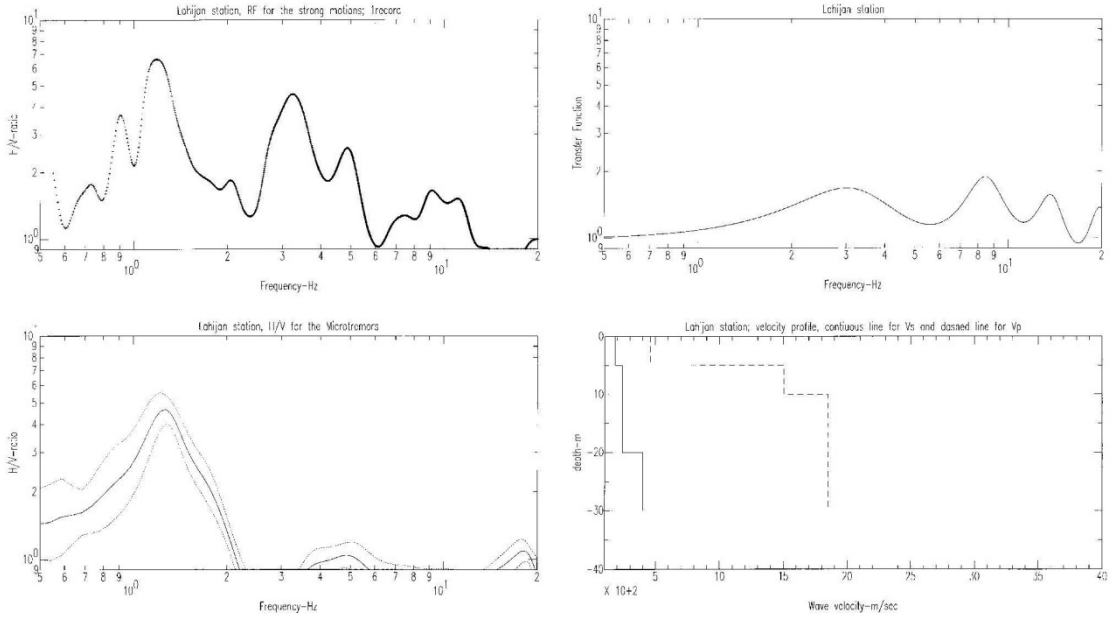

Fig. 7. The results of the site tests in Lahijan station (RF SMS, H/V MTS, transfer function and velocity profile).

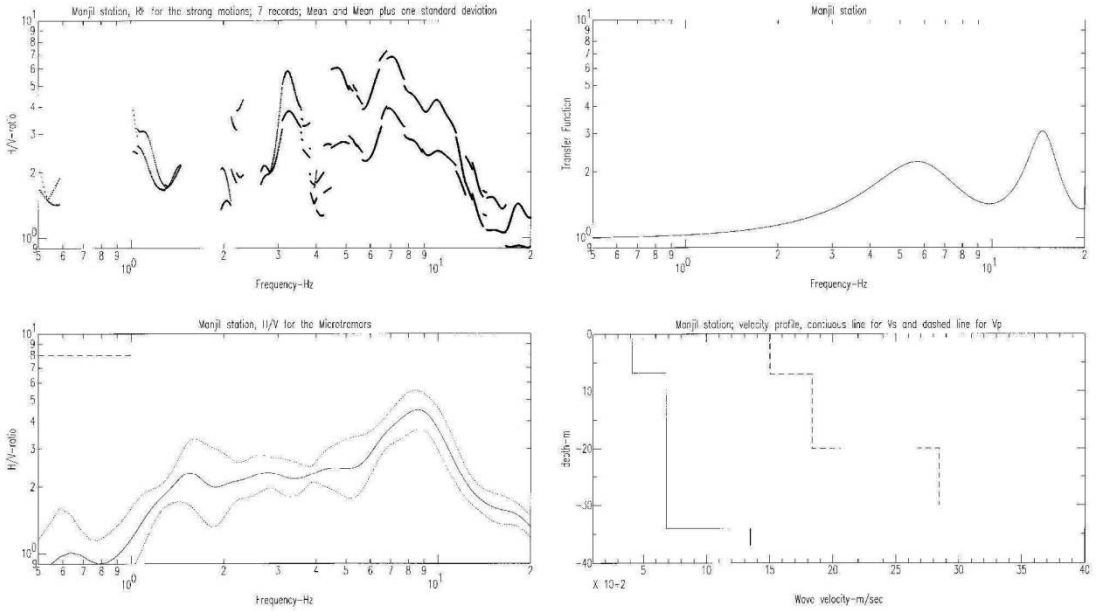

Fig. 8. The results of the site tests in Manjil station (RF SMS, H/V MTS, transfer function and velocity profile).

distinguish between different types of sites through the geoelectric tests. Based on the aforementioned reason the results of geoelectric tests will neither be presented here nor be used in the site categorization.

In the absence of down-hole arrays and rock outcrop motions, we have used the H/V method having then an idea of the response of each site to a strong ground motion.

Most of the strong motion sites in Iran are installed on foothills, for the sake of better climate and topographic situations in most areas of the country. On the other hand,

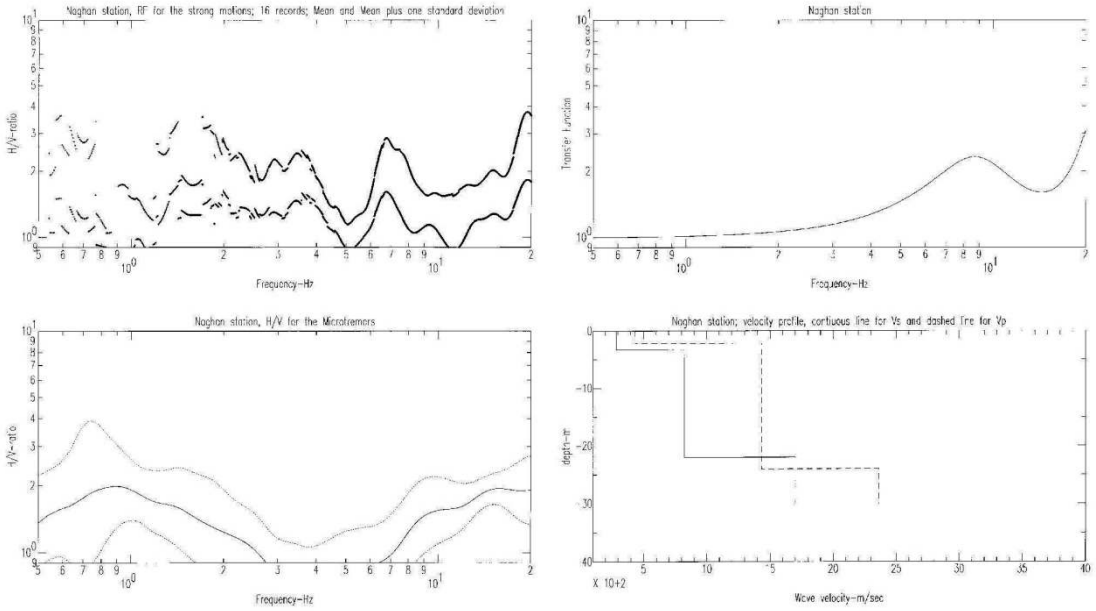

Fig. 9. The results of the site tests in Naghan station (RF SMS, H/V MTS, transfer function and velocity profile).

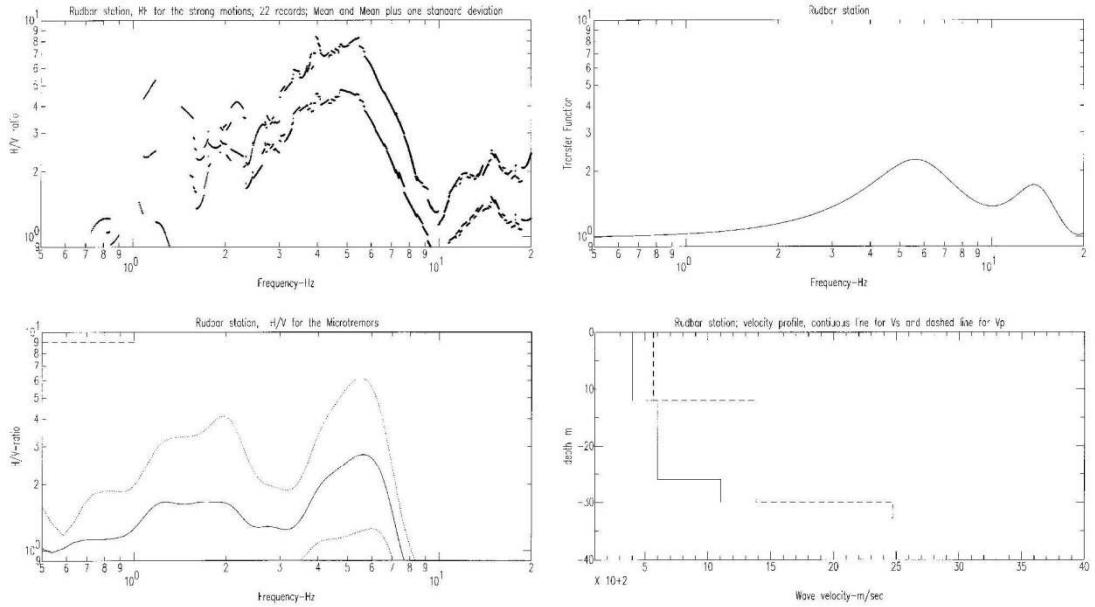

Fig. 10. The results of the site tests in Rudbar station (RF SMS, H/V MTS, transfer function and velocity profile).

in most cases, the sites are alluvial or firm grounds and the soft soil sites may be found only near the coast (Lahijan, Rudsar and Tonkabon) or in the plains (Talesh, Golbaf, Shiraz and south Tehran). A summary of the tests performed in each of the 50 sites is presented in Table 1. As is shown in the table, in most of these sites a microtremor test was done and in each of the local geological situations were observed. The comparison of the local geological observations with the results of the tests may show us the degree of reliability of these observations in each place.

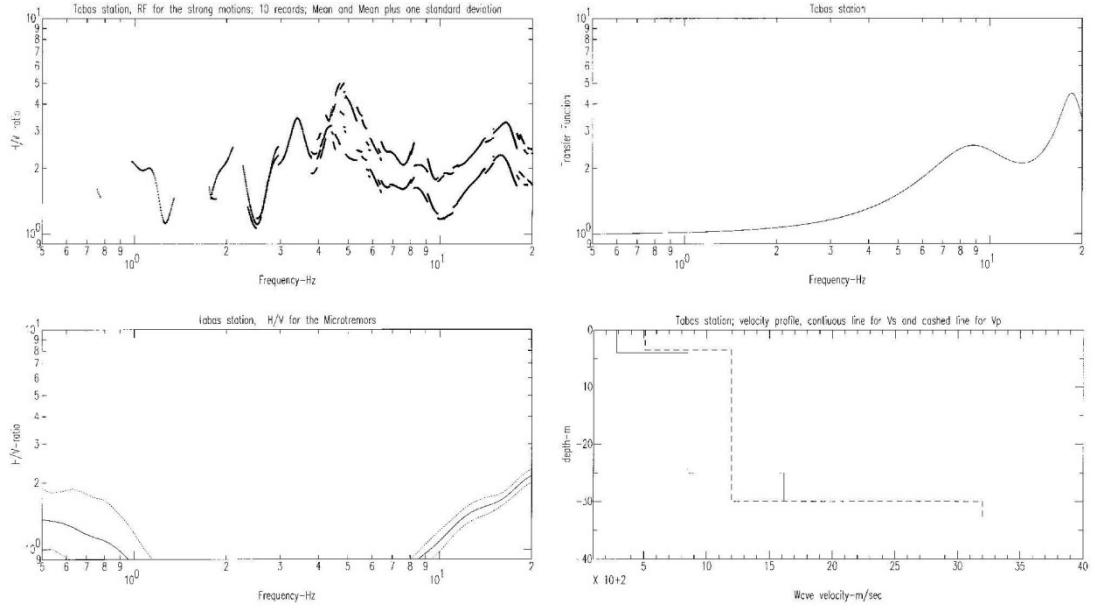

Fig. 11. The results of the site tests in Tabas station (RF SMS, H/V MTS, transfer function and velocity profile).

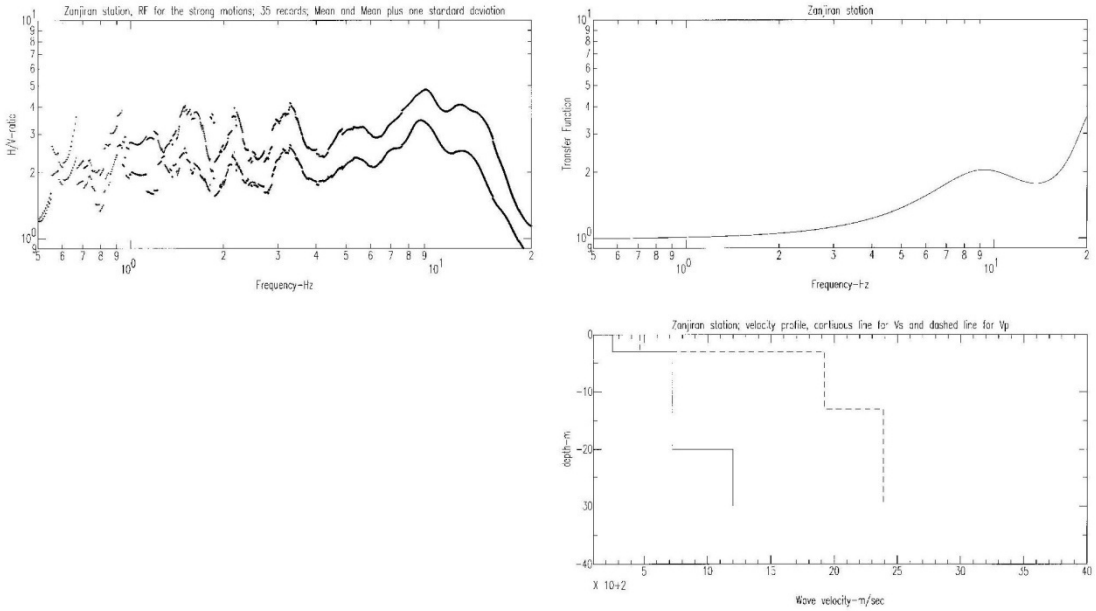

Fig. 12. The results of the site tests in Zanjiran station (RF SMS, transfer function and velocity profile).

3.1. Receiver function method for strong motions

Since there are no station pairs located (one on soil and another on rock) in a nearby distance, and as there is no down-hole array in the country, we had to use single-station estimates of H/V ratio for site effects. This method, also called the receiver function technique, was shown to be efficient [12,13] in pointing out the site fundamental frequency and its stability making it applicable, in principle, even when one single three-component recording is avail-

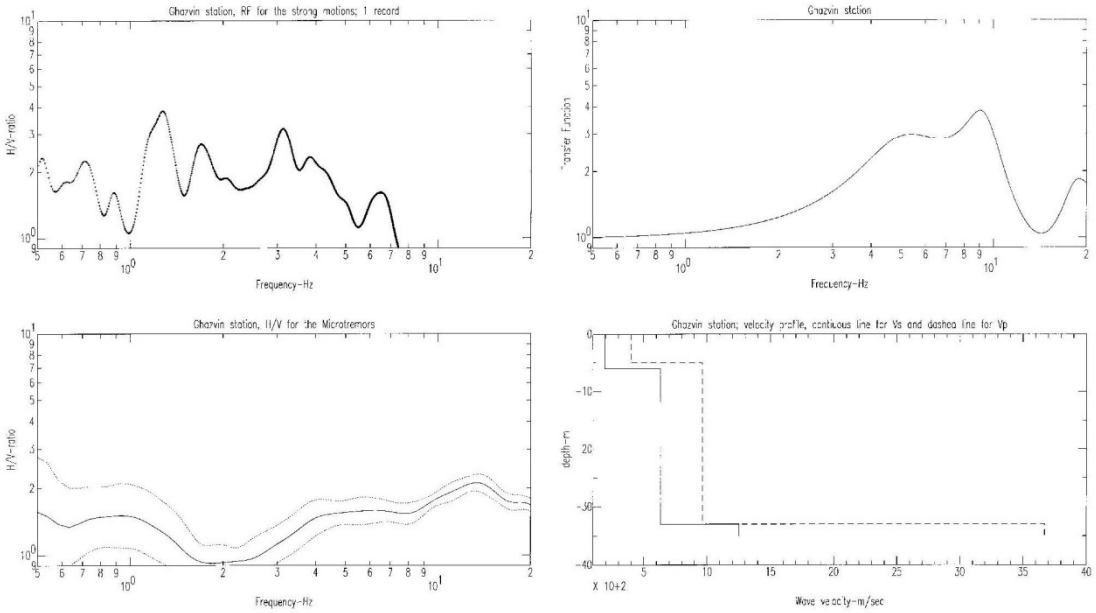

Fig. 13. The results of the site tests in Ghazvin station (RF SMS, H/V MTS, transfer function and velocity profile).

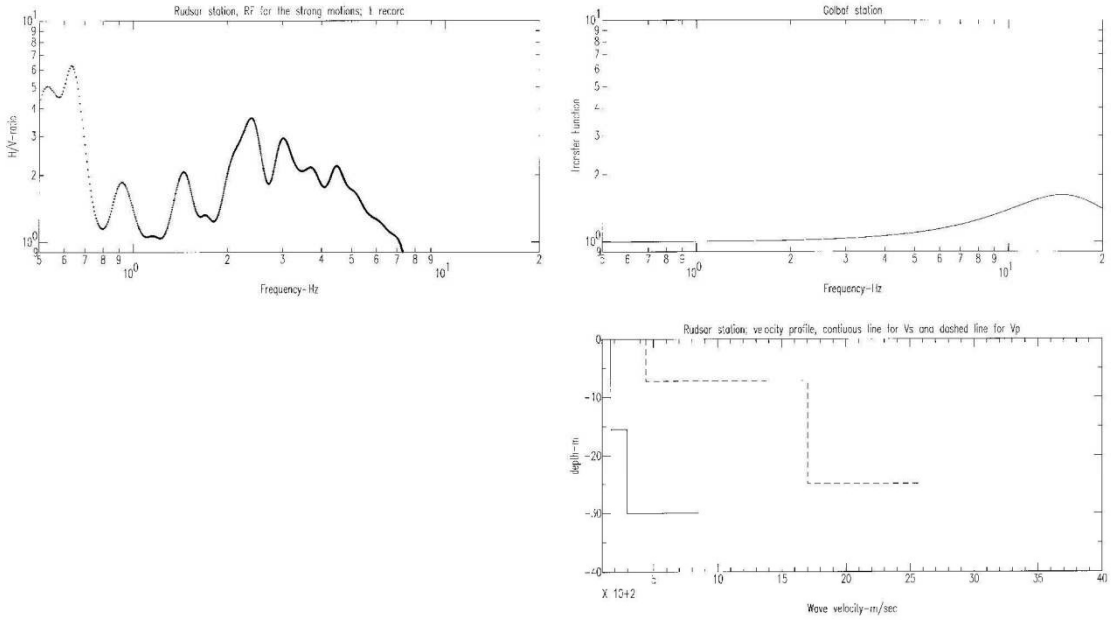

Fig. 14. The results of the site tests in Rudsar station (RF SMS, transfer function and velocity profile).

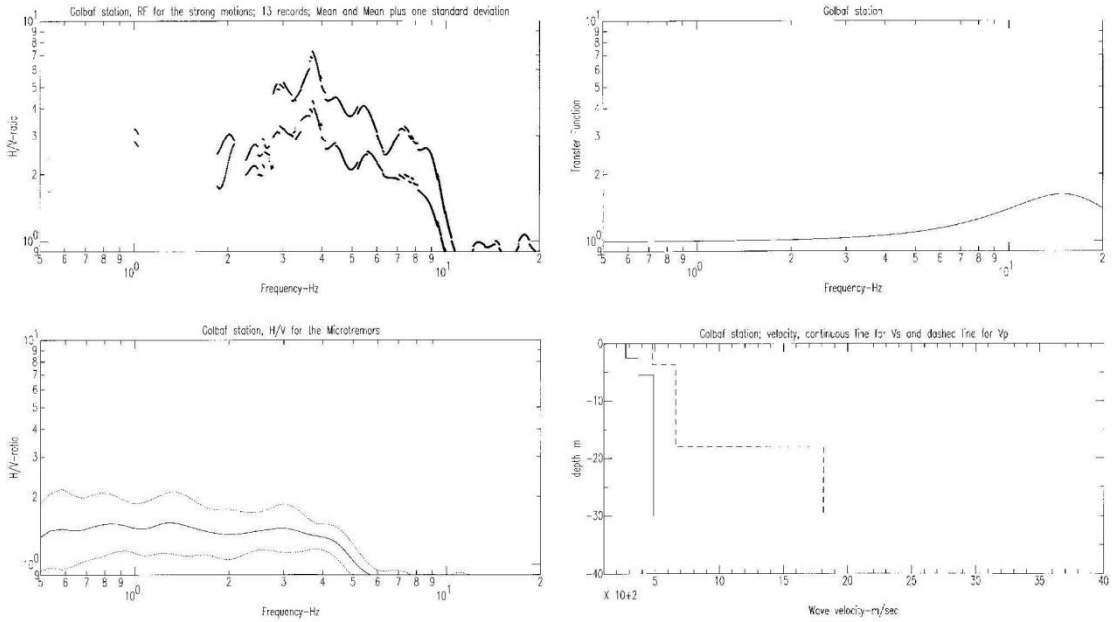

Fig. 15. The results of the site tests in Golbaf station (RF SMS, H/V MTS, transfer function and velocity profile).

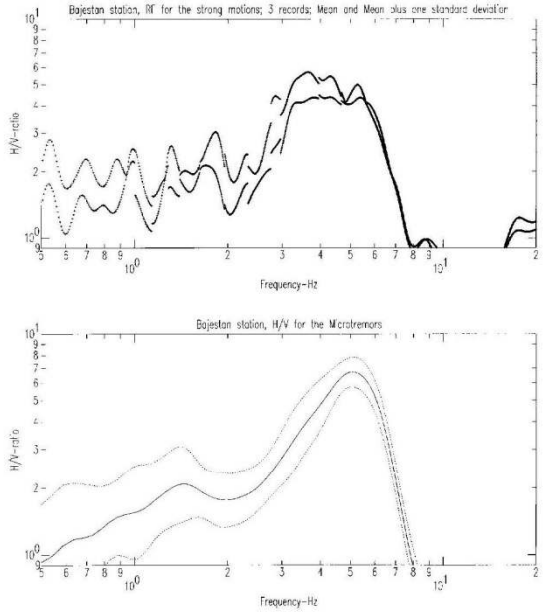

Fig. 16. The H/V ratio results in Bajestan station (RF SMS, H/V MTS).

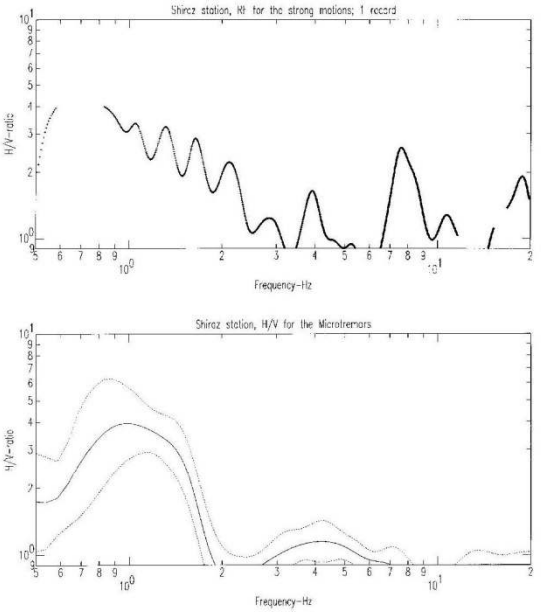

Fig. 18. The H/V ratio results in Shiraz station (RF SMS, H/V MTS).

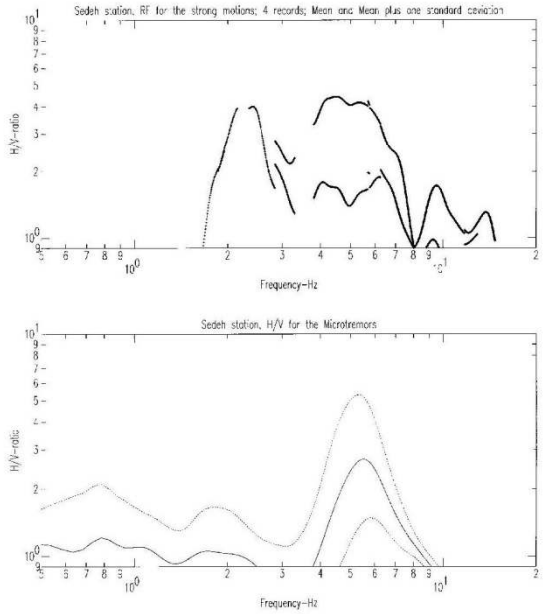

Fig. 17. The H/V ratio results in Sedeh station (RF SMS, H/V MTS).

able. The formulation used for the H/V method is based on the spectral ratio (R_{hv}) between the smoothed horizontal components and the smoothed vertical component:

$$R_{hv} = \frac{\sqrt{\frac{S_{H1}^2}{2\sqrt{T_{H1}}} + \frac{S_{H1}^2}{2\sqrt{T_{H1}}}}}{\frac{S_v(f)}{\sqrt{T_V}}}$$

where T_{H1}, T_{H2} and T_V are the signal duration for the horizontal and vertical components, respectively. Since the same time windows are used the same for all of the components, this relationship might be simplified as;

$$R_{hv} = \frac{\left[\frac{1}{2}(S_{H1}(f) + S_{H2}(f))\right]}{S_v(f)}$$

In this study, this ratio was considered to be significant only when the signal to noise ratio R_{sn} for both components exceeds a given threshold value, taken equal to 3. The signal to noise ratio (R_{sn}) is computed as:

$$R_{sn} = \frac{\frac{S(f)}{\sqrt{t_1}}}{\frac{N(f)}{\sqrt{t_2}}}$$

where t_1 and t_2 are the window duration for the signal and noise parts, respectively. A R_{sn} ratio over 3 is selected as the proper ratio to distinguish the signal from the noise. The resultant R_{sn} ratios for two horizontal components are

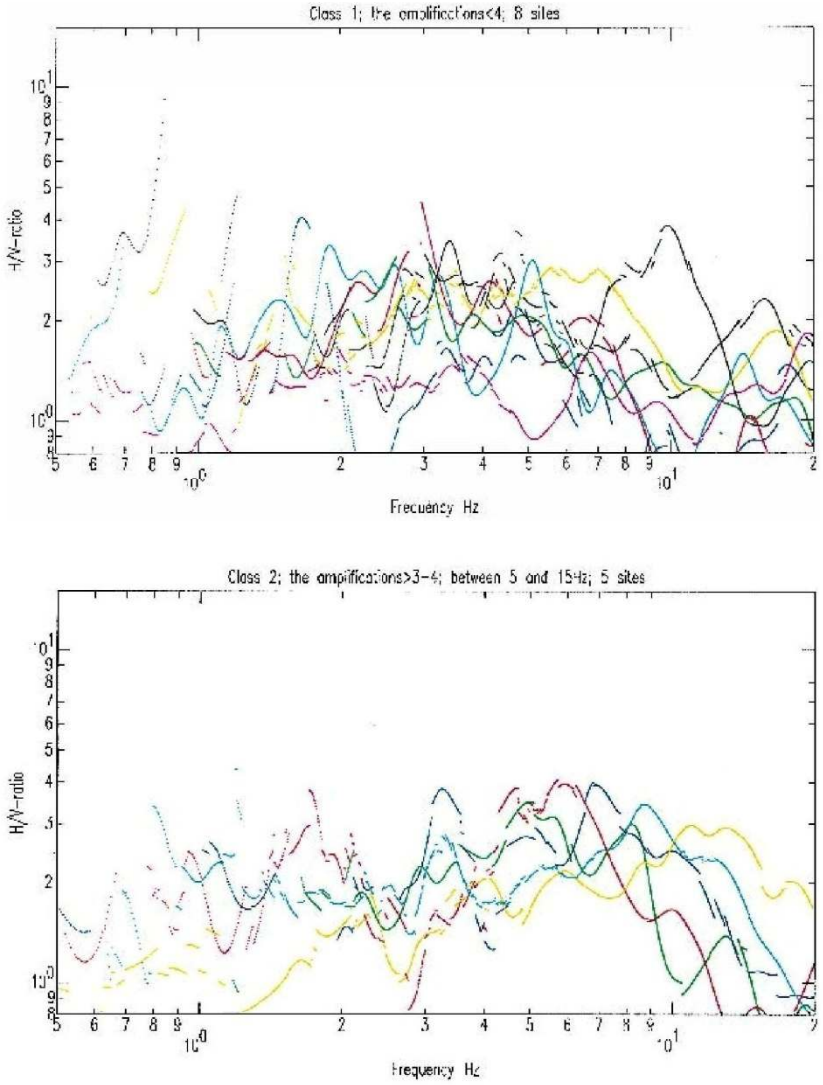

Fig. 19. The comparison of the receiver function for the strong motions in four site classes (the results of 26 sites with the most records).

compared with the same ratio calculated for the vertical component in different frequencies.

The implied smoothing is the smoothing proposed by Konno and Ohmachi [10], which keeps corrects amplitudes whatever the frequency. The stability is found acceptable especially in the sites with many records. The standard deviation of this ratio (RF SMS) is found to be about 1.5. The standard deviations of the digital and the analog records for the RF SMS method are shown in the sites with more than 10 records (Fig. 2). This figure shows that the standard deviations for the digital records are less than the analog ones and on the other hand in most cases the standard deviations do not pass 2. Therefore, it may be concluded that the use of RF SMS as the main criteria to distinguish the site responses was reliable.

3.2. Microtremors

The microtremor tests are performed in 47 sites, using SSR-1 sensors with a minimum sensitivity of 0.1 Hz. Five windows of 3 min duration are selected in each site. In each coordinate, only the best stationary parts of the tremors are considered. The spectral ratio (R_{hv}) formulation for the microtremors are the same as the strong motions. The H/V MTS are compared in each site with the relative RF SMS.

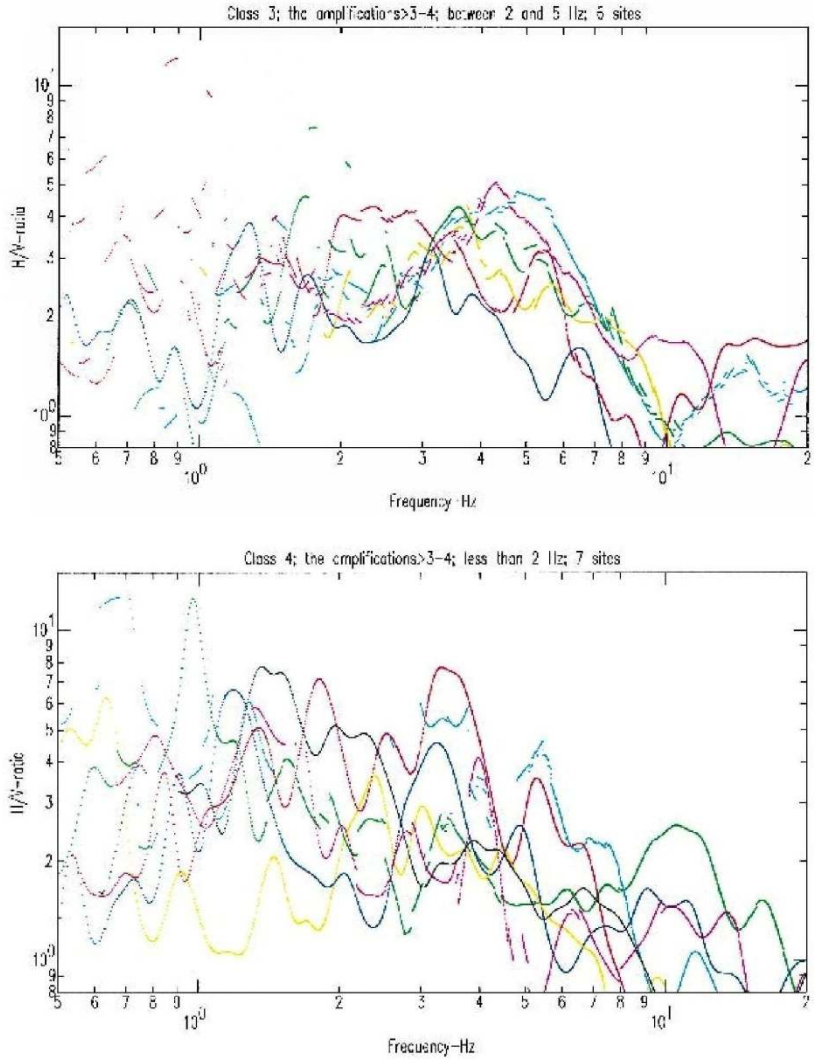

Fig. 19. Continued.

3.3. Geoseismic tests

The geoseismic tests in 26 sites displayed the compressional and shear wave velocities in the superficial first 30 m of depth using the refraction method. The theoretical transfer function (TTF) could then be computed in each case with 1D programs based on the geoseismic results in each case. There were some cases where the S-wave velocities at depth were low (Golbaf, Lahijan). In these cases no velocity contrast may be seen in these depths, meanwhile the receiver function showed the amplifications in low and middle frequencies. No damping measurement was done at the studied sites.

Since it is necessary to place a row of 24 geophones with the interval distances of 4–5 m to do the geoseismic tests, and according to the location of the stations which are mainly in the central parts of the cities, the tests were not always possible to be done in the same place of the stations. In these cases we have tried to do this test in the nearest possible place. Therefore, the velocity profile tests in Deyhuk, Firouzabad, Ghaen Ghazvin, Golbaf, Kavar, Rudbar, Rudsar, Saadabad, Shabankareh, Tabas, Tonkabon and Zarrat are performed in distances of 200–1000 m away from the location of strong motion accelerographs. This problem might be the source of the incoherence between the strong motion and geoseismic results. The rest of the tests are performed in distances of less than 200 m to the stations.

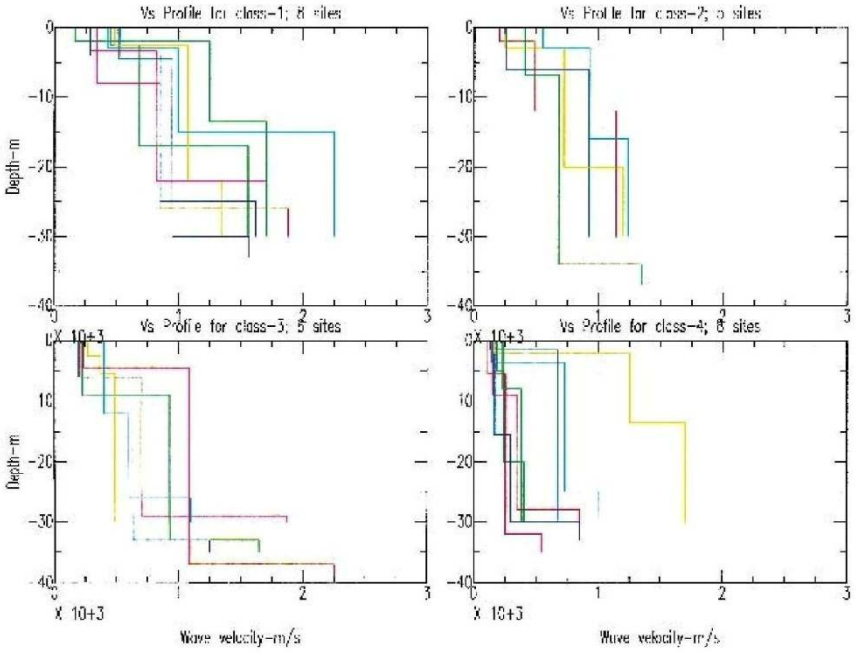

Fig. 20. The comparison of shear wave velocity profiles in four site classes.

4. The results of the geoseimic tests, microtremors and h/v for strong motions

For 26 sites shown in Fig. 1, some information from the receiver functions, the noise recordings, and the velocity profiles could be simultaneously found from which a theoretical 1D-transfer function for vertically incident S-waves could be computed. The sites where the most important earthquakes were recorded, were considered. Meanwhile, in three sites (Maku, Shabankareh, Tonkabon) reliable

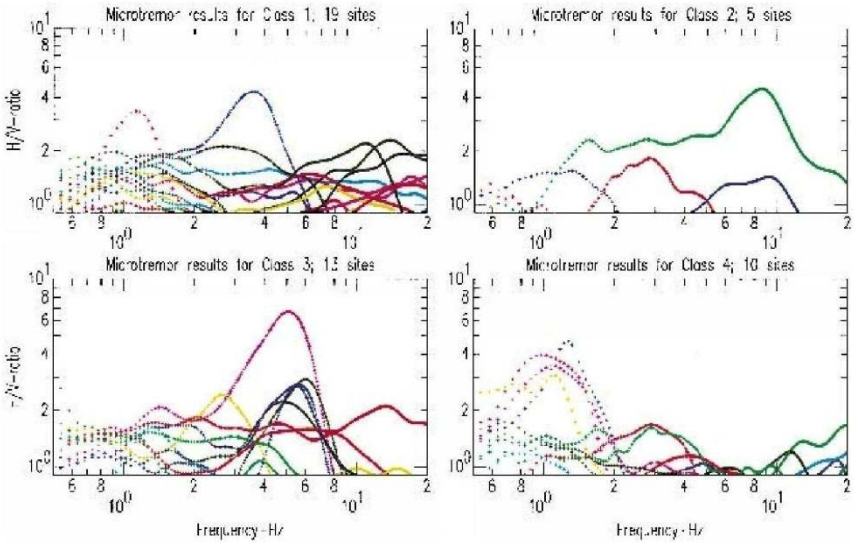

Fig. 21. The comparison of the H/V ratio for the microtremors in four site classes.

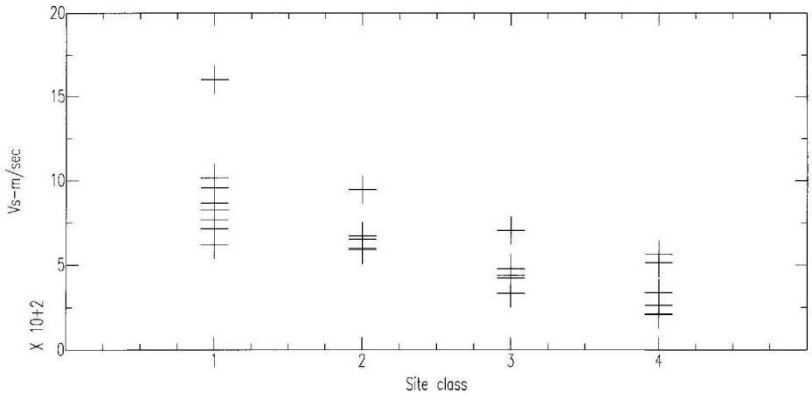

Fig. 22. The distribution of Vs_{30} for four site classes.

results were not obtained on the vertical component and, thus, the microtremor results were eliminated. In 23 other sites, only microtremor tests were performed in order to compare them with RF SMS. For some of the sites, a good consistency between all three techniques could be observed, while for some others the agreement was not so close. In particular, the noise results were very disappointing compared with studies made in other countries [12,7,1,11].

4.1. Sites with a satisfactory agreement between the results of the different methods

A satisfactory similarity between the different methods was obtained only for less than one half of the studied sites. The sites with the best similarities for the different tests are, for instance, Fin (Fig. 3), Firouzabad (Fig. 4), Ghaen (Fig. 5), Jovakan (Fig. 6), Lahijan (Fig. 7), Manjil (Fig. 8), Naghan (Fig. 9), Rudbar (Fig. 10), Tabas (Fig. 11) and Zanjiran (Fig. 12). This means that the factors affecting the amplifications were very different. In almost all cases, the peaks on the H/V MTS had low amplitude, much lower than those of the H/V ratio strong motion spectra (RF SMS) and the theoretical transfer functions (TTF). However, poor agreement was observed at Lahijan (Fig. 7) between RF SMS and TTF because the S-wave velocity profile was not deep enough. The presence of the low velocity surface

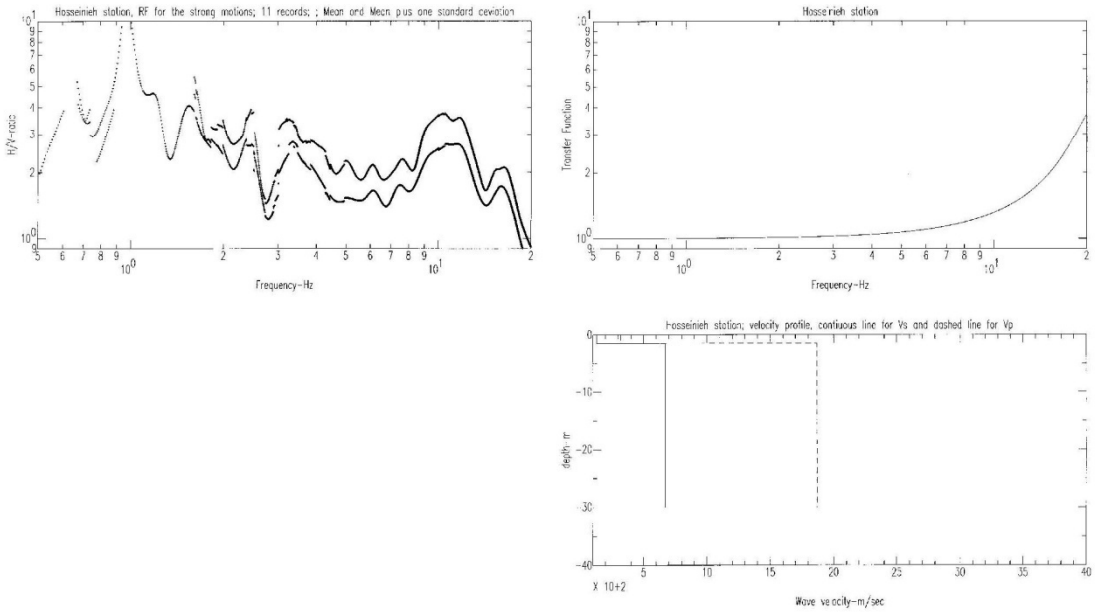

Fig. 23. The results of the site tests in Hosseinieh-Olia station (RF SMS, transfer function and velocity profile).

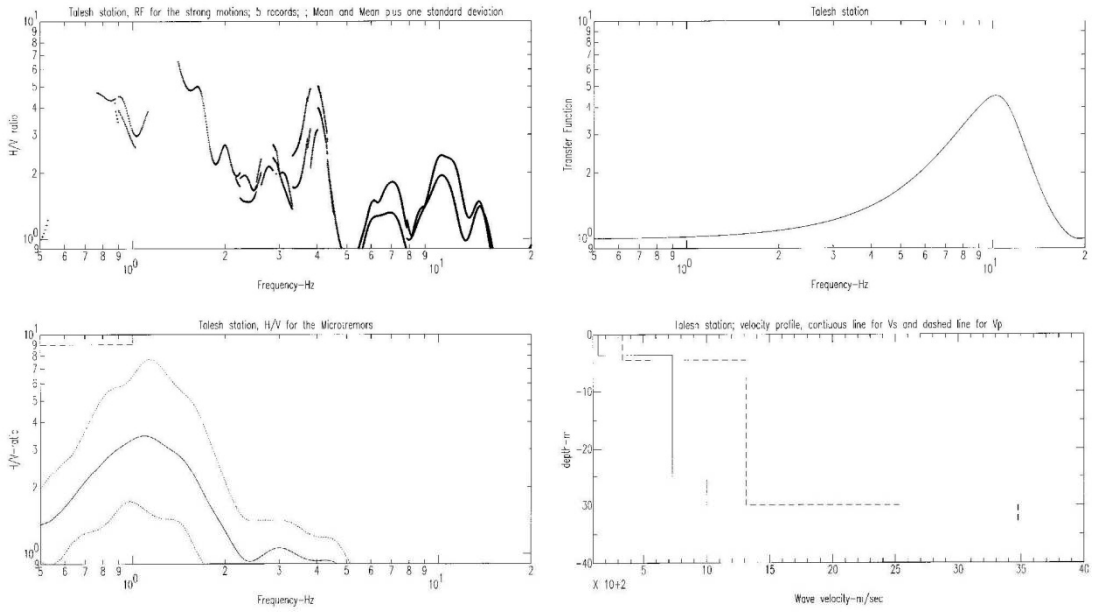

Fig. 24. The results of the site tests in Talesh station (RF SMS, H/V MTS, transfer function and velocity profile).

Table 2
Average velocities for each site, in each category

No	Site	Class	Vs_{30}
1	Abbar	1	621
2	Deyhuk	1	826
3	Ghaen	1	867
4	Jovakan	1	1017
5	Kakhk	1	1602
6	Naghan	1	768
7	Saadabad	1	958
8	Tabas	1	715
9	Kavar	2	946
10	Maku	2	652
11	Manjil	2	589
12	Vendik	2	597
13	Zanjiran	2	627
14	Fin	3	480
15	Firouzabad	3	478
16	Ghazvin	3	424
17	Golbaf	3	439
18	Rudbar	3	334
19	Zarrat	3	704
20	Abhar	4	263
21	Hosseinieh	4	563
22	Lahijan	4	264
23	Rudsar	4	215
24	Shabankareh	4	337
25	Talesh	4	514
26	Tonkabon	4	209

layer was essential to find a satisfactory agreement between methods.

4.2. Sites without agreement: failure of the microtremor technique

Based on the present studies, the results of the microtremor test appear to be reliable just for sites exhibiting significant amplifications at low and/or intermediate frequencies (less than 5 Hz) caused by a low velocity superficial layer. In some of the sites the thick alluvium deposits caused the amplifications in low and middle frequencies (less than 5 Hz) on RF SMS, the H/V MTS did not exhibit the same peaks, for instance in Ghazvin (Fig. 13). In Rudsar (Fig. 14) the velocity of the transfer function has not shown the peaks in low frequencies (evident on RF SMS). In the soft soil sites, it seems that a high contrast in the superficial layers is needed to cause the evident amplifications in H/V MTS. For example in Golbaf (Fig. 15) which shows a low average velocity in the first 30 m (439 m s^{-1}) the amplifications on the RF SMS may not be seen on the same spectra for the microtremors. A high contrast in about 40 m depth, with a Vs velocity of about 1500–200 m s^{-1} is sufficient to explain this low frequency amplification in RF SMS of this site.

There are cases for which there were not each result, however it was possible to compare the amplifications, which may be measured through the H/V MTS and RF SMS. The similarities between H/V ratios for noise and strong motions are observed for instance in Bajestan (Fig. 16), Sedeh (Fig. 17), and Shiraz (Fig. 18). These sites show total accordance between the RF SMS and H/V MTS.

Table 3
The four class site categorization

Group	Frequency band of the amplification	Vs_{30} m s^{-1}	Sites
1	F > = 15 Hz	Vs_{30} > = 700	Abbar, Deyhuk, Ghaen, Jovakan, Kakhk, Naghan, Saadabad, Tabas
2	5 = < 15 Hz	500 = < Vs_{30} < 700	Kavar, Maku, Manjil, Vendik, Zanjiran
3	2 = < 5 Hz	300 = < Vs_{30} < 500	Fin, Firouzabad, Ghazvin, Golbaf, Rudbar, Zarrat
4	F < = 2 Hz	Vs_{30} < 300	Abhar, Lahijan, Hosseinieh, Rudsar, Shabankareh, Tonkabon, Talesh

4.3. A preliminary conclusion on the results of the different methods

Among the methods that are used to study the site conditions, the only method that may reveal the site response to ground motions is to study the three component strong motion records (RF SMS). The benefit gained from this method is that we had at least one record in each of the stations and this is the only method that may be applied at each location. On the other hand, the RF SMS is a method that does not have the limitations of the other methods. The velocity profiles measured by the geoseismic methods are limited to the first 30–35 m, the microtremors have shown the important amplifications in only the soft soil sites and the geoelectric tests do not give the precise measurements to distinguish the different sites. The study on the amplifications based on the three component records has another benefit. In the sites where there are thick alluvial layers on the surface (with a thickness of more than 30 m) on a very high velocity layer at greater depths, the RF SMS is the only way to observe such amplification in low frequencies. In this case the other methods will show just the high velocity alluvium with some amplifications in high to very high frequencies (more than 15 Hz). In addition, the RF SMS is a very stable method (Fig. 24)

5. A site categorization

The relatively good relationship between the S-wave velocity profiles and the RF results allowed us to propose a multi-class site categorization based on the RF curves. This classification is simply based on the amplitude and level of the highest peak on the RF curve:

1. Site category #1 corresponds to flat RF curves (i.e. peak amplitude below 3–4), or those presenting a peak with an amplitude larger than 3–4 at frequencies beyond 15 Hz.
2. Site category #2 corresponds to RF curves presenting a peak with an amplitude larger than 3–4 at frequencies between 5 and 15 Hz.
3. Site category #3 corresponds to RF curves presenting a

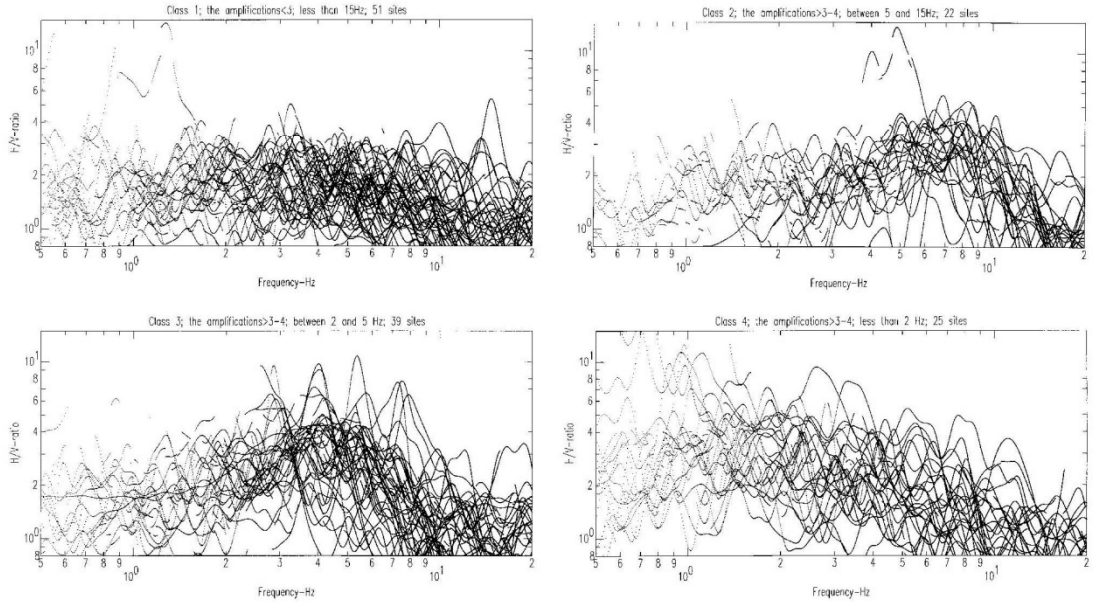

Fig. 25. The results of the RF SMS for all of the 138 sites in four classes.

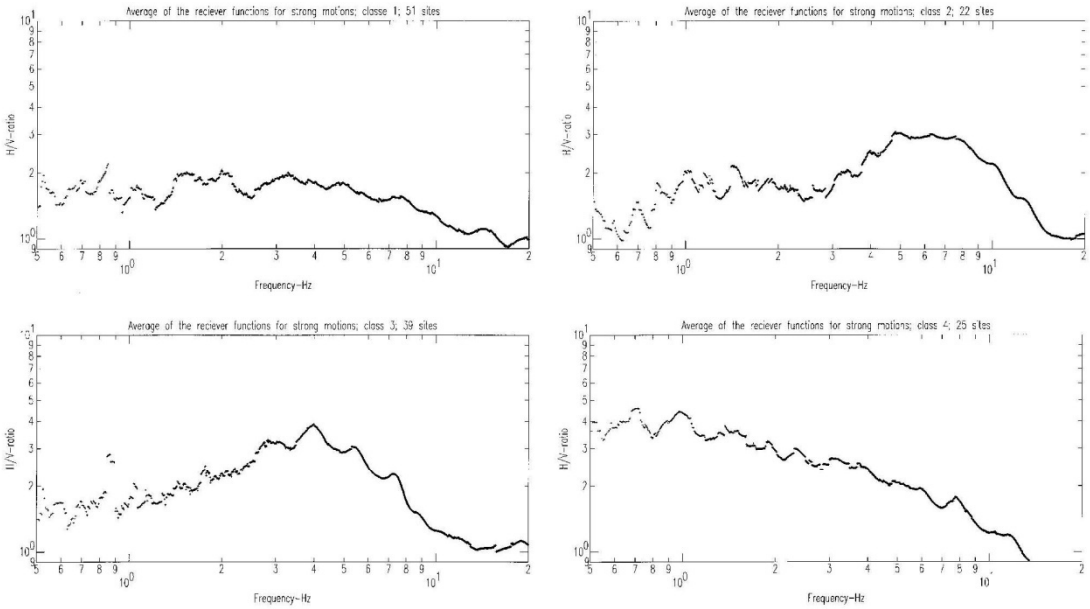

Fig. 26. Average spectra for four site classes (using the RF SMS of all 138 sites).

peak with an amplitude larger than 3–4 at frequencies between 2 and 5 Hz.

4. Site category #4 corresponds to RF curves presenting a peak with an amplitude larger than 3–4 at frequencies below 2 Hz.

According to these criteria, the 26 studied sites are classified and presented later (Section 5.1). The RF curves for these sites of each class are depicted in Fig. 19.

On the other hand, there are the cases where the RF amplitude is not equal to 4 (as it is defined earlier), but passes 3. In these cases it observes the results of other tests (if available) to distinguish the site conditions. In such intermediate cases, we have used the Vs and Vp profiles and the microtremor results to decide on the case. However, if the peaks did not approach 3 at all, that site is classified as rock site (class 1).

The measured velocity profiles corresponding to each of these classes are grouped in Fig. 20. The main characteristic of category 1 is that the S-wave exceeds 700 m s^{-1} at depths beyond 5 m, although the values may be much lower at very shallow depths (thin layers with resonance frequencies exceeding 15 Hz). On the opposite, the velocity profiles in category 4 exhibit low velocities at the surface (below 250 m s^{-1}) and at depth (below 500 m s^{-1} down to 30 m) except for three 'exceptional' sites for which there was a clear discrepancy between velocity profile and RF curve, that we checked several times and could not interpret. Velocity profiles for categories 2 and 3 are intermediate.

The microtremor H/V spectra corresponding to each of these 4 categories are displayed in Fig. 21. It clearly shows that, to the contrary of many published studies, microtremors could not, in our case, point out the fundamental frequency, this negative result may perhaps be related to the absence of strong impedance contrasts in velocity profiles, except for some class 4 sites. In any case, it requires further work, and probably new measurements, before it can be understood.

5.1. The average of vs for upper 30 m

The average value of shear wave velocity over the topmost 30 m was proposed as a criterion to distinguish the site characteristics in response to the ground motions [2–4]. Such a criterion has certainly some drawbacks, since it does not take into account the velocity profile at greater depths, which may have a prominent influence on the low frequency response. However, since there was not any other information for the Iranian sites, the relationship between our site categorization and these average velocities Vs_{30} are tested. This average shear wave velocity Vs_{30} is defined as:

$$\frac{30}{Vs_{30}} = \frac{h_1}{Vs_1} + \frac{h_2}{Vs_2} + \ldots + \frac{h_n}{Vs_n}$$

with,

$$h_1 + h_2 + h_3 + \ldots + h_n = 30 \text{ m}$$

The corresponding values for our 26 sites are listed in Table 2, and the distribution of Vs_{30} for different site classes

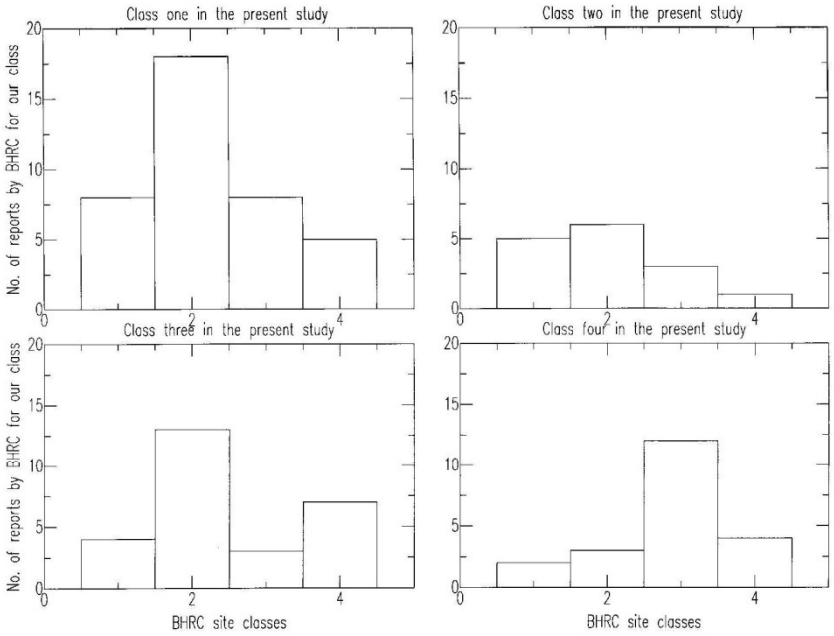

Fig. 27. The comparison of the site classification in this study and that of BHRC (1993), the BHRC site classes are compared to each of the four classes defined in the present study.

is shown in Fig. 22. Although the values at depth are much less reliable than at the near surface, we are rather confident in our estimate of Vs_{30} since the 'deep' values have only a limited influence in the result. Table 2 thus points out a rather clear correlation between Vs_{30} and our definition for the site classes 1–4, based on RF SMS, our criteria on RF SMS may therefore be almost equivalently replaced by the criteria on Vs_{30}, as indicated in Table 3, the correspondence turns out to be valid for 20 out of our 26 studied sites (i.e. 77% of the cases).

5.2. The discrepancies from the defined criteria

There exist some cases where peaks on RF SMS appear in a frequency band that is not consistent with Vs_{30}. The most important reasons for these discrepancies may be considered in different ways. The source effects may in some cases affect the H/V ratio [for instance, when a station was very close to the earthquake source (such as in Tabas)]. In some other cases one may think that a high velocity layer may be found at depths greater than 30 m, which could not be imaged by geoseismic methods (i.e. for an average surface velocity of 500 m s^{-1} there may exist significant amplifications at low frequencies ($f < 1$ Hz) if the corresponding thickness exceeds 125 m).

In the Hosseinieh-Olia station the peaks on RF SMS were observed in the frequency band of less than 2 Hz but the Vs_{30} is more than 500 m s^{-1} (563 m s^{-1}) (Fig. 23). The low frequency high amplifications on RF SMS (which may be seen on RF MTS as well) in Talesh (Fig. 24) and Vs_{30} = 508 m s^{-1} is also inconsistent with the limits observed for most of the other sites. The most important reasons for these discrepancies may be considered in different ways. The source effects may be more effective than site effects, where the station was very close to the earthquake, the Saadabad records which are obtained in the epicentral distances of 8–16 km [18] shows low frequency amplifications which may be associated with directivity effects or near field pulses. The high contrast of a superficial low velocity layer with a higher velocity sub-layer may cause the lower average value of Vs_{30} in Hosseinieh. There is a superficial layer with Vs = 130 m s^{-1} and a thickness of 1.5 m situated adjacent to a hard sub-layer with Vs = 672 m s^{-1}. In Talesh a high velocity layer might be found at depths greater than 30 (for a velocity of 730 m s^{-1} a depth of about 100 m to have the amplification of 0.8–1 Hz, would be expected). The same situation may be expected for Ghazvin which shows the lower amplifications in 1–2 Hz. If this situation is to be justified with the site effects, a high contrast in a depth of more than 100 m is needed.

5.3. Application to all of the Iranian strong motion data

The RF SMS method is performed to determine the site conditions for all of the Iranian strong motion data. The result of this application for 138 sites (comprising the studied sites) is shown in Table 1. This criterion is applied to categorize the Iranian sites for which strong motion

records are available with satisfactory quality. The final statistics corresponding to the 138 sites is as follows: 51 sites are in class 1 (37%), 22 sites in class 2 (16%), 39 sites in class 3 (29%) and 25 sites in class 4 (18%) (Fig. 25Fig. 26).

5.4. Quality factor for the site determination

To determine the quality of the information that is developed in this study we have used a quality factor in four steps ordered from the best to the worst quality: A to D. If there existed all of the data for a site; the 'A' quality was assigned. The order is subdivided to A1 for the coordination between the different results, and A2 for the cases when the H/V MTS or the Vs_{30} contradicted the RF SMS. Otherwise, when there were not the velocity profiles but there were all of the other results (H/V MTS and RF SMS) then the 'B' quality is marked. If there was just the RF SMS, the 'C' is assigned, and in the worst case (when the quality of the record and consequently the quality of the RF SMS was not reliable) 'D' is used. These assignments are shown in Table 1.

6. Conclusions

We conclude that the 26 sites considered in this study may be grouped in four classes: class 1 corresponds to an average velocity Vs_{30} larger than 700 m s^{-1}, and no site amplification below 15 Hz; class 2 corresponds to an average velocity Vs_{30} between 500 and 700 m s^{-1}, and an RF curve exceeding 3–4 between 5 and 15 Hz; class 3 corresponds to an average velocity Vs_{30} between 300 and 500 m s^{-1}, and a RF curve exceeding 3–4 between 2 and 5 Hz; finally class 4 corresponds to soft sites with an average velocity Vs_{30} below 300 m s^{-1}, and an RF curve exceeding 3–4 below 2 Hz.

This new record based classification may be compared to the previous 4 class classification performed by BHRC [6] on a pure geological basis: it shows that pure surface geological observations are very poor in assessing the real response of the sites to strong motions. In our study, in just 22 cases (over the 138 sites; i.e. 16%) the surface geological observations agree with the detailed sites studies (Table 3, Fig. 27). In this figure it is shown that the determination of the sites classes based on the surface observation may result in very biased conclusions, such that each site classes may be mistaken for another one.

We insist that the RF SMS method seemed stable for a lot of the studied sites, therefore we have applied this method for the first time as our essential criteria to classify the site responses. Meanwhile the microtremors studies were not consistent with the strong motion results in our studies in Iran, which might be justified with the dry-arid climate mountainous conditions in most parts of Iran, in any case the further microtremor tests should be performed. Similar studies might also be conducted in the neighbouring countries of Iran, such as Turkey, Pakistan, Afghanistan, Iraq, Caucasus and central Asian republics to develop and extrapolate the hazard mitigation results for this seismogenic region. In Iran, future developments of the strong motion network should favour the installation of instruments pairs; one on the rock outcrop and another on nearby soil. This will provide the possibility to compare the H/V results with classical site to reference ratio. Other developments may be proposed in the form of 'local arrays' for site studies in regions with high seismicity rate, and an important industrial and urban situations. We propose the first array of these series around the important city of Shiraz in southern Iran, where there is a high seismic activity, while a great part of the east of this city is located on soft soils and the underground water level is very high. Another local array with first priority of importance may be proposed for the city of Rasht on the shorelines of the Caspian sea in northern Iran (near the epicentre of the Manjil earthquake of 1990; Mw7.3).

Acknowledgements

In this study many individuals have assisted us, most notably Messrs Shirazian, Azadmanesh, Akbari and Mohseni (in IIEES) who assisted this project in the field studies, and Mirzaei-Alavijeh, Mahmoudi and Jalali in BHRC (Building and Housing Research Center, Tehran) who have completed the geoelectric tests. The financial support in Iran was provided by IIEES, and in France (for the first author) was provided by a French scholarship (Ministère Français des Affaires Etrangères), which are both duly acknowledged. The first author wants to thank F. Zoueshtiagh who has given some suggestions for article layout. Our thanks also go to Douglas McLean who has proof-read this text and has given comments to correct the orthography.

References

[1] Bard P-Y, Duval A-M, Lebrun B, Lachet C, Riepl J, Hatzfeld D, Reliability of H/V technique for site effects measurement: an experimental assessment. SDEE97, Presented at the Eighth International Conference on Soil dynamics and Earthquake Engineering, Istanbul, 1997. Soil Dynamics and Earthquake Engineering, submitted.

[2] Boore MB, Joyner WB, Fumal TE. Equations for estimating horizontal response spectra and peak acceleration from western north American earthquakes. Seismological Research Letters 1997;68(1):128–153.

[3] Boore MB, Joyner WB, Fumal TE, Estimating of response spectra and peak acceleration for western north American earthquakes, Interim report, US Geological Survey, Open-File Report, 1993. pp. 93–509.

[4] BSSC, NEHRP Recommanded provisions for seismic regulations for new buildings, part 1 provisons, Federal Emergency Management Agency, 1994. 222A, 290p.

[5] Building and Housing Research Center. Accelerograms of the Manjil Iran Earthquake of 20 June 1990, vol. 2, Pub. No#143, 1992.

[6] Building and Housing Research Center. A Collection of the Accel-

erogram Network of the Islamic Republic of Iran, Pub. No#179, 1993. 173p.

[7] Duval AM, Détermination de la réponse dun site aux séisme à l'aide de bruit de fond: evaluation expérimental, Thése de Doctorat, Université Pierre et Marie Curie, Paris, 1994.

[8] Jafari MK, Kamalian M, Chamanzad M. Microzonation of the Tehran Region. In: Proceedings of the Second International Conference on Seismology and Earthquake Engineering (SEE-2), Tehran, vol. 2, 1995, pp. 1301–1311.

[9] Jafari MK, Kamalian M, Chamanzad M. Microzonation study in the Tehran region. In: Proceedings of the Eleventh World Conference on Earthquake Engineering (WCEE), Accopolco, paper no.895, 1996.

[10] Konno K, Ohmachi T. Ground motion characteristics estimated from spectral ratio between horizontal and vertical components of microtremors. Bulletin of the Seismological Society of America 1998;88(1):228–241.

[11] Lachet C, Hatzfeld D, Bard P-Y, Thodulidis N, Papaioannou C, Savvaidis A. Site effects and microzonation in the city of Thessaloniki (Greece) comparison of different approaches. Bulletin of the Seismological society of America 1996;86(6):1692–1703.

[12] Riepl J, Bard P-Y, Hatzfeld D, Papaioannou C, Nechtschein S. Detailed evaluation of site response estimation methods across and along the sedimentary valley of Volvi (EURO-SEISTEST). Bulletin of the Seismological society of America 1998;88(2):488–502.

[13] Theodulidis N, Bard P-Y. (H/V) Spectral ratio and geological conditions: an analysis of strong motion data from Greece and Taiwan (SMART-1). Soil Dynamics and Earthquake Engineering 1995;14:177–197.

[14] Zaré M. The study of site effects on the strong ground motions during earthquakes, a case-study on the Manjil 1990 earthquake, MSc. Thesis, Engineering Geology Dept. Tarbiat-Modarres University, Tehran, 1994. 214p (in Persian).

[15] Zaré M. Site dependent attenuation of strong motions for Iran. In: 5th International Conference on Seismic Zonation, Nice, Paris: Ouest Pub, vol. 2, 1995. pp. 1227–1236.

[16] Zaré M. Deux exemples de mouvements de forts séismes en champ proche en Iran. In: 4ém Colloque National en Génie Parasismique, AFPS, Paris, Proc. vol.1, 1996. pp. 112–119.

[17] Zaré M. The soft soil site responses to the Manjil, Iran (1990) earthquake. In: Proceedings of the Eleventh World Conference on Earthquake Engineering (WCEE), Acoppolco, paper no. 1475, 1996.

[18] Zaré M, Bard P-Y, Ghafory-Ashtinany M. The Iranian accelerometric data bank, a revision and data correction. Journal of Seismology and Earthquake Engineering 1998;1(1):1–22.